ESO ASTROPHYSICS SYMPOSIA
European Southern Observatory

Series Editor: Bruno Leibundgut

I. Saviane V.D. Ivanov J. Borissova (Eds.)

Groups of Galaxies in the Nearby Universe

Proceedings
of the ESO Workshop held
at Santiago de Chile, December 5-9, 2005

Springer

Volume Editors

Ivo Saviane
Valentin D. Ivanov
ESO
Av. de Cordova 3107
Santiago, Chile

Jordanka Borissova
Universidad de Valparaiso
Av. Gran Bretana 1111
Casilla 5030
Valparaiso, Chile

Series Editor

Bruno Leibundgut
European Southern Observatory
Karl-Schwarzschild-Str. 2
85748 Garching
Germany

ISBN-13 978-3-540-71172-8 Springer Berlin Heidelberg New York

Library of Congress Control Number: 2007922597

Springer is a part of Springer Science+Business Media
springer.com

Typesetting: by the authors and techbooks using a Springer LaTeX macro package
Cover design: WMXDesign, Heidelberg

Printed on acid-free paper SPIN: 11971788 55/techbooks 5 4 3 2 1 0

Preface

This volume contains the proceeding of an international conference held in Santiago, Chile, in December 2005. The meeting was attended by nearly a hundred active researchers in the field. The following is the reproduction of an article that appeared in the March 2006 issue of the ESO Messenger.

Groups of Galaxies in the Nearby Universe

For every galaxy in the field or in clusters, there are about three galaxies in groups. Therefore, the evolution of most galaxies actually happens in groups. The Milky Way resides in a group, and groups can be found at high redshift. The current generation of 10-m class telescopes and space facilities allows to study members of nearby groups with exquisite detail and their properties can be correlated with the global properties of their host group. Finally, groups are relevant for cosmology, since they trace large-scale structures better than clusters, and the evolution of groups and clusters may be related.

Strangely, there are three times less papers on groups of galaxies than on clusters of galaxies, as revealed by an ADS search. Organizing this conference was a way to focus the attention of the community on the galaxy groups. We also wanted to offer a venue where people coming from various research fields could meet and discuss groups from different perspectives. All this happened in a friendly atmosphere created by hotel Torremayor in Santiago.

The discussion was organized in seven sessions, introduced by invited reviews: Eva Grebel (Local Group vs. Nearby Groups), Vince Eke (Groups Searches and Surveys), Chris Conselice (The Evolution of Galaxies in Groups – Observations), Gary Mamon (The Evolution of Galaxies in Groups – Theory), Ann Zabludoff (Evolution of Groups as Systems), Trevor Ponman (Interstellar Medium and Intragroup medium), Stefano Borgani (Groups in a Cosmological context), and finally Ken Freeman (Conference Summary). There were almost 50 contributed talks and 30 posters. In the following text we give a short summary of the main conference ideas, mostly based on the invited reviews.

All You Wanted To Know About Groups (But You Were Afraid To Ask)

Groups are bound structures with masses in the range $m = 10^{12-14}\mathcal{M}_{\odot}$ (Eke), containing less than 50 galaxies (Conselice), and with typical sizes of

a few Mpc. Groups detected in X-rays have luminosities of $L_X = 10^{41-43}$ erg sec^{-1} and gas temperatures of $kT = 0.1 - 3$ keV (Ponman). Most of the stellar mass in the present universe is in groups similar to the Local Group with masses $2 \times 10^{12} \mathcal{M}_\odot$ and only 2% is in clusters with $m > 5 \times 10^{14} \mathcal{M}_\odot$ (Eke). Groups were already present at redshifts $z > 1$ (Conselice). Cosmological simulations predict a much larger number of galaxy satellites than observed, and HI high velocity clouds cannot fill in this gap (Pisano). Groups follow a fundamental plane (Muriel) and the most massive ones have an X-ray halo with an extended component (Zabludoff).

A special class of groups are the so-called 'fossil groups' – isolated ellipticals with properties similar to a group, which could be the final stage of a collapsed group. However, most isolated ellipticals are not collapsed groups (Forbes). There are only 15 fossil groups known to date.

The evolution of low velocity dispersion groups is dominated by mergers, which could explain the bimodal mass function of the X-ray faint groups (X-ray faint groups tend to have low velocity dispersion and vice versa), if intermediate-mass members merge to build the largest group members (Raychaudhury). The bimodal mass function, similar to that of clusters, is confirmed in compact groups (Bomans). Compared to compact groups, the loose ones tend to have fewer low-mass members.

The results presented here were obtained thanks to large observational efforts (Table 1). Historically, the first group catalogs were biased toward compact groups, which are the easiest to identify from imaging surveys. Modern redshift surveys allow selections including recession velocities, and finding algorithms can be tested on mock catalogs generated with dark matter (DM) simulations (Eke).

Galaxies in Groups

Galaxies in groups can be affected by processes like ram pressure stripping, interactions and harassment, mergers, group tidal field, gas loss and suppressed star formation (also known as strangulation or suffocation). Merging is the most important of these because of the low relative velocities of galaxies in groups in comparison with the galaxies in clusters. Simulations show that mergers induce an intense and brief (of the order of a hundred Myr) surge of star formation before the final coalescence into a spheroid, which evolves passively afterwards. Simultaneously, mergers transfer momentum from the interacting galaxies to the group as a whole, thereby increasing the group velocity dispersion. Indeed, observations show that there are more spheroids in groups with higher velocity dispersion (Zabludoff).

Eventually, the feedback from the residual black-hole and active galactic nucleus (AGN) reduces the star formation by a factor of ten or more. At least 50% of galaxies in compact groups are low-luminosity AGNs (Martinez), while the field fraction is only 30%. Moreover, the cores of X-ray groups are often disturbed, which could be additional evidence for AGN feedback (O'Sullivan).

The selective suppression of star formation in larger group members could explain the downsizing phenomenon – the decrease of the maximum luminosity of star-forming galaxies at lower redshifts. Mergers occur mostly at redshifts $z > 1$, for example at $z = 2.5$ about 50% of bright galaxies are undergoing mergers, while today only 2% of galaxies merge per Gyr (Conselice). Most of the stars in group members also formed between redshifts $z = 2.5$ and 1.

Locally, environmental effects can be traced directly by reconstructing star formation histories of individual galaxies. For example, the fraction of intermediate-age stars of Milky Way dwarf satellites depends on their distance from the Galaxy. On the contrary, this fraction is constant in M81 satellites (Da Costa) probably due to the compactness of the M81 group, where multiple close encounters have homogenized their star formation histories.

The Evolution of Groups

The origin of groups is probably related to large-scale gaseous filaments at high redshift. Before virialization, smooth accretion, super novae and AGN activity enhance the entropy, and the metal-enriched gas cannot be retained by the shallow potential of pre-collapse groups (Ponman, Borgani). During the virialization, the central spheroidals grow via mergers. Early-type stars and enriched gas become part of the intragroup environment. Eventually, a common dark matter and a hot (X-ray) gas halos are formed (Zabludoff). The X-ray emission increases, and the X-ray halo becomes more and more regular. Later, the diffuse DM distribution will reduce the merger rate and moderate the evolution of groups. At least a fraction of groups end their lives as fossil groups.

Most low-redshift groups are just detaching from the Hubble flow, as suggested by the time evolution of the virial mass to light ratio (Mamon). In particular, the detachment for the Local Group occurred at $z < 0.7$ (Freeman). The mass-temperature and mass-luminosity distributions in the X-rays for clusters and groups can constrain the cosmological parameters (Borgani).

To summarize, as a group evolves, the dwarf-to-giant ratio, early-type galaxy fraction, intragroup starlight and metallicity, the velocity dispersion, and the mass of the central giant elliptical grow. The metallicity of the intragroup medium also increases thanks to the intragroup stars, whose ejecta do not have to overcome galactic potential wells (Zabludoff).

Observations are consistent with this scenario. As mentioned above, groups with higher velocity dispersions have higher fractions of early type galaxies. And the intragroup medium can be responsible for stripping, e.g. of NGC 2276 in the NGC 2300 group (Ponman). In turn, stripping enhances the fraction of passive galaxies in groups. Further observational support for this evolutionary scheme are the constant radial profiles of velocity dispersion, which point to a common DM halo. Next, if the early enrichment history of the intragroup gas is dominated by type II supernovae, and the late history by

type Ia supernovae, then this could explain the observed decrease of the overall metallicity toward the outskirts of the group and the alpha-enhancement in the outer parts of groups (Rasmussen) because the early ejecta had time to spread across the group.

Groups and Clusters of Galaxies

It was realized during the conference that groups are important for the evolution of clusters as well. Clusters may grow by accretion of groups, as exemplified by the Eridanus Super-group infalling toward Fornax (Brough). Therefore, some cluster properties might be explained by groups, like the X-ray medium, high dwarf to giant galaxy ratio, brightest cluster galaxies and the early-types galaxy fraction (especially in more massive groups).

Likewise, the evolution of galaxies in clusters might be dominated by group-scale environment, driving, e.g. the morphology-environment relation, the Butcher-Oemler effect, and the brightest cluster galaxies formation. For example, the intra-cluster light in Virgo probably originates in tidal interactions inside group-size structures (Mihos), favoured by their low velocity dispersion. Since tidal features are erased as clusters evolve, the presence of such features would indicate that the cluster is dynamically young, still 'fragmented' in groups.

Although mergers can happen both in clusters and groups, the high velocity dispersion in clusters leads to less efficient orbital-decay-type mergers, while more efficient, direct head-on mergers are common in groups, especially the evolved, X-ray bright ones (Mamon). This can explain the higher fraction of early type galaxies in this class of groups compared to the field and clusters.

These few paragraphs could only give a brief sense of the stimulating discussion during the five days of the conference, and we hope that all participants went away with fresh views on the current status of galaxy groups studies. The entire proceedings of the symposium are presented in this volume.

We would like to express our gratitude to the members of the SOC, and especially of the SOC Chair Duncan Forbes, for their efforts that made it possible to organize this meeting. Last but not least, the success of the conference would have been impossible without the excellent work of Maria Eugenia Gómez, Paulina Jiron and Ismael Martínez, and the financial support of ESO.

Santiago de Chile
November 2006

Ivo Saviane
Valentin D. Ivanov
Jordanka Borissova

Contents

Part I Local Group versus Nearby Groups

Local Group(s)
E.K. Grebel 3

The Local Group Dwarfs Compared
E.D. Skillman 21

Galaxy Groups in the Local Volume: An HI Perspective
B.S. Koribalski 27

HI in Local Group Analogs: What does it Tell Us about Galaxy Formation?
D.J. Pisano, D.G. Barnes, B.K. Gibson, L. Staveley-Smith, K.C. Freeman and V.A. Kilborn 33

Stellar Metallicities and Ages in Leo I dSph
M. Gullieuszik, I. Saviane, E.V. Held and L. Rizzi 39

Globular Clusters in M31 and the Local Group
S.C. Kim, M.G. Lee, D. Geisler, A. Sarajedini, W.E. Harris, H.S. Park, H.S. Hwang and J.C. Seguel 41

Properties of RR Lyrae Stars in the Inner Regions of the Large Magellanic Cloud. II. The Extended Sample
J. Borissova, D. Minniti, M. Rejkuba and D. Alves 45

Diffuse Ionized Gas in the Dwarf Galaxy DDO 53
N. Flores-Fajardo and A.M. Hidalgo-Gámez 47

Part II Groups Searches and Surveys

Galaxy Group Searches and Surveys
V. Eke 53

Baryon Budget in 2 keV Galaxy Groups
A. Hornstrup, A. Vikhlinin, R. Burenin, H. Ebeling, O. Kotov, K. Pedersen, H. Quintana and J. Rasmussen 67

Isolated Compact Groups of Galaxies in the 2dF Galaxy Redshift Survey
J. Saucedo-Morales and P. Loera-González 73

Environmental Effects on Galaxy Evolution Based on the Sloan Digital Sky Survey
T. Goto 79

DPOSS II Compact Groups: The EMMI/NTT Survey
E. Pompei, A. Iovino and R.R. de Carvalho 85

The Low-luminosity Galaxy Population in the NGC 5044 Group
S.A. Cellone and A. Buzzoni 91

The Galaxy Evolution Multi-wavelength Study (GEMS) Project
D.A. Forbes 97

A Search for Ultra-compact Dwarf Galaxies in the NGC 1023 Group of Galaxies
S. Mieske, M.J. West and C.M. de Oliveira 103

Dwarf Galaxies in the Antlia Cluster: First Results
A.V.S. Castelli, L.P. Bassino, S.A. Cellone, T. Richtler, B. Dirsch, L. Infante, C. Aruta and M. Gómez 109

Compact Groups: A Statistical Analysis
E. Díaz, C. Ragone, H. Muriel 111

Study of Intracluster Diffuse Light within the Fornax Cluster
A.C. Cárdenas, S.A. Cellone and J.C. Forte 113

BVRI Photometric Analysis for the Galaxy Group NGC 4410
J.A.P. Grana, S.N. Kemp, A.C. Katsiyannis, E. de la Fuente, A. Franco-Balderas and J. Meaburn 115

Photometric and Kinematical Study of Nearby Groups of Galaxies Around IC 65 and NGC 6962
J. Vennik and E. Tago 119

Part III Evolution of Galaxies in Groups – Observational

The History of Galaxy Formation in Groups: An Observational Perspective
C.J. Conselice 123

Deep Optical Imaging of ESO 383–45: A Galaxy Undergoing Ram-pressure Stripping, or a Tidal Merger Remnant?
S.N. Kemp, E. de la Fuente, A. Franco-Balderas and J. Meaburn 139

Morphologies and Star Formation in $z \sim 0.5$ Group Galaxies
D.J. Wilman, M.L. Balogh, R.G. Bower, J.S. Mulchaey, A. Oemler Jnr and R.G. Carlberg 145

Formation and Evolution of Early-type Galaxies
C. Chiosi and E. Merlin 151

Dwarf Galaxies in Hickson Compact Groups
D.J. Bomans, E. Krusch, R.-J. Dettmar, V. Müller and C. Taylor . . . 157

Low Luminosity Activity in Hickson Compact Groups
M.A. Martinez, A. del Olmo, J. Perea and R. Coziol 163

Dwarf Elliptical Galaxies in Cen A Group
M. Rejkuba 169

Stellar Populations in Compact Group Elliptical Galaxies
I.G. de la Rosa, R.R. de Carvalho, A. Vazdekis and B. Barbuy 175

***Spitzer* 4.5 μm Luminosity-Metallicity and Mass-Metallicity Relations for Nearby Dwarf Irregular Galaxies**
H. Lee, E.D. Skillman, J.M. Cannon, D.C. Jackson, R.D. Gehrz, E. Polomski and C.E. Woodward 181

Shapes and Galaxy Flows Around Clusters and Groups of Galaxies
N. Padilla 187

Infrared Surface Brightness Analysis of Galaxies in Compact Groups
I. Plauchu-Frayn, R. Coziol and H. Bravo-Alfaro 193

Size and Orientation of the 'Z' in ZRGs
C. Zier 195

IMF Model Sampling and the Emission Lines in Star Forming Galaxies
G. Magris C., F. Molina and A. Parravano 197

Part IV Evolution of Galaxies in Groups – Theoretical

The Evolution of Galaxy Groups and of Galaxies Therein
G.A. Mamon 203

Diffuse Starlight and the Evolution of Groups and Clusters of Galaxies
J.C. Mihos 221

Simulating Diffuse Light in Galaxy Clusters
C.S. Rudick, J.C. Mihos and C. McBride 227

Lensing by Groups
O. Möller, M. Kitzbichler, V.R. Eke and P. Natarajan 233

The Role of Tidal Interactions in Driving Galaxy Evolution
J. Pérez, P.B. Tissera, D.G. Lambas, C. Scannapieco and M.E. De Rossi 239

Chemical and Photometric Evolution of NGC 6822 in a Cosmological Context
L. Carigi, P. Colín and M. Peimbert 241

Evolution of the Luminosity-Metallicity-Stellar Mass Correlation in a Hierarchical Scenario
M.E. De Rossi, P.B. Tissera and C. Scannapieco 243

Part V Evolution of Groups as Systems

Groups: The Rich, the Poor and the Destitute
A. Zabludoff 249

The Eridanus Supergroup
S. Brough 261

ClG J1205 + 4429, the Most Distant Fossil Group at z = 0.59
F. Durret, M.P. Ulmer, C. Adami G. Covone and G.B. Lima Neto 267

Past and Future of CG J1720-67.8: Constraints from Observations and Models
S. Temporin and W. Kapferer 273

The Optical and Near-infrared Properties of Nearby Groups of Galaxies
S. Raychaudhury and T.A. Miles 279

Halo Shapes, Dynamics and Environment
M. Plionis, C. Ragone and S. Basilakos 285

II Zwicky 23 and Family
E.H. Wehner, J.S. Gallagher, G.C. Rudie and P.J. Cigan 291

Dynamical Analysis of NGC 5128 and the Centaurus Group
K.A. Woodley 297

Seyfert's Sextet (HGC 79): An Evolved Stephan's Quintet?
A. Durbala, J. Sulentic, M. Rosado, A. del Olmo, J. Perea and H. Plana 301

Part VI Interstellar Medium and Intragroup Medium

The HI Content of a Sample of Groups with Different Dynamical Ages
E.E. Freeland 307

Neutral Hydrogen in Galaxy Groups
V.A. Kilborn 313

Environmental Effects on Clusters at z = 0.2: Strong Galaxy Disruption in A 2667 and A 1689
H. Bravo–Alfaro, L. Cortese, G. Covone and J.-P. Kneib 319

Metallicity Structure in X-ray Bright Galaxy Groups
J. Rasmussen and T.J. Ponman 325

An X-ray View of the Cores of Galaxy Groups: Effects of AGN and Mergers on the IGM
E. O'Sullivan and J.M. Vrtilek 331

Active Galaxies, Thermal Conduction and Entropy of Gas in Galaxy Groups and Clusters
S. Roychowdhury 337

Stellar and Ionized Gas Kinematics of Peculiar Virgo Cluster Galaxies
J.R. Cortés, J.D.P. Kenney and E. Hardy 343

ISM of Galaxies in Extremely Different Environments: Isolated vs Compact Groups
L. Verdes-Montenegro, M. S. Yun, S. Borthakur, D. Espada, I. Sellim, E. Athanassoula, G. Bergond, A. Bosma, F. Combes, E. Garcia, W.K. Huchtmeier, S. Leon, U. Lisenfeld, S. Odewahn, T. Ponman, J. Rasmussen, J. Sabater, J. Sulentic and S. Verley 349

Comparing Semi-Analytical and Numerical Modelling of the ICM Chemical Enrichment
S.A. Cora, L. Tornatore and S. Borgani 355

Part VII Groups in a Cosmological Context

Groups and Clusters of Galaxies in Cosmological Context
S. Borgani 361

The Association of Compact Groups of Galaxies with Large-scale Structures
H. Andernach and R. Coziol 379

Probing the Environment with Galaxy Dynamics
A.J. Romanowsky 385

Index 391

The Internal Dynamics of A115 Nearby Cluster of Galaxies
R. Barrena, W. Boschin and M. Girardi 391

Dynamics of the Radio–halo Cluster A2744: An Optical Study
W. Boschin, R. Barrena, M. Girardi and M. Spolaor 393

Dynamics and Shape of Brightest Cluster Galaxies
H. Andernach, K. Alamo-Martínez, R. Coziol and E. Tago 395

Author Index 397

List of Contributors

Andernach Heinz
Universidad de Guanajuato
Mexico
heinz@astro.ugto.mx

Barrena Rafael
Instituto de Astrofisica de Canarias
Spain
rbarrena@iac.es

Bassino Lilia
Universidad Nacional de La Plata
Argentina
lbassino@fcaglp.unlp.edu.ar

Bomans Dominik
Ruhr-University Bochum
Germany
bomans@astro.rub.de

Borgani Stefano
Universita di Trieste
Italy
borgani@oats.inaf.it

Borissova Jordanka
ESO
Chile
jborisso@eso.org

Brasileiro Francisca
IAG
Univ. de Sao Paulo
Brazil
chica@astro.iag.usp.br

Bravo-Alfaro Hector
Universidad de Guanajuato
Mexico
hector@astro.ugto.mx

Brough Sarah
Swinburne University
Australia
sbrough@astro.swin.edu.au

Carigi Leticia
Instituto de Astronomia - UNAM
Mexico
carigi@astroscu.unam.mx

Cellone Sergio
Universidad Nacional de La Plata
Argentina
scellone@fcaglp.unlp.edu.ar

Chiosi Cesare
Padova University
Italy
chiosi@pd.astro.it

Chomiuk Laura
University of Wisconsin-Madison
chomiuk@astro.wisc.edu

Cifuentes Cárdenas Alejandro
Universidad Nacional de La Plata
Argentina
acifuentes@fcaglp.unlp.edu.ar

Coenda Valeria
IATE, Obs. Astron. de Cordova
Argentina
vcoenda@oac.uncor.edu

Conselice Christopher
University of Nottingham
UK
cc@astro.caltech.edu

Cooray Asantha
University of California
Irvine
USA
acooray@uci.edu

Cora Sofia Alejandra
Inst. de Astr. de La Plata, CONICET
Argentina
sacora@fcaglp.unlp.edu.ar

Cortes Juan
Universidad de Chile
jcortes@das.uchile.cl

Da Costa Gary
Mt Stromlo Obs. RSAA
ANU
Australia
gdc@mso.anu.edu.au

De Rossi Maria Emilia
IATE
Obs. Astron. de Cordova
Argentina
maribblue@hotmail.com

Diaz Eugenia
IATE
Obs. Astron. de Cordova
Argentina
euge@mail.oac.uncor.edu

Durret Florence
IAP
France
durret@iap.fr

Eke Vincent
University of Durham
UK
v.r.eke@durham.ac.uk

Flores Nahiely
Instituto de Astronomia - UNAM
Mexico
nahiely@astroscu.unam.mx

Forbes Duncan
Swinburne University
Australia
dforbes@swin.edu.au

Freeland Emily
University of Wisconsin
USA
freeland@astro.wisc.edu

Freeman Ken
Mt Stromlo Obs.
RSAA
ANU
Australia
kcf@mso.anu.edu.au

Garcia de la Rosa I.
IAC (Spain) - IAG (Brazil)
ignacio@astro.iag.usp.br

Gastaldello Fabio
University of California
Irvine
USA
gasta@uci.edu

Geisler Doug
Universidad de Concepción
Chile
dgeisler@astro-udec.cl

Giovanelli Riccardo
Cornell University
USA
riccardo@astro.cornell.edu

Goto Tomotsugu
Japan Aerospace Exploration
Agency
Japan
tomo@ir.isas.jaxa.jp

Grebel Eva K.
University of Basel
Switzerland
grebel@astro.unibas.ch

Gullieuszik Marco
Padova University/ESO
Italy
gullieus@pd.astro.it

Hau George
Durham University
UK
george.hau@durham.ac.uk

Hernandez-Martinez L.
Instituto de Astronomia - UNAM
Mexico
lhernand@astroscu.unam.mx

Hibbard John
NRAO
USA
jhibbard@nrao.edu

Hornstrup Allan
Danish National Space Center
Denmark
allan@spacecenter.dk

Infante Leopoldo
Pontificia Universidad Catolica
Chile
linfante@astro.puc.cl

Ivanov Valentin
ESO
Chile
vivanov@eso.org

Jeltema Tesla
Carnegie Observatories
USA
tesla@ociw.edu

Kemp Simon
Universidad de Guadalajara
Mexico
snk@astro.iam.udg.mx

Kilborn Virginia
Swinburne University
Australia
vkilborn@swin.edu.au

Kim Sang Chul
Astr. and Space Science Inst.
Korea
sckim@kasi.re.kr

Koribalski Baerbel S.
Austr. Tel. Nat. Facility
Epping
Australia
Baerbel.Koribalski@atnf.csiro.au

Lares Marcelo
IATE
Obs. Astron. de Cordova
Argentina
mlares@mail.oac.uncor.edu

Lee Henry
University of Minnesota
USA
hlee@astro.umn.edu

Lynam Paul
ESO
Chile
plynam@eso.org

Magris Gladis
CIDA
Venezuela
magris@cida.ve

Mamon Gary
IAP
France
gam@iap.fr

Martinez Carballo M. A.
Instituto de Astrof. de Andalucia-CSIC
Spain
geli@iaa.es

Mazzotta Pasquale
CfA, USA – Univ. of Roma "Tor Vergata"
Italy
mazzotta@roma2.infn.it

Mieske Steffen
ESO/Garching
Germany
smieske@eso.org

Mihos Christopher
Case Western Reserve Univ.
Cleveland
USA
mihos@case.edu

Möller Ole
MPA
Garching
Germany
ole@mpa-garching.mpg.de

Motta Veronica
Pontificia Universidad Catolica
Chile
vmotta@astro.puc.cl

Muriel Hernan
IATE
Obs. Astron. de Cordova
Argentina
hernan@oac.uncor.edu

Oliveira C. M. de
Universidade de Sao Paulo
Brazil
oliveira@astro.iag.usp.br

O'Mill Ana Laura
IATE
Obs. Astron. de Cordova
Argentina
aomill@oac.uncor.edu

O'Sullivan Ewan
CfA
USA
eosullivan@head.cfa.harvard.edu

Padilla Nelson
Pontificia Universidad Catolica
Chile
npadilla@astro.puc.cl

Paz Dante
IATE
Obs. Astron. de Cordova
Argentina
dpaz@oac.uncor.edu

Perez Grana Arturo
Universidad de Guadalajara
Mexico
rivenzhell@yahoo.com

Perez Maria Josefa
Universidad Nacional de La Plata
Argentina
jperez@fcaglp.unlp.edu.ar

Plauchu-F. Ilse
Universidad de Guanajuato
Mexico
plauchuf@astro.ugto.mx

Plionis Manolis
INAOE-Mexico & NOA-Greece
mplionis@inaoep.mx

Pompei Emanuela
ESO
Chile
epompei@eso.org

Ponman Trevor
University of Birmingham
UK
tjp@star.sr.bham.ac.uk

Ragone F. Cinthia
IATE
Obs. Astron. de Cordova
Argentina
cin@oac.uncor.edu

Rasmussen Jesper
University of Birmingham
UK
jesper@star.sr.bham.ac.uk

Raychaudhury Somak
University of Birmingham
UK
somak@star.sr.bham.ac.uk

Rejkuba Marina
ESO/Garching
Germany
mrejkuba@eso.org

Rodriguez-Gonzalez Ary
INAOE-Mexico
ary@inaoep.mx

Romanowsky Aaron
Universidad de Concepcion
Chile
romanow@astro-udec.cl

Rosado Margarita
Instituto de Astronoma - UNAM
Mexico
margarit@astroscu.unam.mx

Roychowdhury Suparna
Raman Research Institute
Bangalore
India
suparna@rri.res.in

Rudick Craig
Case Western Reserve Univ.
Cleveland
USA
craig@fafnir.astr.cwru.edu

Saucedo-Morales Julio
Universidad de Sonora
Mexico
jsaucedo@astro.uson.mx

Saviane Ivo
ESO
Chile
isaviane@eso.org

Skillman Evan D.
University of Minnesota
USA
skillman@astro.umn.edu

Smith Analia
Universidad Nacional de La Plata
Argentina
asmith@fcaglp.unlp.edu.ar

Vennik Jaan
Tartu Observatory
Estonia
vennik@aai.ee

Verdes-Montenegro L.
Inst. de Astrof. de Andalucia-CSIC
Spain
lourdes@iaa.es

Wehner Elizabeth
McMaster University
Canada
wehner@astro.wisc.edu

Wilman David
MPI f. Extraterrestrial Physics
Germany
dwilman@mpe.mpg.de

Woodley Kristin
McMaster University
Canada
woodleka@physics.mcmaster.ca

Zabludoff Ann
University of Arizona
USA
azabludoff@as.arizona.edu

Zandivarez Ariel
IATE
Obs. Astron. de Cordova
Argentina
arielz@mail.oac.uncor.edu

Zier Christian
Raman Research Institute
Bangalore
India
chzier@rri.res.in

Zimer Marc
MPE / University of Vienna
Austria
zimer@astro.univie.ac.at

Local Group(s)

E.K. Grebel

Astronomical Institute of the University of Basel, Department of Physics and Astronomy, Venusstrasse 7, CH-4102 Binningen, Switzerland
grebel@astro.unibas.ch

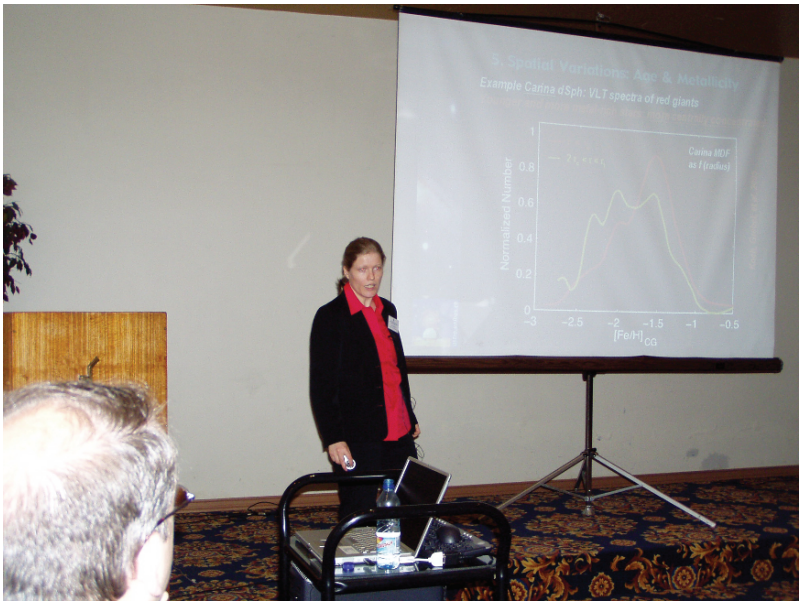

Summary. The properties of the galaxies of the Local Group are reviewed, followed by a brief discussion of nearby groups. The galaxy groups in our vicinity – the M81 group, the Cen A group, and the IC 342/Maffei group – are in many respects Local Group analogs: Their luminosity functions, galaxy content, fractional galaxy type distribution, crossing times, masses, and zero-velocity surface radii are similar to those of the Local Group. Also, the nearby groups usually consist of two subgroups, some of which approach each other and may ultimately merge to form a fossil group. These poor groups contrast with the less evolved, loose and extended galaxy "clouds" such as the Scl group and the CVn I cloud. These are characterized by long crossing times, are dominated by gas-rich, late-type galaxies, and lack gas-deficient, low luminosity early-type dwarfs. These clouds may be groups still in formation. The local Hubble flow derived from the clouds and groups is very cold.

1 Why are galaxy groups interesting?

The most conspicuous gatherings of mass and luminous matter in the Universe are galaxy clusters. However, the majority of nearby galaxies – about 85% [205, 110] – is observed to be located outside of clusters and can be found mainly in galaxy groups. While galaxy clusters reveal the location of the highest concentration of visible and dark matter, these less massive galaxy agglomerations trace the distribution of the filaments of the cosmic web and hence the extended distribution of dark matter in less dense regions. In terms of luminous matter, the fraction of mass locked up in stars increases with decreasing group size [44]. Most of the stellar mass is in groups of the size of our Local Group, whereas massive clusters only contain 2% of the stellar mass in the Universe [44].

Galaxy groups come in a variety of different morphologies, shapes, and sizes, including, for instance, seemingly unbound "clouds" and "spurs" [205], loose groups, poor groups, compact groups, rich groups, etc. Precisely what constitutes a group is a question of definition and depends primarily on how many galaxies down to a certain limiting magnitude are found within a certain volume. Common usage often considers an agglomeration of some 30 galaxies within a radius of one to two Mpc a galaxy group, but this broad definition is usually adjusted to the practical needs of the actual application; for instance, when searching for groups in redshift surveys (e.g., [107, 5]).

The different types of richness and compactness of groups permit us to study galaxy evolution and environmental effects in lower-density regions, and to contrast the results with the properties and the evolutionary state of galaxies observed in the field or in rich clusters. The degree of clustering of groups increases with increasing group luminosity [179]. Within groups, the earlier-type galaxies are more strongly clustered and tend to lie closer to the centers of the groups [59], similar to the well-known morphology-density relation in galaxy clusters [41, 10]. The final stage of evolution within groups may be represented by fossil groups, which are dominated in light and mass by a large central elliptical galaxy, presumably the end product of major mergers [103, 40]. The different types of groups appear to epitomize different stages from early to advanced structure formation.

Members of galaxy groups and ensembles of groups are kinematic tracers that can be useful for mass determinations and that help to uncover the local properties of large-scale galaxy flows, such as the local Hubble flow. It has even be suggested that they may reveal the effects of dark energy on small scales (>7 Mpc; e.g., [118, 121, 148]).

The title of this contribution as assigned to me can be interpreted in two ways: Apart from the Local Group, one may understand it to cover galaxy groups that are local, i.e., nearby, or one can interpret it as referring to galaxy groups that are counterparts of the Local Group. In fact, the nearby galaxy groups often combine these two properties. Thus in this review I will concentrate mainly on the Local Group and nearby Local Group analogs.

Our own Milky Way is a member of a poor groups of galaxies, the Local Group. The nearest neighboring group, the Sextans-Antlia group, is a an even poorer group consisting only of dwarf galaxies – sometimes also referred to as a dwarf group [210], [208]. Additional poor groups are located in our vicinity. In a number of ways we live in a fairly average extragalactic neighborhood.

2 The Local Group

The Local Group is the home to two large spiral galaxies, our Milky Way and M31. The Local Group is the only place where we can study the ages, chemistry, star formation history, and kinematics of a range of different galaxies in exceptional detail based on their resolved stellar populations. Here we can truly connect stellar and extragalactic astrophysics. We can compare our observational findings with the predictions of cosmological models or, vice versa, test those predictions through targeted observations. Owing to our ability to resolve and study even the oldest populations and very faint stars in the closest galaxies and in our own Milky Way, we can conduct near-field cosmology [51], uncovering their detailed evolutionary histories based on their resolved fossil stellar record.

2.1 The Local Group census and galaxy distribution

In spite of their proximity and in spite of the large efforts invested into studying them over the past decades, the galaxies of the Local Group continue to provide surprises. As has also been found in other groups, the number of faint galaxies in the Local Group lies below theoretical expectations by about two orders of magnitude, a deficiency also known as the missing satellite problem or the cosmological substructure problem [128, 168]. A number of solutions to solve this problem have been proposed, but none has proved fully satisfactory until now. This problem remains one of the key questions in structure formation in standard cold dark matter (CDM) models. Nonetheless, considerable progress has been made in recent years in identifying new Local Group members. Within a zero-velocity radius of approximately 1 Mpc [118] the current Local Group census comprises at least 42 galaxies (including the tidal streams of Sagittarius around the Milky Way and the great stellar stream around M31, [96, 97]).

The three most luminous Local Group members are its spiral galaxies, which form two subgroups: The M31 plus M33 subgroup and the Milky Way subgroup. In terms of mass and luminosity, the Milky Way and M31 are the two dominant galaxies and may be similarly massive [45]. Each of these two galaxies is surrounded by an entourage of mainly low-mass, gas-deficient galaxies. In close proximity to M31, one compact elliptical and three dwarf elliptical (dE) galaxies are found. M31 is the only Local Group galaxy with dE companions. The remaining low-mass early-type dwarfs in the Local Group

are all dwarf spheroidal (dSph) galaxies, the least massive (total masses estimated to be a few times 10^7 $M_\odot$), least luminous ($M_V > -14$) type of galaxy known. (For a more detailed description of the different galaxy types of the Local Group, see [211, 65, 80].) The dSphs and the dEs are almost all found within a 300 kpc radius around the two dominant spirals. This radius also roughly corresponds to the size of the dark matter density profile of $\sim L_\star$ galaxies (e.g., [163, 187]). The gas-rich, late-type irregular and dwarf irregular (dIrr) galaxies, in contrast, show a much less concentrated distribution and and are the most frequent galaxy type at larger distances from the spirals.

This biased distribution is also apparent when considering the H I mass of dwarf and satellite galaxies as a function of distance to the nearest principal galaxy: The upper limits for the H I masses of dSphs are typically of the order of 10^5 $M_\odot$ or less, whereas dIrrs usually have H I masses of at least 10^7 $M_\odot$ [80]. In between, the so-called dIrr/dSph transition-type galaxies are located. These low-mass dwarf galaxies share some of the properties of dIrrs (such as a measurable gas content and recent star formation) and of dSphs (such as prominent old populations and low luminosities). Morphological segregation akin to that within the Local Group is also observed in other groups and indicates that environment plays an important role in shaping galaxy properties (e.g., [42]). The distribution of the galaxies in the Local Group is illustrated in, e.g., [61, 63].

More than half of the Local Group's galaxies are dSph galaxies. At present, we know of 22 dSphs in the Local Group. Three of the M31 dSph companions were only detected and confirmed approximately seven years ago [1, 2, 111, 71]. Two more M31 dSph companions were discovered during the past two years in the Sloan Digital Sky Survey (SDSS) and confirmed through follow-up observations by [227, 87, 229]. They are among the least luminous, lowest surface brightness dwarfs known. Altogether eight confirmed or likely dSph companions of M31 are now known. Additional faint dSphs may yet to be found, whereas other features (e.g., [169, 228]) are likely part of the giant stellar stream around M31 [98, 46]. Recent additions to the Milky Way dSph census include three extremely low surface brightness dwarfs also found the SDSS [218, 7, 230], which increases the number of Galactic early-type companions to 12. The new dSph Boo is the faintest galaxy known so far with $M_V \sim -5.7$ [7], and the new CVn dSph seems to have the lowest surface brightness of any of these dwarfs ($\mu_V \sim 28$ mag arcsec^{-2}; [230]). The recent detections beg the question whether there is a lower-mass cut-off for dwarf galaxies with luminous baryonic matter. Finally, some seven years ago a new *isolated* Local Group dSph was discovered by [213], raising the number of these rare objects to two. Isolated dSphs are of particular interest since they seem to defy commonly held ideas about the creation of dSphs through, e.g., tidal or ram pressure stripping by massive galaxies. On the other hand, since we do not know the orbits of these more distant dSphs, we cannot exclude that they may once have had close encounters with the massive galaxies.

All recent galaxy discoveries added more objects to the faint end of the Local Group's luminosity function. It is generally believed that the census is fairly complete for brighter galaxies (with the possible exception of the zone of avoidance.) Additional very low surface brightness objects may be uncovered in the coming years using large imaging sky surveys. We may expect that nearby groups also host a number of comparatively faint objects that have escaped detection so far. In spite of the recent impressive improvements in the census of nearby galaxies (see, e.g., [113, 132] and references therein) the numbers are still far too small to resolve the substructure crisis. It seems doubtful at present that new searches will add the hundreds of objects required to solve this problem – if the missing dark matter halos contain luminous matter as well.

Another promising avenue is the search for stellar streams in the halos of massive galaxies (e.g., [14, 172, 173, 220, 158, 193, 105, 183, 219, 8]), which may ultimately permit us to constrain the number of past accretion events, esp. once full phase-space information is added – one of the objectives of ESA's Gaia satellite mission [184].

Interestingly, the companions of the Milky Way do not seem to show a random distribution. Instead, they appear to be arranged along one or two polar great planes (e.g., [143, 109, 150, 52, 142]). An investigation of the satellite distribution around M31 revealed that most of its early-type companions lie along one single, almost polar great plane with high statistical significance [78, 136], see also [162]). As shown by [136], this plane does not coincide with the great stellar stream around M31. It is unclear whether these apparent satellite anisotropies have a deeper physical significance. If the satellites orbit within the planes – a requirement if the planes have any physical reality – then the satellites may have formed following interactions or the break-up of a more massive progenitor (see, e.g., [143, 109, 196, 13]). Another possibility is that the planes are indicators of a prolate dark halo of the Milky Way and M31 (e.g., [89, 171, 226]). Or we may be seeing the left-over effects of matter accretion along large-scale dark matter filaments (see [129, 226, 146] for a more detailed discussion) [136] found that the M31 polar plane includes also M33 and points in the direction of the M81 group. – In the absence of actual orbits it remains difficult to assess the meaning of the observed polar alignments, if any. For the M31 subsystem the planar alignment comprises only a subsample of the total number of its satellites [136], which may lend support to the suggestion by [226] that such distributions may also originate from random samples. Unfortunately, the distance uncertainties for galaxies in nearby groups are still too large, preventing us from conducting a similar study there.

2.2 A few remarks about star formation histories

The star formation histories of the galaxies of the Local Group have been reviewed fairly frequently (e.g., [211, 64, 67]). Here we will only summarize some interesting characteristics that have emerged in recent years.

Old populations are ubiquitous in the galaxies of the Local Group, but their fractions vary [64, 73]. For instances, horizontal branches are an unmistakable tracer of old populations and have been identified in all Local Group galaxies with sufficiently deep photometry. Here "old" refers to old Population II stars with ages >10 Gyr. We have no evidence for the existence of possible Population III stars in external galaxies. For galaxies with deep main-sequence photometry (mainly Galactic populations and satellites of the Milky Way) there is evidence for a common epoch of early (Population II) star formation. Within the currently available accuracy of the age dating techniques (<1 Gyr), the oldest detectable populations in the Milky Way and its surroundings are coeval [73]. Moreover, there is no evidence for the suppression of star formation in the low-mass galaxies of the Local Group after the end of reionization [73], contrasting predictions of certain cosmological models that suggest that low-mass halos experience complete photo-evaporation [4, 48, 201].

All Local Group galaxies show evidence for extended star formation histories, but no two galaxies share the same star formation history, not even within the same morphological type (e.g., [61]). The spirals, irregulars, and dIrrs all show evidence for active star formation over a Hubble time. In dwarf galaxies star formation proceeded largely continuously with amplitude variations. Strongly episodic star formation with long pauses in between is only seen in the Carina dSph (e.g., [167]). Even dSph galaxies with seemingly entirely old populations show large abundance spreads of more than 1 dex in [Fe/H] (e.g., [197]), which require star formation and enrichment over several Gyr [99, 157, 47]. In contrast to many dIrrs, which are able to continue to form stars for another Hubble time [94], dSphs do not show any ongoing star formation activity and appear to be devoid of gas [54] and references therein). This is unexpected, since even simple mass loss from red giants should lead to detectable amounts of gas (e.g., [221]). The Milky Way is surrounded by several dSphs with substantial intermediate-age (2 to 10 Gyr) star formation activity. One of the Galactic companions, the Fornax dSph, even ended its star formation activity only as recently as about 200 Myr ago [74]. For a more detailed discussion of the gas loss problem see [80].

Population gradients are obvious in spiral galaxies, but also many dwarf galaxies show spatial variations in their star formation histories (e.g., [63, 64]). Essentially all galaxies have extended "halos" of old Population II stars (e.g., [165]). DIrrs tend to also show extended intermediate-age populations as traced by, e.g., carbon stars (e.g., [108]). Generally, the density distributions of different populations in irregular galaxies become increasingly more regular and extended with increasing age (e.g., [20, 223]), whereas the many scattered

young star-forming regions are responsible for the irregular appearance. Large star-forming regions may remain active for several 10 to 100 Myr, revealing a complex substructure in ages (e.g., [37, 70, 212, 72, 35, 36]).

DE and dSph galaxies have usually experienced continuous star formation with decreasing intensity. Star formation tends to be longest-lasting in the centers of these galaxies, and in a number of cases radial age (and possibly metallicity) gradients are observed (see [61, 199, 95, 32, 194, 203, 137] for individual cases and [85] for a comprehensive study). Subpopulations may also be asymmetrically distributed (e.g., [199]). Overall, the Galactic dSph companions show a trend for increased intermediate-age population fractions with increasing Galactocentric distance, possibly indicating that star-forming material might have been removed earlier from closer companions [209, 61]. However, neither the fairly isolated Local Group dSphs Cetus and Tucana fit this pattern, nor do the M31 low-surface-brightness companions [81].

In the past star formation histories of galaxies with resolved stellar populations were primarily based on photometry, and on the modelling of the observed color-magnitude diagrams (as pioneered by [204, 82]). Limitations of modelling techniques are discussed in [55]. Additional complications may arise from rotation, multiplicity, unrecognized extinction effects, and transformation problems (e.g., [69, 192, 77, 224, 135, 60, 225]). While in many cases no other information but photometric data are available, information on special types of stars can provide important additional clues (e.g., [61, 63, 12, 5, 39, 86, 88]). Special types of stars can be identified photometrically if, e.g., they exhibit unique spectral features that can be traced by special filter combinations (e.g., [25, 26, 75, 62, 151, 174, 125, 21, 90, 86, 126, 134]) or if they are variable (e.g., [159, 140, 161, 141, 39, 189]).

Photometric systems with improved metallicity sensitivity have been employed to break the photometric age-metallicity degeneracy (e.g., Washington and Strömgren photometry, [56, 57, 68, 76, 92, 22]). However, this degeneracy can best be addressed spectroscopically. This is now a realistic prospect for nearby galaxies (e.g., [28, 84, 197, 186, 203, 23, 137, 138]), largely thanks to the routine availability of optical 8 to 10-m telescopes.

2.3 A few remarks on abundances

While the absorption-line measurements for stellar abundances tend to require large telescopes and long integration times, emission lines can relatively easily be measured with medium-sized telescopes. In galaxies with active star formation the metallicity of young populations can be determined by measuring the emission lines of H II regions. This has not only been done for gas-rich galaxies such as dIrrs in the Local Group and its surroundings (e.g., [200, 195, 106, 133], but is routinely carried out also for much more distant galaxies with sufficiently strong emission lines (e.g., [131]). These measurements yield the present-day abundances, and individual element abundance ratios give us information about the modes of star formation.

Also nebular abundances derived from planetary nebulae can be obtained with only a modest investment of telescope time, yielding metallicity estimates for mainly intermediate-age populations (e.g., [191, 100]), which can be age-dated within certain limits [133, 16]. Combining ages with the results from nebular abundances as well as stellar abundance measurements supports the existence of an age-metallicity relation, i.e., increasing enrichment with decreasing age (e.g., [31, 202, 66, 133, 137]). The comparison with chemical evolution models can then provide fairly detailed information about the enrichment history as well as the relative importance of closed-box evolution vs. outflows and galactic winds (e.g., [164, 31, 144, 145, 91, 137]).

For a given age, a given dIrr galaxy is usually assumed to be chemically well-mixed and homogeneous. However, there are indications in a few dIrrs for a metallicity spread in populations of similar ages based on age-datable star clusters [30] or on differing nebular abundances in H II regions [133]. For dSphs, we do not yet have data that would permit us to quantify possible abundance spreads within populations of the same age, but as noted earlier dSphs exhibit large metallicity spreads overall, even in galaxies dominated entirely by old populations (e.g., [197]).

Interestingly, high-resolution studies of individual red giants in nearby dwarf galaxies indicate that at a given [Fe/H] their [α/Fe] ratios are on average lower by $\sim$0.2 dex than those of equally metal-poor stars in the Galactic halo (e.g., [93, 197, 198, 11, 58, 188]). This makes these *present-day* dwarf galaxies – dIrrs and dSphs alike – unlikely major contributors of the build-up of the Galactic halo and hence unlikely survivors of a once much more numerous population of primary Galactic building blocks. However, at low [Fe/H] there is consistency with the abundance ratios observed in the Galactic halo, leaving very early accretion as a plausible option [80, 49].

On global scales, galaxies tend to follow a luminosity–metallicity relation in the sense that more luminous galaxies are more metal-rich. This trend is seen for all Local Group galaxies, but the metallicity–luminosity relations of dSphs and dIrrs are offset from each other [191], an offset that persists even when comparing the same metallicity tracers and the same populations [80]: DSphs have higher mean stellar metallicities at a given optical luminosity, which may imply more rapid star formation and enrichment at early times as compared to dIrrs [80]. This suggests that the old populations in dSphs and dIrrs are intrinsically different. Transitions from gas-rich to gas-poor dwarfs seem plausible only for present-day dIrr/dSphs to present-day dSphs.

2.4 A few remarks on kinematics and dark matter

The internal kinematics of galaxies are not only a valuable tool to differentiate their components, populations, and evolutionary histories, but also provide information about galaxy masses. For the large spiral galaxies, a variety of approaches have been used to constrain their masses, including stellar and gas kinematics, the kinematics of star clusters, and of satellites. These data seem

to suggest that the Milky Way and M31 may be of similar mass [139, 45, 18]. This is somewhat unexpected considering the larger luminosity, larger bulge, larger number of globular clusters, and larger physical size of M31.

While the disks of spiral galaxies exhibit differential rotation, the more massive dIrrs show solid-body rotation. Low-mass dIrrs, dIrr/dSph and dSph galaxies are dominated by random motions and do not appear to be supported by rotation. DSphs may contain large amounts of dark matter (e.g., [53]). This is inferred from the high velocity dispersion and the resulting high mass-to-light ratios derived under the assumption of virial equilibrium [160]. Indirectly, a high dark matter content is also supported by the smooth, symmetrical morphology of some nearby dSphs [176] and by the observed lack of a significant depth extent [127]. The radial velocity dispersion profiles of dSphs tend to be flat and fall off large radii [215, 216]. While detailled modelling is still in progress, the current data favor that dSphs share a common halo mass scale of about $4 \cdot 10^7$ $M_\odot$, are dark-matter dominated, and have cored mass distributions [217].

Evidence for ongoing accretion events in the Local Group have been mentioned already in Section 2.1. Stellar streams may also be contributed by disrupted globular clusters (e.g., [177, 178, 9, 83]) and can provide valuable information about the shape of the massive galaxy's halo (e.g., [170, 14, 34, 183, 104, 152]). The results can be compared to the halo shape derived from other indicators such as the halo globular cluster mass density profile, which seems to be partly of primordial origin [181]. – A well-known example of ongoing interactions is the triple system of the Magellanic Clouds and the Milky Way with the gaseous Magellanic Bridge and Magellanic Stream as interaction signatures. Tidal interactions are also apparent in the S-shaped surface density profile of the Galactic dSph Ursa Minor [180] and in the twisted isophotes of the M31 dE companions M32 and NGC 205 [19]. These galaxies and other dSphs are likely to be accreted eventually. Moreover, dwarf-dwarf interactions and interactions with gas clouds may play an important role (e.g., [214, 33, 24]). The Local Group's wealth in low-mass, gas-deficient early-type dwarfs as well as the radius-morphology relation may both be indicative of the environmental impact on galaxy evolution.

3 Other nearby groups and Local Group analogs

In our immediate cosmic neighborhood we find poor, loose groups and "clouds" or filaments. The spatial and density distribution of nearby galaxies is beautifully illustrated in [207]. A few years ago we initiated a project with the Hubble Space Telescope and ground-based telescopes to study the properties of the groups and clouds within a $\sim$5 Mpc around the Local Group, i.e., in the Local Volume [79]. This project led to an improved galaxy census and resulted in knowledge of the approximate distances, luminosities, luminous stellar content, and approximate metallicities of a large number of nearby

galaxies [112, 113, 114, 115, 38, 116, 117, 119, 153, 194, 120, 154, 122, 123, 124, 106, 130, 155, 133]; see also [27, 17, 102, 3, 182, 190]. Moreover, kinematic properties and global masses were derived, improving the characterization of these nearby groups (see also [29, 118, 121, 206, 110]). Many of the results presented in the following stem from this continuing project.

[185] find that galaxy groups are considerably more elongated than galaxy clusters, a trend that becomes most pronounced in very poor groups of galaxies. They suggest that the poorest groups of galaxies are still in the process of being assembled through galaxy infall, a scenario that is supported by the observed properties of nearby, extended galaxy "clouds" like Sculptor and CVn I [101, 122, 123]: These elongated clouds show several subclumps and are not yet in dynamical equilibrium, since their crossing times are of the order of half a Hubble time. They contain mainly early-type dwarfs, and their luminosity functions show a lack of very low-luminosity dSph galaxies. CVn I may be even less evolved than Scl. CVn I, Scl, and the Local Group form a 10 Mpc filament that appears to be driven by the free Hubble flow [123].

In contrast to the clouds, the nearby, poor groups are Local Group analogs in many respects. They tend to be dominated by two massive galaxies: In the M81 group, the dominant galaxies are the spirals M81 and NGC 2403 [119]. A prominent interaction between M81, and the irregular galaxies M82 and NGC 3077 is currently in progress (e.g., [222]), giving rise to impressive starburst phenomena in M82 (e.g., [175]) and possibly to the formation of tidal dwarfs from material torn out during past close encounters (e.g., [154]). In the Centaurus A group the spiral M83 and the peculiar elliptical Cen A (NGC 5128) dominate the mass distribution [120]. NGC 5128 seems to have experienced various accretion events in the past (e.g., [156, 166]). In the IC 342/Maffei group the main subgroups are centered around the spiral IC 342 and the elliptical Maffei I [124]. In this group the faint galaxy census is still highly incomplete due to the high foreground extinction (e.g., [15]). In any case, all of these nearby groups reveal a "binary" substructure.

Just like the Local Group, the nearby groups also exhibit an increased frequency of early-type dwarfs, particularly of dSphs, and a comparable degree of morphological segregation [66, 67]. The luminosity functions show the familiar rise at the faint end [120, 122]. The differences in the fractional dwarf galaxy type distribution between clouds and Local Group analogs supports the idea of morphological transformations induced by denser environments. In accordance with this picture, transition-type dIrr/dSph galaxies and dIrrs tend to be found at larger distances from massive galaxies (e.g., [80]), and dwarf S0 galaxies are located in the outskirts of groups (and clusters; e.g., [6, 147]). [149] note that star-forming galaxies are more likely on radial orbits and may be falling in for the first time, whereas the orbits of galaxies dominated by older populations are more consistent with isotropy.

In the M81 group, the M81 subgroup and the NGC 2403 subgroup approach each other, similar to what is seen in the Local Group between M31

and the Milky Way. A third, smaller subgroup around the less luminous spiral NGC 4236 in the M81 group appears to be currently receding from the other two subgroups [119]) and may actually even constitute a small group outside of the M81 group. In the Cen A group the two dominant subgroups also appear to be moving away from each other [120]. We have insufficient data on the other groups. – Where subgroups approach each other the final result is expected to be one single large elliptical galaxy (see also [50]) and hence a fossil group [103].

The estimated crossing times in the nearby, poor groups range from 1.8 to 5.9 Gyr with a median around ∼2.3 Gyr [110], suggesting that they are closer to reaching dynamical equilibrium than the unevolved clouds, although they are far from "fossilization". The radii of the zero-velocity surfaces (beyond which galaxies are no longer bound) of the nearby groups and of the Local Group are of the order of 1 Mpc, and the total masses of the groups are approximately a few 10^{12} $M_\odot$ [119, 120, 124]. Within groups, the mass is closely correlated with the luminous matter and concentrated at the location of the massive galaxies (in agreement also with the findings by [163, 187]).

On larger scales, the nearby groups and clouds nicely delineate the local large-scale structure [207]. The centers of the groups lie within a narrow layer with a thickness of only ±0.33 Mpc [110]. The centroids of the groups show a small velocity dispersion with respect to the Hubble flow. Overall the local Hubble flow is remarkably cold [118, 121], indicating a low local matter density [148] suggest that the local Hubble flow is best fit by ΛCDM models with signatures of the impact of dark energy already becoming noticeable at distances >7 Mpc.

4 Summary

In the Local Group, old populations are ubiquitous in all galaxies, but their fractions vary. There appears to have been a common epoch of early (Population II) star formation. All galaxies show evidence for extended star formation episodes, but no two galaxies share the same detailed star formation history. There is no obvious cessation of star-formation activity after re-ionization in low-mass galaxies. The apparent correlation between increasing intermediate-age population fraction in dSph galaxies with increasing distance from the Milky Way is not seen in the M31 dSph companions. The morphological segregation and H I mass – distance correlation in the Local Group and other nearby groups hint at the importance of environment and interactions. This is also indicated by the observed ongoing interactions and by the increased fraction of low-luminosity, early-type dwarfs in groups as compared to loose, unvirialized "clouds" of galaxies. However, there is an offset in the metallicity-luminosity relation even for old populations that shows dSphs to be too metal-rich for their luminosity in comparison to dIrrs, making a simple transformation from dIrrs to dSphs unlikely. The origin and

nature of dSphs remains a puzzle. Also, the meaning (if any) of the seemingly anisotropic distribution of the early-type companions of the Milky Way and of M31 along a polar great plane remains unclear as long as accurate orbits are lacking.

Nearby groups in the Local Volume are Local Group analogs in many respects. Their luminosity functions, galaxy content, and fractional type distribution are reminiscent of the Local Group. They show morphological segregation. Just like the Local Group, they are typically dominated by two luminous galaxies. The crossing times, group masses and radii resemble those of the Local Group. These poor groups may ultimately evolve into fossil groups once their subgroups merge. This stands in contrast to nearby galaxy "clouds", which have long crossing times, are extended, have few early-type dwarfs and are dominated by gas-rich late-type galaxies. These clouds do not show a turn-up at the faint end of the galaxy luminosity function. Perhaps they are groups in formation. – The local Hubble flow is very quiet.

References

1. Armandroff, T. E., Davies, J. E., & Jacoby, G. H.: AJ, **116**, 2287 (1998)
2. Armandroff, T. E., Jacoby, G. H., & Davies, J. E.: AJ, **118**, 1220 (1999)
3. Barazza, F. D., Binggeli, B., & Prugniel, P.: A&A, **373**, 12 (2001)
4. Barkana, R., & Loeb, A.: ApJ, **523**, 54 (1999)
5. Battinelli, P., & Demers, S.: AJ, **120**, 1801 (2000)
6. Beaulieu, S. F., Freeman, K. C., Carignan, C., Lockman, F. J., & Jerjen, H.: AJ, **131**, 325 (2006)
7. Belokurov, V., et al.: ApJ, submitted (astro-ph/0604355) (2006)
8. Belokurov, V., et al.: ApJ, **642**, L137 (2006)
9. Belokurov, V., Evans, N. W., Irwin, M. J., Hewett, P. C., & Wilkinson, M. I.: ApJ, **637**, L29 (2006)
10. Binggeli, B., Tammann, G. A., & Sandage, A.: AJ, **94**, 251 (1987)
11. Bonifacio, P., Sbordone, L., Marconi, G., Pasquini, L., & Hill, V.: A&A, **414**, 503 (2004)
12. Borissova, J., et al.: A&A, **363**, 130 (2000)
13. Bournaud, F., & Duc, P.-A.: A&A, in press (astro-ph/0605350) (2006)
14. Bullock, J. S., Kravtsov, A. V., & Weinberg, D. H.: ApJ, **548**, 33 (2001)
15. Buta, R. J., & McCall, M. L.: ApJS, **124**, 33 (1999)
16. Buzzoni, A., Arnaboldi, M., & Corradi, R. L. M.: MNRAS, **368**, 877 (2006)
17. Caldwell, N., Armandroff, T. E., Da Costa, G. S., Seitzer, P.: AJ, **115**, 535 (1998)
18. Carignan, C., Chemin, L., Huchtmeier, W. K., & Lockman, F. J.: ApJ, **641**, L109 (2006)
19. Choi, P. I., Guhathakurta, P., & Johnston, K. V.: AJ, **124**, 310 (2002)
20. Cioni, M.-R. L., van der Marel, R. P., Loup, C., & Habing, H. J.: A&A, **359**, 601 (2000)
21. Cioni, M.-R. L., & Habing, H. J.: A&A, **402**, 133 (2003)
22. Cole, A. A., Smecker-Hane, T. A., & Gallagher, J. S.: AJ, **120**, 1808 (2000)

23. Cole, A. A., Tolstoy, E., Gallagher, J. S., & Smecker-Hane, T. A.: AJ, **129**, 1465 (2005)
24. Coleman, M. G., Da Costa, G. S., Bland-Hawthorn, J., & Freeman, K. C.: AJ, **129**, 1443 (2005)
25. Cook, K. H., Aaronson, M., & Norris, J.: ApJ, **305**, 634 (1986)
26. Cook, K. H., & Aaronson, M.: AJ, **97**, 923 (1989)
27. Côté, S., Freeman, K. C., Carignan, C., & Quinn, P. J.: AJ, **114**, 1313 (1997)
28. Côté, P., Oke, J. B., & Cohen, J. G.: AJ, **118**, 1645 (1999)
29. Côté, S., Carignan, C., & Freeman, K. C.: AJ, **120**, 3027 (2000)
30. Da Costa, G. S.: in *Extragalactic Star Clusters*, IAU Symp. 207, eds. D. Geisler, E. K. Grebel, & D. Minniti (San Francisco: ASP), 83 (2002)
31. Da Costa, G. S., & Hatzidimitriou, D.: AJ, **115**, 1934 (1998)
32. Da Costa, G. S., Armandroff, T. E., Caldwell, N., & Seitzer, P.: AJ, **119**, 705 (2000)
33. de Blok, W. J. G., & Walter, F.: ApJ, **537**, L95 (2000)
34. Dehnen, W., Odenkirchen, M., Grebel, E. K., Rix, H.-W.: AJ, **127**, 2753 (2004)
35. Dieball, A., & Grebel, E. K.: A&A, **358**, 897 (2000)
36. Dieball, A., Müller, H., & Grebel, E. K.: A&A, **391**, 547 (2002)
37. Dohm-Palmer, R. C., et al.: AJ, **114**, 2527 (1997)
38. Dolphin, A. E., et al.: MNRAS, **324**, 249 (2001)
39. Dolphin, A. E., et al.: AJ, **123**, 3154 (2002)
40. D'Onghia, E., Sommer-Larsen, J., Romeo, A. D., Burkert, A., Pedersen, K., Portinari, L., & Rasmussen, J.: ApJ, **630**, L109 (2005)
41. Dressler, A.: ApJ, **236**, 351 (1980)
42. Einasto, J., Saar, E., Kaasik, A., & Chernin, A. D.: Nature, **252**, 111 (1974)
43. Eke, V. R., et al.: 2004, MNRAS, **348**, 866 (2004)
44. Eke, V. R., Baugh, C. M., Cole, S., Frenk, C. S., King, H. M., & Peacock, J. A.: MNRAS, **362**, 1233 (2005)
45. Evans, N. W., Wilkinson, M. I., Guhathakurta, P., Grebel, E. K., & Vogt, S. S.: ApJ, **540**, L9 (2000)
46. Fardal, M. A., Babul, A., Geehan, J. J., & Guhathakurta, P.: MNRAS, **366**, 1012 (2006)
47. Fenner, Y., Gibson, B. K., Gallino, R., & Lugaro, M.: ApJ, submitted (astro-ph/0602489) (2006)
48. Ferrara, A., & Tolstoy, E.: MNRAS, **313**, 291 (2000)
49. Font, A. S., Johnston, K. V., Bullock, J. S., & Robertson, B. E.: ApJ, **638**, 585 (2006)
50. Forbes, D. A., Masters, K. L., Minniti, D., & Barmby, P.: A&A, **358**, 471 (2000)
51. Freeman, K., & Bland-Hawthorn, J.: ARA&A, **40**, 487 (2002)
52. Fusi Pecci, F., Bellazzini, M., Cacciari, C., & Ferraro, F. R.: AJ, **110**, 1664 (1995)
53. Gallagher, J. S., & Wyse, R. F. G.: PASP, **106**, 1225 (1994)
54. Gallagher, J. S., et al.: ApJ, **588**, 326 (2003)
55. Gallart, C., Zoccali, M., & Aparicio, A.: ARA&A, **43**, 387 (2005)
56. Geisler, D.: 1986, PASP, **98**, 762 (1986)
57. Geisler, D., Claria, J. J., & Minniti, D.: AJ, **102**, 1836 (1991)
58. Geisler, D., Smith, V. V., Wallerstein, G., Gonzalez, G., & Charbonnel, C.: AJ, **129**, 1428 (2005)

59. Girardi, M., Rigoni, E., Mardirossian, F., & Mezzetti, M.: A&A, **406**, 403 (2003)
60. Girardi, L., et al.: A&A, **422**, 205 (2004)
61. Grebel, E. K.: Reviews in Modern Astronomy, **10**, 27 (1997)
62. Grebel, E. K.: A&A, **317**, 448 (1997)
63. Grebel, E. K.: in *The Stellar Content of the Local Group*, IAU Symp. 192, eds. P. Whitelock & R. Cannon (San Francisco: ASP), 17 (1999)
64. Grebel, E. K. 2000, in ESA SP-445: *Star Formation from the Small to the Large Scale*, eds. F. Favata, A. Kaas, & A. Wilson (Noordwijk: ESA), 87
65. Grebel, E. K.: Ap&SSS, **277**, 231 (2001)
66. Grebel, E. K.: in *Origin and Evolution of the Elements*, Carnegie Centennial Symposia, Carnegie Astrophysics Series, eds. A. McWilliam & M. Rauch (Cambridge: CUP), 234 (2004)
67. Grebel, E. K.: in *Stellar Astrophysics with the World's Largest Telescopes*, AIP Conf. Proc. 752, eds. J. Mikołaewska & A. Olech (Melville: AIP), 161 (2005)
68. Grebel, E. K., & Richtler, T.: A&A, **253**, 359 (1992)
69. Grebel, E. K., & Roberts, W. J.: A&AS, **109**, 293 (1995)
70. Grebel, E. K., & Brandner, W.: in *The Magellanic Clouds and Other Dwarf Galaxies*, eds. T. Richtler & J. Braun (Aachen: Shaker Verlag), 151 (1998)
71. Grebel, E. K. & Guhathakurta, P.: ApJ, **511**, L101 (1999)
72. Grebel, E. K., & Chu, Y.-H.: AJ, **119**, 787 (2000)
73. Grebel, E. K., & Gallagher, J. S.: ApJ, **610**, L89 (2004)
74. Grebel, E. K., & Stetson, P. B.: in IAU Symp. 192, *The Stellar Content of the Local Group*, eds. P. Whitelock & R. Cannon (San Francisco: ASP), 165 (1999)
75. Grebel, E. K., Richtler, T., & de Boer, K. S.: A&A, **254**, L5 (1992)
76. Grebel, E. K., Roberts, W. J., & van de Rydt, F.: in *The Local Group: Comparative and Global Properties*, ESO Conf. and Workshop Proceedings, Third CTIO/ESO Workshop on The Local Group, eds. A. Layden, R. C. Smith, & J. Storm (Garching: ESO), 148 (1994)
77. Grebel, E. K., Roberts, W. J., & Brandner, W.: A&A, **311**, 470 (1996)
78. Grebel, E. K., Kolatt, T., & Brandner, W.: in IAU Symp. 192, *The Stellar Content of the Local Group*, eds. P. Whitelock & R. Cannon (San Francisco: ASP), 447 (1999)
79. Grebel, E. K., Seitzer, P., Dolphin, A. E., Geisler, D., Guhathakurta, P., Hodge, P. W., Karachentsev, I. D., Karachentseva, V. E., Sarajedini, A.: in *Stars, Gas, and Dust in Galaxies: Exploring the Links*, ASP Conf. Ser. 221, eds. D. Alloin, K. Olsen, & G. Galaz (San Francisco: ASP), 147
80. Grebel, E. K., Gallagher, J. S., & Harbeck, D.: AJ, **125**, 1926 (2003)
81. Grebel, E. K., Gallagher, J. S., & Harbeck, D.: AJ, submitted (2006)
82. Greggio, L., Marconi, G., Tosi, M., & Focardi, P.: AJ, **105**, 894 (1993)
83. Grillmair, C. J., & Johnson, R.: ApJ, **639**, L17 (2006)
84. Guhathakurta, P., Reitzel, D. B., & Grebel, E. K.: SPIE, **4005**, 168 (2000)
85. Harbeck, D., et al.: AJ, **122**, 3092 (2001)
86. Harbeck, D., Gallagher, J. S., & Grebel, E. K.: AJ, **127**. 145 (2004)
87. Harbeck, D., et al.: ApJ, **623**, 159 (2005)
88. Harbeck, D., Gallagher, J. S., Grebel, E. K., & Guhathakurta, P.: in *Near-field cosmology with dwarf elliptical galaxies*, IAU Coll. 198, eds. H. Jerjen & B. Binggeli (Cambridge: CUP), 30 (2005)

89. Hartwick, F. D. A.: AJ, **119**, 2248 (2000)
90. Helmi, A., et al.: ApJ, **586**, 195 (2003)
91. Hensler, G., Theis, C., & Gallagher, J. S.: A&A, **426**, 25 (2004)
92. Hilker, M.: A&A, **355**, 994 (2000)
93. Hill, V., François, P., Spite, M., Primas, F., & Spite, F.: A&A, **364**, L19 (2000)
94. Hunter, D.: PASP, **109**, 937 (1997)
95. Hurley-Keller, D., Mateo, M., & Grebel, E. K.: ApJ, **523**, L25 (1999)
96. Ibata, R. A., Gilmore, G., & Irwin, M. J.: 1994, Nature, **370**, 194 (1994)
97. Ibata, R., et al.: Nature, **412**, 49 (2001)
98. Ibata, R., et al.: MNRAS, **351**, 117 (2004)
99. Ikuta, C., & Arimoto, N.: A&A, **391**, 55 (2002)
100. Jacoby, G. H., & Ciardullo, R.: ApJ, **515**, 169 (1999)
101. Jerjen, H., Freeman, K. C., & Binggeli, B.: AJ, **116**, 2873 (1998)
102. Jerjen, H., Binggeli, B., & Freeman, K. C.: AJ, **119**, 593 (2000)
103. Jones, L. R., Ponman, T. J., Horton, A., Babul, A., Ebeling, H., & Burke, D. J.: MNRAS, **343**, 627 (2003)
104. Johnston, K. V., Law, D. R., & Majewski, S. R.: ApJ, **619**, 800 (2005)
105. Juric, M., et al.: submitted (astro-ph/0510520) (2005)
106. Lee, H., Grebel, E. K., & Hodge, P. W.: A&A, **401**, 141 (2003)
107. Lee, B. C., et al.: AJ, **127**, 1811 (2004)
108. Letarte, B., Demers, S., Battinelli, P., & Kunkel, W. E.: AJ, **123**, 832 (2002)
109. Lynden-Bell, D.: Observatory, **102**, 202 (1982)
110. Karachentsev, I. D.: AJ, **129**, 178 (2005)
111. Karachentsev, I. D. & Karachentseva, V. E.: A&A, **341**, 355 (1999)
112. Karachentsev, I. D., et al.: A&A, **352**, 399 (1999)
113. Karachentsev, I. D., Karachentseva, V. E., Suchkov, A. A., & Grebel, E. K.: A&AS, **145**, 415 (2000)
114. Karachentsev, I. D., et al.: ApJ, **542**, 128 (2000)
115. Karachentsev, I. D., et al.: A&A, **363**, 117 (2000)
116. Karachentsev, I. D., et al.: A&A, **375**, 359 (2001)
117. Karachentsev, I. D., et al.: A&A, **379**, 407 (2001)
118. Karachentsev, I. D., et al.: A&A, **389**, 812 (2002)
119. Karachentsev, I. D., et al.: A&A, **383**, 125 (2002)
120. Karachentsev, I. D., et al.: A&A, **385**, 21 (2002)
121. Karachentsev, I. D., et al.: A&A, **398**, 479 (2003)
122. Karachentsev, I. D., et al.: A&A, **398**, 467 (2003)
123. Karachentsev, I. D., et al.: A&A, **404**, 93 (2003)
124. Karachentsev, I. D., et al.: A&A, **408**, 111 (2003)
125. Keller, S. C., Grebel, E. K., Miller, G. J., & Yoss, K. M.: AJ, **122**, 248 (2001)
126. Kerschbaum, F., Nowotny, W., Olofsson, H., & Schwarz, H. E.: A&A, **427**, 613 (2004)
127. Klessen, R. S., Grebel, E. K., & Harbeck, D.: ApJ, **389**, 798 (2003)
128. Klypin, A., Kravtsov, A. V., Valenzuela, O., & Prada, F.: ApJ, **522**, 82 (1999)
129. Knebe, A., et al.: ApJ, **603**, 7 (2004)
130. Kniazev, A. Y., et al.: ApJ, **593**, L73 (2003)
131. Kniazev, A. Y., et al.: ApJS, **153**, 429 (2004)
132. Kniazev, A. Y., et al.: AJ, **127**, 704 (2004)
133. Kniazev, A. Y., et al.: AJ, **130**, 1558 (2005)

134. Kniazev, A. Y., Grebel, E. K., Zucker, D. B., Bell, E., & Harris, H.: in *Planetary Nebulae beyond the Milky Way*, ESO Astrophysics Symposia, eds. J. R. Walsh, L. Stanghellini, & N. G. Douglas (Heidelberg: Springer Verlag), 46 (2006)
135. Koch, A., Odenkirchen, M., Grebel, E. K., & Caldwell, J. A. R.: AN, **325**, 299 (2004)
136. Koch, A., & Grebel, E. K.: AJ, **131**, 1405 (2006)
137. Koch, A., et al.: AJ, **131**, 895 (2006)
138. Koch, A., Grebel, E. K., Wyse, R. F. G., Kleyna, J. T., Wilkinson, M. I., Harbeck, D. R., Gilmore, G. F., & Evans, N. W.: The ESO Messenger, **123**, 38 (2006)
139. Kochanek, C. S.: ApJ, **457**, 228 (1996)
140. Kovács, G., & Zsoldos, E.: A&A, **293**, L57 (1995)
141. Kovács, G.: A&A, **375**, 469 (2001)
142. Kroupa, P., Theis, C., & Boily, C. M.: A&A, **431**, 517 (2005)
143. Kunkel, W. E.: ApJ, **228**, 718 (1979)
144. Lanfranchi, G. A., & Matteucci, F.: MNRAS, **345**, 71 (2003)
145. Lanfranchi, G. A., & Matteucci, F.: MNRAS, **351**, 1338 (2004)
146. Libeskind, N. I., et al.: MNRAS, **363**, 146 (2005)
147. Lisker, T., Grebel, E. K., & Binggeli, B.: AJ, **131**, in press (astro-ph/0604216)
148. Macciò, A. V., Governato, F., & Horellou, C.: MNRAS, **359**, 941 (2005)
149. Mahdavi, A., Geller, M. J., Böhringer, H., Kurtz, M. J., & Ramella, M.: ApJ, **518**, 69 (1999)
150. Majewski, S. R.: ApJ, **431**, L17 (1994)
151. Majewski, S. R., Ostheimer, J. C., Kunkel, W. E., & Patterson, R. J.: AJ, **120**, 2550 (2000)
152. Majewski, S. R., Law, D. R., Polak, A. A., Patterson, R. J.: ApJ, **637**, L25 (2006)
153. Makarova, L. N., et al.: A&A, **384**, 72 (2002)
154. Makarova, L. N., et al.: A&A, **396**, 473 (2002)
155. Makarova, L. N., et al.: A&A, **433**, 751 (2005)
156. Malin, D. F., Quinn, P. J., & Graham, J. A.: ApJ, **272**, L5 (1983)
157. Marcolini, A., D'Ercole, A., & Brighenti, F.: MNRAS, submitted (astro-ph/0602386) (2006)
158. Martin, N. F., Ibata, R. A., Bellazzini, M., Irwin, M. J., Lewis, G. F., & Dehnen, W.: MNRAS, **348**, 12 (2004)
159. Mateo, M., Kubiak, M., Szymanski, M., Kaluzny, J., Krzeminski, W., & Udalski, A.: AJ, **110**, 1141 (1995)
160. Mateo, M.: in *The Nature of Elliptical Galaxies*, 2nd Stromlo Symposium, ASP Conf. Ser. 116, eds. M. Arnaboldi, G. S. Da Costa, and P. Saha (San Francisco: ASP), 259 (1997)
161. Mateo, M., Hurley-Keller, D., & Nemec, J.: AJ, **115**, 1856 (1998)
162. McConnachie, A. W., & Irwin, M. J.: MNRAS, **365**, 902 (2006)
163. McKay, T. A., et al.: ApJ, **571**, L85 (2002)
164. Mighell, K. J., Sarajedini, A., & French, R. S.: AJ, **116**, 2395 (1998)
165. Minniti, D., Zijlstra, A. A., & Alonso, M. V.: AJ, **117**, 881 (1999)
166. Mirabel, I. F., et al.: A&A, **341**, 667 (1999)
167. Monelli, M., et al.: AJ, **126**, 218 (2003)
168. Moore, B., et al.: ApJ, **524**, L19 (1999)

169. Morrison, H. L., Harding, P., & Hurley-Keller, D.: ApJ, **596**, L183 (2003)
170. Murali, C., & Dubinski, J.: AJ, **118**, 911 (1999)
171. Navarro, J. F., Abadi, M. G., & Steinmetz, M.: ApJ, **613**, L41 (2004)
172. Newberg, H. J., et al.: ApJ, **569**, 245 (2002)
173. Newberg, H. J., et al.: ApJ, **596**, L191 (2003)
174. Nikolaev, S., & Weinberg, M. D.: ApJ, **542**, 804 (2000)
175. O'Connell, R. W., Gallagher, J. S., Hunter, D. A., & Colley, W. N.: ApJ, **446**, L1 (1995)
176. Odenkirchen, M., et al.: AJ, **122**, 2538 (2001)
177. Odenkirchen, M., et al.: ApJ, **548**, L165 (2001)
178. Odenkirchen, M., et al.: AJ, **126**, 2385 (2003)
179. Padilla, N. D., et al.: MNRAS, **352**, 211 (2004)
180. Palma, C., Majewski, S. R., Siegel, M. H., Patterson, R. J., Ostheimer, J. C., & Link, R.: AJ, **125**, 1352 (2003)
181. Parmentier, G., & Grebel, E. K.: MNRAS, **359**, 615 (2005)
182. Parodi, B. R., Barazza, F. D., & Binggeli, B.: A&A, **388**, 29 (2002)
183. Peñarrubia, J., et al.: ApJ, **626**, 128 (2005)
184. Perryman, M. A. C., et al.: A&A, **369**, 339 (2001)
185. Plionis, M., Basilakos, S., & Tovmassian, H. M.: MNRAS, **352**, 1323 (2004)
186. Pont, F., Zinn, R., Gallart, C., Hardy, E., & Winnick, R.: AJ, **127**, 840 (2004)
187. Prada, F., et al.: ApJ, **598**, 260 (2003)
188. Pritzl, B. J., Venn, K. A., & Irwin, M.: AJ, **130**, 2140 (2005)
189. Pritzl, B. J., Armandroff, T. E., Jacoby, G. H., & Da Costa, G. S.: AJ, **129**, 2232 (2005)
190. Rejkuba, M., et al.: A&A, **448**, 983 (2006)
191. Richer, M., McCall, M. L., & Stasinska, G.: A&A, **340**, 67 (1998)
192. Roberts, W. J., & Grebel, E. K.: A&AS, **109**, 313
193. Rocha-Pinto, H. J., et al.: ApJ, **615**, 732 (2004)
194. Sarajedini, A. et al.: ApJ, **567**, 915 (2002)
195. Saviane, I., Rizzi, L., Held, E. V., Bresolin, F., & Momany, Y.: A&A, **390**, 59 (2002)
196. Sawa, T., & Fujimoto, M.: PASJ, **57**, 429 (2005)
197. Shetrone, M. D., Côté, P., & Sargent, W. L. W.: ApJ, **548**, 592 (2001)
198. Shetrone, M., Venn, K. A., Tolstoy, E., Primas, F., Hill, V., & Kaufer, A.: AJ, **125**, 684 (2003)
199. Stetson, P. B., Hesser, J. E., & Smecker-Hane, T. A.: PASP, **110**, 533 (1998)
200. Skillman, E. D., Terlevich, R., & Melnick, J.: MNRAS, **240**, 563 (1989)
201. Susa, H., & Umemura, M.: ApJ, **600**, 1 (2004)
202. Tolstoy, E., et al.: AJ, **125**, 707 (2003)
203. Tolstoy, E., et al.: ApJ, **617**, L119 (2004)
204. Tosi, M., Greggio, L., Marconi, G., & Focardi, P.: AJ, **102**, 951 (1991)
205. Tully, R. B.: ApJ, **321**, 280 (1987)
206. Tully, R. B.: ApJ, **618**, 214 (2005)
207. Tully, R. B., & Fisher, J. R.: *Atlas of Nearby Galaxies*, CUP (1987)
208. Tully, R. B., Somerville, R. S., Trentham, N., & Verheijen, M. A. W.: ApJ, **569**, 573 (2002)
209. van den Bergh, S.: ApJ, **428**, 617 (1994)
210. van den Bergh, S.: ApJ, **517**, L97 (1999)
211. van den Bergh, S.: *The galaxies of the Local Group*, CUP (2000)

212. Walborn, N. R., Barbá, R. H., Brandner, W., Rubio, M., Grebel, E. K., & Probst, R. G.: AJ, **117**, 225 (1999)
213. Whiting, A. B., Hau, G. K. T., & Irwin, M.: AJ, **118**, 2767 (1999)
214. Wilcots, E. M., & Miller, B. W.: AJ, **116**, 2363 (1998)
215. Wilkinson, M. I., Kleyna, J. T., Evans, N. W., Gilmore, G. F., Irwin, M. J., & Grebel, E. K.: ApJ, **611**, L21 (2004)
216. Wilkinson, M. I., Kleyna, J. T., Evans, N. W., Gilmore, G. F., Read, J. I., Koch, A., Grebel, E. K., & Irwin, M. J.: in *Mass Profiles & Shapes of Cosmological Structures*, XXIst IAP Coll., EAS Publication Series 20, eds. G. A. Mamon, F. Combes, C. Defayet, & Fort, B. (Paris: EDP Sciences), 105 (2006)
217. Wilkinson, M. I., Kleyna, J. T., Gilmore, G. F., Evans, N. W., Koch, A., Grebel, E. K., Wyse, R. F. G., & Harbeck, D.: The ESO Messenger, **124**, in press (2006)
218. Willman, B., et al.: ApJ, **626**, L85 (2005)
219. Wyse, R. F. G., et al.: ApJ, **639**, L13 (2006)
220. Yanny, B., et al. 2003, ApJ, **588**, 824 (2003)
221. Young, L. M.: AJ, **119**, 188 (2000)
222. Yun, M. S., Ho, P. T. P., & Lo, K. Y.: Nature, **372**, 530 (1994)
223. Zaritsky, D., Harris, J., Grebel, E. K., & Thompson, I. B.: ApJ, **534**, L53 (2000)
224. Zaritsky, D., et al.: AJ, **123**, 855 (2002)
225. Zaritsky, D., Harris, J., Thompson, I. B., & Grebel, E. K.: AJ, **128**, 1606 (2004)
226. Zentner, A. R., Kravtsov, A. V., Gnedin, O. Y., & Klypin, A. A.: ApJ, **629**, 219 (2005)
227. Zucker, D. B., et al.: ApJ, **612**, L121 (2004)
228. Zucker, D. B., et al.: ApJ, **612**, L117 (2004)
229. Zucker, D. B., et al.: ApJ, submitted (astro-ph/0601599) (2006)
230. Zucker, D. B., et al.: ApJ, **643**, L103 (2006)

The Local Group Dwarfs Compared

E.D. Skillman

Astronomy Department, University of Minnesota
116 Church St., Minneapolis, MN, 55455, USA
skillman@astro.umn.edu

Summary. I review the differences and similarities between the dwarf irregular and dwarf spheroidal galaxies in the Local Group. New observations are resolving the long-standing problem of the relationship between dwarf elliptical and dwarf irregular galaxies. I will highlight results from an HST Archival Legacy program with the goal of producing secure star formation histories for all of the Local Group galaxies. This program uses color-magnitude diagrams from HST photometry reduced in a uniform manner by Holtzman and Dolphin to produce star formation histories via programs developed by Dolphin. Particular attention is paid to estimating statistical and systematic uncertainties. An important result is that the star formation histories of the dwarf irregular and dwarf spheroidal galaxies in the Local Group are quite similar. Ultimately, environmental influences must play a dominant role in deciding their different evolution paths. Our experience with the

Local Group galaxies guides us in understanding similar types of observations in the nearest groups.

1 Similarities between dEs and dIs

The primary distinction between dE and dI galaxies is the presence or absence of cold gas. This is usually measured through HI emission at 21 cm. The typical values of M(HI)/L for dIs range from 0.1 to 10, while most dEs are non-detections in HI or show ratios of 10^{-3} or less [20]. Otherwise, dE and dI galaxies have many similar properties. Most importantly, it has been known for a long time now that dEs and dIs have similar structures [12, 16, 5, 2].

When trying to understand the possible relationships between dE and dI galaxies, there are several observations to consider. Perhaps most important is the strong morphology – density relationships observed in both the group (e.g., [11]) and cluster (e.g., [3]) environments.

Because of their low masses, both are generally recognized as fragile systems (e.g., [6]). In his summary talk, Ken Freeman took exception to this statement and pointed to work with John Kormendy [17] showing that the lowest mass systems have the highest central densities, and, therefore, should be considered the opposite of fragile! For a long time, dEs were considered to be non-rotating systems, and lack of rotational support distinguished them from the dIs (e.g., [1]). Many dEs in the cluster environment have nuclei (e.g., [4]). In contrast, the typical dI does not show the presence of a nucleus, but centrally concentrated star formation is common (and defines the class of blue compact dwarf galaxies). Finally, almost by definition, dEs and dIs must have different star formation histories (as dEs have no current star formation and almost all dIs do). Although it has been known for quite a while that the Milky Way dSph companions show a great variety of star formation histories (e.g., [18]), it is now emerging that dIs may too (see section 2).

One of the properties which was long thought to separate the dEs from the dIs was rotation. Bender and collaborators found very little evidence of rotation in the few systems that they observed (e.g., [1]). However, recent programs to observe dEs have discovered that a significant fraction of dEs show significant rotational support [7, 8, 19, 13, 14, 23]. Interestingly, [23] find a Tully-Fisher relationship between luminosity and velocity width for the Virgo dEs which do show rotation. It is intriguing that the rotating and non-rotating dEs are not distinguished structurally.

2 Comparing star formation histories of dIrr and dSph galaxies

The section title raises an interesting question. What is the best way to compare the star formation histories of galaxies? Certainly the uniformity of analysis is important. It is also important to concentrate on robust measures (Mario Mateo says that it is important to measure the climate, not the weather). As a result, it is important to keep things simple.

Jon Holtzman and Andy Dophin have constructed an archive of all HST WFPC2 photometry in Local Group galaxies [15]. This is a wonderful resource, as all of the photometry has been compiled in a uniform way. Together with Dan Weisz (a graduate student at Minnesota), we are using this photometry database and Andy Dolphin's programs to produce star formation histories for all of these fields. In addition to taking a uniform approach, we are using only the most modern stellar evolution models, taking care to estimate systematic uncertainties in the isochrones, and quantifying random errors using Monte Carlo techniques. Through the use of well-defined statistical measures we hope to produce true comparisons of star formation histories. Preliminary results of this effort are reported in [10].

One of the diagnostic diagrams that we have come to favor is the plot of cumulative stars formed versus time. In this plot the y-axis spans from 0 to 1, so absolute star formation rates are normalized. Since Jon Holtzman advocated this diagram as meeting many of the criteria set forth above, we are now calling them "Holtzman" diagrams. Figure 1 shows a comparison of several Local Group dSphs in a single Holtzman diagram. Figure 2 shows a comparable Holtzman diagram for several Local Group dIrrs.

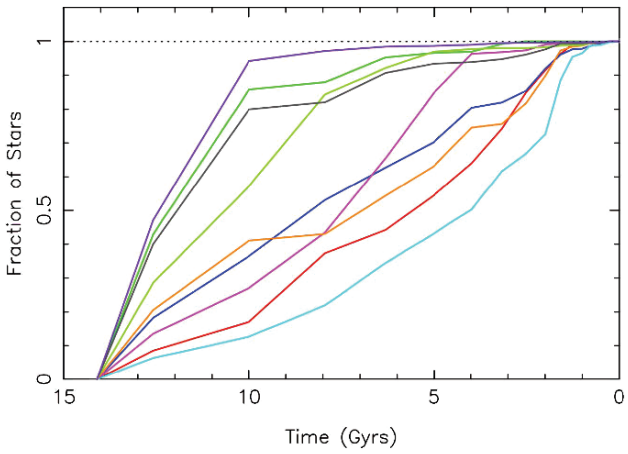

Fig. 1. Comparison of cumulative SFHs for several Local Group dSphs.

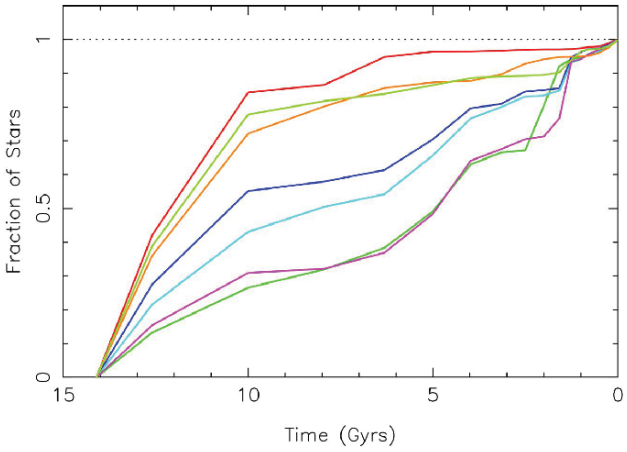

Fig. 2. Comparison of cumulative SFHs for several Local Group dIrrs.

The surprising (to most people) aspect of Figures 1 and 2, is the similarity of the two plots. The large variety of the the SFHs for the Local Group dSphs is now well known. However, it appears that the Local Groupp dIrrs show a similar variety. Even though these two families of galaxies look very different, their star formation histories have much in common. Thus, the appearances of a dwarf galaxy are affected disproportionately by their recent ($\sim$1 Gyr) star formation histories.

Admittedly, the HST field of view can be quite small compared to the angular size of some nearby Local Group galaxies, so it is possible that the HST fields are not truly representative of the whole galaxy. This is especially true since most of these galaxies are known to exhibit radial gradients in their stellar populations (e.g., [9, 22]). Are the star formation histories dominated by local or global variations? Figure 3 addresses this question for the dIrr NGC 6822. Here we compare four fields in this galaxy. Although all four lines are not the same, evidence of rapid increases in the star formation rate happen at the same times in these four independent fields. It would appear from this one example that global influences may be more important than local ones.

Hopefully, with more observations of this type, analyzed in this way, we will begin to be able to identify the factors that are most important in determining the star formation histories of the dwarf galaxies. Most importantly, as proper motions and orbits become available, we can compare the star formation histories with their environmental influences to see to what degree interactions play a role in determining the star formation histories. Future HST ACS observations will be especially important in this regard as they will provide much tighter constraints on the star formation histories.

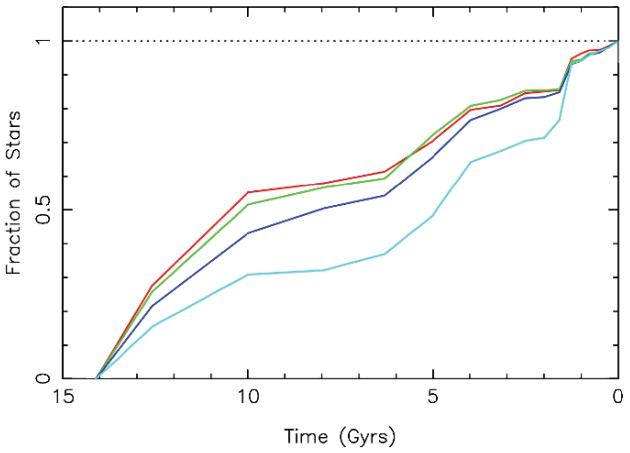

Fig. 3. Comparison of cumulative SFHs for four different fields in the Local Group dIrr NGC 6822.

I wish to thank the LOC for organizing such an exciting conference. The "Star Formation Histories of Local Group Galaxies" HST archival legacy program (PI = Dolphin) is supported by grant HST-AR-09521 from the Space Telescope Science Institute, which is operated by AURA, Inc., under NASA contract NAS5-26555. I am grateful for partial support from a NASA LTSARP grant No. NAG5-9221 and the University of Minnesota. Finally, I wish to thank the Hertzburg Institute of Astrophysics in Victoria, BC, Canada for providing me with visiting worker status.

References

1. Bender, R., Paquet, A., & Nieto, J.-L. 1991, A&A, 246, 349
2. Binggeli, B., & Cameron, L. M. 1991, A&A, 252, 27
3. Binggeli, B., Tarenghi, M., & Sandage, A. 1990, A&A, 228, 42
4. Caldwell, N. 1983, AJ, 88, 804
5. Caldwell, N., & Bothun, G. D. 1987, AJ, 94, 1126
6. Dekel, A., & Silk, J. 1986, ApJ, 303, 39
7. De Rijcke, S., Dejonghe, H., Zeilinger, W., & Hau, G. 2001, ApJ, 559, L21
8. De Rijcke, S., Dejonghe, H., Zeilinger, W., & Hau, G. 2003, A&A, 400, 119
9. Dolphin, A. E., et al. 2003, AJ, 126, 187
10. Dolphin, A. E., Weisz, D., Skillman, E.D., & Holtzman, J. A. 2006, astro-ph 0506430
11. Einasto, J., Kaasik, A., & Saar, E. 1974, Nature, 250, 309
12. Faber, S. M., & Lin, D. N. C. 1983, ApJ, 266, L17
13. Geha, M., Guhathakurta, P., & van der Marel, R. P. 2002, AJ, 124, 3073
14. Geha, M., Guhathakurta, P., & van der Marel, R. P. 2003, AJ, 126, 1794
15. Holtzman, J. A., Alfonso, C., & Dolphin, A. 2006, ApJ, submitted

16. Kormendy, J. 1985, ApJ, 295, 73
17. Kormendy, J., & Freeman, K. C. 2004, IAU Symposium, 220, 377
18. Mateo, M. L. 1998, ARA&A, 36, 435
19. Pedraz, S., et al. 2002, MNRAS, 332, L59
20. Skillman, E. D. 1996, ASP Conf. Ser. 106: The Minnesota Lectures on Extragalactic Neutral Hydrogen, 106, 208
21. Tolstoy, E., et al. 1998, AJ, 116, 1244
22. Tolstoy, E., et al. 2004, ApJL, 617, L119
23. van Zee, L., Barton, E. J., & Skillman, E. D. 2004b, AJ, 128, 2797

Galaxy Groups in the Local Volume: An HI Perspective

B.S. Koribalski

Australia Telescope National Facility, CSIRO, P.O. Box 76, Epping, NSW 1710, Australia
Baerbel.Koribalski@atnf.csiro.au

Summary. The 'Local Volume H I Survey' (LVHIS; Koribalski et al.) is a large project to obtain high-resolution and high-sensitivity H I and 20-cm radio continuum observations of all nearby ($D < 10$ Mpc) galaxies that are detected in the H I Parkes All-Sky Survey (HIPASS). We will obtain detailed maps of the H I distribution, kinematics and environment of all target galaxies, and derive their rotation curves, orientation parameters and star formation rates. By using independent distances we will be able to derive H I mass functions and local star formation densities for the Local Volume as well as nearby galaxy groups such as the Cen A and Sculptor groups. A complementary H-band survey will also allow us to analyse the (baryonic) Tully-Fisher relation.

The 'Local Volume' (the sphere of radius ∼10 Mpc centered on the Local Group) includes at least 500 known galaxies, many of which congregate in well-known groups like the Local Group, the relatively loose Sculptor Group and the more compact Centaurus A group. Now that accurate distances for many of these nearby galaxies are becoming available, mainly by Karachentsev and collaborators [1, 2], it is possible to define a complete distance-limited galaxy sample and study: the true Tully-Fisher relation; the reality of the supposedly quiet Hubble flow in the local Universe; galaxy spin vector alignments; the faint end of the H I mass; the local star-formation rate; and the unbiased properties of the faintest galaxies.

The first catalog of galaxies within 10 Mpc was compiled in 1979 by Kraan-Korteweg & Tammann [3]; it contained 179 galaxies. A decade later Huchtmeier & Richter [4, 5] published Effelsberg H I measurements for almost all non-elliptical galaxies in the sample and presented global parameters, including the Tully-Fisher relation. Following numerous updates, the latest catalog of Local Volume (LV) galaxies was presented in 2004 by Karachentsev et al. [1]; it contains 451 galaxies. About 85% of the LV population are dwarf galaxies which contribute about 4% to the local optical luminosity density and roughly 10–15% to the local H I mass density. Independent distances currently exist for more than half of the LV population within 8 Mpc, either from the luminosity of Cepheids, the tip of the red giant branch (TRGB), or surface brightness fluctuations (SBF).

Figure 1 shows the correlation between Local Group velocity, $v_{\rm LG}$, and distance, D, for ∼400 galaxies as given in the LV catalog [1] and supplemented by HIPASS data [6, 7] for new LV galaxies discovered by the author and her collaborators. The uncertainties of Cepheid, TRGB, and SBF distances are typically around 10%. The Local Group (LG; $D < 1$ Mpc), which consists of two subgroups centred around the Milky Way and Andromeda spirals, has a velocity dispersion similar to that of other nearby groups such as the Cen A/ and M 83 subgroups at ∼3.6 and ∼4.6 Mpc, respectively. We note that Centaurus A itself is the most prominent elliptical galaxy in the Local Volume.

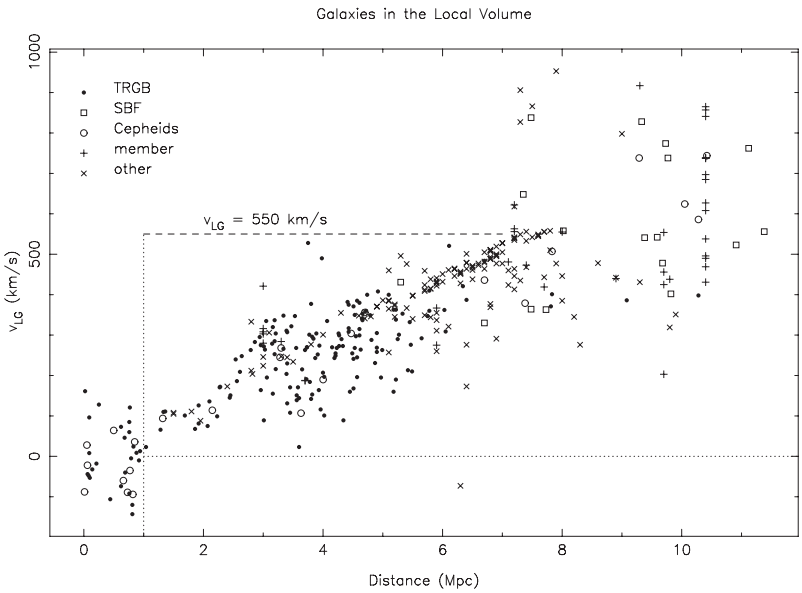

Fig. 1. Local Group velocity, $v_{\rm LG}$ (km s^{-1}), versus independent distance, D (Mpc), for all catalogued galaxies in the Local Volume. The different symbols denote the methods by which the distances were determined.

Beyond ∼6 Mpc we currently lack reliable distances, but many efforts are underway to remedy the situation. While membership distances can be useful in the overall picture, independent distances are needed for all galaxies to determine group memberships and study their 3D distribution as well as their orientation and kinematics with respect to each other.

Figure 2 shows the distribution of Local Volume galaxies on the sky, with symbols indicating distance ranges. There is no doubt that most galaxies live in groups, but the compactness or density of groups varies enormously, with strong implications as to the evolution of individual members and groups as

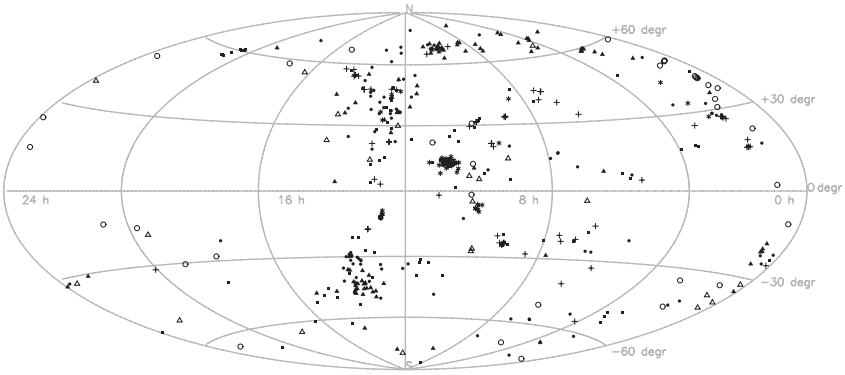

Fig. 2. Distribution of Local Volume galaxies on the sky. The symbols denote the following distance ranges: < 1 Mpc (open circle), 1 – 2.5 Mpc (open triangle), 2.5 – 4 Mpc (filled triangle), 4 – 5.5 Mpc (filled circle), 5.5 – 7 Mpc (filled square), 7 – 9 Mpc (plus sign), and > 9 Mpc (star). In the southern sky, the Cen A group stands out as the densest concentration of galaxies (see also Fig. 3).

a whole. Through sensitive H I observations we have clear evidence for interactions between close neighbours. The Magellanic Bridge and Stream are the most nearby indicators of strong interactions between the Magellanic Clouds and the Milky Way [14]. The network of H I streams and filaments in the M 81–M 82–NGC 3077 group [9] is one of the most spectacular examples of nearby interacting galaxies. And recent ATCA H I observations of the giant spiral galaxy M 83 [10] reveal a prominent tidal arm to the east, clearly indicating previous and on-going tidal interactions with its neighbouring dwarf galaxies.

Several large surveys of nearby galaxies have recently been carried out or are in progress. Most importantly, *'The HI Nearby Galaxy Survey'* (THINGS [11, 12]), which aims at high-resolution ($7''$) H I imaging of initially 36 galaxies north of declination $-30°$, has just been completed at the Very Large Array. The THINGS sample is targeting LV galaxies from *'The Spitzer Nearby Galaxies Survey'* (SINGS [13]).

Using the Australia Telescope Compact Array (ATCA) we have obtained sensitive H I distributions, velocity fields and 20-cm radio continuum maps for a complete sub-sample of ∼70 southern, gas-rich LV galaxies. These data form part of the 'Local Volume H I Survey' (LVHIS[1]; Koribalski et al.). The initial sample lies south of declination $-30°$ and contains all LV galaxies detected in the H I Parkes All-Sky Survey (HIPASS). The HIPASS Bright Galaxy Catalog (BGC [6]), which contains the 1000 H I-brightest galaxies in the southern sky, includes 80 galaxies with $v_{\rm LG} < 550$ km s^{-1}. Of these, 54 lie south of declination $-30°$. To this sample we added fainter HIPASS

[1]The LVHIS webpages are at: www.atnf.csiro.au/research/LVHIS.

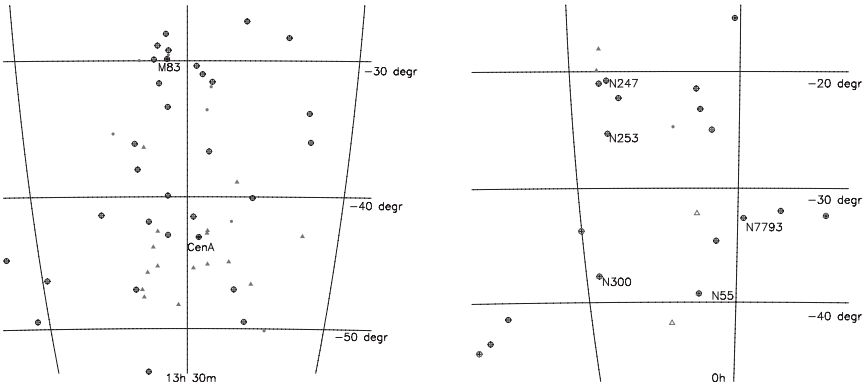

Fig. 3. The two most prominent southern groups are the relatively compact Cen A & M 83 groupings (left) and the loose Sculptor group (right). Galaxies that are known to contain H I emission are marked with an open circle.

galaxies from the Cen A group catalog [14] and HICAT [7]. – We have now observed each galaxy in our sample for 12-h using either the ATCA EW352-m or the EW367-m array and are on track to obtain further full synthesis (12-h) observations in each of the ATCA 750-m and 1.5-km arrays. Our aim is to complete the survey by the end of 2007. In addition, we mosaic galaxies with very extended H I envelopes (such as the prominent Sculptor spirals) in the ATCA H75 array.

Figure 3 shows the distribution of galaxies in the two southern groups, Cen A/M 83 and Sculptor. While M 83 is a giant H I-rich galaxy surrounded by numerous dIrr galaxies, the galaxies around Cen A are predominantly of earlier type. The ATCA H I velocity fields of some of the irregular galaxies near Cen A are shown in Fig. 4. The Sculptor Group, which is dominated by five bright gas-rich spiral galaxies, stretches over a relatively large range of distances and is much less compact than the Cen A/M 83 group. It is often considered to be a filament or loose group. While there are signs of disturbances in individual galaxies, no tidal streams have so far been detected in the Sculptor group. All of the H I-rich galaxies in these groups are being studied in detail as part of the LVHIS project.

My collaborators in the LVHIS project are Lister Staveley-Smith, Jürgen Ott, Erwin de Blok, Helmut Jerjen, Igor Karachentsev and Katie Kern. Our ATCA H I survey of gas-rich galaxies in the Local Volume is a major and very timely contribution to the on-going multi-wavelength campaign to characterise the Local Universe.

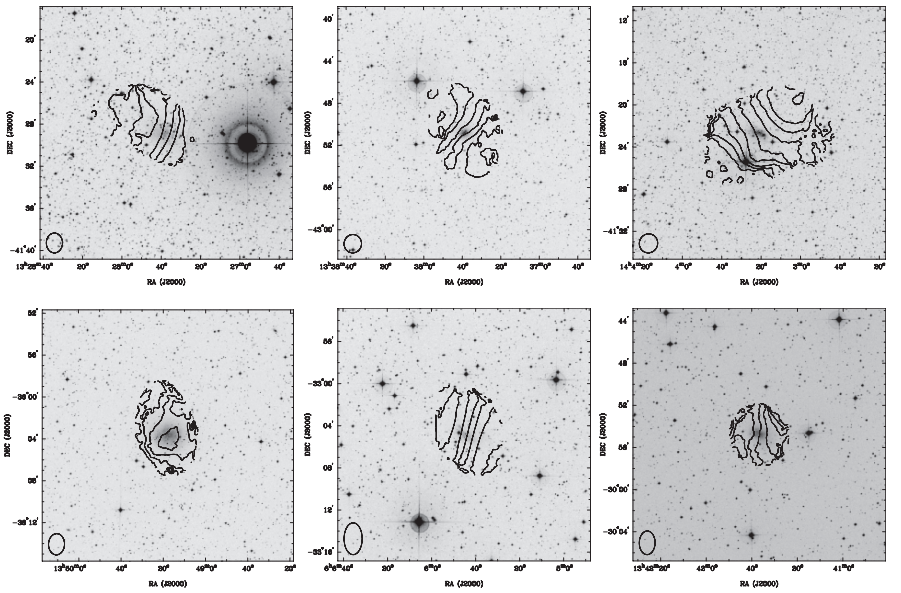

Fig. 4. H I mean velocity fields (contours) of some irregular galaxies in the Local Volume, as obtained from archival ATCA data. Top (left to right): ESO324-G024 (3.73 Mpc), NGC 5237 (3.40 Mpc), and NGC 5408 (4.81 Mpc). Bottom (left to right): ESO383-G087 (3.45 Mpc), ESO364-G?029 (7.7 Mpc), and NGC 5264 (4.53 Mpc). The ATCA synthesized beam is indicated at the bottom left of each panel. The H I velocity fields are overlaid onto *R*-band images from the Digitised Sky Survey (greyscale).

References

1. I.D. Karachentsev et al.: AJ **127**, 2031 (2004)
2. I.D. Karachentsev et al.: AJ **131**, 1361 (2006)
3. R. Kraan-Korteweg & G.A. Tammann: AN **300**, 181 (1979)
4. W.K. Huchtmeier & O.-G. Richter: A&AS **63**, 323 (1986)
5. W.K. Huchtmeier & O.-G. Richter: A&A **203**, 237 (1988)
6. B.S. Koribalski et al.: AJ **128**, 16 (2004)
7. M. Meyer et al.: MNRAS **350**, 1195 (2004)
8. M.E. Putman et al.: Nature **394**, 752 (1998)
9. M.S. Yun, P.T. Ho, K.Y. Lo: Nature **372**, 530 (1994)
10. B.S. Koribalski et al.: in prep. (2006)
11. F. Walter et al.: ASPC **331**, 269 (2005)
12. W.J.G. de Blok et al.: ASPC **329**, 265 (2005)
13. R. Kennicutt et al.: PASP **115**, 928 (2003)
14. G.D. Banks et al.: ApJ **524**, 612 (1999)

HI in Local Group Analogs: What does it Tell Us about Galaxy Formation?

D.J. Pisano[1], D.G. Barnes[2], B.K. Gibson[3], L. Staveley-Smith[4], K.C. Freeman[5] and V.A. Kilborn[6]

[1] Naval Research Laboratory, 4555 Overlook Ave. SW, Washington, DC 20375 USA
pisano@nrl.navy.mil
[2] School of Physics, University of Melbourne, Victoria 3010, Australia
dbarnes@astro.ph.unimelb.edu.au
[3] Centre for Astrophysics, University of Central Lancashire, Preston, PR1 2HE, UK
bkgibson@uclan.ac.uk
[4] Australia Telescope National Facility, P.O. Box 76, Epping NSW 1710, Australia
Lister.Staveley-Smith@atnf.csiro.au
[5] RSAA, Mount Stromlo Observatory, Cotter Road, Weston, ACT 2611, Australia
kcf@mso.anu.edu.au
[6] Centre for Astrophysics & Supercomputing, Swinburne University, Hawthorn, Victoria 3122, Australia
vkilborn@astro.swin.edu.au

Summary. We present the results of our HI survey of six loose groups of galaxies analogous to the Local Group. The survey was conducted using the Parkes telescope and the Australia Telescope Compact Array to produce a census of all the gas-rich galaxies and potential analogs to the high-velocity clouds (HVCs) within these groups down to $M_{HI} \leq 10^7 \mathrm{M}_\odot$ as a test of models of galaxy formation. We present the HI mass function and halo mass function for these analogous groups and compare them with the Local Group and other environments. We also demonstrate that our non-detection of HVC analogs in these groups implies that they must have low HI masses and be clustered tightly around galaxies, including around our own Milky Way, and are not distributed throughout the Local Group.

1 Introduction

As various proceedings from this conference illustrate, the Local Group is the nearest and best studied group of galaxies. We have a census of the dwarf galaxies down to very faint magnitude limits. We can study the resolved stellar populations in Local Group galaxies using HST and large ground-based telescope and re-create their star formation histories. These same data can be used to measure distances to these galaxies. We can now even measure the proper motions of some Local Group galaxies [4]. But just as our position within the Milky Way complicates our studies of it, our position inside

the Local Group leads to similar problems. This is particularly true when studying the gas within the Local Group that is not associated with stars, for example the high-velocity clouds (HVCs) [19].

The HVCs were first discovered over 40 years ago [12] and have remained a mystery since. They are HI clouds which are moving inconsistent with simple Galactic rotation with deviation velocities greater than 90 km s^{-1}. They also lack stars [20], and so we are generally unable to directly infer their distances. Without knowing their distances, we do not know their masses and can not, therefore, divine the physical processes responsible for their origins. Most likely, however, they represent a variety of phenomena. Some are probably related to a galactic fountain powered by supernovae explosions [3] and are located in the lower Galactic halo. Some HVCs are certainly tidal in origin, like the Magellanic Stream [14]. Others may be infalling primordial gas, such as Complex C [18], or gas condensing out of a hot Galactic halo [9]. Finally, some have been suggested to be associated with the low mass dark matter halos predicted to exist by models of cold dark matter (CDM) galaxy formation [1, 2].

CDM models predict that the Local Group should contain ∼300 low mass dark halos, while there are only ∼20 luminous dwarf galaxies known [8, 11]. While this may imply that we lack a complete census of the luminous galaxies in the Local Group, it may also be uniquely deficient in dwarf galaxies. Or, perhaps, the HVCs may populate these dark matter halos and solve this "missing satellite" problem.

The best way to address these questions is to study other groups of galaxies in detail. We can then determine if the population of low mass, gas-rich galaxies in the Local Group typical, or if there are relatively more in analogous groups? If HVCs are the solution to the "missing satellite" problem, then they should be ubiquitous in other groups where we can then directly determine their masses. Our HI survey of six loose groups of galaxies chosen to be analogous to the Local Group attempts to answer these questions.

2 Observations

We selected five of our groups from the optical catalog of [7] and one group from the HIPASS catalog [10]. The resulting groups are between 10.6 and 13.4 Mpc distant, contain between 3–9 bright, spiral galaxies which are separated, on average, by ∼550 kpc, and have diameters of ∼1.6 Mpc; hence the moniker loose groups. These groups were known to contain only spiral and irregular galaxies and no massive elliptical galaxies; just like the Local Group. These groups have no known X-ray emitting gas as is expected to be the case for the Local Group. Their masses, as estimated by the virial theorem, of $\sim 10^{11.7-13.6} M_{\odot}$ are comparable to the mass of the Local Group $\sim 10^{12.4} M_{\odot}$ [5].

We used the Parkes Multibeam and Australia Telescope Compact Array (ATCA) to survey the entire area of each group down to a M_{HI} sensitivity of $5 - 8 \times 10^5$ $M_\odot$ per 3.3 km s^{-1}. All Parkes detections in the groups were confirmed to be real by the follow-up ATCA observations. A total of 64 HI-rich galaxies were detected in the six groups, almost twice the number of optically cataloged group galaxies [7] and 50% more galaxies than were detected by HIPASS in the same fields [10]. All of our detections are associated with optical counterparts and have properties consistent with typical spiral, irregular, or dwarf irregular galaxies. No analogs to the HVCs were detected.

3 Is the Local Group typical?

While our sample of loose groups was chosen to be qualitatively analogous to the Local Group, are the HI properties of these groups quantitatively similar? To answer this, we constructed an HI mass function (HIMF) and a cumulative circular velocity distribution function (CVDF), both shown in Figure 1. For the former we have not made any attempt to quantify the volume observed, so we are simply comparing the slopes. That is, we are comparing the ratio of high-M_{HI} and low-M_{HI} galaxies in our sample to the Local Group. The CVDF is a measure of the dark matter halo mass function as traced by luminous matter, in this case only for HI-rich galaxies. As for the HIMF, we are focusing on the slope of the CVDF and how our groups compare to the Local Group and CDM model predictions.

The HIMF for both the Local Group and our sample of loose groups appears to be flat; there are the same number of massive and low mass galaxies per dex of M_{HI} when our sample is corrected for incompleteness

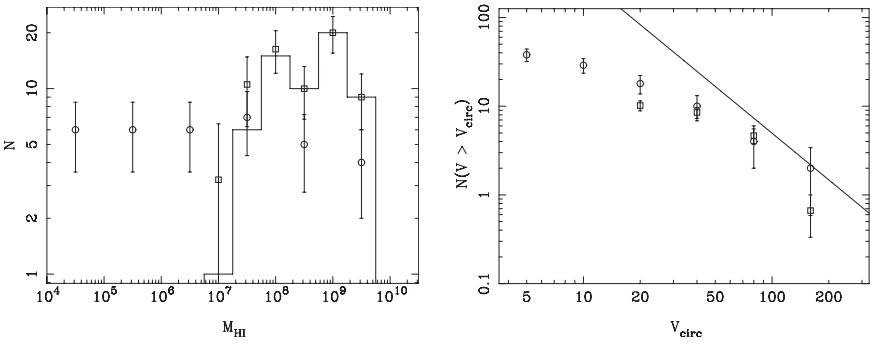

Fig. 1. Left: The HI mass function (HIMF) of the Local Group (circles) and the sum of the six loose groups (solid histogram) corrected for incompleteness (squares). Right: The cumulative velocity distribution function for the Local Group (circles), and the average of the six loose groups (squares). The solid line represents the CDM model from [8], roughly normalized to the second data point.

down to the sensitivity limit of our survey. This is consistent with other results for the HIMF in low density environments. In [22], it was shown that the HIMF flattens in lower density environments with data from HIPASS, although others find an opposite trend [15]. In [17], similar results to [22] were demonstrated from a compilation of optical luminosity functions. This demonstrates that, as far as the M_{HI} distribution goes, the Local Group is not atypical.

The CVDF for the Local Group clearly deviates from the solid line representing the predictions from CDM models [8] below $V_{circ} \sim 80$ km s^{-1}; this is the "missing-satellite" problem. From Figure1, we can see that our loose groups show the exact same deviation and match the CVDF for the Local Group within the statistical errors. Note that this is the CVDF only for the gas-rich galaxies in these groups, and we know that there are more gas-poor systems within the Local Group. These are shown in Figure 1, but typically have lower circular velocities than the gas-rich systems. The CVDF for the loose groups has not been corrected for incompleteness, but we do not expect such corrections to be large. This comparison of CVDFs illustrates, again, that there does not appear to a deficit of dwarf galaxies in the Local Group as compared to other loose groups. The Local Group does not appear to be an atypical loose group.

4 The nature of the High Velocity Clouds

Since we can now be confident that our sample of loose groups is truly analogous to the Local Group, what does our non-detection of HVCs in these groups imply for their nature? To answer this question, we have constructed a simple model with a Monte Carlo simulation for the distribution of the HVCs as described in [13]. For this paper, we use our knowledge of the completeness of our survey as a function of integrated flux and linewidth.

Based on this simulation, our non-detection of any HVC analogs in these six loose groups implies that they must have relatively low average HI masses, $M_{HI} \leq 1.6 \times 10^5$ $M_\odot$, and be tightly clustered around individual galaxies, $D_{HWHM} \leq 100$ kpc. These constraints are consistent with the limits found by others through a variety of other observational and theoretical methods [21, 6, 16]. This also implies that CHVCs are not a major repository of neutral gas, $M_{HI} \leq 10^8$ $M_\odot$, although there may be a large reservoir of ionized gas to fuel star formation in the Milky Way. These limits are independent of the nature of HVCs; they may or may not be associated with dark matter halos [9].

5 Conclusions

We have conducted a deep HI survey of six loose groups of galaxies analogous to the Local Group. The survey yielded detections of 64 HI-rich dwarf galaxies. The slopes of the HI mass function and the luminous, dark matter halo function for the Local Group and our sample of loose groups are consistent with each other. The Local Group, therefore, does not appear to be atypical in its apparent deficit of low mass, dwarf galaxies as compared to the predictions of CDM models of galaxy formation. This does not necessarily imply a failure of CDM, but does require, at least, the suppression of baryon collapse in low mass halos.

Our survey also failed to detect any HI clouds lacking stars; no HVC analogs were detected. This implies that HVCs are not a large reservoir of neutral gas for future star formation in galaxies. This is consistent with many models for the origin of HVCs and with other observational limits. Both deeper HI surveys of the ∼100 kpc environment of individual galaxies and higher resolution and sensitivity observations of Milky Way HVCs will help to better constrain the nature and origin of HVCs.

This research was performed while D.J.P. held a National Research Council Research Associateship Award at the Naval Research Laboratory. Basic research in astronomy at the Naval Research Laboratory is funded by the Office of Naval Research. D.J.P. also acknowledges generous support from the ATNF via a Bolton Fellowship and from NSF MPS Distinguished International Research Fellowship grant AST 0104439.

References

1. Blitz, L., Spergel, D.N., Teuben, P.J. et al.: ApJ **514**, 818 (1999)
2. Braun, R., Burton, W.B.: A&A **341**, 437 (1999)
3. Bregman, J.N.: ApJ **234**, 577 (1980)
4. Brunthaler, A., Reid, M.J., Falcke, H., et al.: Science **307**, 1440 (2005)
5. Courteau, S., van den Bergh, S.: AJ **118**, 337 (1999)
6. de Heij, V., Braun, R., Burton, W.B.: A&A **392** 417 (2002)
7. Garcia, A.M.: A&AS **100** 47 (1993)
8. Klypin, A., Kravtsov, A.V., Valenzuela, O. et al.: ApJ **522**, 82 (1999)
9. Maller, A.H., Bullock, J.S.: MNRAS **355**, 694 (2004)
10. Meyer, M.J., Zwaan, M.A., Webster, R.L., et al.: MNRAS **350**, 1195 (2004)
11. Moore, B., Ghigna, S., Governato, F., et al.: ApJ **524**, L19 (1999)
12. Muller, C.A., Oort, J.H., Raimond, E.: CR Acad. Sci. Paris **257**, 1661 (1963)
13. Pisano, D.J., Barnes, D.G., Gibson, B.K., et al.: ApJ **610**, L17 (2004)
14. Putman, M.E., Gibson, B.K., Staveley-Smith, L., et al.: Nature **394**, 752 (1998)
15. Springob, C.M., Haynes, M.P., Giovanelli, R.: ApJ **621**, 215 (2005)
16. Thilker, D.A., Braun, R., Walterbos, R.A.M., et al.: ApJ **601**, L39 (2004)
17. Tully, R.B., Somerville, R.S., Trentham, N., et al.: ApJ **569**, 573 (2002)
18. Wakker, B.P., Howk, J.C., Savage, B.D., et al.: Nature **402**, 388 (1999)

19. Wakker, B.P., van Woerden, H.: ARA&A **35**, 217 (1997)
20. Willman, B., Dalcanton, J., Ivezic, Z., et al.: AJ **124**, 2600 (2002)
21. Zwaan, M.A.: MNRAS **325**, 1142 (2001)
22. Zwaan, M.A., Meyer, M.J., Staveley-Smith, L., et al.: MNRAS **359**, L30 (2005)

Stellar Metallicities and Ages in Leo I dSph

M. Gullieuszik[1,2], I. Saviane[3], E.V. Held[1] and L. Rizzi[4]

[1] Osservatorio Astronomico di Padova, INAF, Italy
gullieus,held@pd.astro.it
[2] Dipartimento di Astronomia, Università di Padova, Italy
[3] European Southern Observatory, Chile
isaviane@eso.org
[4] Institute for Astronomy, University of Hawaii, USA
rizzi@ifa.hawaii.edu

1 The MDF and the metallicity gradient

We present the first results of a spectroscopic study of Leo I dSph carried out using FORS2 at the ESO VLT, in which we derive metallicities for 78 red giant stars from the equivalent widths of calcium triplet lines.

The metallicity distribution function (MDF), shown in Fig. 1, is well fitted by a Gaussian distribution, centered at [Fe/H] $= -1.46$ and with $\sigma = 0.23$, in good agreement with the result of [1]. A simple closed-box model convolved with the observational errors is unable to fit the observed MDF (solid curve in Fig. 1). In order to reproduce the peak of the MDF we had to adopt an "effective yield" $y = 0.025 Z_\odot$, much lower than the value for the solar vicinity ($y = 1.2 Z_\odot$; e.g. [6]). This is a clear indication of loss of metals [2]. Further, the number of metal-poor stars is largely overestimated by the simple model. The fit can be improved by assuming an early enrichment scenario with an initial metallicity $Z_0 = 0.02 Z_\odot$ ([Fe/H] $= -1.7$). This new model, convolved

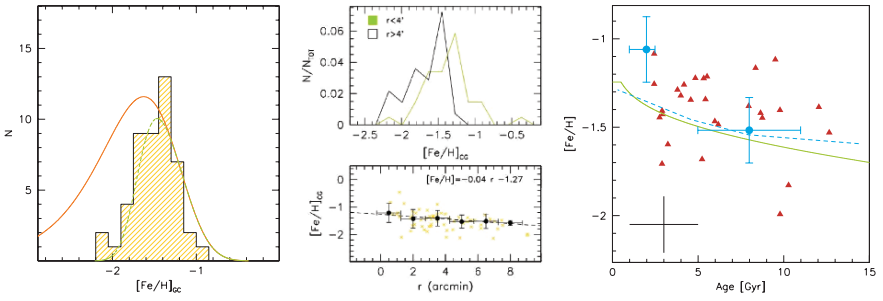

Fig. 1. *Left panel:* the MDF of Leo I together with simple models. *Central panel:* the metallicity gradient. *Right panel:* the age-metallicity relation of stars in Leo I, using our data (triangles) and iron abundance data from [7], plotted together with simple models. Typical uncertainties are represented by the cross on the lower left side.

with the observational errors (dashed curve in Fig. 1) seems to reproduce the MDF reasonably well. Although we do not put much emphasis on this rather ad-hoc model, it provides some qualitative insight on the chemical evolution of this galaxy, to be further explored with more detailed models. This narrow MDF is likely to arise from a combination of initial enrichment from a lost generation of stars, and subsequent loss of metals through outflows.

We also found evidence for a metallicity gradient in Leo I, as shown in the central panel of Fig. 1. The MDF of stars in the inner region is peaked at higher metallicity than the metallicity distribution of stars in the outer region. A Kolmogorov-Smirnov test shows that the distributions are different at a 99% confidence level. The gradient is confirmed by the lower central panel, where the radial trend of [Fe/H] is shown. The original data have been binned in steps of 1.5 arcmin (filled circles with error bars). A fit to the binned data suggests a gradient of -0.04 dex arcmin^{-1}, comparable with those measured in Carina [4] and Sculptor [8].

2 Age-metallicity relation

Using our metallicities and the photometry from [3], we estimated the age of each star by interpolating over theoretical isochrones [5]. In this way we obtained the age-metallicity relation of Leo I shown in Fig. 1 (right panel). The ages and metallicities of two stars based on direct abundance measurements from high-resolution spectroscopy [7], are consistent with our indirect measurements. The solid line represents the model used to reproduce the MDF with a constant SFR $= 0.0015 M_{\odot}\ yr^{-1}$. The result is similar to that obtained by [7] by taking into account the known SFH of Leo I (dashed line). While the measurement errors are too large to allow a detailed discussion of the abundance trend, the indication is that the derived metallicities are nearly constant over the galaxy life.

References

1. Bosler, T. L., Smecker-Hane, T. A., Cole, A., Stetson, P. B., 2004. In: Origin and Evolution of the Elements, from the Carnegie Observatories Centennial Symposia.
2. Hartwick, F. D. A., 1976, ApJ, 209, 418
3. Held, E. V., Saviane, I., Momany, Y., Carraro, G., 2000, ApJ, 530, L85
4. Koch, A., et al., 2006, AJ, 131, 895
5. Pietrinferni, A., Cassisi, S., Salaris, M., Castelli, F., 2004, ApJ, 612, 168
6. Portinari, L., Moretti, A., Chiosi, C., Sommer-Larsen, J., 2004, AJ, 604, 579
7. Tolstoy, E., et al., 2003, AJ, 125, 707
8. Tolstoy, E., et al., 2004, AJ, 617, L119

Globular Clusters in M31 and the Local Group

S.C. Kim[1], M.G. Lee[2], D. Geisler[3], A. Sarajedini[4], W.E. Harris[5], H.S. Park[2], H.S. Hwang[2] and J.C. Seguel[3]

[1] Korea Astronomy and Space Science Institute, Daejeon, Korea
sckim@kasi.re.kr
[2] Astronomy Program, Seoul National University, Seoul, Korea
mglee@astrog.snu.ac.kr, hspark + hshwang@astro.snu.ac.kr
[3] Dept. de Física, Universidad de Concepción, Concepción, Chile
doug@kukita.cfm.udec.cl, jseguel@andromeda.cfm.udec.cl
[4] Department of Astronomy, University of Florida, FL, USA
ata@astro.ufl.edu
[5] Department of Physics & Astronomy, McMaster University, Hamilton ON, Canada
harris@physics.mcmaster.ca

1 A new M31 GC survey

Previous surveys for M31 globular clusters (GCs) have been mainly done by using photographic plates. We have performed a new systematic survey for M31 GCs using imaging by KPNO 0.9 m telescope + 2K CCD + C, M, T_1 filters, and spectroscopy by WIYN 3.5 m telescope + Hydra multifiber spectrograph.

We have found 544 previously known GCs and 620 new GC candidates, and among these new candidates more than 120 objects are believed to be genuine clusters. Most of the GCs have reddening-corrected $(C - T_1)$ values between 1 and 2, while there are still some objects with $(C - T_1)_0 > 2$ and several objects with $(C - T_1)_0 < 1$.

2 Comparison of GC systems in the Local Group

The Milky Way Galaxy (MWG) is known to have at least 153 GCs [2], and there could be 10 ± 3 undiscovered GCs [13]. MWG also has some accretion/merger signals, such as Sagittarius dwarf spheroidal galaxy, Canis Major dwarf galaxy, and ω Centauri [8, 15, 16].

M33 has more than 75 ± 14 GCs [4], the Large and Small Magellanic Clouds have $\geq$13 and 1 GCs, respectively, NGC 205, NGC 185, and NGC 147 have 8, 6, and 4 GCs, respectively, the Fornax dwarf spheroidal galaxy has 5 GCs, the Sagittarius dwarf spheroidal galaxy has four GCs (M54, Arp 2, Ter 7, Ter 8) and possibly some more (Pal 12, NGC 4147, Pal 2 ?), NGC 6822 has two (?) GCs [10], and Canis Major dwarf galaxy has four GCs (NGC 1851, M79(NGC 1904), NGC 2298, NGC 2808).

Table 1. Comparison of the GC systems of MWG and M31

	MWG (Sbc)	M31 (Sb)	References
N(GC)	$153(+10^{+3}_{-3}?)$	> 460	[2, 14]
M_V(galaxy)	-21.3	-21.8	[5]
Galaxy mass	$(1.3-2.5)\times10^{12}M_\odot$	$(0.7-1.2)\times10^{12}M_\odot$	[1, 6, 7, 17]
Blue (young?) GCs	No	Yes	[14]
Intermediate-metallicity GCs	No	Yes	[14]
Metallicity of halo stars	[m/H]~-1.7	[m/H]~-0.5	[9]

Since 2000, it is reported that the mass of M31 is a factor of two smaller than that of the MWG (Table 1). It is not clear why the less massive galaxy, M31, has more GCs, brighter absolute magnitude, and higher value of metallicity for the halo stars. It is also to be answered why only M31 has blue (possibly young?) GCs and intermediate-metallicity GCs. While M31 also has accretion/merger signals such as (i) extended stellar disk [12], (ii) giant stream of metal-rich stars [11], and (iii) intermediate-age (11–13.5 Gyr) metal-poor stars [3], it is yet to be found how many GCs are supplemented to M31 via these processes. There could have been more efficient cluster formation in M31 or higher satelliate and cluster capture rate for M31 compared to the MWG.

References

1. Bellazzini, M.: MNRAS, **347**, 119 (2004)
2. Bica, E., Bonatto, C., Barbuy, B., & Ortolani, S.: A&A accepted (astro-ph/0511788) (2006)
3. Brown, T. M. et al.: ApJ, **592**, L17 (2003)
4. Chandar, R., Bianchi, L., Ford, H. C., & Sarajedini, A.: ApJ, **564**, 712 (2002)
5. Chandar, R., Whitmore, B., & Lee, M. G.: ApJ, **611**, 220 (2004)
6. Evans, N. W., & Wilkinson, M. I.: MNRAS, **316**, 929 (2000)
7. Evans, N. W., Wilkinson, M. I., Guhathakurta, P., Grebel, E. K., & Vogt, S. S.: ApJ, **540**, L9 (2000)
8. Gilmore, G., Wyse, R. F. G., & Norris, J. E.: ApJ, **574**, L39 (2002)
9. Harris, W. E., & Harris, G. L. H.: AJ, **122**, 3065 (2001)
10. Hwang, N. et al.: In: *Near-field Cosmology with Dwarf Elliptical Galaxies*, Edited by H. Jerjen and B. Binggeli, (IAU Colloquium 198) pp. 257–258
11. Ibata, R., Irwin, M., Lewis, G., Ferguson, A. M. N., & Tanvir, N.: Nature, **412**, 49 (2001)
12. Ibata, R. et al.: ApJ, **634**, 287 (2005)
13. Ivanov, V. D., Kurtev, R., & Borissova, J.: A&A, **444**, 195 (2005)
14. Kim, S. C. et al.: in preparation (2006)

15. Lee, Y.-W., Joo, J.-M., Sohn, Y.-J., Rey, S.-C., Lee, H.-c., & Walker, A. R.: Nature, **402**, 55 (1999)
16. Meza, A., Navarro, J., Abadi, M. G., & Steinmetz, M.: MNRAS, **359**, 93 (2005)
17. Sakamoto, T., Chiba, M., & Beers, T. C.: A&A, **397**, 899 (2003)

Properties of RR Lyrae Stars in the Inner Regions of the Large Magellanic Cloud. II. The Extended Sample

J. Borissova[1], D. Minniti[2], M. Rejkuba[3] and D. Alves[4]

[1] European Southern Observatory, Ave. Alonso de Cordoba 3107, Casilla 19, Santiago 19001, Chile
jborisso@eso.org
[2] Department of Astronomy, P. Universidad Católica, Av. Vicuña Mackenna 4860, Casilla 306, Santiago 22, Chile
dante@astro.puc.cl
[3] European Southern Observatory, Karl-Schwarzschild-Str. 2, D-85748 Garching b. München, Germany
mrejkuba@eso.org
[4] 3549 Lynne Way, Sacramento, CA 95821-3722, USA
alvesdavid@ucdavis-alumni.com

Using low-resolution spectroscopy with FORS1,FORS2 and GEMINI-GMOS we have obtained good quality spectra for 99 LMC RR Lyrae, of which 86 are in the field and 13 in the clusters NGC1835 and NGC2019. 15 RR Lyrae stars of ωCen were observed as well for comparison. We measured radial velocities for 87 LMC RR Lyrae, and metallicities for 78 RR Lyrae, nearly tripling the previous sample. These targets are located in 11 fields covering a wide range of distances, out to 2.5 degrees from the center of the LMC. The sample allows us to compare the kinematics of the old and metal-poor stars in the LMC with the rest of the stellar populations.

Our main preliminary result is that the mean LMC RR Lyr velocity dispersion is $\sigma_{RV} = 50 \pm 2$ km/s. This quantity does not appear to vary with distance from the LMC center.

The mean velocities show a larger field to field variation, and our conclusions are weaker for this quantity. They appear to differ systematically from the existing velocities of the HI gas. Within the errors, they do not show any significant bulk rotation.

The metallicity shows a Gaussian distribution, with mean $[Fe/H] = -1.53 \pm 0.02$ dex, and dispersion $\sigma_{[Fe/H]} = 0.20 \pm 0.02$ dex, confirming that they represent a very homogeneous metal-poor population. There is no dependence of the kinematics with metallicity for the field RR Lyrae population.

Based on observations collected with the Very Large Telescope, the New Technology Telescope of the European Southern Observatory and GeminiS of Gemini Observatory within the Observing Programs 64.N-0176(B),70.B-0547(A), 072.D-0106(B), GS-2004A-Q-27.

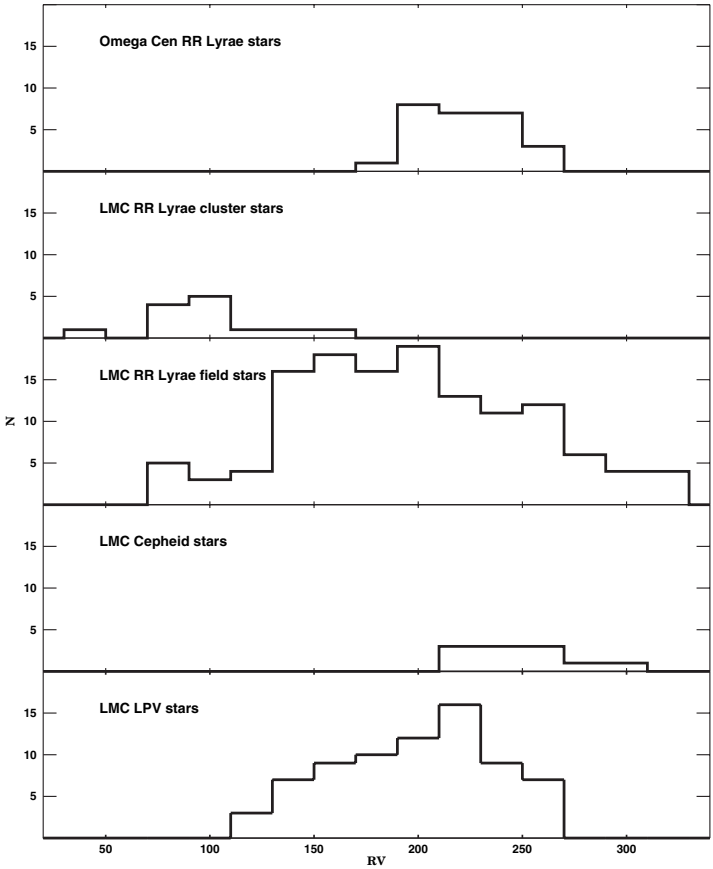

Fig. 1. The radial velocity histogram for ω Cen RR Lyrae, LMC RR Lyrae field, LMC RR Lyrae clusters, Cepheid and LPV star.

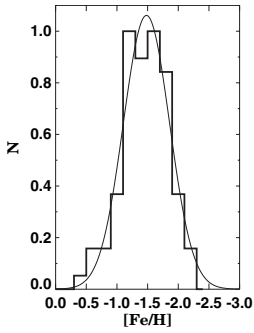

Fig. 2. The metallicity histogram for RR Lyrae stars in our fields. The solid line represents the Gaussian distribution.

Diffuse Ionized Gas in the Dwarf Galaxy DDO 53

N. Flores-Fajardo[1] and A.M. Hidalgo-Gámez[1,2]

[1] Instituto de Astronomía, UNAM, México
nahiely@astroscu.unam.mx
[2] Instituto Politécnico Nacional, México
anamaria@astroscu.unam.mx

We study the diffuse ionized gas (DIG) in the M81 group dwarf irregular galaxy DDO 53. We use long-slit spectroscopy in order to determine the most interesting line ratios. We compare these ratios with classical and leaking photoionization, shocks and turbulent layer models. As other dwarf irregular galaxies, the spectral characteristics are very diferent to those of the DIG in spiral galaxies: the excitation is higher and the [SII/Hα] much lower. A combination of leakage photoionization models plus shocks will be able to explain these characteristics.

1 Introduction

The near group of galaxies M81 is an ideal site for the study of dwarf galaxies because of their proximity. This group has velocity dispersion of $\sigma_v = 91$ km s^{-1} and a radius of $< R_p >= 211$ kpc, which are found to be similar to those of the subgroups around M31 and the Milky Way. Nevertheless, the group around M81 has more galaxies than the other two subgroups given that it has more 29 galaxies so far detected, one wich is DDO 53. This is an irregular dwarf galaxy at a distance of 3.53 ± 0.07 Mpc (Hidalgo-Gámez & Olofsson, 1998), wich have $12 + \log [O/H] = 7.8$ (Hidalgo-Gámez & Flores-Fajardo, in preparation; here after HGG-FF). Hunter & Elmegreen (2004) has estimated an Star Formation Rate of -2.28 $M_\odot$ yr^{-1} and a $\log M_{gas} = 8.39$.

2 Discussion

This investigation is based in observations made at OAN-SPM (México). For more details of the acquisition, reduction and analysis of the data, the reader is refered to HG-FF. The surface brightness in Hα corrected for galactic extinction was used to distinguish between DIG and H II location as previously used for other galaxies, e.g. IC 10 (Hidalgo-G'amez, 2005). Figure 1.a shows a comparison between the data of this work and the diagnostic diagrams of

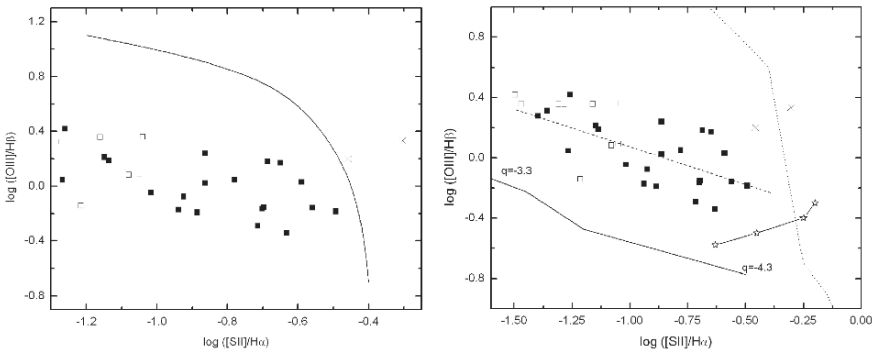

Fig. 1. White squares correspond to the H II regions, black squares to the DIG and the crosses are for two points of DIG that were not corrected by extintion (see HG-FF for details).

Veilleux & Osterbrock (1987). In this plot, the points to the right of the curve are mainly objects whose main source of ionization are shocks while those data at the left of the curve are associated with photoionization sources. Figure 1.b shows the comparison between our data with Rand's models (1998). The continuous black line represents the density bounded model while the radiation bounded model is represented by the dotted line. The model that considers radiation bounded regions with a turbulent mixed layer is represented by continue line with stars. Strictly speaking, none of the models fit the data; nevertheless the data follows the same behavior of the density bounded model. The slope of the dashed line which correspond to our data is $m = -0.427$ with a correlation coefficient of $r = 0.6415$, while the slope of Rand's model is $m = -0.439$. It is important to keep in mind that if the metallicity of the galaxy falls then the excitation increases and the [SII]/Hα decreases. If we make a comparision between the line ratios for DDO 53 and Hoopes & Walterbo's models (2003), we can see that a 40% leakage of photons from a H II with a T_{ion} of 40,000 K would explain most of the line ratios.

3 Acknowledgements

This work was partly supported by CONACyT project 2002-c40366.

References

1. Hidalgo-Gámez A. M., Olofsson K.: A&A **334**, 45 (1998)
2. Hidalgo-Gámez A. M., Olofsson K.: A&A **442**, 443 (2005)
3. Hunter D. A., Elmegreen B. G.: AJ **128**, 2170 (2004)
4. Rand R. J.: ApJ **501**, 137 (1998)
5. Veilleux S., Osterbrock D. E.: ApJS **63**, 295 (1987)


Local Group(s)
ostro.unibas.ch

Galaxy Group Searches and Surveys

V. Eke

Institute for Computational Cosmology, Durham University, Science Laboratories, South Road, Durham. DH1 3LE, England
v.r.eke@durham.ac.uk

Summary. In this contribution I will provide a brief summary of the history of searches for, and surveys of, galaxy groups. This will be split up into two separate parts, searches with and without galaxy redshift measurements. I will conclude with a more detailed look at a recent result from the 2 degree Field Galaxy Redshift Survey (2dFGRS).

1 What is a group?

Before launching into the history of group-finding, a necessary precursor is to define what is meant by the word group. Judging by the broad range of

sizes of object being talked about at this "groups of galaxies" conference, it appears that, if I cannot find a definition that pleases everybody, then I will at least define what I mean by this word.

In a literal sense, a galaxy group ought to be a collection of at least two galaxies located sufficiently near to one another. Given a galaxy survey, these are exactly the structures that typical group-finders pick out as galaxy groups. Note that I have not specified an arbitrary upper limit to the number of galaxies that can comprise a group, so objects that have traditionally been referred to as galaxy clusters would be found by a group-finder. Thus, in any sensible nomenclature, they must be merely big groups.

Of course, as galaxy surveys usually measure galaxies above a minimum flux limit, defining the galaxy groups by their galactic content would mean that a galaxy group at low redshift would not be a galaxy group if moved sufficiently far away that no more than one of its constituent galaxies remained above the flux limit. This is not a very satisfactory situation. It is preferable to have the definition depend only upon the intrinsic properties of an object, rather than how it is viewed. Thus, unless specified otherwise, in the rest of this contribution the word group will refer to any object with a mass of at least $\sim 10^{12.5} h^{-1} M_{\odot}$[1] (this being approximately the mass of two Milky Ways and their associated dark matter haloes). Clusters are the subset of groups with $M > 10^{14} h^{-1} M_{\odot}$.

I should make clear that in this choice of definition, I have made no reference to the physical processes going on within groups. For instance, the larger velocity dispersions in clusters will suppress the interactions between galaxies relative to the situation in smaller groups. However, this does not strike me as sufficient reason to remove clusters from the set of groups by introducing an upper mass limit to the set of galaxy groups.

2 Group searches and surveys

While searches for galaxy groups have typically been performed via emission from the galaxies themselves, it would be remiss of me not to refer to the fact that many surveys find galaxy clusters through the diffuse ionised gas within their deep potential wells. The bremsstrahlung emission from the gas at temperatures of 10^{7-8}K has been detected by X-ray satellites, giving rise both to cluster detections and surveys for the best part of the last 20 years e.g. [1], [2], [3], [4]. Interesting results arising from X-ray studies include how the gas appears to be distributed in two distinct components in smaller groups: one associated with the galaxies themselves, and the other with an extended common halo [8], [9], and the fact that small galaxy groups do not lie on the same luminosity-temperature relation as galaxy clusters [10], implying some non-gravitational physics is becoming important. More recently, the inverse

[1] Hubble's constant, $H_0 = 100h \mathrm{kms}^{-1}\mathrm{Mpc}^{-1}$

Compton scattering of microwave background photons passing through intracluster plasma, known as the Sunyaev-Zel'dovich [5] effect, has also been used to detect clusters [6], [7].

Even if one considers searching for galaxy groups using the galaxies themselves as tracers, there is still the choice of whether or not to use the emission from their cold gas or stars. There are many other contributions at this conference concerning neutral hydrogen (HI) surveys, so I will focus on the group searches and surveys that are based on the integrated stellar emission from the galaxies. As the group-finding techniques differ significantly depending upon whether or not galaxy redshifts are available, this provides a natural way to split the subject.

2.1 Searches without redshifts

The first systematic galaxy group searches used photographic plates as a starting point. An example of one of these is shown in Figure 1. The photographic sky surveys most often used for studies of the galaxy distribution are the Palomar Observatory Sky Survey (POSS) in the northern hemisphere, and the United Kingdom Schmidt Telescope (UKST) Sky Survey for the southern sky. From Figure 1, it is apparent that one must decide which of the splodges on the photographic plate are galaxies before applying any group-finding algorithm. Given this sort of information, the most readily detectable systems would be the largest galaxy clusters, which provide significant local enhancements in the galaxy surface number density.

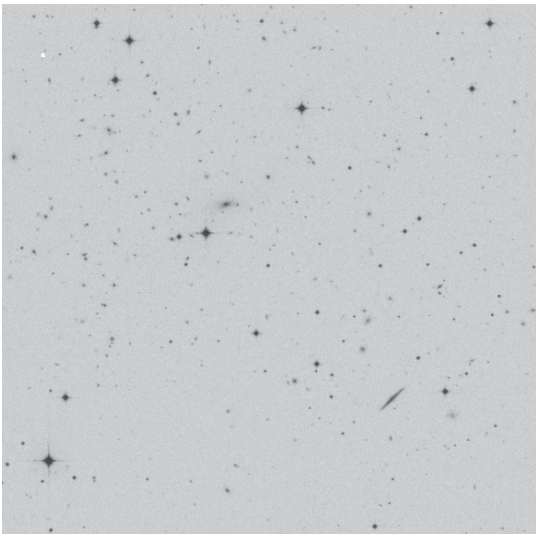

Fig. 1. A SuperCOSMOS scan of a UKST sky survey plate. From www-wfau.roe.ac.uk/sss.

Cluster finding

In the late 1950s and 1960s both Abell, and Zwicky and his collaborators independently visually inspected the POSS plates, found galaxies and then applied their own group-finding algorithms to yield cluster catalogues.

The Abell catalogue [11], which was subsequently extended into the southern sky using the UKST plates by Abell, Corwin & Olowin [12], contained over 1600 clusters with at least 50 galaxies (post background correction):

1. within 2 magnitudes of the third brightest galaxy member
2. within a $1.5h^{-1}$Mpc projected radius at the distance of the cluster.

The cluster distance was estimated from the flux of the 10th brightest member using a relation calibrated with measured redshifts for a few galaxies, and the background correction assumed that the number density of contaminating galaxies was uniform across the survey.

Zwicky et al. [13] used a slightly different cluster definition, requiring that clusters should contain at least 50 galaxies out to the projected radius at which the mean enclosed background-corrected number overdensity of galaxies was 2.

These early studies represented the state of the art in cluster catalogues for about 25 years. In 1985, Schectman introduced a different group-finding technique, which took binned galaxy counts from the Lick Survey plates, applied a smoothing filter and then defined clusters as the resulting peaks above a particular threshold.

The next big steps forward came with the introduction of plate-scanning machines that could automate the galaxy-defining procedure. In 1992, Lumsden et al. [14] used the COSMOS machine scans of UKST plates. By applying a local background correction and a Schectman-like cluster-finding algorithm, they produced the Edinburgh-Durham Cluster Catalogue, containing 737 objects. Dalton et al. followed this with a catalogue of 957 clusters [15] obtained using an Abell-like group-finding procedure on a galaxy catalogue constructed using the APM machine scans of UKST plates. Unlike Abell, Dalton et al. used a projected radius of $0.5h^{-1}$Mpc to define their clusters, arguing that this smaller radius would produce fewer objects that were contaminated by chance superpositions than was the case in the Abell catalogue.

More recently, digitised versions of the POSS have been used as the source for further galaxy cluster catalogues. As they had galaxy fluxes in two different wavebands, Gal et al. [16], [17] used a colour cut to remove excessively red ($g - r > 1.3$) or blue ($g - r < 0.3$) objects. The blue ones were deemed to be likely to be field galaxies, whereas the red objects were dismissed as stars or high redshift galaxies. In this way, the contaminating objects could be filtered out before applying the smoothing and peak-finding algorithms to locate galaxy clusters.

One other cluster-defining technique that has been used on galaxy surveys is the Voronoi Tesselation [18]. This is a purely geometrical method, which

considers only the projected galaxy positions. If for each galaxy, one joins it to every other one and draws onto the sky all of the perpendicular bisectors of those connecting lines, then the size of the area around this galaxy represents the reciprocal of a local projected galaxy number density. Doing this for every galaxy creates a 'crazy paving' pattern of local densities from which a threshold can be chosen to define clusters.

More modern cluster finding techniques typically take advantage of galaxy colours and luminosities when defining clusters. Examples include the matched filter introduced by Postman et al. [19] and the red sequence method [20]. Variants of these methods have more recently been applied to the Sloan Digital Sky Survey (SDSS) by a number of different groups [21], [22], [23], [24].

Finding smaller groups

Turner & Gott [25] found 103 small groups of galaxies in the Zwicky Galaxy Catalogue using the

'blind application of a precisely defined group identification procedure. This procedure only considers the positions of galaxies in the sky. As a result, it sometimes makes "absurd" mistakes, but these are usually too obvious to be misleading. In addition, the shortcomings of the groups defined by our naïve method are offset, we feel, by their objectivity, homogeneity, and completeness.'

The absurd mistakes presumably involved the grouping together of galaxies that for reasons of flux of angular size appeared unlikely to be at a similar distance. Unlike with clusters, where the sheer numbers of galaxies per cluster was large enough that they stood out in projection, small groups are generally not very imposing, and there is a bigger chance that they are just a chance alignment of a few isolated galaxies.

The easiest small groups to identify are those where constituent galaxies are within a few galaxy radii from each other, i.e. compact groups. While a few examples of such associations were known before, the first systematic search for compact groups was conducted by Rose in 1977 [26]. This was followed in 1982 by Hickson's compact group catalogue, containing 100 objects found from the POSS plates. The criteria for a compact group were that:

1. there should be at least 4 galaxies
2. with the centre of the nearest neighbouring group being at least 3 times the group's angular radius away
3. and that the mean surface brightness should be brighter than 26.0 mag/arcsec^2.

These groups, being so compact, were much more reliable than typical small loose groups at tracing real three-dimensional associations. Spectroscopic follow-up of Hickson's sample showed that 69 of the groups did have at least

4 concordant velocities, 23 systems were merely triples, and 8 had two or less galaxies at a similar redshift.

Given that such compact groups have short crossing times and represent the most effective environment in which galaxies merge together, they clearly provide a crucial step in understanding the origin of the currently observed galaxy population. Many subsequent studies have found compact groups, using criteria very similar to Hickson's, from the COSMOS scans of UKST sky survey plates [27], [28], the second digitised POSS [29], [30] and the SDSS [31]. While the criteria for selecting compact groups have hardly changed during this time, the galaxy surveys on which this procedure is being applied have grown such that hundreds of compact groups are now known, out to redshifts of $\sim$0.2 [30].

2.2 Searches with redshifts

The difficulty of finding groups that are merely chance alignments is greatly reduced when redshift information is available to give rough distance estimates to the galaxies in a survey. These are not precise distances because the redshift includes the Doppler shift of spectral features caused by peculiar velocities, which result because galaxies are accelerated by inhomogeneities in the mass distribution around them. This fact complicates the attempt to pull three-dimensional groups out of the two dimensional plus redshift data.

In the last $\sim$5 years, the 2dFGRS and SDSS have greatly increased the size of galaxy redshift surveys such that, rather than having $\sim$10000 galaxies, there are an order of magnitude more objects from which to define galaxy groups. Figure 2 shows the evolution of the number of galaxies in redshift surveys from which galaxy group catalogues have been constructed.

Two different group-finding techniques have been used for the majority of the studies shown in Figure 2. Most frequent is the friends-of-friends method (FOF, [32], with the most commonly used alternative being the hierarchical method [49].

The friends-of-friends method

Given a set of galaxies, the friends-of-friends method finds groups that are roughly bounded by a region with a constant galaxy overdensity. It does this by centring a linking volume on each galaxy. Then, any other galaxies lying within the volume are considered to be friends. The galaxy groups are the distinct collections of connected friends. Once the size and shape of the linking volume is defined, the set of groups is completely specified. In a situation where the 3-dimensional position of the galaxies is precisely known, the linking volume should be spherical. However, in a redshift survey, the peculiar velocities effectively smear structures out along the line of sight. This can be seen in Figure 3, which shows a projection through declination of

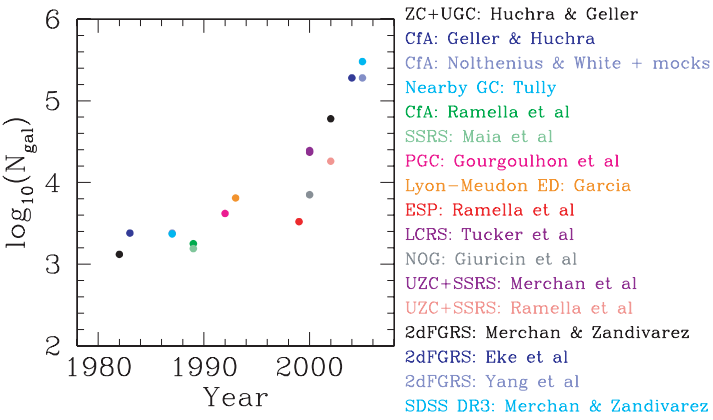

Fig. 2. The evolution of the number of galaxies in the redshift surveys from which group catalogues have been found. The various studies shown here are contained in references [32]–[48].

the two contiguous patches of the 2dFGRS [50]. Consequently an elongated cylinder pointing along the redshift direction is used as the linking volume. For group-finding, the aspect ratio of this cylinder is usually chosen to be ∼10. The size of the linking volume sets the galaxy number overdensity at the edge of the groups. For a flux-limited catalogue, one should therefore scale the linking volume with the reciprocal of the number density of galaxies above the flux limit in order that the same edge would be found if the same group were placed at a different redshift and sampled differently.

In the extreme case of a large linking volume, all galaxies are placed in a single group; this is called percolation. When the linking volume is small, no galaxies are linked together. For intermediate sizes, a more interesting spectrum of groups can be obtained.

The hierarchical method

The hierarchical method involves creating a tree-like data structure where the individual galaxies represent leaves, and they are progressively linked together until a single trunk is left. Groups are then defined as having a particular branch size.

To put some more quantitative measures on this picture, consider the algorithm employed by Tully [35]. Tully defined the separation between two galaxies by assuming that the line-of-sight velocity difference contained no information about true separations if it was less than 300 km/s. For very large separations in velocity space, these are translated directly into line-of-sight spatial separations. The intermediate regime was treated using a simple transformation that went smoothly to these limiting cases. Having defined the galaxy separations, the pair of galaxies with the largest value

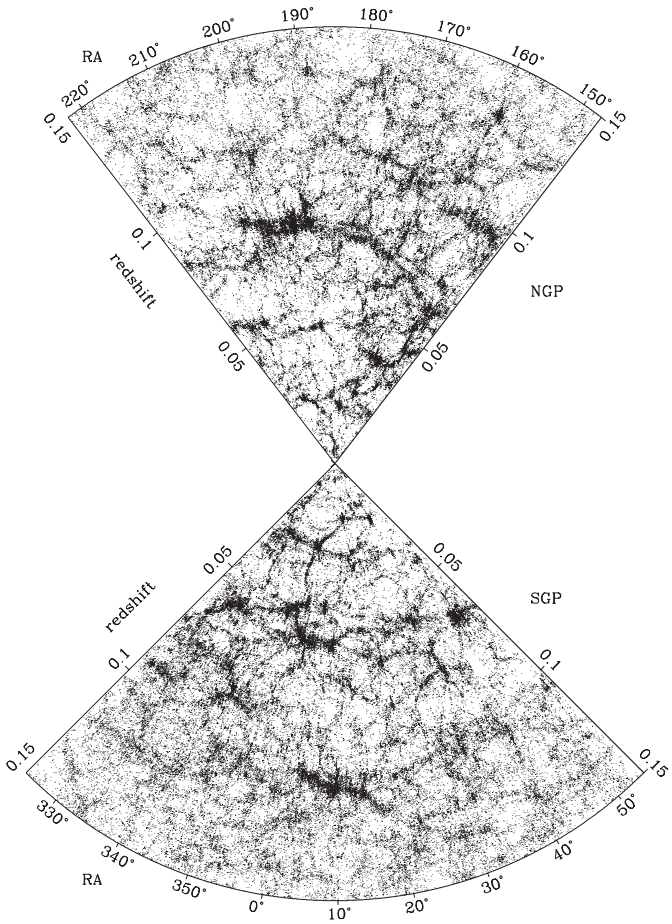

Fig. 3. The 2dFGRS out to $z = 0.15$. Each dot represents a galaxy, and the entire declination range in both the NGP and SGP has been projected through in making this figure.

of luminosity of brighter galaxy/separation^2 were then linked together and replaced with a single node at the centre of luminosity. These two steps were repeated $N_{\rm gal} - 2$ more times to leave a single node. From this dendrogram, the group boundaries were drawn at a particular threshold of luminosity density. If objects in the Universe have a constant mass-to-light ratio within their virialised regions, then a suitably chosen luminosity density threshold should pick out the virialised groups.

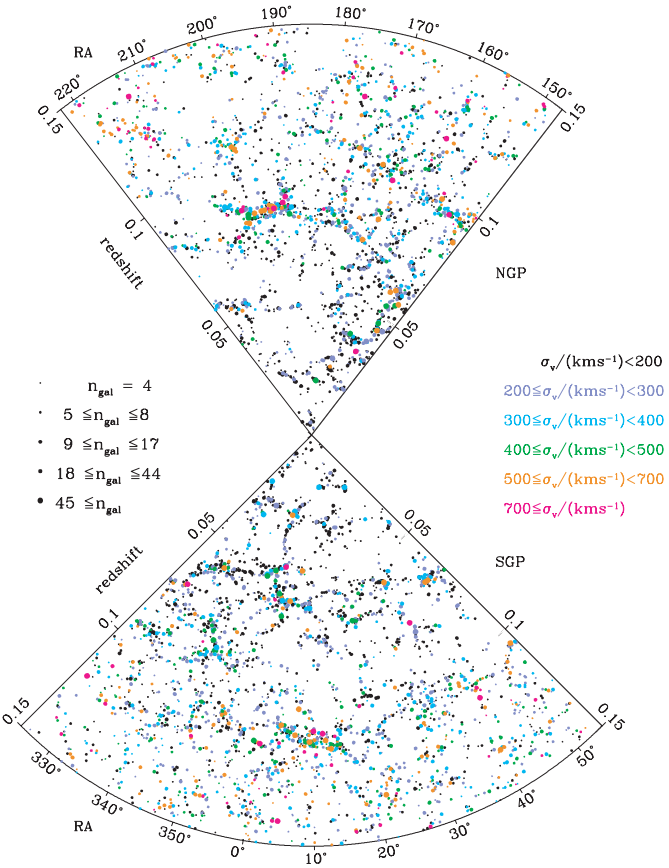

Fig. 4. The 2dFGRS out to $z = 0.15$. Each dot represents a galaxy group. The dot size varies with the number of galaxies per group, and the colour of the dots represents the velocity dispersion of the associated group.

2.3 Compact groups from redshift surveys

Friends-of-friends algorithms have also been applied to galaxy redshift surveys in order to find compact groups [51], [52], [53]. The size and shape of the linking volume is chosen in order to recover groups with similar number densities of galaxies to the Hickson compact group catalogue selected in two dimensions. This involves using a smaller linking volume than is typical for normal group-finding from redshift surveys. Unfortunately for compact group studies, the multi-object spectral capability used to obtain the SDSS and 2dFGRS catalogues was such that fibre clashes preferentially exclude galaxies at small angular separations. Consequently, extra spectroscopic effort to improve the completeness of the galaxy catalogues would be desirable before using these as resources for compact group studies.

3 The 2dFGRS Percolation-Inferred Galaxy Group (2PIGG) catalogue

The 2dFGRS survey consists of a collection of ∼220000 galaxy redshifts down to an apparent magnitude limit of $b_J \approx 19.4$. This survey covers a few percent of the sky, and the majority of this area is within two contiguous strips, shown projected through declination in Figure 3. Eke et al. [46] applied a friends-of-friends algorithm to this galaxy survey to create the 2PIGG catalogue (see Figure 4).

3.1 Mock catalogues

Before applying the group-finding algorithm to the real 2dFGRS, it had been tested on mock catalogues. These were created using semi-analytical models of galaxy formation to place galaxies into the dark matter haloes present in large N-body simulations. This simulation cube filled with galaxies is then 'observed' like the real Universe, allowing a faithful representation of the observational selection function.

Such mock catalogues provide a crucial part of the process of trying to infer properties of the real groups from the data, because they allow a plausible quantification of the systematic errors introduced throughout the whole procedure, right through from deciding which galaxies to target to the allocation of galaxies to groups. Furthermore, they also provide the only effective way of doing any meaningful comparison of the model galaxy groups with those found from the real galaxy survey. This will be seen in the following section where the distribution of stellar mass among groups of different size is calculated.

3.2 Where are the stars?

The galaxy luminosity provides a rough estimate of its stellar mass. However, if the colour of the galaxy is also known, this allows a correction to be made for the age of the stellar population. For instance, at a given luminosity, a redder galaxy will harbour more stellar mass than a blue galaxy that contains a younger, and hence intrinsically more luminous, set of stars. By comparing the 2dFGRS with the 2 Micron All-Sky Survey (2MASS) catalogue of extended sources, Cole et al. [55] were able to estimate the mean density of stellar mass in the local Universe. Bell et al. [56] performed a similar analysis using the SDSS. With the benefit of the mock catalogues, Eke et al. [54] were able to calibrate the method for inferring stellar mass, before calculating how the stellar mass is partitioned between groups of different size.

In estimating a stellar mass from a galaxy luminosity and set of colours, a number of assumptions must be made. These include the values of the metallicity of the stellar population and the dust extinction, the stellar initial

mass function (IMF), a model for stellar evolution, and the star formation rate (SFR) as a function of time. The largest single systematic uncertainty, amounting to about a factor of 2 in stellar mass, arises due to the choice of IMF. However, the set of star formation histories, a different one of which is chosen to match the colours of each galaxy, is also important. Previously, this set had consisted merely of exponentially decaying SFRs, but the mock catalogues showed that these systematically overestimated the stellar mass associated with the galaxy population. The semi-analytical model galaxies have realistically diverse SFRs, reflecting the range of formation histories present in a hierarchically clustering model. Thus, there is no reason why an exponential SFR should better describe their past than those of galaxies in the real Universe. In fact, even the best-fitting exponentially decaying SFR typically led to a $\sim$40% overestimation of the stellar mass because of some late burst making the galaxy look more luminous, while adding little stellar mass. Once the set of allowed SFRs was changed to include the possibility of a late burst of star formation, the mock galaxy stellar masses could be much more accurately inferred.

To estimate the fraction of stellar mass in haloes of a particular size, Eke et al. [54] used a trivariate maximum likelihood procedure to take into account the survey flux limits. The solid lines in Figure 5 show the input model distribution of stellar mass among different sized groups. Dotted lines trace the distribution recovered from the mock catalogues. These show that the size of the systematic errors is small, mainly because the set of groups being used has been carefully selected to ensure this. The symbols in Figure 5 show the results obtained when the real data is used instead of a mock catalogue. It is apparent that there are broad similarities; namely that only a few per cent of all stellar mass lies in clusters, and the most likely halo size to host a randomly selected piece of stellar mass is Local Group-sized. However, there are a few differences in detail. Most notably, more stellar mass is placed in low luminosity systems in the model than is the case in the real data. This is therefore telling us about an area of the semi-analytical modelling, presumably, that needs revising. One should note that, while there is some systematic uncertainty associated with the total stellar mass coming from the choice of stellar IMF, this uncertainty will only propagate into the results shown in Figure 5 if the IMF varies from groups of one size to another.

4 Summary

The majority of group searches have been performed at optical wavelengths, although for bigger groups, also known as clusters, there have been many objects detected via their hot intracluster plasma. These non-optical searches have typically been carried out at X-ray wavelengths, although the Sunyaev-Zel'dovich effect is now beginning to be used for cluster searches.

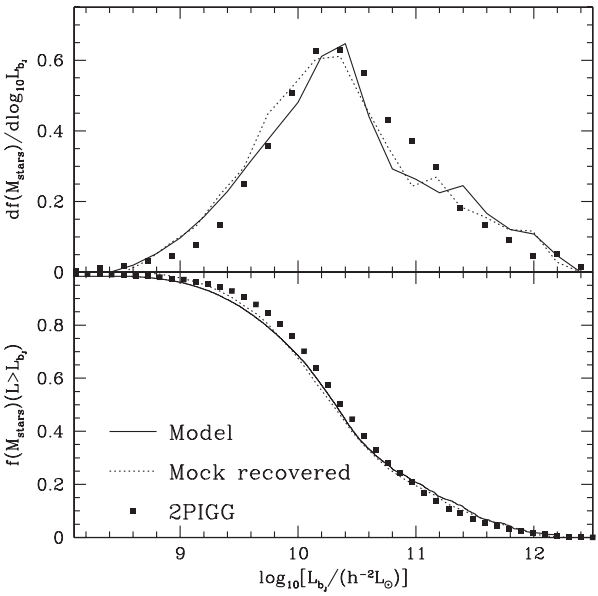

Fig. 5. The distribution of stellar mass among different sized groups, with group size encoded by the total group luminosity in the $b_{\rm J}$ band. The top panel shows the differential distribution of stellar mass, whereas the lower panel is the cumulative version of this, namely the fraction of all stellar mass within systems having a total $b_{\rm J}$ band luminosity at least $L_{b_{\rm J}}$.

Redshift surveys are returning huge quantities of data, from which many galaxy groups can be found. Unfortunately, the physical constraints on fibre positioning in the multi-object spectrographs mean that these surveys are not well suited to finding compact groups. Upcoming surveys will go to higher redshifts, and also probe the less luminous galaxies in local groups. These data will constrain models of galaxy formation. Mock galaxy catalogues will be crucial when comparing models with data, and in understanding what systematic biases are introduced by the group-finding procedure itself.

References

1. I.M. Gioia, J.P. Henry, T. Maccacaro, S.L. Morris, J.T. Stocke, A. Wolter, ApJ, **356**, L35 (1990)
2. A.K. Romer: The Spatial Distribution of X-ray Clusters of Galaxies, University of Edinburgh (1995)
3. H. Ebeling, W. Voges, H. Böhringer, A.C. Edge, J.P. Huchra, U.G. Briel, MNRAS, **281**, 799 (1996)
4. H. Böhringer et al., A&A, **369**, 826 (2001)
5. R.A. Sunyaev, Ya. B. Zel'dovich, Comm. Astrophys. Space Phys., **4**, 173 (1972)

6. M.C. Runyan: A search for galaxy clusters using the Sunyaev-Zel'dovich effect, California Institute of Technology (2003)
7. P.L. Gomez et al.: Sunyaev-Zeldovich Observations of Massive Clusters of Galaxies. In: *The Cool Universe: Observing Cosmic Dawn*, ASP Conference Series, vol 344, ed by C. Lidman, D. Alloin (San Francisco, 2005) pp. 45
8. A. I. Zabludoff, J.S. Mulchaey, ApJ, **496**, 39 (1998)
9. J.S. Mulchaey, A. I. Zabludoff, ApJ, **496**, 73 (1998)
10. T.J. Ponman, D.B. Cannon, J.F. Navarro, Nature, **397**, 135 (1999)
11. G.O. Abell, ApJS, **3**, 211 (1958)
12. G.O. Abell, H.G. Corwin, R.P., Olowin, ApJS, **70**, 1 (1989)
13. F. Zwicky, E. Herzog, P. Wild, M. Karpowicz, C.T. Kowal: *Catalogue of Galaxies and Clusters of Galaxies*, California Institute of Technology (1968)
14. S.L. Lumsden, R.C. Nichol, C.A. Collins, L. Guzzo, MNRAS, **258**, 1 (1992)
15. G.B. Dalton, S.J. Maddox, W.J. Sutherland, G. Efstathiou, MNRAS, **289**, 263 (1997)
16. R.R. Gal, R.R. de Carvalho, S.C. Odewahn, S.G. Djorgovski, V.E. Margoniner, AJ, **119**, 12 (2000)
17. R.R. Gal, R.R. de Carvalho, P.A.A. Lopes, S.G. Djorgovski, R.J. Brunner, A. Mahabal, S.C. Odewahn, AJ, **125**, 2064 (2003)
18. R. van de Weygaert, V. Icke, A&A, **213**, 1 (1989)
19. M. Postman, L.M. Lubin, J.E. Gunn, J.B. Oke, J.G. Hoessel, D.P. Schneider, J.A. Christensen, AJ, **111**, 615, (1996)
20. M.D. Gladders, H.K.C. Yee, AJ, **120**, 2148 (2000)
21. J. Annis et al., AAS, **195**, 1202 (1999)
22. R.S.J. Kim et al., AJ, **123**, 20 (2002)
23. T. Goto et al., AJ, **123**, 567 (2002)
24. N.A. Bahcall et al., ApJ, **585**, 182 (2003)
25. E.L. Turner, J.R. Gott III, ApJS, **32**, 409 (1976)
26. J.A. Rose, ApJ, **211**, 311 (1977)
27. I. Prandoni, A. Iovino, H.T. MacGillivray, AJ, **107**, 1235 (1994)
28. A. Iovino, AJ, **124**, 2471 (2002)
29. A. Iovino, R.R. de Carvalho, R.R. Gal, S.C., Odewahn, P.A.A. Lopes, A. Mahabal, S.G. Djorgovski, AJ, **125**, 1660 (2003)
30. R.R. de Carvalho, T.S. Goncalves, A. Iovino, J.L. Kohl-Moreira, R.R. Gal, S.G. Djorgovski, AJ, **130**, 425 (2005)
31. B.C. Lee et al., AJ, **127**, 1811 (2004)
32. J.P. Huchra, M.J. Geller, ApJ, **257**, 423 (1982)
33. M.J. Geller, J.P. Huchra, ApJS, **52**, 61 (1983)
34. R. Nolthenius, S.D.M. White, MNRAS, **225**, 505 (1987)
35. R.B. Tully, ApJ, **321**, 280 (1987)
36. M. Ramella, M.J. Geller, J.P. Huchra, ApJ, **344**, 57 (1989)
37. M.A.G. Maia, L.N. da Costa, D.W. Latham, ApJS, **69**, 809 (1989)
38. E. Gourgoulhon, P. Chamaraux, P. Fouqué, A&A, **255**, 69 (1992)
39. A.M. Garcia, A&AS, **100**, 47 (1993)
40. M. Ramella et al., A&A, **342**, 1 (1999)
41. D.L. Tucker et al., ApJS, **130**, 237 (2000)
42. G. Giuricin, C. Marinoni, L. Ceriani, A. Pisani, ApJ, **543**, 178 (2000)
43. M.E. Merchán, M.A.G. Maia, D.G. Lambas, ApJ, **545**, 26 (2000)
44. M. Ramella, M.J. Geller, A. Pisani, L.N. da Costa, AJ, **123**, 2976 (2002)

45. M.E. Merchán, A. Zandivarez, MNRAS, **335**, 216 (2002)
46. V.R. Eke et al., MNRAS, **348**, 866 (2004)
47. X. Yang, H.J. Mo, F.C. van den Bosch, Y.P. Ying, MNRAS, **356**, 1293 (2005)
48. M.E. Merchán, A. Zandivarez, ApJ, **630**, 759 (2005)
49. J. Materne, A&A, **63**, 401 (1978)
50. M. Colless et al., MNRAS, **328**, 1039 (2001)
51. E. Barton, M. Geller, M. Ramella, R.O. Marzke, L.N. da Costa, AJ, **112**, 871 (1996)
52. S.S. Allam, D.L. Tucker, AN, **321**, 101 (2000)
53. P. Focardi, B. Kelm, A&A, **391**, 35 (2002)
54. V.R. Eke et al., MNRAS, **362**, 1233 (2005)
55. S. Cole et al., MNRAS, **326**, 255 (2001)
56. E.F. Bell, D.H. McIntosh, N. Katz, M.D. Weinberg, ApJS, **149**, 289 (2003)

Baryon Budget in 2 keV Galaxy Groups

A. Hornstrup[1], A. Vikhlinin[2,3], R. Burenin[3], H. Ebeling[4], O. Kotov[3], K. Pedersen[5], H. Quintana[6] and J. Rasmussen[7]

[1] Danish National Space Center, Juliane Maries Vej 30, 2100 Copenhagen, Denmark
allan@spacecenter.dk
[2] Center for Astrophysics, 60 Garden Street, Cambridge, MA 02138, USA
[3] Space Science Institute, Profsoyuznaya 84/32, Moscow, Russia
[4] Institute for Astronomy, 2680 Woodlawn Drive, Honolulu, HI 96822, USA
[5] Dark Cosmology Center, Juliane Maries Vej 30, 2100 Copenhagen, Denmark
[6] Dpt de A. y A., Pontificia Univ. Catol.de Chile, Casilla 306, Santiago 22, Chile
[7] School of Phys. and Ast., U. Birm., Edgbaston, Birmingham B15 2TT, UK

Summary. We present gas-, total- and galaxy mass profiles from a 2 keV group of galaxies as part of measurements of these quantities from a small series of low-mass clusters and groups, drawn from a new 400 deg^2 X-ray serendipitous survey of Clusters of Galaxies. The aim is to establish robust determinations of the baryon contents in these low-mass systems, and to determine if there is a baryon deficit compared to CMB observations.

1 Introduction

Groups and Clusters of Galaxies are the best systems in the Universe to accurately determine the relative contribution of different components of matter (dark matter, stars, intergalactic gas).

The galaxy groups and poor clusters are both vastly more numerous, and contribute more to the total mass density than do the rich, massive clusters. The commonality of poor clusters and groups makes the study of those systems important for understanding the gravitational and thermal evolution of the bulk of matter in the Universe.

To demonstrate the applicability of cosmological studies using galaxy groups and poor clusters, we need a clear understanding of any non-gravitional processes affecting the global X-ray properties of groups, which we e.g. use to determine gas mass, total mass etc. We need to accurately determine their baryon composition and extend the important scaling relations, such as the mass-temperature relation, from massive clusters to group scales.

Due to their lower mass, the X-ray properties of groups are very sensitive to the presence of any non-gravitional heating of the intergalactic medium, such as early input from SN'e and AGNs ("preheating" see e.g. [1]) radiative cooling and associated energy feedback from star formation see [2] and [3].

Selection of the sample of groups to study is vital to allow statistically safe extrapolations of the results from a few samples to cosmological interpretations. We have for this study drawn a sample of 14 galaxy systems with $T \simeq 2\,\mathrm{keV}$ from a new, unpublished 400 deg^2 survey of X-ray selected galaxy systems.

We assume $\Omega_m = 0.3, \Lambda = 0.7$ and $\mathrm{h} = 0.7$, and X-ray fluxes are in the [0.5–2 keV] band.

2 The 400 deg^2 survey of ROSAT PSPC observations

In 1999–2003, we have performed a large X-ray survey for clusters which were serendipitously detected in a large number of ROSAT PSPC pointed observations with a total sky coverage of 400 deg^2 [4], [5]. This 400 deg^2 survey is an extension to the wellknown 160 deg^2 survey [6], [7].

The criteria for inclusion in the 400 deg^2 catalog were: 1) High galactic latitude to avoid interference with the Milky Way $|b| > 20°$, 2) The hydrogen column $\mathrm{N_H} < 10^{21}\,\mathrm{cm^{-2}}$, 3) Exposure time $\mathrm{t_{exp}} > 1000\,\mathrm{s}$ and 4) The cluster must be 10° away from LMC and SMC.

The detection threshold for the survey is $f_X > 1.4 \times 10^{-13}\,\mathrm{erg\,s^{-1}\,cm^{-2}}$.

Compared to the 160 deg^2 survey, this survey now goes closer to the Milky Way, accepts shorter exposures, and has included the recent archival release of pointings made to cover the original lack of coverage in the ROSAT all-sky survey.

The survey eventually covered 1610 fields (vs 646 in the 160 deg^2 survey), yielding 287 extended objects above the flux limit, a factor of 2.4 increase compared to 160 deg^2.

The survey has a total of 266 galaxy systems, and with the criteria described above, the survey is optimized towards richer, more massive clusters at higher redshifts. However, the 400 deg^2 survey is also very useful for selection of galaxy groups or low-mass (i.e. low $\mathrm{L_X}$) clusters in the nearby Universe, because the survey is complete within $z < 0.2$ and includes therefore also the lower mass galaxy systems. This number may be compared with the ROSAT All-Sky Survey, which is only complete up to $z < 0.04$.

Each cluster in the 400 deg^2 survey has been optically confirmed by imaging, and the redshift of each cluster has been spectroscopically determined based on at least 2 bright galaxies.

2.1 Selection of Groups from the 400 deg^2 survey

We have drawn a sample of 14 systems with $T \simeq 2\,\mathrm{keV}$ (based on $f_X - L_X - T$ using the local $L - T$ relation from [8]) from the 400 deg^2 survey, fulfilling the requirements $0.5 < z < 0.15$, and $f_X > 3 \times 10^{-13}\,\mathrm{erg\,s^{-1}\,cm^{-2}}$. The lower limit in the redshift range allows for X-ray observations using XMM or

Chandra while still having the group's virial radius within the FOV of these telescopes.

3 Analysis of one source: cl1013p4933 at z = 0.134

X-ray observations with XMM

cl1013p4933 was observed with XMM-Newton in 2004.

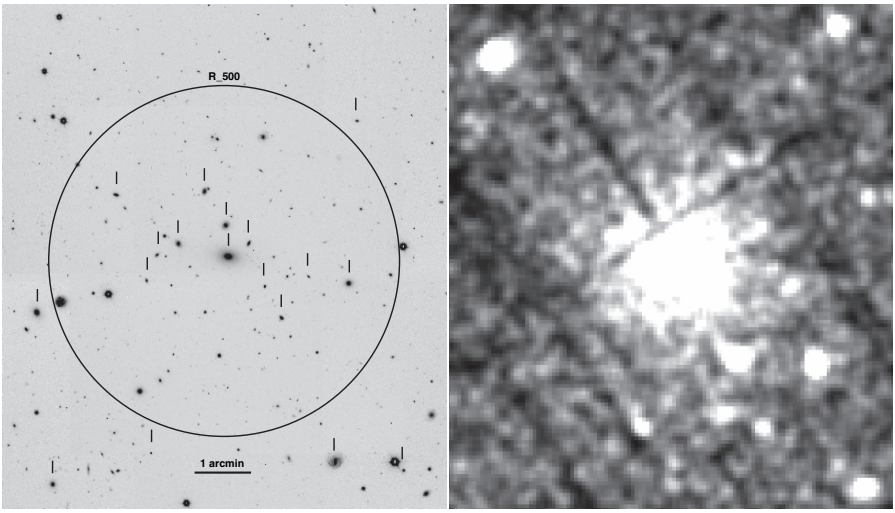

Fig. 1. cl1013p4933 - *left*: R-band image with markings of galaxies spectroscopically identified to belong to the group - *right* The smoothed XMM image to same scale.

Figure 1 shows the X-ray image of cl1013p4933 and the R-band optical image. The X-ray emission indicates a relaxed gas system.

The X-ray surface brightness profile was created from the background corrected image, and fit to the classical β model which, however, turned out to be inadequate to do the fitting. Instead, we used the modified β-model from [9]:

$$n_e n_p = n_0^2 \frac{(\frac{r}{r_c})^{-\alpha}}{(1+\frac{r^2}{r_c^2})^{3\beta-\alpha/2}} \frac{1}{(1+\frac{r^\gamma}{r_c^\gamma})^{\epsilon/\gamma}} + \frac{n_{02}^2}{(1+\frac{r^2}{r_c^2})^{3\beta_2}} \quad (1)$$

which obviously has many degrees of freedom, and fits the data well, see Fig. 2. The interdependence of the parameters makes error estimates difficult. We will here assume that the errors in the mass-estimates mostly come from the T-determination. We trace the X-ray emission to at least R_{500}, which we will use as boundary for all mass-determinations in the following.

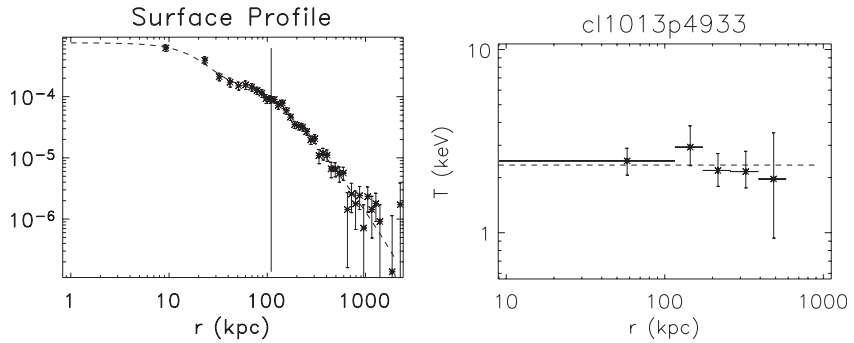

Fig. 2. *Left:* The surface brightness profile and the fit using a modified β-model – *Right:* The X-ray temperature.

Figure 2 shows the temperature profile for the source. The data allows for assuming T_e konstant; we find $T_e = 2.34 \pm 0.40$ keV.

Optical observations with NOT

The object was observed during two runs in 2003. Direct imaging in B, V and R was obtained; part of the R-band image is shown in Fig. 1. Spectra of 20 galaxies in the group were taken.

4 Mass determination and Baryon content

We assume hydrostatic equilibrium and get the total mass as function of radius from the center from the usual $M(r)$ expression. We then derive the gas-density profile, total density profile and gasmass profiles using $M(r)$ and $n_e n_p$ from above.

We derive the galaxy mass profile by first using the relation from [10], which gives the mass of a given galaxy from it's $(B-R)$ and L_R values; after simplified deprojection the profile is achieved. Estimated error is 20%.

In Fig. 3 we show the total-, gas- and galaxy mass profiles.

4.1 Mass and Baryon content of cl1013p4933

CMB observations [13],[14] constrain the baryon content (in our cosmology) to $\Omega_b/\Omega_m = 0.177 \pm 0.023$. The results from our source are shown in fig. 3. At R_{500}, we get $f_{bar} = 0.13 \pm 0.03\, h_{70}^{-3/2}$. The value is within the error of the CMB observations, i.e. there is no strong motivation to include non-gravitational effects to explain the results for this group.

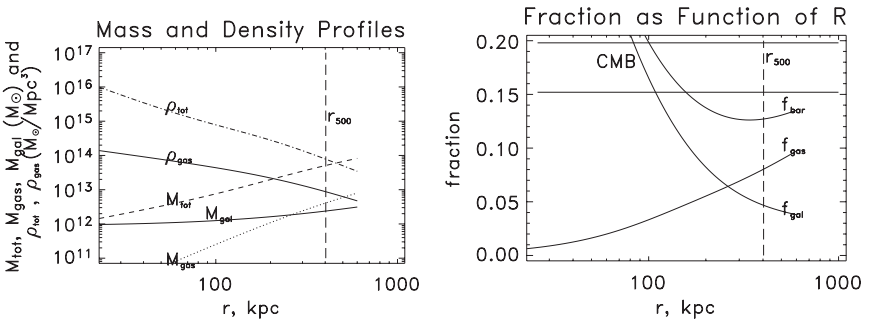

Fig. 3. *Left*: Total and gas masses and densities and galaxy mass up to r_{500} and *Right*: The gas-, galaxy- and baryon fractions.

5 Summary

Our project aims at accurately determine the mass distribution in a sample of low-mass clusters of galaxies and groups, drawn from a new X-ray selected survey of clusters of galaxies, and in particular determine the baryon content.

The preliminary results show, that the values of e.g. $M_{total}, M_{gas}, f_{gas}, f_{gal}$ and σ_r can be determined from these observations.

The f_b values for the first group analyzed are within the errors of the values predicted by the CMB observations; however, more observations and careful analysis are needed to eventually rule out non-gravitional processes.

Optical observations reported here are made with the Nordic Optical Telescope, operated on the island of La Palma jointly by Denmark, Finland, Iceland, Norway, and Sweden, in the Spanish Observatorio del Roque de los Muchachos of the Instituto de Astrofisica de Canarias.

References

1. Cavaliere, A., Menci, N., and Tozzi, P., Astrophys. J., **484**, L21, (1997)
2. Kravtsov, A. V., Nagai, D. and Vikhlinin, A. A., Astrophys J., **625**, 588, (2005)
3. Bryan, G.L., Astrophys. J., **544**, L1, (2000)
4. Burenin, R., et al., in prep. (2006)
5. Hornstrup, A., et al., in prep. (2006)
6. Vikhlinin, A., McNamara, B. R., Forman, W., Jones, C. , Quintana, H., and Hornstrup, A.: Astrophys. J., **502**, 558 (1998)
7. Mullis, C. R., McNamara, B. R., Quintana, H., Vikhlinin, A., Henry, J. P.,Gioia, I. M., Hornstrup, A., Forman, W., and Jones, C., Astrophys. J., **594**, 154, (2003)
8. Markevitch, M., Astrophys. J., **504**, 27, (1998)
9. Vikhlinin, A., Kravtsov, A., Forman, W. R., Jones, C., Markevitch, M., Murray, S. S., and van Speybroeck, L., astro-ph/**0507092**, (2005)
10. Bell, E. F., McIntosh, D., H., Katz, N., and Weinberg, M. D., Astrophys. J. Suppl, **149**, 289, (2003)

11. Poggianti, B. M., Astron. Astrophys. Suppl., **122**, 399, (1997)
12. Helsdon, S. F. and Ponman, T. J., MNRAS, **315**, 356, (2000)
13. Readhead, A. C. S. et al., Science, **306**, 836, (2004)
14. Spergel, D. N. et al., Astrophys. J. Suppl., **148**, 175 (2003)

Isolated Compact Groups of Galaxies in the 2dF Galaxy Redshift Survey

J. Saucedo-Morales[1] and P. Loera-González[2]

[1] Área de Astronomía del Departamento de Investigación en Física, Universidad de Sonora, México
jsaucedo@astro.uson.mx
[2] Departamento de Física, Universidad de Sonora
ploera@astro.uson.mx

Summary. An algorithm that finds isolated compact groups of galaxies in redshift catalogs is presented. It works by sorting the neighbors of each galaxy by projected distance, and forming groups according to chosen parameters of compactness and isolation. This work presents the results for an application of the algorithm to the 2dF Catalog. It has been found that a suitable choice of parameters can yield similar number of groups than those found by the Friends of Friends algorithm. It is important to stress, however, that there are also important differences, whose discussion could be useful to gain insight on the nature of galaxy groups, and to complement the results of other studies.

Aside from obtaining samples of truly compact and isolated groups for later studies of galaxy properties, it is also possible to extract properties of galaxy groups themselves. As an example, the population of groups in the local Universe has been studied. It has been found that for plausible parameters, the percentage of galaxy pairs accounts for less than 40% of the total number of groups.

1 Introduction

The importance of galaxy groups is widely recognized. They can tell us a lot about the evolution of the majority of galaxies and can also be very useful as tracers of large scale structure. The history, as well as the importance of galaxy groups have been discussed at length during this meeting. For the specific scope of this work an excellent introduction may be found in the review by Eke [1], in these proceedings.

A significant advance to our knowledge of the distribution of galaxies in the universe came about with the introduction of galaxy redshift catalogs. The first was the CfA Redshift Survey, which began in 1977 and was completed in 1982 [2]. The availability of redshift catalogs paved the way for systematic searches of galaxy groups. It was in fact in this context that the most successful finding program, the Friends-of-Friends (FOF) algorithm was introduced [3]. Since that time, several investigators have implemented different versions of the FOF. Some of the most recent searches of groups with

the FOF have been done by [4] and [5]. Both of these were based on the 2dF, but [4] used the 100k data release, whereas [5] used the final data release.

In this work, a different method for finding galaxy groups is introduced. The approach relies on the use of the large catalogs of galaxy redshifts presently available (2dF, SDSS, Leda, etc.). The selection criteria adopted is based exclusively on two parameters: the compactness and isolation radius. The motivation for this approach goes back to [6], in which somewhat similar criteria were used for finding the Hickson Compact Groups of Galaxies (HCG) in the POSS plates.

The main motivation for this work, is to study the statistical properties of groups, as well as of the galaxies that reside in them. It is hoped that the isolated and compact groups will be useful to study the evolution of galaxies in such groups.

2 Group finding algorithm

A Fortran program was written to find isolated compact groups. The first step of the finding program is to read the equatorial coordinates and redshifts $(\alpha_i, \delta_i, z_i)$ of all the galaxies in a redshift catalog. Here we present the results for the 2dF, selected for being the more complete and homogeneous currently available. Another argument for using the 2dF, is that it permits us to compare results with those found for the same catalog in [5], and to some extent with those in [4]. The 2dF consists of two parts. The Southern Catalog, which contains 112694 galaxies, and the 2dF Northern, whose total number is 78746. A system of flags is implemented in the code to be able to restrict galaxies whenever appropriate. At the beginning of the program, all the galaxies in the catalog are turned on, by setting their flags equal to one $(flag(k) = 1$, for $k = 1, 2, ..., n)$.

2.1 Calculating and sorting the distances

The next step is to calculate the distances from one particular galaxy to the rest in the catalog, where we are only interested in galaxies reasonably close among themselves. This can be expressed with the restriction $|z_i - z_j| < \Delta z$, where a value of $\Delta z = 0.01$ has been adopted. It is worth mentioning that the purpose of the restriction is merely to reduce computer time, by reducing the number of calculations, but that it should not affect the results unless one chooses a value Δz that is too small. For galaxy i, the angular distances Θ_{ij} from i to j are then calculated for all $j \neq i$ that satisfy the redshift restriction given above, according to the expresion:

$$\Theta_{ij} = acos[sin(\delta_i)sin(\delta_j) + cos(\delta_i)cos(\delta_j)]cos(\alpha_i - \alpha_j). \quad (1)$$

Once the angular separation is known, it is straightforward to calculate the projected distances using the equation $R_{ij} = r_{ij} \times \Theta_{ij}$, where r_{ij} is the mean

distance from us to the galaxies i and j, that one can obtain from Hubble's law. Since we are interested in low redshift galaxies $r_{ij} \sim 0.5(z_i - z_j)c/H_0$. For each galaxy i, the distances R_{ij} are sorted from the first nearest neighbor to the last. The projected distance to the first nearest neighbor is called $s(1)$, $s(2)$ to the second, and so on. Once the distances are sorted, galaxy i is turned off ($flag(i) = 0$). The groups are formed according to the two parameters: r_{comp} (compactness radius) and r_{isol} (isolation radius). A group of 2 galaxies will be considered compact and isolated if the projected distance between them is smaller than r_{comp}, and the next nearest galaxy is outside a circle of radius r_{isol} centered on galaxy i. Thus, the selection criteria for finding a compact and isolated pair of galaxies can be written as follows: $s(1) \leq r_{comp}$ and $s(2) \geq r_{isol}$. Likewise, a group of n galaxies will be defined as compact and isolated if the n galaxies are within a circle of radius r_{comp} around galaxy i, and the next galaxy lies outside a circle with radius r_{isol} centered on galaxy i. This more general selection criteria may be written as follows: $s(n-1) \leq r_{comp}$ and $s(n) \geq r_{isol}$. As galaxies are associated to groups, flags are set to 0 for the group members. This warrants that each galaxy can at most be member of one group, and that the groups will have null intersection.

3 Results

3.1 Selection of the compactness and isolation parameters

The algorithm is capable of forming groups for any given set of parameters. As it turns out, the number and type of groups that are found, vary widely depending on the parameter values. In the absence of a clear theoretical prescription, the parameters are chosen empirically. This can be done for instance, by selecting parameters capable of finding most of the HCGs thought to be true groups. In practice, the selection of parameters involves running the program several times, sampling the 2-parameter space, until it successfully finds the majority of the groups expected to be found. This procedure works rather well in finding the HCGs, since plausible parameters, i.e., a reasonably small value for r_{comp} finds most of the HCGs.

3.2 Results for the 2dF catalog

The 2dF Galaxy Redshift Catalog turns out to be an interesting case for the application of this program. For one thing, the advantage of a large database provides an excellent opportunity to obtain statistically meaningful results. Furthermore, there is a clear advantage of having at hand the results obtained with the FOF algorithm.

As for the case of the HCGs, the two parameters were varied until the total number of groups (pairs + triplets + all the others) turned out to be the same

as that found in [5]. The same number was obtained for $r_{comp} = 1.83Mpc$, and $r_{isol} = 2.0Mpc$. More important, however, is the fact that the pair of parameters is not unique. When trying to fit the number of groups with more than 3 galaxies, the result was $r_{comp} = 1.63Mpc$ (where r_{isol} was set to $2.0Mpc$). Similarly, for the number of groups with more than 4 galaxies, the result was $r_{comp} = 1.60Mpc$, for the same value of r_{isol}. No single pair of parameters was capable of giving the same results for the number of pairs, triplets, and so on. The main reason for this result, is the different nature of this algorithm with that of the FOF. In other words, the FOF groups found in [5] are definitely not compact nor isolated.

3.3 Population of Groups at $z = 0$

Choosing what can be argued to be a reasonable set of parameters $r_{comp} = 1.1Mpc$ and $r_{comp} < 2.0Mpc$, the number of groups were calculated in 5 different redshift bins. To avoid the influence of peculiar velocities nearby, the first bin started a $z = 0.02$. A bin width of 0.05 was selected to make sure there would be enough galaxies in every bin. Thus, the first bin covered the range $(0.02 < z < 0.07)$, the next bin $(0.07 < z < 0.12)$, and so on.

The results are presented in Figure 1. The points on top represent the fraction of pairs (total number of pairs divided by the total number of groups). Only the points for $n = 2, 3, ..., 6$ (top to bottom) are presented, because for $n > 6$, the points would overlap at the bottom. It is easy to see that the fraction of galaxy pairs that are found increases with redshift. In contrast, the number of groups with more than 3 members decreases, whereas galaxy triplets appear to present a mixed behavior. In all cases the groups with less members had a higher percentage than those with more members. In fact this behavior is observed for at least $n = 10$.

A possible interpretation for the results in Figure 1, is that there is a tendency to loose faint group members in the catalog at increasingly higher redshits. If this is the case, an extrapolation to $z = 0$ should tell us what is the representative population of groups at low redshift. The points at $z = 0$ were found, by fitting the other five points of each plot with a second order polynomial. The results for the percentage of groups extrapolated to $z = 0$ are: 39.1% for pairs, 24.6% for triplets ($n = 3$), 16.7% ($n = 4$), 8.4% ($n = 5$), 4.2% ($n = 6$), 3.3% ($n = 7$), 1.9% ($n = 8$), 1.0% ($n = 9$), and 0.3% ($n = 10$).

4 Conclusions

The algorithm presented here, is capable of finding isolated and compact groups of galaxies with any number of members (including isolated galaxies, which were not discussed here), provided the isolation and compactness

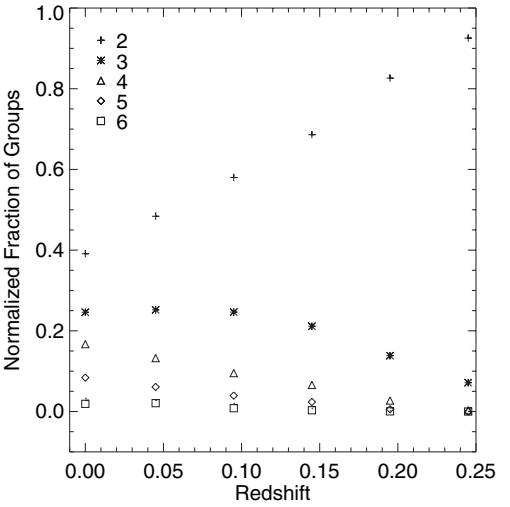

Fig. 1. Fractions of the number of groups, for groups with n galaxies, including $n = 2$ (galaxy pairs), $n = 3$ (triplets), and up to $n = 6$, as a function of redshift. The groups were obtained for the parameters $r_{comp} = 1.1Mpc$, and $r_{isol} = 2.0Mpc$. The points for $z = 0$, were obtained by extrapolation by fitting the data points with a second order polynomial.

parameters are specified. The groups found by this approach may be complementary to those found by FOF. This should be particularly true, if one is interested in studies of the local dynamics of groups.

The results presented for the local population of groups are only preliminary, and require further work. In particular, it would be interesting to find out if these results hold for an application of the algorithm to SDSS data, as well as other galaxy redshift catalogs.

References

1. Eke V.R. (these proceedings)
2. Huchra J.P., Davis M., Latham D., and Tonry J., ApJS **52**, 89 (1983).
3. Huchra J.P., Geller M.J., ApJ **257**, 423 (1982)
4. Zandivarez A., Merchán M. E., Padilla N. D., MNRAS **304**, 247 (2003).
5. Eke V. R. et al., MNRAS, **348**, 866 (2004).
6. Hickson P., ApJ, **255**, 382 (1982).

Environmental Effects on Galaxy Evolution Based on the Sloan Digital Sky Survey

T. Goto

Institute of Space and Astronautical Science, Japan Aerospace Exploration Agency, 3-1-1 Yoshinodai, Sagamihara, Kanagawa 229-8510, Japan
tomo@ir.isas.jaxa.jp

Summary. We have constructed a large, uniform galaxy cluster catalog from the Sloan Digital Sky Survey data. By studying the morphology–cluster-centric-radius relation, we have found two characteristic environments where galaxy morphologies change dramatically, indicating there exist two different physical mechanisms responsible for the cluster galaxy evolution. We also found an unusual population of galaxies, which have spiral morphology but do not have any emission lines, indicating these spiral galaxies do not have any on-going star formation activity. More interestingly, these passive spiral galaxies preferentially exist in the cluster outskirts. Therefore, these passive spiral galaxies are likely to be a key galaxy population being transformed from blue, star-forming galaxies into red, early-type galaxies.

1 The Sloan Digital Sky Survey

The Sloan Digital Sky Survey (SDSS) [1] is both an imaging and spectroscopic survey of a quarter of the sky. Imaging part of the survey takes CCD images of the sky in five optical bands (u, g, r, i and z) [2]. The spectroscopic part of the survey observes one million galaxies. Due to its large quantity and superb quality, the SDSS provides us with an excellent data set to tackle the long standing problems on environmental effects on galaxy evolution.

2 The SDSS Cut & Enhance galaxy cluster catalog

The SDSS Cut & Enhance galaxy cluster catalog (CE)[3] is one of the initial attempts to produce a cluster catalog from the SDSS imaging data. It uses generous color-cuts to eliminate fore- and background galaxies when detecting clusters. Its selection function is calculated using a Monte Carlo simulation. The accuracy of photometric redshift is $\Delta z = 0.015\, at\, z < 0.3$. For a cluster catalog from the spectroscopic sample of the SDSS, see [4][5][6].

3 The morphology-density relation

Using a volume limited sample of 7938 spectroscopic galaxies ($0.05 < \mathrm{z} < 0.1$, $Mr < -20.5$), we investigated the morphology–cluster-centric-radius relation

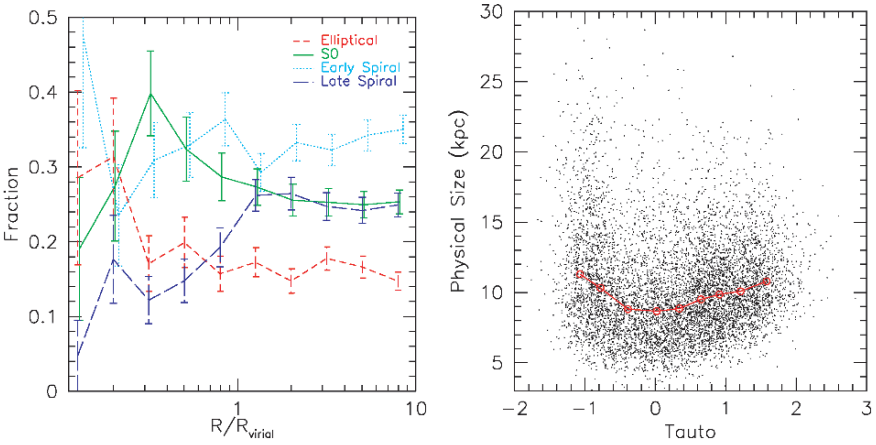

Fig. 1. (*left*) The morphology-radius relation. Fractions of each type of galaxies are plotted against cluster-centric-radius to the nearest cluster. The short-dashed, solid, dotted and long-dashed lines represent elliptical, S0, early-spiral and late-spiral galaxies classified with the automated method ($Tauto$), respectively.

Fig. 2. (*right*) Physical sizes of galaxies are plotted against $Tauto$. Petrosian 90% flux radius in r band is used to calculate physical sizes of galaxies. A solid line shows medians. It turns over around $Tauto \sim 0$, corresponding to S0 population.

in the SDSS [7]. We classified galaxies using the $Tauto$ method, which utilizes concentration and coarseness of galaxies (see [8] for more details of $Tauto$). We measured the distance to the nearest cluster using the C4 cluster catalog [9]. In Fig. 1, morphological fractions of E, S0, Sa and Sc galaxies are shown in the short-dashed, solid, dotted and long-dashed lines as a function of cluster-centric-radius. Around 1 R_{vir}, fractions of Sc start to decrease. Around 0.3 R_{vir}, S0 starts to decrease and E starts to increase. These two changes imply there might be two different physical mechanisms responsible for cluster galaxy evolution. Since a physical size of S0 galaxies ($Tauto = 0$) is smaller than E and Sc ($Tauto = 2$ and -1) in Fig. 2, the results are consistent with the hypothesis that in the cluster outskirts, stripping creates small S0 galaxies from spiral galaxies and, in the cluster cores, the merging of S0s results in a large Es.

4 The passive spiral galaxies

In a similar volume limited sample of the SDSS, we have found an interesting class of galaxies with spiral morphologies (Fig. 3), and without any star formation activity (shown by the lack of emission lines in the spectrum; Fig. 4). These galaxies are called "passive spiral galaxies", and interesting

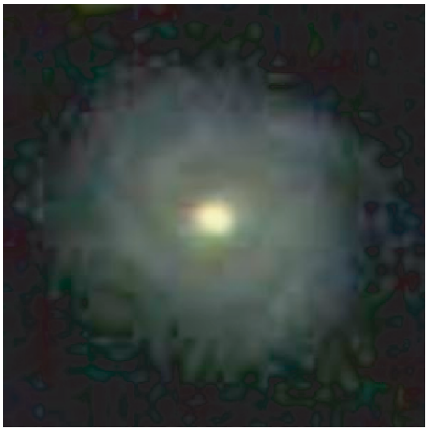

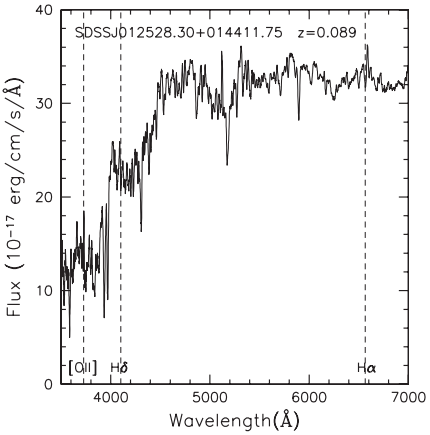

Fig. 3. (*left*) An example image of a passive spiral galaxy. The image is a composite of SDSS g, r and i bands, showing 30"×30" area of the sky with its north up. Discs and spiral arm structures are recognized.

Fig. 4. (*right*) An example restframe spectrum of the passive spiral galaxy. The spectrum is shifted to restframe and smoothed using a 10Å box. The image is shown in Fig. 3.

since they are against currently favored galaxy formation models in which star-formation is sustained by the density waves. Using a volume-limited sample ($0.05< z <0.1$ and $Mr^* < -20.5$; 25813 galaxies) of the SDSS data, we found 73 ($0.28 \pm 0.03\%$) passive spiral galaxies and studied their environments. It is found that passive spiral galaxies exist in a local galaxy density of 1–2 Mpc^{-2} and have a 1–10 cluster-centric virial radius (Figs. 5 and 6; [10]). In other words, passive spirals preferentially exist in the cluster infalling regions. This is the first direct evidence to connect the origin of passive spiral galaxies to cluster related physical mechanisms. These characteristic environments coincide with a previously reported environment where the galaxy star-formation rate suddenly declines [11] and the so-called morphology-density relation turns (See Section 3). It is likely that the same physical mechanism is responsible for all of these observational results in the cluster infalling regions. The existence of passive spiral galaxies suggests that a physical mechanism that works calmly (e.g., gas stripping) is preferred to dynamical origins such as major merger/interaction since such a mechanism would destroy the spiral-arm structures. Passive spiral galaxies are likely to be a key galaxy population in transition between red, early-type galaxies in low-redshift clusters and blue, spiral galaxies more numerous in higher-redshift clusters.

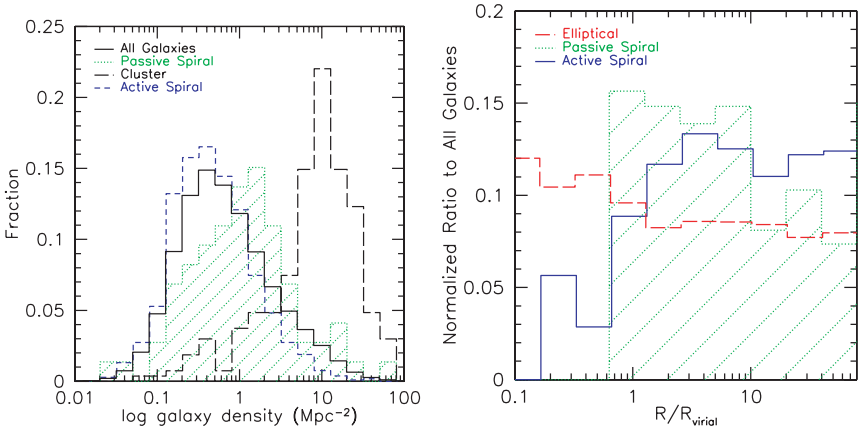

Fig. 5. (*left*) The density distribution of passive spiral galaxies (hashed region) and all galaxies (solid line) in a volume limited sample. Local galaxy density is measured based on the distance to the 5th nearest galaxy within ±3000 km/s. A Kolomogorov-Smirnov test shows distributions of passive spirals and all galaxies are significantly different. A long dashed line shows the distribution of cluster galaxies. A short dashed line shows that of active spiral galaxies. Both of them are statistically different from that of passive spirals.

Fig. 6. (*right*) The distribution of passive spiral galaxies as a function of cluster-centric-radius. The solid, dashed and dotted lines show the distributions of passive spiral, elliptical and active spiral galaxies, respectively. The distributions are relative to that of all galaxies in the volume limited sample and normalized to be unity for clarity. The cluster-centric-radius is measured as a distance to a nearest C4 cluster[9] within ±3000 km/s, and normalized by virial radius [12].

5 Conclusions

We have constructed a large, uniform galaxy cluster catalog from the SDSS data in order to investigate physical mechanisms responsible for the cluster galaxy evolution. By revealing the morphology–cluster-centric-radius relation with the largest statistics to date, we have found two characteristic environments where galaxy morphology changes dramatically, suggesting the existence of two different physical mechanisms in the cluster regions. In addition, we have found unusual galaxies with spiral morphology but without any emission lines. More interestingly, we found that these passive spiral galaxies preferentially exist in the cluster infalling regions, indicating that they are likely to be transition objects between field star-forming spirals and red, cluster early-type galaxies due to the environmental effects in the cluster outskirts.

References

1. Abazajian, K., et al. 2005, AJ, 129, 1755
2. Fukugita, M., Shimasaku, K., & Ichikawa, T. 1995, PASP, 107, 945
3. Goto, T., et al. 2002, AJ, 123, 1807
4. Goto, T. 2005a, MNRAS, 357, 937
5. Goto, T. 2005b, MNRAS, 356, L6
6. Goto, T. 2005c, MNRAS, 359, 1415
7. Goto, T., Yamauchi, C., Fujita, Y., Okamura, S., Sekiguchi, M., Smail, I., Bernardi, M., & Gomez, P. L. 2003a, MNRAS, 346, 601
8. Yamauchi, C., et al. 2005, AJ, 130, 1545
9. Miller, C. J., et al. 2005, AJ, 130, 968
10. Goto, T., et al. 2003b, PASJ, 55, 757
11. Tanaka, M., Goto, T., Okamura, S., Shimasaku, K., & Brinkmann, J. 2004, AJ, 128, 2677
12. Girardi, M., Giuricin, G., Mardirossian, F., Mezzetti, M., & Boschin, W. 1998, ApJ, 505, 74

DPOSS II Compact Groups: The EMMI/NTT Survey

E. Pompei[1], A. Iovino[2] and R.R. de Carvalho[3]

[1] European Southern Observatory, Avenida A. de Cordova 3107, Santiago, Chile
epompei@eso.org,
[2] INAF-OA Brera, via Brera 28, Milano, Italy
iovino@brera.mi.astro.it
[3] Instituto Nacional de Pesquisas Espaciais, DAS, São José) dos Campos, São Paulo, Brazil
reinaldo@das.inpe.br

Summary. We present here the first results from an ongoing spectroscopic survey of candidate compact groups selected in second Digitized Palomar Observatory Sky Survey, DPOSS II. The survey has been carried out at La Silla Observatory and 120 groups out of 261 possible candidates visible from the southern emisphere have been observed. A preliminary analysis of the results show that ∼60% of the candidate are confirmed groups, and that the median redshift of the sample is z ∼ 0.12. Other physical parameters of the confirmed groups, like crossing time, mass and median group radius, are very similar to those measured for the Hickson's compact groups sample in the local universe, suggesting that our new catalogue will be a valuable tool to extend at higher redshifts the investigation of such extreme objects.

1 Introduction

Compact groups (CGs from now onwards) are small (4–8) associations of galaxies characterized by a very high overdensity ($\delta\rho/\rho \sim 80$) and by a low velocity dispersion, of the order of 200–300 km/s. According to classical N-body models [3], the high density and the low velocity dispersion of these structures should make them very short lived, of the order of a small fraction of Hubble time. In addition to this, merging and interactions are expected to be very frequent, making groups an ideal laboratory to study environmentally driven evolution of galaxies. The effects of the CGs extreme environment on group member galaxies and the time scales for CGs eventual coalescence into one fossil remnant are however still question of debate. While detection of diffuse intra-group medium in many CGs confims that these are bound, self-gravitating structures, [12], studies of early type galaxies in CGs [14] show that their stellar population is quite old, suggesting that these objects have been existing for a sizeable fraction of the Hubble time.

One obvious way to try to determine the formation epoch of CGs and establish their evolutionary path is to search for such objects at higher redshifts, possibly going back to look-back times comparable to the expected life-time of compact groups. Depending on the models, this value ranges from 0.1 to

0.5 of the Hubble time (or higher). Searching for these objects at high redshifts is a difficult task: as redshift increases, the typical projected radius of compact groups, 50 Kpc, is projected on an increasing smaller angular scales ($30''$ at z = 0.1) while, at the same time, the fore- and back-ground contamination increases. Furthermore these are extreme and therefore rare objects: one needs to cover a wide area on the sky in order to collect a sizeable sample. There are two photometric surveys which cover a significant part of the sky and are available in the literature: one is the DPOSS II survey, the second one is the Sloan Digital Sky Survey (SDSS). Both surveys have a similar limiting magnitude, r $\sim$ 21.2, and both have been used to produce CGs catalogues using automated algorithms, see [8] and [4] for the DPOSSII and [11] for the SDSS. The SDSS photometric catalogue possess ancillary spectroscopic information, albeit only for a subset of objects. However, as the SDSS spectra have been obtained with a fiber fed spectrograph, whose fiber separation on the sky was $55''$, i.e. nearly twice the size of a compact group at redshift 0.1, the redshift information available at the moment for the SDSS CGs catalogue is not of much help. The search on the DPOSSII catalog produced 459 candidate CGs over an area of 6200 sq. degrees on the sky, with an expected median redshift of 0.12. On this subsample, we started a campaign of spectroscopic follow-up, in order to confirm group membership, to derive the groups's characteristic physical parameters, to study the properties of the member galaxies and to compare our results with the nearby Universe counterparts. We report here the preliminary results from the spectroscopic survey; for more details see also [13].

In the following we assume a ΛCDM cosmology ($\Omega_M = 0.3$; $\Omega_\Lambda = 0.7$) and $H_0 = 67$ km/s

2 Observations and data reduction

The observations were executed in multiple runs during 2004 and 2005 at La Silla Observatory, using the New Technology Telescope (NTT) and the ESO Multi Mode Instruments (EMMI) in low resolution mode (RILD), with grism #2 and a $1.5''$ slit. The dispersion was 3.56 $\mathring{A}$/pixel and the spatial scale $0.33''$/pix. The wavelength range was 3800 to 11000$\mathring{A}$. For each candidate group we observed at least 4 galaxies; in addition each night we observed spectrophotometric standard stars and radial velocity standards taken from the list of Andersen et al. [1]. Data reduction was performed in the standard way, using the MIDAS package, and the final S/N on the reduced spectra was ranging from 15 to 30 per resolution element, depending on the moon phase during the observations.

To measure the redshift of the candidate member galaxies we used the IRAF packages *emsao* and *xcsao*, for more details see [10]. Measured redshifts with a confidence parameter $r \leq 5$ were checked by hand and redshift with a confidence paramter $r \leq 2.5$ were considered not reliable. The final error on

the recession velocity varies between 15 and 100 km/s, taking into account both measurement errors and the error on the dispersion solution. All recession velocities were corrected to heliocentric velocities using the package *rvcorrect* inside IRAF.

After the redshifts of the candidate member galaxies were measured, we decided to consider as *bona fide* confirmed groups all the candidates with at least three galaxies whose velocity difference from the median velocity of the group was Δv $\pm$ 1000 km/s, as in [7]; these were called *concordant* groups. To calculate the median group velocity and radial velocity dispersion, we used the biweight estimators of location and scale [2], which takes into account all relevant cosmological effects. We find that approximately 60% of the candidate groups are indeed bound structures.

Once we selected bound groups, according to our definition, we proceeded to check the surrounding environment, to check whether a group was close on the sky to a larger structure. We browsed the NASA Extragalactic Database (NED) taking into account all the available cluster catalogs. To find neighboring clusters, we adopted a search radius of $15'$, i.e. $\sim 3'$ bigger than the Abell radius of a cluster placed at the distance of the furthest group observed so far, z = 0.148. If we found neighbors, we checked whether there was a measured redshift; if so we refined the search adding a redshift criterion: the group was related to the cluster if the separation among the two was less than $15'$ and if the difference in redshift was less than 0.01. This corresponds to a velocity difference of 3000 km/s, one order of magnitude higher than the typical velocity dispersion of a compact groups and $\sim$2.5 times the highest velocity dispersion measured for a cluster, 1200 km/s [18].

Following the result of the search, we divided our candidate groups in three classes:

- Class A: concordant and isolated groups;
- Class B: concordant groups, but close on the sky to a larger structure, to which they might be associated;
- Class C: systems with less than 3 concordant galaxies. It is interesting to note that the majority of these groups were composed of pairs of galaxies, while the case of 4 discordant redshifts was extremely rare.

In what follows we will consider only targets belonging to classes A and B.

3 Analysis

With a subsample of bound structures in our hands, we proceeded to study their physical characteristics, namely their radius, crossing time, mass and what was the percentage of early and late type galaxies, in order to see how they compare with their nearer counterpart. An average redshift of 0.12 in fact corresponds to a lookback time of 1.56 Gyr, while the average crossing time measured for nearby groups is of the order of 0.2 Gyr: depending on the

preferred merging model one might expect [3] or not [5], to see differences between the nearby ($z \leq 0.03$) groups and their more distant counterpart presented here.

We defined as group radius the median projected separation among the galaxies; we found that the radius distribution peaks around 50 Kpc, which is the typical scale of a compact group, confirming the validity of our selection criteria. Following this, we proceeded to estimate the crossing time following the prescription given in [8]. The median value of the crossing time is 0.018 H_o^{-1}, in good agreement with what was measured for HCGs, 0.016 H_o^{-1}, and corresponding to 0.21 Gyr. We then measured the mass of the groups, using the virial theorem, and assuming as the projected separation between the galaxies the median length of the two-dimensional galaxy-galaxy separation vector, corrected for cosmological effects. As observed by [6], the use of the virial theorem produces the best mass estimate, provided that there are no interlopers or projection effects. In case one of these two effects is present, the current values can be considered an upper limit to the real mass. A good approximation for the mass, in case of isotropic orbits, is given by the projected mass estimator, M_P [6]. We calculated both quantities, M_V and M_P, and found that M_P is a few percent smaller than M_V, but of a comparable order of magnitude. The median value of the group masses, 4.5×10^{12} solar masses, is again in good agreement with the same value measured for the HCGs, 1.5×10^{12} solar masses. Finally we estimated the group luminosity, from the observed magnitudes of the member galaxies, once these were corrected for galactic extinction and k-correction. As reference for the solar magnitude we assumed $M_B = 5.48$ and we found that the mass-to-light ratio (M/L_B) is $92h$, $\sim 50\%$ higher than the median value for the HCGs, $67h$. Both values however are lower than those measured for loose groups, 200-400h, and higher than those measured for single galaxies in HCGs, $7h$ [16]. As last comparison, we investigated the dominant morphological type in the concordant DPOSS II groups. Since we lack good imaging, we adopted the same spectroscopic criteria used by Ribeiro et al. [15]: a galaxy has a late morphological type if it has an EW(Hα)$> 6\mathring{A}$[1]; in addition we assume that a group can be considered dominated by late type galaxies if two or more members are late type objects. We find that 35% of the galaxies show Hα emission and that approximately 40% of the concordant groups are late type systems. This percentage again is in good agreement with the results obtained for HCGs.

4 Discussion and conclusions

All the results we obtained so far show that the confirmed groups have very similar properties to those of HCGs and, with the selection criteria adopted

[1] We assume that an emission line has a positive EW

in defining the DPOSSII CGs candiates sample, no significant evolution can be detected in GCs global properties up to $z \sim 0.12$. This could mean that either something stabilizes the groups longer than we think, or that these high-redshift groups have a very fast evolution, so that what we observe as CGs at $z \sim 0.12$ are not the progenitor of today's CGs.

The first scenario seems to agree well with numerical models which favor an early formation of a common, massive halo, within which individual galaxies form [5]. These models also predict a central concentration of the common halo and a lack of significant perturbation of the halo potential induced by galaxy interactions, unless these interactions are so strong that the perturbation of the potential is comparable with the field of force of the halo. The predictions are in good agreement with observations of nearby compact groups, but the models are unable to explain the high activity and low velocity dispersion ($\sigma\sim$100 km/s) groups observed both in the nearby and not-so-nearby Universe. Moreover, elliptical galaxies showing clear evidence of recent merging, but almost devoid of gas, have been found at redshift z$\sim$0.1 [17]: their physical morphology makes them ideal candidates for the end-product of a compact groups. Observations of similar galaxies in the nearby Universe, clearly identified as fossil groups [9], give strength to the hypothesis of a very fast group evolution.

Clearly the DPOSS II CGs sample, once we will have in our hands the redshift information for the full survey, will provide an important reference sample to which compare CGs of the very nearby universe. However an advance in understanding the evolution of compact groups will come not only from a larger statistics of groups in the optical, but from a detailed multi-wavelength study of groups both at low and high redshift.

References

1. J. Andersen, B. Nordstrom, A. Ardeberg : A&A, 59, 15 (1985)
2. T. Beers, K. Flynn, K. Gebhardt: AJ, 100,32 (1990)
3. P. Carnevali, A. Cavaliere, P. Santangelo: ApJ 249, 449 (1981)
4. R.R. de Carvalho, T.S. Goncalves, A. Iovino et al.: AJ, 130, 425 (2005)
5. M.A. Gomez-Flechoso, R. Dominguez-Tenreiro: ApJ, 549, L187, 2001
6. J. Heinsler, S. Tremaine, J. Bahcall: ApJ, 298, 8 (1985)
7. P. Hickson, C. Mendes de Oliveira, et al.: ApJ, 399, 353 (1992)
8. A. Iovino, R.R. de Carvalho, R.R. Gal et al.: AJ, 125, 1660 (2003)
9. H.G. Khosroshahi, J. Laurence R., T.J. Ponman: MNRAS, 349, 1240 (2004)
10. M.J. Kurtz, D.J. Mink: PASP, 110, 934 (1998)
11. B.C. Lee, S.S. Allam, D.L. Tucker et al.: AJ, 127, 1811 (2004)
12. T.J. Ponman, P.D.J. Bourner et al.: MNRAS, 283, 690 (1996)
13. E. Pompei, A. Iovino, R.R. de Carvalho: A&A, 445, 857 (2006)

14. R. Proctor, D.A. Forbes et al.: MNRAS, 349, 1381 (2004)
15. A. Ribeiro,, R.R. de Carvalho, R.R. Capelato, S.E. Zepf: ApJ, 497, 72 (1998)
16. V. Rubin, D.A. Hunter, W.K. Ford: ApJS, 76, 153 (1991)
17. P. van Dokkum et al.: astro-ph 0506661
18. A.I. Zabludoff, M. Geller, J. Huchra, M. Vogeley: AJ, 106, 1273 (1993)

The Low-luminosity Galaxy Population in the NGC 5044 Group

S.A. Cellone[1] and A. Buzzoni[2]

[1] Fac. de Cs. Astronómicas y Geofísicas (UNLP), Paseo del Bosque, B1900FWA La Plata, Argentina
scellone@fcaglp.unlp.edu.ar
[2] INAF – Osservatorio Astronomico di Bologna, Via Ranzani 1, Bologna, Italy
alberto.buzzoni@bo.astro.it

Summary. Detailed surface photometry for 79 (mostly dwarf) galaxies in the NGC 5044 Group area is analysed, revealing the existence of different morphologies among objects originally classified as early-type dwarfs. Particularly, a significant fraction of bright dwarf "ellipticals" show a distinct bulge+disc structure; we thus re-classify these objects as dwarf lenticulars (dS0). Our finding points at a possible scenario where these systems are the remnants of "harassed" disc galaxies. This is emphasized by the discovery of a few objects with hints for very low-surface brightness spiral-like structure. The colours, structure, and spatial distribution of the different galaxy types suggest that our classification may indeed be separating objects with different origins and/or evolutionary paths.

1 Introduction and observational material

Due to their low luminosities and sizes, a detailed classification of dwarf ($M_B \geq -18$) galaxies is not easy, thus leading to a deceptively simple picture: those objects showing conspicuous signatures of present/recent star formation and interstellar material are called dwarf irregulars (dI), while the remaining smooth-looking, gas-poor objects fall within the dwarf elliptical (dE) designation[3]. However, there is growing evidence for a morphological diversity among dwarfs; in particular, embedded disc structure and/or rotation were discovered within a fraction of dEs [12, 15, 17, 8, 10], which seems to favor the idea that a fraction of the dEs may be remnants of "harassed" disc galaxies [14]. Whether these objects are related to the still poorly known class of dwarf lenticulars (dS0) or not, is still matter of debate [1, 13].

Aiming at a comprehensive study of the low-luminosity galaxy population in the NGC 5044 Group ($m - M = 31.9$) [9] we have gathered multicolour surface photometry for a representative sample, comprising 40 galaxies with Gunn system *griz* imaging data, observed with the ESO 3.6-m telescope (1999–2000), and 57 galaxies observed at CASLEO, Argentina (1996–1999)

[3] Blue compact dwarfs (BCD), at least in groups and clusters, are rare objects, and will not be treated here.

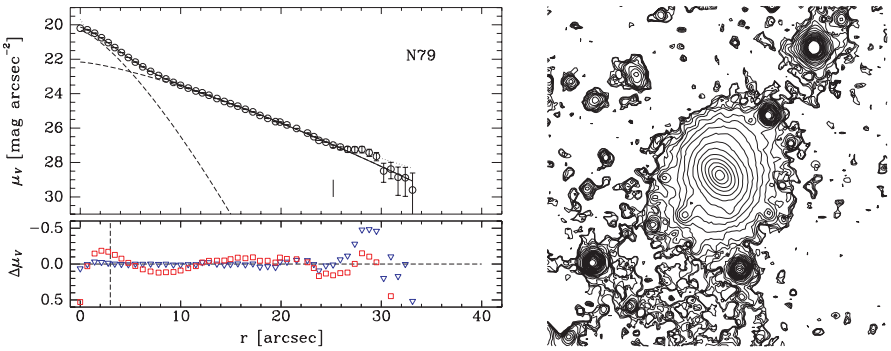

Fig. 1. *Left* – Surface brightness profile for N79 (dS0) showing Sérsic fits to the whole profile and to bulge and disc components (dashed lines); the solid line is the B+D fit. The lower panel shows residuals from a Sérsic fit to the whole profile (squares) and from the B+D fit (triangles). *Right* – Contour plot for N79.

in V and B or R_C with a 2.1-m telescope. There are 18 objects in common between both subsamples, hence we have a total of 79 different galaxies on the NGC 5044 Group area, observed at least in one photometric band. Of these, 74 galaxies have at least one colour information. A subsample of 13 galaxies was also observed spectroscopically at ESO. First results, involving nearly 50% of these data, have been already presented [5, 6, 7].

2 Classification

Background objects were identified by means of morphological criteria when a redshift was not available (see [7]). Group members were classified mostly relying on the behaviour of their surface brightness profiles (SBP), with the aid of colour information and morphological appearance. We were able to assign any individual Group member into one of the following classes:

dE: A Sérsic law [16] gives very good fits to their SBPs. Generally, these galaxies show no isophote twisting.

dE/dS0: These objects are well fit by bulge+disc (B+D) models. They usually show isophote twisting, ellipticity gradients, and/or colour gradients.

dI/dE: Very low surface brightness (LSB) objects, with very extended and nearly exponential SBPs (Sérsic index $n \simeq 1$).

Im: "Magellanic" irregulars.

dSph: Objects (mostly new ones) with $M_g \geq -12$ and central surface brightnesses $\mu_0 \geq 24$ mag arcsec^{-2}.

As an example, Fig. 1 shows the SBP and contour plot for an object (N79) we re-classify as dS0. Trying a single Sérsic fit to the whole useful profile leaves

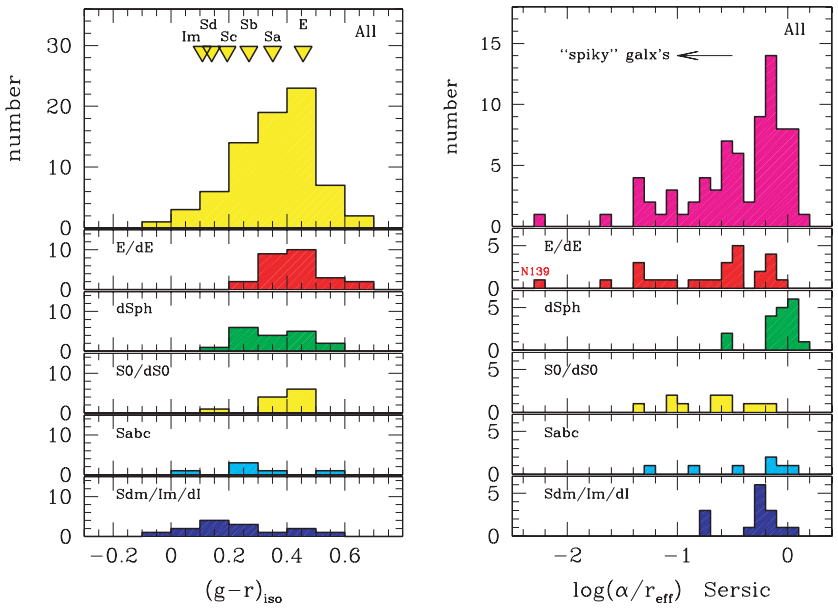

Fig. 2. *Left* - Galaxy colour distribution for the whole sample (top) and for each morphological type. The integrated $(g-r)$ colour refers to g and r galaxy luminosity collected within a $\mu(g) = 27$ mag arcsec^{-2} isophotal aperture. The 15 Gyr template galaxy models from [3, 4] are compared for reference (top triangle markers, as labeled in the upper panel). *Right* - Same as left for the "compactness" parameter $\log(\alpha/r_{\rm eff})$, defined as the ratio between Sérsic pseudo scale-length and galaxy effective radius; compactness increases from right to left. Note the outstanding case of galaxy N139, likely a background cD at $z \sim 0.4$.

both positive and negative systematic residuals ("wave pattern," see [2]). The contour plot (right) clearly shows this galaxy's isophote twisting.

The dI/dE class, in turn, includes a few objects with LSB outer spiral arms [7].

3 Photometric properties

The galaxy colours in our sample show the usual trend with morphological type, with later types having bluer mean colours (Fig. 2, left). The blueing from dE's to dSph's, in turn, is most probably due to a luminosity–metallicity relation. Dwarf spheroidals display a flat and mildly broad distribution, due in part to photometric errors (worse for these faint objects), but probably also reflecting an intrinsic scatter in their origins and star formation histories, as is known for their Local Group counterparts (see e.g. [11]). Also the latest types have a broad color distribution, although in this case the cause may be internal reddening.

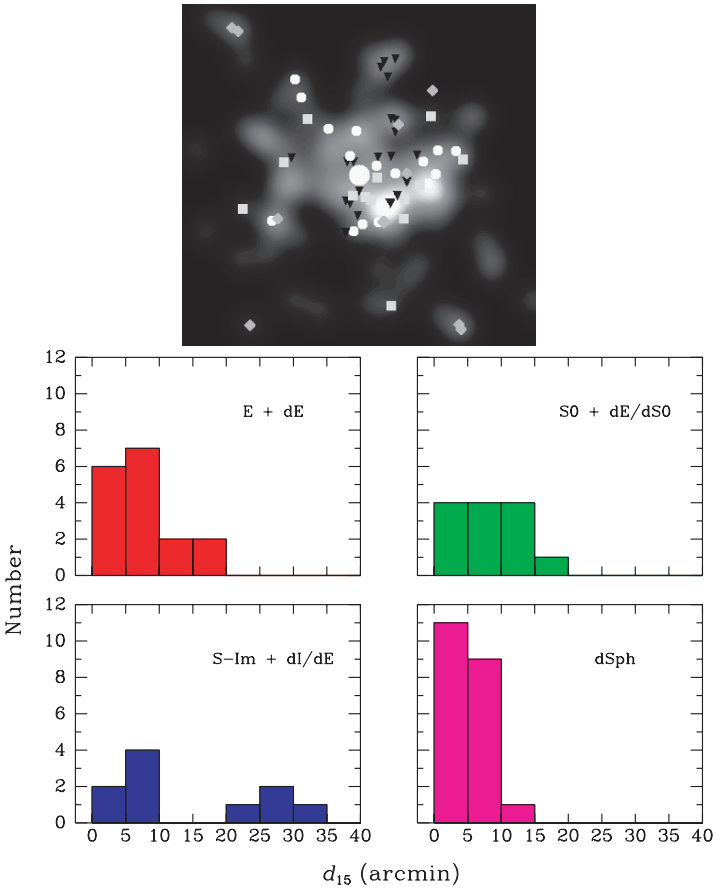

Fig. 3. *Left panel* - Projected number-density map, considering only definite and likely member galaxies from [9]. Superposed is the galaxy distribution from our sample: E+dE (circles); S0+dE/dS0 (squares); S–Im+dI/dE (diamonds); dSph (triangles). The big central dot is NGC 5044. *Lower panels* - Galaxy distribution for different morphological types against distance to the nearest bright ($B_T < 15$ mag) galaxy. Note the striking spatial segregation of dwarf spheroidals, preferentially located around bright group members.

Structural differences between morphological types may be tested by means of a compactness parameter defined as $\alpha/r_{\rm eff}$, where α is the pseudo scale-length in Sérsic's formula, and $r_{\rm eff}$ is the effective radius. Fig. 2 (right) shows the distributions of $\log(\alpha/r_{\rm eff})$ for each morphological type. The dSph galaxy class is characterized by a shallow SBP, clearly distinct from the dE one (but see [7] for possible selection effects). Among the latter, N139 (the most compact object labelled on Fig. 2) stands out for its extremely "spiky"

SBP; our photometric redshift estimate locates this (likely cD) galaxy in the far background at $z \simeq 0.4$.

4 Projected spatial distribution

There is evidence for a morphology – density relation within the NGC 5044 Group, as shown in Fig. 3. While the S0+dE/dS0 galaxies are intermediate between E+dE (more concentrated) and late-type objects (less concentrated), dSph's seem to prefer the highest density regions in the Group. Differences between galaxy types become marginally more significant when the distance to the nearest bright ($B_{\rm T} < 15$ mag) neighbour is considered instead of local number density (see lower panels in Fig. 3). In fact, dSph's are only found in the (projected) vicinity of brighter member galaxies.

Acknowledgement

SC would like to thank the conference organizing committee. This project received partial financial support from CONICET (Argentina) and the Italian INAF, under grant PRIN/05.

References

1. J. A. L. Aguerri, J. Iglesias-Páramo, J. M. Vílchez, C. Muñoz-Tuñón, R. Sánchez-Janssen: AJ **130**, 475 (2005)
2. M. Balcells, A. W. Graham, L. Domínguez-Palmero, R. F. Peletier: ApJL **582**, L79 (2003)
3. A. Buzzoni: AJ **123**, 1188 (2002)
4. A. Buzzoni: MNRAS **361**, 725 (2005)
5. S. A. Cellone: A&A **345**, 403 (1999)
6. S. A. Cellone, A. Buzzoni: A&A **369**, 742 (2001)
7. S. A. Cellone, A. Buzzoni: MNRAS **356**, 41 (2005)
8. S. De Rijcke, H. Dejonghe, W. W. Zeilinger, and G. K. T. Hau: A&A **400**, 119 (2003)
9. H. C. Ferguson, A. Sandage: AJ **100**, 1 (1990)
10. A. W. Graham, H. Jerjen, R. Guzmán: AJ **126**, 1787 (2003)
11. E. K. Grebel, J. S. Gallagher, D. Harbeck: AJ **125**, 1926 (2003)
12. H. Jerjen, A. Kalnajs, B. Binggeli: A&A **358**, 845 (2000)
13. T. Lisker, E. K. Grebel, B. Binggeli: The colours of Virgo dEs as seen by SDSS. In: *IAU Colloq. 198: Near field Cosmology with dwarf elliptical galaxies*, ed by H. Jerjen, B. Binggeli (Cambridge, Cambridge University Press 2005) pp 311
14. B. Moore, G. Lake, N. Katz: ApJ **495**, 139 (1998)
15. S. Pedraz, J. Gorgas, N. Cardiel, P. Sánchez-Blázquez, and R. Guzmán: MNRAS **332**, L59 (2002)
16. J. L. Sérsic: *Atlas de galaxias australes*, (Observatorio Astronómico de Córdoba, Argentina 1968)
17. F. Simien, P. Prugniel: A&A **384**, 371 (2002)

The Galaxy Evolution Multi-wavelength Study (GEMS) Project

D.A. Forbes

Centre for Astrophysics & Supercomputing, Swinburne University, Hawthorn VIC 3122, Australia
dforbes@swin.edu.au

Summary. Here I introduce the GEMS project, our sample and our dataset. Two results in the area of HI mapping and group dynamics are highlighted using the NGC 5044 group as an example. Finally, I briefly discuss a project investigating isolated elliptical galaxies and whether they are the products of merged ('fossil') groups.

1 The GEMS sample and dataset

Galaxy groups are poorly studied relative to their richer cousins – clusters, yet most galaxies are found in the group environment. Groups also appear to be

the density regime in which star formation is strongly suppressed. The physical mechanisms affecting galaxies in groups, and indeed even the processes by which groups themselves evolve are poorly understood.

These processes could include:

- Ram pressure stripping
- Interactions and harassment
- Mergers
- Interaction with the group tidal field
- Strangulation/suffocation
- The presence of overlapping dark matter halos

The GEMS project aims to better understand these processes via a multi-wavelength dataset of 60 nearby groups and mock catalogues from numerical simulations. Details of the GEMS sample and dataset can be found in [2] and [6], with brief details given here. Based on existing optical group catalogues, we selected all groups within $15 <$ Distance < 130 Mpc which have a ROSAT PSPC exposure of $\geq$10,000 sec. This gave a sample of 60 nearby loose and compact galaxy groups, covering a range of evolutionary states and located over the whole sky.

The GEMS dataset consists of:

- ROSAT X-ray imaging (1.5 degrees)
- Wide-field optical imaging (0.5 degrees)
- Parkes HI mapping (5.5 degrees)
- ATCA HI follow-up
- 6dF Galaxy Survey spectra
- 2MASS K-band photometry
- XMM/Chandra X-ray imaging
- Mock catalogues

All 60 groups have X-ray imaging and are included in the 2MASS database, about half have wide-area optical imaging, 16 groups have deep HI observations and all southern groups to $|b > 10^{\circ}|$ are sampled by the 6dF Galaxy Survey.

2 Highlights of GEMS results

Various GEMS results are presented by Ponman, Kilborn, Brough and Raychaudhury at this meeting. Here I briefly mention some other results.

2.1 HI mapping

Our Parkes telescope HI mapping covered 5.5 sq. degrees of 16 southern groups [4]. We sample out to radii of a few Mpc or several virial radii. The

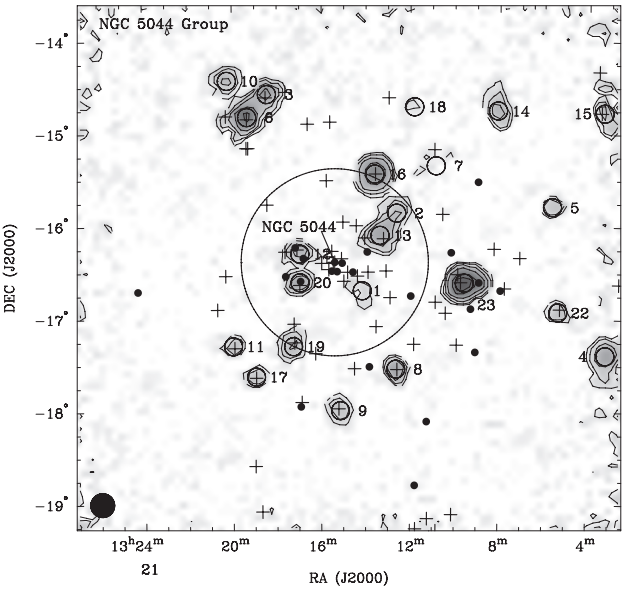

Fig. 1. NGC 5044 group showing HI detections as a grey scale contours previously catalogued group members as crosses from [4]. The large circle shows the r_{500} radius. The Parkes beam size is shown lower left. NGC 5044 itself is indicated.

telescope was scanned across each group in a grid pattern for a total of 16–20 hours. The resulting velocity resolution is ∼2 km s^{-1} (about 10× better than HIPASS) and a mass limit in the range 4–10 × $10^8 M_\odot$ (about 2× better than HIPASS). The bandwidth is 8 MHz with 1024 spectral channels. The final beam size is 15.5 arcmins.

Our HI maps revealed several new group members, including most of the late-type galaxies known to exist in each group. We add about 10% more group members to each previously catalogued group, which has only a small effect on the faint end of the luminosity function (i.e. the so-called 'missing satellites' are not HI-rich, optically-faint dwarf galaxies). An example of our HI mapping is given in Fig. 1, which shows our HI detections and previously known group members for the NGC 5044 group. A 'new' galaxy in the NGC 5044 group was reported in [5]. It has an HI mass of ∼10^9 $M_\odot$ and is associated with an irregular, star forming dwarf galaxy.

2.2 Group dynamics

Another aspect of our GEMS work has been to investigate the dynamics of galaxy groups by combining our HI velocities with velocities from NED and the 6dF Galaxy Survey [1]. After using a friends-of-friends algorithm to define the groups, we calculate the mean group velocity and dispersion. These values are then used to infer the r_{500} radius (∼2/3 of the virial radius), the

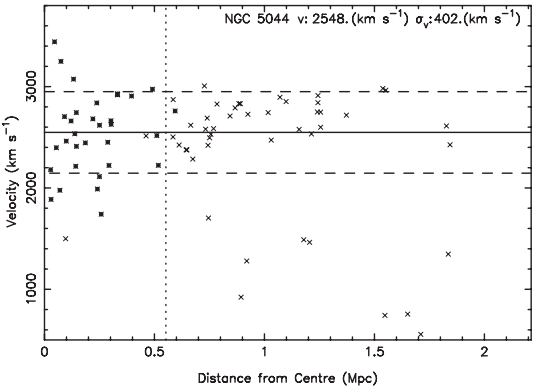

Fig. 2. Velocity vs projected distance from the centre of NGC 5044 from [1]. Filled circles are group members as defined by a friends-of-friends algorithm. Crosses are non-group members. The solid line is the mean group velocity of 2548 km/s and the dashed lines the velocity dispersion of 402 km/s. The vertical dotted line is the r_{500} radius calculated from the velocity dispersion.

virial mass and the crossing time. Using the 2MASS database we are able to calculate the K-band luminosity-weighted spatial centroid of the group.

An example of a velocity–position diagram for the NGC 5044 group is shown in Fig. 2. The vertical line marks the r_{500} radius we calculate, which is very similar to the value found by [6] based on the temperature of the X-ray gas from the intragroup medium of NGC 5044. For small groups, with low numbers of galaxy members, we find that the velocity dispersion is systematically underestimated. The diagram also shows that the velocity dispersion is fairly constant with radius, even out to several virial radii, i.e. beyond the likely boundary of the group. Thus, either groups extend further than we currently believe or galaxies infalling along filaments already have similar velocities to the group that they will soon belong to.

Future GEMS work includes measuring the K-band galaxy luminosity function, high spatial resolution HI follow-up of selected galaxies, examination of the star formation rates via Hα fluxes and understanding the origin of the brightest group galaxies.

Further details of the GEMS project and publications can be found at: http://www.sr.bham.ac.uk/gems/

3 Isolated ellitpicals

Isolated ellipticals are very rare but may hold important clues about galaxy formation. Our aim is to understand whether isolated ellipticals formed early and have remained undisturbed ever since, whether they formed in a recent pair merger, or perhaps they represent a merged group of galaxies (called a 'fossil' group).

With Fatma Reda, George Hau and Ewan O'Sullivan we have defined a new sample of isolated early-type galaxies. Starting with early-type galaxies with a recession velocity $\leq$9,000 km/s and B $<$ 14, we picked those with no neighbours within:

- 700 km/s
- 0.67 Mpc in the plane of the sky
- 2 B magnitudes

In [7] and [8] we show that most isolated ellipticals have a uniform undisturbed morphology but several also reveal signs of a recent merger, eg tidal tails. In general, isolated ellipticals follow the scaling relations of cluster ellipticals but a few of them (with signs of young stellar populations) deviate from the relations in a systematic way. Radial kinematics are presented in [3]. There we show that several galaxies contain kinematically distinct components at their centres – this is indicative of a merger/accretion event or an embedded disk. Only one galaxy (NGC 1132) in our sample is luminous enough in both optical and X-ray emission to be the remnant of a merged group.

References

1. Brough, S., Forbes, D., Kilborn, V., Couch, W., 2006, MNRAS, submitted
2. Forbes, D., et al. 2006, PASA, in press
3. Hau, G., Forbes, D., 2006, MNRAS, submitted
4. Kilborn, V., et al. 2006, MNRAS, in prep.
5. McKay, N., et al. 2004, MNRAS, 352, 1121
6. Osmond, J., Ponman, T., 2004, MNRAS, 350, 1511
7. Reda, F., et al. 2004, MNRAS, 354, 851
8. Reda, F., Forbes, D., Hau, G., 2005, MNRAS, 360, 693

A Search for Ultra-compact Dwarf Galaxies in the NGC 1023 Group of Galaxies

S. Mieske[1], M.J. West[2] and C.M. de Oliveira[3]

[1] ESO, Karl-Schwarzschild-Str. 2, 85748 Garching b. München, Germany
smieske@eso.org
[2] Department of Physics and Astronomy, University of Hawaii, Hilo, HI 96720
westm@hawaii.edu
[3] Instituto de Astronomia, Geofísica, e Ciências Atmosféricas, Departamento de Astronomia, Universidade de São Paulo, Rua do Matáo 1226, Cidade Universitária, 05508-090 São Paulo, SP, Brazil
oliveira@astro.iag.usp.br

Summary. We present a photometric search for UCD candidates in the nearby galaxy group NGC 1023 (d = 11 Mpc) – the poorest environment searched for UCDs yet –, based on wide field imaging with CFHT. After photometric and morphological selection, we obtain a sample of 21 UCD candidates with $-12 < M_V < -11$ mag, if located at NGC 1023's distance. From spectroscopy taken at Calar Alto observatory, we identify the UCD candidate in closest projection to NGC 1023 as an emission line background galaxy. Our photometric data show that in the NGC 1023 group, the mass spectrum of analogs to Fornax/Virgo UCD is restricted to 1/4 of the maximum Fornax/Virgo UCD mass. More spectroscopy is needed to further constrain the mass range of UCDs in this galaxy group.

1 Introduction

In their spectroscopic studies of the Fornax cluster of galaxies, [1]−[3] discovered six isolated compact stellar systems close to the cluster centre with luminosities $-13.4 < M_V < -12$ mag and half-light radii r_h between 15 and 30 pc. They were dubbed "ultra-compact dwarf galaxies" (UCDs) [4]. In [5], metallicities and structural parameters for compact objects in Fornax were derived, indicating that the realm of UCDs in Fornax indeed extends down to about $M_V \simeq -11$ mag. UCDs have also been found in the Virgo and Abell 1689 clusters [6]−[9].

Two main formation scenarios for these puzzling objects have been brought forward. 1. UCDs are tidally stripped "naked" nuclei of dE,Ns [10]. 2. UCDs are merged clusters of massive star clusters created in gas-rich galaxy-galaxy mergers [11].

In order to improve our understanding of UCDs, it is necessary to define their properties in a range of host environments.

In this contribution, we report on a search for UCDs in the nearby galaxy group NGC 1023. This is the poorest environment that has been searched for

UCDs, yet. The galaxy NGC 1023 is of type SB0, has $M_R = -21$ mag [12], and has a distance modulus of 30.29 mag [13]. The NGC 1023 group consists of a few dozen mainly late type galaxies [12],[14]. It has a narrow velocity distribution with $\sigma \simeq 55$ km/s and a virial mass of about $2{\times}10^{12} M_*$.

2 A search for UCDs in NGC 1023

2.1 Data and selection criteria

The imaging data for this investigation were obtained at the 3.6m Canada-France-Hawaii-Telescope (CFHT) at Mauna Kea in service mode between September and November 2004, using the wide-field imager MegaPrime/MegaCam. This camera images a field-of-view of 1×1 degree onto 36 2048×4612 pixel CCDs, which have a pixel scale of 0.187". Four fields around NGC 1023 were imaged (see Fig. 3) in g and i. The seeing-FWHM was between 0.6 and 0.9″. The advantage of the NGC 1023 imaging data is that UCD analogs to those in Fornax and Virgo are resolved, see the Monte Carlo simulations in Fig. 1. This makes the photometric UCD candidate search very effective.

We applied the following criteria to select UCD candidates:

1. i<18.75 mag. At the distance of NGC 1023, this corresponds to $M_V = -11$ mag [15], [16], which is the approximate limit between UCDs and GCs [5].
2. (g-i)<1.40 mag. This corresponds to the red limit $(V-I)_0 \simeq 1.3$ of Fornax UCDs [5], [15], [16], [17].
3. Ellipticity < 0.2. None of the UCDs resolved with HST imaging shows ellipticities larger than 0.2 [3], [6].
4. SExtractor FWHM < 15 pixel. This corresponds to $\simeq 150$ pc at NGC 1023's distance and is chosen to reject significantly extended background sources or cluster members. UCDs are not expected to surpass this size limit, see the Monte Carlo simulations in the right panel of Fig. 1.
5. SExtractor Star Class < 0.05. This limit is applied because analogs to Fornax/Virgo UCDs will be resolved, see Fig. 1. It biases us against detecting UCDs smaller than core radii of about 8pc, which is the very lower limit of UCD sizes in Fornax and Virgo.
6. Morphological selection. The final step was to morphologically reject bulges/nuclear regions of background galaxies, which constitute the major part of the pre-selected sample (Fig. 2). About 90% of the photometrically pre-selected objects were classified by visual inspection as background galaxies, leaving 21 bona-fide UCD candidates.

2.2 Results

The final sample of 21 bona-fide UCD candidates has $-12 < M_V < -11$ mag and is shown in a map and colour-magnitude diagram of the surveyed area

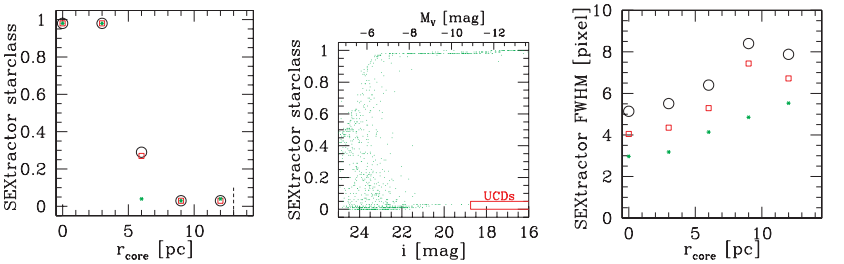

Fig. 1. *Left:* SExtractor star-classsifier plotted vs. core radius r_{core} for simulated UCD-type sources in our CFHT images, projected to NGC 1023's distance. The assumed intrinsic UCD profile is a King profile with concentration parameter c = 1.2 [6]. The profile is convolved with three different PSFs: large black circles denote FWHM = 0.9″; medium sized red squares denote FWHM = 0.7″; small sized green asterisks denote FWHM = 0.5″. The dashed tick at r = 13 pc denotes the mean UCD King core radii from [6]. *Middle:* SExtractor star-classifier plotted vs. apparent i magnitude for 1 out of the 144 imaged CCD chips. Objects plotted are pre-selected according to the UCD colour, size and ellipticity criteria outlined in Sect. 2.1. The rectangle at the lower right corner of the panel indicates the magnitude+starclass selection criteria for UCD candidates. *Right:* Plot is analogous to the one on the left - here the y-axis displays the SExtractor FWHM in pixels instead of the SEXtractor starclass.

in Fig. 3. The most striking feature of this final UCD candidate sample is that there are no UCD candidates with $M_V < -12$ mag. That is, the mass spectrum of possible UCDs in the NGC 1023 group is restricted to about four times lower masses than that of Fornax/Virgo UCDs. This confirms the intuitive expectation that both the number and mass of UCDs scale with host environment properties such as galaxy density and depth of potential well. For example, there are no UCDs known in the Local Group. The spatial distribution of the UCD candidates is clearly not centered on NGC 1023, consistent with a substantial background contamination.

We have obtained a spectrum for the UCD candidate in closest projection to NGC 1023, called f1_15. We were granted 1 hour of observation in DDT mode at Calar Alto observatory using CAFOS (Calar Alto Focal Reducer and Faint Object Spectrograph) mounted at the 2.2m telescope with the G 100 grism (instrumental resolution 7 Å). From the spectrum of f1_15 (Fig. 4) we identify it as an emission line galaxy at z=0.211.

3 Conclusions

Using only photometric data we have been able to show that in the NGC 1023 group the mass spectrum of Fornax/Virgo UCD analogs does not extend beyond about 1/4 of the maximum UCD mass in Fornax/Virgo. More

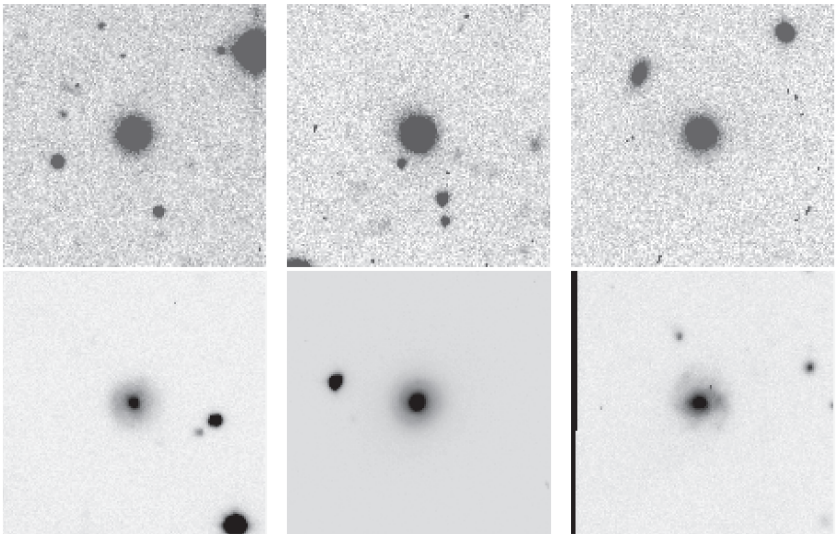

Fig. 2. Thumbnail images of 26×26″ illustrating the morphological selection of UCD candidates. *Top row:* 3 examples for photometrically pre-selected SExtractor detections that morphlogically classify as UCD candidates because of their featureless compactness. *Bottom row:* 3 examples for photometrically pre-selected SExtractor detections that morphologically classify as bulges or nuclear regions of background spirals.

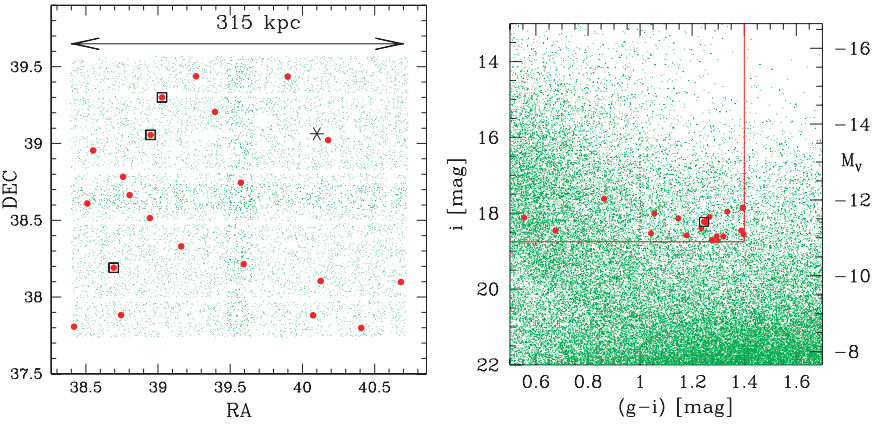

Fig. 3. Left: Map of the investigated area. Red (large) dots indicate positions of UCD candidates. Green (small) dots are pre-selected UCD candidates based only on colour and magnitude. The position of NGC 1023 is indicated by the asterisk. The three UCD candidates marked by squares are those blue-wards of the Fornax/Virgo UCD colour range as indicated in the right panel. **Right:** Green (small) dots show a colour-magnitude diagram of all detected sources in the surveyed area. The solid red lines denote the colour-magnitude selection criteria for UCD candidates. The dashed lines denote the colour-magnitude range of Fornax/Virgo UCDs. The (large) red circles show the UCD candidates. The one source marked by a square is UCD candidate f1_15, which is in closest projected distance to NGC 1023, see left panel.

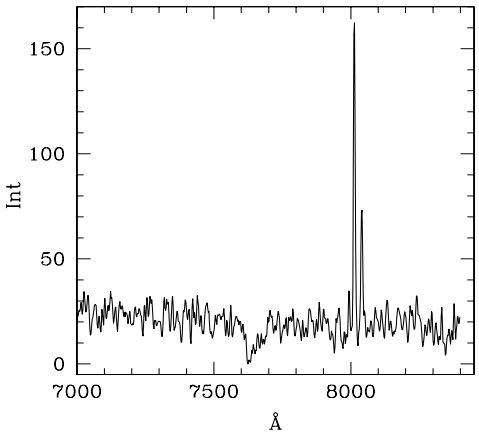

Fig. 4. Excerpt of the spectrum of UCD candidate f1_15, which is the one in closest projection to NGC 1023. We identify the typical Si telluric absorption band at $\simeq$ 7620 Å. The group of three emission lines is identified (in order of decreasing equivalent width) as Hα @ rest-frame wavelength 6562.8 Å, NII @ 6585 Åand NII @ 6549 Å. The corresponding redshift of the source is then z = 0.221.

spectroscopy will be needed to further constrain the mass range of possibly existing UCDs in this group.

References

1. Hilker, M., Infante, L., Vieira, G., Kissler-Patig, M., & Richtler, T. 1999, A&AS, 134, 75
2. Drinkwater M.J., Jones J.B., Gregg M.D., Phillipps S., 2000, PASA 17, 227
3. Drinkwater, M.J., Gregg, M.D., Hilker, M. et al., 2003, Nature, 423, 519
4. Phillipps S., Drinkwater M.J., Gregg M.D., Jones J.B., 2001, ApJ 560, 201
5. Mieske, S., Hilker, M., Infante, L., Jordan, A. 2006, AJ in press, astro-ph/0512474
6. Hasegan, M., Jordán, A., Côté, P. et al. (VCS team) 2005, ApJ, 627, 203
7. Jones, J.B., Drinkwater, M.J., Jurek, R. et al. 2006, AJ, 131, 312
8. Mieske, S., Infante, L., Benítez, N., et al., 2004b, AJ, 128, 1529
9. Mieske, S., Infante, L., Hilker, M. et al. 2005a, A&A, 430L, 25
10. Bekki, K., Couch, W.J., Drinkwater, M.J., Shioya, Y., 2003, MNRAS, 344, 399
11. Fellhauer, M., Kroupa, P., 2002, MNRAS, 330, 642
12. Trentham, N., Tully, B. R. 2002, MNRAS, 335, 712
13. Tonry, J.L., Dressler, A., Blakeslee, J.P. et al. 2001, ApJ, 546, 681
14. Tully, R.B. 1980, ApJ, 237, 390
15. Fukugita, M., Ichikawa, T., Gunn, J.E. et al. 1996, AJ, 111, 1748
16. Schlegel, D.J., Finkbeiner, D.P., & Davis, M. 1998, ApJ, 500, 525
17. Bruzual, G., Charlot, S. 2003, MNRAS, 344, 1000

Dwarf Galaxies in the Antlia Cluster: First Results

A.V.S. Castelli[1,2], L.P. Bassino[1,2], S.A. Cellone[1,2], T. Richtler[3], B. Dirsch[3], L. Infante[4], C. Aruta[4] and M. Gómez[3]

[1] Facultad de Ciencias Astronómicas y Geofísicas, Universidad Nacional de La Plata, Paseo del Bosque s/n, La Plata (1900), Argentina
asmith@fcaglp.unlp.edu.ar
[2] IALP – Conicet, Argentina
[3] Universidad de Concepción, Casilla 160-C, Concepción, Chile (contact address for B.D.)
[4] Pontificia Universidad Católica de Chile, Casilla 306, Santiago 22, Chile

1 Introduction

The Antlia cluster (l = 273°, b = 19°) is the third nearest galaxy cluster (d = 35 Mpc) after Virgo and Fornax. In spite of its proximity, it has been poorly investigated. Its population is dominated by early type galaxies, with dwarf ellipticals being the most abundant galaxy type [1].

Here we present the first results of a project aimed to study the galaxy population of the Antlia cluster. Our results correspond to the identification and classification of dwarf galaxies in the central cluster region, extending the list of [1] (FS90 catalogue), a photographic survey that is complete only up to $B_{\rm T} \simeq 18$ mag ($M_{\rm B} \simeq -14.7$ mag at the Antlia cluster distance).

The final aim of our project is to study the luminosity function, morphology and structural parameters of dwarf galaxies in the Antlia cluster with a more complete sample. We also intend to investigate the kinematics of the cluster (50 spectra have been already obtained).

2 Observations

The observations for the Antlia project were performed with the MOSAIC camera (8 CCDs mosaic imager) mounted at the prime focus of the 4-m Blanco telescope at the Cerro Tololo Inter-American Observatory (CTIO). The field of view is $36' \times 36'$. Kron-Cousins R and Washington C filters were selected due to their known good metallicity resolution [2]. Images from a field located at the cluster center were obtained during April 2002, and three adjacent fields during March 2004. These fields cover 1.5 square degrees of the Antlia cluster. The results presented here refer to the central field.

3 First results

The detection of extended sources on the images was performed with SExtractor [3]. In addition to 70 galaxies from [1], we detected many new dwarf galaxy candidates (dwarf ellipticals, dwarf spheroidals, and irregulars). The faintest candidates have $B_{\rm T} \simeq 23.4$ mag ($M_{\rm B} \simeq -9.3$ mag at the Antlia cluster distance).

We find that those objects identified by SExtractor that were considered as *definite members* of Antlia cluster by [1], follow a well defined relation in the color-magnitude diagram ($\sigma_{color} \sim 0.08$). Also those objects considered as *likely members* by [1], are mostly located within a region of 3σ level dispersion from the relation followed by *definite members* (hereafter, 3σ region). Those objects considered as Antlia cluster *possible members* by [1], tend to lie outside this region.

Until now we have studied 17 objects, four of which are new dwarf candidates and 13 are objects from [1]. Only four of these objects (three from FS90 and one new) depart from the 3σ region. The morphologies of all objects located within the region are consistent with dwarf galaxies.

No clear color gradients are detected for those FS90 objects located into the 3σ region, except for two galaxies (FS90 241 and FS90 188) which seem to become redder towards their centers. This, however, could in part be an effect of the different seeing in the C and R exposures.

The new candidates located within the 3σ region show clearly exponential brightness profiles and none of them seems to posess a nucleus. According to the definition proposed by [4], these new objects are faint enough to be considered as *dwarf spheroidals* ($M_{\rm B} \geq -12.8$).

From its color profile, we are able to confirm that one object classified as Blue Compact Dwarf (BCD) by [1] (FS90 75) is indeed a BCD galaxy: its color gets redder outwards (see e.g. [5]) besides being the bluest object in our sample.

Only three objects of our sample (FS90 68, FS90 72 and FS90 231) are confirmed members of the Antlia cluster through their radial velocities, obtained from the 6dF catalogue [6] ($\langle V_{\rm rad} \rangle_{Antlia} \sim 2900$ km s^{-1}).

References

1. H. C. Ferguson, A. Sandage: AJ **100**, 1 (1990)
2. B. Dirsch, T. Richtler, D. Geisler, J. C. Forte, L. P. Bassino, W. P. Gieren: AJ **125**, 1908 (2003)
3. E. Bertin, S. Arnouts: A&AS **117**, 393 (1996)
4. J. S. Gallagher III, R. F. G. Wyse: PASP **106**, 1225 (1994)
5. A. Gil de Paz, B. F. Madore: ApJS **156**, 345 (2005)
6. D. H. Jones, W. Saunders and 22 coauthors: MNRAS **355**, 747 (2004)

Compact Groups: A Statistical Analysis

E. Díaz[1], C. Ragone[1], and H. Muriel[1]

IATE, Observatorio Astronómico de Córdoba, Laprida 854, Cba, Argentina
euge@mail.oac.uncor.edu

1 The compact group sample

In this work we use an automated searcher of compact groups completely described by [2]. We use the Millennium cosmological numerical simulation combined with a semianalytical model. From this simulation we construct two mock catalogues of different depth (up to $z = 0.20$ and $z = 0.36$.) with the aim of quantify the projection effects. We apply the CG identifier to both catalogues covering an area of 1200 sq deg. We find 1442 (020-CGs) and 5156 CGs(036-CGs) in the nearer and deeper samples respectively. The median properties of our mock CGs are similar to those found in observational catalogues [1]; [2]; [3].

2 Comparison with FOF groups

In order to quantify the concordance of CGs with real groups identified dynamically we perform the group identification in the numerical simulation using a Friend-of-Friends algorithm (FOF). In top panel of Figure 1 it can be seen that the 71% of the quartets in the 020-CGs are real entities, i.e. all their members belong to one FOF group (62% in the 036-CGs). Bottom panel shows the same as the top panel but for compact quintets. In this case the 67% of the 020-compact quintets are real groups (61% in the 036-CGs sample). Taking into account the whole sample of compact groups the 69% of the 020-CGs are associated with a FOF group in the numerical simulation (61% in the 036-CGs). This fact shows that the accuracy of the identifier is diminished ($\sim$10%) when increasing the redshift cut-off. On the other hand, the 19% of the 020-CGs presents just one discordant galaxy (22% for the 036-CGs) The discordant galaxies are spread over the whole sample depht and are identified as a compact member due to a projection effect of the 2-D identification method.

3 Stucture of the real CGs

With the aim of measuring the elongation of these groups we define two axis, a : along the line of sight and b : on the sky plane. We split the groups in

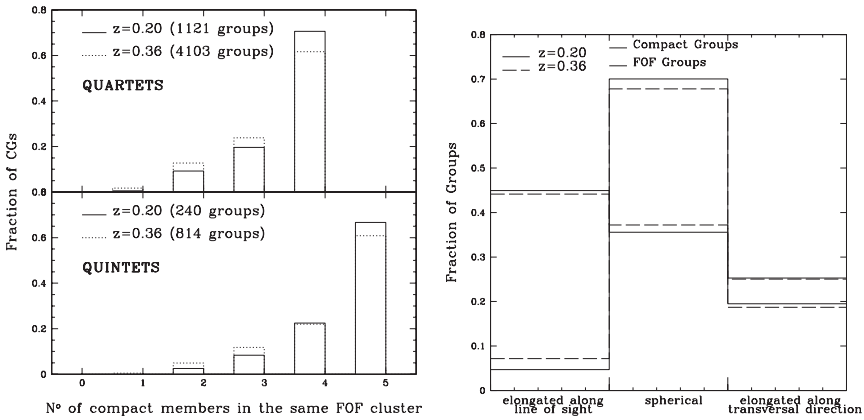

Fig. 1. *Left:* Top (bottom) panel: fraction of compact quartets (quintets)as a function of the number of members per CG that has a counterpart in the FOF groups. *Right:* Thin (thick) histogram: Fraction of CGs (FOF groups) that belong to each subsample of different elongations (see text).

three subsamples according to their ratios b/a: Groups elongated along de line of sight ($b/a < 0.5$), roughly spherical ($0.5 < b/a < 1.5$), and elongated in the transversal direction ($b/a > 1.5$). In Figure 2, it can be seen in thin line that roughly the 50% of the CGs are elongated along the line of sight. The remaining 50% of the realCGs are really compact, it means, compact in a 3-D view. We look for the FOF groups that are the hosts of the real CGs. We also split this FOF group sample in the subsamples mentioned above, the 55% of these groups appear to be spherical (thick line in Figure 2). Then, the apparent elongation present in the CG samples is probably an effect of the identification method.

4 Conclusions

From the comparison with FOF groups we find that the 61% of the CGs in the deeper sample are real entities while this is true for the 69% in the nearer sample. These real CGs are typically elongated along the line of sight but their host FOF groups do not present this characteristic. The ∼20% of the CGs present a galaxy with discordant redshift owing to projections on the line of sight.

References

1. Iovino A: AJ **124**, 2471 (2002)
2. Lee BC et al.: AJ **127**, 1811 (2004)
3. Prandoni I, Iovino A, MacGillivray HT:AJ **107**, 1235 (1994)

Study of Intracluster Diffuse Light within the Fornax Cluster

A.C. Cárdenas, S.A. Cellone and J.C. Forte

Facultad de Ciencias Astronómicas y Geofísicas, Universidad Nacional de La Plata, Paseo del Bosque, La Plata, Argentina
acifuentes@fcaglp.unlp.edu.ar , scellone@fcaglp.unlp.edu.ar
forte@fcaglp.unlp.edu.ar

Summary. Studies of the globular cluster system of the elliptical galaxy NGC 1399, the central galaxy in the Fornax cluster, suggest that many globulars may be associated with the cluster of galaxies potencial, not being bound to any single galaxy but with a diffuse intergalactic medium. However, the galaxies themselves are diffuse objects without any defined edge; this raises a question: is there a true "intergalactic medium?" The goal of this work in to quantify the contribution to the "intergalactic" surface brightness due to the outermost zones of each galaxy in the Fornax cluster and, at the same time, to quantify the surface density of globular clusters associated with this diffuse component.

1 Introduction

The concept of intracluster light (ICL) was proposed by Zwicky [1]. The ICL has low surface brightness, less than 1% the sky brightness in the optical bands. From results to date, the ICL contains between 10% and 70% of the total stellar luminosity of some clusters. Globular clusters may be associated to this component [2]. The correct evaluation of the contribution from all these components requires the determination of the light associated to the most external, very low-surface brightness zones of the galaxies wihtin the cluster. In this work we simulated this diffuse component for the Fornax cluster, estimating its detectability and, at the same time, the number and distribution of its associated globular clusters.

2 Simulation of the astronomical image

Instrumental characteristics were taken from the wide field CCD at the 4m telescope of CTIO: gain = 2 e-/adu, read-out noise = 7e-, sky level = 22.7 mag/arcsec^2≡40000 adu/pix^2, scale = 1.8″/pix. We aimed at solving 1% of the sky brightness, requiring a resolution of 0.1 adu. An integration time of 3600 sec was assumed. We simulated 340 cluster galaxies using data taken from Ferguson's catalogue [3] taking special care to accurately model their surface brightness profiles extrapolating them down to 34.2 mag/arcsec^2.

2.1 Analysis of the simulated image

a) Surface brightness profile: We used the ELLIPSE task within IRAF to obtain the surface brightness profile and the integrated flux of the Fornax cluster, both with and without NGC 1399. We masked-out the central part of each galaxy to better sample the low surface brightness regions. Considering just those regions with surface brightness lower than 22.4 mag/arcsec^2, the Fornax cluster surface brightness profile can be fitted with a single $r^{1/4}$ law. It is thus possible to model the ICL due to the outermost regions of the galaxies within any nearby cluster of galaxies.

b) Aperture photometry: We used IRAF PHOT task to obtain photometry within 2500 apertures of 2 arcmin in radius, in order to evaluate the contribution to the general background of the cluster from the low surface brightness regions of the galaxies. The contribution of the central galaxy to the general background is important. This means that one has to be careful when trying to quantify the genuine sky brightness. This study is useful to locate regions suited to detect ICL in nearby clusters of galaxies.

c) Globular Clusters (GC's): A globular cluster system was generated for each galaxy, with a projected density following a Hubble law propperly scaled to each galaxy luminosity. The position for each globular cluster was ramdomly generated. We took an average specific frequency $S_{\rm N} = 3.3$ and average colour $B - V = 0.7$ for the associated stellar populations. GC's are observed out to $r^{1/4} = 2.6$ arcmin (250 kpc) from the centre of NGC 1399 [4,5]. Between $r^{1/4} = 2.6$ arcmin and $r^{1/4} = 3.3$ arcmin we made an extrapolation of the observed density of GC's. The final population comprises 11900 GC's belonging to NGC 1399 and 12000 GC's belonging to the other galaxies. A single de Vaucouleurs law fits to the whole GC's population. It would not be possible to solve the GC's of NGC1399 from those belonging to the other galaxies. This work could be thus an estimator of the contamination to the NGC 1399 system from those GC's due to the superposition of the other galaxies' systems.

References

1. Zwicky: PASP **63**, 61 (1951)
2. Bassino et al.: A&A **399**, 489 (2003)
3. Ferguson: AJ **98**, 367 (1998)
4. Forte et al.: MNRAS **357**, 56 (2005)
5. Faifer et al.: BAAA **47**, 132 (2004)

BVRI Photometric Analysis for the Galaxy Group NGC 4410

J.A.P. Grana[1,2], S.N. Kemp[1,2], A.C. Katsiyannis[3], E. de la Fuente[1,2], A. Franco-Balderas[4] and J. Meaburn[5]

[1] Departamento de Física, CUCEI, Universidad de Guadalajara Guadalajara Jalisco, México
rivenzhell@yahoo.com
[2] Instituto de Astronomía y Metereología, Universidad de Guadalajara, Guadalajara Jalisco, México
snk@astro.iam.udg.mx, edfuente@astro.udg.iam.mx
[3] Royal Observatory of Belgium, Belgium
T.Katsiyannis@oma.be
[4] Instituto de Astronomía, Universidad Nacional Autónoma de México, México DF, México
alfred@astroscu.unam.mx
[5] Instituto de Astronomía, Universidad Nacional Autónoma de México, Ensenada Baja California, México
jm@ast.man.ac.uk

The interacting group of galaxies NGC 4410 is a peculiar group of twelve galaxies with velocity in the range of 6900-7500 km s^{-1} [7] with four components in obvious interaction: NGC 4410 A-D (Fig. 1). This group lies at a distance of 97 Mpc (using $H_0 = 65$ km $s^{-1}Mpc^{-1}$, which gives a scale of $1'' = 470\,pc$). NGC 4410A ($\alpha = 12^h23^m55^s$, $\delta = 09^o17'40''$, J2000.0) has been classified as a Sab pec asymmetric double lobed radio-galaxy [3], [7]. This galaxy forms a galaxy pair and most probably a future merger [7], [2] with the E? pec or S0? pec galaxy [3], Smith[7] NGC 4410B. This galaxy pair (NGC 4410A/B) has a tidal bridge connected with NGC 4410C, a S0? Hubble type [7]. The four galaxies are connected by two optical bridges, one connecting NGC 4410A/B and NGC 4410C, while the second bridge connects NGC 4410C with NGC 4410D, a SBa Hubble type galaxy. Previous studies in this system suggest a multicolor surface brightness analysis to corroborate facts such as the moderate star formation of 1-4 $M_\odot yr^{-1}$, optical knots [3] and HII regions [2], and possible coincidences of CO, 21 cm and 20 cm observations [7] with dominant stellar populations.

Our data includes a section from a stack of 13 digitally co-added Schmidt films, and three observational periods of direct optical imaging from three different telescopes. CCD direct imaging observations were made on 1999 February 16 with the 1 m Jacubus Kapteyn Telescope (JKT) in the Observatorio del Roque de los Muchachos (La Palma, [8]). During 2001 April 23 to May 1 we carried out more observations with the 0.84 m telescope on the Observatorio Astronómico Nacional de San Pedro Mártir (SPM, BC.). The

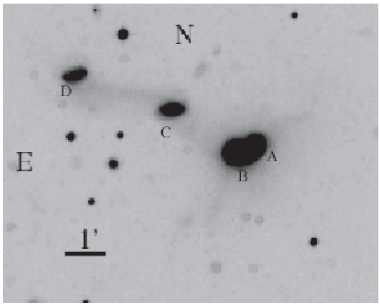

Fig. 1. The four interacting components of the NGC 4410 group: NGC 4410A-D. in a linear B image. The image is part of the co-addition of digital scans of 13 Kodak Tech-Pan Schmidt films (Katsiyannis et al. 1998).

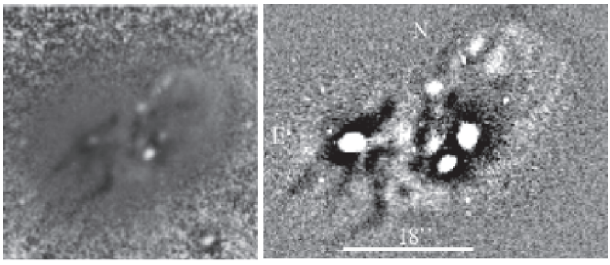

Fig. 2. A $(B - V)$ color map (left) of NGC 4410A/B and a residual image using the unsharp masking process in B for the NGC 4410A/B galaxy pair.

final observational run was made during 2004 April 9-12 with the 2.1 m SPM telescope.

Using color photometry and residual images (Fig. 2) we have found optical counterparts for structures detected in previous studies and images that could indicate the presence of internal structures (Pérez Grana et al. in preparation). We find some evidence of spiral arms within residual images obtained by subtracting the axisymmetric component of the galaxy light [4]. The information obtained was used to discover the predominant stellar populations in order to describe the nature of the bridges and tails within this system.

JAPG and SNK acknowledge receipt of a grant from the LOC to cover the registration fee.

References

1. Barrazza, F. D., Binggeli, B. and Jerjen, H., 2002, A&A 391, 823
2. Donahue, M., Smith, B. and Stocke, J., 2002 AJ. 123, 1922
3. Hummel, E., Kotanyi C. G., and van Gorkom, J. H. 1986, A&A. 155, 161
4. Jerjen, H., Binggeli B. and Kalnajs, A. 2000 A&A 358, 845

5. Katsiyannis, A.C., Kemp S.N., Berry D.S. and Meaburn J., 1998, A&AS, 132, 387
6. Kemp S.N., Katsiyannis, A., Meaburn J., Chavez M. and Berry D.S. *Revista Mexicana de Astronomía y Astrofísica* 14, 70
7. Smith, B.J. 2000, ApJ. 541, 624
8. Tschöcke D., Hensler G. and Junkes N., 1999 A&A 343, 373

Photometric and Kinematical Study of Nearby Groups of Galaxies Around IC 65 and NGC 6962

J. Vennik and E. Tago

Tartu Observatory, 61602 Tõravere, Tartumaa, Estonia
vennik@aai.ee, erik@aai.ee

1 The IC 65 group

The IC 65 group (z = 0.0089) of four late type galaxies – IC 65, UGC 608, UGC 622, and PGC 138291 – has been studied earlier in the 21 cm HI line by van Moorsel (1983, A&AS, 54, 1), who found disturbed HI envelopes of bright group members, and detected a new HI-rich LSB galaxy. We have searched for new dwarf member candidates of this group on the calibrated DSS 2 blue and red frames by means of SExtractor software. Dwarf galaxies were selected using the surface brightness (SB), light concentration, colour and morphological criteria. As a result, we have selected four LSB irregular blue galaxies, which fit the empirical SB – magnitude relation for dwarf galaxies (Ferguson & Binggeli 1994, A&ARv, 6, 67). A detailed surface photometry of selected galaxies has been carried out on the B, R and I CCD frames obtained at Calar Alto (Vennik & Hopp 2004, astro-ph/0409632).

Results for the IC 65 group: The group consists of two dense subgroups with a projected separation of ∼220 kpc (H_0 = 75 km s^{-1} Mpc^{-1} is assumed throughout). The bright group members are rich in HI, their outer HI isophotes generally appear disturbed. Newly found probable dwarf companions are of irregular and/or of the head-tail shape with blue star-forming knots. We conclude that the IC 65 group of galaxies is dynamically young and possibly at the stage of its first collapse with some evidence of (tidal) interactions between its members.

2 The NGC 6962 group

The NGC 6962 group (z = 0.014) is a rich assembly of galaxies, which consists of up to 28 galaxies with concordant redshifts, listed in the NED within 2.6° (∼2.6 Mpc) around the principal galaxy. We have extracted the list of the dwarf galaxy candidates for the group from the *PhotoObjAll* catalog of the SDSS DR4, using the SB, light concentration and isophotal diameter selection criteria. The pre-selected candidates have visually been inspected on the SDSS g, r and i frames and the final membership probability (rated 1–3) has been assigned on the morphological, SB and colour grounds. We

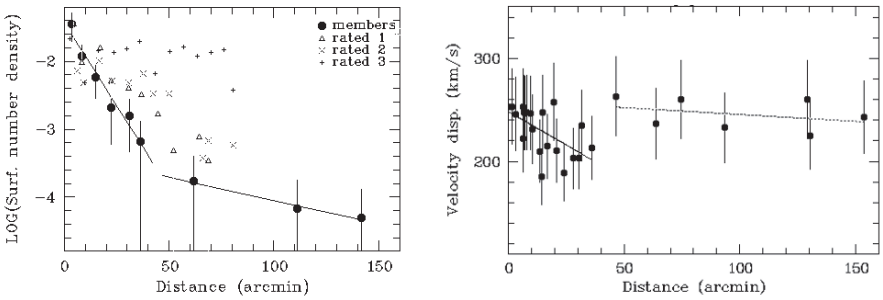

Fig. 1. Number density (*left*) and velocity dispersion (*right*) profiles of true members (•) and dwarf member candidates (rated 1, 2, 3) in the NGC 6962 group.

compared the angular correlation functions (CFs) of true members (reference sample) and newly selected galaxies of different priority classes. The CF of the highest probability (rated 1) candidates could have been reproduced by a mix of 55% of reference sample and 45% of the randomly distributed objects. The rated 2 and 3 ensembles are more severly contaminated by background galaxies. The group displays a dense core + a sparse halo structure. The number density profile (Fig. 1, left) and the radial velocity dispersion (σ_v) profile of a moving window of 9 galaxies (Fig. 1, right) both display a break at $\sim 45'$ (730 kpc), which could be interpreted as a core radius or the rebound radius of the group. Within the rebound radius the σ_v profile is marginally dropping, indicating some dynamical evolution in the core region.

Results for the NGC 6962 group: The group has a well-defined partially relaxed core + halo (or infall region) structure. Further evidence of an evolved group is provided by clear morphological/spectral segregation, with the core being populated mainly by passive S0 and E+ galaxies, except the SXab type principal galaxy. Non-detection of diffuse X-ray emission by RASS indicates that the (supposed) intragroup gas should be in a relatively cold stage.

Table 1. Parameters of the IC 65 and NGC 6962 (core) groups of galaxies

Group	n_{gal}	L_T $10^{10}L_\odot$	R_{harm} kpc	$< R_{ij} >$ kpc	$< v_0 >$ km s^{-1}	σ_v km s^{-1}	$\mathcal{M}_{vt}$ $10^{12}\mathcal{M}_\odot$	$\mathcal{M}_{vt}/L_T$	$t_{cr}H_0$
IC 65	5	5.8 (B)	135	192	2890	77	2.2	38	0.23
NGC 6962	23	13.4 (g)	237	456	4200	238	32.6	242	0.13

Acknowledgments

The reserach was supported by the Estonian Science Foundation grants 6104 and 6106. This study has made use of the NASA/IPAC Extragalactic Database (NED), the STScI Digitized Sky Survey (DSS), and the Sloan Digital Sky Survey (SDSS).

The History of Galaxy Formation in Groups: An Observational Perspective

C.J. Conselice

School of Physics and Astronomy, University of Nottingham, UK

Summary. We present a pedagogical review on the formation and evolution of galaxies in groups, utilizing observational information from the Local Group to galaxies at $z \sim 6$. The majority of galaxies in the nearby universe are found in groups, and galaxies at all redshifts up to $z \sim 6$ tend to cluster on the scale of nearby groups ($\sim$1 Mpc). This suggests that the group environment may play a role in the formation of most galaxies. The Local Group, and other nearby groups, display a diversity in star formation and morphological properties that puts limits on how, and when, galaxies in groups formed. Effects that depend on an intragroup medium, such as ram-pressure and strangulation, are likely not major mechanisms driving group galaxy evolution. Simple dynamical friction arguments however show that galaxy mergers should be common, and a dominant process for driving evolution. While mergers between L_* galaxies are observed to be rare at $z < 1$, they are

much more common at earlier times. This is due to the increased density of the universe, and to the fact that high mass galaxies are highly clustered on the scale of groups. We furthermore discus why the *local* number density environment of galaxies strongly correlates with galaxy properties, and why the group environment may be the preferred method for establishing the relationship between properties of galaxies and their local density.

1 Introduction

Astronomers have known since the time of Messier and the Herschels that the faint nebula, or what we today call galaxies, cluster together. This was before we knew anything else about these systems, including their distances. Galaxy clustering remains one of the cornerstones of cosmology and galaxy formation, and most galaxies are clustered in some form. This is one of the major successes of the Cold Dark Matter model of structure formation, and simulations show that the bulk of large-scale structure is composed of individual groups of galaxies [37]. This is found to be the case observationally [24], and it appears that up to half of all nearby galaxies are in groups or clusters [26].

The fact that a significant fraction of all galaxies are found in groups is likely an important aspect for understanding galaxy formation and evolution. We know that the local environment[1] of a galaxy correlates with most of its properties. The most famous example of this is the morphology-density relation [23], where galaxies with early-type morphologies are more likely found in denser areas, while spirals are more likely found in lower density environments. Galaxies in low local density regions also have a higher star formation rate than those in areas with a higher local galaxy density [40,30]. Whether the relationship between local density and the properties of galaxies is intrinsic, or is a result of physical processes that occur in dense regions after initial galaxy formation is still an unresolved issue.

Galaxy evolutionary effects were also first noticed in the densest areas of the universe – namely galaxy clusters. A high fraction of blue galaxies were found in galaxy clusters at $z \sim 0.5$ compared to local systems [4]. These star forming, or post-star forming galaxies, possibly provide evidence that denser environments induce relatively recent evolution in galaxies. In fact, it is largely unarguable that dense environments such as groups[2] and clusters

[1] We often refer to local and global environments in this paper. The local environment is the density defined by the volume enclosing a galaxy and its nearest bright neighbors. The global environment refers to the type of environment a galaxy lives, whether it be a cluster, a group, or the field, without regards to whether the galaxy is in the core or outer part of a cluster or group. The local environment can be quantitatively measured through a nearest N neighbor approach detailed in e.g., [23,50], or through a friends-of-friend algorithm.

[2] We define a group as a gravitationally bound system of galaxies with less than fifty members all within 1-2 Mpc, and with only a few bright $>L_*$ members.

induce *some* evolution. When these effects occur, and to what degree they alter the evolution of galaxies, is still open for debate.

In this review, we address some of these issues by focusing on the most common environment of galaxies – the galaxy group – and how the cumulative effects of a dense galaxy environment drives the evolution and formation of its members. There are several reasons why the group environment is perhaps the most important for understanding how galaxy formation and evolution occurs. The main reason is due to the fact that most nearby galaxies are in group environments, which we now know extends up to $z \sim 1.4$ [27]. Furthermore, many of the physical processes associated with galaxy formation, e.g., galaxy mergers, can *only* occur in group-like environments. Therefore groups appear to be a gateway environment producing galaxies with drastically different morphological and star forming properties from previous field galaxies.

The outline of this review is as follows: we first describe the final (thus far) evolution of groups of galaxies and their properties by examining nearby groups. We then extended these results to higher redshifts and examine processes, such as star formation and galaxy mergers, and how these might be driven by the group environment. Finally, we draw some conclusions regarding how the group environment might be influencing the evolution of most galaxies. The cosmology $H_0 = 70$ km s^{-1} Mpc^{-1}, $\Omega_\lambda = 0.7$, and $\Omega_m = 0.3$ is used throughout.

2 Groups in the nearby universe

2.1 The Local Group

The nearby universe provides a number of important clues for understanding how galaxies in groups evolved. The best studied example is of course our own Local Group, with its 35+ members, each of which has undergone a distinct formation history (see [31] and the Grebel review in these proceedings). The most effective way to determine when stars in Local Group galaxies formed is to study the resolved stellar populations within these systems. The derived star formation history of the Local Group is clearly very extended and variable, even for the most basic dwarf spheroidals. The star formation in these simple and morphologically indistinct galaxies occurred from roughly the time of reionization until a few Gyr ago [32]. Dwarf irregulars, and the spirals in the Local Group, including our own Milky Way, are by definition still undergoing star formation, but they also have old stars produced likely before reionization.

There are a few more interesting facts about the Local Group worth mentioning in regards to the history of galaxy evolution. While the Local Group

Typically, these systems have masses $\sim 10^{13} - 10^{14}$ M$_\odot$, and velocity dispersions of 150–500 km s^{-1}.

contains four massive members (M31, the Milky Way, M33 and the LMC), it is dominated by lower mass dwarf galaxies. These dwarf galaxies tend to cluster around the two massive members, M31 and the Milky Way. There is also a strong environmental effect occurring within the Local Group dwarf population. The evolved dwarf spheroidal galaxies are located nearest the two giant spirals, while the star forming dwarf irregulars are located away from the giants. This is one example of how the *local* environment of a galaxy correlates with its properties. For more extensive reviews of the star formation history and properties of Local Group galaxies see [31,53].

2.2 Nearby groups and the morphology-density relation

Nearby groups, such as the Sculptor and M66 groups (Figure 1), contain a similar range of morphological and ongoing star formation properties as the Local Group. Because of their distances, it is difficult to reconstruct detailed star formation histories in these nearby groups, but they likely have similar histories as the Local Group.

We can still however use other tools, such as morphologies and ongoing star formation in nearby group members, to understand how these systems are evolving. Star formation is still occurring in both large and small galaxies in group environments. Unless these groups recently formed, this implies that environmental effects that can reduce star formation, such as ram-pressure stripping [44] or the gradual depletion of hot halo gas around galaxies (so-called strangulation or starvation) [38], are not occurring – or at the very least they are not dominating effects. However, we can see environmental effects inducing evolution in the form of induced star formation, and morphological distortions due to galaxy-galaxy interactions, such as between M65 and M66, in the M66 group (Figure 1).

The morphology-density relation for nearby and distant groups and clusters reveals that galaxy formation is sensitive to local environment. This correlation is such that the higher the local projected galaxy surface density, the less likely a galaxy in that area will be a spiral, or undergoing active star formation [49]. However, [55] showed that the morphological-density relation does not hold in a global sense. Zabludoff & Mulchaey [55] found that groups of galaxies can have total early-type fractions as low as in the field, or as high as in clusters (fraction $\sim$0.6), which is independent of the global environment. The local environmental density in which group early-type galaxies are found is as high as the densest environments in clusters of galaxies. The passive or early type galaxies in groups are also found in the centers of groups, where the local galaxy density is highest.

The star formation rate of a galaxy also does not correlate strongly, if at all, with its global environmental density as measured by velocity dispersions [3]. It is not the global environment, such as living in a massive cluster, but the local environment which correlates with galaxy properties. Likewise, gravitational interactions between nearby galaxies only alter morphology, and

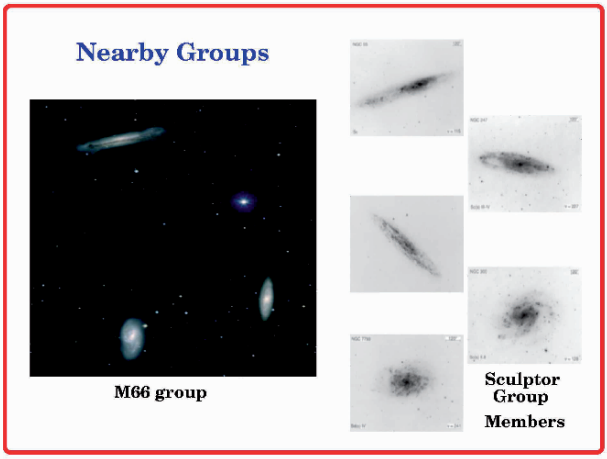

Fig. 1. Examples of galaxies in two of the nearest galaxy groups – the M66 group and the Sculptor group. The galaxies in these groups are similar to the Local Group, with many galaxies undergoing star formation, and in the M66 groups an ongoing interaction between members.

induce star formation, when they are separated by less than a galaxy diameter [34]. Galaxy formation is therefore a local process.

Another nearby galaxy group type that deserve detailed discussion are the so-called compact groups. The compact groups, such as Seyfert's Sextent and Stephen's Quintet, are examples of galaxy groups where the members are within a galaxy diameter, and are likely to merge within about a Gyr. While there is some controversy over the existence of compact groups – some have argued they are chance alignments – the fact that there is a hot intragroup medium associated with these galaxies provides strong evidence that they are bound objects.

An indication that compact groups may be the progenitors of mergers between galaxies are the fossil groups [48], ghost groups, and the AWM groups [1]. These objects are all systems with massive and luminous X-ray emission, but only contain one bright central galaxy. There are some differences, such as the AWM group's central galaxy having a cD like structure. However, what is clear about these 'groups' is that although they consist of only one bright galaxy, they have X-ray profiles and dark matter halos that closely resemble groups. This suggests that these systems are recent merger remnants or the final stages of a galaxy group whose members merged together.

2.3 Galaxy groups up to $z \sim 1.4$

Beyond about $z \sim 0.3$ there have been few searches and systematic studies of groups of galaxies, although this is rapidly changing. The first evidence that galaxy groups at high redshift evolve was provided by Allington-Smith et al.

[1] who discovered populations of galaxies surrounding radio sources at $z \sim 0.5$. They furthermore found that at the same local environmental density, there is a larger amount of star formation in galaxies in groups at $z \sim 0.3$ compared to lower redshift clusters. This is similar to the Butcher-Oemler effect found in clusters, and possibly arises from the same mechanism(s).

The first proper redshift surveys at $z > 0.3$ found significant peaks in galaxy redshift distributions [10,7], suggesting that real over-densities of galaxies exist beyond the local universe. The CNOC2 survey pioneered efforts to characterize the galaxy population in groups at these redshifts [54], which has only recently been superseded by the DEEP2 and VVDS redshift surveys [21,27,36].

The CNOC2 groups at redshift $z \sim 0.5$ display remarkably similar scaling properties as field galaxies at similar redshifts, and in comparison to $z \sim 0$ groups. [54] found a large blue galaxy fraction in both the field and in groups up to $z \sim 0.5$, with a similar rate of decrease in both environments at lower redshifts. However, there are more passive galaxies in group environments at all redshifts, suggesting that the correlation of environment in groups with the properties of its member galaxies existed at least 5-6 Gyr ago.

Redshift surveys with a high velocity resolution, such as DEEP2 and the VVDS, are allowing us to trace how galaxies cluster out to $z \sim 1$. One result of these studies is that galaxies, particularly bright galaxies, cluster strongly out to $z \sim 1.4$ [9]. Using various cluster/group finding techniques such as the Voronoi-Delaunay method, individual groups of galaxies can be identified and studied out to these redshifts [27] (Figure 2).

Once we have found these groups we can then try to determine how environment drives evolution up to $z \sim 1.4$. Bundy et al. [5] have approached this problem recently through using stellar mass functions at different environmental densities and redshifts up to $z \sim 1.4$ (Figure 3). By fitting the spectral energy distributions of galaxies in the BRIJK bands to different star formation histories, [5] calculated the most likely stellar mass to light (M/L) ratio for all galaxies within the DEEP2 spectroscopic survey. Through the use of the observed K-band flux for these galaxies, and the derived stellar M/L ratio, a stellar mass is calculated. The mass function for galaxies in high density environments compared to those in low density environments, as measured through a 3rd nearest neighbor statistic in shown in Figure 3.

Figure 3 shows that mass functions in low and high density environments are similar up to $z \sim 1.4$. This implies that environment in a very broad sense is not a critical component for the formation of galaxies - that is, a galaxy or a potential proto-galaxy's formation by $z \sim 1.4$ does not strongly depend upon whether it is in a dense region or a lower density region. There are however some differences between mass functions in low and high density environments, as galaxies at the extreme ends of the environmental density distribution show significant differences. There are more massive galaxies in higher density environments (cf. [36]), but the overall mass function shape,

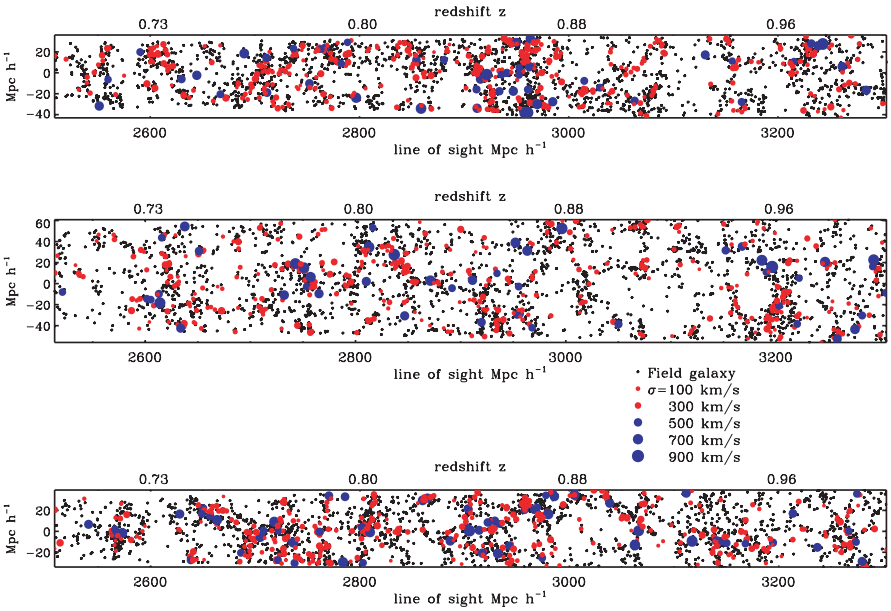

Fig. 2. The distribution of groups in redshift space as seen in the DEEP2 redshift survey [27]. The larger symbols represent groups/clusters with larger velocity dispersions, with groups at dispersions of $z < 300$ km s^{-1} labelled as the smaller (and red) points. (Courtesy of Brian Gerke)

and the characteristic masses of star formation galaxies (i.e., the downsizing) are similar. This furthermore implies that environmental processes that could trigger, or halt, star formation in groups are not major effects, at least since $z \sim 1.4$. This is partially simply another way of saying that most galaxy stellar mass is formed by $z \sim 1.4$. However, there is some star formation evolution in both field and group/cluster galaxies as observed through direct measures [41], as well as increased blue fractions (i.e., Butcher-Oemler). However, this additional star formation does not induce large amounts of new star formation in massive galaxies, and most star formation is occurring in low-mass galaxies at $z < 1.4$ in both low and high density environments.

2.4 Young galaxies at $z > 2$

Large samples of galaxy groups at redshifts larger than $z \sim 1.4$ do not yet exist. What we do have is considerable evidence that $z > 2$ galaxies appear to be clustered, and are in environments that are either group-like, or forming into groups. In fact, there is considerable evidence that higher redshift galaxies are strongly clustered, with the most massive galaxies (examples shown in Figure 4) the most clustered [28,20,39].

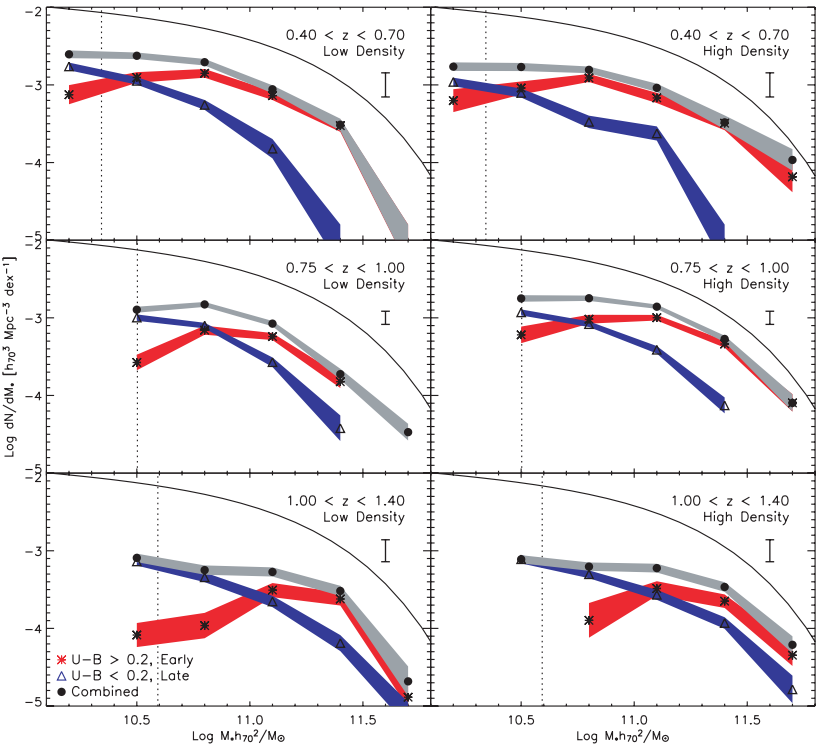

Fig. 3. The stellar mass function from [5] plotted as a function of density and redshift (time). The mass functions are furthermore divided into red and blue galaxies. The transition between blue and red galaxy dominance, i.e., when $M_{blue} > M_{red}$ does not change with a broad environmental density cut.

Examples of this clustering can be seen all the way back to where the earliest galaxies are seen. For example, deep Hubble Space Telescope (HST) imaging of bright $z \sim 6$ QSOs show an excess of red $(i - z)$ galaxies surrounding these systems [56]. If these QSOs are the sites of massive galaxy progenitors, then it seems likely that they and their companion galaxies will evolve to become a virialized system – perhaps a group or a cluster. Making the connection between these 'groupings', and modern clusters/groups is not as difficult as it might seem. The large statistical excess of objects with red $(i-z)$ colors strongly suggests that these objects are spatially associated with each other. They are furthermore found within a projected radius of a Mpc or so – which is the typical size of a group or cluster core.

Although we can detect galaxy clustering through various techniques out to $z \sim 6$, often we know very little about the formation modes of these galaxies, except that they are undergoing star formation. Internal galaxy properties as observed with HST, and integral field units, can only be studied

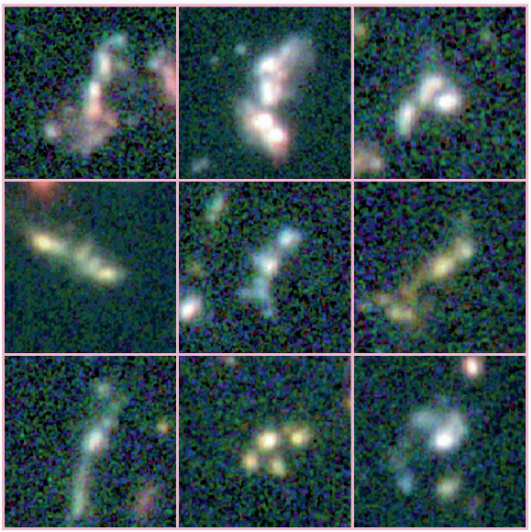

Fig. 4. Examples of high redshift bright galaxies as seen in the Hubble Deep Field. These types of galaxies are the most clustered and often shown direct signs through color gradients, and structures, for a recent merger origin.

in large numbers at $z < 3$. There is now abundant information about these young galaxies which suggests that their clustering, and perhaps grouping, is driving their formation and evolution.

Galaxies at $z > 1.4$ are generally found to cluster quite strongly on small ($\sim$1 Mpc) scales. A recent example of this comes from the Great Observatories Origins Deep Survey (GOODS; 29). Due to the high quality and depth of the GOODS Hubble Space Telescope imaging it is possible to use the Lyman drop-out technique to find galaxies undergoing unobscured star formation at $z \sim 3$ and $z \sim 4$. The correlation function for these systems has an excess at small scales over a power-law. This excess can be explained by a two component model for galaxy clustering, such that a large scales galaxies are in single halos, where as at small scales two galaxies per halo are needed to explain the excess [39]. There is also a luminosity dependence to this clustering, such that the most luminous galaxies are the most clustered [28,39]. We will address in the later part of this review how this clustering might be driving the formation of galaxies found in early groups.

3 Physical processes in groups

3.1 Possible formation mechanisms

Galaxy evolution occurs via both internal and external drivers. The environments of galaxies should have some effect on how galaxies evolve. For

example, if galaxies are surrounded by other galaxies then gravitational interactions and mergers can induce the formation of new stars, remove stars/gas from galaxies due to tides, increase the masses of galaxies through accretion of satellites, decrease the number of galaxies from mergers, and change the morphological types of galaxies. Furthermore, if there exists an intragroup or intracluster medium then gas can be removed from member galaxies through processes such as ram-pressure stripping and strangulation [38]. All of these processes are going on, but their strength and time-scales are still very much debated. We discuss each of these processes below, and why it appears that galaxy mergers are likely the dominate method by which galaxies in groups are evolving in the early universe ($z > 1.5$).

The efficiency of these various processes can be characterized by the velocity dispersion σ of an environment. Ram pressure stripping has an induced pressure force $\sim\rho\sigma^2$, where ρ is the density of the intergroup medium. As the velocity dispersion of groups are typically $\sim 250-400$ km s^{-1}, the efficiency of this process in groups is likely not great, and its influence in clusters of galaxies where both ρ and σ are both high is also not clear. Likewise high speed galaxy interactions, such as galaxy harassment [46], are unlikely to produce significant effects in groups due to the low relative velocities of member galaxies. This type of process is most efficient in rich clusters of galaxies where the velocity dispersion is high, and galaxies are rapidly interacting with cluster members [45]. Interactions between a group galaxy and the potential of its group [6] are also unlikely to be very effective given the low masses of groups.

Strangulation/starvation is the processes whereby hot gas is removed from a galaxy's halo after it enters a hot medium. This is proposed to halt the star formation in the accreted galaxy, as eventually no hot gas is left to cool and form new stars. It is however not a fast process, and has a time-scale of roughly a Gyr in clusters. It also requires a removal mechanism, which is usually an intracluster medium, that interacts and removes hot gas from orbiting galaxies. These mechanisms cannot be effective however as we see star formation occurring in groups. Unless these groups are young, the time-scale for truncation of star formation via ram-pressure and strangulation must be longer than a Hubble time. This leaves galaxy mergers and low velocity interactions, and non-gravitational processes, such as AGN feedback, as major effects that drive the evolution of group members.

3.2 Galaxy mergers

Galaxy mergers should be common in groups of galaxies. This is due to the low velocity dispersion of galaxies in groups, and the close proximity of members. Various types of nearby groups, such as the compact groups and the fossil groups, are possibly the result of the merger process. A simple way to understand this is through dynamical friction effects which have a time-scale that varies roughly as as $\tau_{\rm merge} \sim \sigma^3$. Lower velocity dispersion groups therefore have a shorter time scale for mergers than galaxies in clusters. This

is one reason why galaxy-galaxy mergers in the centers of massive clusters are rare. Simple calculations show that groups with velocity dispersions > 300 km s^{-1} will not have a significant number of mergers over a Hubble time. This is one reason why galaxy mergers, almost by definition, must occur in groups of galaxies.

Galaxy mergers and interactions are sometimes observed in nearby groups, which may be a common way to induce star formation in these systems. However, galaxy mergers in nearby groups, and in groups up to $z \sim 1$, are not expected to be common. Simulations and analytical calculations of the dynamical friction process show that galaxies in groups become more centrally concentrated by about a factor of two since $z \sim 1$ [8], but do not necessarily merge. The effect is strongest for groups with lower velocity dispersions, < 150 km s^{-1}. [8] argues that merging in groups at $z \sim 0.4$ should be low, about 2% per Gyr per group. Observations tend to agree that the merger fraction for massive galaxies is not high (but does increase) at redshifts $z \sim 0-1$ [13,42,43].

The merger rate for galaxies in groups should increase significantly at earlier times, that is at $z > 2$. The reason is simply because the universe was denser and galaxies were physically closer together, and should thus merge more often. A simple argument shows this to be the case. In a Λ-dominated universe, the mass density increases as the Hubble parameter squared, or $H^2 \sim (1+z)^3$, with a merger rate $\sim\sqrt{(}H^2) \sim (1+z)^{1.5}$. This merger rate explains why we see a mix of galaxy types in groups, such as early types and spirals with bulges. These spheroidal components were formed when systems underwent mergers early in the universe, with disk/bulge systems the spheroids who were able to re-acquire a disk via gas accretion from the intergalactic medium.

Finding mergers and calculating the merger rate at $z > 1$ has been carried out using deep Hubble Space Telescope imaging [13]. The merger fraction evolution out to $z \sim 3$ has been computed utilizing structural methods, such as the CAS system [11,15,16], and rest-frame optical observations of galaxies with NICMOS imaging of the Hubble Deep Field [22]. This imaging revealed that galaxy morphology changes gradually from normal ellipticals and spirals to peculiar galaxies at $z \sim 0$ to $z \sim 3$ [18]. In the nearby universe most of the bright $M_B < -20$ galaxies are normal Hubble types – spirals and ellipticals. However, when we view younger galaxies at higher redshifts we find that the fraction, and number densities, of peculiars rises at the expense of normal galaxies [47]. This morphology-redshift relation has been interpreted as an increase in the merger fraction with time [13].

The merger fraction varies with magnitude and stellar mass, such that the brightest and most massive galaxies have the highest merger fractions at $z \sim 2.5$. This merger fraction declines steeply with redshift approximately as a power-law, $f_m \sim (1+z)^{3-5}$ (Figure 5). The merger rate can be calculated using N-body models of the merger process to obtain the time-scale for merg-

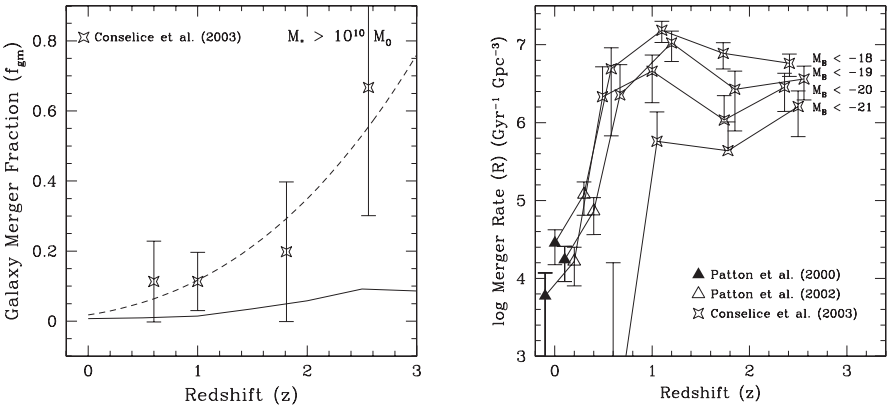

Fig. 5. *Left panel*: The galaxy merger fraction evolution for systems with $M_* > 10^{10}$ $M_\odot$ as a function of redshift [13]. *Right panel*: The galaxy merger rate in units of Gyr^{-1} and Gpc^{-3} as a function of redshift. The merger rate at $z > 1.5$ is very high for galaxies at all luminosities. The merger fraction for the most massive galaxies is also high – around 50% [19].

ers to occur as seen through the CAS system [19]. Using models with various orbital properties and viewing angles, the time-scale for identifying mergers in the CAS method is roughly 0.38±0.1 Gyr for galaxies with stellar masses $> 10^{10}$ $M_\odot$. Knowing this time-scale allows us to calculate the merger rate evolution for galaxies as a function of time and stellar mass. The result of this is shown in Figure 5.

Integrating the merger rate with time lets us determine the number of major mergers a galaxy with a given initial stellar mass has undergone since $z \sim 3$. This simple calculation, explained in detail in Conselice (2006) [19], results in $4.4^{+1.6}_{-0.9}$ major mergers since $z \sim 3$ for galaxies with initial masses $> 10^{10}$ $M_\odot$. This allows galaxies with stellar masses of $\sim 10^{10}$ $M_\odot$, which tend to be among the most massive galaxies at $z > 2$, to grow by a factor of 10-15 to contain as much stellar mass as the most massive galaxies in the local universe. Most of this merger activity occurs at $z > 1.5$, with on average no mergers occurring at $z < 1$ for the most massive systems.

What does an increase in the merger rate with redshift have to do with galaxy evolution in groups? We unfortunately do not yet know how the merger rate varies with redshift *and* environment, but through a chain of observations, we can argue that these mergers are occurring in group-like environments. The argument is simple – the mergers we see occurring at $z > 2$ are in the most massive galaxies, which previously must of been bound pairs or groups. These massive galaxies are also clearly the most clustered, as shown by [28] and [39]. The scale of this excess clustering is small – about 1 Mpc - similar to the size of a group.

4 Discussion

4.1 Environmental correlations

As we have already described in this review, there are several environmental correlations between the local density of a galaxy and that galaxy's properties. Perhaps one of the most interesting characteristics of these correlations is that there is little to no global environmental influence on the evolution of galaxies. This can be shown in a number of ways, including the fact that the star formation rate of galaxies, measured through Hα equivalent widths, correlates with the local projected surface density of galaxies. What is surprising is that this is independent of global environment, such that the correlation is nearly the same in both clusters with $500 < \sigma < 1000$ km s^{-1} and within groups with $\sigma < 500$ km s^{-1} [3].

What is the origin of local density sensitive properties of galaxies? This relates to the classic 'nature vs. nurture' debate about whether galaxy properties are imprinted early in their history, or whether they are transformed by their environment. We can argue now with some confidence that the observed correlation between galaxy properties and local density is likely a 'nature' process at low redshift, but a minor one that largely involves halting star formation in accreted spirals. Except for low mass systems [45], it is unlikely that environment induces significant morphological effects outside of mergers. At higher redshifts where most star formation and morphological evolution occurs, the eventually properties of a galaxy are sealed by its local environment.

We can argue this through observational properties of galaxies and basic theory. First, areas of higher density are predicted to form earlier than those in lower density areas, as simple density arguments and simulations show [51]. This implies that the first galaxies should form in higher density areas. This however does not necessarily imply that galaxies in high density regions should be different (other than age) from galaxies in lower density areas. Observationally, we know that the most massive galaxies at $z > 2$ tend to have peculiar morphologies, and average stellar masses of $z \sim 10^{10}$ M$_\odot$ [18,47]. Elliptical and spiral morphologies were not in place until $z \sim 1 - 1.5$, and the morphology-density relation is already in place by then [49]. The seeds of the morphology-density relation therefore must have occurred even earlier when massive galaxies are already highly clustered.

Galaxies in higher density regions in the early universe are rapidly merging with each other. The progenitors of these galaxies are not spirals, but simply post-mergers, with multiple mergers occurring in a short time interval of a few Gyr [19], providing no time for the establishment of a stable morphology. Disk galaxies are likewise able to form after the merger epoch has ended. In this sense the morphology and stellar mass of a galaxy is set by the local density in which it forms. The global density is less important for driving galaxy evolution, as merging activity is the dominant process. By

their nature, mergers are a local process driven by potentials dominated by a few massive systems, or what we call in the local universe galaxy groups.

The fact that the star forming properties of galaxies only depend upon local environment, and not global environment, is a strong indicator that whatever process is driving the decrease in star formation with local environment is not related to the total velocity dispersion (or density) of the system where a galaxy is located [35, 3], nor to the density of the intracluster or intragroup medium. The quenching of star formation in massive galaxies is however perhaps not driven entirely by environmental effects. The star formation properties of a galaxy appear to correlate with galaxy mass more strongly than with environmental density. The internal properties of galaxies, either through regulation with an active nucleus [33], or from the time-scale for the exhaustion of gas must be responsible for shutting down star formation. What is not yet clear is why massive galaxies do not reestablish a cold gas supply, nor have their hot gas cool and form stars. This is perhaps related to the galaxy downsizing whereby star formation is truncated in higher mass galaxies before lower mass systems at $z < 1$ [5].

4.2 Dwarfs and the global environment

One galaxy property that does not simply correlate with local environment is the faint end of the luminosity function, or the ratio of dwarf to giant galaxies. This correlation is such that in higher density global environments, the number of low mass galaxies per giant galaxy is much higher than in lower density environments [25]. This tells us first of all that galaxy clusters cannot form through the mergers of lower mass galaxy groups. This implies that in *global* high density environments there are processes that somehow produce low mass galaxies. There is no definitive agreement on how this occurs, with both a primordial origin suggested [52], as well as scenarios in which dwarfs are formed after clusters are in place [12,14]. For a more detailed discussion of this issue see [17].

5 Summary

Various observational techniques allow us to study the evolution of galaxies in groups, and in group-like environments up to $z \sim 6$. By studying galaxies in groups at various redshifts we can determine the modes by which most galaxies evolved. Four main features of galaxies in groups suggest how evolution has occurred in this most common environment.

I. The morphological and star forming properties of galaxies in low redshift galaxy groups reveal that multiple galaxy formation modes have occurred. This is due to the presence of star forming galaxies, such as spirals and irregulars, as well as evolved galaxies, namely ellipticals and dwarf ellipticals.

There are also several examples of galaxies evolving in nearby groups through interactions/mergers.

II. Groups, in a traditional sense of having a measured velocity dispersion and found within a small volume, can be identified out to $z \sim 1.4$. Out to these redshifts we know that the group environment is very common with as much as 50% of all galaxies located in groups.

III. Galaxies in groups out to $z \sim 0.5$ evolve in a similar manner as the field, although groups tend to have a more evolved population at all redshifts thus far probed. This implies that the galaxy formation process, or at least residual star formation, is halted more quickly in groups than in the field. This may however be an effect of groups containing more massive galaxies, which end their star formation earlier than low mass systems. What triggers the star formation in galaxies in groups is still not resolved, and the cause may not differ from what is triggering star formation in field galaxies.

IV. At higher redshifts, there is evidence for groups in the form of strong galaxy clustering, and merging, which produces larger galaxies. The universe was denser at high redshift by a factor H^2, and thus galaxies were closer together. The time-scale for these systems to merge is fairly quick, and this is likely the method whereby most early type galaxies and bulges were formed. This is also a natural method for putting the morphology-density relation into place. What remains a mystery is what causes the end to star formation in the most massive galaxies, and why no further star formation occurs.

I thank the organizers of the ESO conference on galaxy groups for their invitation to present this review, for their support, and their forbearance while it was written up. I also thank Meghan Gray for valuable comments which improved the presentation of this review, and Brian Gerke for providing Figure 2. This work was supported by a National Science Foundation Astronomy & Astrophysics Fellowship and by PPARC.

Invited review, 16 pages, to be published in ESO Conference on Nearby Galaxy Groups"

References

1. Albert, C., White, R., & Morgan, W. 1977, ApJ, 211, 309
2. Allington-Smith, J., et al. 1993, ApJ, 404, 521
3. Balogh, M., et al. 2004, MNRAS, 348, 1355
4. Butcher, H., & Oemler, A. 1984, ApJ, 285, 426
5. Bundy, K., Ellis, R., Conselice, C., et al. 2005, astro-ph/0512465
6. Byrd, G., & Valtonen, M. 1990, ApJ, 350, 89
7. Carlberg, R.G., et al. 2001, ApJ, 552, 427
8. Carlberg, R.G. 2004, in "Clusters of Galaxies: Probes of Cosmological Structure and Galaxy Evolution", p. 343.
9. Coil, A., et al. 2004, ApJ, 609, 525

10. Cohen, J., et al. 2000, ApJ, 538, 29
11. Conselice, C.J., et al. 2000, ApJ, 529, 886
12. Conselice, C.J., et al. 2001, ApJ, 559, 791
13. Conselice, C.J., et al. 2003a, AJ, 126, 1183
14. Conselice, C.J., et al. 2003b, AJ, 125, 66
15. Conselice, C.J. 2003, ApJS, 147, 1
16. Conselice, C.J., et al. 2004, ApJ, 600, 139L
17. Conselice, C.J. 2005, IAUS, 198, 277, astro-ph//0512497
18. Conselice, C.J., et al. 2005, ApJ, 628, 160
19. Conselice, C.J. 2006, ApJ, 638, 686
20. Daddi, E., et al. 2004, ApJ, 600, 127L
21. Davis, M., et al. 2003, SPIE, 4834, 161
22. Dickinson, M., et al. 2000, ApJ, 531, 624
23. Dressler, A. 1980, ApJ, 236, 351
24. Eke, V., et al. 2004, MNRAS, 348, 866
25. Ferguson, H.C., & Sandage, A. 1991, AJ, 101, 765
26. Geller, M.J., & Huchra, J.P. 1983, ApJS, 52, 61
27. Gerke, B.F., et al. 2005, ApJ, 625, 6
28. Giavalisco, M. & Dickinson, M. 2001, ApJ, 550, 177
29. Giavalisco, M., et al. 2004, ApJ, 600, 93
30. Gomez, P.L., et al. 2003, ApJ, 584, 210
31. Grebel, E.K. 1999, IAUS, 192, 17
32. Grebel, E., & Gallagher, J., 2004, ApJ, 610, 89L
33. Grogin, N. et al. 2005, ApJ, 627, 97L
34. Hernandez-Toledo, H., et al. 2005, AJ, 129, 682
35. Hogg, D., et al. 2003, ApJ, 585, 5L
36. Ilbert, O. et al. 2006, astro-ph/0602329
37. Jenkins, A., et al. 2001, MNRAS, 321, 372
38. Larson, R.B., Tinsley, B.M., & Caldwell, C.N. 1980, ApJ, 237, 692
39. Lee, K.-S., et al. 2005, ApJ, 642, 63L
40. Lewis, I., et al. 2002, MNRAS, 334, 673
41. Lilly, S., et al. 1996, ApJ, 460, 1L
42. Lin, L., et al. 2004, ApJ, 617, 9L
43. Lotz, J., et al. 2006, astro-ph/0602088
44. Marcolini, A., Brighenti, F., & D'Ercole, A. 2003, MNRAS, 345, 1329
45. Mastropietro, C. et al. 2005, MNRAS, 364, 607
46. Moore, B., Lake, G., & Katz, N. 1998, ApJ, 495, 139
47. Papovich, C., et al. 2005, ApJ, 631, 101
48. Ponman T., et al. 1995, Nature, 369, 462-64
49. Postman, M., & Geller, M. 1984, ApJ, 281, 95
50. Postman, M. et al. 2005, ApJ, 623, 721
51. Sheth, R., & Tormen, G. 1999, MNRAS, 308, 119
52. Tully, R, et al. 2002, ApJ, 569, 573
53. van den Bergh, S. 2000, "The Galaxies of the Local Group", Cambridge University Press
54. Wilman, et al. 2005, MNRAS, 358, 71
55. Zabludoff, A., & Mulchaey, J. 1998, ApJ, 496, 39
56. Zheng et al. 2006, ApJ, 640, 574

Deep Optical Imaging of ESO 383–45: A Galaxy Undergoing Ram-pressure Stripping, or a Tidal Merger Remnant?

S.N. Kemp[1], E. de la Fuente[1], A. Franco-Balderas[2] and J. Meaburn[3,4]

[1] Instituto de Astronomía y Meteorología, Universidad de Guadalajara, Avenida Vallarta 2602, Col. Arcos Vallarta, CP 44130, Guadalajara, Jalisco, México
snk@astro.iam.udg.mx, edfuente@astro.iam.udg.mx

[2] Instituto de Astronomía, Universidad Nacional Autónoma de México, Apartado Postal 70-264, 04510-México, México DF
alfredo@astroscu.unam.mx

[3] Jodrell Bank Observatory, Department of Physics and Astronomy, University of Manchester, Macclesfield, Cheshire SK11 9DL, UK
jm@ast.man.ac.uk

[4] Instituto de Astronomía, Universidad Nacional Autónoma de México, CP 22800, Ensenada, Baja California, México

Summary. We present deep Schmidt plate and CCD images of ESO 383–45, an S0 galaxy in A3565 which possesses an extended halo and system of filaments. We discuss whether these structures may be formed by gravitational interaction with other galaxies or ram-pressure stripping by the intergalactic medium.

ESO 383–45 (also known as MCG–05-32-053; [1]) is an edge-on lenticular galaxy. It lies ∼15 arcmin northeast of IC 4296, the giant elliptical galaxy in the centre of the cluster A3565, and its radial velocity of 3914 ± 19 km s^{-1} [2] indicates that it is a member of this cluster of galaxies. Using a Hubble constant of 65 km s^{-1} Mpc^{-1}, the distance to the group, and hence to the galaxy, is ∼56 Mpc. [1] examined the structure of this galaxy using data extracted from a $\sim 4.5^\circ \times 4.5^\circ$ array of aligned and digitally co-added Automatic Plate Measuring (APM) Facility scans of eight IIIaJ/GG395 United Kingdom Schmidt Telescope (UKST) plates centred on the A3565 cluster of galaxies. A high contrast image of ESO 383–45 from the co-added Schmidt data is shown in Figure 1a. The large oval-shaped halo detected has an extent of at least 45 kpc, 4 times the diameter of the disk within. This halo has trails of material emanating from it (to the S, NW, N, NNE, and NE; see Fig. 1a). Three of these trails were first noticed by [3] using scans of a smaller area of the same Schmidt plates lated used in our digital co-addition.

CCD observations of a field containing ESO 383–45 were obtained on 1993 March 1 at the 3.9m Anglo-Australian Telescope (AAT) in photometric conditions as part of the AAT Service Programme. A Tetronix CCD (1024×1022 pixels) was used as the detector at the f/3.3 prime focus. This gave a 6.7×6.7 arcmin^2 field of view with each pixel 0.39×0.39 arcsec^2. Exposures of 600s in B and V were obtained of the field containing ESO 383–45. The

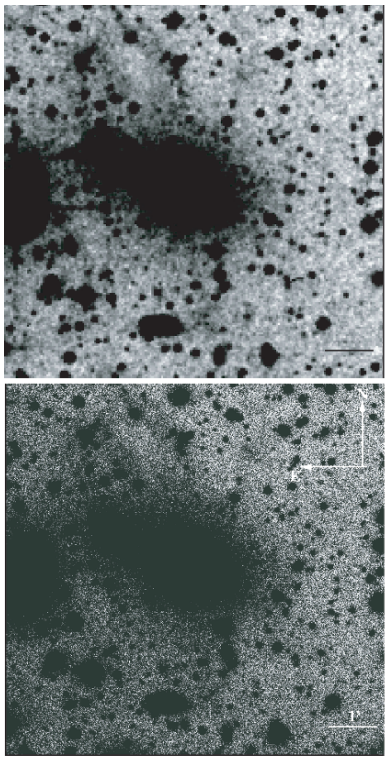

Fig. 1. (a) High-contrast B_J-band image of a field containing ESO 383–45 from the co-added array of 8 IIIaJ Schmidt plates. N is to the top and E to the left. A bar corresponding to 1 arcmin is shown at bottom right. The pixel size is 2×2 arcmin^2. The center of ESO 383–45 is at R.A. = 13 37 39.5, Decl. = –33 48 40 (J2000.0). (b) High-contrast V-band image of the CCD field. The field is 6.7×6.7 arcmin^2. The pixel size is 0.39×0.39 arcsec^2.

high contrast V band image of the CCD field containing ESO 383–45 is shown in Figure 1b. The section of the co-added Schmidt data shown in Fig. 1a corresponds to the same field. The filaments and extended halo are clearly seen, while the smaller pixel size of the CCD data helps to show that the central northern filament splits into two at about 3 arcmin north of the centre of the galaxy. The NW filament appears considerably fainter than the others. In spite of the different waveband and pixel sizes of the two images, the correlation of the fine structure of the filaments, the brighter areas within them, and the distribution of diffuse background emission are excellent. In both cases the background is brighter to the NE, E and S of the galaxy, hinting that this represents genuine IGM emission. In Figure 2 we show two representations of the summed B- and V-band images. Fig. 2a is at intermediate contrast while Fig. 2b has a logarithmic intensity scale,

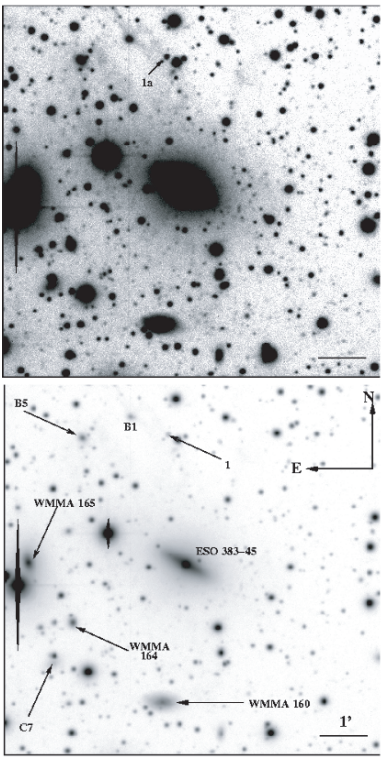

Fig. 2. (a) Sum of the B and V CCD images of ESO 383–45 displayed at intermediate contrast. The orientation and field size are the same as in Fig. 1. (b) The same image displayed with a logarithmic intensity scale. Some other galaxies in the field are labelled on the image [4]

clearly showing the inner S0 disk and bulge structures of ESO 383–45. In comparison with other disk galaxies seen in high-contrast images, e.g. [1], the relative sizes of the extended halo and inner disk structure of ESO 383–45 are remarkable.

We also carried out a digital unsharp-masking treatment (not shown), which shows well the disk-bulge structure, generated a B–V color map (not shown) which shows redder colors in the disk and bulge B–V of 1.1–1.2, with a blueward gradient into the halo, with the filaments slightly bluer still $B - V \sim 0.5$. We also generated a self-correlated image (not shown) which shows the filament structure well. These images can be found in [4] which also contains the surface brightness and color profiles.

ESO 383–45 is situated near the center of the IC 4296 group of galaxies, 15 arcmin NE of the giant E0 IC 4296. Figure 3 shows a larger area of sky in this direction, with IC 4296 at bottom right and ESO 383–45 left of and above the center of the field. We nore several more areas of diffuse emission

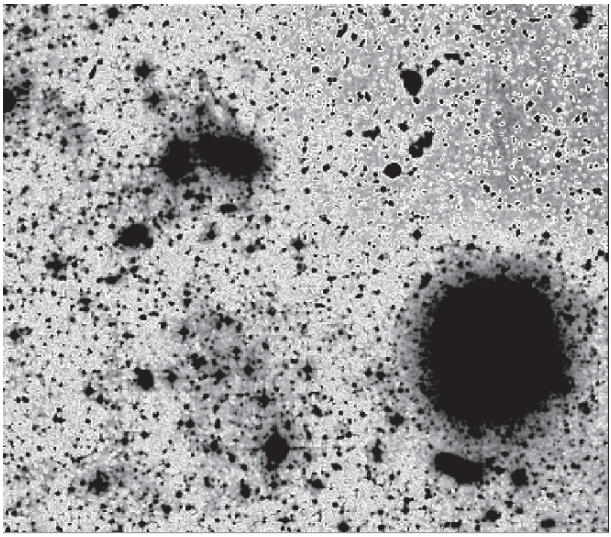

Fig. 3. Self-correlated image of a 29×25 arcmin^2 region from the B_J digitally co-added Schmidt plate data. N is to the top and E to the left. IC 4296 is the giant elliptical galaxy in the SW quadrant, ESO 383–45 is NE of the center of the field.

in this field: the fainter NW trail of ESO 383–45 continues beyond the area of the CCD field, while there are large areas of detached faint emission 9 arcmin ENE and 5 arcmin ESE of ESO 383–45, plus a larger area 10 arcmin S of ESO 383–45 and 11 arcmin E of IC 4296. These areas of diffuuse emission, together with the known pair of radio jets and lobes of IC 4296 and X-ray emission associated with the group [5], [6], indicate the presence of an extensive IGM near thhe center of the A3565 cluster. The curvature of the filaments of ESO 383–45 may indicate a direction of motion of this galaxy to the SW in the plane of the sky (if the filaments are made of ionised gas and are curved by interaction with a dense IGM), while the opposite sense of curvature of the radio jets of IC 4296 may indicate a movement of IC 4296 to the NE [5].

The colors of the filaments are consistent with them being formed of stars, and stars may be moved outside galaxies by tidal interactions between galaxies, or formed as a result of compression of gas clouds during tidal interactions. However there is no obvious candidate galaxy that may be participating in a tidal interaction with ESO 383–45. Many nearby objects (e.g. WMMA 160 and 165, see Fig. 2b) have much higher redshifts, ESO 383–49 (small E 6 arcmin to SE) appears undisturbed, while IC 4296 is 15 arcmin away and may be approaching ESO 383–45. However ESO 383–45 may be a merger product, the filaments contain 'knots' (e.g. 1 and 1a in Fig. 2) which may be tidal dwarf galaxies in formation. The simulations of the mergers of two disk galaxies by [7] produce S0 galaxies with thick disks which look similar to the disk and extended halo of ESO 383–45 (though without the filaments).

However, given the dense cluster environment and the likely direction of motion of ESO 383–45 through it, it is possible that ESO 383–45 is losing gas by ram-pressure stripping, leaving behind the filaments, in which either enhanced star formation has somehow taken place, or the filaments are composed of ionized gas (making the knots in them giant HII regions). The S0 morphology of ESO 383–45 suggests that it is near the end of thiis process of conversion from spiral to lenticular.

Further observations in HI 21cm, optical narrow-band imaging, and spectroscopy will locate the neutral and ionized gas and their kinematics, and discover the nature of the knots. Simulations will show whether a tidal interaction or ram-pressure stripping can explain the form of the galaxy, or whether both processes are needed.

SNK acknowledges receipt of a grant from the organisers of the conference to cover the registration fee.

References

1. Kemp, S.N., & Meaburn, J., 1993, A&A, 274, 19
2. Willmer, C.N.A., Maia, M.A.G., Mendes, S.O., Alonso, M.V., Rios, L.A., Chaves, O.L., & de Mello, D.F., 1999, AJ, 118, 1131
3. Marston, A.P., 1988, MNRAS, 230, 97
4. Kemp, S.N., de la Fuente, Eduardo, Franco-Balderas, A., & Meaburn, J., 2005, ApJ, 624, 680
5. Killeen, N.E.B., & Bicknell, G.V., 1988, ApJ, 324, 198
6. Kemp, S.N., 1994, A&A, 282, 425
7. Naab, T., & Burkert, A., 2003, ApJ, 597, 893

Morphologies and Star Formation in $z \sim 0.5$ Group Galaxies

D.J. Wilman[1], M.L. Balogh[2], R.G. Bower[3], J.S. Mulchaey[4], A. Oemler Jnr[4] and R.G. Carlberg[5]

[1] Max-Planck-Institut für extraterrestrische Physik, Giessenbachstraße, D-85748 Garching, Germany
dwilman@mpe.mpg.de
[2] Department of Physics, University of Waterloo, Waterloo, Ontario, Canada.
[3] Physics Department, University of Durham, South Road, Durham, U.K.
[4] Observatories of the Carnegie Institution, 813 Santa Barbara Street, Pasadena, California, U.S.A.
[5] Department of Astronomy, University of Toronto, Toronto, ON, Canada.

Summary. As groups today contain ∼60% of the galaxy population [1], and are the first step in the hierarchical growth tree which dominates structure formation, these environments must have a critical influence on the evolution of star formation in the Universe as a whole. Indeed their dynamics make them the ideal environments to foster galaxy–galaxy interactions and mergers, leading to a dramatic transformation of galaxy properties. To study the evolution of galaxies in groups requires highly complete, targetted, deep spectroscopic surveys. At intermediate redshift, the only such is our sample of 26 groups at $0.3 < z < 0.55$, selected from the CNOC2 redshift survey [2], with additional targetted spectroscopy using the Magellan 6.5m and VLT telescopes providing a complete kinematic description to a depth of $\sim M_* + 3$ at $z = 0.4$. [3]. Our full multiwavelength dataset will include HST-ACS, GALEX UV, Chandra, XMM and Spitzer imaging, with the power to ultimately reveal the importance of the group environment in controlling the evolutionary fate of a galaxy. In this contribution, we present some of the more recent and illuminating analysis, revealing evolution in the group environment and the dependence of star–formation and galaxy morphologies upon environment and stellar mass. Finally we discuss the important role Spitzer will play in revealing the processes actively transforming galaxies in the group environment.

1 Results and analysis

Colours and Star Formation: The bimodality of the galaxy colour distribution is a powerful statistical tool which can be used to statistically separate blue galaxies with ongoing or recent star–formation from red, passive galaxies (the red sequence). Locally the distribution can be accurately parameterized using a double–gaussian fit [4]. We establish independently volume-limited bins of luminosity in the CNOC2 spectroscopic survey, and apply a double–gaussian fitting procedure to each bin:[6] the double–gaussian fit works remarkably well, resulting in 5 basic parameters: the mean colour and standard

[6] Galaxy luminosities and colours are computed using a SED fitting technique.

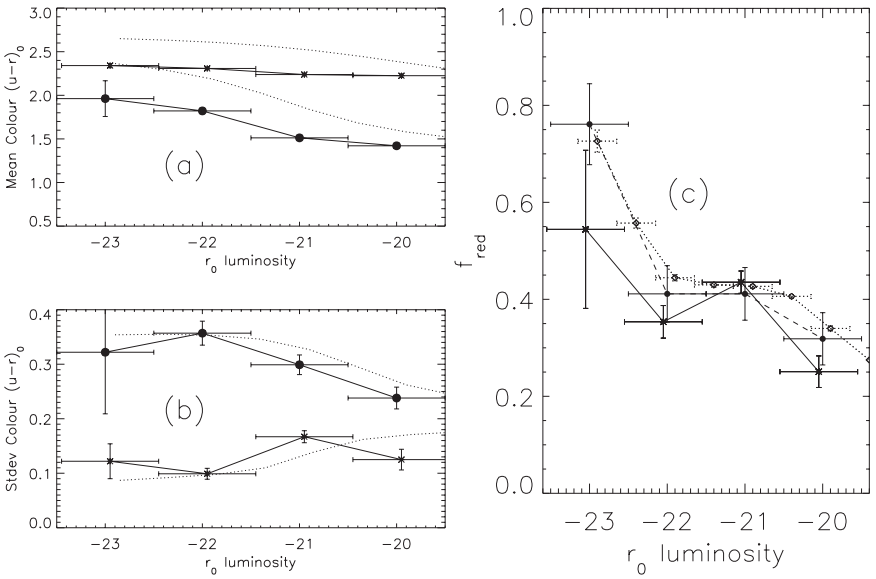

Fig. 1. A double gaussian fitting technique [4] is applied to the distribution of CNOC2 galaxy colours in bins of luminosity. **(a)** The Mean Colour of each peak (red and blue), **(b)** Standard deviation (width), and **(c)** The fraction of galaxies in the red peak f_{red}. each as a function of r-band luminosity (**solid** line) and contrasted with the local SDSS sample (*dotted* line, identical sample selection and fitting method). The **dashed** line in **(c)** represents the fit for CNOC2 group galaxies only. See the main text for discussion.

deviation for each of the blue and red peaks, and the fraction of galaxies in each peak. In Figure 1, we show how each parameter depends upon galaxy luminosity in CNOC2 (solid line), and locally in the SDSS DR3 (dotted line, following an identical procedure). The mean and width of the colour distributions suggest that both blue and red galaxies were bluer at $z \sim 0.4$ than they are today, but with similar scatter. However, this is sensitive to the details of the k–correction (mean and width) and magnitude errors (width). More robustly we show that the fraction of galaxies in the red peak (f_{red}) is lower at $z \sim 0.4$ than at $z \sim 0$, indicating that more galaxies have found their way onto the red sequence (truncated star–formation) in the intervening time ($\sim$4 Gyrs). The influence of the group environment is shown by restricting the CNOC2 analysis to group members only (dashed line), in which the fraction of red galaxies is significantly higher than the global population.

These results are consistent with the strong evolution we have previously seen in f_p, the fraction of galaxies with little or no current star formation, as inferred using the [OII]λ3727 emission line (selected to have EW[OII] $< 5\mathring{A}$). This evolution is strong both in group and field environments [5] but is low

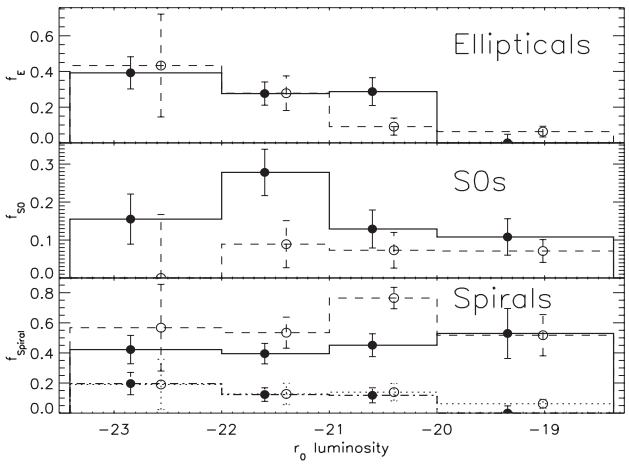

Fig. 2. Morphological fractions for group (solid lines/points) and field (*dashed* lines, open points) galaxies, divided into 3 bins of luminosity and with Jackknife errors. For spirals we also show the contribution with EW[OII]$< 5\AA$ (group and field: dot-dashed and dotted lines respectively). Note an overall deficit of [OII]-strong spirals in groups which instead host an excess of bright S0s and faint ellipticals.

in cluster cores, where the passive galaxy population was probably already established prior to $z \sim 1$ [6].

Morphological Composition: With deep HST ACS (Hubble Space Telescope – Advanced Camera for Surveys) F775W filter observations of our CNOC2 groups, Augustus Oemler Jnr has visually classified galaxies with $0.3 < z_{spec} < 0.55$ in 16 of 20 ACS fields to date, including 21 of 26 groups and a total sample of 158 group and 124 field galaxies. Figure 2 shows the fraction of ellipticals, S0s and spiral galaxies in groups (**solid** lines/points) and in the lower density field (*dashed* lines, open points), divided into 3 bins of luminosity and with Jackknife errors. For all luminosities, we use a bootstrapping method to determine there is a 3-σ deficit of spirals and a 2.7-σ excess of ellipticals in groups relative to the field. Interestingly, we note that the excess elliptical fraction is confined to fainter luminosities (whilst significantly more bright galaxies in the group sample means that most massive ellipticals are in groups – see [3] for details of group and field luminosity functions). In contrast, the brightest 16 S0s in our sample are all in groups, which corresponds to a 3.5-σ significant excess of bright S0s in groups. At $f_{S0} \sim 20\%$, the S0 population matches that in the $z \sim 0.5$ MORPHS clusters [7], suggesting that transformations of spiral galaxies into S0s probably favour the group environment. Accordingly, the increase to $f_{S0} \sim 40\%$ in local clusters would be directly related to processes active in infalling groups.

Figure 2 also shows the contribution of [OII]-weak (EW[OII]$< 5\AA$) spirals to the overall spiral fraction (group and field: dot-dashed and dotted lines

respectively). The fraction of spirals which are [OII]-weak increases with luminosity and correlates strongly with group–centric radius, increasing to ∼80% in the inner ∼100 kpc. However, this statistic must also be intricately bound–up with both the overabundance of more luminous galaxies in groups, and the deficit of [OII]-strong spirals in groups. Indeed, the **overall fraction** (as seen in Figure 2) of [OII]-weak spirals in group and the field is almost identical in each luminosity bin. In addition, preliminary Spitzer analysis indicates that there is significant dust–obscured star formation ongoing in *some* (but not all) of these objects. Therefore it will be essential to disentangle the roles of the mass function and dusty star–formation from group–related processes which *directly* influence the star-formation of spiral galaxies, and with associated morphological transformations which are likely to result in early-type galaxies, probably S0s. This we will do using Spitzer data.

Clues in the Infrared: We have matched our catalogue to archival Spitzer-IRAC coverage of part of the CNOC2 survey. Figure 3 shows the distribution

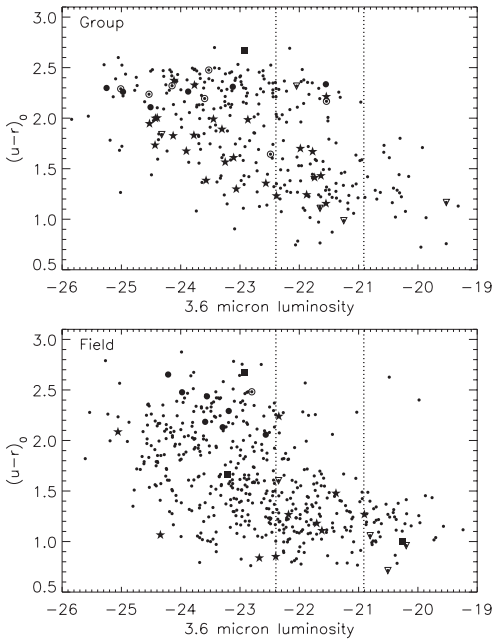

Fig. 3. Colour–(3.6μ luminosity) plots for all $0.3 < z < 0.55$ CNOC2 group and field galaxies with existing IRAC coverage. 3.6μ luminosity is a close tracer of stellar mass and is computed assuming a k–correction for a typical passive galaxy. The 2 vertical dotted lines represent the luminosity corresponding to a stellar mass of $3{\times}10^{10} M_{\odot}$ (the local *transition mass*) with the minimum (starburst) and maximum (passive) possible values of $M/L_{3.6\mu}$. We highlight the location of morphologically classified ellipticals (filled circles), S0s (bullseyes), spirals (stars), irregulars (triangles) and mergers (squares) in this parameter space.

of the resulting group and field galaxy sample in optical colour – k-corrected 3.6μ luminosity parameter space. In the local Universe, the galaxy population makes a fairly sharp transition from mostly star forming below a stellar mass of $3 \times 10^{10} M_{\odot}$ to mostly passive above this mass [8]. The 2 vertical lines in Figure 3 represent the equivalent luminosity for minimum (starburst) and maximum (passive) possible values of $M/L_{3.6\mu}$. The relatively small uncertainty converting $L_{3.6\mu}$ to stellar mass allows us to confirm that there are many more massive star–forming (blue) galaxies in both groups and field environments, still common at $z \sim 0.4$. This is a representation of the well-known *downsizing* effect of star-forming activity. Where this sample overlaps our ACS sample, we indicate morphologies in Figure 3. Most interesting to note is that spiral galaxies occupy a wide distribution of optical colour, roughly equivalent to the blue gaussian peak. [OII]-weak spirals are found predominately at the intermediate–red end of this colour distribution, but in many cases with a strong IRAC band 4 flux which is likely to pick up the 6.2μ (rest-frame) PAH feature suggesting some level of obscured star–formation. In some of these galaxies we even detect 24μ warm dust emission in shallow MIPS coverage, suggesting that this obscured star formation can be quite strong.

To conclude, multiwavelength analysis of our unique sample of targetted, kinematically selected groups at $0.3 < z < 0.55$ is revealing the important role that galaxy groups must play in galaxy evolution and will allow us to distinguish which processes are active in groups.

DJW would like to thank the LOC for organising a stimulating conference, and for financial support.

References

1. Eke, Baugh, Cole, Frenk, Norberg, Peacock et al: MNRAS, **348**, 866 (2004)
2. Carlberg, Yee, Morris, Lin, Hall, Patton et al: ApJ, **552**, 427 (2001)
3. Wilman, Balogh, Bower, Mulchaey, Oemler, et al: MNRAS, **358**, 71 (2005)
4. Baldry, Glazebrook, Brinkmann, Ivezić, Lupton, Nichol, & Szalay: ApJ, **600**, 681 (2004)
5. Wilman, Balogh, Bower, Mulchaey, Oemler, et al: MNRAS, **358**, 88 (2005)
6. Nakata, Bower, Balogh, & Wilman, MNRAS, **357**, 679 (2005)
7. Dressler, Oemler, Couch, Smail, Ellis, Barger et al: ApJ, **490**, 577 (1997)
8. Kauffmann, Heckman, White, Charlot, et al: MNRAS, **341**, 54 (2003)

Formation and Evolution of Early-type Galaxies

C. Chiosi and E. Merlin

Department of Astronomy, University of Padova, Vicolo dell'Osservatorio 2, 35122 Padova, Italy
chiosi@pd.astro.it; merlin@pd.astro.it

1 Introduction

One of the major challenges of modern astrophysics is to understand the origin and evolution of galaxies, the bright elliptical ones (EGs) in particular. In a Universe dominated by Cold Dark Matter (CDM) and, as recent observations seem to suggest, by some kind of Dark Energy in the form of a non-zero Cosmological Constant Λ, and containing a suitable mix of baryons and photons, cosmic structures are formed by the gravitational collapse of Dark Matter (DM) and are organized in a hierarchy of complexes (halos) inside which Baryonic Matter (BM) dissipates its energy and collapses to form luminous systems. In this context, modelling the formation of EGs with simulations taking into account the dynamics of DM halos and BM (gas), radiative cooling of baryons, star formation (SF), and gas loss by galactic winds can be reduced to following schemes:

(1) The *monolithic* scenario of galaxy formation supposes and predicts that all EGs form at high redshift by rapid collapse and undergo a single prominent star formation episode [13, 22, 1, 7] ever since followed by quiescence. In favour of this view are observational data of different kind that convincingly hint for old and homogeneous stellar populations, see [28], [10], and [27] for recent reviews of the subject.

(2) The *hierarchical* scenario suggests instead that massive EGs are the end product of several mergers of smaller subunits, over time scales almost equal to the Hubble time in the particular cosmological model used; as the *look back time* increases, the density in comoving space of bright (massive) EGs should decrease by a factor 2 to 3 [36, 15]. In favour of this scenario are some observational evidences that the merger rate likely increases with $\sim(1+z)^3$ [26] together with some hint for a colour-structure relationship for E & S0 galaxies: the colour becomes bluer at increasing complexity of a galaxy structure. This could indicate some SF associated to the merger event. In addition, there are the many successful numerical simulations of galaxy encounters, mergers and interactions [2]. Nevertheless, contrary to the expectation from this model, the number density of EGs does not seem to decrease with the redshift, at least up to $z \simeq 1$ [14].

(3) There is a third scheme named *dry merger view*, in which bright EGs form by encounters of quiescent, no star forming galaxies. This view

is advocated by [3] who finds that the B-band luminosity density of the red peak in the colour distribution of galaxies shows mild evolution starting from $z \simeq 1$. As old stellar populations would fade by a factor 2 or 3 in this time interval, and the red colour of the peak tells us that new stars are not being formed in old galaxies, he argues that this mild evolution hints for a growth in the stellar mass of the red sequence coming from the blue-peak galaxies, and claims the necessity of "dry mergers".

(4) Finally, a fourth hybrid scenario named *revised monolithic* has been proposed by [28], who suggests that a great deal of the stars in EGs are formed very early-on at high z and the remaining few ones at lower z. The revised monolithic ought to be preferred to the classical one, as some evidences of star formation at $0.2 \leq z \leq 2$ can be inferred from the presence of the emission line of [OII], and also as the number frequency of EGs up to $z \simeq 1$ seems to be nearly constant.

However, a sharp distinction among the various scenarios could not exist in reality. As pointed out by [23] early-type galaxies in isolation and in interaction (such as pair and shell galaxies) share the same distribution in diagnostic planes such as $H\beta$ vs [MgFe]. This means that secondary episodes of star formation may not only occur in merging (dynamically interacting) galaxies, but also in the isolated ones because of internal processes, thus supporting the revised monolithic scheme. Captures (mergers) of small satellites by a galaxy born in isolation according to the monolithic scheme are reasonably possible (e.g. the Milky Way which is currently capturing the Sagittarius dwarf galaxy). In any case, as thoroughly discussed by [10], [12], [31] and [32], the age and intensity of the last episode of SF, as measured by the fractionary mass engaged in newly formed stars, cannot exceed some stringent limits, a few per cent and before about one third of the Hubble time even in a massive elliptical, otherwise the typical broad band colours cannot be matched; they would be too blue compared to observations.

In addition to all this, EGs are known to obey to a colour-magnitude relation (CMR): the colours become redder at increasing luminosity (and hence mass) of galaxies [6]. According to [6] there was an early and short star forming period during which the vast majority of stars were formed at $z > 2$. Subsequent activity, if any, should have occurred at $z \geq 0.5$. It can be shown that the CMR stems from a mass-metallicity sequence and not an age sequence, e.g. [21], [12], and references therein.

Long ago, [22] advocated the supernova driven galactic wind model to explain the CMR. He argued that massive galaxies retain gas and form stars for longer periods of time, and become richer in metals than the low-mass ones. In any case the star forming period even in the most massive galaxies seemed to be confined at very early epochs (say within the first Gyr to be generous). This kind of model has been extensively used to describe and predict the chemo-spectro-photometric properties of EGs [7, 8, 33, 34, 11].

Over the years, the situations became more intrigued because (i) the [22] model got in contrast with the observational constraint that massive elliptical have on the average [α/Fe] ratios higher (super-solar) than the low mass ones (solar or below solar), thus implying the opposite trend for the duration of the star forming period as amply discussed by [11], [10], and [12]; (ii) the results from absorption line indices, which seem to indicate that large age difference could exist [8, 34, 30, 31, 32]. The point of inconsistency of the [22] model has been cured by the numerical simulations of galaxies by [12] thanks to the dependence of the SF history on the galaxy mass (see below) and the refinement of the galactic wind description.

Out of those studies the following picture emerges: all elliptical galaxies have been formed far back in the past, but have undergone different histories of SF. Massive ellipticals had a single burst-like episode of stellar activity ever since followed by passive evolution. In contrast, the low mass galaxies stretched their SF history over long periods of time in a series of bursts. This view has been supported by the N-Body TSPH simulations of [12] who find that the duration and mode of SF is driven by the total mass (DM plus BM) and/or the initial density of the galaxy. It is also supported by the most recent Spitzer-data (and SIRTF) in the far infrared, which have revealed the existence of very massive galaxies already in place at redshift $z \sim 6$; in addition to data HST observations have also brought into evidence galaxies in place at $z \sim 7 - 8$ [5]. All this can be understood within a model ruled by *violent relaxation* taking place in the remote past thanks to which aggregates of just born stars can merge together into even denser agggregates (e.g. [24]).

In this context it is also worth mentioning that according to [9] (i) the mass of star forming galaxies decreases with redshift (*"downsizing"*) thus strongly weakening the hierarchical scenario as the main mechanism for forming giant ellipticals; and (ii) even if "dry mergers" clearly occur [35], they cannot play an important role in the assembling history of massive quiescent galaxies as the expected number density of massive galaxies at low redshift does not agree with observational data. Furthermore the mass-downsizing of star forming galaxies seems to be almost independent of the environmental density, whereas one would expect a strong density dependence in the dry merger rate. Therefore, either classical or revised monolithic scenarios seem to be the right frame for the galaxy formation mechanism [27, 28].

2 What drives star formation? The gravitational pot

The study of [12] has clarified the tight correlation between the kind of SF (whether a single prominent initial burst or a series of episodes continuing for long periods of time) and the total initial mass and initial density of a galaxy. More precisely, massive elliptical galaxies, independently of their initial density, show a single burst of SF, whereas the low mass ones have a varied SF history. It is early and monolithic in the high initial density systems, and

irregular and intermittent in the low density ones. *Why such different SF histories?* This is the end product of a complex interplay among SF, gas heating and cooling, and the gravitational potential of the system. In a galaxy with a deep gravitational potential well (such as in the case of high density and/or high total mass), despite the energy injection by supernova explosions and stellar winds, gas tends to remain inside the regions of deepest gravitational potential. A sort of equilibrium between heating and cooling is established forcing SF to completion in a single dominant episode till the heated up gas, whose gravitational binding energy gets smaller and smaller, becomes so hot that it can escape from the galaxy, thus terminating further stellar activity. In contrast, in a system with a shallow gravitational potential well (the case of low density, low mass systems), the same processes heat up the gas pushing it toward the galaxy outskirts of low mass density (from where, once cooling has taken place, it may fall back toward the centre), or even outside the potential well. Due to the temporary decrease in gas density in the regions of the highest SF activity, this latter cannot be sustained at the same efficiency, so that it becomes intermittent. As a consequence of it, SF can occur for much longer periods of time although at low efficiency till once again gas is definitely lost in galactic winds. In this scheme, the gravitational potential well of BM+DM drives the whole process and dictates the efficiency and duration of the SF process. *The galaxy, thanks to its gravitational potential well, knows in advance the kind of stellar populations (very old or spanning a large age range) it is going to build up.*

3 Early assembling of galaxies

One the weak aspects of the [12] was the kind of initial conditions they assumed, i.e. virilized halos of DM in which BM is let collapse. This has been cured by [25] who, following previous studies (e.g. [16, 18, 17, 19] and [20]), derived the initial conditions from large spatial grids simulating the Universe using the public software GRAFIC2 by [4]. The cosmological background is the Standard Cold DM (CDM) Universe with $\Omega(z) = \Omega_0$, the matter density at the present time. Therefore, the basic parameters of the model are H_0, Ω_0, and σ_8 (the rms mass fluctuations of the present-day Universe that normalizes the density fluctuations and fix the initial redshift of the simulations via the amplitude of the density fluctuations). These models do not consider the Cosmological Constant Λ perhaps indicated by the W-MAP data [29]. This is less of a problem here, because at the redshifts we are interested in the effect of Λ of the dynamical evolution of galaxies is likely to be small.

In these grids, at a certain (high) redshift a massive perturbation made of DM and BM is detached from the Hubble flow and let collapse on its own toward a virialized structure. It becomes a proto-galaxy, rich of substructures which moving inside the common gravitational potential well merge, form stars and eventually give rise to a single entity (the galaxy). The process

turns out to complete at high redshift and from now on the galaxy evolves in "isolation"; subsequent captures of small satellites are possible without significantly altering the overall structure and evolution. In the case of a low-mass perturbation the stellar activity is prolonged over longer time scales. The numerical simulations show that the SF is completed within the first 3-4 Gyr or for an Hubble constant H = 50 km/s/Mpc at redshift greater than about 2. The models conform to the revised monolithic scheme, because mergers of substructures have occurred very early in the galaxy life. The present-day mass density gradients, mean metallicity and metallicity gradients fairly agree with current observational data. Finally, conspicuous galactic winds are found to occur.

4 Conclusions

Putting together the results of all the studies we have been referring to the following picture emerges:

(i) Simulations of galaxies originating from realistic initial conditions in a CDM universe show that high density perturbations may end up as galaxies whose formation and stellar activity is completed early on. In perturbations of low initial density the galaxy assembling and the star formation history most likely last longer, the latter in a series of bursts. The gravitational pot is the basic engine driving the efficiency and mode of SF.

(ii) Galaxies generated by perturbations of high initial density are expected to contain a dominant population of α-enhanced stars. The situation is more varied in galaxies generated by perturbations of low initial density. They are definitely less enhanced than those of high initial density. However the high mass galaxies are more enhanced than those of low mass see [30] for more details.

(iii) Galactic winds do actually occur but differently from what envisaged by [22] thus removing the inconsistency between the Larson picture and the chemical properties. In brief there no precise age at which the galactic wind has to occur and the degree of enhancement reached by a galaxy is simply related to the duration of the SF activity.

(iv) Galaxy models according to the monolithic scheme successfully reproduce the Fundamental Plane, the CMR, the $(M/L_B)_\odot$ vs σ_{0B} relation, the small scatter in the observational colours (e.g. B–V) of bright EGs, and the mass-metallicity relationship, see [12] for a thorough discussion of the various topics. All these well-behaved observational trends require a sort of general rule which galaxies seem to obey. The rule is ascribed to SF and its dependence on the initial density and total mass of the galaxy. Only in low-mass, low-density systems recent SF can take place, whereas in high mass EGs the initial period of intense activity is followed by quiescence during most of the Hubble time. This is indeed the opposite of what expected to be observed in high mass systems if they are the result of subsequent mergers with likely

companion SF randomly occurring all over the Hubble time. It goes without saying that mergers or captures of smaller galaxies can occasionally occur.

To conclude, even if mergers between two galaxies may occur giving rise to spectacular events, they are not the basic mechanism for assembling massive EGs.

References

1. N. Arimoto, Y. Yoshii: A&A **173**, 23, (1987)
2. J.E. Barnes, L. Hernquist: ApJ, **471**, 115 (1996)
3. E.F. Bell, C. Wolf, K. Meisenheimer et al.: ApJ, **608**, 752 (2004)
4. E. Bertschinger: ApJS, **137**, 1 (2001)
5. R. J. Bouwens, R. I. Thompson, G.D. Illingworth et al.: ApJL, **616**, L79 (2004)
6. R.G. Bower, J.R. Lucey, R. S. Ellis: MNRAS, **254**, 601 (1992)
7. A. Bressan, C. Chiosi, F. Fagotto: ApJS, **94**, 63 (1994)
8. A. Bressan, C. Chiosi, R. Tantalo: A&A, **311**, 425 (1996)
9. K. Bundy, R.S. Ellis, C. J. Conselice et al.: AASA, **207** (2005)
10. C. Chiosi: ASP Conf. Ser. **192**, 251 (2000)
11. C. Chiosi, A. Bressan, L. Portinari et al.: A&A, **339**, 355 (1998)
12. C. Chiosi, G. Carraro: MNRAS, **335**, 335 (2002)
13. O. J. Eggen, D. Lynden-Bell, A. R. Sandage: ApJ, **136**, 748 (1962)
14. M. Im, R.E. Griffiths, K.U. Ratnatunga et al.: ApJL, **461**, L79 (1996)
15. G. Kauffmann, S.D.M. White, B. Guiderdoni: MNRAS, **264**, 201 (1993)
16. D. Kawata: PASJ, **51**, 931 (1999)
17. D. Kawata: ApJ **548**, 703 (2001a)
18. D. Kawata: ApJ **558**, 598 (2001b)
19. D. Kawata, B. K. Gibson: MNRAS, **340**, 908 (2003)
20. C. Kobayashi: MNARS, **361**, 1216 (2005)
21. T. Kodama, N. Arimoto: A&A, **320**, 41 (1997)
22. R.B. Larson: MNRAS, **173**, 671 (1975)
23. M. Longhetti, A. Bressan, C. Chiosi et al.: A&A, **353**, 917 (2000)
24. F. Macchetto, M. Pastoriza, N. Caon et al.: A&AS, **120**, 463 (1996)
25. E. Merlin, C. Chiosi: A&A, submitted (2006)
26. D. R. Patton, C. J. Pritchet, H.K.C. Yee et al.: ApJ, **475**, 29 (1997)
27. P. J. E. Peebles: PASP Conf. Ser. **283**, 351, (2002)
28. D. Schade, S. J. Lilly, D. Crampton et al.: ApJ, **525**, 31
29. D. M. Spergel, L. Verde, H.V. Peiris et al.: ApJS, **148**, 175 (2003)
30. R. Tantalo, C. Chiosi: A&A, **338**, 396 (2002)
31. R. Tantalo, C. Chiosi: MNRAS, **353**, 917 (2004a)
32. R. Tantalo, C. Chiosi: MNRAS, **353**, 405 (2004b)
33. R. Tantalo, C. Chiosi, A. Bressan et al.: A&A, **311**, 361 (1996)
34. R. Tantalo, C. Chiosi, A. Bressan et al.: A&A, **335**, 823 (1998)
35. P. G. van Dokkum: AJ, **130**, 2647 (2005)
36. S. D. M. White, M. J. Rees: MNRAS, **183**, 341 (1978)

Dwarf Galaxies in Hickson Compact Groups

D.J. Bomans[1], E. Krusch[1], R.-J. Dettmar[1], V. Müller[2] and C. Taylor[3]

[1] Astronomical Institute of the Ruhr-University Bochum, Universitätstr. 150, 44780 Bochum, Germany
bomans@astro.rub.de, dettmar@astro.rub.de
[2] Astrophysikalisches Institut Potsdam, An der Sternwarte 16, 14482 Potsdam, Germany
vmueller@aip.de
[3] California State University, Sacramento, 6000 "J" Street Sacramento, CA 95819-6041, USA
ctaylor@csus.edu

Summary. We observed 5 Hickson Compact Groups with the ESO/MPI 2.2m telescope and WFI to investigate the dwarf galaxy content and distribution in these galaxy groups. Our deep imaging and careful selection of the candidate galaxies revealed a rich population of mainly passively evolving dwarf galaxies, which is spatially much more extended than the originally defined Hickson Compact groups. The composite luminosity function of the 5 groups shows a bimodal structure with a very steep rise in the low luminosity regime. The faint end slope is close to the predictions of CDM theory for the slope of the Dark Matter halo mass function.

1 Dwarf galaxies in compact groups

Hickson Compact Groups (HGCs) are tight groups of galaxies selected by Hickson on POSS-I plates based galaxy density and isolation criteria as described e.g. in [2]. Analysing the environments of HGCs it soon becomes clear, that the cores Hickson classified are often not isolated, but embedded into larger structures. As an example we found in HGC 16 an spiral galaxy with the same redshift, which is located just outside the radius defined in Hickson's isolation criterium.

Searches for dwarf galaxies in HGCs which were conducted up to now were either deep, but limited to the area of the compact group itself (e.g. [3]) or wide field, but rather shallow (e.g. [9, 13]. We used this as a starting point to investigate the dwarf galaxy content of HGCs and to map out the structure of HGCs and their envelopes.

2 Observations and sample selection

We observed nearby HGCs (distance < 50 Mpc) using the ESO/MPI 2.2m telescope at La Silla with its wide field of view (0.57 by 0.54 deg), high

sensitivity, good spatial sampling (0.24 arcsec per pixel), and generally good seeing conditions. Especially important is the good sampling and resolution, which allows us to select dwarf galaxy candidates belonging to the HGCs against the background of more distant large galaxies. We observed HGC 16, 19, 30, 31, and 42 in B and R band, under seeing conditions between 0.8 and 1 arcsec.

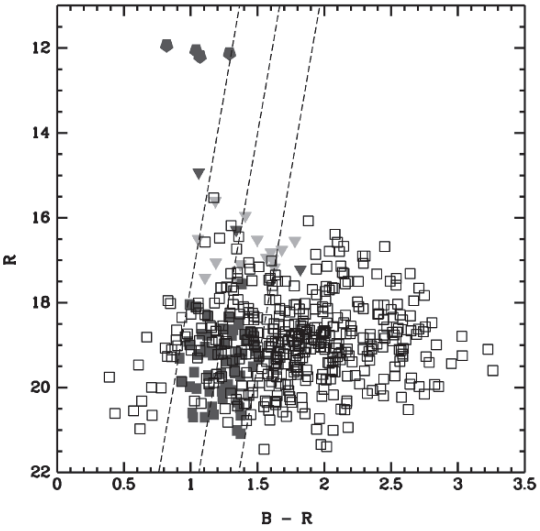

Fig. 1. Color-magnitude diagram of HGC 16 derived from our photometry. Hexagons denote the original HGC 16 members, dark and light triangles denote spectroscopic members and non-members from the literature, filled and open squares denote members and not-members based on our selection criteria.

The data were reduced using IRAF/mscred and some routines developed at Bochum. The final images allowed us to search for galaxies as faint as $M_B = -11$ in all observed compact groups. Object detection was done using SExtractor, and we set a lower size limit consistent with the size of the smalles Local Group dwarf galaxy shifted to the distances of the observed HGCs. This first selection gave 200–500 dwarf galaxy candidates per field. We constructed color-magnitude diagrams (CMDs) for our fields and used all available sources for spectroscopic redshifts. An example of the resulting CMDs is given in Fig. 1. We find very few blue dwarf galaxy candidates, while the region of the red sequence [11] is very well populated. These galaxies are therefore candidate dE/dSph galaxies belonging to the HGCs. With the good seeing and well sampled images, we can further test this assumption similar to [1] by classifying all galaxy by eye (select for low surface brightness, irregular shape, no spiral arms, and no bulge/disk structure). We also analysed the light

profiles with surface photometry package in IRAF/STSDAS for exponential profiles.

3 Dwarf galaxies in compact groups

The galaxies which passed the selection process described above showed a clear concentration towards the HGCs centers, which reassured, that we generated samples of high probability dwarf galaxy members of the HGCs. The spatial extend of these dwarf galaxy population varied from group to group, but did not reach the typical background level at a radius of 200 kpc (limited by the size of our WFI fields) for at least HGC 16, 30, and 42.

With the assumption of membership for all our final selection dwarf galaxy candidates, we generate a composite luminosity function (LF) by converting all measurements to a common distance. Given the relatively small differences in the distance of our target groups this will not induce a large spread in observed properties. The resulting LF is plotted in Fig. 2.

The small number statistics at the bright end precludes an analysis of this part and also a formal fit to the whole LF. What is still obvious from the diagram is the steep rise in the dwarf galaxy regime ($M_B < -16$ mag) and that the whole LF is not consistent with a single Schechter function [10], but implies a bimodal LF. The observed decline at luminosities fainter than $M_B = -12$ mag is most probably due to the completeness limit of our data.

Similar bimodal LFs were recently presented by [6] for X-ray dim groups and are present in the LF of passively evolving field galaxies from the 2dFRS

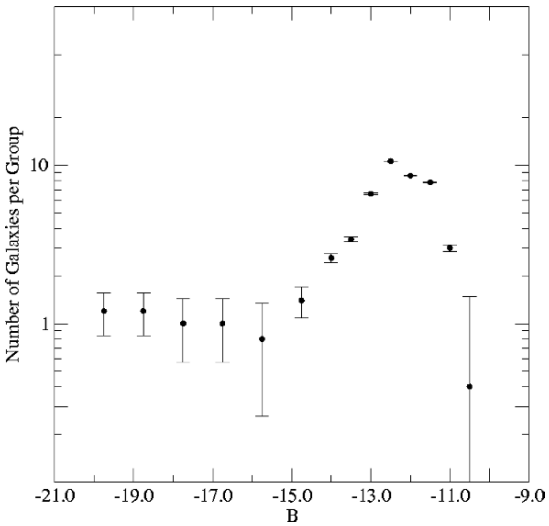

Fig. 2. Composite luminosity function of all 5 observed HGCs (HGC 16, 19, 30, 31, and 42).

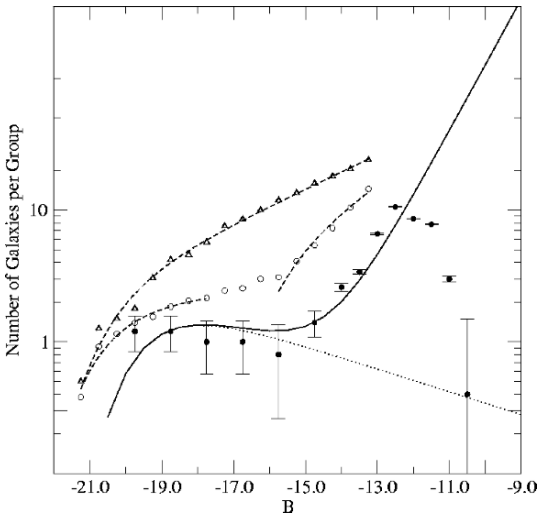

Fig. 3. Our measured luminosity function (points with error bars) is overplotted with the LF for massive (dotted line) and dwarf (solid line) passively evolving galaxies from the 2dFRS [5]. Also plotted are the measurements for X-ray bright (triangles) and X-ray faint (circles) group galaxies from [6].

[5]. Especially the LF derived by [5] provides a good agreement for the luminosity of the break in our observed LF of HGCs and the extrapolated faint end slope a decent description of our data, as shown in Fig. 3.

Our data therefore imply a large population of passively evolving dwarf galaxies in HGCs. Such a steep faint end slope dominated by dE/dSph galaxies was up to now only found in galaxy clusters, e.g. [12]. In galaxy groups, dE/dSph are generally only found orbiting massive galaxies. Actually, the numbers in the Local Group dwarf galaxies seems to be very low compared to the predictions from CDM theory (the substructure crisis [4, 7]). In the general field, dSph are exceedingly rare or even absent. Just recently one object was detected which may be the best case yet for a field dSph [8]. The steep faint end of the LF we observe in HCGs is hard to understand, since the conditions in HGCs are cluster-like only in the very dense cores of HGCs, and not in the outer envelopes where we find most of the dwarf galaxies. Here the galaxy densities resemble more those of loose groups.

The faint end slope of our observed LF is very steep and may add a new aspect to the ongoing discussion on the formation, evolution, and survival of dwarf galaxies. The measured LF slope of our HGCs ($\alpha \sim -1.7$) is strikingly similar to the slope of the mass function of dark matter halos, see Fig. 4. This would imply that in compact galaxy groups most DM halos would have been populated with baryons, in contradiction the results for the Local Group, where an overabundance of DM halos without baryons seems to be present.

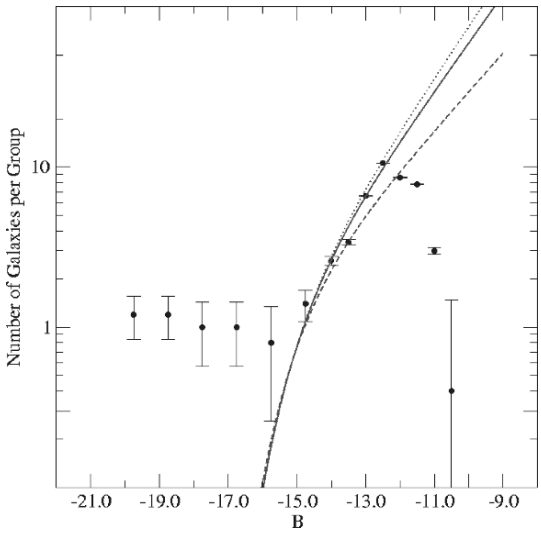

Fig. 4. Same luminosity function as plotted in Fig. 2 compared with faint end slopes of $\alpha = -1.74$ (solid line: best fit to our data), $\alpha = -1.6$ and $\alpha = -1.8$ (dashed and dotted lines) overplotted.

We recently got the first VIMOS spectroscopy of the dwarf candidates in two of our HCGs, providing redshifts of a large number of the dwarfs. This will also allow us to study the dynamics of the dwarf galaxy population and the internal properties of the confirmed dwarf members.

References

1. Conselice, C. J. (2002). *ApJL*, **573**, L5–L8.
2. Hickson, P. (1997). *ARA&A*, **35**, 357–388.
3. Hunsberger, S. D., Charlton, J. C., and Zaritsky, D. (1996). *ApJ*, **462**, 50.
4. Klypin, A. et al., (1999). *ApJ*, **522**, 82–92.
5. Madgwick, D. S. et al., (2002). *MNRAS*, **333**, 133–144.
6. Miles, T. A. et al., *MNRAS*, **355**, 785–793.
7. Moore, B. et al., (1999). *ApJL*, **524**, L19–L22.
8. Pasquali, A. et al., (2005). *AJ*, **129**, 148–159.
9. Ribeiro, A. L. B., de Carvalho, R. R., and Zepf, S. E. (1994). *MNRAS*, **267**, L13–L16.
10. Schechter, P. (1976). *ApJ*, **203**, 297–306.
11. Secker, J. and Harris, W. E. (1997). *PASP*, **109**, 1364–1376.
12. Trentham, N., Sampson, L., and Banerji, M. (2005). *MNRAS*, **357**, 783–792.
13. Zabludoff, A. I. and Mulchaey, J. S. (2000). *ApJ*, **539**, 136–148.

Low Luminosity Activity in Hickson Compact Groups

M.A. Martinez[1], A. del Olmo[1], J. Perea[1] and R. Coziol[2]

[1] Instituto de Astrofisica de Andalucia(IAA),CSIC, Granada (Spain)
geli@iaa.es,chony@iaa.es,jaime@iaa.es
[2] Departamento de Astronomia, Universidad de Guanajuato (Mexico)
rcoziol@astro.ugto.mx

Summary. With the aim of studying the influence of environment on the nuclear activity of galaxies, we have selected a well defined sample of 65 Compact Groups of galaxies with concordant redshift in the Hickson Catalogue [5]. In this proceeding, we present the results of the classification of nuclear activity for 42 galaxies, based on newly obtained spectral observations. In this subsample, 71% of the galaxies turned out to have emission lines in their nuclei. 73% of these emission-line galaxies were found to have characteristics consistent with low luminosity AGN (LLAGN), which makes compact groups extremely rich in such objects.

1 Introduction

Although environment is suspected to play an important role on the formation and evolution of galaxies, including mass assembly, star formation, morphological evolution and AGN activity, the physical details on how such connection is established are not yet well determined.

To study the connection between environment and nuclear activity (AGN or HII), systems with high galaxy density and low velocity dispersion, where the influence of gravitational encounters are optimized, are in need. In principle, these two conditions can be found in Hickson Compact Groups of galaxies (HCG). Evidence for gravitational interaction in these systems take the forms of morphological and kinematical perturbations [6] [11], the existence of tidal features such as tails or shells [10], the presence of intergalactic gas emission observable in X-rays [8] and the perturbed distribution of molecular and atomic gas [12].

For our study of nuclear activity we have selected all the groups with concordant redshift in the Hickson catalogue [5] with $\mu_G \leq 24.4$ (group compactness) and $z \leq 0.045$ (redshift completeness), which resulted in a statistically complete sample of 65 groups (283 galaxies).

2 New observations and data reduction

New optical spectroscopic data for 42 galaxies were obtained with the CAFOS spectrograph, during a seven night run (November 2004) on the 2.2m telescope of the Calar Alto Observatory (Almeria, Spain). The detector used was a 2048 × 2048 SITE CCD, with a plate scale of 0.53arcsec/pixel. Specifications for the two grisms used to obtain the required wavelength range can be found in Table 1.

Table 1. Instrumental parameters

Grism	Dispersion	Resolution	Spectral Range
B100	2Å/px	3.74Å/arcsec	3200Å-5800Å
G100	2.12Å/px	3.97Å/arcsec	4900Å-7800Å

The spectra were reduced using standard procedures in IRAF and SIPL packages. After overscan and bias subtraction, flat fielding correction was performed using internal flats (taken with a quarz lamp). A correction for the different illumination along the slit was done using sky flats. Finally, cosmic-rays were removed by a median combination of different images (at least three). During each night we also obtained arc (HgCdAr, He and Rb) expositions for wavelength calibration and observed three blue and three or four red spectrophotometric standard stars for flux calibration. Using our observation of standard stars, an extinction curve was determined for each night, which resulted in photometric errors less than 5% on the calibrated fluxes. The sky contribution was calculated by selecting two bands on both sides of the target galaxy. After sky subtraction we made the alignment of the spectra along the spatial axis. In Figures 1 and 2 we show some examples of spectra obtained after addition of the three central spatial sections of each galaxy and after joining the spectra obtained with the two grims.

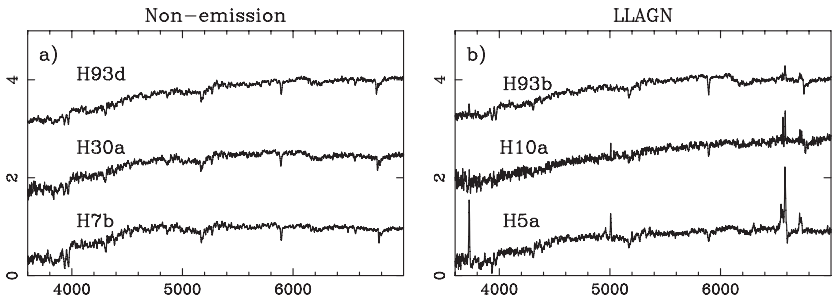

Fig. 1. Some examples of our new spectra. The flux scale is normalized to 1 and the spectra are shifted for ease of presentation.

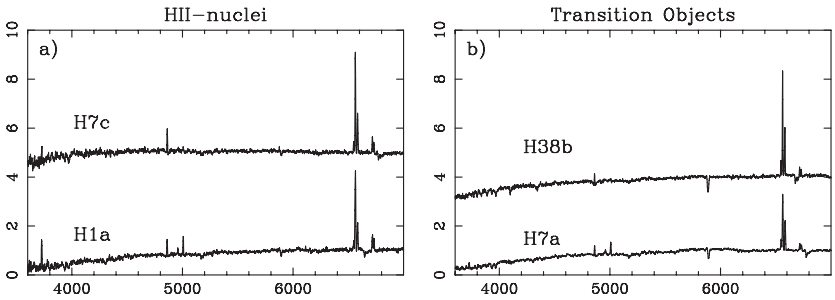

Fig. 2. Some examples of emission line galaxies.

3 Results and analysis

The classification of activity type of the emission line galaxies was done using standard diagnostic diagrams [1], [9]. For our classification, we use the line ratios $\log([\mathrm{OIII}]/H_\beta)$ and $\log([\mathrm{NII}]/H_\alpha)$, which are not affected by reddening and are largely insensible to errors in the photometry. In Figure 3 we plot the diagnostic diagram for all the analyzed objects (the 42 spectra obtained in Calar Alto together with 68 galaxies previously classified by Coziol et al. [3][4]). In this figure we uses the empirical separation between starburst galaxies and AGNs as determined by Veilleux and Osterbrock [9], and the separation defined by Coziol [2] to distinguish between Seyfert and LINERs. Note that in cases where only one line ratio is available, we tentatively classify the object as AGN based on a value of $[\mathrm{NII}]/H_\alpha > 0.6$ [7].

To summarize our classification, we have found four different types of spectra (as shown in Figures 1 and 2):

- Non-emission galaxies, where only stellar absorptions features such as the CaII lines, G band, 4000Å break or Mg band are observed (Fig. 1a).
- Galaxies hosting nuclear AGN activity, mainly in the form of Low Luminosity AGNs. In Figure 1b, emission lines in HCG 93b are obviously diluted by intermediate age stellar population which leaves visible only the [NII] lines. In HCG 10a, on the other hand, the emission lines are more intense and the stellar contribution probably lower, but the intensity of [NII] lines are also quite strong, comparable to the intensity of H_α, which also suggest an AGN nature. At it was previously shown [3][4] such spectral characteristics are typical of LLAGN, and usually remain even after subtracting a stellar contribution from their spectra.
- Galaxies with star formation in their nuclei, where, as we can see in Figure 2a, the strong emission lines are detected over a featureless continuum.
- Transition objects between HII/LINER (Fig. 2b).

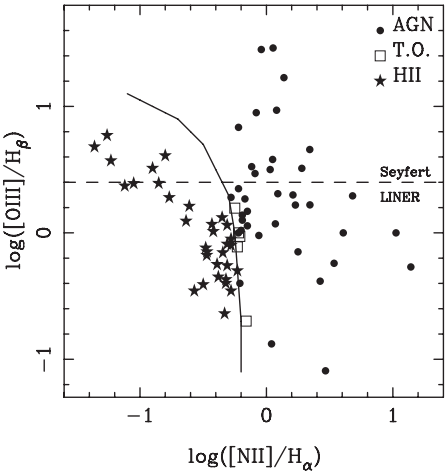

Fig. 3. Diagnostic diagram for the classified objects. The solid lines indicates the empirical separation between starburst galaxies and AGNs, as determined by Veilleux & Osterbrock [9]. The dashed line establishes a distinction between Seyfert2 galaxies and LINERs as determined by Coziol [2].

In diagnostic diagrams, transition objects (TO; open squares in our diagnostic diagram) are located at the limit between LINER and HII-nuclear region, and are consequently thought to share features proper to both types. For instance, they show H_α lines which are more intense than the [NII] lines, although not as intense as in HII-nuclear galaxies. They also show a continuum which is not strong enough to mask emission lines. It has been suggested by Ho et al. [7] that these galaxies could be the host of an AGN (LINER or Seyfert 2) with a circumnuclear star formation region. Our present classification of these objects should be considered temporary, until a proper stellar population subtraction is performed.

It is interesting to note that in the whole subsample classified here, we find only one galaxy, HCG 5a (in Figure 1b), with a wide component in H_α and H_β characteristic of a Seyfert 1.5.

4 Conclusions

Of the 42 galaxies studied in this work, only 8 galaxies do not show any apparent emission. In 30 galaxies emission-lines are clearly observed, while a weak presence of [NII] or H_α is detected in four more. The percentage of emission line galaxies in our present sample amount therefore to at least 71%. Within the 30 emission galaxies in our sample, 8 are classified as HII/star-forming nucleus, 17 (57%) show characteristics consistent with low luminosity AGNs with a LINER type, while the rest (5 galaxies) could represent transition like

objects or TO. If TO really turn out to possess an AGN in their nucleus, that would increase the number of AGNs in our sample to 73%.

If we add to our sample the 68 galaxies previously studied by Coziol et al. [3][4] the fraction of emission-line galaxies would amount to 67% and 60% of these would be classified as AGN (mostly LLAGN). From these results we conclude therefore that compact groups of galaxies are particularly rich in AGNs.

References

1. J.A. Baldwin, M.M Phillips & R. Terlevich: PASP **93**, 5B (1981)
2. R. Coziol: A&A **309**, 345 (1996)
3. R. Coziol, A.L.B. Ribeiro, R.R. de Carvalho & H.V. Capelato: ApJ **493**, 563 (1998)
4. R. Coziol, E. Brinks, H. Bravo-Alfaro: AJ **128**, 68c (2004)
5. P. Hickson: ApJ **255**, 382 (1982)
6. P. Hickson: Ann. Rev. A&A **35**, 357 (1997)
7. L.C. Ho, A.V. Fillipenko & W.L.W. Sargent: ApJ **417**, 63 (1993)
8. T.J. Ponman, P.D.J. Bourner, H. Ebeling & H. Bhringer: MNRAS **283**, 690P (1996)
9. S. Veilleux & D.E. Osterbrock: ApJ **63**, 295 (1987)
10. L. Verdes-Montenegro, A. Del Olmo, J.I. Iglesias-Paramo, J. Perea, J.M. Vilchez, M.S. Yun, & W.K. Huchtmeier: A&A **326**, 815 (2002)
11. Verdes-Montenegro, A. Del Olmo, M.S. Yun & J. Perea: A&A **430**, 443 (2005)
12. M.S. Yun, L. Verdes-Montenegro, A. del Olmo & J. Perea: ApJ **475**, 21 (1997)

Dwarf Elliptical Galaxies in Cen A Group

M. Rejkuba

European Southern Observatory, K.-Schwarzschild-Str. 2, D-85748
Garching, Germany
mrejkuba@eso.org

The analysis of the red giant stellar populations in Cen A group dwarf elliptical galaxies AM 1339-445 and AM 1343-452 is presented based on deep optical and near-IR photometry. The distances and average metallicities have been derived from the magnitudes and colors of the red giant branch (RGB) stars. The presence of stars brighter than the RGB tip, is an evidence of extended star formation. The luminosities of these bright red giants imply ages of the last significant star formation episodes occurring 6.5 ± 1 Gyr ago in AM 1339-445 4 ± 1 Gyr ago in AM 1343-452. The near-IR integrated colors and the central surface brightness magnitudes are compared with other nearby dwarf galaxies.

1 Introduction

The nearby Centaurus A group presents a different environment to its members with respect to the Local Group (LG). Its central dominant member is Cen A, the nearest easily observable giant elliptical galaxy ($D = 3.84$ Mpc, [1]), which hosts an AGN and shows evidences of the recent merger. Furthermore, this group is more compact than the LG, and probably contains twice as many galaxies [2]. It is thus of interest to study in detail the stellar populations of its dwarf galaxy population in order to investigate the influence of the environment on the star formation in these small systems. To this end we have conducted the observations of 14 Cen A group dwarf galaxies with ISAAC near-IR array at the ESO VLT. The results for the two galaxies AM 1339-445 and AM 1343-452 that have archival optical HST images available have been published by [3] and are described shortly here. The analysis of the rest of the sample will be published elsewhere (Rejkuba et al., in preparation).

2 Data and color-magnitude diagrams

The near-IR observations of AM 1339-445 and AM 1343-452 were taken between May and July 2004 using the short wavelength arm J_s and K_s filters of ISAAC near-IR array on the Antu VLT. The K_s observations were taken

on two different epochs, each amounting to 2352 s observation on source and the single epoch J_s observation had 2100 s. After the standard reduction of near-IR images within IRAF, the PSF fitting photometry was performed using the suite of DAOPHOT, ALLSTAR and ALLFRAME programmes.

The HST archival data consist of single 600 s exposures with $F606W$ and $F814W$ filters taken as part of the HST WFPC2 snapshot programme 8192. These filters correspond closely to Cousins V and I bands. The photometry was performed using HSTphot package [4] on pipeline processed images. For the details of the data reduction and photometry for both optical and near-IR data the interested reader is referred to [3].

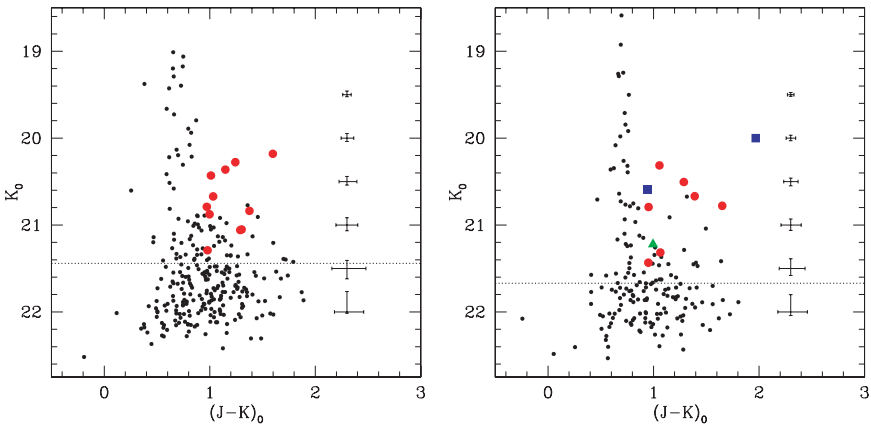

Fig. 1. Near-IR CMDs for AM 1339-445 (left) and AM 1343-452 (right). The horizontal dotted line indicates the expected magnitude of the RGB tip. The large symbols indicate candidate upper-AGB intermediate-age stars that are brighter than RGB tip in both optical and near-IR CMDs. Large square and triangle symbols indicate probable long period variable stars.

The near-IR color-magnitude diagram (CMD) for AM 1339-445 is shown in the left panel of Fig. 1, and for AM 1343-452 is in the right panel. The horizontal line at $K_{0,TRGB} = 21.4$ and $K_{0,TRGB} = 21.7$ indicates the expected magnitude for the red giant branch (RGB) tip, calculated using the Eqs. 7 and 9 from [5] and assuming the metallicities and distance moduli from the optical data. The large number of stars with colors bluer than $(J-K)_0 = 0.95$ belong to the foreground Galactic population.

The optical CMDs are shown in Fig. 2. Overplotted are fiducial RGB loci for Galactic globular clusters with metallicities [Fe/H] $= -2.17, -1.62, -1.36,$ and -0.71 dex, from blue to red. Bright stars found above the RGB tip in both optical and in near-IR CMDs that have near-IR colors redder than the Galactic stars have been plotted with large symbols in Figs. 1 and 2. These are candidate intermediate-age upper-asymptotic giant branch (AGB) stars.

3 Ages and metallicities

Tip of the RGB is a sharp feature in the I-band luminosity functions. It is a well known distance indicator as its absolute magnitude shows only very mild age and metallicity dependence for old metal-poor populations like the ones observed in dwarf elliptical (dE)galaxies [6]). Using the calibration of the method from [6], and the tip of the RGB detection at $I_{TRGB} = 23.95 \pm 0.15$ in AM 1339-445 and at $I_{TRGB} = 24.10 \pm 0.15$ in AM 1343-452, the distance moduli of $(m - M)_0 = 27.74 \pm 0.20$, and $(m - M)_0 = 27.86 \pm 0.20$ were derived for the two galaxies respectively, in agreement with previous measurements from the literature [7], [2].

As can be seen from Fig. 2, the $(V - I)_0$ color depends on metallicity. Hence the mean color of the RGB can be used as an indicator of metallicity provided that the mean age of the population is similar to that of the Galactic globular clusters. Adopting this assumption the average metallicity is $\langle[\mathrm{Fe/H}]\rangle = -1.4 \pm 0.2$ for AM 1339-445 and $\langle[\mathrm{Fe/H}]\rangle = -1.6 \pm 0.2$ for AM 1343-452. As it is below argued that a small fraction of intermediate-age population is present in these galaxies, which would then have bluer colours, and thus would mimic the lower metallicity giants, the average metallicities might be systematically too low by up to ∼0.2 dex.

There is a significant number of stars brighter than the RGB tip in both optical and near-IR CMDs. Based on their magnitudes and colours, as well as indications that at least some of them may be variable it is highly probable that these belong to the intermediate-age upper-AGB population.

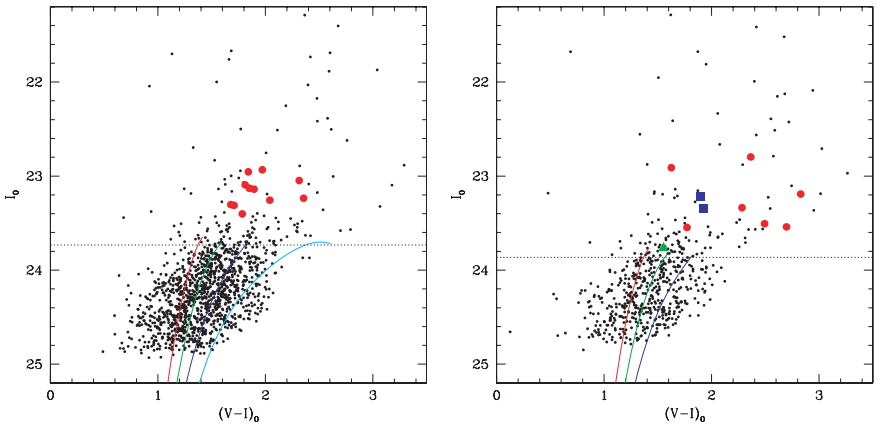

Fig. 2. Optical VI CMDs for AM 1339-445 (left) and AM 1343-452 (right). The horizontal dotted line indicates the expected magnitude of the RGB tip. Overplotted are fiducial red giant branches for Galactic globular clusters M 15 ([Fe/H] = −2.17), M 2 (−1.62), NGC 1851 (−1.36), and only for AM 1339-445 (left) 47 Tuc (−0.71). Bright upper-AGB intermediate-age candidate stars are plotted with larger symbols.

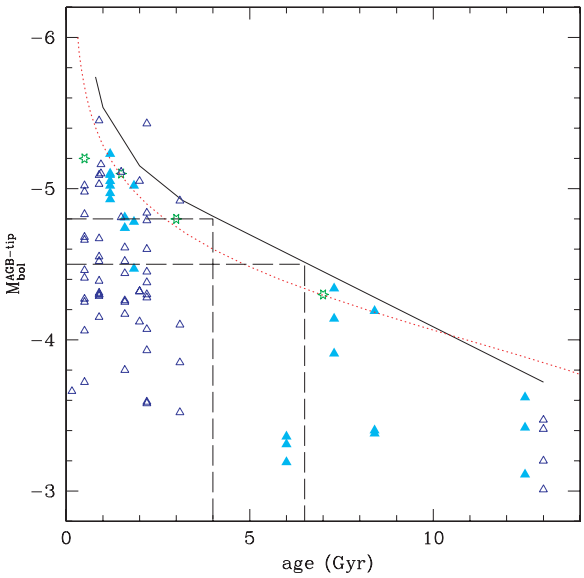

Fig. 3. The empirically determined relation between the AGB tip luminosity and age using the LMC (open triangles), and SMC (filled triangles) data is shown with solid line. The dotted line is the theoretically determined relationship from [8]. The long dashed lines indicate the measured average AGB tip bolometric magnitudes in AM 1339-445 and AM 1343-452 and their inferred ages. For comparison the AGB tip magnitudes and the ages of the last star formation epoch for Leo I, Fornax, Carina and Leo II are also plotted (open star symbols). For details see [3].

The bolometric magnitude of the brightest AGB stars in any given stellar population is a strong function of age, while it depends much less on metallicity. The empirically determined AGB tip-age relation is shown in Fig. 3 with solid line. It is based on the AGB tip magnitudes and ages for well observed LMC (open triangles) and SMC (filled triangles) clusters (for details see [3]). For comparison the AGB-tip magnitudes and ages for the latest star formation episodes are plotted for the LG galaxies Leo I, Fornax, Carina and Leo II (open star symbols) and the dotted line is a theoretical AGB-tip vs. age relation from [8]. Adopting I-band bolometric corrections from [6], and K-band bolometric corrections from [9], the average bolometric magnitude for the three brightest AGB candidate stars are -4.5 mag in AM 1339-445 and -4.8 in AM 1343-452. Hence the age of the last significant star formation episode for these two dE galaxies is 6.5 ± 1 Gyr and 4 ± 1 Gyr, respectively, as indicated with dashed lines in Fig. 3.

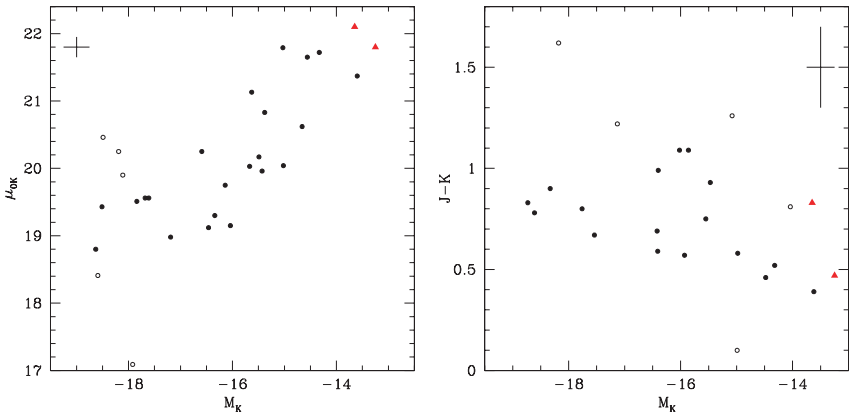

Fig. 4. Correlation of the central surface brightness and near-IR color with luminosity for nearby dwarfs [10]; circles) and Cen A dEs (triangles).

4 Comparison with nearby dwarf galaxies

In Fig. 4 the near-IR global properties for the two Cen A dEs (filled triangles) are compared with nearby dwarfs [10]; circles): correlation of the central surface brightness with luminosity is shown in the left panel, and the right panel shows the correlation of the $J-K$ color with K-band luminosity. These correlations show that less luminous galaxies have fainter cores and bluer colors, which imply lower metallicity. It should be noted that the comparison sample [10] contains dwarf irregular galaxies which are different from dEs studied in the present work, because of the presence of HI gas and varying degrees of recent star formation. However, as these authors argue the near-IR light probes primarily the old and intermediate-age stellar populations, similar to the populations observed in AM 1339-445 and AM 1343-452.

Acknowledgments. I would like to thank my collaborators, in particular Gary Da Costa and Helmut Jerjen, for their contribution to this work.

References

1. M. Rejkuba: A&A, **413**, 903 (2004)
2. I.D. Karachentsev, M.E. Sharina, A.E. Dolphin, et al.: A&A, **385**, 21 (2002)
3. M. Rejkuba, G.S. Da Costa, H. Jerjen, et al.: A&A, **448**, 983 (2006)
4. A.E. Dolphin: PASP, **112**, 1383 (2000)
5. E. Valenti, F.R. Ferraro & L. Origlia: MNRAS, **354**, 815 (2004)
6. G.S. Da Costa, & T.E. Armandroff: AJ, **100**, 162 (1990)
7. H. Jerjen, K.C. Freeman, & B. Binggeli: AJ, **119**, 166 (2000)
8. A.W. Stephens, & J.A. Frogel: AJ, **124**, 2023 (2002)
9. E. Costa, & J.A. Frogel: AJ, **112**, 2607 (1996)
10. O. Vaduvescu, M.L. McCall, et al.: AJ, **130**, 1593 (2005)

Stellar Populations in Compact Group Elliptical Galaxies

I.G. de la Rosa[1,2], R.R. de Carvalho[3], A. Vazdekis[1] and B. Barbuy[2]

[1] Instituto de Astrofísica de Canarias, E-38200 La Laguna, Tenerife, Spain
irosa@iac.es, vazdekis@iac.es
[2] Instituto Astronômico e Geofísico - USP, 04301-904 São Paulo, Brazil
barbuy@astro.iag.usp.br
[3] Instituto Nacional de Pesquisas Espaciais - DAS, São José dos Campos - SP - Brazil
reinaldo@das.inpe.br

Summary. Elliptical galaxies in Hickson Compact Groups (HCGs) are compared with their counterparts in the field. The stellar populations have been studied with two alternative models and reduction strategies to ensure the robustness of the results. Furthermore, great care has been taken to correct for emission contamination by Balmer lines, used to determine the ages of the galaxies. We find that, compared to the field, galaxies in HCGs are systematically older and more metal-poor, in agreement with previous works. For the first time, we show that the less massive galaxies in HCGs show an enhanced [Mg/Fe] abundance ratio compared to the field. This enhancement is interpreted as a relic of an event which truncated the galactic star formation, when the abundance ratio was still high. Recent hydrodynamical simulations predict such truncation after a galaxy merger, believed to be a common interaction in HCG environments.

1 Introduction

Compact groups of galaxies, with their high spatial densities and low velocity dispersions, are potentially ideal locales for interactions and mergers. Although mergers are generally associated with enhanced SF [1], the galaxies in HCGs have not matched these simple expectations. Despite abundant traces of interactions [2] enhanced SF levels have not been observed [3] [4] [5] [6] [7]. Nevertheless, recent hydrodynamical simulations of galaxy mergers [8] find that, after a brief starburst, the feedback from active galaxy nuclei (AGN) depletes the gas and quenches star formation, producing a red and dead spheroid. In this context, the lack of enhanced SF in HCGs does not seem so unexpected. One of the best tools for investigating the history of a galaxy is the study of its stellar populations. Among the extracted parameters, the [Mg/Fe] abundance ratio is especially suitable for disentangling the SF history, because the enrichment of α and Fe elements have different timescales. In the present study we apply this technique to look for traces

of past SF truncation events in early-type galaxies within HCGs. The identification of galaxy mergers as the mechanism responsible for SF quenching would be an important piece of evidence to understand the deficit of SF observed in dense environments [9], as well as the global trend of a decreasing SF rate to the present day [10]. In this study, we use a homogeneous set of early-type galaxies belonging to two different environments, HCGs and the field or very loose groups. Our aim is to study how their stellar population properties depend on the environment. Most stellar population studies suffer from a variety of limitations, which we address using two methodological approaches. First, we apply two alternative reduction schemes, those of [11] (hereafter TMB03) and [12] (hereafter Vaz99), to minimize and understand systematic effects introduced by the models.

2 Observations and reduction

Our sample consists of 34 early-type galaxies, 22 of them located in HCGs and the remainder in the field. Long-slit spectra were obtained at the KPNO 2.1 m telescope with the GoldCam CCD spectrometer, with an intermediate 4.25 Å FWHM spectral resolution and a median Signal-to-Noise Ratio (SNR) of 55. Details about the sample and basic reduction were published in [13]. For the present study, $R_{eff}/8$ and $R_{eff}/2$ apertures were extracted.

2.1 Emission correction

The emission contamination of the Balmer lines, generally used to estimate the ages of the populations, is a potential source of bias for the present work, because the emission contamination is expected to differ between the two studied environments. We have carried out a careful decontamination of this emission, by combining the results of two independent methods. The first method, proposed by [14], obtains an empirical relation between the [OIII]λ5007 Å and Hβ_{emiss} indices, measured in a residual spectrum (contaminated - template). By measuring the [OIII]λ5007 index one can readily calculate the Hβ_{emiss} and correct for the emission contamination. The second method follows several steps which are detailed in [15]. In summary, it measures the Hα_{emiss} with the help of the *Rose index* [Hn/Fe] and calculates the Hβ_{emiss} by using the decrement ratios proposed by [16]. Although both methods are based in rather scattered relations, there is a good match between their results and the average emission correction is adopted.

2.2 The stellar population studies

In the TMB03 approach, our spectra are first broadened to the low spectral resolution of the Lick/IDS system and compared with 12 galaxies in common

with the [14] study, in order to guarantee correct conversion to that system. A further broadening correction is needed to convert the indices into the three stellar population parameters: age, metallicity and [Mg/Fe] abundance ratio. This approach takes non-solar abundance ratio effects into account and an iterative process is used to extract the stellar population parameters from a [MgFe]' vs Hβ grid.

The main advantage of the Vaz99 approach is that the high resolution models are adapted to the data, instead of the reverse. Only emission corrections are applied here because the models are now broadened to the σ_{tot} of the data $(\sigma^2_{instr} + \sigma^2_{gal})^{1/2}$. These models do not take the non-solar abundance ratios into account and the [Mg/Fe] parameter has to be calculated by dividing the [Mg/H] by the [Fe/H] metallicities.

By comparing the results of both methods we can assess the systematic effects introduced by the models and understand their origin. TMB03 ages are, on average, 16% lower than those obtained with the Vaz99 approach, while TMB03 metallicities are 0.16 dex larger. Vaz99 [Mg/Fe] ratios are systematically larger and the discrepancy increases with the overabundance. Fortunately, our study is not vulnerable to this effect because it compares two subsamples extracted from a single homogeneous set.

3 Results

The stellar population parameters depend both on the galaxy mass and on its environment. We have chosen the σ_0 to represent mass and the *crossing time* to characterize the environment. Several trends have been found.

(i) *Galaxies in HCGs are 1.3 Gyrs older, on average, than their counterparts in the field.* Qualitatively similar results has been already reported in the literature [18] [19] [20].

(ii) *Total metallicities [Z/H] of the field galaxies are 0.10 dex larger, on average, than in HCGs.* This result, also reported by [18] [19] [20], is complemented by the observation of an increase of [Z/H] with σ_0, interpreted as the larger resistence of massive galaxies to lose their enriched gases through supernovae winds [21].

(iii) *The [Mg/Fe] abundance ratio increases with σ_0 for the field galaxies.* This result, shown in Figure 1(b), coincides with previous findings by e.g. [22], interpreted as a *downsizing*, in which low-mass galaxies display more extended SF histories.

(iv) *Galaxies in HCGs show an anomalous trend in [Mg/Fe] vs log σ_0.* This result, shown in Figure 1(a), is a novel finding of this study. Encircled points show the largest departures from the corresponding field behaviour, which cannot be explained by the error bars. The encircled star corresponds to HCG 59b, whose [Mg/Fe] is a lower limit while the solid square corresponds to HCG 76d, taken from [20], in a similar study made with the TMB03 approach. This effect, which is detected with both TMB03 and Vaz99 approaches, is

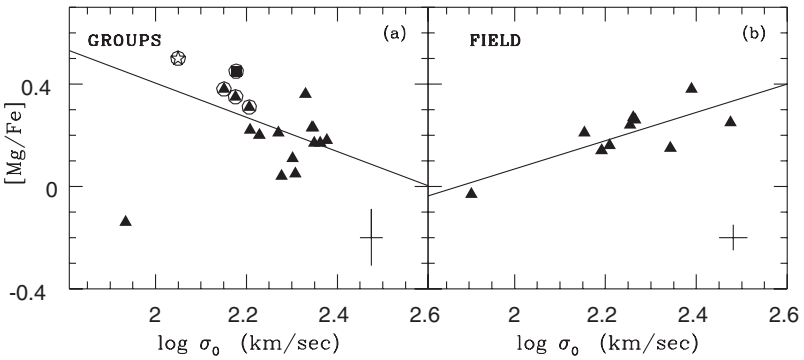

Fig. 1. Trends of [Mg/Fe] abundance ratios with log σ for (a) HCG and (b) field environments. Values were obtained with the TMB03 approach for central ($R_{eff}/8$) apertures. The encircled points in (a) represent galaxies with *anomalous* abundance ratios. The solid square (HCG 76d) has been taken from [20] and the encircled star corresponds to galaxy HCG 59b, whose [Mg/Fe] value is only a lower limit. Average error bars are represented at the low right corners.

especially prominent in the central apertures ($R_{eff}/8$) and weaker in the global ones ($R_{eff}/2$).

A further proof that the encircled points make a distinct group is that they also share different properties, when compared with the rest of the HCG sample galaxies. Encircled points show, in average, lower masses and fainter luminosities, more nuclear activity, more extended profiles, disky isophotes and reside in dynamically evolved groups, with shorter *crossing times*.

4 Discussion

The anomalous behaviour of the [Mg/Fe] abundance ratio of the low-mass HCG galaxies can be interpreted as a result of a *merger + SF truncation* process. Soon after the SF has started in a galaxy, the [Mg/Fe] attains its maximum value, which steadily decreases as the Fe is incorporated to the new formed stars. Low-mass galaxies in the field evolve undisturbed until the SF has been completed and the [Mg/Fe] attains a minimum value. A field galaxy falling into the dense compact group environment, would likely merge and see their gas depleted by the feedback of the central supermassive black hole, as shown by the simulations [8]. Without the gas, the SF is truncated and the stellar populations of the galaxy stop their Fe enrichment, keeping an enhanced [Mg/Fe] abundance ratio. As observed in Figure 1(a), both the massive and the dwarf galaxies are exceptions to the SF truncation process. Due to the downsizing, the more massive galaxies have completed their SF long ago and nothing remains to be truncated after the merger. The dwarf galaxies, on the contrary, are actively forming stars, but the feedback of the of

the central black hole is not powerful enough to deplete the gas. The *merger + SF truncation* can possibly be the process modeled by [23] to interpret the hostility to SF observed in dense environments.

References

1. Barnes, J.E., Hernquist, L.: ARA&A. **30**, 705 (1992)
2. Mendes de Oliveira, C., Hickson, P.: ApJ. **427**, 684 (1994)
3. Zepf, S. E., Whitmore, B. C., Levison, H.F.: ApJ. **383**, 524 (1991)
4. Allam, S., Assendrop, R., Longo, G., Braun, M., Richter, G.: A & ApS. **117**, 39 (1996)
5. Verdes-Montenegro, L., Yun, M.S., Perea, J., del Olmo, A., Ho, P.T.P.: ApJ. **497**, 89 (1998)
6. Iglesias-Páramo, J., Vílchez, J.M.: ApJ. **518**, 94 (1999)
7. Coziol, R., Iovino, A., de Carvalho, R.R.: AJ. **120**, 47 (2000)
8. Di Matteo, T., Springler, V., Hernquist, L.: Nature **433**, 604 (2005)
9. Dressler, A.: ApJ. **236**, 351 (1980)
10. Madau, P., Ferguson, H.C., Dickinson, M.E., Giavalisco, M., Steidel, C.C., Fruchter, A.: MNRAS **283**, 1388 (1996)
11. Thomas, D., Maraston, C., Bender, R.: MNRAS **339**, 897 (2003)
12. Vazdekis, A.: ApJ. **513**, 224 (1999)
13. de la Rosa, I.G., de Carvalho, R.R., Zepf, S.E.: ApJ. **122**, 93 (2001)
14. González, J.J.: Line-strength gradients and kinematic profiles in elliptical galaxies. Ph.D. Thesis, University of California, Santa Cruz (1993)
15. Caldwell, N., Rose, J.A., Concannon, K.D.: AJ. **125**, 2891 (2003)
16. D.E. Osterbrock: *Astrophysics of Gaseous Nebulae and Active Galactic Nuclei*, (Mill Valley, CA, University Science Books) (1989)
17. Hickson, P., Mendes de Oliveira, C., Huchra, J.P., Palumbo, G.G.C.: ApJ. **399**, 353 (1992)
18. de la Rosa, I.G., Coziol, R., de Carvalho, R.R., Zepf, S.E.: A&SS **276**, 717 (2001)
19. Proctor, R.N., Forbes, D.A., Hau, G.K.T., Beasley, M.A., de Silva, G.M., Contreras, R., Terlevich, A.I.: MNRAS **349**, 1381 (2004)
20. Mendes de Oliveira, C., Coelho, P., González, J.J., Barbuy, B.: ApJ. **130**, 55 (2005)
21. Arimoto, N., Yoshii, Y.: A&A. **173**, 23 (1987)
22. Thomas, D., Maraston, C., Bender, R., Mendes de Oliveira, C.: ApJ. **621**, 673 (2005)
23. Wilman, D.J., Balogh, M.L., Bower, R.G., Mulchaey, J.S., Oemler, A., Carlberg, R.G., Eke, V.R., Lewis, I., Morris, S.L., Whitaker, R.J.: MNRAS **358**, 88 (2005)

Spitzer 4.5 μm Luminosity-Metallicity and Mass-Metallicity Relations for Nearby Dwarf Irregular Galaxies

H. Lee[1], E.D. Skillman[1], J.M. Cannon[2], D.C. Jackson[1], R.D. Gehrz[1], E. Polomski[1] and C.E. Woodward[1]

[1] Dept. of Astronomy, Univ. of Minnesota, 116 Church St. S.E., Minneapolis, MN 55455 USA
(hlee, skillman, djackson, gehrz, elwood, chelsea@astro.umn.edu)
[2] Max-Planck-Institut für Astronomie, Königstuhl 17, D-69117 Heidelberg, Germany
(cannon@mpia.de)

Summary. For a sample of 25 dwarf irregular galaxies with distances $D \lesssim 5$ Mpc and measured oxygen abundances, we present results derived from galaxy luminosities at 4.5 μm and stellar masses from near-infrared imaging with IRAC on the *Spitzer Space Telescope*. We have constructed the appropriate luminosity-metallicity (L–Z) and mass-metallicity (M–Z) relations, and compared these relations with their corresponding relations from the Sloan Digital Sky Survey (SDSS). We obtain the following results. 1. The dispersion in the near-infrared L–Z relation is reduced with respect to the dispersion in the optical L–Z relation, which agrees with expectations for reduced variations of stellar mass-to-light ratios at longer wavelengths compared to optical wavelengths. 2. The dispersion in the optical L–Z relation is similar over approximately 11 mag in optical luminosity. 3. With our constructed M–Z relation, we have extended the SDSS M–Z relation to lower masses by about 2.5 dex in stellar mass. 4. The dispersion in the M–Z relation appears to be comparable over a range of 5.5 dex in stellar mass.

1 Near-infrared luminosity-metallicity relation

The luminosity-metallicity (L–Z) relation for nearby dwarf irregular galaxies has been studied traditionally at optical wavelengths (e.g., [7, 11, 9, 5, 13]). However, the dispersion in the optical L–Z relation is affected by variations in stellar mass-to-light ratios, which are caused by variations in the current star formation rate among galaxies. To minimize the effects of these variations, we determine the L–Z relation at near-infrared wavelengths where stellar populations dominate the emission. The sensitivity of the *Spitzer Space Telescope* provides an excellent opportunity to observe the total near-infrared emission from the stellar populations in nearby dwarf galaxies. The present results are based on observations taken with IRAC in channel 2 (4.5 μm); we assume that the contribution from warm and/or small dust grains at 8 μm is negligible in dwarf galaxies [3].

We have measured 4.5 μm luminosities for 25 galaxies taken from GTO program 128 (P.I. R. D. Gehrz) and the *Spitzer* archive. Located within the Local Group and other nearby groups, these galaxies have measured distances ($D \lesssim 5$ Mpc) and oxygen abundances. The optical and near-infrared L–Z relations [6] are plotted in Figs. 1a and b, respectively. The dispersion in the L-Z relation is reduced at near-infrared wavelengths compared to the dispersion in the optical relation. By comparison with the optical L–Z relation for more massive galaxies [12] from the Sloan Digital Sky Survey (SDSS), it appears that the dispersion in the optical L–Z relation is similar ($\simeq 0.16$ dex) over 11 magnitudes in optical luminosity.

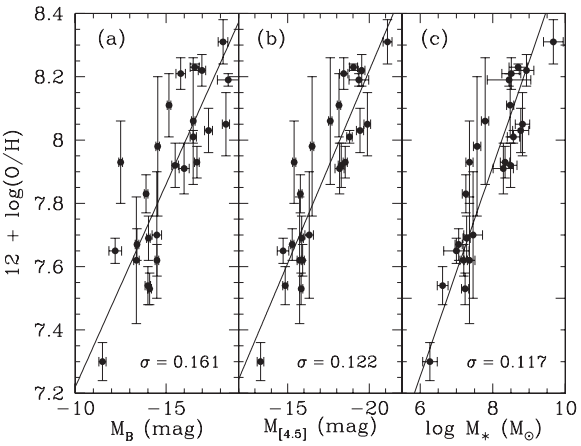

Fig. 1. Panel (a): optical (B) luminosity-metallicity relation with dispersion $\sigma = 0.16$ dex. Panel (b): near-infrared (4.5 μm) luminosity-metallicity relation with dispersion $\sigma = 0.12$ dex. Panel (c): stellar mass-metallicity relation with dispersion $\sigma = 0.12$ dex. In each panel, the solid line represents a linear least-squares fit to the data.

2 Stellar mass-metallicity relation

With measured luminosities at 4.5 μm, we have derived stellar masses for our sample of dwarf irregular galaxies. We have used the models from Bell & de Jong [1] to determine stellar mass-to-light ratios as functions of $B-K$ color, and we have applied a correction for nonzero $K-[4.5]$ color in late-type dwarf galaxies (e.g., [8]). We have also adjusted the derived stellar masses to the Kroupa [4] stellar initial mass function; additional details of the derivation are provided in [6].

The stellar mass-metallicity (M–Z) relation [6] is shown in Fig. 1c. The M–Z relations for dwarf galaxies and for massive galaxies from the SDSS

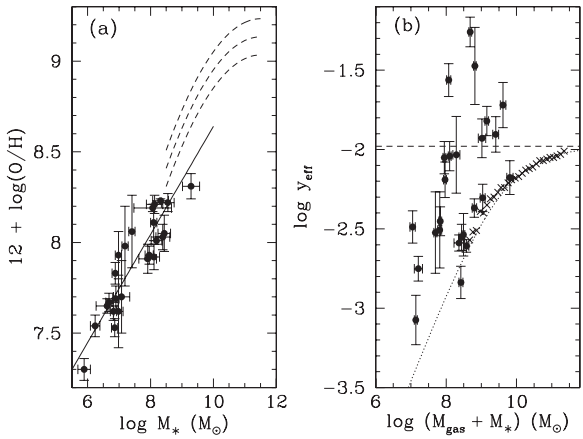

Fig. 2. Panel (a): Stellar mass-metallicity relation over 5.5 dex in stellar mass. The filled circles and solid line represent the present sample of dwarfs and the best fit, respectively. The relation from the SDSS and the ~ 0.10 dex curves from [12] are shown as dashed lines. Panel (b): Effective yield versus total baryonic mass. The crosses represent the median of the SDSS data in mass bins of 0.1 dex [12]. An empirical fit is shown as a dotted line, and the asymptotic yield ($y_{\rm eff} = 0.0104$) is shown as a horizontal dashed line.

are shown in Fig. 2a. With the present sample of dwarf galaxies, we have extended the SDSS M–Z relation to lower stellar mass by 2.5 decades. We find that the dispersion in the M–Z relation is comparable ($\approx$0.10–0.12 dex) over a range of 5.5 decades in stellar mass, although we have not performed a homogeneous treatment of gas-phase metallicities and stellar masses for the SDSS sample; see [6] and [12] for details.

We have plotted the effective yield as a function of total baryonic mass in Fig. 2b. The simple closed-box model of chemical evolution (see, e.g., [10]) predicts that the effective yield is equal to the true yield for all masses. However, that the effective yield decreases at lower baryonic mass is commonly interpreted as a signature of either outflow or dilution from the infall of metal-poor gas. We find that the present sample of dwarf galaxies exhibits a much larger variation in the effective yield at a given total baryonic mass. The large variation in the effective yield is difficult to explain if galaxy outflows are dominant in low-mass dwarf galaxies; see [12] for a countering view.

3 Stellar iron abundances vs. near-infrared luminosity

Stellar masses for our sample of dwarf galaxies have been derived from near-infrared luminosities under the assumption that the emission is dominated by the populations of older stars. Iron abundances are a good tracer of the chemical evolution for these stars integrated over the entire history of past star

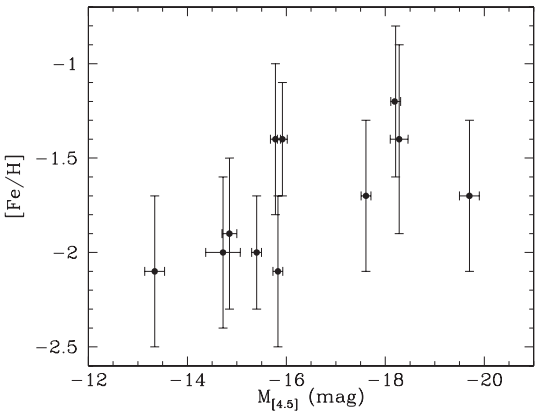

Fig. 3. Stellar photometric iron abundances vs. absolute magnitude at 4.5 μm. The iron abundances were taken from [2].

formation. We have constructed an L–Z relation using photometric stellar iron abundances from the literature to examine if the correlation is comparable to the relation constructed using gas-phase metallicities. The iron abundance-luminosity relation is shown in Fig. 3. Unfortunately, the photometric iron abundances have large uncertainties or spreads. Nevertheless, there appears to be a trend between the mean photometric iron stellar abundance and the measured galaxy luminosity at 4.5 μm in the same sense as that found in Fig. 1.

4 Final remarks

The challenge is explaining the relatively uniform scatter in both the L–Z and M–Z relations. Additional near-infrared imaging and spectroscopy for a large number of dwarf galaxies within the Local Volume can test whether the scatter in the L–Z and M–Z relations holds over a large range in luminosity and mass. The growing interest in determining the redshift-evolution of the L–Z and M–Z relations provides good impetus to exploring galaxy formation models that incorporate varying degrees of galaxy outflows and can predict the slope and the scatter in the L–Z and M–Z relations over large dynamic range.

References

1. E. F. Bell, & R. S. de Jong: ApJ **550**, 212 (2001).
2. E. K. Grebel, J. S. Gallagher, & D. Harbeck: AJ **125**, 1926 (2003).
3. D. C. Jackson, J. M. Cannon, E. D. Skillman, H. Lee, R. D. Gehrz, C. E. Woodward, & E. Polomski: ApJ, submitted (2006).

4. P. Kroupa: MNRAS **322**, 231 (2001).
5. H. Lee, M. L. McCall, R. L. Kingsburgh, R. Ross, & C. C. Stevenson: ApJ **125**, 146 (2003).
6. H. Lee, E. D. Skillman, J. M. Cannon, D. C. Jackson, R. D. Gehrz, E. F. Polomski, & C. E. Woodward: ApJ, submitted (2006).
7. J. Lequeux, M. Peimbert, J. F. Rayo, A. Serrano, & S. Torres-Peimbert: A&A **80**, 155 (1979).
8. M. A. Pahre, M. L. N. Ashby, G. G. Fazio, & S. P. Willner: ApJS **154**, 235 (2004).
9. M. Richer & M. McCall: ApJ **445**, 642 (1995).
10. L. Searle, & W. L. W. Sargent: ApJ **173**, 25 (1972)
11. E. Skillman, R. Kennicutt, & P. Hodge: ApJ **347**, 875 (1989)
12. C. Tremonti et al.: ApJ **613**, 898 (2004).
13. L. van Zee, E. D. Skillman, & M. Haynes: ApJ **637**, 269 (2006)

Shapes and Galaxy Flows Around Clusters and Groups of Galaxies

N. Padilla

Departamento de Astronomía y Astrofísica, Universidad Católica de Chile, Vicuña Mackenna 4860, Casilla 306, Santiago, Chile
npadilla@astro.puc.cl

Summary. We present results from three recent works, one on the shapes of groups in the 2dFGRS and SDSS catalogues [5], and the others on the dynamics around clusters and groups of galaxies, in a theoretical framework [6] and from observational data [1]. Our results for the shapes of groups of galaxies indicate that more massive groups are more elongated than less massive groups, in accordance with expectations from cosmological numerical simulations and in contrast with previous observational results for the 2dFGRS groups [7]. As for the dynamics around groups, the results from numerical simulations indicate that more massive groups show much higher infall velocities than low mass groups, by up to a factor of 10, reaching infall velocities as high as 1000km/s. We also find important differences in the infall velocities of simulation particles lying in different environments indicating that particles in filaments (higher local density) show a larger infall toward the group centres [6]. On the observational side, we develop and apply a novel method for measuring the infall of galaxies towards groups, using the peculiar velocity data from the SFI catalogue [2] and the UZC groups [4]. Our observational results allow us to find larger infall velocities for more luminous, or equivalently, more massive groups, in agreement with our studies of infall velocities in numerical simulations [1].

1 Shapes of haloes

Cluster and groups of galaxies provide invaluable information on the formation and evolution of structure in the Universe. These systems, also denominated haloes, represent the largest gravitationally bound systems in the universe. It has been shown that these systems are mildly aspherical with orientations related to the surrounding structures such as filaments and large scale walls as shown by [3] (see also references therein), who combined large volume and high resolution simulations, to find a systematic trend with halo shape: a larger ratio of minor to major semi-axes is obtained when larger halo masses are considered.

On the observational side, [7] find a trend of shape with cluster size that is opposite to that seen in simulations [3]. From 1168 groups in the UZC-SSRS2 galaxy group catalogue, Plionis et al. concluded that poor groups are more elongated than rich ones, with 85% of poor groups having a projected semi-axis ratio lower than 0.4.

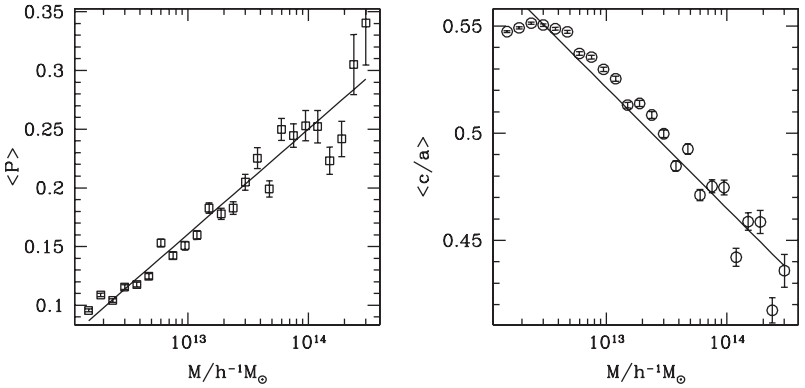

Fig. 1. Triaxiality parameter P, and c/a ratios as a function of halo mass (symbols in left and right panels respectively). The lines show the best fitting log-linear relations to the measurements from the numerical simulation (Equations 1 and 2). Figure from [5].

Our results are shown in Figure 1 (extracted from [5]) where it can be seen that the halos in the numerical simulation tend to be more prolate as the halo mass increases (both shown by the triaxiality parameter P and the minor to major axis ratio c/a). This can also be detected by means of another statistical parameter; the projected semi-axis ratios b/a show a clear decrement with halo mass. The relations that describe the log-linear fits in the figure correspond to

$$\langle c/a \rangle = -(0.056 \pm 0.003) \log_{10}(M) + (0.70 \pm 0.01), \tag{1}$$

$$\langle P \rangle = (0.089 \pm 0.005) \log_{10}(M) - (0.11 \pm 0.01). \tag{2}$$

In Paz et al., we also demonstrated that low number statistics tend to bias the measured shapes toward oblate shapes. Performing a Monte-Carlo analysis, we show that the smaller semi-axes are more affected by noise, and consequently, prolate shapes, characterised by two small semi-axes, are more distorted.

On the observational side, we take into account our result from numerical simulations on the important systematic effects produced by the use of different numbers of tracers per dark matter halo [5]. When this effect is not taken into account, our results are consistent with those of [7]; however, Figure 2 shows the results by considering a fixed number of members per group. As can be seen, the trend of 2dFGRS group shapes is of rounder objects for higher group masses, in agreement with the numerical simulation results.

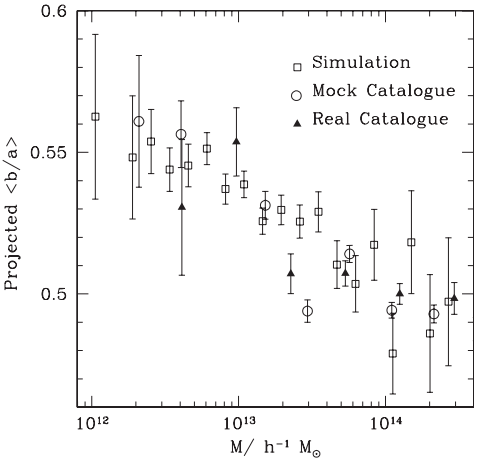

Fig. 2. Dependence of average b/a ratios as a function of mass for haloes from the numerical simulation (circles), groups from the 2PIGG mock and real catalogues (squares and triangles, respectively). In all cases, only 10 randomly selected group members were used when calculating the projected group shape. Figure from [5].

2 Galaxy flows around groups and clusters

The large-scale velocity field provides a significant source of information on the distribution of mass fluctuations in the Universe. Moreover, the relation between peculiar velocities and mass is simple, providing a direct indication of the distribution of mass independent of assumptions about the bias factor of different galaxy types.

Here we summarise the simulation results on infall of dark-matter particles towards massive haloes we presented in [6]. Our main results, shown in Figure 3, indicate that more massive haloes induce much higher infall velocities than low mass haloes, as expected qualitatively from linear theory. More interestingly, the marked difference in infall amplitudes for dark-matter particles embedded in different environmental densities indicates that the flows toward halo centres occur preferentially in filaments (higher densities than average).

Obtaining the infall velocities of galaxies toward groups using real data is somewhat difficult. In [1], we developed a method for directly measuring it using peculiar velocity data and galaxy group catalogues. In this case, the use of a mock catalogue was necessary to ensure that the method provided reasonably accurate results. The method consists on measuring the average deprojected radial infall velocity toward group centres (from the UZC catalogue compiled by [4]) from peculiar velocities (extracted from the SFI peculiar velocities, [2]). In Ceccarelli et al. we find reasonable agreement between the results of mock catalogues and the underlying numerical simulation, indicating that the method is viable. When applied to real data, our results are

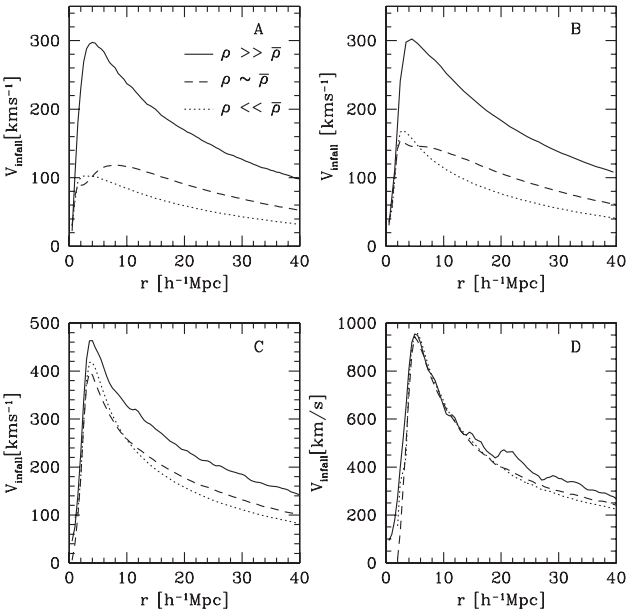

Fig. 3. Mean infall velocity as a function of scale. Halo samples correspond to S1, S2, S3 and S4, and are defined in Table 1 (panels A, B, C and D). The different lines show the average infall patterns of particles in regions with density $\rho \gg \bar{\rho}$ (solid line), $\rho \sim \bar{\rho}$ (dashed line) and $\rho \ll \bar{\rho}$ (dotted line). Figure from [6].

Table 1. Description of our samples of dark-matter haloes corresponding to different ranges of mass and the number of groups identified.

Sample	Mass interval $[h^{-1}M_{\odot}]$	Number of groups
S1	$3.4 \times 10^{12} - 6.8 \times 10^{12}$	73509
S2	$6.8 \times 10^{12} - 6.8 \times 10^{13}$	72465
S3	$6.8 \times 10^{13} - 6.8 \times 10^{14}$	6097
S4	$> 6.8 \times 10^{14}$	92

consistent with the numerical simulation results in that more massive groups show higher infall velocities. This represents the first direct measurement of the infall of galaxies toward galaxy groups, and of the scaling between group mass and galaxy infall.

3 Conclusions

We presented recent results on the shapes of groups in the 2dFGRS and SDSS catalogues [5] and on the dynamics around clusters and groups of galaxies, both in a theoretical framework [6] and from observational data [1].

Our study of halo shapes in [5] on numerical simulations, indicates that dark-matter haloes are preferentially prolate, with a prolateness increasing with the dark-matter halo mass; this result is in good agreement with previous numerical simulation studies (e.g. [3]). When translated into a two-dimensional halo shape, more massive haloes show more elongated shapes. When analysing observational samples of groups, we also find such a trend, in very good agreement with the numerical simulations, but in clear contrast with previous observational analyses of the 2dFGRS groups [7]. We also find that this controversy is only due to a systematic effect arising from using different numbers of tracers to measure the shape of a group of galaxies [5].

We also summarise recent measurements of the dynamics around groups and clusters of galaxies, both in numerical simulations and in observations. The results from numerical simulations we presented in Pivato, Padilla & Lambas, indicate that more massive groups show much higher infall velocities than low mass groups, by up to a factor of 10, reaching infall velocities as high as 1000km/s. They also find important differences in the infall velocities of simulation particles lying in different environments which indicate that particles in filaments (higher local densities) show a larger infall toward the group centres. On the observational side, we developed and applied a novel method for measuring the infall of galaxies toward groups in [1], using the peculiar velocity data from the SFI catalogue [2] and the UZC groups [4]. These observational results show larger infall velocities for more luminous, or equivalently, more massive groups, in agreement with the numerical simulation results, and the hierarchical clustering scenario.

References

1. L. Ceccarelli, C. Valotto, D. Lambas, N. Padilla, et al.: ApJ, 622, 853 (2005)
2. R. Giovanelli, M. Haynes: ApJ, 571, L107 (2002)
3. S. Kasun, A. Evrard: ApJ in press, astro-ph/0408056 (2005)
4. M. Merchán, M. Maia, D. Lambas: ApJ, 544, 2 (2000)
5. D. Paz, D. Lambas, N. Padilla, M. Merchán: MNRAS, 366, 1503 (2006)
6. M. Pivato, N. Padilla, D. Lambas: submitted to MNRAS, astro-ph/0512160 (2005)
7. M. Plionis, S. Basilakos, H. Tovmassian: MNRAS, 352, 1323 (2004)

Infrared Surface Brightness Analysis of Galaxies in Compact Groups

I. Plauchu-Frayn, R. Coziol and H. Bravo-Alfaro

Departamento de Astronomía, Universidad de Guanajuato, Apdo. Postal 144, 36000 Guanajuato, México
plauchuf@astro.ugto.mx, rcoziol@astro.ugto.mx, hector@astro.ugto.mx

Observations were carried out during seven nights at the 2.12m telescope of the Observatorio Astronómico Nacional, located in Baja Califormia, México. The images were obtained with the NIR Camera CAMILA using J and K' filters for seven groups (Plauchu-Frayn et al. 2006).

Our analysis follows the method described in Barth et al. (1995). We used the program ELLIPSE in IRAF to fit ellipses to NIR isophotes. The program yields the ellipticity, position angle and variation of ellipticity through the higher-order harmonics a4 and b4. Strong deviations from ellipticity and of position angle indicate inhomogeneous mass distributions related to tidal interactions (plumes and tail), mergers, bars or presence of a companion.

In general, the level of perturbation (a4) is well correlated with the level of activity. The trends observed seem to follow the spectroscopic classification found by Coziol et al. (2004): the level of perturbation decreases from A to B to C. The CGs of types A and B look much less "evolved" than those of type C, which suggests they formed more recently.

The lack of perturbation in HCG 74 may suggest the galaxies are located in deeper potential wells, which would be consistent with the high velocity dispersion of the group. This is as expected if they are the results of past mergers, also consistent with the earlier morphological types and absence of gas. However, our analysis does not exclude the possibility of an ongoing merger phase, only that interactions need more time to produce visible perturbations. Alternatively, massive systems are expected to form first in more massive dark matter haloes, and the galaxies could thus be in equilibrium. More observations of CGs of this type will be necessary to distinguish between the two possibilities.

References

1. C. S. Barth, R. Coziol and S. Demers: MNRAS **276**, 1224 (1995)
2. R. Coziol, E. Brinks and H. Bravo-Alfaro: AJ **128**, 68 (2004)
3. I. Plauchu-Frayn et al. 2006 in preparation

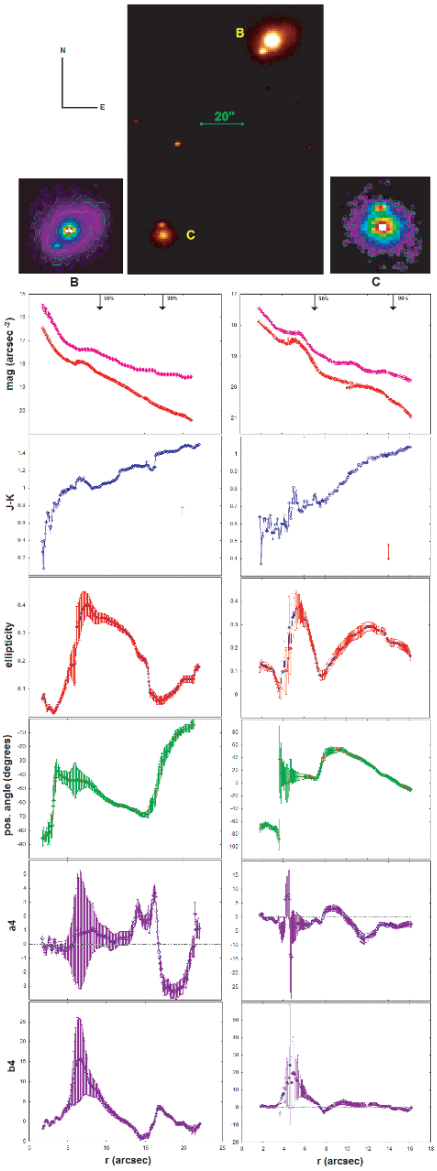

Fig. 1. One example of our analysis: members b y c of HCG88 (type A) in J band and two of its members (b and c) in false colours and isophotes. The green line indicates the image scale. From top to bottom we plot the surface brightness, colour index and geometrical parameters: ellipticity, position angle and harmonics a4 y b4, as a function of the semimajor axis length r. The 50% (R50) and 90% (R90) isophotal radii are also indicated. Both b and c show signs of merger with a small companion within R90 and R50, respectively. In the c member, the high level of perturbations is correlated with a strong starburst activity. Both members also present strong perturbations beyond R90 due to star formation in the disks.

Size and Orientation of the 'Z' in ZRGs

C. Zier

Raman Research Institute, Bangalore (India)
chzier@rri.res.in

1 Introduction

X-shaped radio galaxies (XRGs) form a small subclass of radio galaxies with two misaligned pairs of radio lobes and radio luminosities close to the FR I/II transition. Assuming that the jets are aligned with the spin of the black hole (BH) at their origin these sources can be explained by rapid realignment of the jet: The coalescence of a supermassive black hole binary (BHB), a product of a galaxy merger, quickly realigns the jet ($\lesssim 10^7$ yr), with the spin of the merged black hole being dominated by the orbital angular momentum of the BHB [3, 4, 5, 1]. In at least two XRGs (NGC 326 and 3C 52) the ridges of the secondary lobes have been observed to be offset from each other laterally by about their width, hence showing a Z-shaped symmetry about the nucleus. As the galaxy merger proceeds and the captured galaxy spirals to the common center it induces a rotational stream-field in the ISM on large scales. If its trajectory passes through the polar regions of the primary galaxy, the ram pressure of the rotating ISM bends the original jet into Z-shape [2].

2 Deprojection of ZRGs and results

Because the pre-merger spin of the primary BH and the orbital angular momentum of the merging BHB are not correlated the distribution of the angle between them is $\propto \sin\theta_{\rm jet}$, peaking at 90°. Since the post-merger spin is dominated by the orbital angular momentum, the angle between pre- and post-merger jet follows the same distribution. This corresponds to the requirement that in Z-shaped radio galaxies (ZRGs) the secondary's trajectory passes through the polar regions of the primary galaxy. Spiralling inwards the ram pressure of the rotating ISM balances that of the jet in a distance r and the jet, with a power close to the FR I/II transition, will be bent into a Z-shape.

With the observed projected lateral offset of the ridges $y_{\rm p}$ in the known distance D of the galaxy we can determine the angle $\theta_{\rm jet}$ between the pre- and post-merger jets in dependence on the bending radius r and the angle $\theta_{\rm los}$ between our line of sight (LOS) and the post-merger jet. There are three possible orientations of the jets and the LOS relative to each other. The

requirement of $\theta_{\rm jet}$ and $\theta_{\rm los}$ to be large ($\gtrsim 60°$) imposes certain limits on the bending radius: Only for $r \gtrsim y_{\rm p}/2$ first the orientation with both, the LOS and the receding part of the pre-merger jet in the same hemisphere, which is defind by the post-merger jet as polar axis, becomes possible. At $r \approx y_{\rm p}\sqrt{3}/2$ also both other orientations enter the region of allowed angles, but are less likely. For NGC 326 and 3C 52 we obtain the limiting radii 10, 17 kpc and 25, 43 kpc respectively [6]. This result, based on geometrical arguments only, is consistent with the location of ∼50 kpc where the ram pressure of a FR I/II-jet equates that of the rotating ISM. The peoperties of the gas stream which are required to bend the jet in Z-shape ($M \approx 10^9\,M_\odot, v \approx 200\,{\rm km/s}, r \approx$ 30–100 kpc) are also in very good agreement with observations and numerical simulations of galaxy mergers (see references in [6]).

3 Discussion and conclusions

Our results strongly support to the merger model for XRGs, and ZRGs as a special subclass with $\theta_{\rm jet} \approx 90°$. They also strengthen the conjecture that a jet is aligned with the spin of the BH at its base and that the jet flips into the direction of the orbital angular momentum of the pre-merger BHB. We also could restrict the bending radius to the range 30–100 kpc. Another important result is that most likely the LOS and the receding part of the pre-merger jet are in the same hemisphere whose polar axis is defined by the post-merger jet. Knowing the correct orientation we also know the sense of rotation and consequently the direction of the spin of the post-merger BH. These conclusions have also an important impact on the conjecture favoured by some authors that after a merger of two galaxies the decay of the BHB stalls due to the depletion of the so-called loss cone. In contradiction the existence of XRGs and ZRGs proves that the binary has merged. In ZRGs it probably merges on timescales of some 10^8 yr after the bending of the jet in a distance of about 50 kpc. Thus, in a way, the bending starts a stop watch for the rest of the merger. For figures and detailed calculations see [6].

References

1. M. Chirvasa: MA Thesis, University of Bukarest, Bukarest (2002)
2. Gopal-Krishna, P. L. Biermann & P. J. Wiita: ApJ **594**, 103 (2003)
3. H. Rottmann: PhD Thesis, Bonn University, Bonn (2001)
4. C. Zier & P. L. Biermann: A&A **377**, 23 (2001)
5. C. Zier & P. L. Biermann: A&A **396**, 91 (2002)
6. C. Zier: MNRAS **364**, 583 (2005)

IMF Model Sampling and the Emission Lines in Star Forming Galaxies

G. Magris C.[1], F. Molina[1,2] and A. Parravano[2]

[1] Centro de Investigaciones de Astronomía (CIDA), Apdo. Postal 264, Mérida, Venezuela
magris@cida.ve, fmolina@cida.ve

[2] Facultad de Ciencias, Universidad de Los Andes, La Hechicera, Mérida, Venezuela
parravan@ula.ve

Summary. We present a model for the H II emission line spectrum in galaxies, where the initial stellar mass distribution is calculated as a function of the cluster size, allowing a stochastic dispersion around a preselected initial mass function. This translates in an upper mass limit cutoff in the resulting initial mass distribution that depends on the size of cluster. We obtain the Hα, Hβ, [O II]λ3727 and [O III]λ5007 luminosities and we compare them with the results of previous models.

1 Introduction

With the exception of the closer galaxies, for which is possible to resolve individual H II regions, present-day observations allow us only to obtain the integrated spectrum of all H II regions present in individual galaxies (superimposed to the stellar and other non-stellar components). Conventional models assume an equivalent H II region that represents the global emission of the galaxy [4], [3], [7]. In this work we explore the impact of including a size distribution of H II regions, as is suggested by the Hα luminosity function of a sample of nearby galaxies [5], in the integrated galaxy spectrum.

2 Model and results

We assume that star formation occurs in individual clusters of variable size, N, following an universal powerlaw distribution: $\mathrm{n}(N) \propto N^{-\alpha}$, and that in each cluster of N stars ($m \geq 8$ M$_\odot$), the stellar masses are distributed with the [9] IMF: $\phi(m)dm \propto m^{-2.35}$, with 8 M$_\odot \leq m \leq$ 120 M$_\odot$ (see [6], and [8]). Additionally, we use a Monte Carlo approach, allowing fluctuations around these distributions. The main results are: 1) many stellar clusters have only low mass stars, and 2) only in large clusters the most massive star is near the upper limit of 120 M$_\odot$. We calculate the time evolution of the H and He ionizing photons for each star inside each new born stellar cluster. We assume

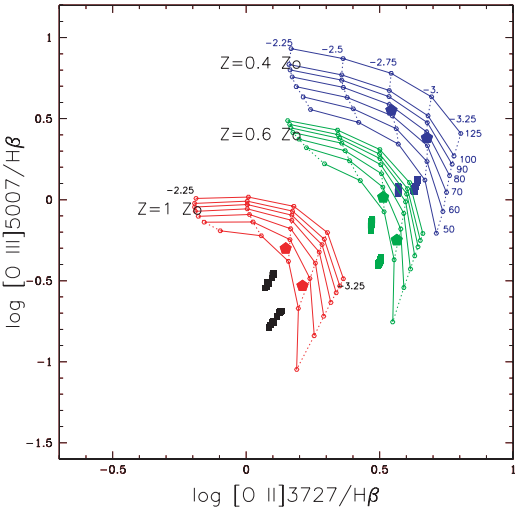

Fig. 1.

that each generation of high mass stars has an associated H II region that last for a maximum of 10 million years. We use the stellar evolutionary tracks and the atmosphere models compiled by [2]. We calculate the emission line luminosities using the photoionization code MAPPINGS I [1] and follow its evolution in time. The total emission line luminosity is obtained by adding the luminosity of all simultaneously living H II regions at the sampling time. We use the stellar track corresponding to the metal abundance of the gas phase. Figure 1 shows, in the [O II]/Hβ, [O III]/β diagnostic diagram, the results of this model, compared to the result of the [7] conventional model. The theoretical grids correspond to [7] H II regions models calculated with the labeled ionization parameter log U, and m_{up}, the upper stellar mass limit in the IMF. Each group is for the indicated metallicity. The pentagon is for the integrated galaxy model with a continuous star formation rate of the same metallicity and U, as the underlying grid. After 10^7 yr, a steady population of stars is established with an ionizing spectrum characterized by the indicated m_{up}. The set of squares indicates the Montecarlo simulation for the present model. We can see that the [O II]/Hβ, [O III]/Hβ line ratios are diminished with respect to the value predicted by conventional models, and hence, the abundance derived from these ratios is overestimated. It can be showed that the ([O II]+[O III])/Hβ ratio predicts an oxygen over-abundance of approximately 15 % if the correct sampling of the IMF is not taken into account.

References

1. L. Binette, M.A. Dopita, I.R. Tuhoy: ApJ. **297**, 476 (1985)
2. G. Bruzual A., S. Charlot: MNRAS. **344**, 1000 (2003)
3. S. Charlot, M. Longhetti: MNRAS. **323**, 887 (2001)
4. M.L. García-Vargas, R.S. Sutherland, A.I. Díaz: A&AS. **112**, 13 (1995)
5. R.C. Kennicutt, B.K. Edgar, P.W. Hodge: ApJ. **337**, 761 (1989)
6. C.F. McKee, J.P. Williams: ApJ. **476**, 144 (1997)
7. G. Magris C., L. Binette, G. Bruzual A.: ApJS. **149**, 313 (2003)
8. A. Parravano, D.J. Hollenbach, C.F. McKee: ApJ. **584**, 797 (2003)
9. E.E. Salpeter: ApJ. **121**, 161 (1955)

The Evolution of Galaxy Groups and of Galaxies Therein

G.A. Mamon

IAP, 98 bis Bd Arago, F–75014, Paris, France
gam@iap.fr

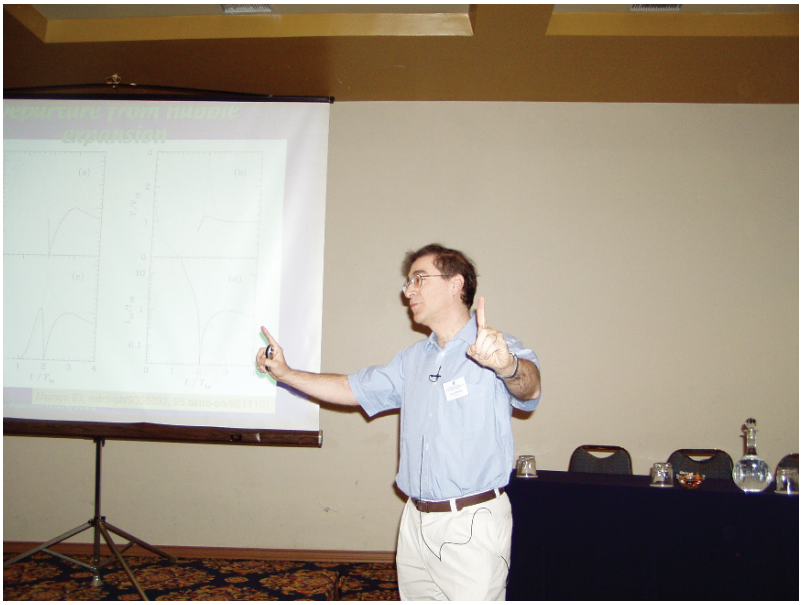

Summary. Properties of groups of galaxies depend sensitively on the algorithm for group selection, and even the most recent catalogs of groups built from redshift-space selection should suffer from projections and inclusion of infalling galaxies. The cosmo-dynamical evolution of groups from initial Hubble expansion to collapse and virialization leads to a fundamental track in virial-theorem estimated M/L vs crossing time. The increased rates of mergers, both direct and after orbital decay by dynamical friction, in (low velocity dispersion) groups relative to clusters, explain the higher fraction of elliptical galaxies at given local number density in X-ray selected groups, relative to clusters, even when the hierarchical evolution of groups is considered. Galaxies falling into groups and clusters should later travel outwards to typically 2 virial radii, which is close to but somewhat less than the outermost radius where galaxy star formation efficiencies are observed to be enhanced relative

Table 1. Typical scales of groups

	$\log M_{200}$ ($M_\odot$)	r_{200} (Mpc)	$r_{\rm ta}$ (Mpc)	σ_v (km s^{-1})	kT (keV)
Minimum	12.5	0.3	1.1	140	0.2
Maximum	14.0	1.0	3.4	450	2

to field galaxies of same morphological type. An ongoing analysis of the internal kinematics of X-ray selected groups suggests that the radial profiles of line of sight velocity dispersion are consistent with isotropic NFW distributions for the total mass density, with higher concentrations in massive groups than ΛCDM predictions and lower concentrations in low mass groups. The critical mass, at $M_{200} \approx 10^{13} M_\odot$ is consistent with possible breaks in the X-ray luminosity-temperature and Fundamental Plane relations. The internal kinematics of groups indicate that the $M - T$ relation of groups should agree with that extrapolated from clusters with no break at the group scale. The analyses of observed velocity dispersion profiles and of the fundamental track both suggest that low velocity dispersion groups (compact and loose, X-ray emitting or undetected) are quite contaminated by chance projections.

1 Introduction

The attractive nature of gravity tends to assemble galaxies together in groups. With typical grouping algorithms, roughly half of all galaxies reside in groups. A smaller fraction of galaxies live in virialized groups of at least 4 bright galaxies, and a considerably smaller fraction live in the more massive virialized clusters.

Given typical scaling relations, defining the virial radius of groups where the mean density is 200 times the critical density of the Universe, groups of galaxies have ranges of mass within the virial radius, virial and turnaround radii (all assuming $H_0 = 70\,{\rm km\,s^{-1}\,Mpc^{-1}}$), velocity dispersion and temperature shown in Table 1. More massive objects can be called clusters. Of course, the limiting mass between groups and clusters is arbitrary and historical. The more massive groups have properties (e.g. $L_X - T$ [1] and Fundamental Plane [2] relations) expected from the extrapolation of clusters, while the less massive groups do not appear to follow such extrapolations, with the separation between massive cluster-like and low mass groups occurring at $M_{200} \approx 10^{13}\,M_\odot$.

Groups of galaxies thus provide an important laboratory to understand how the density of the environment affects the properties of galaxies. In turn, the modulation with environment of galaxy properties serves as an important constraint for (semi-)analytical models of galaxy formation.

This review focusses on several dynamical and cosmological aspects of the evolution of groups and of their constituent galaxies.

2 The evolution of groups

2.1 Group expansion, collapse and virialization

Groups are difficult to define from galaxy catalogs, because the selection of nearby galaxies in redshift space causes frequent interlopers and spurious groups [3, 4] (also Eke, at this meeting). This problem of interlopers and spurious groups is probably worsened by the use of the Friends of Friends grouping algorithm, which tends to produce filamentary structures when there are less than a dozen objects (it would be worthwhile to compare the efficiency of the Friends-of-Friends algorithm with other grouping methods, based upon cosmological simulations).

While virialized structures in a ΛCDM Universe with $\Omega_m = 0.24$ [5] have a mean density $\Delta = 384$ [6] times the mean density of the Universe, i.e. 94 times the critical density of the Universe, groups have been selected in the past with Friends-of-Friends linking lengths corresponding to an overdensity of only 20 [7] or 80 [8, 9, 10]. In comparison, the mean density at the turnaround radius in a ΛCDM Universe with $\Omega_m = 0.24$ is 14 times that of the Universe (Mamon, in preparation). Overdensities of 80 relative to the mean Universe density thus roughly correspond to the geometric mean between the virial and turnaround radii, and thus, *in most catalogs, group galaxies are selected out to the region of rapid infall, and the infalling galaxies bias the group definition, mass estimate and properties*. Given very large galaxy samples, such as SDSS, group selection should be done at $\Delta = 384$.

In the extreme, all galaxies of a selected group could be in the infalling region. The departure of such a group from virialization has an important effect on the derived virial mass of the system [11, 12, 13]. Indeed, while it is difficult to compare groups of different scale and cosmo-dynamical state (expansion, collapse, virialization), I had realized that the dimensionless crossing time, $R/(\sigma_v t)$, and the dimensionless mass bias, that is mass from the virial theorem divided by true mass, $R\sigma_v^2/(GM)$, provide a plane in which the evolution of isolated systems in an expanding Universe follow a *fundamental track* (FT), which is independent of their mass [11, 12, 13]. This track is estimated for the case of a binary system of two extended subgroups of very different masses, with no specific angular momentum. The velocity dispersion of a system can be expressed as $\sigma_v^2 = (\dot{R})^2 + (\sigma_v)^2_{\rm proper}$. The FT, shown in the left panel of Figure 1, was derived assuming that the velocity dispersion of the expanding/collapsing group is dominated by the $\dot{R}$ term, with the proper velocity dispersion dominating after the full collapse.

The left panel of Figure 1 shows that the true mass is usually severely underestimated by application of the virial theorem. During the early stages of collapse, this occurs because the velocity dispersion of the system is still low (as $\dot{R}$ is small). Near full collapse, the galaxies decouple from their dark matter halos: while the virial theorem measures the mass at the radius of the group where lie the galaxies, there is dark matter beyond that radius. The

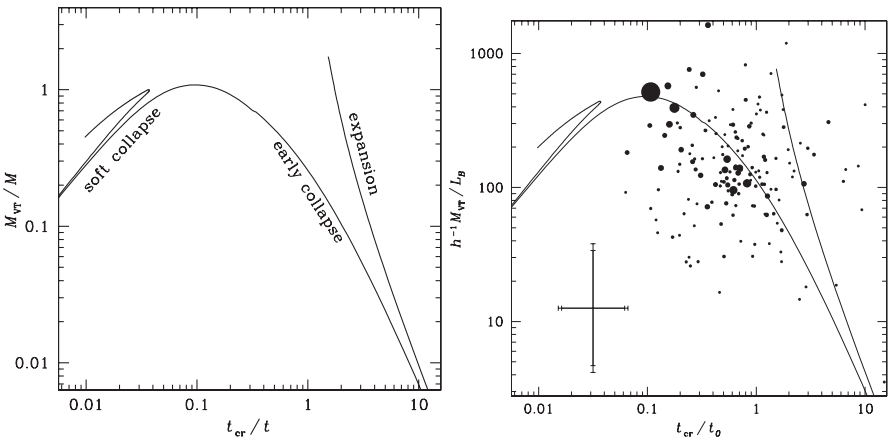

Fig. 1. Cosmo-dynamical evolution of galaxy systems (adapted from [11]). The left panel shows the theoretical evolution of an isolated binary with no specific angular momentum and small mass ratio. The right panel shows observed groups [14, 15], with increasingly larger symbols for richer groups. The *thin* and *thick error bars* are for the quartets and typical [14, 15] groups, respectively. The *largest symbol* is the Virgo cluster. The fundamental track was drawn assuming $M_{\rm true}/L_B = 440\,h$.

FT diagram (left panel of Fig. 1) also indicates that while the crossing time is to first approximation a good estimator of the cosmo-dynamical evolution of a group, it suffers from degeneracies between the expansion and early collapse phases, and also between the full collapse and rebound phases. These degeneracies can be lifted in part by combining crossing times with the virial to true mass ratio. Note that the precise evolution of a system after full collapse is not well known and probably varies from group to group, depending on the specific angular momentum of the binary.

The right panel of Figure 1 shows how observed groups relate to this FT. Since we do not know the true masses of groups, we assume, as a first order approximation that the optical luminosity of a group is proportional to its true mass. The true mass-to-light ratio is a free parameter and is fitted with the highest multiplicity groups, yielding $M_{\rm true}/L_B = 440\,h$ (where $h = H_0/\left[100\,{\rm km\,s^{-1}\,Mpc^{-1}}\right]$), while the median $M_{\rm VT}/L_B$ is 4 times smaller (because it is dominated by low multiplicity groups near turnaround).

Interestingly, *most groups lie near the fundamental track*. The large scatter for the low multiplicity groups is partly due to larger errors in estimating the plotted quantities given small numbers of galaxies, but the errors are not sufficient in explaining the large number of low-multiplicity groups well below the FT, unless these groups, either have lower $M/L_B < 440\,h$ (because of an intrinsic M/L increase with group luminosity, or because the galaxies in these particular groups are undergoing bursts of star formation), or are

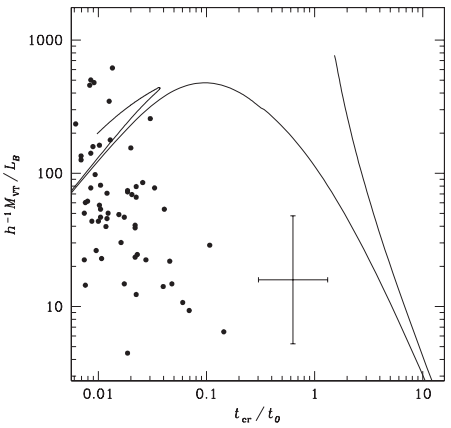

Fig. 2. Same as right panel of Figure 1, with the same $M_{\rm true}/L_B = 440\,h$, but for Hickson compact groups [16, 17]. Velocity dispersion increases from lower right to upper left.

caused by chance alignments of galaxies along the line-of-sight (for which the group radius is underestimated, while the velocity dispersion is not).

Figure 2 displays the positions of Hickson's compact groups [16, 17] relative to the FT. The high velocity dispersion compact groups agree with the predicted FT for $M_{\rm ture}/L_B = 440\,h$, while the low velocity dispersion compact groups do not. The strong offset of the low σ_v compact groups relative to the FT can be explained either by bursts of star formation (making L_B a poor estimator of the true mass) or by chance alignments of galaxies along the line of sight within large collapsing groups [11] (for which the compact group radius is a severe underestimate of the parent group radius).

3 The evolution of galaxies in groups

3.1 The many physical processes at work

Dense environments are expected to alter the properties of galaxies. A variety of physical mechanisms are at work in groups and clusters: basically gravitational and hydrodynamical. We highlight below those processes that alter the morphologies, gas content (and briefly star formation efficiency) of galaxies in groups.

Major galaxy mergers drastically alter the galaxy morphologies, destroying the disks of spirals galaxies and producing a merger remnant that resembles an elliptical galaxy, not only in its surface brightness profile [18], but in the details of its internal kinematics [19]. Minor mergers are expected to build up the bulges of spirals at the expense of their disks [20]. But repeated minor mergers can have the effect of a single major merger [20]. Similarly, repeated minor encounters (merging or not) will "harass" a galaxy enough

to substantially transform it [21]. Rapid non-merging encounters also play an important role: the tidal force at closest approach (pericenter) produces a quadrupolar perturbation on the shape of the galaxy, and in extreme cases does the same on its giant molecular clouds. The latter tidal force thus accelerates star formation, while the former can help gas fall into the galaxy core, thus driving an episode of active galactic nucleus (AGN) [22]. In addition to these collisional tides, the galaxy is affected by the mean tidal field of its cluster [23] or dense group [24], where this global tide is more efficient at altering galaxies than the tides from galaxy encounters [24]. The mean tidal field of the group or cluster does not simply limit the galaxy extent and mass, but by pumping energy into the reservoir of outer gas, it suppresses gas infall onto galaxy disks, thus severely reducing long-term star formation [25], a process often called disk strangulation.

Gas can be removed from its parent galaxy through ram pressure ($P \, \rho_e \, v^2$, where ρ_e is the gas density of the environment). This idea was first applied to colliding spiral galaxies [26], and later it became clear that the hot intracluster gas provides an important ram pressure [27]. After losing its gas, a spiral galaxy would see its disk fade and resemble a lenticular (S0) galaxy. It is not yet clear that S0s are indeed produced by ram pressure gas stripping, or are simply systems with large bulge to disk ratio. Ram pressure stripping produces the correct local and global trends in clusters [28], but cannot explain the presence of S0s in groups, where the lower velocities are unable to produce sufficiently high ram pressure [29, 30]. On the other hand, if the large bulges of S0s are built up by minor mergers, the fraction of S0s is clusters are found to be lower in semi-analytical models of galaxy formation [31] than observed. However, the inclusion of ram pressure stripping (in very simplistic schemes) does not increase enough the S0 fraction in semi-analytical models [32, 33].

The morphological segregation of galaxies in groups and clusters obviously leads to color segregation, where the redder galaxies lie in the dense central regions, but interestingly, the galaxy colors are redder for given morphological type in clusters than in the field [34], which can be simply explained by the tidal dissipation of the gas reservoirs of spirals [35].

Most of the processes listed here work best in dense environments. On the contrary, for very loose groups such as the Local Group, which are still in the collapse phase, major interactions have not yet altered the more massive galaxies. Only the low mass satellites of massive galaxies are affected by the presence of their more massive companion.

3.2 How frequently do group galaxies merge?

The merger rate per unit volume of equal mass galaxies in a group is obtained by integrating over a merger cross-section:

$$k(m) \equiv k(m,m) = \langle vS(v) \rangle = \int_0^\infty vS(v) f(v) \, dv \ , \qquad (1)$$

where $S(v) = \pi\, p_{\rm crit}^2(v)$ is the relative-velocity dependent merger cross-section and $f(v)$ is the distribution of relative velocities. For a linear $p_{\rm crit}(v)$ [36], one finds [37]

$$k = b\,\frac{r_h^2\,\sigma_g^4}{\sigma_e^3}\ , \tag{2}$$

where r_h and σ_g are the half-mass radius and (1D) velocity dispersion of the galaxies, σ_e is the velocity dispersion of the environment, and with now old cross-sections scalings [36, 38] one has $b \simeq 200$. With $\sigma_g^2 \simeq (0.4/3)\,Gm/r_h$ [39], one then gets [37]

$$k(m) = a\,\frac{G^2\,m^2}{\sigma_e^3}\ , \tag{3}$$

where $a \simeq 3.5$. The merger rate has also been derived directly [40] from fairly realistic N-body simulations of the mergers of equal mass Hernquist [41] models, and this rate is essentially identical to my analytical prediction [37], as shown in a previous review of mine [42], despite my neglect of gravitational focussing and my use of merger cross-sections based upon very primitive N-body simulations [36, 38].

In my previous review [42], I've adapted equation (2) to estimate the merger rates for unequal mass galaxies, and integrating over the mass function of field galaxies I derived a merger rate as a function of galaxy mass:

$$\frac{dN_m}{dt} = {\rm cst}\, n_*\frac{G^2 m_*^2}{\sigma_e^3}\,\mathcal{R}\left(\frac{m}{m_*}\right)\ , \tag{4}$$

where m_* and n_* are the break in the galaxy mass function and a fiducial number density, while $\mathcal{R}(m)$ is a dimensionless function of mass which, for major mergers, increases with mass, reaches a maximum near $m = m_*$ and decreases sharply for $m > m_*$. The normalization is such that m_* galaxies in typical $\sigma_v = 300\,{\rm km\,s^{-1}}$ groups should suffer a few major mergers per Hubble time [42]. I also estimated merger rates as a function of position in the group or cluster and found that the direct merger rate outside of the the central galaxy is maximum at $\simeq 0.1\,R_{200}$ [42]. An increasing number of observational constraints on the galaxy merger rate and its evolution are now arising (see Conselice in these proceedings and [43]) and need to be compared with the predictions given here.

3.3 Do we understand the morphology-density relation in groups and clusters?

The predictions above on the rates of direct mergers versus environment can be compared to the global morphological mix and its local variations (the morphology-density relation, hereafter MDR) observed in groups and clusters. While an early analysis [44] concludes to a universal MDR as a function of local galaxy density, a closer look reveals various problems with

groups of galaxies: Hickson's [16] compact groups, assumed as dense in 3D as they appear in 2D, have much higher spiral fractions than expected from the universal MDR [45]. Conversely, these compact groups are spiral-poor relative to other systems of the same velocity dispersion [46], but with a very strong inverse correlation of spiral fraction and velocity dispersion [47], also seen in general SDSS groups [48].

Recently, Helsdon & Ponman [30] compared the local morphological mix of their sample of X-ray emitting groups to that of clusters [49]. After statistical correction for projections, X-ray emitting groups appear to be spiral-poor relative to clusters of the same local 3D density, by an amount just as expected from the σ_e^{-3} scaling of equations (2) and (3) [30]. In other words, the true groups, as selected by their X-ray emission, have less spirals than clusters because their lower velocity dispersions lead to slow enough encounters to lead to major mergers that transform spirals into ellipticals.

This simple understanding of the MDR of groups vs clusters has 3 caveats:

1. Major mergers are probably more often the result of orbital decay by dynamical friction than of direct slow collisions. The orbital decay time scales as the dynamical friction (df) time [13], which scales as

$$\left(\frac{dN_m}{dt}\right)_{\rm df} \propto \tau_{\rm df}^{-1} \propto \frac{G^2\, m\, \rho}{\sigma_e^3}\, \ln\left(\frac{M(R)}{m}\right) . \qquad (5)$$

   Comparing equations (4) and (5), one finds that the rate of direct to frictional mergers scales as $\ln(M(R)/m)/f$, where f is the mass fraction of the group/cluster in galaxies. This small (logarithmic) dependence on the mass of the environment means that *to first order, the ratio of frictional to direct mergers is independent of the environment*, with direct mergers slightly more (less) important in groups (clusters).
2. When two groups or clusters merge, violent relaxation might cause their galaxy populations to mix sufficiently to erase their MDRs. However, N-body simulations indicate that when two systems merge, there is a strong correlation between initial and final binding energies [50], so that the most bound galaxies in the initial groups or clusters, mostly ellipticals, will end up as the most bound galaxies, thus preserving the MDR.
3. Our analysis pertains to instantaneous merger rates. Since we live in a hierarchical Universe where the rich clusters today were built of smaller groups, we still need to check that the ratio of instantaneous merger rates in groups and clusters is equal to the ratio of the time-averaged merger rates in groups and clusters. But since the merger rates scales as σ_e^{-3}, hence as one over the mass of the environment, the ratio at any time between the merger rates of the main progenitors of present-day groups and clusters will scale as $M_{\rm group}(t)/M_{\rm cluster}(t)$. Since massive clusters are rare objects, they must form recently, because otherwise they would be even more extreme objects in the past. However, this effect

is not too severe: from cosmological N-body simulations and analytical predictions of the mass assembly history of cosmic systems [51], I infer that the elapsed time for the doubling in mass of (the main progenitors of) present-day groups ($z = 0.9$) is only 1/3 greater than that of present day clusters ($z = 0.4$). Therefore, the average mass ratio of the group to cluster progenitors decreases only slightly with time, so that *to first order the time averaged ratio of merger rates of group and cluster progenitors is close to the ratio of present-day merger rates.*

Therefore, none of the caveats is serious, and it does appears that *the increased rate of galaxy mergers indeed explains the larger local fractions of ellipticals in X-ray selected groups relative to clusters.*

Since compact groups in general are spiral-rich [45], while X-ray selected groups are spiral-poor [30], then *the compact groups that are not in the GEMS sample must be nearly devoid of early-type galaxies*, i.e. the spiral fractions of these groups should be as high or higher than in the average field. The non-X-ray emitting compact groups are typically low velocity dispersion groups, which as we saw, do not fit the FT, so it is tempting to conclude that *low velocity dispersion compact groups are mostly caused by chance projections.*

3.4 How far out should galaxies feel the group environment?

The decreased star formation rate for group/cluster galaxies of given morphological type is visible out to $2\,r_{200}$ [34], i.e. $\approx 2.6\,r_{100}$. Regardless of whether the mass assembly of groups and clusters is viewed in a monolithic spherical infall context or in a hierarchical merging one, the effects of the group/cluster on the galaxies should thus be seen out to the maximum *rebound* or *backsplash* radius. If this radius is assimilated to the radius of mixing in the spherical infall model, one finds $r_{\rm reb} \approx r_{\rm vir}$ [52]. If one assumes values for the ratio of the (lagrangian) rebound to turnaround radius (e.g. 1/2), and for the corresponding ratio of rebound to turnaround times (e.g. 3/2), one can solve in the context of a flat Universe with a cosmological constant for the rebound radius, and we find $r_{\rm reb}/r_{100} \approx 1$ with a maximum of 2.5 for the most favorable case (rebound radius equals turnaround radius and rebound time equals twice the turnaround time) [52]. Deriving reasonable ratios from particle trajectories of an ΛCDM simulation [53], we obtain $r_{\rm reb}/r_{100}$ ranging from 0.55 to 1.25 [52]. Finally we considered the final output ($z = 0$) of a GALICS galaxy formation simulation [54] built on top of a dark matter only ΛCDM cosmological simulation, where galaxies penetrating groups and clusters are selected by empty halos (a feature of GALICS is that when halos merge, galaxies remain with the more massive halo). We then found that galaxies (empty halos) travel out to $1.7\,r_{100}$ [52]. These numbers were confirmed through an analysis of the particle trajectories in ΛCDM halos, which shows that particles that penetrate deep into their halo travel out to $2\,r_{100}$ [55] $\simeq 2.6\,r_{200}$. These maximum rebound radii are thus somewhat larger (by

30%) than the observed maximum radius for decreased star formation, but consistent this value.

4 The internal kinematics of groups

Clusters of galaxies are beginning to reveal their mass profiles, through analyses of their internal kinematics, X-ray gas or lensing properties. Kinematical analyses are often based upon the Jeans equation of hydrostatic equilibrium, relating the divergence of the anisotropic dynamical pressure tensor with the tracer density times the gradient of the gravitational potential. In spherical symmetry this becomes

$$\frac{\mathrm{d}\left(\nu\sigma_r^2\right)}{\mathrm{d}r} + 2\,\beta\,\frac{\nu\sigma_r^2}{r} = -\nu\frac{GM(r)}{r^2}\ , \tag{6}$$

where $\nu(r)$, $M(r)$ and $\beta(r)$ are the radial profiles of tracer number density, total mass, and velocity anisotropy $\beta = 1 - \sigma_\theta^2/\sigma_r^2$ (where $\beta = 1, 0$, and $\to -\infty$ corresponds to radial, isotropic and circular orbits, respectively). Since the data are seen in projection, one has to couple the Jeans equation with the anisotropic projection equation [56]

$$\Sigma(R)\,\sigma_{\rm los}^2(R) = 2\,G\int_R^\infty \left(1 - \beta\,\frac{R^2}{r^2}\right)\nu\sigma_r^2\,\frac{r\,\mathrm{d}r}{\sqrt{r^2 - R^2}}\ , \tag{7}$$

where $\Sigma(R)$ is the surface number density as a function of projected radius R, and $\sigma_{\rm los}(R)$ is the line of sight velocity dispersion profile (hereafter VDP).

For example, assuming isotropic to moderately radial orbits, the mass profile of clusters is consistent with being proportional to the galaxy number density profile [57], which itself was consistent with the cuspy NFW [58] profile. Recently, the mass-anisotropy degeneracy, inherent in the Jeans equation, was recently (partially) lifted: the early type galaxies in clusters follow isotropic orbits [59, 60], galaxy velocities are isotropic in groups and somewhat radial in clusters [61].

Andrea Biviano and I are currently performing a similar analysis for groups of galaxies, as we wish to check if various types of groups (hot vs. cold, etc.) display similar mass profiles and concentrations. For this, we use the GEMS group sample [1], which considers all groups for which there have been X-ray pointings. In this review, we focus on the groups with diffuse X-ray emission distinct from diffuse emission around the central bright elliptical.

We selected group member galaxies with NED (which at the time included the SDSS-DR4 and the 6dFGS-DR2), searching out to twice (to be conservative) a 1st-order estimate of their virial radius, r_{200} (where the mean density is 200 times the critical density of the Universe) using $r_{200}/\mathrm{Mpc} = \sigma_v/450\,\mathrm{km\,s^{-1}}$, as appropriate for pure NFW models with $c = 8$ and $H_0 = 70\,\mathrm{km\,s^{-1}\,Mpc^{-1}}$ (when $\sigma_v < 300\,\mathrm{km\,s^{-1}}$, we used $\sigma_v = 300\,\mathrm{km\,s^{-1}}$

to be conservative) and out to $\pm 5\,\sigma_v$. We then computed the velocity dispersion and iterated with a $\pm 3\,\sigma_v$ depth.

4.1 Which is the best estimator of virial radius?

Since groups have few galaxies, we need to stack them, normalizing the radii to their virial radius, r_{200} (as first done by [62]), and similarly stack their velocities to V_{200}, the circular velocity at r_{200}. We have considered several estimators of the virial radius: 1) the velocity dispersion, assuming an isotropic pure NFW model with a ΛCDM concentration parameter, σ-NFW; 2) the K-band total galaxy luminosity, taken from the 2MASS survey, corrected for incompleteness, using an $M - L_K$ relation [63]; 3) the X-ray emission-weighted temperature, using $M-T$ relations from several authors [64, 65, 66]. For each of our r_{200} estimators, we performed the interloper removal, first group per group, then on the stacked pseudo-group. We also removed a few groups contaminated by nearby groups or clusters and thse with <5 members. In the stacking, we have weighted the galaxies inversely proportional to the number of galaxies in the group out to the virial radius. This weighting gives equal weight to each group in the stacked pseudo-group.

Figure 3 compares the measured VDPs with the expectation from the isotropic Jeans equation [67]:

$$\Sigma(R)\,\sigma^2_{\rm los}(R) = 2\,G\,R\int_R^\infty \sqrt{1-\frac{R^2}{r^2}}\,\nu(r)\,M(r)\,\frac{{\rm d}r}{r}\ . \tag{8}$$

We are also investigating other simple anisotropy profiles for which the term in the square root is replaced by other kernels given by [68], and alternatively, we are directly estimating the mass profile for given anisotropy profiles using the recently discovered mass inversion technique [69].

The Sanderson et al. [65] $M-T$ relation, which predicts lower mass groups than when extrapolated from cluster $M - T$ relations, appears inconsistent with isotropic NFW models, as the virial radius and velocity dispersion appear to be overestimated by a factor 1.3, i.e. the mass is a factor of 2 higher than predicted from their $M - T$ relation. A maximum likelihood analysis at β = cst suggests that the Sanderson et al. $M - T$ relation can only be reconciled with a highly concentrated ($c \approx 100$) and tangentially anisotropic ($\beta \approx -2$) system. On the other hand, the virial radii built upon $M - T$ relations derived for hot clusters [66] or cosmological simulations [64] produce velocity dispersion profiles that are consistent with isotropic NFW models. Therefore, *the $M - T$ relation of groups of galaxies appears to lie in the extrapolation of that of clusters*, with no break at $\approx 10^{13} M_\odot$.

4.2 Constraints on group mass profiles

We have subdivided the G groups into subclasses according to their velocity dispersion, σ_v, temperature, T, ratio of galaxy orbital to gas thermal

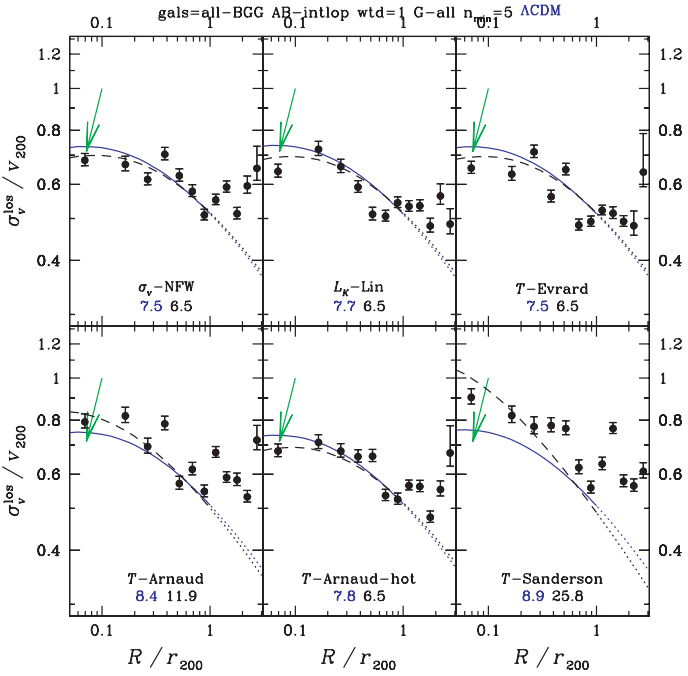

Fig. 3. Line-of-sight velocity dispersion profiles for GEMS groups with diffuse emission, drawn for 6 samples stacked using different methods for estimating the virial radius. The curves are the predictions (eq. [8]) for isotropic systems with NFW profiles: total mass and number number densities following ΛCDM predictions (*solid/blue*), as well as different NFW fits to total mass and number density profiles (*dashed/black*). The *dotted curves* show the extrapolations beyond the last fitted radius ($R = r_{200}$). The *arrows* indicate the effect of underestimating the virial radius by a factor 1.4. The *labels* at the bottom indicate the method to estimate r_{200}, where T-Arnaud-hot refers to the fit to the hotter clusters of the Arnaud et al. sample. The *numbers under the labels* indicate the concentration parameters for the ΛCDM model and the best NFW fit to the total mass density.

energies $\beta_{\rm spec} = \sigma_v^2/(kT/\mu m_p)$, X-ray luminosity, L_X and K-band luminosity, L_K. Figure 4 shows plots analogous to those in Figure 3, but when the sample is subdivided into dynamically hot ($\sigma_v > 300\,{\rm km\,s^{-1}}$) and cold ($\sigma_v \leq 300\,{\rm km\,s^{-1}}$) groups. Regardless of the method used to estimate r_{200}, *the dynamically hot (cold) groups are always more (less) concentrated in total mass than the ΛCDM prediction for isotropic orbits*. While clusters of galaxies display mass concentrations that are consistent with the ΛCDM predictions [66] using X-rays and [70, 59, 60, 71] using internal kinematics), the richer (high velocity dispersion) groups appear to be more concentrated than ΛCDM predictions, while the poorer (low velocity dispersion) groups appear to be less concentrated than ΛCDM predictions. The high concentrations of

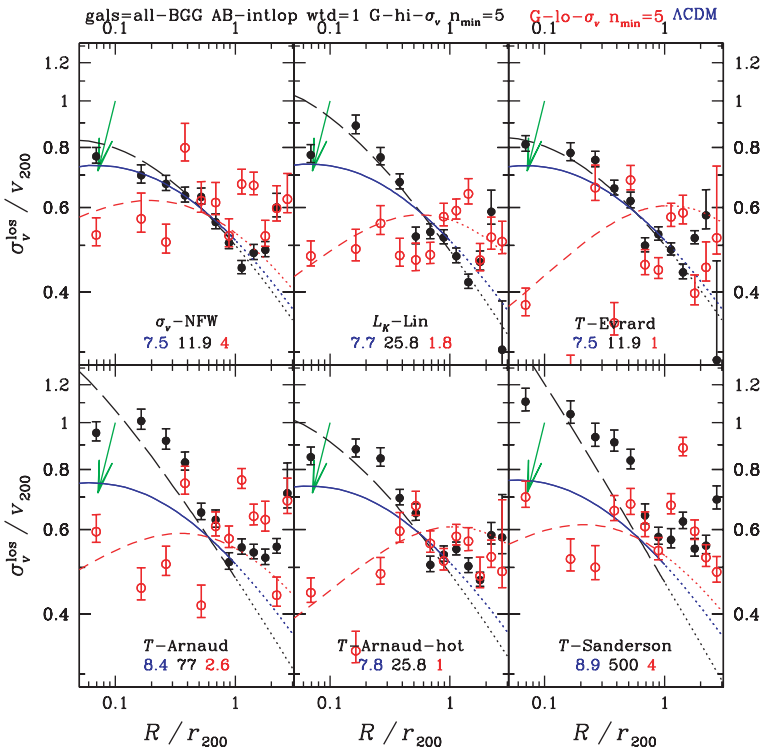

Fig. 4. Same as Figure 3, with *long-dashed (black)* and *short-dashed (red) curves* displaying the fits for the dynamical hot ($\sigma_v > 300\,\mathrm{km\,s^{-1}}$) and cold ($\sigma_v \leq 300\,\mathrm{km\,s^{-1}}$) groups. The *three numbers under the labels* give the NFW concentration parameters for the ΛCDM model as well as the best fit to the total mass density profiles of the dynamical hot and cold groups, respectively.

the hot groups are caused in part by fitting the total mass density profile, while the more concentrated baryonic (Sérsic) component gives the illusion of high total mass concentrations [72]. Note that the galaxy distribution is even more concentrated, leading to rising mass over number ratio, consistent with what was derived on an optically selected sample [62]. Alternatively, hot (cold) groups could have ΛCDM mass profiles, with radial (tangential) galaxy orbits. Finally, the strong scatter in the VDPs of the dynamically cold groups suggests that *dynamically cold groups are contaminated by unreal groups.*

There are also strong differences between groups with high and low β_{spec}, and X-ray luminosity, but smaller differences when subdividing groups into classes of high and low X-ray temperature or K-band luminosity.

4.3 The fundamental track of groups selected to the virial radius

Figure 5 shows the FT of GEMS groups, which were selected out to the virial radius, here defined with the L_K luminosity. The rich groups cluster

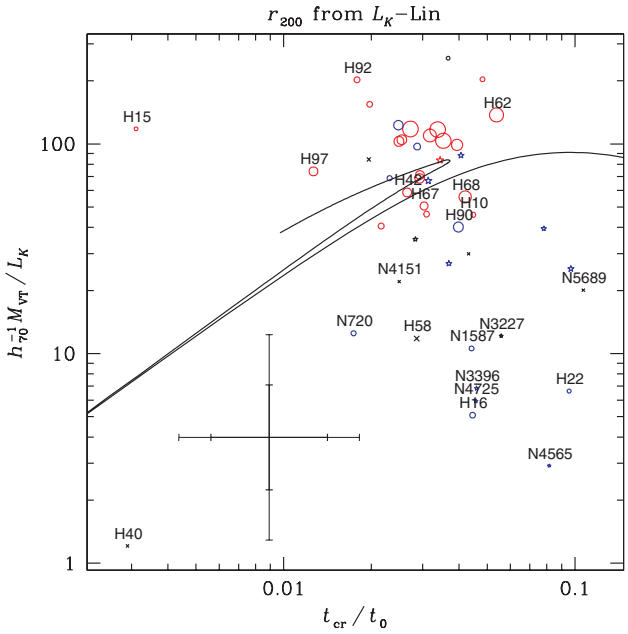

Fig. 5. Same as right panel of Figure 1, for GEMS groups selected out to the virial radius (defined with the K-band luminosity [63]). The *open symbols*, *stars* and *crosses* indicate the GEMS G (extended X-ray emission distinct from central galaxy emission), H (extended X-ray emission indistinguishable from that of central galaxy) and U (undetected extended X-ray emission) groups, respectively. The *red*, *blue* and *black symbols* are for high (>0.5), low (≤0.5) and undefined (unavailable temperature) $\beta_{\rm spec}$, respectively. The FT was placed assuming the universal value $M/L_K = 84\,h_{70}$ as derived from the K-band luminosity density of the 6dFGS galaxies [73]. The *symbol sizes* are proportional to the square root of the number of galaxies within r_{200}. Outliers to the FT and Hickson compact groups are highlighted.

near the position expected for virialized systems (the kink of the FT at $t_{\rm cr} = 0.035\,t_0$). Interestingly, the groups that lie off the FT (at lower $M_{\rm VT}/L_K$) have typically low $\beta_{\rm spec}$, but also longer crossing times. This suggests that these low velocity dispersion groups are not simply low mass-to-light ratio systems, but that there is an intrinsic property that takes them off the FT. The simplest explanation is that *low velocity dispersion groups (compact or not) are chance alignments of galaxies along the line of sight, i.e. prolate groups in real space.*

5 Concluding thoughts

Our understanding of the evolution of groups and of galaxies therein is making rapid progress thanks to the advent of 1) large galaxy surveys such as the 2dFGRS and SDSS, 2) multi-wavelength observations of groups, and 3) high resolution cosmological N body simulations. Many of the results presented here need to be confirmed with these large data sets and simulation outputs.

I am grateful to my collaborator, Andrea Biviano, for allowing me to mention our work in progress. I also thank Ivo Saviane, Valentin Ivanov and Jordanka Borissova for organizing a very exciting and high-level meeting and for being extremely patient with the manuscript.

References

1. J.P.F. Osmond, T.J. Ponman: MNRAS **350**, 1511 (2004)
2. R. Schaeffer, S. Maurogordato, A. Cappi, F. Bernardeau: MNRAS **263**, L21 (1993)
3. B. Moore, C.S. Frenk, S.D.M. White: MNRAS **261**, 827 (1993)
4. A. Diaferio, G. Kauffmann, J.M. Colberg, S.D.M. White: MNRAS **307**, 537 (1999)
5. D.N. Spergel, R. Bean, O. Doré, et al.: ApJ submitted, arXiv:astro-ph/0603449 (2006)
6. T. Kitayama, Y. Suto: ApJ **469**, 480 (1996)
7. M.J. Geller, J.P. Huchra: ApJS **52**, 61 (1983)
8. M. Ramella, M.J. Geller, J.P. Huchra: ApJ **344**, 57 (1989)
9. M. Merchán, A. Zandivarez: MNRAS **335**, 216 (2002)
10. M.E. Merchán, A. Zandivarez: ApJ **630**, 759 (2005)
11. G.A. Mamon: Dynamical theory of groups and clusters of galaxies. In: *Gravitational Dynamics and the N-Body Problem*, ed by F. Combes, E. Athanassoula (Obs. de Paris, Paris 1993) pp 188–203, arXiv:astro-ph/9308032
12. G.A. Mamon: The galaxy group/cosmology connections. In: Moriond Astrophysics Mtg number 14, *Clusters of Galaxies*, ed by F. Durret, A. Mazure, S.D.M. White, J. Trânh Thanh Vân (Frontières, Gif-sur-Yvette 1994) pp 291–296, arXiv:astro-ph/9406043
13. G.A. Mamon: The dynamics of groups and clusters of galaxies and links to cosmology. In: 3rd Paris cosmology colloq, ed by H. de Vega, N. Sánchez (World Scientific, Singapore 1995) pp. 95–119, arXiv:astro-ph/9511101
14. P. Fouqué, E. Gourgoulhon, P. Chamaraux, G. Paturel: A&AS **93**, 211 (1992)
15. E. Gourgoulhon, P. Chamaraux, P. Fouqué: A&A **255**, 69 (1992)
16. P. Hickson: ApJ **255**, 382 (1982)
17. P. Hickson, C. Mendes de Oliveira, J.P. Huchra, G.G. Palumbo: ApJ **399**, 353 (1992)
18. J.E. Barnes: ApJ **331**, 699 (1988)
19. A. Dekel, F. Stoehr, G.A. Mamon, T.J. Cox, G.S. Novak, J.R. Primack: Nature **437**, 707 (2005)
20. F. Bournaud, C.J. Jog, F. Combes: A&A **437**, 69 (2005)

21. B. Moore, N. Katz, G. Lake, A. Dressler, A. Oemler, Jr.: Nature **379**, 613 (1996)
22. G.G. Byrd, M.J. Valtonen, L. Valtaoja, B. Sundelius: A&A **166**, 75 (1986)
23. D. Merritt: ApJ **276**, 26 (1984)
24. G.A. Mamon: ApJ **321**, 622 (1987)
25. R.B. Larson, B.M. Tinsley, C.N. Caldwell: ApJ **237**, 692 (1980)
26. L.J. Spitzer, W. Baade: ApJ **113**, 413 (1951)
27. J.E. Gunn, J.R. Gott: ApJ **176**, 1 (1972)
28. J.M. Solanes, E. Salvador-Solé: ApJ **395**, 91 (1992)
29. A. Dressler: ApJ **301**, 35 (1986)
30. S.F. Helsdon, T.J. Ponman: MNRAS **339**, L29 (2003)
31. V. Springel, S.D.M. White, G. Tormen, G. Kauffmann: MNRAS **328**, 726 (2001)
32. T. Okamoto, M. Nagashima: ApJ **587**, 500 (2003)
33. B. Lanzoni, B. Guiderdoni, G.A. Mamon, J. Devriendt, S. Hatton: MNRAS **361**, 369 (2005)
34. M.L. Balogh, D. Schade, S.L. Morris, H.K.C. Yee, R.G. Carlberg, E. Ellingson: ApJL **504**, L75 (1998)
35. M.L. Balogh, J.F. Navarro, S.L. Morris: ApJ **540**, 113 (2000)
36. N. Roos, C.A. Norman: A&A **76**, 75 (1979)
37. G.A. Mamon: ApJL **401**, L3 (1992)
38. S.J. Aarseth, S.M. Fall: ApJ **236**, 43 (1980)
39. L. Spitzer: ApJL **158**, L139 (1969)
40. J. Makino, P. Hut: ApJ **481**, 83 (1997)
41. L. Hernquist: ApJ **356**, 359 (1990)
42. G.A. Mamon: Theory of galaxy dynamics in clusters and groups. In: 15th IAP Astrophys. Mtg., *Dynamics of Galaxies: from the Early Universe to the Present*, vol 197, ed by F. Combes, G.A. Mamon, V. Charmandaris (ASP, San Francisco 2000) pp. 377–387, arXiv:astro-ph/9911333
43. C.J. Conselice: ApJ **638**, 686 (2006)
44. M. Postman, M.J. Geller: ApJ **281**, 95 (1984)
45. G.A. Mamon: ApJ **307**, 426 (1986)
46. P. Hickson, H.J. Rood: ApJL **331**, L69 (1988)
47. P. Hickson, E. Kindl, J.P. Huchra: ApJ **331**, 64 (1988)
48. S.M. Weinmann, F.C. van den Bosch, X. Yang, H.J. Mo: MNRAS **366**, 2 (2006)
49. A. Dressler, A.J. Oemler, W.J. Couch, et al.: ApJ **490**, 577 (1997)
50. J.E. Barnes: ApJ **393**, 484 (1992)
51. F.C. van den Bosch: MNRAS **331**, 98 (2002)
52. G.A. Mamon, T. Sanchis, E. Salvador-Solé, J.M. Solanes: A&A **414**, 445 (2004)
53. T. Fukushige, J. Makino: ApJ **557**, 533 (2001)
54. S. Hatton, J. Devriendt, S. Ninin, F.R. Bouchet, B. Guiderdoni, D. Vibert: MNRAS **343**, 75 (2003)
55. S.P.D. Gill, A. Knebe, B.K. Gibson: MNRAS **356**, 1327 (2005)
56. J. Binney, G.A. Mamon: MNRAS **200**, 361 (1982)
57. R.G. Carlberg, H.K.C. Yee, E. Ellingson: ApJ **478**, 462 (1997)
58. J.F. Navarro, C.S. Frenk, S.D.M. White: ApJ **462**, 563 (1996)
59. E.L. Łokas, G.A. Mamon: MNRAS **343**, 401 (2003)
60. P. Katgert, A. Biviano, A. Mazure: ApJ **600**, 657 (2004)
61. A. Mahdavi, M.J. Geller: ApJ **607**, 202 (2004)

62. R.G. Carlberg, H.K.C. Yee, S.L. Morris, et al.: ApJ **552**, 427 (2001)
63. Y.T. Lin, J.J. Mohr, S.A. Stanford: ApJ **591**, 749 (2003)
64. A.E. Evrard, C.A. Metzler, J.F. Navarro: ApJ **469**, 494 (1996)
65. A.J.R. Sanderson, T.J. Ponman, A. Finoguenov, E.J. Lloyd-Davies, M. Markevitch: MNRAS **340**, 989 (2003)
66. M. Arnaud, E. Pointecouteau, G.W. Pratt: A&A **441**, 893 (2005)
67. P. Prugniel, F. Simien: A&A **321**, 111 (1997)
68. G.A. Mamon, E.L. Łokas: MNRAS **363**, 705 (2005)
69. G.A. Mamon, G. Boué: MNRAS to be submitted (2006)
70. A. Biviano, M. Girardi: ApJ **585**, 205 (2003)
71. E.L. Łokas, R. Wojtak, S. Gottlöber, G.A. Mamon, F. Prada: MNRAS **367**, 1463 (2006)
72. G.A. Mamon, E.L. Łokas: MNRAS **362**, 95 (2005)
73. D.H. Jones, B.A. Peterson, M. Colless, W. Saunders: MNRAS **369**, 25 (2006)

Diffuse Starlight and the Evolution of Groups and Clusters of Galaxies

J.C. Mihos

Case Western Reserve University, Cleveland, OH
mihos@case.edu

Summary. Using a combination of numerical simulations and observation data, I explore the use of intracluster light (ICL) as a tool to study the evolution of groups and clusters of galaxies. Groups are particularly effective at "feeding" the ICL of larger clusters, as interactions in the group environment begin to liberate tidal material, a process which is then amplified by the cluster potential. Observational surveys of galaxy clusters are beginning to reveal complex ICL structures, suggesting a connection between ICL morphology and cluster dynamical state. This complex structure is illustrated through deep wide-field imaging of the Virgo cluster, which shows an intricate web of diffuse ICL, including long tidal streams, galaxies with extended stellar halos, and groups embedded in diffuse common envelopes of light.

1 Forming intracluster light

The classic picture for the formation of intracluster light is through tidal stripping of galaxies orbiting within the potential well of a massive cluster. While this mechanism is undoubtedly at play, the hierarchical nature of cluster accretion means that other dynamical processes must contribute as well to the formation of ICL. Clusters grow not simply through the slow one-by-one addition of galaxies, but through the accretion and coalescence of smaller galaxy groups. These groups have a smaller velocity dispersion than do massive clusters, meaning that interactions on the group scale can be slow and damaging, as opposed to the impulsive high speed encounters on the cluster scale. These slow interactions can tidally strip material from the galaxies into loosely bound tidal structures, which are then easily and completely stripped into the intracluster medium when the groups coalesce or fall into a more massive cluster [6]. In this manner, interactions in the group environment act to "prime the pump" for forming ICL in more massive clusters.

Because of the complexity and interdependency of the differing processes liberating ICL (slow galaxy interactions, slow stripping by the cluster potential, heating from fast encounters, the time-dependent gravitational potential of a cluster in formation), fully self-consistent N-body simulations (e.g., [3], [8], [11], [10]) are needed in order to produce detailed, quantitative descriptions of the morphological and kinematic properties of the ICL.

Our own such simulations (see [9] and Rudick et al., this volume for more details) illustrate clearly the link between the group and cluster environments in generating intracluster light. To generate these simulations, we first run a large 50^3 Mpc^3 ΛCDM cosmological volume and select low mass ($\sim 10^{14}$ M$_\odot$) clusters at $z = 0$. We then identify galaxy scale halos ($M > 10^{11}$ M$_\odot$) at $z = 2$ which are destined to end up in the $z = 0$ cluster, and replace these halos with high-resolution spiral and elliptical galaxy models, with a spatial resolution in the stellar component of ~ 300 pc. The substituted galaxies are inserted in the dark matter halos using the HOD formalism [1], and using a morphology-density relationship to determine the spiral/elliptical mix. After galaxy insertion, the clusters are then re-simulated to $z = 0$ to study the production of their ICL.

An example of one such cluster is shown in Figure 1. At $z = 1$, galaxies in the proto-cluster have already begun interacting strongly within several distinct groups, drawing out a myriad of distinct filaments and plumes from the interacting galaxies. As the groups subsequently coalesce to form the cluster, these tidal features are dynamically heated and mix together to create a diffuse ICL halo that permeates the cluster. The models predict a clear link between the ICL and the dynamical state of the cluster – as clusters accrete and grow, the ICL should evolve from a system of distinct, relatively high surface brightness tidal features to a smoother, more diffuse ICL halo. During this process, the fraction of cluster luminosity in the ICL component increases as well, as starlight is continually stripped from galaxies by the various dynamical processes at work.

2 Finding intracluster light

To test this predicted link between cluster dynamical state and ICL properties, we have been conducting a survey (see [5], [4]) for ICL in galaxy clusters ranging from clusters dominated by a massive central cD galaxy to irregular clusters with several comparably luminous galaxies in their core. To the extent that cluster morphology can be used as a proxy for dynamical state – cD clusters being more highly evolved than irregular clusters in the process of merging, for example – these different cluster types should possess markedly different ICL properties. Using the KPNO 2.1m telescope and observing in Washington M to suppress variable night sky emission lines, we use a combination of super sky flats and aggressive masking of stars and background objects to obtain cluster images with a limiting surface brightness of $\mu_V = 27$.

Figure 2 shows two clusters from our survey. The left panel shows the $z = 0.14$ cD cluster Abell 1413, after the smooth cD envelope has been subtracted off. This residual image shows very little in the way of small-scale ICL features; the small arcs near the core of the cluster are radially unresolved and are likely due to gravitational lensing (an interpretation further supported by

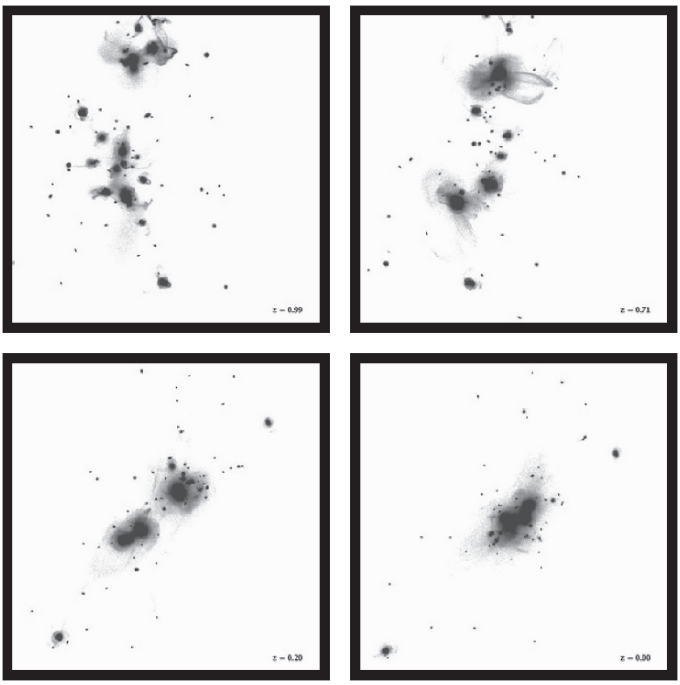

Fig. 1. The evolution of the ICL in a simulated galaxy cluster [9]. Each frame is 4 Mpc on a side, and redshift evolves from upper left ($z = 1$) to lower right ($z = 0$).

HST imaging of the cluster). In this case, the ICL *is* the extended cD envelope which has been subtracted off, and little else remains, reminiscent of the smooth diffuse ICL envelopes shown in the simulated clusters late in their dynamical history.

In contrast, the right panel of Figure 2 shows the irregular cluster Abell 1914 ($z = 0.17$), likely undergoing a cluster merger event. In this cluster, a number of discrete, extended ICL features can be seen at surface brightnesses of $\mu_V = 26-27$. These features contain a significant amount of starlight – the northwest plume has a luminosity of 3.0×10^9 $L_\odot$, while the eastern plume has a luminosity of 2.8×10^{10} $L_\odot$. The plumes also appear dynamically young – the western arc is thin and shows a small scale bifurcation along its length, while the southernmost edge of the southern plume is very sharply cut off. Clearly, Abell 1914 is experiencing an era of strong ICL production, likely associated with the dynamical processes of cluster coalescence.

These examples support the notion that the structure of the ICL in clusters does indeed reflect their dynamical state – the less evolved, irregular cluster shows significant ICL substructure, while the evolved cD cluster shows an ICL characterized by a smooth extended cD envelope. An trend of increasing

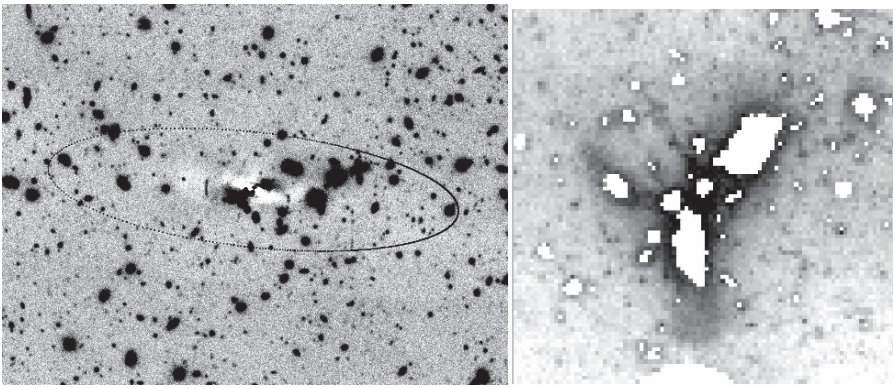

Fig. 2. *Left:* Deep image of the cD cluster Abell 1413, after subtraction of the smooth cD envelope [5]. The limits of the cD halo subtraction are shown by the drawn ellipse, and the cluster shows little sign of any ICL substructure. *Right:* Deep image of Abell 1914, smoothed to highlight low surface brightness features [4]. In both images, north is up and east is to the left.

fractional amount of ICL with cluster dynamical stage is also suggested by the compilation of ICL properties by Ciardullo et al. [2].

3 Close to home: ICL in the Virgo cluster

To study the formation of ICL in more detail, over the past several years we have used Case's Burrell Schmidt wide-field telescope to survey the Virgo Cluster for ICL. Imaging Virgo's faint ICL presents a number of technical challenges related to flat fielding and sky subtraction over large angular scales, challenges which the Burrell is ideally configured to meet. The telescope images a 1.5×0.75 degree field of view onto a single CCD, simplifying the flat fielding by reducing the need for mosaicing. The telescope's closed tube design minimizes off-axis scattered light, and we have taken significant steps to further reduce scattered light through extensive baffling and flocking of the telescope tube.

Figure 3 shows the inner 2.25 square degrees of the Virgo Cluster core, with a limiting surface brightness of $\mu_V = 28.5$, nearly 1.5 mag/arcsec^2 deeper than previous photographic studies. The image reveals several long (>100 kpc) tidal streamers, as well as a myriad of smaller-scale tidal tails and bridges between galaxies. The diffuse halo of M87 is traced out to nearly 200 kpc, appearing very irregular on these scales, while significant diffuse light is also detected around the M84/M86 pair. Several galaxies in the core are embedded in common envelopes, suggesting they are true physical subgroups. The complex substructure of Virgo's diffuse ICL reflects the hierarchical nature of

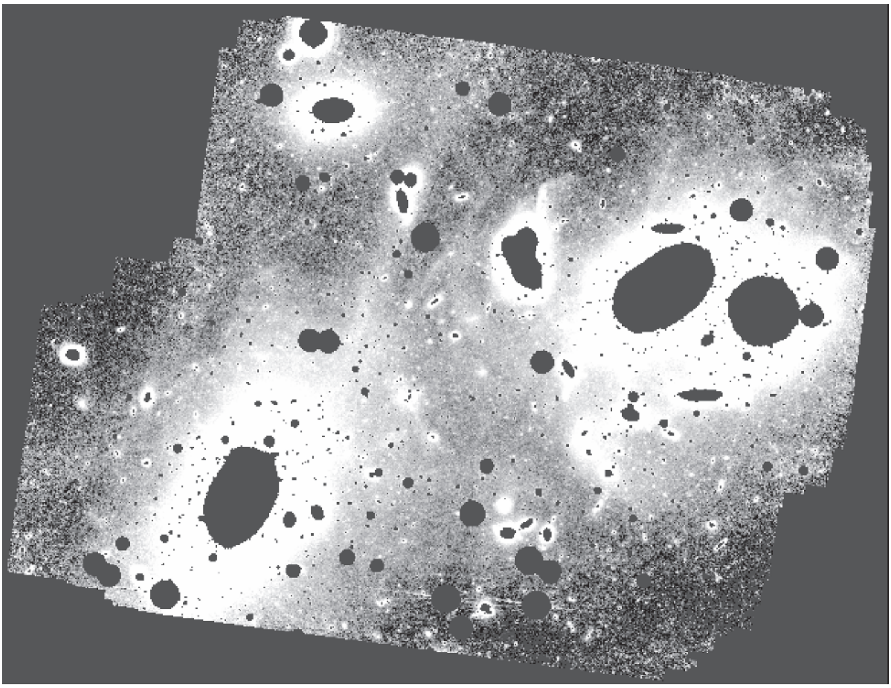

Fig. 3. Deep image of the Virgo cluster, taken with Case's Burrell Schmidt telescope [7]. North is up; east is to the left. The white levels saturate at $\mu_V \sim 26.5$, while the faintest features visible have a surface brightness of $\mu_V \sim 28.5$.

cluster assembly, rather than being the product of smooth accretion around a single central galaxy.

This research has been supported by the National Science Foundation and Research Corporation.

References

1. Berlind, A. A., & Weinberg, D. H. 2002, ApJ, 575, 587
2. Ciardullo, R., Mihos, J. C., Feldmeier, J. J., Durrell, P. R., & Sigurdsson, S. 2004, IAU Symposium, 217, 88
3. Dubinski, J. 1998, ApJ, 502, 141
4. Feldmeier, J. J., Mihos, J. C., Morrison, H. L., Harding, P. H., Kaib, N., & Dubinski, J. 2004, ApJ, 609, 617
5. Feldmeier, J. J., Mihos, J. C., Morrison, H. L., Rodney, S. A., & Harding, P. H. 2002, ApJ, 575, 779
6. Mihos, J. C. 2004, in Clusters of Galaxies: Probes of Cosmological Structure and Galaxy Evolution, 277
7. Mihos, J. C., Harding, P. H., Feldmeier, J. J., & Morrison, H. L. 2005, ApJ, 631, L41

8. Murante, G., et al. 2004, ApJ, 607, L83
9. Rudick, C., Mihos, J. C., & McBride, C. 2006, ApJ, in press
10. Sommer-Larsen, J., Romeo, D. A., & Portinari, L. 2005, MNRAS, 357, 478
11. Willman, B., Governato, F., Wadsley, J., & Quinn, T. 2004, MNRAS, 355, 159

Simulating Diffuse Light in Galaxy Clusters

C.S. Rudick[1], J.C. Mihos[1] and C. McBride[1,2]

[1] Department of Astronomy, Case Western Reserve University, 10900 Euclid Ave, Cleveland, OH 44106
craig@fafnir.astr.cwru.edu, mihos@case.edu
[2] Now in the Department of Physics and Astronomy, University of Pittsburgh

Summary. Using N-body simulations, we have modeled the production and evolution of low surface brightness, diffuse intra-cluster light (ICL) in galaxy clusters. By creating simulated observations of the clusters we have measured the evolution of the ICL luminosity throughout the dynamical history of the clusters. We find that ICL production tends to occur in short, discrete events, which correlate very strongly with strong, small-scale interactions and accretions between groups within the clusters.

1 Simulated deep imaging of galaxy clusters

Diffuse, intra-cluster starlight (ICL) has been observed in numerous galaxy clusters in the local universe (see [1] for more on ICL observations). As the product of tidal interactions between cluster galaxies, this very low surface brightness material has the potential to reveal a great deal about the nature of dynamical interactions within the cluster. In order to better understand the processes which create the observed ICL, we have created N-body simulations of the evolution of luminous galaxies in clusters, in the context of a ΛCDM universe (see [2] for more information on our simulation techniques). We have modeled three such clusters, each approximately $10^{14} M_{\odot}$ (referred to as clusters C1, C2, and C3 respectively, henceforth).

In order to examine the evolution of the ICL in our clusters, we have created simulated deep photometric images of the clusters evolving from $z = 2$ to $z = 0$. First, we smoothed the distribution of discrete particles into a continuous mass distribution. This was done by first projecting the three-dimensional particle positions onto a two-dimensional plane, then smoothing the particles using an adaptive two-dimensional Gaussian smoothing kernel.

We obtained luminosity distributions of the clusters by applying a mass-to-light ratio (M/L) to the smoothed mass distribution. Our N-body simulations, however, have not modeled gas physics, and therefore star formation and stellar evolution, in any way. We have therefore chosen to adopt a global M/L of $5 M_{\odot}/L_{\odot}$ in the V-band, a value characteristic of older stellar populations in the local universe, such as we expect to dominate in the dense cluster environments we have simulated. This M/L has been applied to all

images at all evolutionary times. While it is certainly unphysical to expect to see similar stellar populations at $z = 2$ and $z = 0$, this method has several advantages which aid in the interpreting dynamical changes within the cluster. Most importantly, the global M/L means that all changes seen in the luminosity distribution as the cluster evolves are the direct result of gravitational dynamics alone. Secondly, we are not attempting to simulate cosmological observations of the clusters at distant redshifts, but rather observing the clusters in their given dynamical state as they would appear in the local universe.

2 Evolution of the ICL

2.1 Defining ICL

Most previous theoretical work has defined ICL as stellar particles which are bound to the cluster potential, but unbound to any individual galaxy in the cluster (e.g. [3], [4]). In general, however, the specific binding energy of individual stars is not a readily observable feature of the ICL. We have therefore adopted a more observationally tractable quantity as our definition of ICL: luminosity which is at surface brightness fainter than 26.5 mag/sq.arcsec. We chose $\mu_V = 26.5$ mag/sq.arcsec specifically as our surface brightness cut-off because in both our simulated images and in direct observations [5], [6] this appeared to be approximately the surface brightness limit where the isophotal contours no longer simply outlined those of higher galaxian surface brightness, but seemed to take on a distinct morphology.

2.2 Changes in ICL luminosity

Using our observational definition of ICL, we have calculated the fraction of each cluster's luminosity which is at ICL surface brightness (f_{ICL}) as a function of time [3], as shown on the top row of Fig. 1. The most immediately obvious feature of this analysis is that, in general, the fraction of ICL luminosity increases as a function of time in each of the clusters. However, it is apparent that this increasing ICL fraction is far from smooth or monotonic, including several examples of large increases in f_{ICL} on short timescales, as well as significant, extended decreases. In order to better understand the changing ICL luminosity fraction, we have calculated the fractional change in f_{ICL} per unit time (Δf_{ICL}), plotted as a function of time on the bottom row of Fig. 1. This plot shows even more clearly that increases in the ICL luminosity fraction tend to come in short, discrete events, often preceded by significant f_{ICL} decreases.

[3] The units of time used are such that $t = 1$ is the current age of the universe.

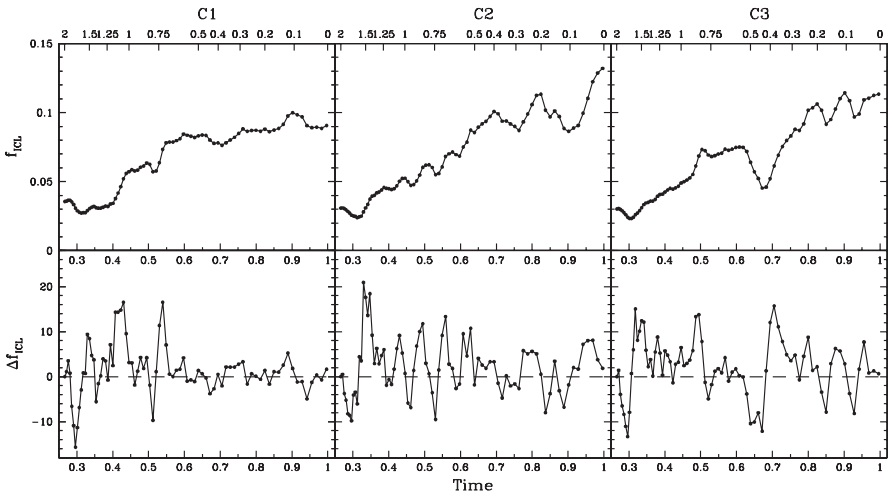

Fig. 1. *Top:* The fraction of luminosity in each cluster which is at ICL surface brightness ($\mu_V > 26.5$ mag/arcsec^2) as a function of time (f_{ICL}) for each of the three clusters. The top axis shows the corresponding nominal redshift. *Bottom:* The fractional change in ICL luminosity per unit time as a function of time (Δf_{ICL}).

By following the evolution of our clusters using the simulated images, shown in Fig. 2, we see that large increases in the ICL luminosity fraction are highly correlated with small scale interactions and accretion events between groups within the clusters. Additionally, f_{ICL} decreases are the result of temporary increases in the projected density of luminous material which are a part of the accretion process. The following sections show a representative example of this behavior from each cluster.

Cluster C1

The top row of Fig. 2 shows simulated images of a short segment of the evolution of cluster C1, along with the f_{ICL} and Δf_{ICL} functions during this time period. At $t = 0.6$, the cluster consists of three distinct galaxy groups. However, at $t = 0.8$ these same three groups still exist within the cluster, relatively unaltered. The groups simply orbit one another, resulting in little accretion or strong inter-group interactions. During this period, the fraction of the cluster's luminosity at ICL surface brightness remains roughly constant.

Cluster C2

The middle of Fig. 2 shows a segment of the evolution of cluster C2. Here, we see a significant increase in the ICL luminosity fraction over a very short time period. The small group which is below and to the left of the cluster

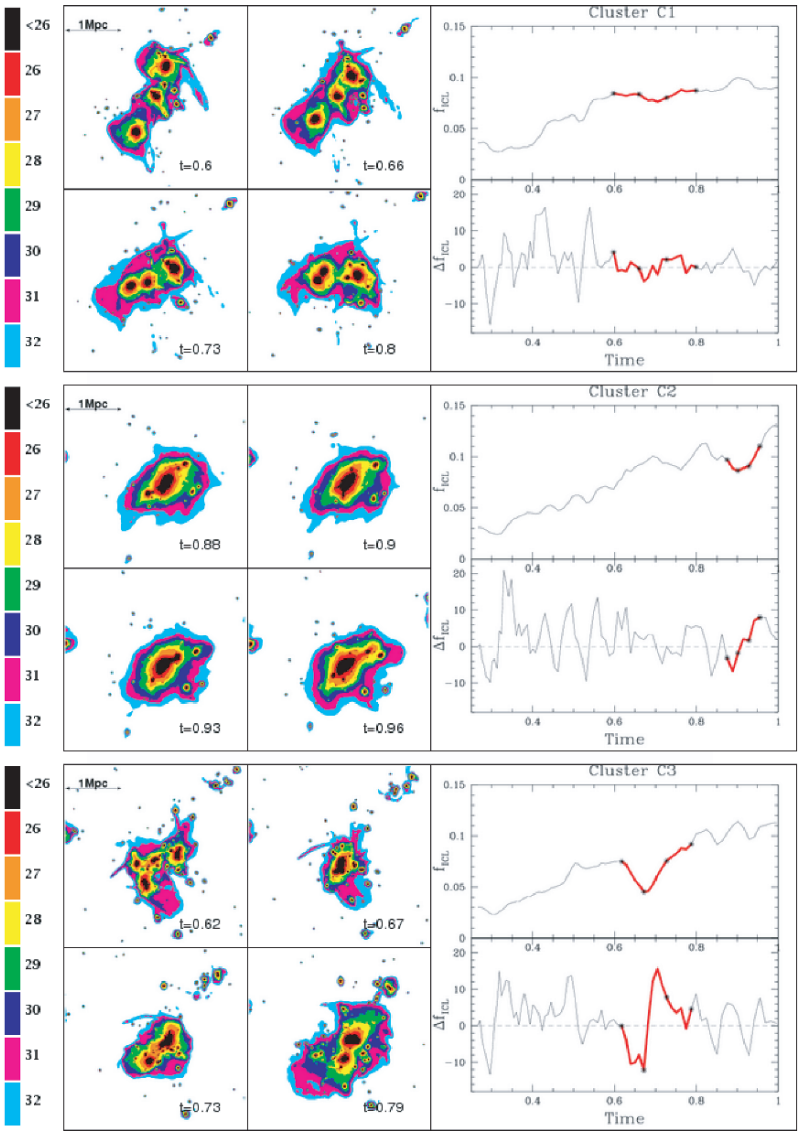

Fig. 2. Simulated images of short segments of the evolution of each of our clusters (*top:* C1; *middle:* C2; *bottom:* C3). The length scale in physical units is shown in the upper left. The evolutionary time of each images is labeled in its lower right corner. The simulated images are color-coded by V-band surface brightness, as shown by the color key at the far left. Black represents all luminosity at $\mu_V < 26.0$ mag/arcsec^2; each other color represents a bin of one mag/arcsec^2: red is $\mu_V = 26.0 - 27.0$, orange is $\mu_V = 27.0 - 28.0$, etc. On the right are the f_{ICL} and Δf_{ICL} plots for each cluster. The red segments highlight the time period shown in the simulated images; the stars mark the specific timepoints shown in the images.

core at $t = 0.88$ plunges through the central mass concentration, emerging to the upper right. As the group enters the core, the projected luminous density increases temporarily, thus creating the drop in ICL luminosity. However, as the group exits the cluster core, the tidal field strips material from the group, thus moving it to lower surface brightness, increasing the ICL luminosity fraction

Cluster C3

In cluster C3, we see our most dramatic example of an ICL production event, shown at the bottom Fig. 2. At $t = 0.62$ the cluster consists of no less than four distinct galaxy groups. At $t = 0.67$ all of these groups have collapsed together, resulting in a very large loss in the ICL luminosity fraction. As the groups separate again, huge amounts of material are stripped from the groups, resulting in the single largest ICL production event observed in any of these three clusters.

3 Conclusions

By modeling the dynamical evolution of luminous cluster galaxies, we have been able to trace the evolution of the clusters' diffuse ICL using simulated broadband images of clusters. We find that not only does the fraction of cluster luminosity at ICL surface brightness increase with dynamical time, but that the ICL evolution is tightly linked to the specific dynamical histories of the clusters. Major increases in ICL luminosity are highly correlated with small scale interactions and accretions between groups within the clusters. Because the features of ICL production observed in these simulations are so tightly correlated with specific evolutionary events within the clusters, observations of this low surface brightness material has the potential to reveal a great deal of hitherto inaccessible information about the dynamical history of galaxy clusters.

This research has been supported by the National Science Foundation, Research Corporation, and the Jason J. Nassau Graduate Fellowship Fund.

References

1. J. C. Mihos: this volume
2. C. S. Rudick, J. C. Mihos, C. McBride: in press
3. B. Willman, F. Governato, J. Wadsley, & T. Quinn: MNRAS **355**, 159 (2004)
4. J. Sommer-Larsen, D. A. Romeo, & L. Portinari: MNRAS **357**, 478 (2005)
5. J. J. Feldmeier, J. C. Mihos, H. L. Morrison, S. A. Rodney, & P.H. Harding: ApJ **575**, 779 (2002)
6. J. C. Mihos, P. H. Harding, J. J. Feldmeier, & H. L. Morrison: ApJ **631**, L41 (2005)

Lensing by Groups

O. Möller[1], M. Kitzbichler[1], V.R. Eke[2] and P. Natarajan[3]

[1] Max-Planck-Institute for Astrophysics, Karl-Schwarzschild-Str. 1, Postfach 1317, 85741 Garching b. München
ole@mpa-garching.mpg.de
[2] Department of Physics, Univ. of Durham, South Road, Durham DH1 3LE
[3] Astronomy Department, Yale University, PO Box 208101, New Haven, CT 06520-8101

Summary. Determining the mass content and distribution of galaxy groups is crucial for a better understanding of their rôle in structure and galaxy formation and evolution. Here we discuss, using the sample of groups in the 2dF as an example, how the mass properties of groups from large surveys can be constrained using gravitational lensing. We show that realistic mass models of 2dF groups predict detectable weak lensing signals and that the total mass as well as the mass distribution can be constrained from the weak lensing signal of $\sim 10-100$ of the more massive groups in the 2dF. We also show that a number of $\sim 65\%$ of all strong lens galaxies with $z < 0.2$ are expected to lie in groups, with a fraction of $\sim 70\%$ of lenses being satellite galaxies.

1 Introduction

Groups of galaxies as bound systems on scales smaller than clusters of galaxies, have been the focus of an ever increasing amount of research (e.g. the articles in this volume). This is strongly motivated by the fact that most galaxies appear to reside in groups of galaxies and that group environments are very important in galaxy evolution processes. Understanding both the properties of groups in terms of their physical parameters and also their rôle in galaxy evolution is an observational and theoretical challenge. Observations at various wavelengths have already provided important information regarding luminosity functions and the nature of some physical processes in groups. What is very difficult to determine observationally however, is the masses, mass distributions and the mass evolution of groups. Studies in the X-ray and dynamical methods can provide some important measurements of these, but often rely on assumptions about the relation between baryonic and dark mass. Gravitational lensing provides a means to determine the mass properties of such systems that is in principle independent of such assumptions. Here, we will discuss the applications of lensing to groups in two different regimes: weak and strong lensing. In the first case, the effect is common but very weak; all background galaxies are affected by the foreground mass distribution so as to be distorted slightly. Previous studies have shown

that this weak lensing effect in groups is detectable (e.g. [5]). Using mass models of groups based on large simulations, we will show here how the mass distribution of groups in extended catalogues of objects, like the 2PIGG [3] can be determined using weak lensing. Specifically we show that the expected signal depends strongly on the relative fraction of mass that resides within a common group halo and the mass that is associated with galaxies. In the strong lensing regime, we calculate how many group member galaxies in the 2dF are expected to be lens galaxies. We show that the expected fraction of lenses that are satellite galaxies is high.

2 The mass models

To model the mass distribution of groups, we combine the results of a large N-body simulation, the Millennium Run [10] with the 2dF group catalogue 2PIGG [4]. For each galaxy in the 2PIGG galaxy catalogue we assign an NFW host halo and model the baryonic component as an isothermal sphere. Given the luminosity of a galaxy from the catalogue, we assign the velocity dispersion using the Faber-Jackson relation $\sigma = \sigma_*(L/L_*)^{0.25}$, with $\sigma_* = 160\,\mathrm{km\,s^{-1}}$ and $L_* = 1.6 \times 10^{10} L_\odot$ [1]. To assign a dark matter halo, we use two probability distribution functions that we measure from the Millennium Run in combination with a semi-analytic model of structure formation [2]. The first is the distribution of dark matter halo virial masses and luminosities, $n(M_{\rm vir}, L)$. The second is the distribution of halonumbers as function of virial and maximal velocity of the DM halo, $n(V_{\rm vir}, V_{\rm max})$. Given a luminosity L, we draw randomly from the corresponding distribution $n(M_{\rm vir}|L)$. The virial velocity of the dark matter halo is directly related to its mass by $\log V_{\rm vir}/\mathrm{km\,s^{-1}} = \frac{1}{3}\left(\log M_{\rm vir}/10^{11} M_\odot + \alpha + \log \rho_c\right)$, where $\alpha = 4.38$ and ρ_c is the cosmological critical density in units of $10^{11}\mathrm{M}_\odot/\mathrm{kpc}^3$. Having determined $V_{\rm vir}$ in this way, we sample the maximum velocity $V_{\rm max}$ from $n(V_{\rm max}|V_{\rm vir})$. The concentration parameter is then given by the solution of $c/\left(\ln(1+c) - c/(1+c)\right) = 4.7 V_{\rm max}^2/V_{\rm vir}^2$. In this way we can assign a unique dark matter halo to each galaxy in the 2PIGG catalogue, that statistically fulfills the predicted association criteria of dark and luminous components. Since we wish to investigate the effect of the mass distribution in groups on the weak and strong lensing properties, we allow the relative dark matter contributions of satellite galaxies to host galaxies to vary (schematically illustrated in Fig. 1). In this way, we can represent the different degrees of halo stripping that may have occurred in groups, in a similar way to that observed in clusters [9].

Note that we keep the total mass in all models fixed, and only vary the fraction of the dark mass $\Gamma = M_{\rm gal}/M_{\rm tot}$ that is associated with satellite galaxies themselves. We do not vary the baryonic component.

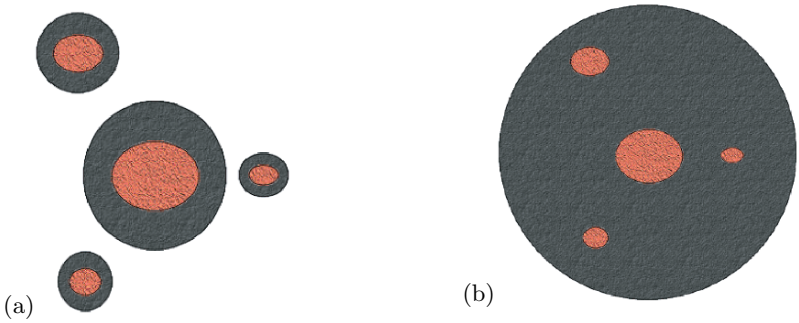

Fig. 1. The two mass distributions in groups: in the first model, all the mass resided with the individual galaxies – no common group halo has formed. In the second case, all dark matter is in a common group halo into which the baryonic components of the galaxies are embedded.

3 Weak lensing

For each group, we calculate the expected weak lensing signal taking into account all group members. At each position on a plane we calculate the shear, which we then average radially to obtain the radial shear around a given point. We repeat this for the 10 most massive groups in the 2PIGG that have between 4 and 20 member galaxies and average the final radial shear curves together. The average shear around the central galaxy is shown in Fig. 2a). The solid line shows the result for massive satellites, $\Gamma = 1$, whereas the dotted line shows the result for $\Gamma = 0.1$. The shear signal is in general high, $\sim 5\%$ at 50 arcsec distance. Space observations can achieve a background density of

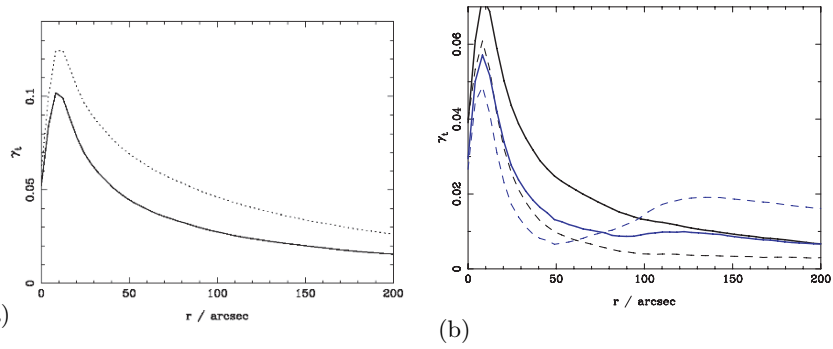

Fig. 2. The shear around the central galaxy (a) and the satellite galaxies (b) for the two mass distributions in groups. In the left panel, the solid curve is for $\Gamma = 1$ and the dotted curve for $\Gamma = 0.1$. In panel (b) the (black) upper solid curve is for $\Gamma = 1$, the upper dashed one for $\Gamma = 0.1$. The solid and dashed lower (blue) curves are for satellites within 200 kpc of the central group galaxy only.

galaxies of $\sim$40 arcmin^{-2}, and hence could measure the average background galaxy shape within such a radius for 10 groups to $\sim$1% accuracy – the effect would thus be detectable. In a smaller survey the weak lensing effect of groups has indeed been detected [5], and the lensing signal around individual galaxies is now routinely measured (e.g. [6]). Measuring the shear around the central group galaxies enables a determination of the total mass in the group, but it is not the best way to determine its mass distribution. This can be achieved if the tangential shear around the individual satellite galaxies is measured. Here it is important to note that purely isolated galaxies produce a tangential shear signal, whereas galaxies that are offset within a deeper potential well, as satellite galaxies in groups are, have a lowered tangential shear due to the proximity of another massive galaxy, that induces a strong radial shear component. We show the tangential shear, again for $\Gamma = 1$ and $\Gamma = 0.1$ in Fig. 2b). As can be seen a higher mass fraction in the central group halo produces a much lower average tangential shear around galaxies within $\sim$20$-$100 arcsec (or $\sim$40$-$200 kpc). Measuring the average tangential shear signal at small and large radii of satellite galaxies of the 10–100 most massive galaxy groups in the 2dF therefore can distinguish different group mass models.

4 Strong lensing

Close to compact objects, mass contrasts are high enough to cause background sources to be multiply imaged. This strong lensing regime in principle allows the reconstruction of the mass distribution of the lens on small scale of a few kpc. In many known lens systems the effect is complicated due to the presence of nearby structures, and a significant number of strong lens systems are in fact found close to groups of galaxies (e.g. [11]). We use our mass models of the 2PIGG catalogue to predict the properties of such group lenses. Using a strong lensing ray-tracing code [7] we calculate for all groups in the 2PIGG what the expected cross section for strong lensing should be. Due to the low redshift of the groups we found that the effect of the nearby masses is less pronounced than expected for higher redshift group lenses, at $z \sim 0.3-0.6$ [8], but that there is still a significant effect for the most compact groups, which produce shears of a few %. Depending on the assumed mass distribution within the groups, this external shear can vary by factors of a few. Therefore, for lenses in compact groups, the lens mass models need to correctly model the details of the mass distribution in groups. From the cross sections for lensing, we determine what fraction of lenses are expected to lie in groups, and which fraction of these is expected to be lensed by satellite galaxies. The results for the two different assumptions about the mass distribution in groups is summarised in Table 1, together with the observational results from [11]. Using our calculation of lensing cross sections, we also es-

Table 1. Strong lensing in groups

	% of lenses in groups	% central lenses	% satellite lenses	typical luminosity
Williams et al. (2005)	67	25	75	$\sim 0.5 L_*$
No massive group halo ($\Gamma = 1$)	70	25	75	$\sim L_*$
Massive group halo ($\Gamma = 0.1$)	60	35	65	$\sim L_*$

timate that a fraction of $\sim 2 \times 10^{-4}$ of all sources at $z \sim 1$ will be lensed by 2dF groups.

5 Conclusions

Determining the mass distribution of groups of galaxies is important if the rôle of groups in galaxy and structure formation is to be understood fully. Both weak and strong lensing can help to constrain the mass properties of groups. In particular, measuring the weak lensing signal around satellite galaxies in the more compact groups in the 2PIGG group catalogue would allow constraints on the total mass and mass distribution in these groups. In the strong lensing regime, we found that about $\sim$65% of all lenses that are expected to be found in surveys like the 2dF are members of groups, with a fraction of $\sim$30% of those being central group galaxies. These numbers agree well with observations and vary by a few per-cent depending on the assumed mass distribution in groups.

Future, deep observations of a selected sample of groups will allow constraints on the masses and mass distributions from weak and strong lensing.

References

1. M. Bernardi, R.K. Sheth, J. Annis, D.J. Eisenstein et al.: AJ, **125**, 1866 (2003)
2. D.J. Croton, V. Springel, S.D.M. White, G. De Lucia et al.: MNRAS, **365**, 11 (2006)
3. V.R. Eke, C.M. Baugh, S. Cole, C.S. Frenk et al.: MNRAS, **348**, 866 (2004)
4. V.R. Eke, C.S. Frenk, C.M. Baugh, S. Cole et al.: MNRAS, **355**, 769 (2004)
5. H. Hoekstra, M. Franx, K. Kuijken, R.G. Carlberg: ApJ, **548**, 5 (2001)
6. R. Mandelbaum, P. McDonald, U. Seljak, R. Cen: MNRAS, **361**, 1287 (2005)
7. O. Möller, P. Natarajan, J.-P. Kneib, A.W. Blain: ApJ, **573**, 562 (2002)
8. O. Möller, A.W. Blain: MNRAS, **299**, 845 (1998)
9. P. Natarajan, A. Loeb, J.-P. Kneib, I. Smail: Apj, **580**, 17 (2002)
10. V. Springel, S.D.M. White, A. Jenkins, C.S. Frenk et al.: Nature, **435**, 629 (2005)
11. K.A. Williams, I. Momcheva, C.R. Keeton, A.I. Zabludoff et al.: astro-ph, **11598** (2005)

The Role of Tidal Interactions in Driving Galaxy Evolution

J. Pérez[1,2], P.B. Tissera[2,3], D.G. Lambas[3,4], C. Scannapieco[2,3] and M.E. De Rossi[2,3]

[1] Facultad de Ciencias Astronómicas y Geofísicas, UNLP, Argentina
jperez@fcaglp.unlp.edu.ar
[2] Instituto de Astronomía y Física del Espacio, Argentina
[3] CONICET
[4] Observatorio Astronómico de Córdoba, Argentina

Summary. We carry out a statistical analysis of galaxy pairs selected from chemical hydrodynamical simulations with the aim at assessing the capability of hierarchical scenarios to reproduce recent observational results for galaxies in pairs. Particularly, we analyse the effects of mergers and interactions on the star formation (SF) activity, the global mean chemical properties and the colour distribution of interacting galaxies. We also assess the effects of spurious pairs.

In order to determine the effects of interactions on the SF activity, we have used a cosmological Λ-CDM simulation ($\Lambda = 0.7$, $\Omega = 0.3$, $H_0 = 100$ h km s^{-1}Mpc^{-1}, h = 0.7) run with the chemical GADGET-2 code [7] which includes the enrichment of the interstellar medium by SNIa and SNII. In agreement with observations [3], our results indicate that close encounters (with relative projected separation (r_p) smaller than 25 kpc h^{-1}) can enhance the SF activity to levels higher than those observed for galaxies without a close companion (or control sample). We also find that the triggering of SF activity by interactions depend on the internal properties of galaxies, described by the depth of their potential wells and gas reservoirs [5]. Currently passive star forming pairs (systems with SF levels lower than that measured for the control sample) are older and more evolved objects, with deeper potential wells and less leftover gas than active star-forming systems.

We constructed a 3D and a projected 2D galaxy pair catalogs to study the effects of spurious pairs. Consistently with observations [4], we estimated a $\sim$27% of contamination by projection for systems with $r_p < 100\,\mathrm{kpc\ h^{-1}}$, and a $\sim$19% of spurious pairs for close systems ($r_p < 25\,\mathrm{kpc\ h^{-1}}$). However, comparing the 2D and 3D simulated galaxy pair samples, we find that these levels of contamination by projection do not affect significantly the correlations between the SF activity and the relative separation, colour distributions and global chemical properties.

The analysis of colours for galaxy pairs shows a clear bimodal distribution [1] with a blue peak populated basically by the closest pairs with a currently strong or recently past SF activity induced by interactions. Instead, the red peak is more consistent with currently passive star forming systems, older

and more evolved than those of the blue peak. The analysis of merging and interacting pairs shows that the former contribute with a larger fraction of stellar mass to the blue colours than the latter, demostrating the role of interactions in driving the colour bimodality.

Finally, we study the global mean chemical abundance of the stellar populations (SP) and the interstellar medium (ISM) of galaxies in pairs. The analysis of the chemical abundance as a function of the projected separation shows that while the SP are enriched with respect to galaxies without a close companion, regardless of their current SF activity or relative separation, the ISM stores record fossils of the interactions. Galaxies with a close companion but passively forming stars show a clear correlation of their ISM chemical abundances with distance, fossils of previous past interactions. Conversely, galaxies in pairs with active SF show an enhancement of their ISM abundances as expected. We also analyse the luminosity-metallicity and mass-metallicity relations in order to determine if interactions modify the observed relations [2]; [8]. Our results show the same trends for galaxy pairs and the control sample, indicating that these correlations might not be strongly affected by interactions. This point will be addressed in more detail by Pérez et al. [6].

Acknowledgements

MJP thanks the LOC of this conference for their financial support. This work was partially funded by Fundación Antorchas, CONICET and LENAC.

References

1. Balogh M. L., Eke V., Miller C., et al., 2004, MNRAS 348, 1355
2. Kobulnicky H. A. & Kewley L. J., 2004, ApJ 617, 240
3. Lambas, D. G., Tissera, P. B., Alonso, M. S. Coldwell, G. 2003, MNRAS 346, 1189
4. Mamon G.A., 1986, ApJ, 307, 436
5. Perez J., Tissera, P. B., Lambas, D. G.& Scannapieco C., 2005, A&A accepted (astro-ph/0510327)
6. Perez J., Tissera P. B., Scannapieco C., Lambas D. G. & De Rossi M. E., 2006, in preparation
7. Scannapieco C., Tissera P.B., White S.D.M. & Springel V., 2005, MNRAS 364, 552
8. Tremonti, C. A., Heckman T. M., Kauffmann G. et al., 2004, ApJ 613, 898

Chemical and Photometric Evolution of NGC 6822 in a Cosmological Context

L. Carigi[1], P. Colín[2] and M. Peimbert[1]

[1] Instituto de Astronomía, UNAM, Apdo. Postal 70-264, México 04510 D.F., Mexico
carigi,peimbert@astroscu.unam.mx
[2] Centro de Radioastronomía y Astrofísica, UNAM, Apdo. Postal 72-3, 58089 Morelia, Michoacán, Mexico
p.colin@astrosmo.unam.mx

We have derived a robust star formation history (SFR) for NGC 6822, an irregular galaxy of the Local Group, based on observations and photometric evolution models. That SFR can be used for different applications related to NGC 6822. Our photometric model computed with GALAXEV code of Bruzual and Charlot (2003) and based on the adopted SFR, the IMF by Kroupa, Tout & Gilmore (1993, KTG), and the metallicity evolution, $Z(t)$ obtained by the chemical evolution model predicts absolute magnitudes and colors that agree with the observed ones at the one σ level.

Based on the adopted SFR we present our best chemical evolution model for NGC 6822. The model evolves according to the mass assembly history of non baryonic mass predicted by a cosmological context. The adopted total mass for the model presented in Fig. 1 is 2.6×10^{10} $M_\odot$.

We have assumed that during accretion the universal baryon fraction is only reduced by reionization. If the model does not include well mixed outflows, it is not successful in reproducing the observational constraints because the amount of baryonic gas accreted by the galaxy is higher than the amount of baryonic matter derived from observations. Moreover based on our adopted SFR the thermal heating produced by SNe, under the assumption of no outflows, is considerably larger than the binding energy of the observed gas content. These two results imply that the presence of outflows of well mixed material is needed. We argue that these outflows most likely occurred early on in the history of the galaxy.

In order to comply with the presence of an early outflow, and the observed O/H and C/H values, we have computed our best model that have a KTG IMF with m_{up} of 60 $M_\odot$ while for the solar vicinity m_{up} amounts to 80 $M_\odot$ (see Carigi et al. 2005). That is the number of SN of Type II per generation of stars has to be smaller in NGC 6822 than in the solar vicinity. A lower value of m_{up} for NGC 6822 than for the solar vicinity is in agreement with recent results on dwarf galaxies by others authors (e.g. Goodwin & Pagel 2005 and Weidner & Kroupa 2005).

The fractions of C produced by MS ($m > 8$ $M_\odot$), LIMS ($m < 8$ $M_\odot$), and SNIa amount to 34%, 65%, and 1%, respectively. On the other hand, in the

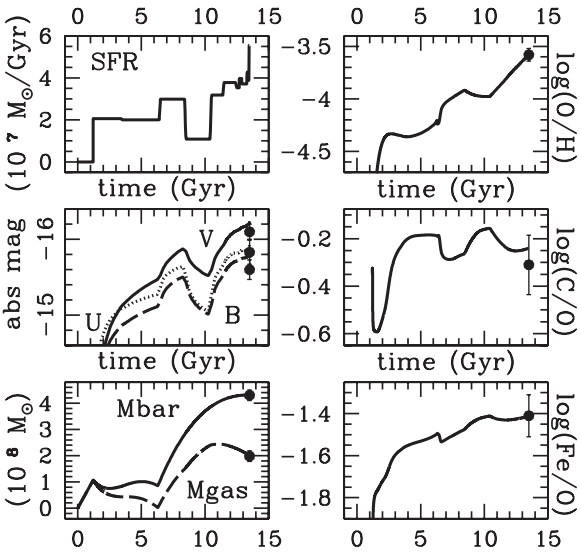

Fig. 1. Evolution of the: i) derived star formation rate, ii) U, B, and V absolute magnitudes, iii) baryonic mass, iv) gaseous mass, and v) abundance ratios. The present-day observational constraints (filled circles) are presented for comparison.

solar vicinity, these values amount to 48%, 50%, and 2%, respectively (see Carigi et al. 2005).

More details of this model and other models are presented in Carigi, Colín, & Peimbert (2006).

References

1. Bruzual, G., Charlot, S. 2003, MNRAS, 344, 1000
2. Carigi, L., Colín, P., Peimbert, M. 2006, Apj, 644, 924
3. Carigi, L., Peimbert, M., Esteban, C., García-Rojas, J. 2005, ApJ, 623, 213
4. Goodwin, S. P., Pagel, B. E. J. 2005, MNRAS, 359, 707
5. Kroupa P., Tout C.A., Gilmore G. 1993, MNRAS, 262, 545 (KTG)
6. Weidner, C., Kroupa, P. 2005, ApJ, 625, 754

Evolution of the Luminosity-Metallicity-Stellar Mass Correlation in a Hierarchical Scenario

M.E. De Rossi[1,2], P.B. Tissera[1,2] and C. Scannapieco[1,2]

[1] Consejo Nacional de Investigaciones Científicas y Técnicas, Argentina
[2] Instituto de Astronomía y Física del Espacio, Ciudad de Buenos Aires, Argentina
derossi@iafe.uba.ar

Summary. We study the evolution of the Stellar Mass-Metallicity Relation and the Luminosity-Metallicity Relation by performing numerical simulations in a cosmological framework. We find that the slope and the zero point of the Luminosity-Metallicity Relation evolve in such a way that, at a given metallicity, systems were $\sim$3 mag brighter at $z = 3$ compared to galaxies in the local universe, which is consistent with the observational trend. The local Stellar Mass-Metallicity Relation shows also a good agreement with recent observations. We identify a characteristic stellar mass $M_{\rm c} \sim 10^{10.2} M_{\odot} h^{-1}$ at which the slope of the Stellar Mass-Metallicity Relation decreases for larger stellar masses. Our results indicate that $M_{\rm c}$ arises naturally as a consequence of the hierarchical building up of the structure.

1 Results and discussion

The Luminosity-Metallicity Relation (LMR) has been widely studied during the last two decades. In the local universe there is a clear correlation between the luminosity and the chemical abundance of galaxies in such a way that brighter systems tend to be more metal rich (e.g. [3]). Futhermore, recent observations have suggested that this correlation evolves with redshift (e.g. [2]). At a given luminosity systems seem to be less enriched in the past. Because of the difficulties in obtaining stellar mass, most studies have used galaxy luminosity as a surrogate. Recently, though, the relation between oxygen chemical abundance and stellar mass (MMR) has been estimated for local galaxies finding a well defined correlation [6]. In this work we study the MMR and the LMR by using chemo-dynamical simulations in a cosmological scenario, which allow us to follow the non-lineal growth of structure together with the chemical enrichment of the interestellar medium.

We have performed chemo-dynamical simulations by employing the chemical GADGET-2 [4]. A ΛCDM universe ($\Omega = 0.3, \Lambda = 0.7, \Omega_b = 0.04$ and $H_0 = 100h^{-1}$ km s^{-1}Mpc$^{-1}, h = 0.7$) was assumed. The simulated volume corresponds to a periodic cubic box of a comoving 10 Mpc h^{-1} side length. We have considered two runs initially resolved with 2×160^3 and 2×80^3 particles (for details see De Rossi et al. 2006 in preparation).

Our simulations predict a local LMR which is in good agreement with the observational findings (e.g. [2] among others). The slope and the zero point of the LMR evolve with time in such a way that systems, at a given chemical abundance, are ∼3 mag brighter at $z = 3$ compared with local ones. The major variations in chemical abundance are driven by the faintest systems. We have also analysed the MMR obtaining similar trends to those encountered by [6] for SDSS galaxies but with a displacement of ~ -0.25 dex in the zero point. This discrepancy may be due to the fact that the SDSS explores only the central regions of galaxies leading to an overestimation of the metal content of the systems. We also observe an excess of metals at lower masses for the simulated MMR which may be probably associated to the lack of strong energy feedback in our numerical model.

The metallicity of galactic systems tends to increase with stellar mass in a non-linear way. We have determined a characteristic mass $M_c \sim 10^{10.2} M_\odot h^{-1}$ where the slope of the MMR decreases and the relation starts to flatten for larger masses [5]. It is important to note that this mass is independent of redshift and has been previously mentioned in the literature as a characteristic mass for galaxy evolution [1]. By examining the history of evolution of each individual galactic system, we found that those with stellar masses $M_* > M_c$ have experienced important merger events at high redshift causing an acceleration in the transformation of gas into stars. At lower redshifts these systems are saturated of stars and hence, while their stellar mass significantly increases during a merger event, their metallicity remains almost the same. On the other hand less massive systems form their stars in a more passive way or by rich gas mergers leading to a more tight correlation between stellar mass and metallicity. Thus, the patterns of the MMR are closely related to the hierarchical aggregation of structure in a ΛCDM universe and hence it might be considered a fossil of this process.

MEDR thanks the LOC of this conference for their financial support. This work has been partially supported by CONICET, Fundación Antorchas and LENAC.

References

1. G. Kauffmann, T.M. Heckman, S.D.M. White, S. Charlot, C. Tremonti et al.: MNRAS **341**, 33 (2003)
2. H.A. Kobulnicky, C.N.A. Willmer, A.C. Phillips, D.C. Koo, et al.: ApJ **599**, 1006 (2003)
3. F. Lamareille, M. Mouhcine, T. Contini, I. Lewis, S. Madox: MNRAS **350**, 396 (2004)
4. C. Scannapieco, P.B. Tissera, S.D.M. White, V. Springel: MNRAS **364**, 552 (2005)
5. P.B. Tissera, M.E. De Rossi, C. Scannapieco: MNRAS **364**, 38 (2005)
6. C.A. Tremonti, T.M. Heckman, G. Kauffmann, J. Brinchmann, S. Charlot et al.: ApJ **613**, 898 (2004)

Groups: The Rich, the Poor and the Destitute

A. Zabludoff

University of Arizona, Steward Observatory, 933 N. Cherry Ave., Tucson, AZ, 85750, USA
azabludoff@as.arizona.edu

Summary. I discuss recent observational results that suggest an evolutionary path for groups in which galaxy tidal interactions and mergers strip stars, dark matter, and gas from galaxies. As the group evolves, its velocity dispersion increases, the brightest group galaxy grows and moves toward the center of the potential, other giant galaxies merge, concentrating and/or creating their dwarf satellite populations, group members evolve from late to early types, and intragroup stars are drawn out of their host galaxies. Dark matter and gas are stripped from the galaxies' outer halos and dispersed into a common group halo. The ultimate evolution of this group may be an isolated elliptical or "fossil group". In this process, some evolved groups acquire the characteristics of rich clusters. Given that clusters themselves evolve via the accretion of poor groups from the field, there is evidence that galaxy evolution in groups dominates the evolution of the galaxies that ultimately end up as cluster

members and that evolutionary mechanisms associated with clusters, such as ram pressure stripping or strangulation, are relatively unimportant.

1 Introduction

I have been asked to discuss the evolution of groups as systems. This is a bit more difficult than I would like in that there are few direct measurements of group evolution to date. However, given the many on-going, ambitious surveys for groups in the local Universe and at higher redshifts, as well as the growing sophistication of simulations of group formation and evolution, this talk should become easier to present in the next few years. For the time being, I will discuss what observational evidence we do have – most of it indirect – for the evolution of the galaxy, dark matter, and X-ray components of groups. Because groups are major building blocks for richer clusters, and we do actually observe clusters growing by accreting groups, I will then speculate on how the evolution of these components in groups may ultimately affect their evolution in clusters.

2 Classes of Groups

Let me start by defining what I mean by poor group. I will talking about systems with five or fewer L^* or brighter galaxies. Such groups have a continuum of properties, but it is easiest to divide them into three principal classes based on their masses, X-ray morphologies, and fraction of early-type galaxies. Groups such as NGC 533 have total masses of $\sim 10^{14}\ M_{\odot}$, symmetric and luminous X-ray halos coincident with a giant, central elliptical, and bright early-type fractions comparable to those in rich clusters. Groups like the Local Group are factors of 10–100 lower in mass, are not X-ray luminous, and have no early type galaxies among their brighter members. In between are groups like HCG 90, which could be dynamically evolving between these two extremes: its mass is a few $\times 10^{13}\ M_{\odot}$, its hot, X-ray emitting gas is not relaxed or centered on any galaxy, and its brightest galaxies are late types that are tidally interacting.

There is now evidence for a fourth class of group, which is perhaps the endpoint of some or all group evolution. In the case of these "fossil groups" (e.g., Ponman et al. 1994, Jones et al. 2003) or "isolated ellipticals" (Mulchaey & Zabludoff 1999), we see a single gE, occasionally embedded in an extended X-ray halo (Figure 1). The properties of the X-ray halo, including morphology, extent, luminosity, temperature, metallicity, and gas mass, are all consistent with those of X-ray luminous groups. The total mass derived from the gas kinematics is also like that of such groups. In addition, isolated ellipticals

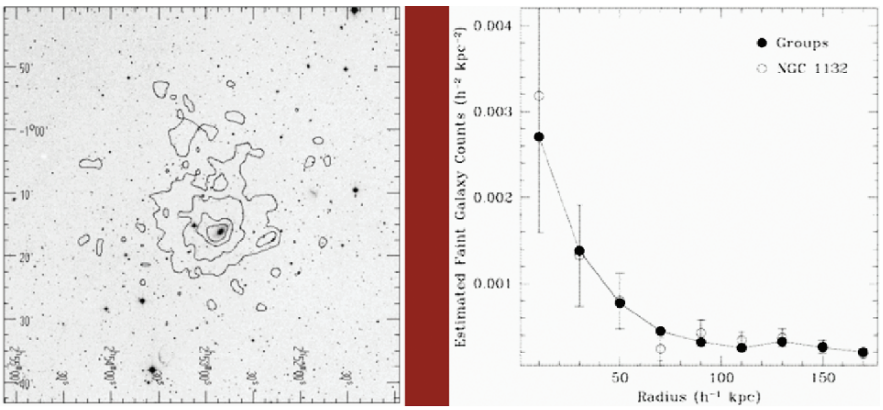

Fig. 1. *Left:* The isolated elliptical NGC 1132 with a group-like X-ray emitting halo (Mulchaey & Zabludoff 1999). *Right:* The projected radial profile and counts of the faint galaxies around NGC 1132 (open circles) are also consistent with those of poor, X-ray luminous groups (solid circles).

with luminous X-ray halos have satellite dwarf populations whose spatial distribution and number density are consistent with those of X-ray luminous groups.

3 An evolutionary sequence?

The classes of groups suggests that they may represent an evolutionary sequence. Of course, groups such as the Local Group, which are collapsing for the first time, could not have been exactly like the progenitors of today's X-ray luminous, high velocity dispersion, gE-dominated, virialized groups, but the initial collapse of what we now call dynamically evolved groups might have looked something like Figure 2.

In this admittedly simplistic scenario, galaxy tidal interactions and mergers strip stars, dark matter, and gas from galaxies, affecting measurable quantities. As the group evolves, its velocity dispersion increases, its gE grows and falls to the center of the potential, the dwarf-to-giant ratio increases as the most massive galaxies merge, concentrating and/or creating their dwarf satellite populations, the morphologies of galaxies evolve to earlier types, and intragroup stars are stripped from their host galaxies. These intragroup stars may evolve in time, spewing their metals into the intragroup medium directly, increasing the metallicity of the gas there. The dark matter and some gas are stripped from the outer halos of the galaxies and dispersed into a common group halo, which eventually equilibrates.

The resulting dynamically evolved group may have an isolated elliptical as its endpoint – the more massive galaxies merge more quickly than the dwarfs,

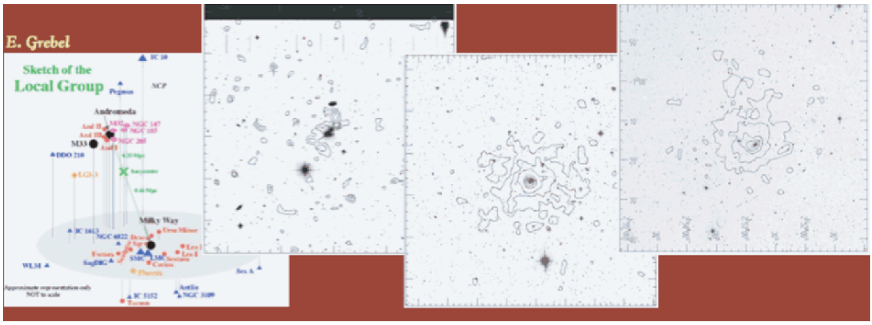

Fig. 2. A schematic of the Local Group (E. Grebel), and the optical/X-ray images of HCG 90, NGC 2563, and NCG 1132, respectively, from left to right (Mulchaey & Zabludoff 1998). Do these four classes of groups represent one possible group evolutionary sequence?

the X-ray halo has a cooling time longer than a Hubble time. At any rate, this scenario predicts than some groups will end up resembling the cluster that may accrete them. As we shall see, this resemblance has consequences for our understanding of cluster evolution as well.

How reasonable is this picture, if very short on details?

Galaxy evolution via mergers in groups

Galaxy mergers are favored in groups, because the internal velocity dispersions of the galaxies are comparable to that of the group. Simulations have long predicted that mergers in groups transform the morphologies, star formation histories, kinematics, and gas properties of late type galaxies into early types, but only recently has work on "E+A" or "k+a" or "post-starburst" galaxies revealed these transformations (e.g., Zabludoff et al. 1996; Norton et al. 2001; Chang et al. 2001; Yang et al. 2004, 2006).

What about the more general evolution of the galaxy population in groups as the group evolves? Here the evidence for the scenario described above is indirect. We observe a strong correlation between early-type fraction and velocity dispersion of groups (Figure 3). Do groups form this way or evolve along this relation? Evidence favoring the latter (nurture) instead of nature comes from a naïve extrapolation of this relation to a cluster-like velocity dispersion of 1000 km/s. At 1000 km/s, we would predict that clusters have unphysical early-type fractions of 120%. Therefore, the relation must turn up (saturate) around 400–500 km/s, a velocity dispersion that would allow two L^* galaxies in a group to merge within a Hubble time. The saturation point in this relation, where some groups start looking like rich clusters, suggests that mergers drive group evolution along this sequence.

There is also indirect evidence that the dwarf-to-giant ratio and the size and centralization of the brightest group galaxy increase as the group evolves.

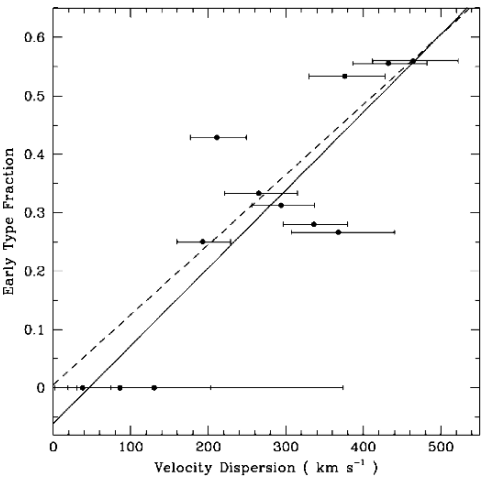

Fig. 3. The group velocity dispersion versus early type fraction relation for poor groups (Zabludoff & Mulchaey 1998). To reproduce the early type fractions of rich clusters (60–80%) with velocity dispersions of about 1000 km/s, this relation turns up (saturates) at 400–500 km/s, also the value that would allow two L^* galaxies in a group to merge within a Hubble time. The saturation point in this relation, where some groups start looking like rich clusters, suggests that mergers drive group evolution along this sequence.

For example, the phase-space diagram (radial velocity vs. projected radius) of the members of a composite X-ray luminous group (Zabludoff & Mulchaey 2000) shows that the brightest group galaxy, a gE, lies in the center of the group's potential well. The dwarf group members tend to cluster about the gE, whereas the other giant galaxies lie on different orbits than the dwarfs. The giant and dwarf populations have not mixed, implying different average formation times. Recent observations at higher redshifts find some low velocity dispersion groups where the gE is offset relative to the group centroid, suggesting that those groups and their gE's are still dynamically evolving (Williams et al. 2006; Momcheva et al. 2006).

Evolution of the dark matter halo in groups

In the previous section, I discussed the evolution of the galaxy component as the group evolves. Here I would like to review what we know about the dark matter halo of a group and the implications for group evolution. The phase-space diagram for the members of a composite X-ray luminous group reveals that the group velocity dispersion is constant with projected radius to at least the virial radius (∼0.5 Mpc; Figure 4).

If all the mass in the group were associated with individual galaxies, most of the mass would be tied to the central gE and the velocity dispersion

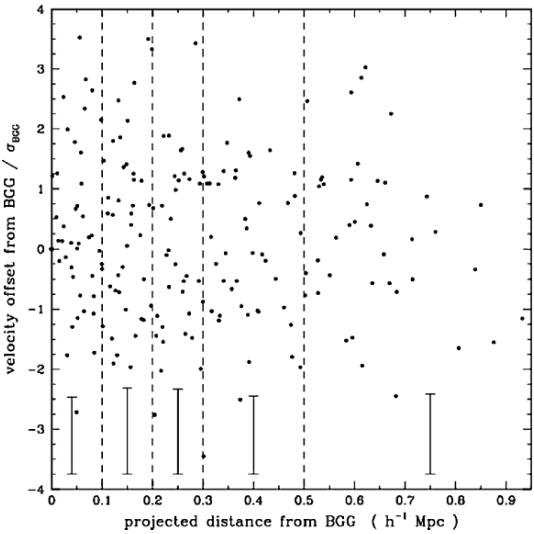

Fig. 4. Phase-space diagram for galaxies in a composite X-ray luminous group (Zabludoff & Mulchaey 1998). The x-axis shows the projected radial offset of each group member from the central gE, the y-axis shows the member's velocity offset from the central gE. The velocity dispersion in each radial bin is roughly constant out to the virial radius of 0.5 Mpc, indicating that the galaxies occupy a common dark matter halo.

would decrease in a Keplerian fashion by a factor of two over this range. The constant velocity dispersion implies that the group mass is increasing with projected radius and that the dark matter is distributed in a common group halo. Early mergers and tidal stripping may have removed dark matter from individual galaxies and re-distributed it in the group halo. The common halo may explain why there are so many poor groups – groups are longer-lived than expected because the galaxy cross-sections to later mergers are smaller than at early times. Unlike these X-ray luminous groups, the Local Group has yet to collapse and its members still retain their individual dark matter halos.

Evolution of the X-ray halo in groups

As for the hot gas component of groups, we might expect that some of it, like the dark matter, may come from the tidally stripped halos of galaxies. The X-ray halo heats to detectable levels as the group velocity dispersion rises and the gas attains hydrostatic equilibrium.

In evolved groups (and in at least some clusters), the X-ray surface brightness profiles have two components: the inner one associated with the central gE and the outer with the diffuse intragroup medium (Mulchaey & Zabludoff 1998; Figure 5). The properties of the outer component are consistent with

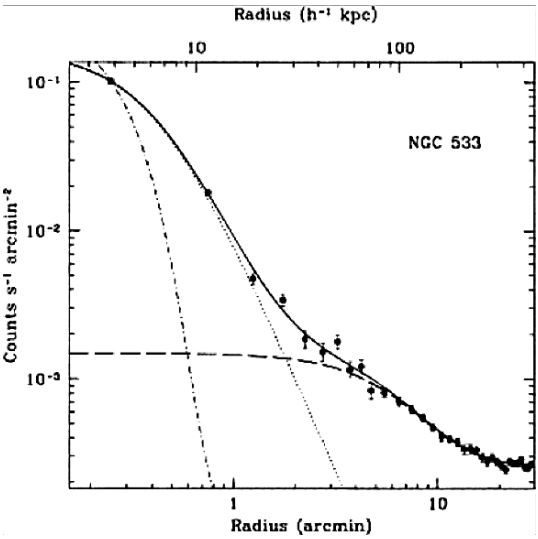

Fig. 5. The two-component X-ray surface-brightness profile of the poor group NCG 533 (Mulchaey & Zabludoff 1998). The PSF is shown by the dot-dashed line.

its being a scaled-down analog of the intracluster medium in richer systems. In particular, the relations among velocity dispersion, X-ray luminosity, and temperature are similar for clusters and X-ray luminous groups, suggesting that the gas and galaxies trace the same potential per unit mass, that the gas lies in hydrostatic equilibrium, and that the intragroup and intracluster media evolve in the same way. Less is known about lower velocity dispersion, X-ray faint or undetected groups, which are naturally more difficult to observe, and claims still vary about whether these less evolved groups lie on the cluster relations.

Evolution of intragroup starlight

The two-components observed in the X-ray surface brightness profiles of groups and some clusters is mirrored in the optical stellar profiles (Figures 6 and 7). We have found that a two-component model (a double de Vaucouleurs profile) is the best fit to deep images of the stellar surface brightness distribution in groups and clusters (Gonzalez et al. 2005; Figure 7). The inner component is associated with the central gE and the outer component with intragroup stars, the latter possessing a color, spatial distribution, and ellipticity like the group galaxies from which it may have been stripped. This intragroup light is a distinct, ubiquitous component of evolved groups, 10–40× larger and more elliptical than the gE component, with which it is

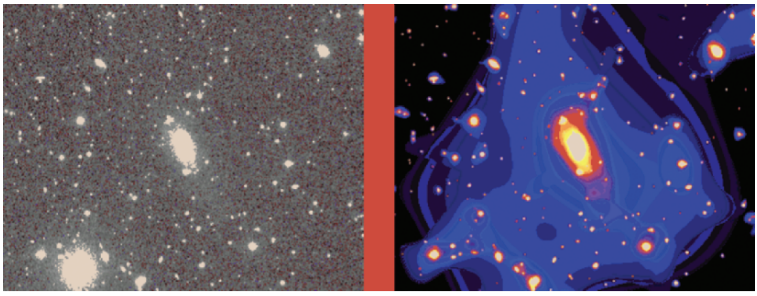

Fig. 6. *Left:* Optical image of the cluster Abell 2955, centered on the brightest cluster galaxy. *Right:* Wavelet smoothed image of the same cluster showing the intracluster starlight (Gonzalez et al. 2005). Intragroup stars make up an even higher fraction of the total optical light in poor groups (Gonzalez et al. 2006, in prep.).

closely aligned. The intragroup stars could be a significant source of metal enrichment for the intragroup medium (Sivanandam et al. 2006, in prep.), a scenario that does not rely on the metals being ejected from group or cluster galaxies.

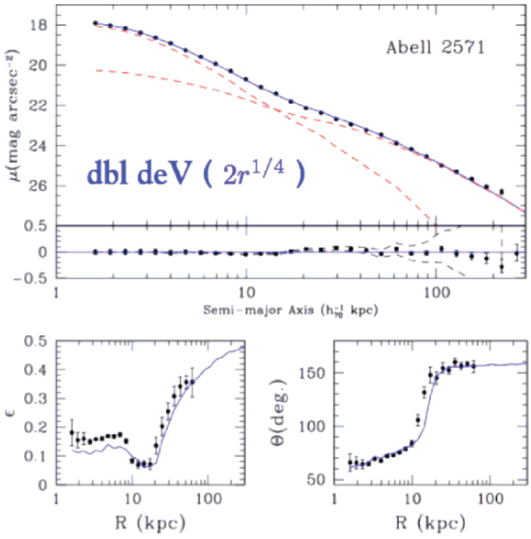

Fig. 7. *Top:* Optical surface brightness profile of the cluster Abell 2571 showing that the intracluster starlight is best fit by a two-component model, just as in the X-ray case. *Bottom:* The double de Vaucouleurs model here also fits the ellipticity and position angle profiles well.

4 Importance of group evolution to galaxies in *clusters*

If mergers and stripping are in part responsible for the evolution of group galaxies, dark matter, intragroup stars, and some of the properties of the hot intragroup medium, *and* clusters form from groups, then the evolution of these group components must affect those in clusters as well. If we consider the galaxy component for starters, it is particularly interesting, as we saw before, that the early-type fractions of some evolved groups look like clusters and that late-to-early type transitional galaxies are found mostly in groups.

There are other revealing observations: 1) the dwarf-to-giant ratios of the quiescent galaxies in X-ray luminous groups and clusters are similar (as parameterized by their luminosity functions; Zabludoff & Christlein 2006, in prep.), 2) the brightest gE is coincident with the centroid of evolved groups, whereas it generally occupies the center of a subcluster (accreted group) in rich clusters, 3) the internal velocity dispersion of the brightest group or cluster galaxy maxes out at about 400 km/s, the velocity dispersion of a group (and one in which, as I discussed before, an L^* galaxy could have merged within a Hubble time), and 4) the break in the normalized star formation rate-local density relation (Lewis et al. 2002, Gomez et al. 2003) occurs at a few galaxies per Mpc^2, roughly the surface density of a poor group.

These "saturation points" suggest that the principal driver for galaxy evolution lies in groups, before and during their accretion by clusters, and that the cluster environment is less important in transforming galaxies. What is the dominant mechanism for this evolution? I have argued above that mergers and tidal stripping of interacting galaxies are both favored and observed in groups, and are less likely to occur in clusters once the galaxies in an accreted group are assimilated by the cluster.

Is what happens to the galaxy in the group more important that any subsequent effect – such as ram pressure stripping or galaxy strangulation – associated with the cluster? These cluster-based mechanisms transform by fading a galaxy's disk, whereas galaxy-galaxy interactions are more likely to grow a galaxy's bulge. We can therefore ask whether early type galaxies can form via fading the disks of late types. Christlein and Zabludoff (2004) show that bulges grow brighter from late to early types, but that the disks do not grow fainter. They also show that the morphology-environment relation arises mostly from bulges getting brighter in denser environments, not from disks getting fainter. These results suggest that galaxy-galaxy interactions, presumably in accreted groups/subclusters, dominate any environment-driven galaxy evolution in clusters.

5 Conclusions

In summary, I conclude that mergers and stripping are important to group evolution. As the group evolves, the dwarf-to-giant ratio, early type fraction,

intragroup starlight, and gE grow (and the gE moves toward the center of the potential). Dark matter and hot gas are stripped from galaxies and end up in a common, relaxed halo. Isolated giant ellipticals ("fossil groups") may be the endpoint of the dynamical evolution of some, if not all, groups. There are many "saturation points" where the properties of groups look like clusters, but unlike the more rarefied field. Group galaxy evolution via mergers and tidal interactions among galaxies may dominate the evolution of galaxies in clusters. In fact, the morphology-environment relation, the Butcher-Oemler effect, and brightest cluster galaxy formation may all arise in groups prior to and during accretion by the parent cluster.

I have focused the above statements on how the evolution of galaxies in groups ultimately affects galaxies in clusters. Is the group environment similarly important for the other components of clusters: the dark matter halo, the X-ray gas, and the intracluster starlight? Rudick et al. (2006) present interesting simulations arguing that intracluster stars are stripped from galaxies in groups prior to their infall into clusters. Does this picture imply that the enrichment of what will be the intracluster medium also occurs first in groups? Careful analysis of new and improved X-ray data may refine the velocity dispersion-metallicity relation for groups and clusters and provide some clues.

Hopefully, some of this speculation will be tested when we observe galaxy evolution in groups *directly*. Because groups have smaller surface density contrasts, X-ray luminosities, and lensing effects than rich clusters, it has been difficult to find many groups at higher redshifts to establish a real timeline. However, ambitious X-ray and optical surveys are gradually adding to the database of intermediate redshift groups. My collaborators and I have adopted the following approach to find distant groups: we identify those strong gravitational lens systems in which the lensing models fail in a manner that suggests there is an unaccounted-for, group-sized dark matter halo. We then obtain images and spectroscopy for the galaxies in the field of the lens galaxy to determine if the lens does lie in a group. So far, we have identified roughly 25 groups with redshifts of 0.3–0.8 (Momcheva et al. 2006, in prep.). We are presently characterizing the properties of these group members over this wide evolutionary baseline.

References

1. T.-C. Chang et al.: AJ, **121**, 1965 (2001)
2. D. Christlein & A.I. Zabludoff: ApJ, **616**, 192 (2004)
3. P.L. Gomez et al.: ApJ, **584**, 210 (2003)
4. A.H. Gonzalez, A.I. Zabludoff & D. Zaritsky: ApJ, **618**, 195 (2005)
5. L.R. Jones et al.: MNRAS, **343**, 627 (2003)
6. I. Lewis et al.: MNRAS, **334**, 673 (2002)
7. I. Momcheva et al.: ApJ, **641**, 169 (2006)

8. J.S. Mulchaey & A.I. Zabludoff: ApJ, **496**, 73 (1998)
9. J.S. Mulchaey & A.I. Zabludoff: ApJ, **514**, 133 (1999)
10. S.A. Norton et al.: ApJ, **557**, 150 (2001)
11. T.J. Ponman et al.: Nature, **369**, 462 (1994)
12. C. Rudick et al.: ApJ, **648**, 936 (2006)
13. K. Williams et al.: ApJ, **646**, 85 (2006)
14. Y. Yang et al.: ApJL, **646**, L33 (2006)
15. Y. Yang et al.: ApJ, **607**, 258 (2004)
16. A.I. Zabludoff & J.S. Mulchaey: ApJ, **539**, 136 (2000)
17. A.I. Zabludoff & J.S. Mulchaey: ApJ, **496**, 39 (1998)
18. A.I. Zabludoff et al.: ApJ, **466**, 104 (1996)

The Eridanus Supergroup

S. Brough

Centre for Astrophysics and Supercomputing, Swinburne University of Technology, Hawthorn, VIC 3122, Australia
sbrough@astro.swin.edu.au

Summary. We examine a supergroup in the direction of the Eridanus constellation using 6dF Galaxy Survey second data release (6dFGS DR2) positions and velocities. We also examine the colours and morphologies of the galaxies in the region with respect to their local projected surface density. We find that the colours of the galaxies redden with increasing density and the morphologies of the galaxies show a strong morphology-density relation. The colours and luminosities of the galaxies in the supergroup are already similar to those of galaxies in clusters.

1 Introduction

The paradigm of hierarchical structure formation leads us to expect that clusters of galaxies are built up from the accretion and merger of smaller structures like galaxy groups [4]. Although we observe clusters of galaxies accreting galaxy group-like structures along filaments (e.g. [12]) we lack clear examples of groups merging together to form clusters – a 'supergroup'. We define a supergroup to be a group of groups that will merge to form a cluster.

The concentration of galaxies in the region behind the Eridanus constellation is a possible supergroup in the local Universe. These galaxies lie at a distance of ∼21 Mpc and form a filamentary structure with the Fornax cluster. The concentration includes two optically classified groups of galaxies (NGC 1407; [8] and NGC 1332; [3]) which are at similar recession velocities.

ROSAT data is available for both the NGC 1407 and NGC 1332 groups from the Group Evolution Multi-wavelength Study (GEMS; [2]). The X-ray emission around the NGC 1407 galaxy is emitted from the intra-group gas, confirming the presence of a massive structure. In contrast, the X-ray emission from the NGC 1332 group is associated with the NGC 1332 galaxy, not with intra-group gas. [14] suggest that there is intra-group gas associated with NGC 1395, a large elliptical in this region, however no optically selected group has previously been associated with this galaxy.

This region is therefore a prime candidate for a supergroup.

2 Data

The 6dF Galaxy Survey (6dFGS; [10]) is a wide-area (the entire Southern sky with $|b| > 10°$), primarily K_s-band selected galaxy redshift survey. The catalogue provides positions, recession velocities, and spectra for the galaxies. Galaxy data were obtained from the second data release of the 6dFGS [11] for an area of radius 15 degrees, centred on the position of NGC 1332, in the velocity range 500–2500 km s^{-1}. This provides a sample of 135 galaxies.

The 6dFGS is not yet complete. We therefore obtained further sources from the NASA/IPAC Extragalactic Database (NED) with known recession velocities between 500 and 2500 km s^{-1}. This added an additional 378 galaxies. All 513 6dFGS DR2 and NED galaxies are illustrated in (Figure 1).

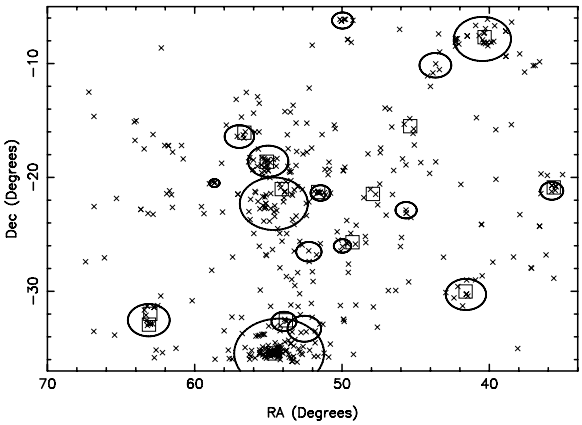

Fig. 1. Spatial distribution of the 6dFGS DR2 and NED galaxies in the Eridanus region. The squares indicate the positions of previously optically catalogued groups in this region with known velocities and the Fornax cluster (RA ∼55; Dec ~ -35). The ellipses indicate the radial extent of the 17 groups found.

It was unfeasible to obtain new photometric data so we used the HyperLyon-Meudon Extragalactic DAtabase (HyperLEDA; [15]) to obtain total B-band magnitudes and morphological T-types for the galaxies brighter than the 2MASS apparent-magnitude limit ($m_K \sim 13.1$). This resulted in 193 galaxies with both B-band magnitudes and T-types.

3 Group properties

In order to study the dynamics of the region it is important to determine which galaxies are associated with each structure. We used the 'friends-of-friends' (henceforth FOF; [9]) percolation algorithm. This method finds group

structures in galaxy data based on positional and velocity information and does not rely on any *a priori* assumption about the shape of groups.

Our FOF analysis has determined that the region is made up of three individual groups (Figure 1). The NGC 1407 group is a massive group with intra-group X-ray emission centred on the large central elliptical galaxy, implying that this is a dynamically mature group. In contrast, the Eridanus group is a low-mass, irregular group with a high spiral fraction. It is not centred on any one galaxy and the spatial offset of the X-ray emission from the centre of the group signifies that this group is dynamically young. The NGC 1332 group is a compact, low-mass group with a low spiral fraction, however there is no X-ray emission associated with this group, only with the central galaxy NGC 1332.

A detailed analysis of the possibility that these groups are bound is presented in [5]. In summary, we find that it is unlikely that the three Eridanus groups form a gravitationally bound structure. However, the Eridanus and NGC 1407 groups and, at a lesser level, the NGC 1407 and NGC 1332 groups are individually bound. A two-body orbital analysis then suggests that the Eridanus and NGC 1332 groups are falling into the NGC 1407 group. We therefore conclude that these groups do form a supergroup, that will merge in the future by dynamical friction to form a cluster.

Although one expects clusters to form from the merging of small galaxy group sized structures, this is expected to happen predominantly at high redshifts, $z \sim 1$. However, the properties of the groups studied here argue that the supergroup consists of one massive, relaxed group (NGC 1407) that formed at those epochs and now has two less massive groups falling in to form a cluster-mass structure, consistent with the predictions of hierarchical structure formation in a ΛCDM Universe.

The three groups in the Eridanus region form a rare, local example of a supergroup. It is, therefore, important to examine the properties of its constituent galaxies.

4 Galaxy properties

The importance of studying the properties of galaxies with respect to their environment is stressed clearly throughout this conference. Studying such a large area of sky means that our galaxy sample encompasses a wide range of environments with which to examine environmental dependences.

We calculated the local galaxy density of each galaxy as the projected surface density of the 5 nearest neighbours to that galaxy within ± 1000 km s^{-1} (Σ_5; [2, 16]). We deal with the effects of edges following [2, 16]. Densities of 75–250 Mpc^{-2} correspond to the centre of the Fornax cluster whilst $\Sigma_5 \sim 100$ Mpc^{-2} corresponds to the density around the NGC 1407 galaxy, $\sim$50 Mpc^{-2} to the NGC 1332 galaxy and $\sim$25 Mpc^{-2} around the NGC 1395 galaxy.

We use the apparent-magnitude limited sample of galaxies with which to examine the distribution with environment of their morphologies and colours. Figure 2 shows the clear morphology-density relationship with galaxies in the most dense environments consisting almost solely of early-type galaxies.

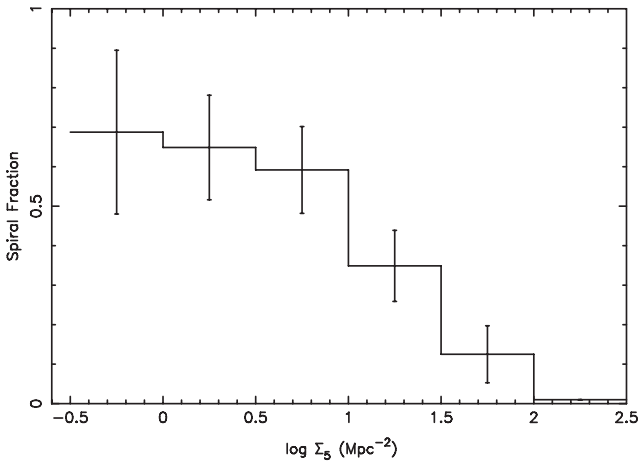

Fig. 2. The fraction of spiral galaxies (T-types >0.0) in each projected local galaxy density bin, the error bars indicate the poisson error in each bin.

We also examine the colours of the galaxies with their projected surface density in Figure 3. The colours of the galaxies are corrected to the colour they would possess at a magnitude of $M_K = -20$, using the colour-magnitude relation fitted to these data. A shallow trend of redder colour with increasing galaxy density is observed. A non-parametric Spearman rank correlation gives a correlation coefficient of $r_s = 0.25$. For 183 galaxies, the Student's t-test rejects the null hypothesis that there is no correlation at >99 per cent confidence level. Thus galaxies in the densest environments are redder than those in the least dense environments.

The relationship between colour and density does not show a sharp transition as observed by [12] and [16]. It is somewhat surprising that we do not observe this sharp transition as we study the same range of projected surface densities. However, the previous studies all had samples at least ∼100 times larger (e.g. [16] with 19714 galaxies) than that available here.

We therefore examined the data to determine whether there is a density at which the colours of the galaxies in denser environments are significantly different to those in less dense environments. We find that at a projected local surface density of ∼2.5 galaxies Mpc^{-2} the probability that the high- and low-density samples are not drawn from the same parent population is 99.98 per cent. This dividing density is in agreement with previously observed densities of sharp colour transitions and is equivalent to the density of galaxies

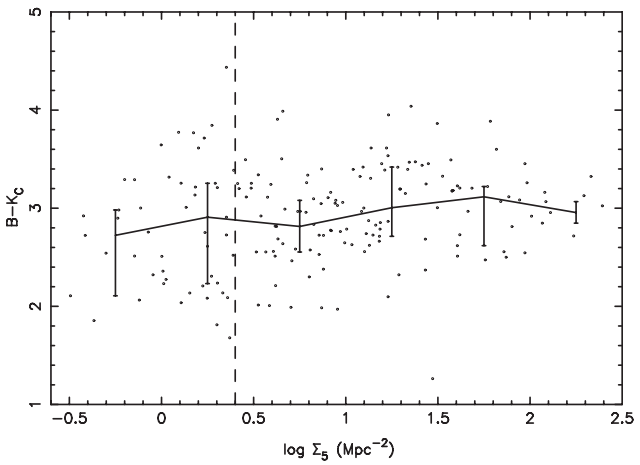

Fig. 3. Variation in colour with local projected galaxy density (Σ_5). The colours are normalised to $M_K = -20$. The solid line represents the loci of the median colours and the error bars indicate the ± 25 percentile colours. The dashed line indicates the density at which the colours of the galaxies in the lower and higher density environments are most different (2.5 galaxies Mpc^{-2}).

on the outskirts of the supergroup structure. The colours of galaxies in the supergroup are therefore already similar to those in clusters.

5 Conclusion

This is a rare example of a supergroup in the local Universe. The mass ratios and properties of the individual groups are consistent with the predictions of hierarchical structure formation. The properties of the constituent galaxies indicate that they are already similar to those of a cluster and that this is likely to be a result of merging or strangulation processes in group density environments. More details of our analysis are given in [5].

References

1. Baker R. H., Shapley H., 1933, Annals of the Astronomical Observatory of Harvard College, 88, 77
2. Balogh M. L. et al., 2004, MNRAS, 348, 1355
3. Barton E., Geller M., Ramella M., Marzke R. O., da Costa L. N., 1996, AJ, 112, 87
4. Blumenthal G. R., Faber S. M., Primack J. R., Rees M. J., 1984, Nature, 311, 517
5. Brough S., Forbes D. A., Kilborn V. A., Couch W., Colless M., 2006, MNRAS, in press

6. da Costa, L. N. et al., 1988, ApJ, 327, 544
7. Forbes D. A. et al., 2006, PASA in press
8. Garcia A. M., 1993, A&AS, 100, 47
9. Huchra J. P., Geller M. J., 1982, ApJ, 257, 423
10. Jones D. H. et al., 2004, MNRAS, 355, 747
11. Jones D. H., Saunders W., Read M., Colless M., 2005, astro-ph/0505068
12. Kodama T., Smail I., Nakata F., Okamura S., Bower R. G., 2001, ApJ, 562, 9
13. Lacey C. G., Cole S., 1993, MNRAS, 262, 627
14. Omar A., Dwarakanath K. S., 2005, JApA, 26, 1
15. Paturel G. et al., 1997, A&AS, 124, 109
16. Tanaka M., Goto T., Okamura S., Shimasaku K., Brinkmann J., 2004, AJ, 128, 2677

ClG J1205 + 4429, the Most Distant Fossil Group at z = 0.59

F. Durret[1], M.P. Ulmer[2], C. Adami[3] G. Covone[4] and G.B. Lima Neto[5]

[1] Institut d'Astrophysique, CNRS, Université Pierre et Marie Curie – Paris 6, 98bis Bd Arago, F 75014 Paris, France
durret@iap.fr
[2] Department Physics & Astronomy, Northwestern University, Evanston, IL 60208-2900, USA
m-ulmer2@northwestern.edu
[3] OAMP, Marseille, France
christophe.adami@oamp.fr
[4] INAF, Osservatorio Astronomico di Capodimonte, Naples, Italy
covone@na.astro.it
[5] IAG, São Paulo, Brazil
gastao@astro.iag.usp.br

Summary. We present the main properties of ClG J1205 + 4429, the most distant fossil group known up to now.

1 Introduction

ClG J1205 + 4429 (hereafter Cl 1205) was detected as part of the Bright SHARC survey search for extended X-ray sources in ROSAT PSPC fields (Adami et al. 2000, Romer et al. 2000, 2001). An optical follow up in two bands with the 3.5m ARC telescope then showed that it contained mostly very red galaxies (with colours i'$-K_s$ around 3), suggesting it could be a distant cluster with a redshift $z \sim 1$. We obtained XMM-Newton and Chandra observations for this object, and coupled these data with an optical HST image and a radio map taken from the archives. Cl 1205 turned out to be by far the most distant fossil group of galaxies known, and we present our main results here. A detailed analysis of this object can be found in Ulmer et al. (2005).

2 Morphological characteristics

The HST image in the F702W filter is displayed in Fig. 1. It reveals the presence of a very bright galaxy, surrounded by notably fainter ones. The magnitude difference between the brightest and second brightest galaxies is

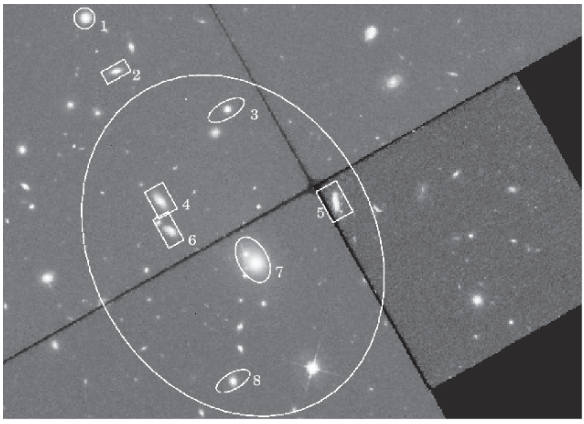

Fig. 1. Zoom of HST image in the F702W filter. North is up and east to the left. The field is $\sim 0.97 \times 0.72$ arcmin^2. The galaxy labeled 1 is likely to be an AGN not related to the group. The galaxies marked with rectangles are late types and those with ellipses are early types. The large ellipse represents the approximate extent of the X-ray emission, see Fig. 2.

almost 2 magnitudes (i' = 18.50 and 20.43 for objects labeled 7 and 4 respectively, in Fig. 1), suggesting that this group is a fossil one, following the definition given by Jones et al. (2003).

Though various time allocation committees have not given us telescope time to gather optical spectra for the galaxies of this group, the mean group spectroscopic redshift of 0.59 was kindly given to us by J. Mulchaey (private communication). The rest of our analysis will be based on this value. With z = 0.59, the absolute magnitude of the central galaxy in the R band is found to be very bright: $M_R \sim -24.1$ (assuming $H_0 = 70$ km s^{-1} Mpc^{-1}, $\Omega_\Lambda = 0.7$ and $\Omega_m = 0.3$ throughout this paper).

The HST image, onto which Chandra X-ray and VLA FIRST radio contours are superimposed is shown in Fig 2. The brightest galaxy coincides with the centroid of the Chandra X-ray emission, confirming that it is indeed at the center of the group. The Chandra emission (see Ulmer et al. Fig. 11) may show two peaks, but the small number of photons detected prevents from making any accurate decomposition. The VLA radio map reveals the existence of a double lobed source which has no obvious relation with the X-ray emission (see Ulmer et al. Fig. 11).

3 X-ray properties

The spectra obtained with the three instruments MOS1, MOS2 and PN on XMM-Newton are shown in Fig. 3 together with the Chandra spectrum. In spite of XMM exposure times between 16500 and 21200s (after eliminating

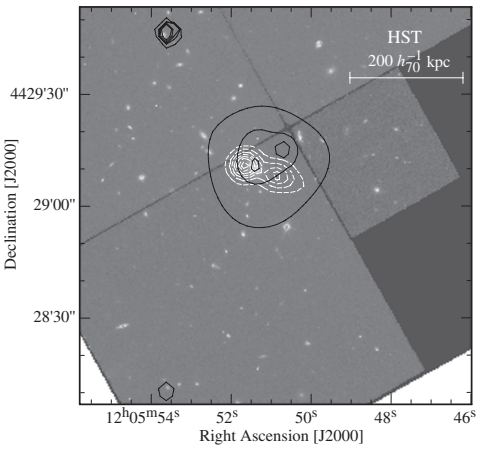

Fig. 2. HST image in the F702W filter, with Chandra X-ray contours superimposed in black and VLA radio contours in white. North is up and east to the left.

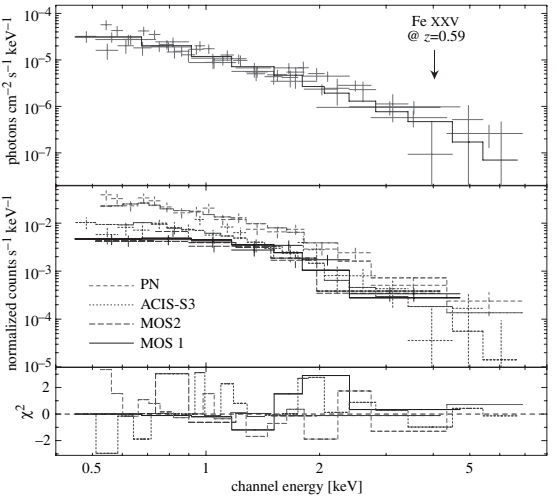

Fig. 3. *Top*: XMM-Newton flux in photons cm^{-2} s^{-1} keV^{-1} with the best fit superimposed (black line). The expected position of the FeXXV line at the group redshift is indicated. *Middle*: fluxes in counts s^{-1} keV^{-1} for all cameras: full line, MOS1; long dashed line, MOS2; dotted line, PN; short dashed line, ACIS-S3. The differences among best fit spectra come from the different detector responses. *Bottom*: residuals given as the χ^2 contribution of each energy bin.

flares), the signal to noise is rather poor. If we fix the metallicity to the typical value found in clusters ($0.3Z_\odot$) and the neutral hydrogen absorption $N_{\rm H}$ to the galactic value, a thermal fit gives a mean temperature $kT = 3.0^{+0.3}_{-0.3}$ keV. This value is typical of a poor cluster, and warmer than that of fossil groups (Jones et al. 2003).

The bolometric X-ray luminosity is then (9.2 ± 0.7) 10^{43} erg/s, corresponding to an X-ray gas mass of 1.9 10^{12} $M_\odot$ and to a total mass of 1.0 10^{13} $M_\odot$. Here also, values are closer to those of poor clusters rather than groups.

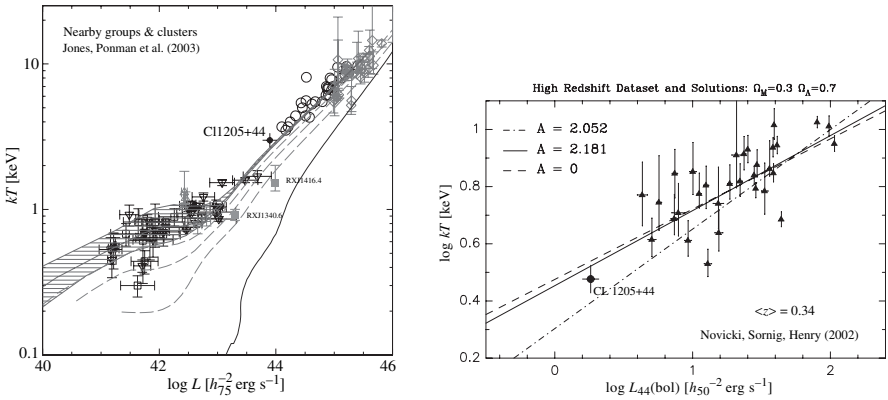

Fig. 4. $L_X - T_X$ relations drawn by Jones et al. (2003) for clusters and groups (left), and by Novicki et al. (2002) for <z> = 0.34 clusters (right).

The intermediate nature of Cl 1205 is confirmed by its position in the $L_X - T_X$ relations drawn by Jones et al. (2003) for clusters and groups, and by Novicki et al. (2002) for <z> = 0.34 clusters, as illustrated in Fig. 4.

4 A formation and evolution scenario for Cl 1205

Cl 1205+44 is the highest redshift known fossil group, and therefore its study is of great importance to gain insight on the evolutionary mechanisms of this peculiar class of galaxy groups. Numerical simulations predict that a merged group can relax to form a single elliptical galaxy (e.g. Barnes 1989), and the timescales for the brightest group members to merge into an elliptical are smaller than a Hubble time (Zabludoff & Mulchaey 1998). Recent N-body/hydrodynamical simulations (D'Onghia et al. 2005) have shown that in galaxy groups the magnitude gap between the first two brightest galaxies is directly related to the formation epoch of the system. Fossil groups appear to have assembled more than half of their $z = 0$ total mass at redshift higher than 1, and were likely already "fossilized" at $z \sim 1$ or before. The discovery of Cl 1025+44 at z = 0.59 supports this view based on cosmological simulations. A likely scenario for Cl 1205 is therefore the following: an initial potential well created by dark matter was present, into which energy injection took place (supernovae, radio galaxies, ULIRGs etc.). The group then "fossilized" at redshift higher than 1, with later little infall of bright galaxies onto the

group from the surrounding environment. Gas-rich galaxies that did fall into the group by $z \sim 2$ have probably lost gas by ram pressure stripping, and star formation was therefore suppressed in these galaxies, making them appear almost as red as early type ones. Many galaxies have then been cannibalized by the central galaxy, explaining why this object is so much brighter than the surrounding ones. The entire evolutionary process is expected to have lasted about 4 Gyr.

5 Comparison with other fossil groups

A nice summary of the properties of the 15 fossil groups known up to now can be found in Mendes de Oliveira et al. (2005). If we look at their Table 4, we can see that Cl 1205 is by far the most distant, and the second brightest in X-rays. Note that one object is missing: RX J0419.6+0225 (Böhringer et al. 1998)

Cl 1205 is obviously quite comparable to other fossil objects such as RX J1340.6+4018 (Ponman et al. 1994), NGC 1132 (Zabludoff & Mulchaey 1999), OLEGs (Vikhlinin et al. 1999) or the five fossil groups analyzed by Jones et al. (2003). The latter gave the presently accepted definition of fossil groups: spatially extended X-ray sources with a bolometric X-ray luminosity $L_{X,bol} > 10^{42}$ erg/s, and a difference in optical magnitude larger than 2.0 between the brightest and second brightest galaxies.

If the merger interpretation is correct, fossil groups have seen little infall since their collapse. They can therefore be important for studying the formation and evolution of galaxies and of the intragroup medium in isolated systems. Fossil groups may be a way to explore the possible link between ellipticals and compact galaxy groups, and more generally they offer a peculiar environment to test the predictions of the hierarchical galaxy formation scenario. The detection of the $z \simeq 0.6$ fossil group Cl 1025+44 shows both that a relatively large population of FGs should already be in place at $z \sim 1$ (in agreement with recent cosmological simulations) and that it is now possible to detect them (or their direct progenitors) at $z \sim 1$, for instance through deep imaging of the X-ray extended sources found in the XMM data archive with 10-m class telescopes.

References

1. Adami C., Ulmer M.P., Romer A.K. et al. 2000, ApJS 131, 391
2. Barnes J.E. 1989, Nature 338, 123
3. Böhringer H., Guzzo L., Collins C. et al. 1998, The Messenger 94, 21
4. Jones L.R., Ponman T.J., Horton A. et al. 2003, MNRAS 343, 627
5. Mendes de Oliveira C., Cypriano E. & Sodré L. 2005, astro-ph/0509884, AJ in press

6. Novicki M.C., Sornig M., Henry J.P. 2002, AJ 124, 2413
7. D'Onghia E., Sommer-Larsen J., Romeo A.D. et al. 2005, ApJ 630, L109
8. Ponman, T.J., Allan, D.J., Jones, L.R. 1994, Nature 369, 462
9. Romer A.K., Nichol R.C., Holden B.P. et al. 2000, ApJS 126, 209
10. Romer A.K., Viana P.T.P., Liddle A.R., Mann R.G. 2001, ApJ 547, 594
11. Ulmer M.P., Adami C., Covone G. et al. 2005, ApJ 624, 124
12. Vikhlinin A., McNamara B.R., Hornstrup A. et al. 1999, ApJ 520, L1
13. Zabludoff A.I. & Mulchaey J.S. 1998, ApJ 498, L5
14. Zabludoff A.I. & Mulchaey J.S. 1999, ApJ 514, 133

Past and Future of CG J1720-67.8: Constraints from Observations and Models

S. Temporin[1,2] and W. Kapferer[1]

[1] Institut für Astro- und Teilchenphysik, Leopold-Franzens University Innsbruck, Technikerstraße 25, A-6020 Innsbruck
giovanna.temporin@uibk.ac.at, wolfgang.e.kapferer@uibk.ac.at
[2] INAF - Brera Astronomical Observatory, Via Brera 28, I-20121, Milano

Summary. We discuss the evolution of the peculiar, nearby (z = 0.045), compact galaxy group CG J1720-67.8, by interpreting a large amount of observational information on the basis of our recent results from spectrophotometric evolutionary synthesis models and new N-body/SPH simulations. The group, that is composed of two spiral galaxies with a mass ratio approximately 4:1 and an S0 galaxy in a particularly compact configuration, is undergoing an active pre-merging phase. Several tidal features are signposts of the complex dynamics of the system. We suggest that the observed structure of the tidal features can be explained only if all three galaxies are involved in a strong interaction process.

Key words: Galaxies: Interactions; Galaxies: Evolution

1 Introduction

Several catalogues of compact galaxy groups (CGs) have been compiled during the last 20 years (e.g. V. Eke, this volume). Many studies have been/are devoted to understand the nature of CGs and their evolution from both an observational and a theoretical point of view (see e.g. the contributions by J. Hibbard, G. Mamon, E. Pompei, this volume). Nevertheless, we do not have yet a clear understanding of how groups evolve and what the product of their evolution is. The study of individual groups in differing evolutionary phases might be useful in this respect, in particular for rarely observed phases, like the pre-merging state represented by extremely compact systems. This is the main motivation of our detailed studies of such a compact system, CG J1720-67.8. In fact, this group gives us the rare opportunity to gather information on the evolutionary stage that precedes the coalescence and provides us with an indication of the processes that might be at play at higher redshifts. In the last few years we collected a large amount of observational information on this system to disentangle its evolutionary history. The application of evolutionary synthesis models allowed us to date the latest bursts of star formation, that are related to the most recent galaxy encounters. In the following we summarize some of the most significant results concerning this

system, and discuss its evolution on the basis of the comparison – presented here for the first time – with N-body/hydrodynamical simulations.

2 A very evolved galaxy group

The group CG J1720-67.8 [5, 6], composed of two spiral galaxies (G1 and G4), one S0 galaxy (G2), and a number of tidal dwarf galaxy candidates in a very compact configuration (Fig. 1), appears to be next to the final merging [7]. All components show significant star formation activity. In fact the group has a total (uncorrected) Hα luminosity of 3.7×10^{41} ergs s^{-1} and the total star formation rate derived from the 20 cm radio continuum emission – which is largely unaffected by extinction – is 18 M$_\odot$ yr^{-1}. The prominent tidal features, which account for about one third of the optical luminosity and of the Hα emission of the group, indicate that the galaxies have recently undergone violent interactions. The age of the most prominent tidal tail, based on its projected length and on the kinematics of G4, is estimated to be approximately 200 Myr. This is indicative of the age of the latest strong interaction event.

The velocity field of the group (Fig. 3) obtained from the Hα emission line gives evidence of its complex kinematics. The kinematic center is offset from the center of G4 by about 5 kpc. Galaxies G1 and G4, and the bridge of ionized gas between them have similar systemic radial velocities. Radial velocities gradually increase along the tidal tail from south to north, with a strong gradient in the northern part, near G4 and G2. There is no visible sign of return of tidal material to the parent galaxy. The deficiency of neutral hydrogen in compact groups has been suggested as an indicator of their evolutionary state [9]. The lack of detected neutral hydrogen in CG J1720-67.8, which gives an upper limit to the HI content of 2.3×10^9 M$_\odot$, would suggest

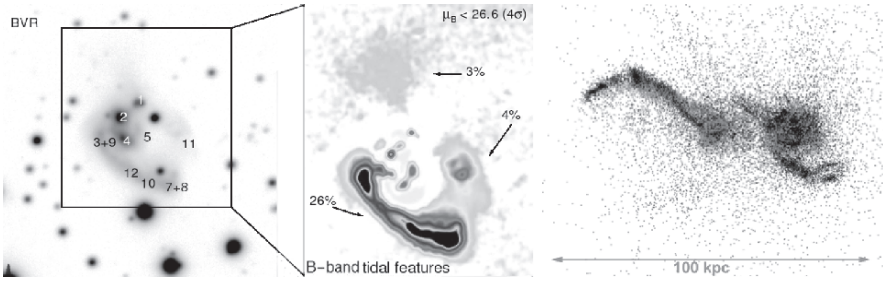

Fig. 1. *Left.* Composite BVR image of CG J1720-67.8. The galaxies and tidal dwarf candidates are labeled. *Middle.* Zoom on the tidal features on the B image after subtraction of the stars and bi-dimensional galaxy models. *Right.* A timestep of the simulation of a prograde encounter between two unequal mass galaxies. The stellar component is plotted in grey and the gaseous component in black (see Sect. 3).

that the group is HI-deficient, if compared with the total B luminosity [7]. However, in this case the B-band luminosity is particularly enhanced due to the star formation activity, hence it leads to an overestimate of the expected neutral hydrogen content of the group. The small size of the galaxies (diameters of ≈8 and 14 kpc for G1 and G4), following [2], suggest an expected HI mass $\leq 2 \times 10^9$ $M_\odot$, comparable to our estimated upper limit. The diameters of these strongly interacting galaxies are ill-defined, however, the whole galaxy group with its tidal features, has an optical size comparable to that of our Galaxy, so it is expected to have a similar content of neutral gas. As a consequence, in this case the available upper limit to the HI mass is not sufficient to establish whether the group is HI-deficient or not.

2.1 Results from evolutionary synthesis models

The application of chemically-consistent spectrophotometric evolutionary synthesis models to the three main galaxies of CG J1720-67.8 provided us with information about the age and strength of the latest interaction-induced bursts of star formation [8]. According to the best-fit models, the two spiral galaxies underwent a strong burst of star formation 40–180 Myr ago. An older burst of star formation in the S0 galaxy accompanied either a merger event or an interaction with the companions, ≤1 Gyr ago. The total (stars + gas) masses of the galaxies implied by the best-fit models are $3.4 - 7 \times 10^{10}$ $M_\odot$ (depending on the considered model) for G2, $4 - 6 \times 10^9$ $M_\odot$ for G1, and 2×10^{10} $M_\odot$ for G4. Therefore, the total stellar plus gaseous mass of the galaxies involved, without taking into account the material in the tidal tail(s), is $\geq 6 \times 10^{10}$ $M_\odot$. The visible mass of the final group remnant is expected to be on the order 10^{11} $M_\odot$.

3 Clues from hydrodynamical simulations

Observations alone are not sufficient to establish the interaction history of the group, although they give important indications. Extensive numerical simulations are required for this purpose. Here we present a first exploration of the possible evolutionary paths that could explain the observed galaxy configuration, on the basis of combined N-body/SPH simulations. For the modelling we used GADGET-2 [4]. For general assumptions and technical details of the simulations we refer the reader to [3] and references therein. Since the two spiral galaxies G1 and G4 have similar systemic velocities and appear to be connected by a bridge of ionized gas, we first compared the observations with an encounter between two unequal mass disks. The best-fit evolutionary synthesis models imply for these two galaxies a mass ratio ≈1:3 or 1:4, hence a 1:3 mass ratio was adopted in the simulations. The properties of the simulated galaxies are similar to those listed in table 1 of [3]. Both fast prograde encounters and retrograde encounters between the two disks

produce a knotty tidal tail departing from the more massive galaxy, but also a relatively prominent counter-tail departing from the less massive galaxy (see e.g., the timestep shown in Fig. 1). The latter is not observed in CG J1720-67.8. This points to a non-negligible role of the S0 galaxy in the interaction. The presence of the third galaxy could suppress the formation of the counter-tail in the smaller spiral. To test this hypothesis, we introduced the S0 galaxy in our simulation. The formation of the S0 galaxy was simulated through an equal mass disk merger. After 1 Gyr a massive disk approaches the S0 and starts a burst of star formation accompanied by galactic winds (Fig. 2, left). The encounter of this spiral with the merger remnant produces a knotty tidal arm and a bridge of stars and gas toward the S0 (Fig. 2, top-right). Another 15 Myr later, in turn, the less massive disk undergoes an encounter with the S0, is strongly distorted by it, without producing any significant tidal tail (Fig. 2, bottom-right), and starts an induced burst of star formation. Some residual star formation activity is still present at the center of the S0. Although this simulation thus not reproduce the galaxy configuration of CG J1720-67.8, it shows several features similar to the observed ones concerning the morphological distortions, the tidal tails, and the induced star formation. Also the velocity field, projected along a hypothetical line-of-sight, has some similarities with the observed one, as shown in Fig. 3.

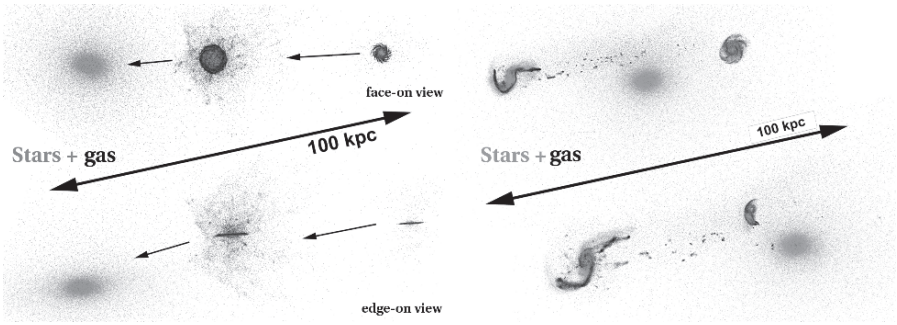

Fig. 2. *Left.* N-body/SPH simulation of the encounter between two disks and an early-type galaxy. At this time-step the larger spiral has started the interaction. *Right.* Subsequent timesteps of the simulation after the encounter of the S0 with the larger spiral (top) and with the smaller spiral (bottom).

4 Conclusions

We found several observational evidences that CG J1720-67.8 is in a late pre-merging phase. The evolutionary stage of the group is similar to that of HCG 31, which is claimed to have started its merging process [1]. According to evolutionary synthesis models the latest interaction episode for the

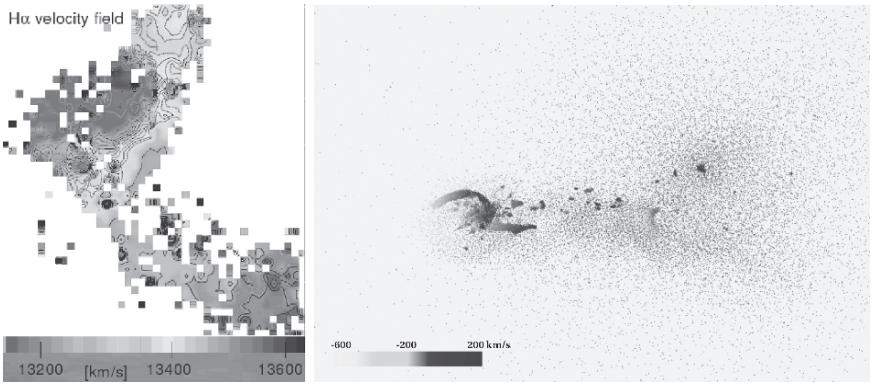

Fig. 3. *Left.* Isovelocity contours overlaid to the velocity field of the gaseous component (from [7]). *Right.* Projected radial velocity distribution of the gas in the N-body/SPH simulation at the last timestep shown in Fig. 2.

two spiral galaxies took place <200 Myr ago. Another interaction or merger event appears to have involved the S0 galaxy less than 1 Gyr ago. Our first comparisons with N-body/hydrodynamical simulations indicate that the observed tidal features cannot be simply the result of the interaction between the two spiral galaxies. Therefore, we suggest that all three galaxies have been involved in the latest interaction. The extreme compactness and low radial velocity dispersion suggest that the group coalescence will be fast. A simulation in which an S0 galaxy is formed through an equal mass merger and about 1 Gyr later undergoes an encounter with both spiral galaxies produces results that approach the observed properties of the group. The properties of CG J1720-67.8 suggest that sufficiently gas-rich groups might undergo a particularly active star-forming phase before final coalescence.

Acknowledgments

ST is grateful to R. Giovanelli for useful discussions during the meeting. The authors acknowledge financial support by the Austrian Science Fund (FWF) under projects P17772 and P15868.

References

1. P. Amram, C. Mendes de Oliveira, H. Plana et al.: Astrophys. J. Lett. 612, L5 (2004)
2. M.P. Haynes, R. Giovanelli: Astron. J. 89, 758 (1984)
3. W. Kapferer, A. Knapp, S. Schindler et al.: Astron. and Astrophys. 438, 87 (2005)

4. V. Springel: Month. Not. Royal Astron. Soc. 364, 1105 (2005)
5. S. Temporin, R. Weinberger, G. Galaz et al.: Astrophys. J. 584, 239 (2003a)
6. S. Temporin, R. Weinberger, G. Galaz et al.: Astrophys. J. 587, 660 (2003b)
7. S. Temporin, L. Staveley-Smith, F. Kerber: Month. Not. R. Astron. Soc. 356, 343 (2005)
8. S. Temporin, U. Fritze-v. Alvensleben: Astron. and Astrophys. 447, 843 (2006)
9. L. Verdes-Montenegro, M.S. Yun, B.A. Williams et al.: Astron. and Astrophys. 377, 812 (2001)

The Optical and Near-infrared Properties of Nearby Groups of Galaxies

S. Raychaudhury and T.A. Miles

School of Physics & Astronomy, University of Birmingham, UK

Summary. We present a study of the optical (BRI) and near-infrared (JHK) luminosity fuctions (LFs) of the GEMS sample of 60 nearby groups of galaxies between $0.01 < z < 0.04$, with our optical CCD photometry and near-IR photometry from the 2MASS survey. The LFs in all filters show a depletion of galaxies of intermediate luminosity, two magnitudes fainter than L_*, within $0.3\,R_{500}$ from the centres of X-ray faint groups. This feature is not as pronounced in X-ray bright gropus, and vanishes when LFs are found out to R_{500}, even in the X-ray dim groups. We argue that this feature arises due to the enhanced merging of intermediate-mass galaxies in the dynamically sluggish environment of low velocity-dispersion groups, indicating that merging is important in galaxy evolution even at $z \sim 0$.

1 Introduction

Observational studies of the environmental dependence of galaxy evolution mostly concentrate on galaxies in rich clusters, even though <5% of galaxies are found in such environments. Most galaxies are found in groups, and arguably the group environment plays an important role in their evolution. In groups, galaxies could be transformed by their interaction with the intragroup medium, or with other galaxies by means of a variety of processes (e.g. stripping, tidal interaction) or through merging with other galaxies. Here we seek to study the optical and near-IR properties of galaxies in groups to find whether they support the relative importance of any of these processes.

2 Luminosity functions of GEMS groups

We explore the optical properties of galaxies in a sample of 60 nearby groups, known as the Group Evolution Multi-wavelength Study (GEMS, detailed descriptions in [1, 2]. This sample represents a variety of groups over a large range of evolutionary stages, and are all in the fields of >10 ks of ROSAT PSPC observations (some of them are not detected). As a description of the Group environment, we use their bolometric X-ray luminosity L_X, and divide the sample into two subsamples: X-ray bright if $L_X > 10^{41.7}$ erg s^{-1},

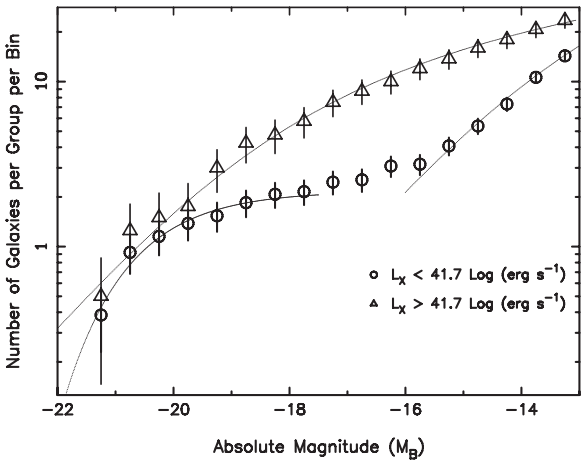

Fig. 1. Cumulative B-band Luminosity Function of 25 GEMS galaxy groups, divided into two categories: X-ray bright groups ($L_X > 10^{41.7}$ erg s^{-1}, plotted as triangles and X-ray dim groups ($L_X < 10^{41.7}$ erg s^{-1}), plotted as circles. Only the LF of X-ray bright groups can be fit with a single Schechter function.

and X-ray dim if less (including the undetected ones). This X-ray luminosity refers to that of the group plus any central galaxy that might exist (for more details, see [3]).

2.1 B(VR)IJHK photometry

The optical subsample consists of 25 GEMS groups: 17 of them were observed at the 2.5m INT, La Palma, with the WFC, imaging an area of $4 \times 22.5 \times 11.3$ arcmin of sky with BVI filters. Another 8 groups were observed with the 2.2m ESO/MPI telescope at La Silla, Chile, using the WFI, with a field of 34×33 arcmin, with broadband BRI filters. For each group, we went out to a radius of $0.3\,R_{500}$ from their centres.

Furthermore, we extracted JHK magnitudes of all 60 GEMS groups from the 2MASS All-Sky Extended Source Catalog (2MASX), going out to a radius R_{500} of its centre for each group, down to a limiting magnitude of $M_K = 13.75$. The adopted group centres, values of R_{500} and distances to these groups can be found in [1], and details of member selection and data reduction in [3, 4].

2.2 Stacked luminosity functions

In Fig. 1, we show the cumulative B-band luminosity function (LF) for our optical subsample (25 GEMS groups), evaluated by co-adding galaxies of several groups in equally spaced bins of absolute luminosity, with galaxies chosen from within $0.3\,R_{500}$ from the centre of each group. This reveals that

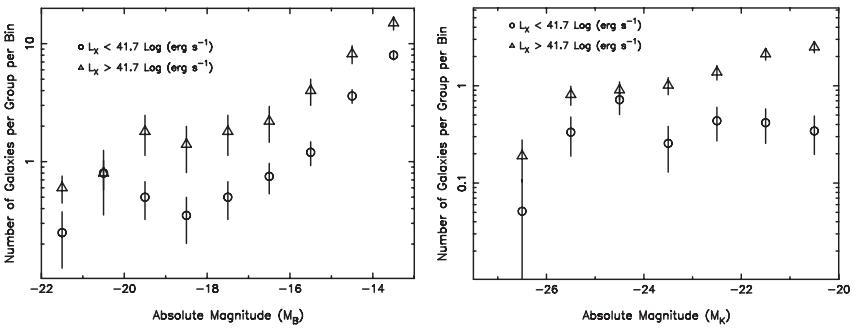

Fig. 2. The mean differential Luminosity functions of GEMS Groups, within $0.3R_{500}$ from their respective centres, *(Left:)* in the B-band, for a subsample of 25 groups, and *(Right:)* K-band (2MASS), for all 60 GEMS groups. They are divided into X-ray bright groups ($L_X > 10^{41.7}$ erg s^{-1}, triangles) and X-ray dim groups (circles), stacked together to form composite LFs for the respective subclasses. The LFs of the dim groups show "dips" between $-19 < M_B < -17$ and $-24 < M_K < -23$.

the LF of the X-ray dim groups ($L_X < 10^{41.7}$ erg s^{-1}) is significantly different from that of the X-ray brighter groups. Fig. 2 shows the differential LFs, (left) for the B-band, within $0.3\,R_{500}$ (same data as Fig. 1), and (right) for the K-band, within R_{500}. The differential LFs reveal the nature of the difference, in the form of a prominent dip, at around $M_B = -18$ and $M_B = -23.5$ (more details of observational data in [3, 4, 5]).

We interpret this deficiency of intermediate luminosity galaxies as evidence of rapid evolution through merging. In the low velocity dispersion environment, as in X-ray dim groups, dynamical friction would facilitate more rapid merging, thus depleting intermediate luminosity galaxies to form more giant central galaxies. Since the collision cross-section depends on the size of a galaxy, the dwarf galaxies at the faint end of the LF are more likely to merge with a giant galaxy, than merge with each other. This ensures galaxies in a range of intermediate luminosities are preferentially depleted, thus enhancing the bright end of the LF.

We suggest that X-ray dim (or low velocity dispersion) groups are the present sites of rapid dynamical evolution rather than their X-ray bright counterparts, and may be the modern precursors of fossil groups. Such LF features are seen in some clusters as well, such as Coma (e.g. [6]), which we would argue has resulted from recent merger with groups.

The optical LFs are determined only out to $0.3\,R_{500}$ of each group, but we can investigate the nature of the LF in their outer parts from the near-IR LFs from the 2MASS survey. We consider three ranges of radial distance in finding the the mean K-band LF in Fig. 3. The dip between $-24 < M_K < -23$ seen in the LF in the central regions of the groups gradually disappears as

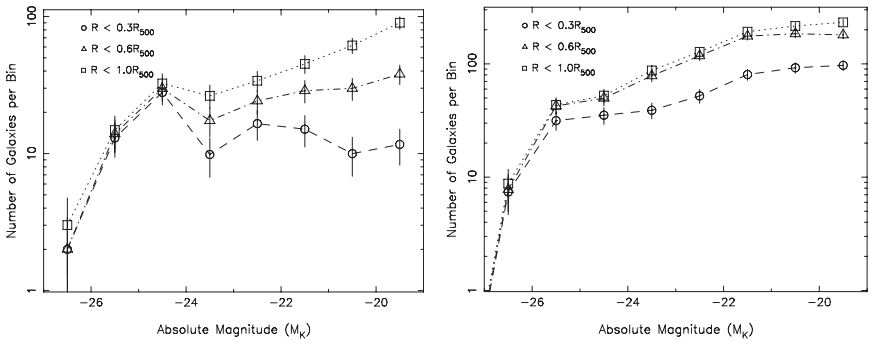

Fig. 3. Differential K-band luminosity functions of *(Left:)* all X-ray dim GEMS groups ($L_X < 10^{41.7}$ erg s^{-1}), out to a fraction of the projected group radius. *(Right:)* The same for all X-ray bright groups ($L_X > 10^{41.7}$ erg s^{-1}). The three plots in each case go out to 0.3, 0.6 and 1.0 times R_{500} respectively. The intermediate luminosity dip feature is more prominent in the inner regions of the X-ray dim groups. The LF of the X-ray bright groups remains similar in shape at all radii.

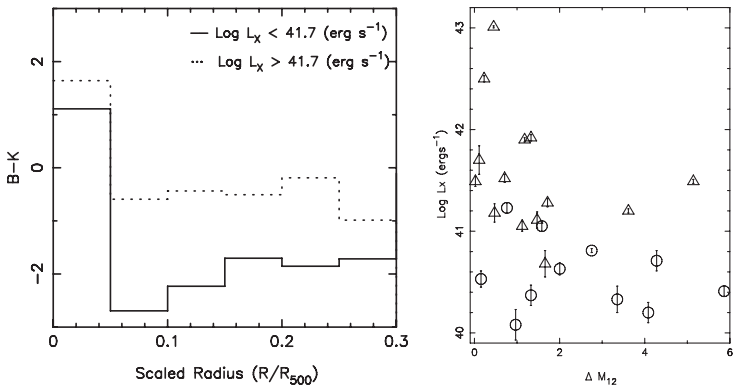

Fig. 4. *Left:* The average $B-K$ colour of galaxies as function of distance (scaled by R_{500}) from the centre of the parent group. X-ray dim groups have redder central galaxies. *Right:* The X-ray luminosity of our GEMS groups, as a function of the difference in magnitude between in the brightest and second brightest galaxies in each group. The biggest values for ΔM_{12} are in the X-ray dim groups.

the LF is averaged out to larger radii, approaching R_{500}, where the LFs of both X-ray bright and dim groups are of a similar shape.

2.3 Brightest group galaxies

One of the consequences of this scenario is that the brightest group galaxies in the X-ray dim groups are expected to be more massive and brighter than those in X-ray bright groups. Fig. 4 shows the colour of galaxies as a function

of radial distance, stacked in radial bins scales by R_{500}, to reveal that X-ray dim groups have redder central galaxies. It also shows that in X-ray bright groups, the difference in B-magnitude between their brightest and second brightest galaxies is in general smaller than in X-ray faint groups. The X-ray bright groups have several galaxies of comparable luminosity (and mass) at the bright end, possibly being the end-products of earlier mergers on smaller scales in sub-groups that were incorporated in the virialised systems we observe today.

3 Conclusions

We argue that the missing intermediate-luminosity galaxies in the optical and near-infrared luminosity functions of X-ray dim groups indicate that, in the dynamically sluggish environment of such groups (which have low velocity disperison), dynamical friction would facilitate more rapid merging, thus depleting intermediate-luminosity galaxies to form a few giant central galaxies. We also show that this effect is seen only in the interior regions of the groups ($R < 0.3\,R_{500}$), and vanishes as one approaches R_{500}. rather than a bright-end enhancement caused by excess star formation. In [4], we show that this feature cannot arise due to enhanced star formation in the brightest galaxies, or due to a varying morphological mix of galaxies in various groups.

It is often suggested (e.g. [7]) that mergers are not an important ingredient of galaxy evolution in the recent Universe ($z < 1$). Here we have shown that in nearby poor groups, merging is still an important process. This picture of galaxy evolution leads to a definite prediction. If X-ray dim groups are indeed systems undergoing rapid dynamical evolution, the stellar populations in their galaxies would be significantly younger than those in X-ray bright groups in case of dissipative merging. This can be observationally verified.

Acknowledgements

We thank Trevor Ponman, Duncan Forbes, Paul Goudfrooij and other members of the GEMS team for their contributions to this work, and the organisers for a very stimulating meeting.

References

1. J. P. F. Osmond, T. J. Ponman: MNRAS **350**, 1511 (2004)
2. D. A. Forbes, T. J. Ponman, F. Pearce, J. P. F. Osmond, V. Kilborn, S. Brough, S. Raychaudhury, C. Mundell, T. A. Miles, K. Kern: PASA **23**, 38 (2006)
3. T. A. Miles, S. Raychaudhury, D. A. Forbes, P. Goudfrooij, T. J. Ponman, V. Kozhurina-Platais: MNRAS **355**, 785 (2004)

4. Miles, T. A., Raychaudhury, S., Russell, P. A.: MNRAS, in press (2006)
5. T. A. Miles: *The Evolution of groups of galaxies*, PhD Thesis, University of Birmingham, Birmingham UK (2006)
6. R. B. Tully: Proceedings of IAUC 198 "Near-Field Cosmology with Dwarf Elliptical Galaxies", astro-ph/0505047 (2005)
7. C. J. Conselice: *The history of galaxy formation in groups: an observational perspective,* this volume (2006)

Halo Shapes, Dynamics and Environment

M. Plionis[1], C. Ragone[2] and S. Basilakos[3]

[1] Institute of Astronomy & Astrophysics, NOA, Athens, Greece & INAOE, Puebla, México
[2] IATE, Observatorio Astronómico, Córdova, Argentina
[3] Kapteyn Institute, University of Groningen, the Netherlands

Summary. In the hierarchical structure formation model cosmic halos are supposed to form by accretion of smaller units along anisotropic direction, defined by large-scale filamentary structures. After the epoch of mass aggregation (which depend on the cosmological model), violent relaxation processes will tend to alter the halo phase-space configuration producing quasi-spherical halos with a relatively smooth density profiles.

Here we attempt to investigate the relation between halos shapes, their environment and their dynamical state. To this end we have run a large ($L = 500\ h^{-1}$ Mpc, $N_p = 512^3$ particles) N-body simulation of a flat low-density cold dark matter model with a matter density $\Omega_{\rm m} = 1 - \Omega_\Lambda = 0.3$, Hubble constant $H_\circ = 70\,{\rm km\ s^{-1}\ Mpc^{-1}}$ and a normalization parameter of $\sigma_8 = 0.9$. The particle mass is $m_{\rm p} \geq 7.7 \times 10^{10}\, h^{-1}\, M_\odot$ comparable to the mass of one single galaxy. The halos are defined using a friends-of-friend algorithm with a linking length given by $l = 0.17\bar{\nu}$ where $\bar{\nu}$ is the mean density. This linking length corresponds to an overdensity $\rho/\rho_{\rm mean} \simeq 200$ at the present epoch ($z = 0$) and the total number of halos with more than 130 particles ($M > 3 \times 10^{13}\, h^{-1}\, M_\odot$) is 57524.

1 Halo shapes and environment

Halo shapes are defined by diagonalizing the moments of inertia from which we derive the eigenvalues and eigenvectors of the best ellipsoidal halo fit. The principal axes a, b, c are related to the square root of the eigenvalues such that $a > b > c$. Our results, in agreement with other studies, indicate that although halos are triaxial they are significantly more prolate than oblate. This is quantified by using the so called triaxiality index [5] defined as $T = (a^2 - b^2)/(a^2 - c^2)$, which has limiting values of $T = 1$ and $T = 0$ for the case of a pure prolate and oblate spheroid, respectively. Our results show that the fraction of halos with pronounced prolatness (i.e., large Ts) is significantly higher than that of oblate-like halos. Overall we obtain from our simulated halos that $\langle T \rangle \simeq 0.73$.

An interesting question, especially for observational studies, is whether the 3D halo shape distribution can be inferred from the projected (2D) shapes. This is an inversion problem for which, under the assumption of random halo orientation with respect to the line of sight and purely oblate

or prolate spheroidal halos, there is a unique relation between the projected and intrinsic axial ratio distributions. This is described by a set of integral equations, first investigated by [6] and given by [15]:

$$\hat{f}(q) = \frac{1}{q^2}\int_0^q \frac{\beta^2 \hat{N}_p(\beta)\mathrm{d}\beta}{(1-q^2)^{1/2}(q^2-\beta^2)^{1/2}} \ , \ \hat{f}(q) = q\int_0^q \frac{\hat{N}_\circ(\beta)\mathrm{d}\beta}{(1-q^2)^{1/2}(q^2-\beta^2)^{1/2}} \tag{1}$$

with β representing the intrinsic axial ratio while $\hat{N}_o(\beta)$ and $\hat{N}_p(\beta)$ the intrinsic prolate and oblate axial ratio distributions, respectively. The continuous function $f(q)$ is derived from the discrete axial ratios frequency distribution using the so-called kernel estimators (for details see [14] and references therein). Inverting then the above equations gives us the distribution of true axial ratios as a function of $f(q)$ (e.g. [4]). Nevertheless, if halos are a mixture of the two spheroidal populations or they have triaxial configurations there is no unique inversion [12]. However, all may not be lost and although the exact shape distribution may not be recovered accurately one could possibly infer whether the 3D halo shapes are predominantly more prolate or oblate-like. Let us see this in more detail using our simulated intrinsically triaxial ellipsoidal halos which are however dominated by prolate-like shapes ($\langle T\rangle \simeq 0.73$). The important point here is that in order for the inverted distribution to be physically meaningful it should be positive for all β's. Negative values indicate that the assumed model for the intrinsic halo shape is unacceptable.

In Fig. 1 (left panel) we present the discrete and continuous - $f(q)$ - distributions of the projected in 2D axial ratios for halos of two mass ranges (indicated in the plot). In the middle and right panels we present the inverted 3D axial ratio distributions (continuous lines) for the prolate and oblate models, respectively. It is evident that the inverted oblate-model distribution has many negative values which is an important indication that this model is unacceptable, while the opposite is true for the prolate-model distribution. Furthermore, we plot as histograms the intrinsic axial ratio distribution of the "average" prolate or oblate spheroidal fit to the 3D halo. These fits are realized by estimating the corresponding axial ratios by $\beta_{\rm P} = (b+c)/2a$ and $\beta_{\rm O} = 2c/(a+b)$. It is evident that the purely oblate model fails miserably to even come close to the inverted distribution while the prolate model fits relatively well the corresponding inverted 3D prolate-model distribution. This agrees with the higher prolatness of the 3D halo shapes. We therefore conclude that applying the previously discussed inversion method to observational data (e.g. [13], [11]) we can infer, even in the event of triaxial ellipsoidal halo shapes, the dominance of prolate or oblate-like 3D shapes.

Another interesting fact, shown in recent high-resolution simulations of the concordance model, is the correlation between halo mass and halo flattening, with more massive halos being flatter (e.g. [1], [8], [7]). This is counter-intuitive in the sense that the massive halos should collapse faster than lower mass halos of roughly the same formation age and thus they should have

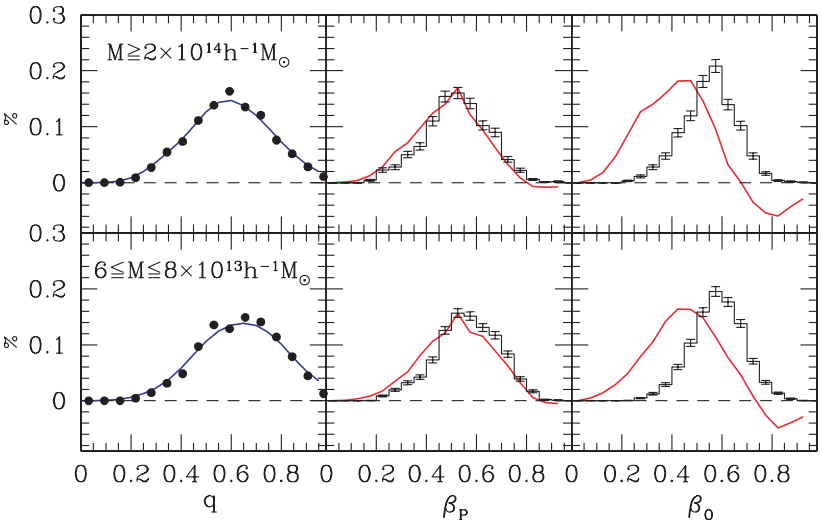

Fig. 1. *Left Panel:* The projected axial ratio distributions for two different halo mass thresholds with the nonparametric kernel estimator fit (solid line). *Central Panel:* The inverted intrinsic halo axial ratio distribution (continuous line) for the prolate model together with distribution of "average" prolate spheroidal fit to the 3D halos. *Right Panel:* the corresponding distributions for the oblate case.

more time to dynamically evolve and virialize, a process that should reduce their initial ellipsoidal configuration. However, halo formation ages vary and secondary infall, which if important it could affect the halo outskirts, can produce such elongated halo geometry. However, even in such a case the inner parts of the most massive halos should be virialized and thus nearly spherical, which however does not seem to be the case (e.g. [1] their Figure 7). Note that these results are based on dissipationless simulations while baryonic dissipation has been shown to affect halo shapes, producing significantly rounder halos (e.g. [9]). Also one may expect that halos in low-density regions, where tidal effects, accretion and merging are minimal to be less elongated, as indeed has been found (e.g. [2]).

2 Halo dynamics and environment

In order to define the dynamical state of a halo we use the Δ-deviation substructure statistic [3], which looks for deviations of the local velocity mean and dispersion around their overall halo values. For each halo particle we find its N_{nn} nearest neighbors from which we calculate their local velocity mean and dispersion which we then compare with their overall halo values. The local deviations are defined by: $\delta_i^2 = \frac{N_{nn}}{\sigma_v^2}\left[(\bar{v}_{local} - \bar{v})^2 + (\sigma_{v,local} - \sigma_v)^2\right]$ while the individual halo Δ-statistic is given by the sum $\Delta = \sum \delta_i$. It has

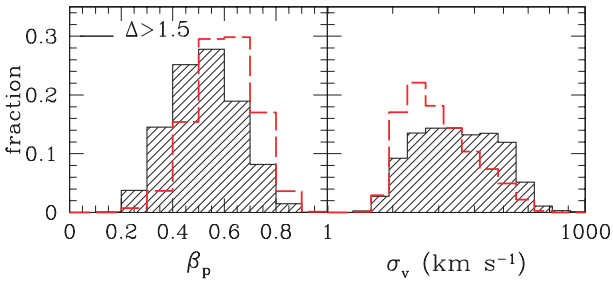

Fig. 2. Normalized axial ratio and velocity dispersion distributions. Hatched histograms represent halos with significant substructure while the dashed-line histograms represent the overall halo population.

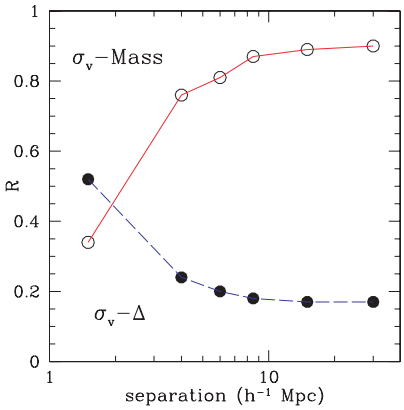

Fig. 3. Spearman correlation coefficient for the σ_v vs Mass and σ_v vs Δ correlations as a function of host-halo distance.

been found that a robust measure of the substructure index is given when using $N_{nn} = 25$ [10], which is the value that we use. In Figure 2 we show the velocity dispersion (right panel) and β_P axial ratio (left panel) distributions for halos in the mass range $3 \times 10^{13} < M < 8 \times 10^{13}\ h^{-1}\ M_{\odot}$. Those that have a substructure index $\Delta > 1.5$ are shown as hatched histograms while the overall halo distributions as dashed-line histograms. *It is evident that dynamically young halos (i.e., those with significant substructure) are more elongated and have a higher velocity dispersion than the overall halo population.*

Furthermore, we investigate the correlation between halo velocity dispersion and halo mass. From our halo identification procedure we expect that most halos should be nearly virialized and thus their velocity dispersion should be strongly correlated with their mass via the virial theorem. Indeed, there is a strong correlation between the velocity dispersion and the halo mass, measured by summing the member DM particles masses, with a

Spearman correlation coefficient of $R \sim 0.9$. We find however, that this strong correlation breaks down in the vicinity of large halo hosts. In Figure 3 we show with open points the correlation coefficient between halo σ_v and Mass as a function of distance to their nearest massive ($M > 2{\times}10^{14}\ h^{-1}\ M_{\odot}$) host neighbor. The monotonic drop of the correlation coefficient with decreasing halo-host separation is evident. We also find that there is a significant although weaker correlation between σ_v and the substructure index (Δ), which increases as the halo-host distance decreases. This probably implies that halos near large hosts are either disrupted due to the presence of strong tidal fields or more probably that the excess density of sub-halos near hosts induce strong inter-halo gravitational interactions and merging. These results have important consequences for observational studies and put important limits on the validity of using the virial theorem to estimate group or cluster masses in the vicinity of massive clusters.

References

1. Allgood et al., ApJ, *in press*, `astro-ph/0508497`
2. Avila-Reese, V., et al., ApJ, **634**, 51 (2005)
3. Dressler, A. & Shectman, S.A., AJ, **95**, 985 (1988)
4. Fall, M. & Frenk, C. S., ApJ, **88**, 1626 (1983)
5. Franx, M., Illingworth, G., de Zeeuw, T., ApJ, **383**, 112 (1991)
6. Hubble, E.P., ApJ, **64**, 321 (1926)
7. Jing, Y.P. & Suto, Y., ApJ, **529**, L69 (2002)
8. Kasun, S.F. & Evrard, A.E., ApJ, **629**, 781 (2005)
9. Kazantzidis, S. et al., ApJ, **611**, L73 (2004)
10. Knebe, A., Müller, V., A&A, **354**, 761 (2000)
11. Paz, D.J., Lambas, D.G., Padilla, N., Merchan, M., MNRAS, *in press* (2006)
12. Plionis M., Barrow J.D., Frenk, C.S., MNRAS, **249**, 662 (1991)
13. Plionis M., Basilakos, S., Tovmassian, H., MNRAS, **352**, 1323 (2004)
14. Ryden, B.S., ApJ, **461**, 146 (1996)
15. Sandage, A., Freeman, K.C. & Stokes, N.R., ApJ, **160**, 831 (1970)

II Zwicky 23 and Family

E.H. Wehner[1], J.S. Gallagher[2], G.C. Rudie[3] and P.J. Cigan[2]

[1] McMaster University, Department of Physics and Astronomy, Hamilton, ON L8S 4M1, Canada
wehnere@physics.mcmaster.ca
[2] University of Wisconsin, 475 N. Charter St., Madison, WI 53706
jsg@astro.wisc.edu, pjcigan@students.wisc.edu
[3] Dartmouth College, Department of Physics and Astronomy, 6127 Wilder Laboratory, Hanover, NH, 03755
gwen.c.rudie@dartmouth.edu

Summary. II Zwicky 23 (UGC 3179) is a luminous ($M_B \sim -21$) nearby compact narrow emission line st arburst galaxy with blue optical colors and strong emission lines. We present a photometric and morphological study of II Zw 23 and its interacting companions using data obtained with the WIYN 3.5-m telescope in Kitt Peak, Arizona. II Zwicky 23 has a highly disturbed outer structure with long trails of debris that may be feeding tidal dwarfs. Its central regions appear disky, a structure that is consistent with the overall rotation pattern observed in the Hα velocity field measured from Densepak observations obtained with WIYN. We discuss the structure of II Zwicky 23 and its set of companions and possible scenarios of debris formation in this system.

1 Introduction

II Zwicky 23 (Mkn 1087, UGC 03179) is a blue compact galaxy currently undergoing a global starburst. It was until recently thought to have one companion, KPG103a. However, recent work [7] has identified several tidal dwarfs around this system, as well as one dwarf galaxy that appears to pre-date the tidal dwarf galaxies (TDGs). There are several indicators suggesting that these group members are currently interacting. The presence of tidally forming dwarfs, and tidal streamers of stellar debris all suggest that the enhanced star formation rates (SFRs) in the two main members may have been triggered by an earlier collision with another group member. It is unlikely that KPG103a and II Zwicky 23 have experienced a direct collision with each other. More likely they have been perturbed by a collision with a dwarf companion or a weak interaction with each other, since there is evidence of disk structure in both II Zwicky 23 and KPG 103a.

2 II Zwicky 23 et al.: Family traits

2.1 II Zwicky 23

II Zwicky 23 has $cz \sim 8320$ km s^{-1} [9] and lies at a distance of 115 Mpc ($H_0 = 72$ km s^{-1} Mpc^{-1}). II Zwicky 23 qualifies as a luminous, blue, compact galaxy, and its SFR is clearly enhanced.[2] The 1.4 GHz radio data [1, 7] suggest a SFR $\sim$4.65 M$_\odot$ yr^{-1} for M $>$ 5 M$_\odot$ and including stars down to M $>$ 0.1 M$_\odot$ brings the SFR$_{1.4GHz}$ up to 25.8 M$_\odot$ yr^{-1}. The far-infrared fluxes [5, 3, 7] yield a SFR $\sim$11.5 M$_\odot$ yr^{-1}, and long slit spectroscopy suggests SFR$_{H\alpha}$ = 4.5 M$_\odot$ yr^{-1}[7].

II Zwicky 23 has an inclination of $i = 37$ degrees, and the northern side is moving away from us, while the southern side is approaching us. [7] In this case, the tidal debris tails emanating from the right of II Zwicky 23 in Figure 1 are polar extensions, and the debris to the north is roughly in the plane of the disk.

2.2 KPG103a

KPG103a is the less well-studied companion of II Zwicky 23. It lies 81 kpc to the southwest and has a very similar velocity ($cz = 8313$ km s^{-1}) [8]. It has been classified an Sb, HII galaxy and is characterized by the presence of a weak, two-armed spiral structure [8]. In optical images, there appear to be three knots in the center of the galaxy, possibly the nucleus and a circumnuclear ring, or multiple nuclei left over from an unrelaxed collision. There also appear to be some diffuse, low surface brightness extensions. These properties, along with what appears to be an enhanced SFR, suggest that KPG103a has recently undergone some type of tidal interaction.

2.3 Tidal debris, dwarfs and knots

A thorough analysis of the knots and regions of interest in II Zwicky 23 can be found in [7]. We initially developed our own labeling scheme, and our region labels are shown along with theirs in Figure 1. However, we have attempted to follow their numbering scheme whenever possible. The regions have been overlaid on our B-band image. Regions 1 and 3 are tidal dwarf galaxies (TDGs) and region 7 is most likely a giant HII region [7], rather than an infalling galaxy, as originally proposed by [4]. While not noted as being tidal dwarfs, regions 11 and 12, along the polar extensions, do show signs of some new star formation in addition to what appears to be material stripped from II Zwicky 23 [7].

Region N/K (hereafter, region N) has a distinct rotational pattern and a lower $[O/H]$ ratio than expected for a tidally forming galaxy. Therefore N is thought to be an independent group member, not formed as a result of any recent collision [7].

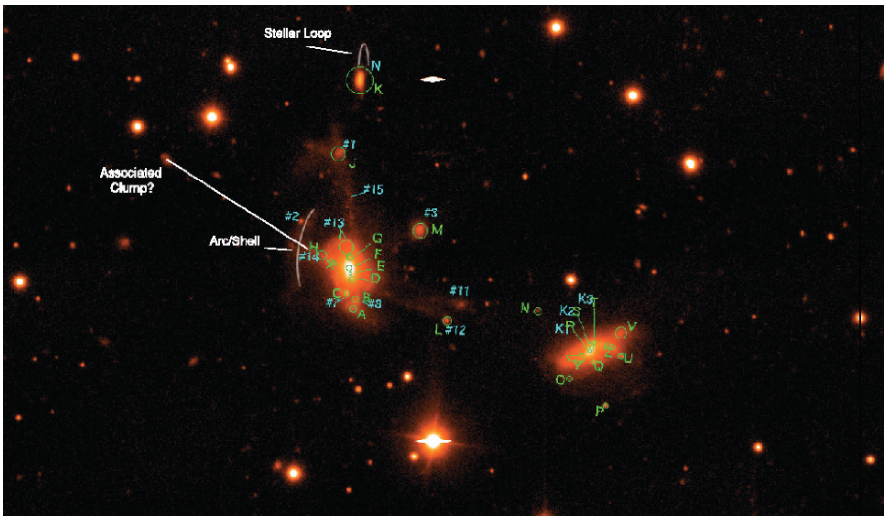

Fig. 1. *B*-band image from the WIYN 3.5m telescope in Kitt Peak, Arizona. II Zwicky 23 is on the left, and KPG103a is on the right. Our region labels are alphabetical, while those region labels containing numbers follow the notation in [7].

3 Observations and reductions

We observed II Zwicky 23 and its companions using the MiniMosaic camera on the WIYN 3.5m telescope in Kitt Peak, Arizona. Data were taken on two different runs. On November 17, 2000, we obtained broadband B and R-band data. We also observed II Zwicky 23 on February 9, 2005 using the DensePak instrument at the Cassegrain focus of the WIYN 3.5m telescope. We obtained 2200s total, centered around the Hα line.

4 Results

4.1 Broadband imaging

In addition to those described in previous works (see Section 2), there are several new and interesting features in our deep B-band image, shown in Figure 1. The first is the small, stellar arc, marked in Figure 1. For an inclination of 37 degrees [7], the inner edge of this ripple lies approximately 18 kpc from the center of II Zwicky 23 and in the plane of the disk, and is therefore most likely a shell-like debris structure. There is also a stellar extension that appears to connect the center of II Zwicky 23 with the shell. These stars could be the remains of a disrupted companion galaxy, which plunged through II Zwicky 23 and created the shell. Considering the uncertainties in projection, it could extend out of the plane of the disk, unconnected to the disk ripple.

It is interesting to note the presence of stellar clumps further out, that lie along a line (as shown in Figure 1) that continue this stellar extension. These clumps lie at distances (uncorrected for projection) of 35 and 42 kpc from II Zwicky 23. However, without further data, we cannot conclusively determine whether these clumps are associated with this group.

KPG103a, also shown in Figure 1, exhibits many signatures of interaction. In the B-band image there appears to be a weak 2-armed spiral pattern, although it is somewhat distorted. The northeastern arm curves briefly clockwise, before proceeding to turn counter-clockwise. While the other arm is more well-behaved, there is an obvious diffuse stellar clump to its immediate upper right. This clump could be the remains of a merged galaxy or part of KPG103a's own disk that was pulled out by tidal forces during an interaction. This disk has clearly been disrupted by a collision with another galaxy.

Also interesting are the two bright and roughly circular knots in the center of this galaxy. These knots may also contain the remains of a merged galaxy, and may even be its nucleus. KPG103a also has a larger, more diffuse low-surface brightness component extending from the west/northwest. This is most likely material pulled from KPG103a during a tidal interaction.

Another feature of note is in the neighborhood of the dwarf galaxy, N. In our deep B-band image, there is a visible loop extending from region N to the north. This loop, while fainter in the shallower data, is visible in all our wavebands and is therefore most likely a loop of stellar material. One possible interpretation is that region N is in the process of disrupting, leaving stars in its wake. In this case, the northern tip of the loop may be where N reached its peak distance from II Zwicky 23 and turned around in its orbit. If we then use this peak, as its maximum orbital distance from II Zwicky 23, and assume a simple orbit, then its last close encounter with II Zwicky 23 was 1.4 Gyr ago - a time much too distant to have caused the current central starburst, which is thought to be only ∼6 Myr old [7].

4.2 DensePak

The DensePak array contains 91 fibers, each of which spans 3 arcseconds. The entire array covers 30 × 40 arcseconds on the sky. For each fiber with detectable Hα, we fit a gaussian to the line to find the location of its peak. From this, we calculated the velocity of the gas in each fiber. We then assigned the velocity range to a color table and plotted the velocity for each fiber, as shown in Figure 2.

Despite its obvious signs of disturbance, we find a fairly smoothly rotating disk, supporting II Zwicky 23's classification as a spiral disk galaxy. We measure a $\Delta v = 230$ km s^{-1} across the disk, or a maximum rotation speed of $v_{rot} \sim 117$ km s^{-1}. It is possible that this number is an overestimate, since it includes fibers such as that on region 7/C, which may represent the remains of an incoming, disrupting dwarf galaxy [4].

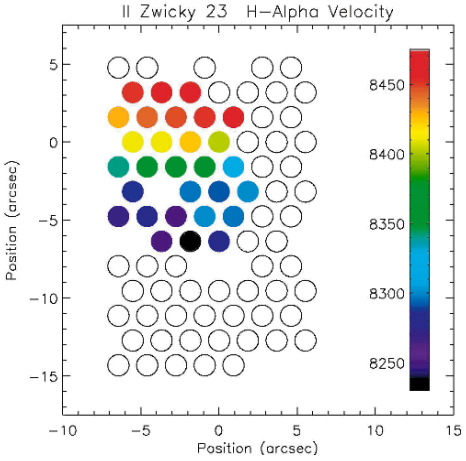

Fig. 2. DensePak data for II Zwicky 23 centered on the Hα line. The velocity for each fiber is represented by its color.

5 Discussion

II Zwicky 23 and its companions are a group in turmoil; there is now extensive evidence that this system is being affected by numerous collisions. The disruption of region N, the ongoing starburst, and tidal arms of debris extending out of the disk all suggest ongoing interactions between the members of this group. In addition, the presence of shells in II Zwicky 23, as well as the possible double nuclei in KPG103a support the idea that collisions with former dwarf companions have recently occurred. However, despite all this, the ionized component of II Zwicky 23's disk has maintained a smoothly rotating structure. This system is an excellent example of intra-group interactions driving galaxy evolution, and merits future study.

References

1. Condon, J. J., Cotton, W. D., & Broderick, J. J. 2002, AJ, 124, 675
2. Hunter, D.A. & Gallagher, J. S. 1985, AJ, 90, 1457
3. Iras Point Source Catalog, 1996
4. Keel, W. C. 1988, A&A, 202, 41
5. Kennicutt, R. C. 1998, ApJ, 498, 541
6. Landolt, A. 1992, AJ, 104, 340
7. López-Sánchez, Á. R., Esteban, C. & Rodríguez, M. 2004, A&A, 428, 425
8. Marzke, R. O., Huchra, J. P., & Geller, M. J. 1996, AJ, 112, 1803
9. Sargent, W. L. W. 1970, ApJ, 160, 405
10. Springel, V. & Hernquist, L. 2005, ApJ, 622, L9

Dynamical Analysis of NGC 5128 and the Centaurus Group

K.A. Woodley

Dept. of Physics and Astronomy, McMaster University, Hamilton, ON, Canada L8S 4M1
woodleka@physics.mcmaster.ca

Summary. NGC 5128 and NGC 5236, separated by ∼1Mpc, are the brightest members of the nearby groups, Centaurus and M83, repectively. Populated with over 60 galaxies, the boundaries of these two groups are still quite uncertain. Since these groups are nearby (3.9 Mpc from the Milky Way), they provide a rare comparison of the globular cluster (GC) system dynamics within its halo to the dynamics of the Centaurus and M83 groups.

1 Rotation amplitude and rotation axis

A kinematic analysis of 343 GCs in NGC 5128 has determined the GCs rotation amplitude and rotation axes in the halo of this galaxy. The same kinematic analysis was applied to the Centaurus and M83 groups, including 42 galaxies with an assumed center of mass of NGC 5128. Figure 1 shows that the rotation axis and the rotation amplitude defined by the 42 satellite galaxies are the same as the outer halo of NGC 5128.

2 Mass and mass/light ratio

The total mass and mass-to-light ratio determined for NGC 5128 and the two groups are continually increasing with radius, shown in Figure 2, indicating a dark matter halo extending past the group members.

3 Conclusions

The dynamics of the halo of NGC 5128 appears to extend to the satellite galaxies in the Centaurus and M83 groups, suggesting the brightest member and the surrounding galaxies are part of the same large-scale structure, consistent with cold dark matter models. The kinematics of the halo of NGC 5128 matching those of the nearby satellites suggests NGC 5128, as an initial large "seed" galaxy, could have formed from the merger of many nearby small satellites. Alternatively, if NGC 5128 formed from the merger of a very small number of large galaxies, it would not as easily explain the kinematic similarities shown in this study.

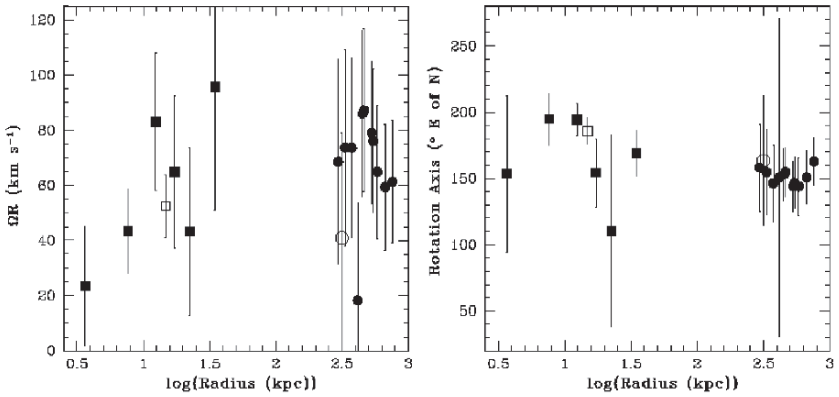

Fig. 1. Rotation amplitude (*left*) and rotation axis (*right*) as a function of the projected radius from NGC 5128 plotted for radially binned GCs (*solid squares*), all 343 known GCs (*open square*), and NGC 5128 with 13 confirmed group members [2] (*open circle*). The *solid circles* represent the 15 galaxies nearest NGC 5128 in angular distance, increasing successively to 42 galaxies with radial velocities from [3]. The mean rotation amplitude is 62 ± 5 km s^{-1} and the mean rotation axis is $159 \pm 4^{\circ}$ E of N. For clarity of the plots, only half of the solid circles are plotted.

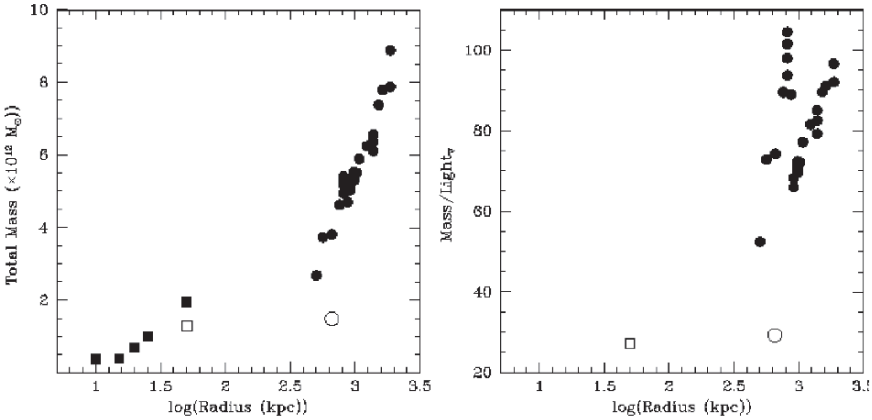

Fig. 2. Total mass and mass-to-light ratio as a function of projected radius from the center of NGC 5128. The symbols are the same as Fig. 1. The total mass is the pressure supported mass determined with the Tracer Mass estimator [1] plus the rotationally supported mass. The typical mass and mass-to-light uncertainties for the galaxies are 1.2×10^{12} M$_{\odot}$ and 19.2, per point.

References

1. N.W. Evans, M.I. Wilkinson, K.M. Perrett, & T.J. Bridges: The Astrophysical Journal **583**, 752 (2003)
2. I.D. Karachentsev, M.E. Sharina, A.E. Dolphin, et al.: Astronomy & Astrophysics **385**, 21 (2002)
3. I.D. Karachentsev, V.E. Karachentseva, W.K. Huchtmeier, & D.I. Makarov: The Astronomical Journal. **127**, 2031 (2004)

Seyfert's Sextet (HGC 79): An Evolved Stephan's Quintet?

A. Durbala[1], J. Sulentic[1], M. Rosado[2], A. del Olmo[3], J. Perea[3] and H. Plana[4]

[1] University of Alabama, USA
durba001@bama.ua.edu
[2] Instituto de Astronomía, UNAM, México
margarit@astroscu.unam.mx
[3] Instituto Astrofísico de Andalucía, Spain
chony@iaa.es
[4] D.C.E.T., Universidade Estadual de Santa Cruz, Brazil

Summary. Scanning Fabry-Perot interferometers MOS/SIS (3.6m CFHT)+PUMA (2.1m OAN-SPM, México) and the long-slit spectrograph ALFOSC (2.5m NOT, La Palma) were used to measure the kinematics of gas and stars in Seyfert's Sextet (HCG79). We interpret it as a highly evolved group that formed from sequential acquistion of mostly late-type galaxies that are now slowly coalescing and undergoing strong secular evolution. We find evidence for possible feedback as revealed by accretion and minor merger events in two of the most evolved members.

1 Gas kinematics in Seyfert's Sextet

Seyfert's Sextet (SS) is composed of three or four early-type members (HCG 79a, b, c and NE tail?) and one spiral galaxy (HCG79d). This compact group shows extreme isolation and compactness with linear diameter $D \sim 22$ kpc. It shows a luminous and hence massive stellar halo that suggests significant secular evolution has taken place.

We detect gas in the nuclear regions of (lenticular) galaxy A that may be partly rotating in the same sense as the stars plus a more extended layer of gas that appears to be infalling. Figure 1 shows stellar (from [1]) and Hα (from PUMA [2]) rotation curves for lenticular galaxy B. The gas is found to be counter-rotating relative to the stars with an amplitude of $\sim$100–160 km s^{-1} implying a mass of $\sim 10^9$ M$\odot$ similar to the observed HI mass of the entire group.

2 Discussion and conclusions

Our working hypothesis views SS as a highly evolved analog of Stephan's Quintet. Given the extreme isolation of SS [3] we assume that it is formed

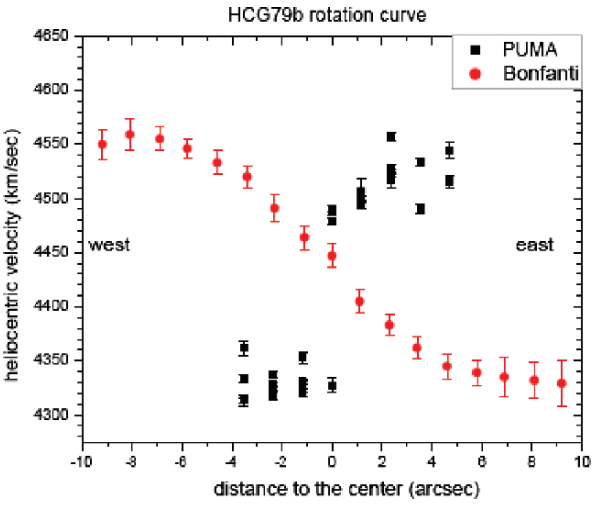

Fig. 1. Galaxy B rotation curves of gas and stars.

out of an extreme field population. Recent work on a very isolated galaxy sample (AMIGA [4]) suggests a probability $P \sim 0.14$ for one member of SS to show early-type (E/S0) morphology. Thus we assume that all or most of the 3-4 E/S0 members in SS entered the group as spirals and were stripped in analog to the ongoing processes observed (NGC7319 and 7320) in Stephan's Quintet (SQ). Stripping in compact groups also leads to suppression of star formation and transformation of spiral members into E/S0 galaxies [5].

If this hypothesis is correct then the halo of SS may be dominated by the stripped disk components of the (formerly) spiral members. A recent measure of halo colors [6] supports this hypothesis indicating that the halo is bluer $(B–R) = 0.9 \pm 0.2$ than the early-type galaxies which we interpret as the remnant bulges of the stripped spirals. Further support for our hypothesis comes from analysis of diameters and luminosities [7], [8] of components a, b and c (the lone spiral d is interpreted as the most recent unstripped intruder). We find that the galaxies are remarkably luminous for their size. Both the colors and sizes are consistent with these galaxies interpreted as the bulge remnants of the stripped spirals that formed the SS halo.

We note that these results indicate that SS is NOT merging in the conventional sequential sense; instead the galaxies are slowly "dissolving" into the luminous halo. This is likely a more quiescent process than conventional mergers perhaps explaining the low IR and X-rays luminosities of SS.

This contribution was done with financial support from grants 40095-F from CONACYT and IN120802 and IN100606 from DGAPA-UNAM.

References

1. P. Bonfanti et al.: A&ASS **139**, 483 (1999)
2. M. Rosado et al.: RevMexAASC **3**, 263 (1995)
3. J.W. Sulentic: ApJ **322**, 305 (1987)
4. J.W. Sulentic: ApJ **in press**, (2005)
5. J.W. Sulentic et al.: AJ **122**, 2993 (2001)
6. C. Da Rocha & C. Mendes de Oliveira: MNRAS **in press**, (2005)
7. P. Hickson et al.: ApJS **70**, 687 (1989)
8. D. Bettoni & G. Fassano: AJ **105**, 1291 (1993)

The HI Content of a Sample of Groups with Different Dynamical Ages

E.E. Freeland

University of Wisconsin, 475 N. Charter St., Madison, WI 53706
freeland@astro.wisc.edu

Summary. I present the results of an HI study of a sample of groups of galaxies with different spiral fractions. The focus is on the distribution of H I rich galaxies with respect to the dynamical center of the groups, the interaction rate as a function of evolutionary status, the amount of intergalactic H I, and the H I properties of individual galaxies. I use this data to compile an H I mass function for groups of galaxies.

1 Motivation

The vast majority of galaxies, including our own Milky Way, reside in loose groups which are small dynamical systems typically containing a handful of large ($\sim L_*$) galaxies and a large number of smaller ones. According to [1], some 70% of nearby galaxies reside in groups, while another 20% are in looser associations. They occupy a key place in the hierarchical structure of the Universe with dark matter distribution intermediate between those of individual galaxies and those of giant clusters [2] and references therein). Groups are the basic building blocks of large scale structure, contributing to the growth of giant clusters via infall [3], and defining the extent and orientation of giant filaments.

Our current understanding of the evolution of groups is derived from observed correlations between the fraction of a group's galaxies that are elliptical and the presence of a diffuse X-ray emitting halo [4], and numerical simulations that suggest that galaxies within a group eventually merge to form large ellipticals [6]. Thus, the dynamical evolution of a group should be marked by a series of interactions that tidally remove H I from the individual galaxies, dumping it into the intragroup medium where it can be heated to X-ray emitting temperatures [7], and/or trigger enhanced star formation within the individual galaxies that leads to the feedback of diffuse hot gas into the intragroup medium [8]. The role of H I observations is to document the interaction/merger rate and map the content and distribution of H I throughout the group as a function of evolutionary stage, and, therefore, shed light onto the evolution of the gas content of loose groups of galaxies. I use the fraction

of group members that are spiral galaxies as a measure of the dynamical age of the group.

The shape of the HI mass function (HIMF), particulary below 10^8 $M_\odot$, continues to be scrutinized. A handful of recent large HI surveys have attempted to accurately determine the slope of the low mass end of the HI mass function. There is some evidence that the low mass slope changes with environment. Cosmological and galaxy evolution models depend on knowledge of the behaviour of the HI mass function how much mass is tied up in low HI mass galaxies.

2 The sample

The following groups have been observed with the Very Large Array (VLA) except for NGC 7582 which was observed with the Australia Telescope Compact Array (ATCA). In all cases mosaics were used to increase the areal coverage and region of uniform sensitivity in the data cubes. New group members are discovered in HI for each group in the sample. A Hubble constant of $H_0 = 75$ km sec^{-1} Mpc^{-1} was used in all distance-dependent calculations.

Table 1. The Sample of Galaxy Groups

Group Name	α(2000)	δ(2000)	N	f_{sp}	σ_v	D (Mpc)	X-rays?
NGC 664	01 44 02.7	+04 19 02	3	1.0	106	72	no
NGC 7582	23 18 54.5	−42 18 28	8	1.0	38	21	no
HCG 58	11 42 09.0	+10 16 30	10	$\geq$0.90	168	84	yes?
GH 40	09 08 43.2	+37 36 07	7	$\geq$0.80	177	94	no
NGC 2563	08 20 24.4	+21 05 46	29	0.59	336	65	yes
GH 109	12 35 45.3	+26 37 23	7	0.57	568	96	no
GH 98	12 04 06.2	+20 14 06	17	$\leq$0.53	388	94	yes
NGC 5846	15 05 47.0	+01 34 25	20	0.50	368	25	yes

3 The distribution of HI rich galaxies

HI rich galaxies are found farther from the group center in dynamically evolved groups compared with younger groups. This can be explained by tidal interactions stripping HI from the galaxies into the intragroup medium where the gas is heated. Strong tidal interactions and large amounts of intergalactic neutral hydrogen are found in some of the dynamically young groups. In dynamically evolved groups the distribution of HI rich galaxies is more asymmetric than in younger groups. Most detections in evolved groups

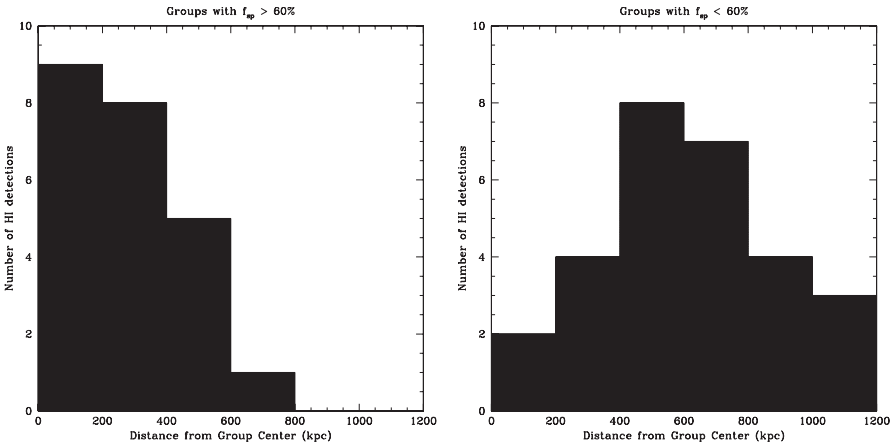

Fig. 1. The distribution of HI rich galaxies as a function of projected distance on the sky from the group center for dynamically young (left) and dynamically evolved (right) groups. The HI rich galaxies are found farther from the group center in dynamically evolved groups than they are in dynamically young groups.

are outside of the extent of X-ray emitting gas in the group. This characteristic mimics what is seen in clusters and even in the Local Group, where most of the gas-rich dwarfs lie at large distances from the Milky Way and M31.

4 The HI mass function

Recent large HI surveys have attempted to determine the low mass slope of the HI mass function. The authors in [9] used the 1000 brightest galaxies from the HI Parkes All-Sky Survey (HIPASS) to construct an HI mass function and derived a low mass slope of $\alpha = -1.30$. Using 265 galaxies from the Arecibo Dual-Beam Survey (ADBS) [10] find a low mass slope of $\alpha = -1.53$. The HI mass functions in both the Centaurus A and Sculptor groups are inconsistent with a slope steeper than $\alpha = -1.5$ [11]. Recently [12] carried out a sensitive search for HI companions to otherwise isolated spiral galaxies. Their survey covered a total of 31.6 Mpc^3 around 41 different spirals, and their results are consistent with slopes flatter than $\alpha \leq -1.3$. The flattest mass function to date comes from a deep survey of the Ursa Major group by [13], whose mass function is flat at the low mass end. The observed differences may reflect that the HI mass function is different in different environments, becoming shallower in high density regions.

Low HI mass galaxies are not detectable throughout the entire volume surveyed. To account for this a volume correction is applied to the lowest three mass bins when making the HIMF. To determine this correction for a given cube I calculate the actual volume over which a galaxy with a certain

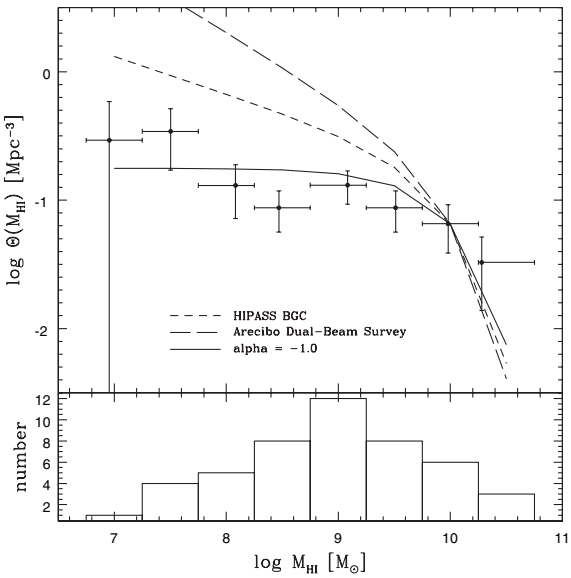

Fig. 2. The loose group HI mass function overlaid with Schechter functions fit from larger surveys. Upper Panel: Horizontal error bars indicate bin widths, vertical error bars indicate Poisson noise. Each point is plotted according to the average of all the HI masses within that bin. The HIPASS Bright Galaxy Catalog (BGC) HIMF is from Zwaan et al. 2003 and the Arecibo Dual-Beam Survey HIMF is from Rosenberg & Schneider 2002. A flat HIMF with faint end slope $\alpha = -1.0$ is plotted for reference. Lower Panel: The number of detections per mass bin.

mass based on the noise level and size of the cube could be detected using the standard HI mass equation.

$$M_{HI} = 2.36 \times 10^5 d^2 \int S_v dv \tag{1}$$

In this equation, d is the distance in Mpc and the integral which has units of Jy $\times$ km/s will be replaced by the 3σ noise in three channels. The HIMF is then produced by dividing the total number of detections in a mass bin by the combined volume surveyed in all the cubes that corresponds to that bin.

I have used this HI data to create an HI mass function for loose groups of galaxies. This HIMF uses 47 HI detected galaxies and surveys a volume of 90 Mpc^3 at masses $\geq 10^{8.5}$ M$_\odot$ with smaller volumes surveyed at smaller masses. This loose group HI mass function is essentially flat and inconsistent with the HIPASS Bright Galaxy Catalog and Araceibo Dual-Beam Survey HI mass functions.

References

1. Tully, R. B. 1987, ApJ, 321, 280
2. Carlberg, R. G. et al. 2001, ApJ, 552, 427
3. Neumann, D. M. et al. 2001, A&A, 365, L74
4. Mulchaey, J. S., Davis, D. S., Mushotzky, R. F., & Burstein, D. 2003, ApJS, 145, 39
5. Mulchaey, J. S, & Zabludoff, A. I. 1998, ApJ, 496, 39
6. Athanassoula, E., Makino, J., & Bosma, A. 1997, MNRAS, 286, 825
7. Verdes-Montenegro et al. 2001, A&A, 377, 812
8. Marcum, P. 1994, Star Formation Structure and Evolution of Galaxies in Loose Groups: the Environmental Connection, Ph.D. Thesis (University of Wisconsin, Madison)
9. Zwaan, M. A., et al. 2003, AJ, 125, 2842
10. Rosenberg, J. L., & Schneider, S. E. 2002, ApJ, 567, 247
11. de Blok, W. J. G., Zwaan, M. A., Dijkstra, M., Briggs, F. H., & Freeman, K. C. 2002, AAP, 382, 43
12. Pisano, D. J., Wilcots, E. M., & Liu, C. T. 2002, ApJS, 142, 161
13. Verheijen, M. A. W., Trentham, N., Tully, R. B., & Zwaan, M. A. 2000, ASP Conf. Ser. 218: Mapping the Hidden Universe: The Universe behind the Mily Way – The Universe in HI, 218, 263

Neutral Hydrogen in Galaxy Groups

V.A. Kilborn

Swinburne University, Hawthorn, Vic, 3122, Australia
vkilborn@swin.edu.au

Summary. We have conducted a wide-field neutral hydrogen (HI) survey of 16 galaxy groups, as part of the Group Evolution Multiwavelength Study (GEMS). We found 204 HI detections in the sixteen groups, and of these, 10 were previously uncatalogued, and 11 were in optical catalogues, but had no redshifts. We find that >98% of the neutral hydrogen mass we detect is associated with galaxies. The majority of our HI detections could be matched with an optically visible galaxy, however in the NGC 3783 galaxy group we find an HI cloud that appears to have no stellar emission associated with it. The origin and nature of this HI cloud is unclear. We look at the properties of all the groups combined, and find that the HI content of a galaxy group depends on its X-ray properties, such that those groups with extended X-ray emission tend to have less HI than those with no X-ray emission.

1 Introduction

HI surveys of groups can reveal the effects of tidal interactions in these environments [2]. One of the best examples of this is the VLA survey of the M81 group by [12]; while the galaxies of this group look quiescent in the optical, the HI distribution shows many streams and tidal tails indicating gravitational interactions. Studies of neutral hydrogen (HI) in groups have previously concentrated almost exclusively on Hickson Compact Groups (e.g. [8]; [11]), as they require small observing regions. Studies of loose groups, which are more extended, are much fewer in number. Pointed HI surveys of groups and clusters of galaxies have found a trend for galaxies to be HI deficient as a function of distance from the group/cluster centre. [11] found in a homogeneous survey of 48 Hickson Compact Groups (HCGs) that HCGs contained only 40% of the expected HI mass, based on the optical properties of the individual galaxies. [9] analysed the HI properties of 18 clusters, and found that two-thirds of their sample were HI deficient in the central regions (within the Abell radius). However it is not known whether loose galaxy groups show this same behaviour.

We have conducted wide-field HI observations as part of the Group Evolution Multiwavelength Study (GEMS) [7, 3], of ∼60 groups selected to have existing ROSAT PSPC X-ray observations. GEMS combines multiwavelength data (optical, X-ray, HI) to determine the characteristics of groups, and the

survey is introduced by Forbes in these proceedings. Sixteen of the GEMS groups in the southern hemisphere were surveyed for neutral hydrogen. The main aims of this HI survey are to provide a census of the HI gas in groups, to find new group members and possible intergalactic HI clouds, and to make a direct comparison between hot and cold gas in the group environment for the first time.

2 Observations and data reduction

Our observations of the sixteen groups follow the approach described in [1, 5, 3]. We scanned a field of dimensions $5.5^\circ \times 5.5^\circ$ using the Parkes 64 m radiotelescope with the 21 cm Multibeam Receiver [10] installed at the prime focus. Scans were made at a rate of one degree per minute, along lines of equatorial latitude and longitude separated by 4 arcmin. A total of ∼200 scans were acquired for each group.

Data were reduced using the LIVEDATA and GRIDZILLA components of the AIPS++ package. Data reduction steps are detailed in [3]. The gridded cubes were smoothed in the spectral domain with a Hanning filter three channels wide, and every second channel was discarded. The rms noise in the final cubes range from $\sim 15 - 20$ mJy per channel. The final gridded beamsize is 15.5 arcminutes, and the pixel size is 4 arcmin square. The final observing and cube parameters are summarised in Table 1.

Table 1. Narrow-band observing and cube parameters.

Number of groups observed	16
Gridded beam size	15.5 arcmin
Total observing time	∼18.5 hr
Channel width	1.65 km s^{-1}
Velocity resolution	2.6 km s^{-1}
rms noise per channel	15-20 mJy

The HI datacubes were searched visually for sources, using the KARMA visualisation suite. We smoothed the datacubes to a velocity resolution of $13.2\,\mathrm{km\,s^{-1}}$ for searching purposes, and then catalogued sources which appeared in several channels at approximately 3σ above the noise of the datacubes. Each datacube was searched three times in R.A–Dec, R.A.–velocity and Dec.–velocity projection, and two people searched each datacube for sources. The sensitivity of each datacube was determined by inserting Gaussian sources of known velocity width and peak flux into each datacube and noting the detection rate. While an estimate of the HI mass sensitivity of a datacube can be determined via the rms noise of the cube, variations in the data quality across the cubes, and the peak flux density versus velocity width of sources affects their detectability, so a better estimate of the HI

mass sensitivity of a cube is determined via calculating the detection rate of fake sources [6]. The HI mass sensitivity of our datacubes ranges from $\sim 1 - 8 \times 10^8 M_\odot$.

Once the sources were catalogued as above, an interactive fitting program based on MIRIAD routines was used to determine the central position, heliocentric velocity, velocity widths (50% and 20%), integrated flux, peak flux density, and rms noise of the spectrum. Firstly MOMENT was used to make a flux integrated HI distribution map of each source, and IMFIT was then invoked to determine the central position and extent of the source by fitting a 2-dimensional Gaussian profile to the HI distribution. This central position was then used in the task MBSPECT to determine all the other parameters for the source.

We used the NED and 6dFGS databases to match HI sources with previously known optical detections. There were ten galaxies we were unable to match with previously catalogued optical detections, and a further eleven sources where our HI detection provided the first redshift for the source.

3 Results

We catalogued 204 HI detections in the 16 groups, including 10 HI detections that did not match with any previously catalogued optical galaxy, and 11 HI detections that provided the redshift for previously catalogued galaxies, where the redshift was not previously known. Thus we find ∼10% new group members in our survey.

Figure 1 shows a velocity-integrated HI intensity map of two of our galaxy groups, NGC 1407 and NGC 1332. The NGC 1407 group displays group

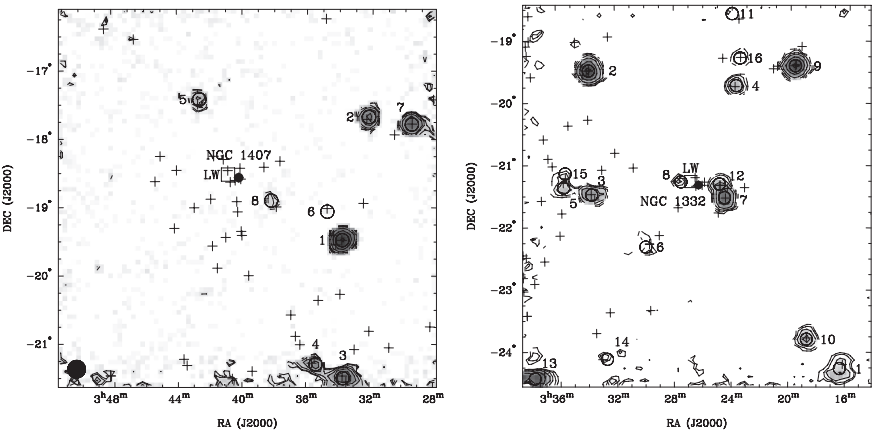

Fig. 1. Velocity-integrated HI maps of the galaxy groups NGC 1407 (left) and NGC 1332 (right). The contours show the HI emission, and crosses show previously catalogued sources near the group velocity. See Brough et al. in these proceedings for more information on these two groups.

X-ray emission at the centre of the group, and thus as it is a more evolved group, with a high early-type fraction, there is little (or no) HI detected near the centre of this group. In comparison, the NGC 1332 group is less evolved, has a high spiral fraction, and neutral hydrogen is found in galaxies throughout the group. We find a trend for this behaviour, i.e. the more evolved groups, that have extended, intra-group X-ray emission, tend to have a lower neutral hydrogen content than those groups that have no X-ray emission. The HI content of the groups depends more upon the total X-ray temperature, rather then the extent of the X-ray emission in the groups. This indicates that the deeper the potential well of the group (and hence the higher X-ray emission), the more evolved the group is, and thus the less neutral hydrogen it contains.

3.1 The HI cloud NGC_3783_2

We discovered one 'cloud' of neutral hydrogen, that does not appear to be associated with any optical emission. This HI cloud, GEMS_N3783_2, was found on the outskirts of the NGC 3783 group. We obtained ten hours of higher resolution HI imaging on the Australia Telescope Compact Array (ATCA) on 2004 March 3 of GEMS_N3783_2. We also obtained Keck imaging in the B and R-bands of the region around the cloud. The resulting HI image, and Keck optical imaging are shown in Figure 2. No extended optical emission that could be associated with GEMS_N3783_2 can be seen in the Keck imaging. The origin of this HI detection is unclear. The nearest HI detection we

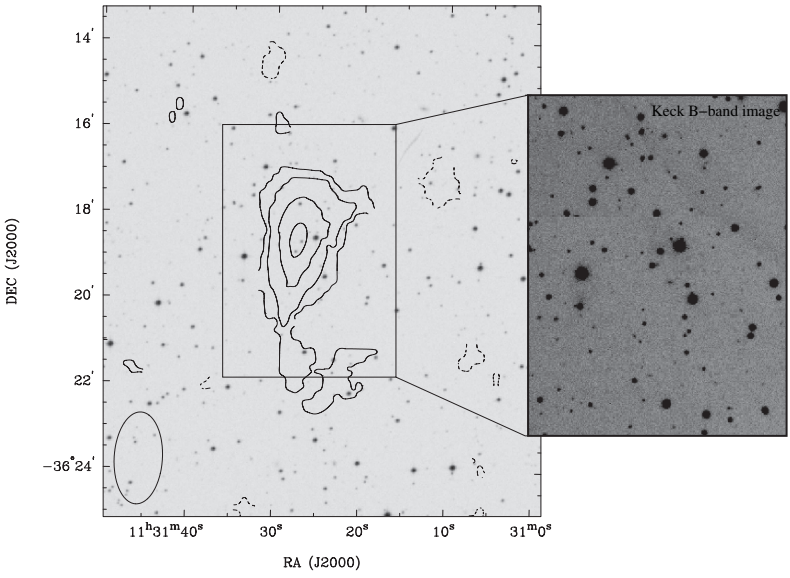

Fig. 2. Velocity integrated HI map of NGC_3783_2 (left) overlaid on the DSS $B-$band image. Right is a $B-$band image from Keck.

found in our data to this source is nearly 460 kpc away, the spiral galaxy ESO 378-G 003. Lying between ESO 378-G 003 and NGC_3783_2 is the early-type galaxy NGC 3706. NGC 3706 has some shells noted optically [4], perhaps indicating a past merger event. Whether GEMS_N3783_2 is a remnant from this past merger event, or an example of the much sought after 'dark galaxies', which comprise purely of dark matter (and in this case, neutral hydrogen) requires further observations to elucidate.

4 Conclusions

We have conducted wide-field neutral hydrogen imaging of 16 groups as part of the GEMS survey. We found ∼10% new group members in the survey, and that most of the HI we detected was gravitationally bound to galaxies. We found one region of HI that apparently does not have any optical emission. The origin of this detection, GEMS_N3783_2, is unclear, and we require further imaging to determine its nature.

References

1. Barnes, D. G., Staveley-Smith, L., de Blok, W. J. G. et al. 2001, MNRAS, 322, 486
2. Haynes M. P., Giovanelli R., Chincarini G. L. 1984, ARAA, 22, 445
3. Kilborn V. A., Koribalski B. S., Forbes D. A., Barnes D. G., Musgrave R. C. 2005, MNRAS, 356, 77
4. Malin, D. F., Carter, D. 1983, ApJ, 274, 534
5. McKay, N. F., et al. 2004, MNRAS, 352,1121
6. Meyer M. J. et al. 2004, MNRAS, 350, 1195
7. Osmond J. P. F. & Ponman T. J. 2004, MNRAS, 350, 1511
8. Shostak, G. S., Allen, R. J., Sullivan, W. T III 1984, A&A, 139, 15
9. Solanes J. M., Manrique A., Garcia-Gomez C., Giovanelli , R., Haynes M. P. 2001, ApJ, 548, 97
10. Staveley-Smith, L. et al. 1996, PASA, 13, 243
11. Verdes-Montenegro L., Yun M. S., Williams W. K., Huchtmeier W. K., Del Olmo A.,Erea J. 2001, A&A, 377, 812
12. Yun M. S., Ho P. T., Lo K. Y. 1994, Nature, 372, 530

Environmental Effects on Clusters at z = 0.2: Strong Galaxy Disruption in A 2667 and A 1689

H. Bravo–Alfaro[1], L. Cortese[2], G. Covone[3] and J.-P. Kneib[3]

[1] Departamento de Astronomia, Universidad de Guanajuato. Apdo. Postal 144, Guanajuato 36000. Mexico
hector@astro.ugto.mx
[2] School of Physics and Astronomy, Cardiff University, 5, The Parade, Cardiff CF24 3YB, Wales, UK
[3] LAM, Traverse du Siphon, 13012 Marseille, France

Summary. We show first results on the study of two spiral galaxies in the process of being strongly disrupted in the rich Abell clusters A 1689 (z = 0.18) and A 2667 (z = 0.23). Hubble Space Telescope images show a spectacular rupture of the spiral arms in both galaxies, one of which appears with no obvious neighbor. Extended trails composed by blue bright knots are associated with both systems. The extraordinary features observed in these two galaxies indicate that gravitational interactions are not rare in medium redshift clusters. The mean ages of the knots, between 10 Myr and 1 Gyr, suggest a tidal interaction scenario where the knots had been stripped from their parent galaxy.

1 Introduction

It is well established that clusters of galaxies represent hostile environments for member galaxies what strongly influences their evolution. At least two different mechanisms are present in clusters: those produced by the interaction of the hot intracluster medium (ICM) with the galactic interstellar medium, and those of gravitational origin. Nowadays it is generally accepted that more than one single physical mechanism is at work in clusters, but there still remain open questions about the specific mechanisms driving the star formation history and the morphological transformations suffered by single galaxies (for references see [6] and [14]).

In recent years some individual galaxies have been reported as candidates to be suffering strong tidal stripping, and the study of their stripped matter, of gaseous and/or stellar origin, is helping to fully understand the environmental effects exerted within the clusters. In this context, the diffuse intracluster light (ICL) has became a key piece on the dynamical history puzzle of clusters and their member galaxies. By far, the most accepted hypothesis remains that the debris of tidally disrupted galaxies are at the origin of the ICL (e.g. [15], [4], [1]). However, only few examples have been reported

to be caught during the process of being stripped. In fact, most of the cases only report the observation of tidal debris or filaments of very low surface brightness seen in nearby clusters such as Virgo, Centaurus and Coma [4], [7], [13], [8], [12].

In this work we report what may be the first galaxies observed during a major process of disruption, showing very bright filaments and knots. These two galaxies, 131124-012040 and 235144-260358, are members of the clusters A 1689 and A 2667, both at a redshift of z = 0.2 (hereafter we named these galaxies as A 1689:13.2-01.3 and A 2667:23.9-26.1 respectively). Their positions and magnitudes are listed in Table 1. No redshift information is avalaible for the galaxy in A 2667, while that in A 1689 has a similar redshift than the cluster itself [9]. These two objects are projected at 2.7′ NW and 3.7′ SW from their respective cluster centers; the equivalent distances in Mpc[4] are given in the last column of Table 1.

Table 1. Observational parameters

ID	α (J2000)	δ (J2000)	Mag F475W	Dist Mpc
A1689:131124-012040	$13^h11^m24^s.9$	-01° 20′ 39.9″	20.71	0.69
A2667:235144-260358	$23^h51^m44^s.1$	-26° 03′ 58.2″	18.70	0.83

2 The data

The photometric data are extracted from deep *HST* images. A 2667 was observed on October 2001, using the WFPC2 through the F450W, F606W and F814W filters. A total exposure time of 12000s in the F450W band and of 4000s in the F606W and F814W filters respectively, was obtained [5]. The $3\,\sigma$ limit detection for point sources are 26.00, 25.97 and 24.94 in the filters F450W, F606W, F814W, respectively.

Deep observations of A 1689 were obtained with the Wide Field Camera (WFC) in June 2002. A total of 20 orbits were taken in the three passbands F475W, F625W and F850LP [3]. The $3\,\sigma$ limit detection for point sources are 29.70, 29.23 and 28.33, in the filters F475W, F625W, F850LP, respectively.

Detection and analysis of sources was performed using *SExtractor* [2]. Source detection was done on an average of three bandpasses, and magnitudes were determined from aperture photometry on each single filter. All magnitudes are in the VEGAMAG systems with the following zero points: 26.17

[4]Throughout this paper we assume a cosmology with $\Omega_m = 0.3$, $\Omega_\lambda = 0.7$ and $H_0 = 70$ km s^{-1} Mpc^{-1}

(F475W), 25.73 (F625W), 24.33 (F850LP), 22.01 (F450W), 22.92 (F606W), 21.67 (F814W). No correction for Galactic extinction was performed, as it is negligible at the position of these objects.

3 Preliminary results

3.1 A 2667:23.9-26.1

Figure 1 shows an RGB image of A 2667:23.9-26.1, projected at ∼0.70 Mpc from the cluster center. This galaxy displays a striking morphology with clear evidences of stripping, even within its optical disk. Moreover a dozen of bright extragalactic blue knots extend from the optical disk to a projected distance of ∼ 75 kpc, forming a sort of trail of stripped material. These bright knots have a F450W magnitude in the range 23.5–25.5 mag, lying between super massive star clusters and dwarf galaxies. In addition to the bright knots, extended blue low surface brightness features are observed throughout the trail supporting the stripping scenario. No redshift is available for the blue knots nor for the bright galaxy itself, however the morphology of the whole system and the similar colors observed in all the knots, independently from their distance to the galaxy, strongly suggests that all these features are physically associated to A 2667:23.9-26.1.

In order to determine the mean age of the blue knots we compute the time evolution of the $F450W - F606W$ and $F606W - F814L$ colours, using

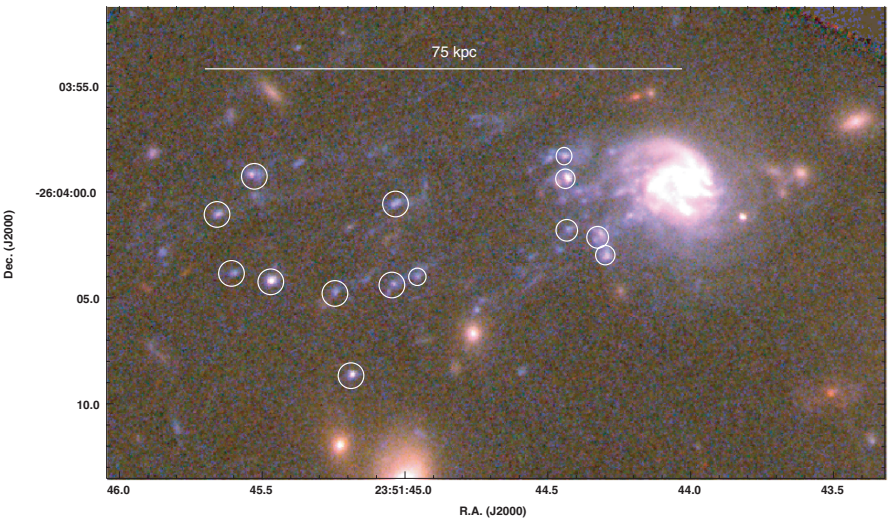

Fig. 1. RGB colour image of 235144-260358 in Abell2667. White circles indicate the knots for which photometry was obtained.

*Starburst*99 [10], and assuming a Salpeter IMF with solar metallicity and a burst or continuum star formation history. The typical colors of the knots are consistent with a continuum star formation activity and an age between 8-500 Myr.

3.2 A 1689:13.2-01.3

Figure 2 shows an RGB image of A 1689:13.2-01.3. It lies at 0.83 Mpc from the cluster center, and it is ∼2 mag fainter than A 2667:23.9-26.1. A tail long of some 20 kpc, formed of at least six blue knots, appears associated with this galaxy. The bright knots have a F475W magnitude in the range 26.2-28.3 mag, typical of stellar clusters and significantly fainter than the knots observed in A 2667:23.9-26.1.

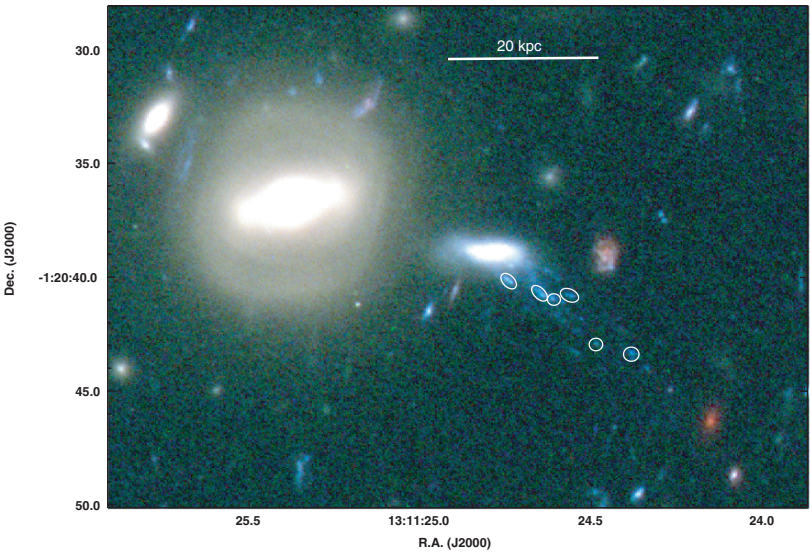

Fig. 2. RGB colour image of 131124-012040 in Abell 1689. White circles indicate the knots for which photometry was obtained.

In order to determine the mean age of the blue knots we computed the time evolution of the $F475W - F625W$ and $F625W - F850LP$ colours as in the previous case. In this case most of the blue knots lie between the modeled tracks of an instantaneous burst (with an age in the range 4-20 Myr), and those tracks of the model of continuum star formation history (age in the range 10-1000 Myr). The estimated dynamical age of the 20 kpc trail (∼18 Myr) suggests that the knots have been stripped from the parent galaxy.

4 Discussion

Our photometric analysis suggests that the blue knots in both galaxies have been stripped from their parent galaxies, supporting a gravitational interaction scenario. It is interesting to note that in A 1689:13.2-01.3 the stripped trail is ∼4 times shorter and its knots are 3 magnitudes fainter than the ones associated to A 2667:23.9-26.1, suggesting that the interaction is younger and/or milder than the one experienced by the later. The difference in 20 cm radio continuum flux confirm this fact, as will be shown in a future work.

About the fate of the knots, it is unlikely that they will fall back onto their parent galaxy. Therefore, those which are dynamically bound could be associated with the origin of ultracompact dwarfs galaxies, as those recently observed in A 1689 [11]. On the other hand, the knots that are not self-gravitationally bound will disperse their gas and stars into the intracluster medium, contributing to the ICL and to the ICM enrichment. In a forthcoming paper we analyze the 20 cm radio continuum data of both galaxies (from NVSS and the VLA-archive data) in order to measure the star formation activity associated with these peculiar systems. From X-ray data, we estimate the amount of ram-pressure stripping exerted by the ICM at each -projected-galaxy position, with the aim to predict the future of the stripped blue knots.

References

1. Adami, C., Slezak, E., Durret, F. et al.: Astron. & Astrophys. **429**, 39 (2005)
2. Bertin, E., & Arnouts, S: 1996, Astron. & Astrophys. Suppl. Ser. **117**, 393 (1996)
3. Broadhurst, T., Benítez, N., Coe, D: et al. ApJ, **621**, 53 (2005)
4. Calcáneo-Roldán, C., Moore, B., Bland-Hawthorn, J., Malin, D. & Sadler, E.M: MNRAS, **314**, 324 (2000)
5. Covone, G., Adami, C., Durret, F., et al.: Astron. & Astrophys. in press (2006)
6. Dressler, A.: Star-forming Galaxies in Clusters. In: *Clusters of Galaxies: Probes of Cosmological Structure*, vol 3, ed by J.S. Mulchaey, A. Dressler, and A. Oemler (Carnegie Observatories Astrophysics Ser. 2004), pp 206–226
7. Gavazzi, G., Boselli, A., Mayer, L. et al.: ApJ, **563**, L23 (2001)
8. Kemp, S. N., de la Fuente, E., Franco-Balderas, A. & Meaburn, J: ApJ, **624**, 680 (2005)
9. Kneib, J.-P. Private communication 2005.
10. Leitherer, C., Schaerer, D., Goldader, J. D., et al.: ApJS, **123**, 3 (1999)
11. Mieske, S., Infante, L., Benitez, N., et al.: AJ, **128**, 1529 (2004)
12. Mihos, J. C., Harding, P., Feldmeier, J., Morrison, H.: ApJ, **631L**, 41 (2005)
13. Oosterloo, T. & van Gorkom, J. H: Astron. & Astrophys. **437**, L19 (2005)
14. van Gorkom, J.H.: Interaction of galaxies with the ICM. In: *Clusters of Galaxies: Probes of Cosmological Structure*, vol 3, ed by J.S. Mulchaey, A. Dressler, and A. Oemler (Carnegie Observatories Astrophysics Ser. 2004), pp 305–321
15. Vílchez-Gómez, R., Pelló, R. & Sanahuja, B: Astron. & Astrophys. **283**, 37 (1994)

Metallicity Structure in X-ray Bright Galaxy Groups

J. Rasmussen and T.J. Ponman

School of Physics and Astronomy, University of Birmingham, Edgbaston, Birmingham B15 2TT, UK
jesper@star.sr.bham.ac.uk

Summary. Using *Chandra* X-ray data of a sample of 15 X-ray bright galaxy groups, we present preliminary results of a coherent study of the radial distribution of metal abundances in the hot gas in groups. The iron content in group outskirts is found to be lower than in clusters by a factor of $\sim$2, despite showing mean levels in the central regions comparable to those of clusters. The abundance profiles are used to constrain the contribution from supernovae type Ia and II to the chemical enrichment and thermal energy of the intragroup medium at different group radii. The results suggest a scenario in which a substantial fraction of the chemical enrichment of groups took place in filaments prior to group collapse.

1 Introduction

Hot X-ray emitting gas constitutes the dominant baryonic component in groups and clusters of galaxies. The chemical enrichment of this intracluster medium (ICM) is believed to originate mainly in material ejected from group and cluster galaxies by supernovae, with a smaller portion driven out by galaxies through galaxy–galaxy and galaxy–ICM interactions. The spatial distribution of metals reflect the action of such processes, providing insight into the mechanisms, other than gravity, that have shaped the thermodynamic properties of gas in groups and clusters.

Iron and silicon comprise the major diagnostic elements for studies of the abundance distribution in groups and clusters, as these elements give rise to the most prominent lines in the soft X-ray spectrum of thermal plasmas, and are among the elements for which there is a distinctively different yield in type Ia and type II supernova explosions according to standard supernova (SN) models. Whilst iron is predominantly produced by SN Ia, silicon is more evenly mixed between the two SN types. The ratio of Si to Fe abundance therefore provides valuable information on the relative importance of SN II vs. SN Ia in enriching the intragroup medium.

Abundance profiles of massive clusters have received considerable attention. Due to their lower X-ray luminosities, the situation in lower-mass systems is much less clear, despite their relatively larger importance for the cosmic baryon and metal budgets. With the current generation of X-ray telescopes, however, the ability to perform spatially resolved X-ray spectroscopy has improved dramatically, enabling detailed mapping of the metal distribution also in groups. Here we utilize this to derive radial profiles of the abundance of Fe and Si from *Chandra* observations of a sample of 15 groups. The sample size allows us to explore statistical trends within the sample and obtain a clearer picture of the content and behaviour of metals in group outskirts, where most of the intragroup gas resides but where the low X-ray surface brightness often prohibits robust constraints to be obtained for individual systems.

2 Sample and analysis

Our sample is based on the 25 GEMS groups that show group-scale extended X-ray emission (the 'G' sample of [1]). Only groups with *Chandra* archival data featuring more than 6,000 net counts and being more distant than 20 Mpc were selected, while at the same time discarding obviously unrelaxed groups. We added four more groups conforming to these criteria, leaving a sample of 15 reasonably relaxed groups with high-quality *Chandra* data.

All data sets were subjected to standard screening criteria and cleaned for periods of high background, with blank-sky background data filtered in

Table 1. Basic X-ray properties of the group sample, with mean temperatures $\langle T \rangle$ in keV, abundances $\langle Z \rangle$ in $Z_\odot$, and r_{500} in kpc

Group	$\langle T \rangle$	$\langle Z \rangle$	r_{500}	Group	$\langle T \rangle$	$\langle Z \rangle$	r_{500}
NGC 383	$1.65^{+0.04}_{-0.06}$	$0.39^{+0.07}_{-0.07}$	578	**NGC 4125**	$0.33^{+0.12}_{-0.05}$	$0.19^{+0.17}_{-0.07}$	259
NGC 507	$1.30^{+0.03}_{-0.03}$	$0.40^{+0.07}_{-0.06}$	513	**NGC 4325**	$0.99^{+0.02}_{-0.02}$	$0.39^{+0.08}_{-0.06}$	448
NGC 533	$1.22^{+0.05}_{-0.05}$	$0.28^{+0.07}_{-0.06}$	497	**HCG 62**	$1.00^{+0.03}_{-0.03}$	$0.12^{+0.02}_{-0.03}$	450
NGC 741	$1.42^{+0.14}_{-0.12}$	$0.16^{+0.08}_{-0.06}$	536	**NGC 5044**	$1.12^{+0.03}_{-0.03}$	$0.25^{+0.04}_{-0.03}$	476
NGC 1407	$1.01^{+0.07}_{-0.09}$	$0.15^{+0.09}_{-0.06}$	452	**NGC 5846**	$0.66^{+0.04}_{-0.03}$	$0.16^{+0.06}_{-0.05}$	366
NGC 2300	$0.78^{+0.04}_{-0.03}$	$0.17^{+0.07}_{-0.05}$	397	**NGC 6338**	$2.13^{+0.19}_{-0.07}$	$0.25^{+0.08}_{-0.05}$	657
HCG 42	$0.80^{+0.05}_{-0.05}$	$0.25^{+0.31}_{-0.10}$	402	**NGC 7619**	$1.06^{+0.07}_{-0.03}$	$0.23^{+0.05}_{-0.05}$	463
NGC 4073	$1.78^{+0.07}_{-0.09}$	$0.49^{+0.07}_{-0.07}$	600				

an identical manner. Background-subtracted spectra were extracted in annuli and fitted with a VAPEC model in XSPEC using Solar abundances from [2]. All elements were tied together, except for Fe and Si. To put all groups on an equal footing, all radii were normalized to r_{500}, the radius enclosing a mean density of 500 times the critical density, using an empirical relation based on the temperature of the group [3]. The temperature profiles themselves reveal that most of the groups feature a central region of cool gas, referred to here as the group core. For each group, Table 1 lists r_{500} and the mean temperature and abundance derived outside the cool core in the radial range 0.1–0.3 r_{500}.

3 Fe and Si radial profiles

Profiles of Fe and Si abundance for all groups combined are shown in Fig. 1a. Fe is seen to decline outside the group core, converging towards a value of $\sim$0.1 $Z_\odot$ at r_{500}. We note that this value is lower than that seen in cluster outskirts by a factor of $\sim$2 (e.g. [4]), even though the Fe abundance in group cores is comparable to cluster levels. Si is more spatially uniform than Fe, declining less steeply outside the core. Intrinsic scatter is most prominent in the core, where non-gravitational processes are expected to be important.

These features are all confirmed by Fig. 1b, where the data have been binned into radial bins of 20 measurements, to help illustrate any radial trends. Adopting the SN model yields of [5, 6], the Si/Fe ratios suggest that the enrichment in group cores can be attributed to a mixture of SN Ia and SN II which is similar to that in the Solar neighbourhood. At large radii the Si/Fe ratio suggests an increasing predominance of SN II, with the abundance pattern being consistent with pure SN II enrichment at r_{500}.

As the intrinsic scatter in abundances outside the group cores is fairly small, we made simple parametrizations of the binned profiles shown in Fig. 1b, in order to obtain prescriptions for $Z_{\rm Fe}(r)$ and $Z_{\rm Si}(r)$ that can be seen as representative for the entire group sample. These are shown as dashed lines

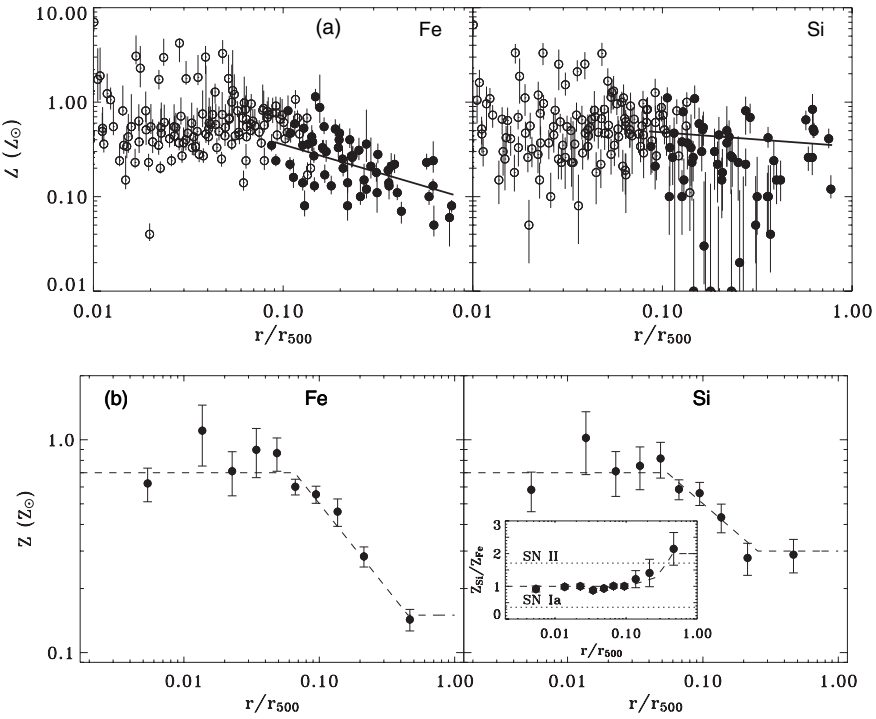

Fig. 1. (**a**) Radial abundance profiles for all groups. Filled circles represent data points outside the cool group cores, empty circles those within. Solid lines represent the results of regression fits to the data outside the group cores. (**b**) The same data, binned into radial bins of 20 data points. The inset shows the resulting Si/Fe ratio, with dotted lines marking the expectations from pure SN Ia and SN II enrichment.

in Fig. 1b, with the resulting (parametrized) ratio $Z_{\rm Si}(r)/Z_{\rm Fe}(r)$ conforming to the range allowed by the adopted SN yields.

4 Implications

4.1 Metal masses and the role of SN Ia vs. SN II

Based on gas density profiles for each group taken from the literature, the parametrized Fe and Si profiles were decomposed into contributions from SN Ia and SN II. The result, shown in Fig. 2a, indicates that about half of the iron in group cores is provided by SN Ia, but that SN II products are much more widely distributed than those of SN Ia, similarly to results for clusters. The total iron mass released by SN within r_{500} spans the range 3×10^7–$3 \times 10^9\,{\rm M}_\odot$ across the sample.

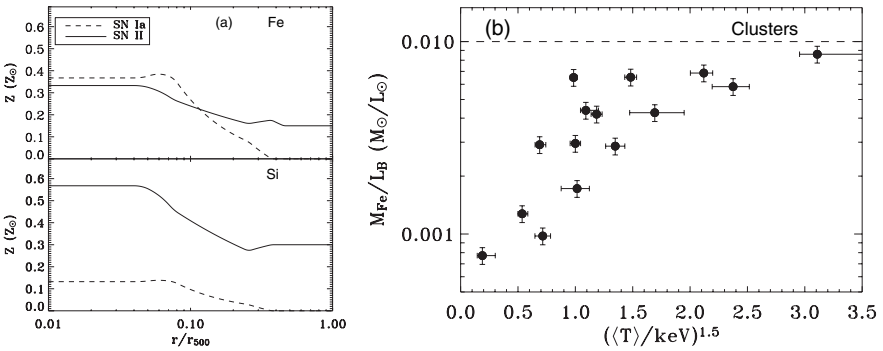

Fig. 2. (**a**) Contribution to the total abundance of Fe and Si from SN Ia and SN II. (**b**) Fe mass-to-light ratio within r_{500} as a function of group 'mass' $M \propto \langle T \rangle^{1.5}$. The dashed line shows the typical cluster value [4].

Using optical luminosities derived as in [1], total iron mass-to-light ratios within r_{500} are shown in Fig. 2b (results for Si are very similar). The low Fe abundance in group outskirts compared to clusters is reflected in lower Fe M/L ratios. Even across the fairly narrow range in total group mass studied here (estimated assuming an empirical mass-temperature relation $M \propto \langle T \rangle^{1.5}$ [7]), there is a clear tendency for lower-mass groups to contain relatively lower amounts of enriched material for their optical luminosity.

Assuming each SN releases 10^{51} erg directly into the ICM, the total SN energy range displayed by the groups of 2×10^{59}–2×10^{61} erg is comparable to the total thermal energy contained in the ICM, with the clear majority of it (∼95%) provided by SN II.

4.2 The chemical enrichment history of groups

Figures 1 and 2 show that the metals are not completely mixed throughout the ICM. This applies particularly to the metals attributed to SN Ia, of which a considerable fraction is likely to be associated with prolonged enrichment from the stellar population of the central galaxy present in all the groups. As also discussed by [4] on the basis of a small sample of three groups, the much wider distribution of SN II products suggests a scenario of SN II–dominated enrichment at an early stage in the formation of the groups, leaving time for the enriched material to mix well throughout the ICM.

In the group outskirts, the inferred energy per particle imparted to the IGM by SN II is of order 0.5 keV. Coupled with the above, this indicates that galactic winds associated with an early phase of strong starburst activity could have contributed substantially to pre-heating of the ICM in groups. It is likely that much of this preheating and the associated chemical enrichment took place before the gas collapsed into groups, while still located in filaments of low overdensities [8]. Some fraction of the SN ejecta should have been able

to escape from low-mass filaments, giving rise to the trend of increasing iron mass-to-light ratio with present-day group mass. The inferred central rise in SN II products can then be explained if some of these metals were released after the group collapsed, possibly facilitated by galaxy–galaxy and galaxy–ICM interactions, and potentially with an additional contribution associated with stellar wind loss from the central elliptical galaxy.

We are grateful to Stephen Helsdon for his contribution to the early stages of this work. JR acknowledges the support of an EU Marie Curie Intra-European Fellowship under contract no. MEIF-CT-2005-011171.

References

1. J.P.F. Osmond, T.J. Ponman: MNRAS **350**, 1511 (2004)
2. N. Grevesse, A.J. Sauval: Space Sci. Rev. **85**, 161 (1998)
3. A. Finoguenov, T.H. Reiprich, H. Böhringer: A&A **368**, 749 (2001)
4. A. Finoguenov, L.P. David, T.J. Ponman: ApJ **544**, 188 (2000)
5. K. Nomoto, et al.: Nucl. Phys. A **616**, 79 (1997)
6. K. Nomoto, et al.: Nucl. Phys. A **621**, 467 (1997)
7. A. Vikhlinin, A. Kravtsov, W. Forman, C. Jones, M. Markevitch, S.S. Murray, L. Van Speybroeck: ApJ submitted (astro-ph/0507092)
8. T.J. Ponman, D.B. Cannon, J.F. Navarro: Nature **397**, 135 (1999)

An X-ray View of the Cores of Galaxy Groups: Effects of AGN and Mergers on the IGM

E. O'Sullivan and J.M. Vrtilek

Harvard-Smithsonian Center for Astrophysics, 60 Garden Street, MS-67, Cambridge, MA 02138, USA
eosullivan,jvrtilek@head.cfa.harvard.edu

Summary. Using data from *XMM-Newton* and *Chandra*, we have studied a number of X-ray luminous galaxy groups in order to investigate the effects of mergers and AGN activity on their properties. We here present results from four disturbed systems with particularly interesting features. These groups provide examples of AGN heating preventing runaway cooling and mixing enriched gas from the dominant elliptical with the surrounding intra-group medium. We also show that under standard assumptions of hydrostatic equilibrium and relaxation, X-ray analysis may underestimate the gravitational mass of disturbed systems.

1 Introduction

Studies of the X-ray halos of galaxy groups can provide useful insights into the structure and history of these systems. Metal abundance measurements provide an excellent method for investigating star formation history and enrichment of the intra-group medium (IGM). Mergers between groups can be very visible in the X-ray, as can AGN activity and interactions between AGN jets and gas. The central cool cores seen in many groups can be used as a basis for estimating the time since the groups were last disturbed and the gas heated. The halos also provide one of the best tools for investigating the total mass profiles of groups, thereby allowing investigation of the dark matter content and its distribution. However, there are a number of important issues relating to groups halos which are only now being addressed. While many groups have very short central cooling times, classical cooling flows appear to be rare; the mechanism preventing runaway cooling is not yet certain. It is also unclear whether metals in the IGM are partially produced *in situ* by an intra-group stellar population, but it seems likely that some or all of them must originate within galaxies. The question of how material could be transported to, and mixed with, the group halo has yet to be answered.

There are also some technical issues relating to the way in which X-ray observations of groups are analysed. In galaxy clusters, the halo can usually be traced to large radii, and so the central region can be ignored if is disturbed or rapidly cooling. Galaxy groups tend to be less luminous, and so only relatively nearby systems can be observed in detail, and the halo cannot be traced to

large radii. The central region is typically retained, despite disturbances, and it is unclear what effect this has on analysis. Mass estimation from X-ray data depends on a number of assumptions, most importantly that the halo is relaxed and in hydrostatic equilibrium, and it is therefore important to determine whether this is actually the case in most X-ray bright groups.

2 Sample and results

In order to investigate the properties of group halos, we have examined a sample of 25 nearby, X-ray luminous galaxy groups which have been observed by *Chandra* or *XMM-Newton*. Of the 11 systems with highest quality data, 6 show signs of serious disturbance in their cores. We present results from 4 systems, showing the effect of AGN activity and mergers on the group halos.

2.1 NGC 4636: AGN heating and gas mixing

Often considered an example of a "typical" elliptical galaxy, NGC 4636 is the dominant elliptical of a small group [1] on the outskirts of the Virgo cluster. The group halo is extensive and highly luminous ($L_X \sim 2{\times}10^{41}$ erg s^{-1}, kT$\sim$1 keV [2]) and the galaxy hosts a weak radio jet source [3]. A *Chandra* ACIS-S observation revealed a number of unusual structures in the galaxy core, most notably "spiral arms" of high surface brightness emission, thought to be shocks caused by a previous AGN outburst [4]. Detailed spectral analysis of these data suggested the presence of a cavity to the west of the core [5].

We analysed both the *XMM* and *Chandra* observations of NGC 4636 (see [6] for a full description and figures), and created spectral maps from the two datasets. These are images in which each pixel represents the temperature or abundance measured from a spectral fit to the surrounding region (see Fig. 1 for an example). The maps reveal a 30 kpc plume of cool, high abundance gas extending SW from the galaxy centre, with a small region of higher temperatures marking the previously suggested cavity. We interpret this plume as the result of repeated AGN outbursts; each period of activity produces cavities in the X-ray gas, filled with radio plasma from the AGN jets. These rise buoyantly, entraining gas behind them, drawing the cool, highly enriched material from the galaxy core outwards. This provides mechanisms for enrichment of the IGM and prevention of runaway cooling, through both direct heating and gas mixing.

2.2 NGC 3411: AGN outburst or galaxy–group merger?

The NGC 3411 group is quite similar to NGC 4636, with a relaxed halo and weak central radio source. We examined the available *XMM-Newton* and *Chandra* observations of the group and found a very unusual temperature

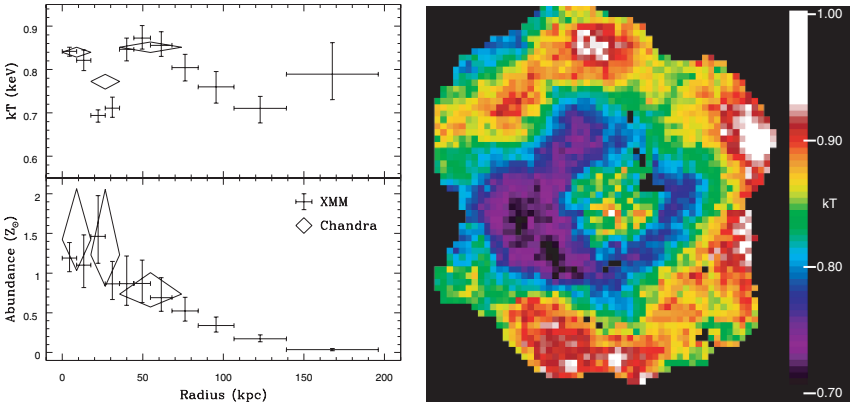

Fig. 1. *Left*: Deprojected temperature and abundance profiles for NGC 3411. Both *XMM* and *Chandra* show a dip in temperature at ∼25 kpc. *Right*: *XMM* temperature map of NGC 3411, showing the shell of cool gas.

profile. Most groups have a central temperature drop, as the high densities in the core lead to rapid cooling. NGC 3411 has a central temperature peak in the middle of this cool region (see Fig. 1). Spectral mapping confirms that there is a roughly circular hot central region, coincident with the galaxy core and radio source, surrounded by a ring of cooler emission.

Two possible scenarios can be suggested to explain this highly unusual structure. The first is that NGC 3411 is the product of a recent galaxy-group merger; if a large elliptical, falling into the group, were stripped of its X-ray halo, the stripped gas would fall through the group until it reached entropy equilibrium with its surroundings. It would then spread along the surface of equal entropy, forming a shell around the core of the group. This model would explain the temperature features quite well, but there is no candidate for the stripped galaxy; the small ellipticals neighbouring NGC 3411 are unlikely to have produced enough gas ($\sim 3.5 \times 10^9$ $M_\odot$ is required). AGN activity provides an alternative. If we have caught the AGN just after the beginning of its activity cycle, we might expect to see a small heated region in the centre of the cooling flow which fueled the outburst. To try to distinguish between these two possibilities we have acquired high resolution VLA data which should reveal whether AGN jets are interacting with the inner halo.

2.3 NGC 507: Group–group merger

NGC 507 is dominant elliptical of one of the largest and most X-ray luminous groups in the local universe (kT = 1.25 keV, log $L_X = 9 \times 10^{42}$ erg s^{-1} [7]), and an FRI radio galaxy. Recent *Chandra* observations have shown strong surface brightness "edges", coincident with regions of low temperature and high abundance gas [8]. We analysed an *XMM* observation of NGC 507, and

spectral mapping confirmed these features, showing them to be correlated with the AGN jets. It appears that the jet activity has disturbed the inner halo, moving enriched gas out to the NE, and severely distorting the temperature distribution. This may be related to the ongoing merger between the NGC 507 and NGC 499 groups. The X-ray halos of the two systems overlap, with a ridge of bright emission linking the two X-ray peaks. Unfortunately, dynamical studies do not reveal whether the two groups are falling together for the first time or whether they have already passed, and current X-ray data do not cover the important ridge area. We have successfully proposed a further *XMM* study, in order to determine whether the AGN activity and disturbance in NGC 507 has been caused by the merger.

2.4 NGC 741: Galaxy collision in a group core

The NGC 741 group is less luminous than the systems described above, but high resolution *Chandra* data has revealed a unique structure in its core. The dominant elliptical has a smaller elliptical neighbour, NGC 742, separated by only a few arcseconds and having a concordant redshift. VLA imaging shows that both galaxies host radio point sources, and that they are linked by a narrow filament of radio emission. Analysis of the *Chandra* data shows a similar filament of bright X-ray emission, linking the two galaxies slightly to the south of the radio filament. One interpretation of the features is that NGC 741 and NGC 742 are an X-ray analogue of the "taffy galaxies", UGC 12914/5. This pair of spiral galaxies appear to have suffered a recent head-on collision [9]. As the two disks passed through one another and moved apart, a bridge of magnetic fields and gas was drawn out between them. In the case of NGC 741/2, magnetic fields associated with AGN may have linked to form filaments filled with radio and X-ray plasma between the two galaxies. If so, we estimate the collision happened a few 10^7 yr ago, and note that the core of NGC 742 still contains cool gas despite this violent interaction.

3 Discussion and conclusions

The systems described above provide examples of the kinds of interactions which occur in the cores of galaxy groups. They also suggest answers to some of the questions posed in section 1. NGC 3411, NGC 507 and in particular NGC 4636 all show how AGN activity may be responsible for heating group cores and preventing runaway cooling, and for transporting enriched gas out into the IGM. Results from galaxy clusters suggest that AGN are an important factor across a wide mass range [10]. However, one worrying issue is the effect that the disturbances we observe may have on X-ray analysis.

Figure 2 shows mass-to-light ratio for a number of groups from our sample, using gravitational mass profiles determined from the X-ray data using standard assumptions, notably hydrostatic equilibrium. For two of the most

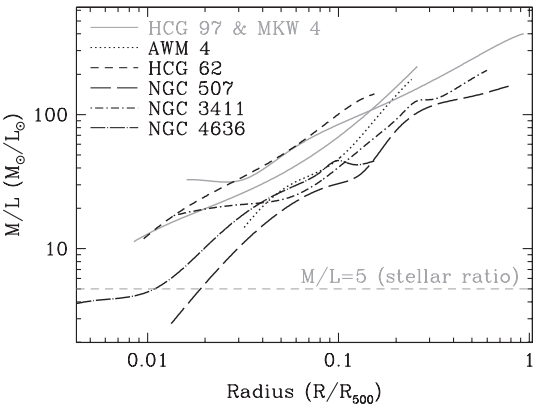

Fig. 2. Mass-to-light ratio profiles of 8 groups in our sample. HCG 97 and MKW 4 are essentially relaxed, all others have signs of disturbance in their cores.

disturbed systems, NGC 507 and NGC 4636, the mass-to-light ratio drops below that expected for stars in the inner core. This suggests that the total mass may be underestimated, most likely because our assumptions about the gas are invalid. We note that a similar result has been seen in other groups and elliptical galaxies [11], and that while it is clearest in the most disturbed systems, we are likely to miss disturbances in many systems which have only poor quality X-ray data available. While X-ray studies of groups provide a wealth of information about their history and structure, comparison with mass estimates from independent techniques is clearly desirable.

References

1. R. Nolthenius: ApJS **85**, 1 (1993)
2. W. Forman, C. Jones, W. Tucker: ApJ **293**, 102 (1985)
3. M. Birkinshaw, R. L. Davies: ApJ **291**, 32 (1985)
4. C. Jones, W. Forman, A. Vikhlinin et al.: ApJ **567**, L115 (2002)
5. A. Ohto, N. Kawano, Y. Fukazawa: PASJ **55**, 819 (2003)
6. E. O'Sullivan, J. M. Vrtilek, J. C. Kempner et al.: MNRAS **357**, 1134 (2005)
7. J. S. Mulchaey, D. S. Davis, R. F. Mushotzky et al.: ApJS **145**, 39 (2003)
8. R. P. Kraft, W. Forman, E. Churazov et al.: ApJ **601**, 221 (2004)
9. J. J. Condon, G. Helou, D. B. Sanders et al.: AJ **105**, 1730, (1993)
10. W. Forman, P. Nulsen, S. Heinz et al.: ApJ **635**, 894, (2005)
11. P. J. Humphrey, D. A. Buote, F. Gastaldello et al.: astro-ph/0601301 (2005)

Active Galaxies, Thermal Conduction and Entropy of Gas in Galaxy Groups and Clusters

S. Roychowdhury

Raman Research Institute, Sadashivnagar, Bangalore - 560080, Karnataka, India
suparna@rri.res.in

Summary. Galaxy clusters harbour large amounts of hot gas which make them luminous in X-rays. The temperature of this gas is mostly thought to be determined by the gravitational potential of the dark matter. Recent detailed X-ray observations have also determined its entropy, and found evidence of non-gravitational heating of this gas. We study the role of buoyant bubbles from active galaxies and thermal conduction in clusters to explain these excess entropy observations at large radii ($r > 0.5r_{\rm vir}$. In addition, we also examine the effect of such AGN heating on the Sunyaev-Zeldovich angular power spectrum.

1 Introduction

Clusters and groups of galaxies contain dark matter and hot, diffuse gas called the intracluster medium. Predictions from the hierarchical structure formation scenario led us to believe that this intracluster gas would follow a self-similar scaling relation. However, recent observations of clusters and groups of galaxies have shown that the scaling relations are not self-similar. The observed relations of different physical parameters of the ICM such as density, X-ray luminosity and entropy have mostly confirmed the requirement for non-gravitational processes like AGN heating and radiative cooling [7], [11], [12]. Many theoretical models have been proposed to explain these X-ray observations like heating from supernovae [18]; [19], quasar outflows [9], and "effervescent heating" [14].

Here, we have studied the evolution of the ICM due to "effervescent heating" via buoyant bubbles which deposit energy into the ICM as they rise and expand in the cluster atmosphere (RRNB04) along with cooling and thermal conduction. In addition, we also focus on the Sunyaev-Zeldovich angular power spectrum of the CMB.

We assume throughout the paper $\Omega_\Lambda = 0.71$, $\Omega_0 = 0.29$, $\Omega_{\rm b} = 0.047$ and $h = 0.71$ which are the best fit parameters from WMAP [16].

2 AGN heating, radiative cooling and thermal conduction

The effervescent heating mechanism is a gentle heating mechanism in which the cluster gas is heated by buoyant bubbles of relativistic plasma produced by central AGN [1], [15]. The average volume heating rate is a function of the ICM pressure gradient and is given by

$$\mathcal{H} = -h(r) P_{\rm gas}^{(\gamma_{\rm b}-1)/\gamma_{\rm b}} \frac{1}{r} \frac{d \ln P_{\rm gas}}{d \ln r}, \tag{1}$$

where $P_{\rm gas}$ is the ICM pressure, $\gamma_{\rm b}$ is the adiabatic index of buoyant gas in the bubbles and $h(r)$ is the normalization function, which is fixed by a time-averaged luminosity of the central AGN and an exponential cut-off at an inner heating radius, where the bubbles originate.

The volume cooling rate is calculated using a fit [9] to the normalized cooling function $\Lambda_{\rm N}(T)$ for a metallicity of $Z/Z_{\odot} = 0.3$, as calculated by [17].

The motivation behind including thermal conduction was to remove out the negative gradients in the temperature and entropy profiles in clusters, which arise due to heating by a central AGN. The flux due to thermal conduction $F_{\rm cond}$ is given by

$$\mathbf{F}_{\rm cond} = -f \kappa \nabla T, \tag{2}$$

where κ is the Spitzer conductivity. f is the supression factor which comes in due to the presence of magnetic fields. Recent theoretical works by [10], [2], [5] and several others suggests that conduction could be as high as 10% to 20% of the Spitzer value in the presence of a tangled and turbulent magnetic field. Motivated by these results we adopt the suppression factor $f = 0.1$.

Next, we describe the evolution of the ICM due to heating, cooling and thermal conduction. The intracluster gas is assumed to be in quasi-hydrostatic equilibrium at all times since cooling is not precipitous at these radii and the heating is mild. The total time available for the simulation is the Hubble time, $t_{\rm H}$. The initial state of the ICM is given by the universal temperature profile [6], [13]. The gas is evolved in time-steps of Δt by updating its entropy by heating, cooling and thermal conduction. The system relaxes to a new state of hydrostatic equilibrium with a new density and temperature profile after each time-step. The boundary conditions imposed to evaluate the new density and temperature profiles are that (1) $P\,(r_{\rm out}) =$ constant $= P_{\rm gas0}(r_{200})$, and (2) $M_{\rm g}(r_{\rm out}) = M_{\rm g0}(r_{200}) = 0.1333 M_{\rm dm}(r_{200})$. It is important to note here that $r_{\rm out}$ increases as the cluster gas gets heated and spreads out.

The observed gas entropy $\mathcal{S}(r)$ at $0.1r_{200}$ and at r_{500} is then calculated using

$$\mathcal{S}(r) \equiv T(r)/n_{\rm e}^{2/3}(r). \tag{3}$$

After a time $t_{\rm heat}$, the heating source is switched off, putting $\mathcal{H} = 0$ and the gas is allowed to evolve with cooling and thermal conduction until the total simulation time. for a duration of $t_{\rm H}$, the Hubble time. Note that $r_{\rm out}$ decreases during this time since the intracluster gas loses entropy and shrinks.

The only free parameters in our calculation are the energy injection rate $\langle L \rangle$ and the time $t_{\rm heat}$ over which the "effervescent heating" of the ICM takes place. Thus, we explore the parameter space of $\langle L \rangle$ and $t_{\rm heat}$ or rather a single free parameter, i.e. the total energy, $E_{\rm agn} = \langle L \rangle t_{\rm heat}$ for different cluster masses so that the entropy (after $1.35{\times}10^{10}$ years) at $0.1r_{200}$ and r_{500} matches the observed values.

In addition, we also calculate the poissonian contribution to the Sunyaev-Zeldovich angular power spectrum, $C_\ell(P)$ as a function of ℓ.

3 Results and discussion

The primary aim of this work was to study the implications AGN heating and thermal conduction on the global properties of groups and clusters of galaxies including the Sunyaev-Zeldovich effect.

Left Panel of Figure (1) shows the permitted total injected energy range as a function of the mass of cluster for heating times between $t_{\rm heat} = 5 \times 10^8$ years and $t_{\rm heat} = 5 \times 10^9$ years required to satisfy entropy observations at both radii. The thin solid line and the thick dashed line represent non-linear relations between the total energy injected to the cluster by AGN and the mass of the cluster with exponent of 1.5 and 5/3 respectively. This relation can be translated to a halo-black hole mass relation. In fact, based on the $M - \sigma$ relation and cosmological simulations, [4] derive a relation between the mass of the black hole and the mass of the galactic halo of the form $M \propto M_{\rm gh}^{1.65}$. The slope of this relation is very similar to the one considered here.

The right panel of Figure (1) shows the time evolution of scaled entropy profiles of a cluster of mass $M_{\rm cl} = 6 \times 10^{14} M_\odot$ for $\langle L \rangle = 5.25{\times}10^{45}$ erg s^{-1}. We use the same method of emissivity weighting as in [13] to calculate the average quantities. The inclusion of conduction removes the negative gradient in the scaled entropy profiles in the central regions of the cluster (within $0.5r_{200}$. These entropy profiles do not show any flat entropy core unlike in [14] (left panel in their Figure 2). Thus, this probably indicates that thermal conduction is a more plausible process in ICM than covection for such gentle AGN heating. Unlike in the case of previously proposed models, we found that isentropic cores are not an inevitable consequence of preheating. This is consistent with observations of groups that do not show large isentropic cores [11].

In a recent study [3] presented the luminosity-temperature relation for groups and separated the sample into "radio loud" or "quiet" objects. They showed that "radio loud" groups deviated more from the self-similar scaling

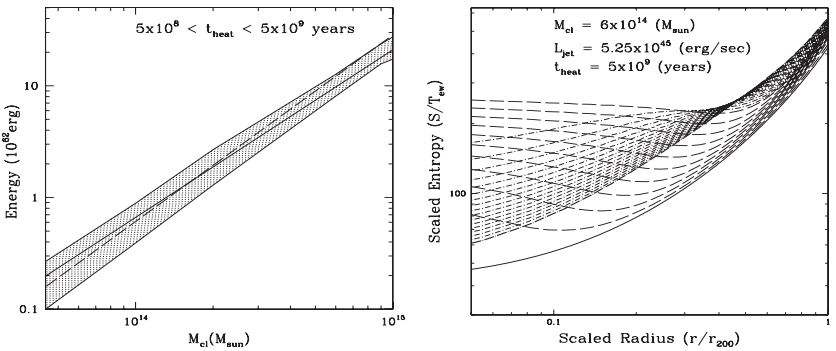

Fig. 1. *Left panel:* This figure shows the permitted total injected energy range as a function of the cluster mass for ICM heating times between $t_{\rm heat} = 5\times10^8$yr (upper envelope) and $t_{\rm heat} = 5\times10^9$yr (lower envelope). The shaded region corresponds to values of $E_{\rm agn}$ that are able to match the entropy observations at *both* $0.1r_{200}$ and r_{500}. The thin solid line represents a non-linear relation between the total energy injected into the cluster by AGN and the mass of the cluster with an exponent of 1.5. The thick long-dashed line represents a non-linear relation between the total energy injected into the cluster by AGN and the mass of the cluster with an exponent of 5/3. The permitted parameter space comes from the sum of permitted regions that satisfy the entropy constraints at both radii for fixed $t_{\rm heat}$. *Right panel:* Scaled entropy profiles as a function of scaled radius for a cluster of mass 6×10^{14} $M_\odot$ heated by an AGN with $\langle L\rangle = 3\times10^{45}$ erg s^{-1}. The scaled entropy profiles are plotted at intervals of 5×10^8 years. The dashed lines correspond to times when heating is on and the dot-dashed lines correspond to times when heating has been switched off. They are seen to rise as the gas is heated and then fall as the gas cools. It is seen here that the final entropy profiles (after hubble time) has neither negative entropy gradient nor any entropy core in the central regions, as compared to Figure (2) in [14]. Initial states correspond to the solid curves.

relation than the radio quiet ones. This argument adds more credibility to the idea that AGNs are responsible for the entropy "floor" and deviations from self-similar scaling relations.

Finally, we examine the effect of the universal temperature profile and AGN heating on the Poisson part of the angular power spectrum. In Figure (2), we note that the peak of the SZ power spectrum is somewhat sensitive to the amount of heating that is added to the cluster gas. The peak of C_ℓ is at a lower ℓ for a larger $t_{\rm heat}$ and at a higher ℓ for a smaller $t_{\rm heat}$. Also, the effect due to heating is larger for higher values of ℓ. In our case the suppression takes place because the gas depletion from the central regions is more efficient in low mass groups than in rich clusters. Therefore, the SZ signal is suppressed more efficiently at smaller scales and, thus, larger ℓ (as seen by some other authors).

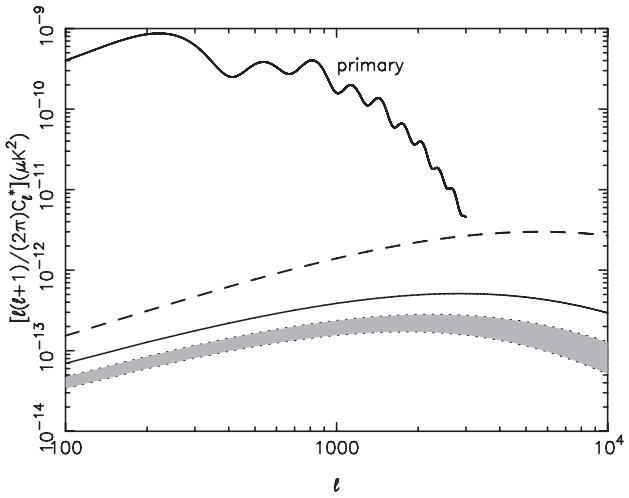

Fig. 2. The Poisson contribution to the angular power spectrum ($C^*_{\rm ell}$) of the SZ fluctuations is plotted here as a function of ℓ. The thick solid line is for the primary temperature anisotropy expected in the Rayleigh-Jeans band. The thin solid line is for the angular power spectrum (Poisson) due to the "universal temperature profile" of the cluster ICM and the dashed line is the expectation from a β–profile and isothermal temperature profile. The region shaded in grey represents the spread in C^*_ℓ (which corresponds to the spread in AGN energy injection shown in Fig. 4) that is required to satisfy the observed entropy excess at both radii.

References

1. Begelman, M.C. 2001, in Gas and Galaxy Evolution, APS Conf. Proc., vol. 240, ed. Hibbard, J. E., Rupen, M.P., van Gorkom, J.H., p. 363, (astro-ph/0207656)
2. Chandran, B., & Maron, J., ApJ, 2001, 602, 170
3. Croston, J.H., Hardcastle, M.J. & Birkinshaw, M., MNRAS, 2005, 357, 279
4. Ferrarese, L., & Ford, H., Space Science Reviews, 2005, 116, 523
5. Loeb, A., New Astronomy, 2002, 7, 279
6. Loken, C., Norman, M.L., Nelson, E., Bryan, G.L., Motl, P., ApJ, 2002, 579, 571
7. Lloyd-Davies, E.J., Ponman, T.J., Cannon, D.B., MNRAS, 2000, 315, 689
8. Nath, B.B., Roychowdhury, S., MNRAS, 2002, 333, 145
9. Nath, B. B., MNRAS, 2003, 339, 721
10. Narayan, R., Medvedev M.V., ApJ, 2001, 554, 1255
11. Ponman, T.J., Sanderson, A.J.R., Finoguenov, A., MNRAS, 2003, 343, 331
12. Pratt G. W., Arnaud M., A&A, 2005, 429, 1
13. Roychowdhury, S., Nath, B.B., MNRAS, 2003, 346, 199
14. Roychowdhury, S., Ruszkowski, M., Nath, B.B., Begelman, M.C., ApJ, 2004, 615, 681

15. Ruszkowski, M., Begelman, M.C., 2002, ApJ, 581, 223
16. Spergel, D.N. et al., ApJS, 2003, 148, 195
17. Sutherland, R. S., Dopita, M. A., 1993, ApJS, 88, 253
18. Valageas, P., Silk, J., A&A, 1999, 350, 725
19. Wu, K.K.S., Fabian, A., Nulsen, P.E.J., MNRAS, 2000, 318, 889

Stellar and Ionized Gas Kinematics of Peculiar Virgo Cluster Galaxies

J.R. Cortés[1], J.D.P. Kenney[2] and E. Hardy[3]

[1] Departamento de Astronomía, Universidad de Chile
jcortes@das.uchile.cl
[2] Astronomy Department, Yale University
kenney@astro.yale.edu
[3] National Radio Astronomy Observatory
ehardy@nrao.edu

Summary. We present the results of the stellar and ionized gas kinematics of 13 bright peculiar Virgo cluster galaxies. The stellar velocity field are mostly consistent with a rotation pattern, but some of them shows interesting features such as; S-shaped stellar isovelocity contours in NGC 4064, and signatures of kinematical distinct components in NGC 4429, and NGC 4698. This latter galaxy and NGC 4424 exhibit extremely low $(V/\sigma)^*$ values suggesting that these galaxies are the result of mergers. The ionized gas velocity fields are more disturbed than the stellar velocity fields, displaying non-circular motions. Most galaxies in the sample reveals kinematical signatures that can be associated to gravitational interactions such as; mergers or tidal interactions, being specially clear in the "truncated/compact" galaxies. Moreover, most of the sample galaxies show evidence for both gravitational interactions, and ICM-ISM stripping. Thus the evolution of a significant fraction of cluster galaxies is likely strongly impacted by both effects.

1 Introduction: morphological evolution of cluster galaxies

It is well known that the environment affects the morphological types of galaxies in clusters. Observational facts such as the "morphology-environment" relation, "Butcher-Oemler effect", as well as the results of the MORPHS collaboration (Dressler et al. 1997), suggest that galaxies in clusters evolve morphologically, with spirals becoming lenticular and redder as the result of environmental effects.

Several mechanisms have been proposed for driving galaxy evolution, including processes that affect the gas and not the existing stellar stellar content (e.g., ICM–ISM stripping; Gunn & Gott 1972; Schulz & Struck 2001; Vollmer et al. 2001), and those interactions (Toomre & Toomre 1972) that affect both the star and the gas (e.g., mergers; Hernquist 1992) However, it is still largely unknown which processes do actually occur and which among them are dominant in driving the morphological evolution of cluster galaxies.

Detailed studies of the stellar and ionized gas kinematics could help to discriminate between interacting processes. With this purpose in mind, we make a study of the stellar and ionized gas kinematics of thirteen peculiar Virgo cluster galaxies using integral-field spectroscopy techniques. Peculiar galaxies are natural targets for studying galaxy evolution, since they are "snapshots" of the galaxy evolution process. Moreover, the Virgo cluster is an ideal place for making this kind of studies, since it has a moderately dense ICM, is dynamically young with on-going sub-cluster mergers and infalling galaxies, and it has a significant population of galaxies characterized by truncated star formation morphologies (Koopmann & Kenney 2004).

2 The galaxy sample

The sample consists in thirteen peculiar Virgo cluster galaxies spanning a variety of optical morphologies. Morphological selection was made using the R, and Hα atlas of Virgo cluster galaxies of Koopmann et al. (2001), whereas the kinematical selection made use of the published Hα kinematics on 89 Virgo cluster spirals by Rubin et al. (1999). While the sample selection is not uniform, it is designed to include bright Virgo spirals whose peculiarities are most poorly understood, and to include representatives of the different Hα types identified by Koopmann & Kenney (2004).

3 Morphology of peculiar Virgo cluster galaxies

Optical imaging in the B, and R-band and Hα narrow band was obtained using the Kitt Peak WIYN 3.5m telescope with the Mini-mosaic imager. A summary of the observed morphologies is displayed in Figure 1. The results show that six galaxies of the sample display disturbed outer stellar disks (NGC 4293, NGC 4351, NGC 4424, NGC 4569, NGC 4606 and NGC 4651), suggesting the action of gravitational interactions. Signatures of triaxial structures such as bars and lenses are found in NGC 4064, NGC 4450, and NGC 4457, whereas gross deviations from ellipticity such as heart-shaped isophotes, and non-elliptical isophotes are found in NGC 4293, NGC 4424, NGC 4429, NGC 4606, and NGC 4694.

At least, six galaxies have disturbed dust distributions; NGC 4064, NGC 4293, NGC 4424, NGC 4569, NGC 4606, and NGC 4694. Most of them show disturbed outer stellar disks, so they are probably the result of gravitational interactions. On the other hand, three galaxies do not exhibit any optical evidence for a recent gravitational interaction. These are NGC 4429, NGC 4457, and NGC 4580.

Most of the galaxies exhibit a depletion in their ionized gas, presenting truncated Hα distributions. NGC 4457, and NGC 4569 have truncated disks

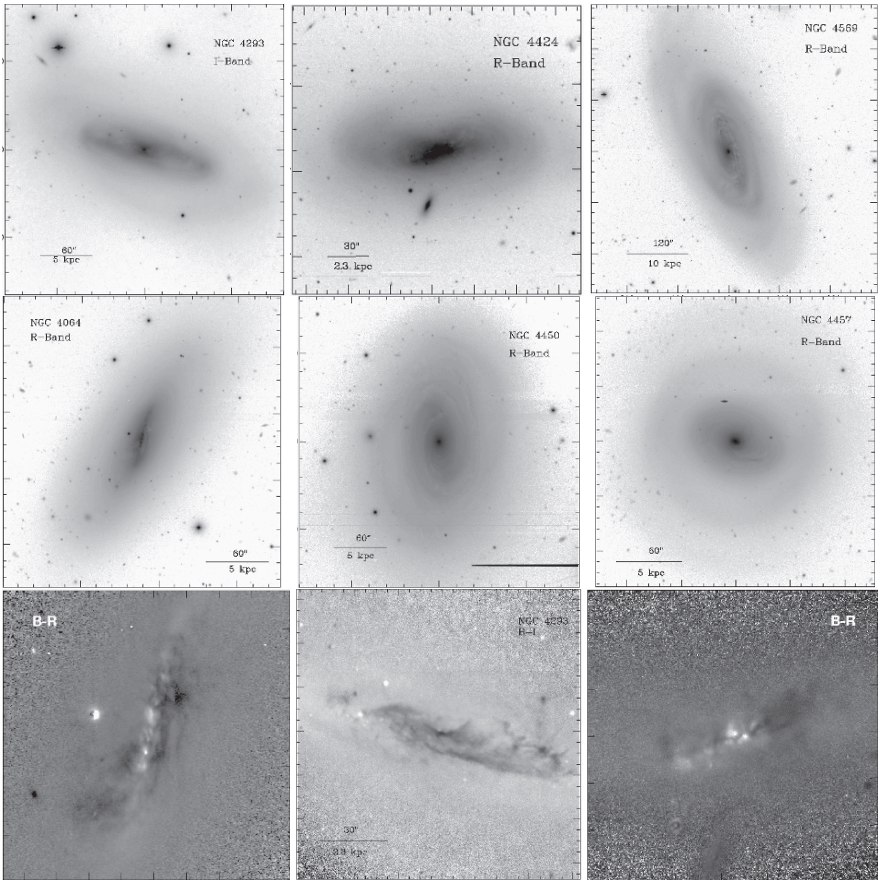

Fig. 1. Morphology of peculiar Virgo cluster galaxies. *Top row:* galaxies with disturbed outer stellar isophotes; NGC 4293, NGC 4424 and NGC 4569. *Middle row:* barred and lensed galaxies; NGC 4064, NGC 4450, and NGC 4457. *Bottom row:* disturbed dust distribution in NGC 4064, NGC 4293 and NGC 4424.

and peculiar Hα arms, suggesting an ongoing or recent ICM–ISM interaction. NGC 4580 has a truncated Hα disk with no peculiar Hα arm or Hα asymmetry, but it does have strong stellar spiral arms in the outer disk suggesting a recent ICM–ISM interaction. In the rest of the sample the cause of the depletion is not well understood with the present data, although most of them could have suffered the action of ICM wind sometime during their lifetime, as most of the galaxies in clusters, excepting the case of NGC 4651, which displays a fairly normal Hα disk.

4 Stellar and ionized gas kinematics

We have mapped the stellar velocity fields, stellar velocity dispersion fields, and ionized gas velocity fields using the DensePak Integral-field unit installed at the 3.5m WIYN telescope at Kitt Peak. Each galaxy was observed in the 4500 to 5000 Å, allowing us to obtain the ionized gas kinematics using the Hβ and [O III] $\lambda\lambda$4959, 5007 lines, and the stellar kinematics using the Magnesium triplet.

The stellar velocity fields in the galaxy sample are mostly consistent with a rotational pattern, but they also exhibit a variety of interesting structures (Figure 2). Some galaxies display misalignments between the photometric and kinematical major axes, which suggest the presence of non-axisymmetric structures, starting from the clear kinematical misalignments in the stellar kinematics of NGC 4293 to the S-type shape found in the isovelocity contours of NGC 4064 as consequence of the existence of the stellar bar, which contrasts with the CO velocity field (Cortés et al. 2006; Figure 2) which displays strong non-circular motions consistent with the infalling of gas to the center.

Signatures of a cold stellar disk (Figure 2) are found in NGC 4429, they characterize by peaks in velocity field correlated with peaks in h_3, and coincident with an undisturbed and axisymmetric dust disk, sugggesting that this cold stellar disk was probably formed by gas accretion. Finally a remarkable

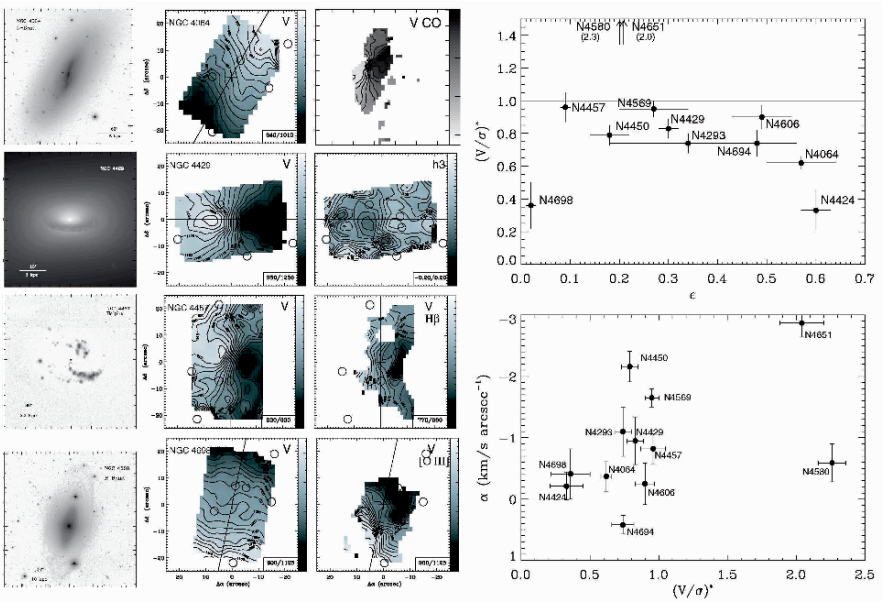

Fig. 2. Stellar and Ionized gas kinematics. *Left*: Stellar and ionized gas velocity fields for a set of sample galaxies. *Right*: $(V/\sigma)^*$–ϵ diagram, and $(V/\sigma)^*$ versus the slope of the velocity dispersion α for all the sample galaxies.

twisting in the isovelocity contours is found in NGC 4698 (Figure 2) which corresponds to a second kinematical component identified previously as an orthogonally rotating core by Bertola et al. (1999).

The ionized gas velocity fields, also exhibit a variety of structures, and in general look more disturbed than the stellar velocity fields. Non-circular motions are found in galaxies such as NGC 4064, NGC 4351, and NGC 4457. In this last galaxy, their are specially important along the anomalous Hα arm (Figure 2), suggesting the action of ICM–ISM stripping on a tilted gas disk (e.g; Schulz & Struck 2001). Signatures of counter-rotation in the gas are found in NGC 4424, and evidence of a warped gas disk is found in NGC 4698 (Figure 2).

To understand the kinematics of the sample galaxies within the inner 2 kpc, we constructed a $(V/\sigma)^*$–ϵ diagram which is shown in Fig. 2. This shows that NGC 4580, and NGC 4651 are systematically well above the oblate isotropic rotator line, showing that their inner kinematics are dominated by the disk. On the other hand, NGC 4424, and NGC 4698 are extraordinary cases, lying well below the line and indicating that these objects have more elliptical-like kinematics favoring a merger scenario. We also have found that $(V/\sigma)^*$ correlates with the slope of the slope of the stellar velocity dispersion α (Figure 2), suggesting that dynamically hot systems tend to have flat velocity dispersion profiles in their inner 3 kpc. The fact that some of these have small C_{30}, all the Truncated/Compact galaxies defined by Koopmann & Kenney (2004), and some with large C_{30} suggest that the origin of this correlation should be due to an external cause, in particular to mergers.

5 Morphological evolution in peculiar cluster galaxies

Our results in the morphology and kinematics indicate that most of the sample galaxies show evidence for both ICM-ISM stripping and gravitational interactions. Two sample galaxies show evidence for recent ICM-ISM stripping, but no strong recent gravitational interaction, just one galaxy show evidence for a recent minor merger but no ICM-ISM stripping, and one does not show any evidence of recent gravitational interaction or ICM-ISM stripping.

With the present evidence, results suggest that gravitational interactions play an important role in altering the morphologies toward a more lenticular stage (e.g. Bournaud et al. 2004) and driving gas inwards, but also drive gas outwards in the form of tidal tails (e.g. Barnes & Hernquist 1991), so they are not responsible for the gas depletion in outer parts. ICM-ISM stripping seems to play a key role in the depletion of gas in the outer disk. Moreover, gravitational interaction can facilitate the action of ICM wind over the ISM (e.g. NGC 4424). ICM-ISM stripping plays an important role in "pre-process" spiral galaxies in the core of the cluster, where merger or gravitational interactions are more unlikely due to the high relative velocities. Finally, these

combined effects seems to be crucial in objects with "Truncated/Compact" star formation as NGC 4064, and NGC 4424.

References

1. J. E. Barnes, & L. Hernquist: ApJ, **370**, L65 (1991)
2. F. Bournaud, F. Combes, & C. J. Jog: A&A, **418**, L27 (2004)
3. F. Bertola, E. M. Corsini, J. C. Vega-Beltrán et al.: ApJ, **519**, L127 (1999)
4. J. R. Cortés, J. D. P. Kenney, & E. Hardy: AJ, **131**, 747 (2006)
5. A. Dressler, A. Jr. Oemler, W. J. Couch et al.: ApJ, **490**, 577 (1997)
6. J. E. Gunn, & J. R. Gott: ApJ, **176**, 1 (1972)
7. L. Hernquist: ApJ, **400**, 460 (1992)
8. R. A. Koopmann, J. D. P. Kenney, & J. Young: ApJS, **135**, 125 (2001)
9. R. A. Koopmann, & J. D. P. Kenney: ApJ, **613**, 866 (2004)
10. V. C. Rubin, A. H. Waterman, & J. D. P. Kenney: AJ, **118**, 236 (1999)
11. S. Schulz, & C. Struck: MNRAS, **328**, 185 (2001)
12. A. Toomre, & J. Toomre: ApJ, **178**, 623 (1972)
13. B. Vollmer, V. Cayatte, C. Balkowski et al.: ApJ, **561**, 708 (2001)

ISM of Galaxies in Extremely Different Environments: Isolated vs Compact Groups

L. Verdes-Montenegro[1], M. S. Yun[2], S. Borthakur[2], D. Espada[1], I. Sellim[3], E. Athanassoula[4], G. Bergond[1], A. Bosma[4], F. Combes[5], E. Garcia[1], W.K. Huchtmeier[6], S. Leon[1], U. Lisenfeld[7], S. Odewahn[8], T. Ponman[9], J. Rasmussen[9], J. Sabater[1], J. Sulentic[10] and S. Verley[5,1]

[1] Instituto de Astrofísica de Andalucía, CSIC, Apdo. 3004, 18080 Granada, Spain
lourdes@iaa.es,daniel@iaa.es,gilles@iaa.es,garcia@iaa.es,jsm@iaa.es, simon@iaa.es
[2] Department of Astronomy, University of Massachussetts, Amherst, MA 01003, USA
myun@bonito.astro.umass.edu,sanchayeeta-lg@yahoo.com
[3] National Research Institute of Astronomy and Geophysics, Cairo Egypt
ibrahimselim@hotmail.com
[4] Observatoire de Marseille, 2 Place le Verrier, 13248 Marseille Cedex 4, France
lia@oamp.fr,bosma@oamp.fr
[5] LERMA, Observatoire de Paris, 61 Av. de l'Observatoire, 75014 Paris, France
Simon.Verley@obspm.fr
[6] Max-Planck-Institut für Radiostronomie, Auf dem Hügel 69, 53121 Bonn, Germany
p083huc@mpifr-bonn.mpg.de
[7] Departamento de Física Teórica y del Cosmos, Facultad de Ciencias, Universidad de Granada, Spain
ute@ugr.es
[8] sco@astro.as.utexas.edu
[9] tjp@xun0.sr.bham.ac.uk,jesper@star.sr.bham.ac.uk
[10] Department of Astronomy, Univ. of Alabama, AL 35487, USA
giacomo@merlot.astr.ua.edu

Summary. We present a study of the HI, CO and FIR emission properties of galaxies in dense groups and compare with those of the reference sample of extremely isolated galaxies defined in the AMIGA project. We have previously proposed an evolutionary scenario in which the amount of HI decreases with the secular evolutionary state of a group. A key question involves the fate of the HI in stripped galaxies, and how it affects the other ISM components. In order to investigate the process leading to HI deficiency, we imaged HI in a redshift limited sample of compact groups using the VLA. Surprisingly, some of these groups show little HI emission down to a column density as low as 10^{19} cm^{-2}. We find a trend for the most HI deficient groups to be also deficient in CO and FIR emission, and we propose that when HI is removed from the galaxies the molecular gas is not replenished, inhibiting future star formation activity.

1 AMIGA reference sample of isolated galaxies

It is widely believed that galaxy interactions stimulate secular evolutionary effects, but the amplitude of the effects and driving physical processes are not well quantified [6], [7]; [17]. As an example ubiquitous tidal interactions among Hickson Compact Groups (HCG) galaxies predict enhanced star formation (SF) activities, but their observed CO and FIR luminosites are surprisingly low [13]. There is no clear consensus on whether SF enhancement depends mainly on the parameters of the tidal encounter or the pre-existing gas reservoirs in the galaxies. These uncertainties reflect the lack of a statistically useful baseline. The main goals of the AMIGA project (Analysis of the interstellar Medium of Isolated GAlaxies, `http://www.iaa.es/AMIGA.html`) are the identification and parameterization of a local statistically significant sample of the most isolated galaxies. By quantifying the properties of different phases of the interstellar medium in isolated galaxies, the effects of the denser environment on the evolution of galaxies can be better understood.

1.1 Sample selection and refinement

Our base sample is the Catalog of Isolated Galaxies (CIG: [3]) which includes 1051 objects. In order to achieve our goals a careful refinement has been performed: positions have been revised [4], more distances have been retrieved (N = 956 galaxies[11], the isolation has been checked and its degree quantified [15], and the morphologies have been revised [9].

1.2 Multiwavelength study

Our optical study of the CIG sample has shown that the AMIGA sample is reasonably complete (∼80%) up to $m_{B-corr} \sim 15.0$ [12]. We emphasize the nonstellar material that is particularly sensitive to the effects of external stimuli. Data have been obtained or compiled from the bibliography for neutral (HI), molecular (CO), and ionized (Hα) gas, and radiocontinuum emission as an extinction-free tracer of current SF rate and AGN diagnostic tool when combined with FIR data. FIR data from IRAS and the blue Zwicky magnitudes complete our data set for this sample.

One specific investigation on the impact of environment has been the galaxies with HI asymmetry. We have identified a well-defined sample of the most isolated galaxies showing significant asymmetries in their HI profiles and obtained VLA-HI images in order to look for signs of external interactions (Espada et al., in prep). One of the most interesting galaxies in our

[11] This number is being updated in the electronic table at http://www.iaa.csic.es/AMIGA.html when new data are available.

VLA sample is CIG 96 (NGC 864), a spiral galaxy well isolated from similarly sized companions, that presents an intriguing asymmetry in its integral HI spectrum. The asymmetry in the HI profile is associated with a strong kinematical perturbation in the gaseous envelope of the galaxy, where at one side the decay of the rotation curve is faster than Keplerian [1]. We detected a small companion in HI close to CIG 96, although it is probably not massive enough to have caused the observed perturbations. We also discussed accretion of a gaseous companion at a radial velocity lower than the maximum.

2 Hickson Compact Groups

We have analysed the total HI contents in 72 HCGs and investigated the detailed distribution and kinematics of the HI in a subset of 16 groups using high resolution VLA observations [14], [11], [12]; [8]; [16]. This sample was not complete in any sense since it was assembled by combining our new observations with already available data from archive/bibliography. These groups contain, on average, only about 40% of the HI expected for their optical luminosities and morphological types. We proposed an evolutionary scenario in which the amount of HI decreases with the secular evolutionary state [14] and the HI stripped from spiral galaxies is then transformed (via shocks) into the surrounding hot intergalactic gas. We also found a lower molecular gas content than expected for the galaxies in HI deficient groups, suggesting that the HI stripping by frequent tidal interactions breaks the balance between the disruption of molecular clouds by SF and the replenishment from the ambient HI. The most HI deficient galaxies are also strongly deficient in molecular gas, and their FIR emission was not enhanced with respect to their optical luminosity, indicating that no SF was triggered by the interaction. A global comparison of FIR emission and HI content in a significant sample of HCGs could not be performed due to a low overlapping of the available data.

For the next step in our VLA imaging, we expanded the sample with the following uniform selection criteria: a) have 4 or more group galaxies (i.e. triplets and false groups excluded); b) contain at least one spiral galaxy (so that the HI deficiency can be determined meaningfully); and c) are located at a distance ≤ 100 Mpc (for $H_0 = 75$ km s^{-1} Mpc^{-1}). This yields a sample of 22 systems. We sorted these groups according to their HI content, which would presumably correspond to an evolutionary scenario as proposed in [14]. So far we have mapped the HI distribution in 17 groups using the VLA in C- and/or D-array, including recent new VLA observations of 8 HI deficient groups (HCG 15, 30, 37, 48, 58, 93, 97,100). We have been allocated additional VLA time to map HI in HCGs with a mild level of deficiency.

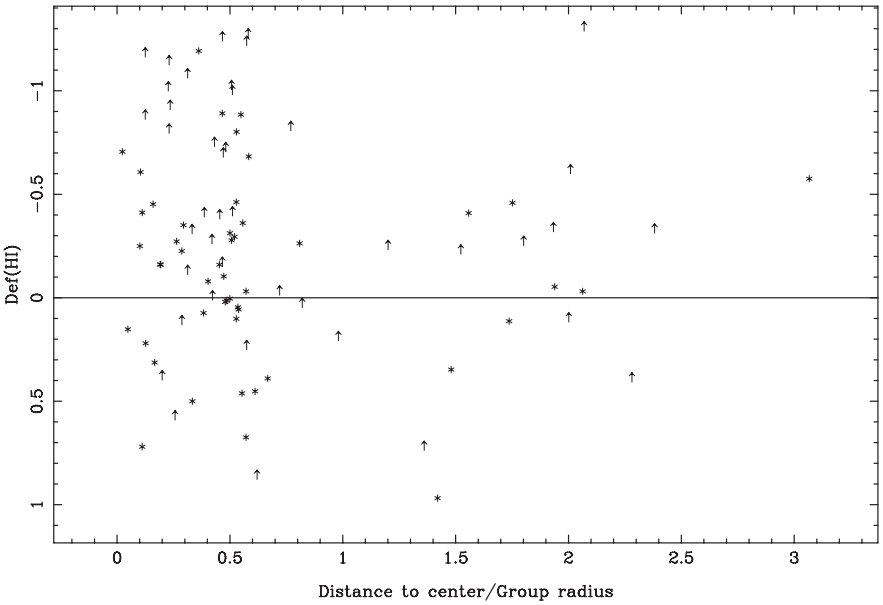

Fig. 1. HI deficiency versus of distance to the center, normalized to the group size.

Our analysis of the new data has revealed that the most HI-deficient galaxies are concentrated within one group radius (Fig. 1). This shows that the mechanism responsible for the HI deficiency is operating most actively at the group center. This result is nicely complemented by the comparison of HI and X-ray data for the most HI deficient HCGs. In HCG 37 and HCG 40, the hot gas mass derived from the X-ray data is similar to the one missing in HI. HCG 37 and HCG 97 also show anticorrelated HI and X-rays distributions (Fig. 2 for the HI, see [5] for the X-ray). Heating of the gas might be in some cases the cause of the HI deficiency as in HCG 92 [10].

We have also analyzed the deficiency in HI, molecular gas, and FIR emission (Fig. 3) using the new expanded database. The trend previously found at 3σ level is now visible as a stronger correlation albeit with a high dispersion, indicating that the more deficient groups in HI tend also to have a lower H_2 content. The same trend is found when the HI deficiency is compared with the FIR luminosity. These results suggest that when HI is removed from galaxies the molecular gas is not replenished, inhibiting the SF activity and suppressing the FIR emission level. This is also consistent with the absence of enhanced Hα emission [2].

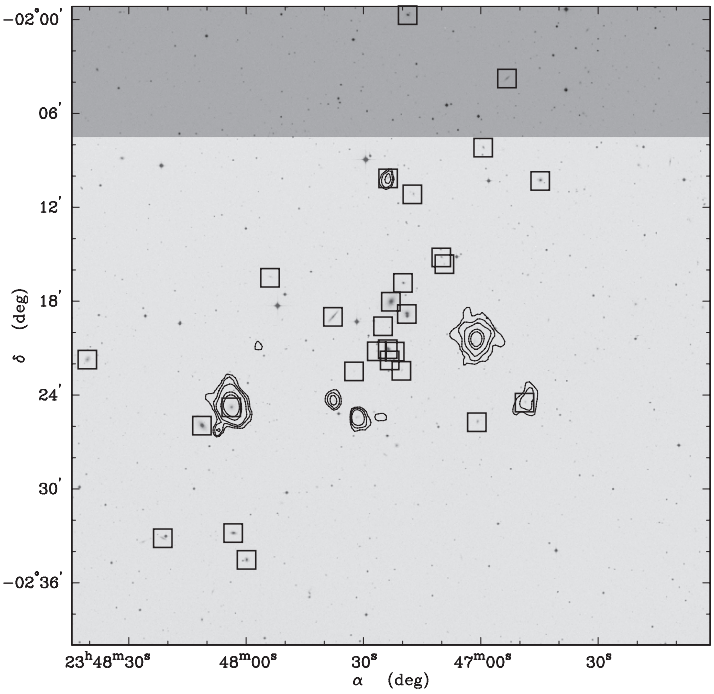

Fig. 2. HI column density contours on a POSSII image of HCG 97. The squares correspond to galaxies at the same redshift as the group.

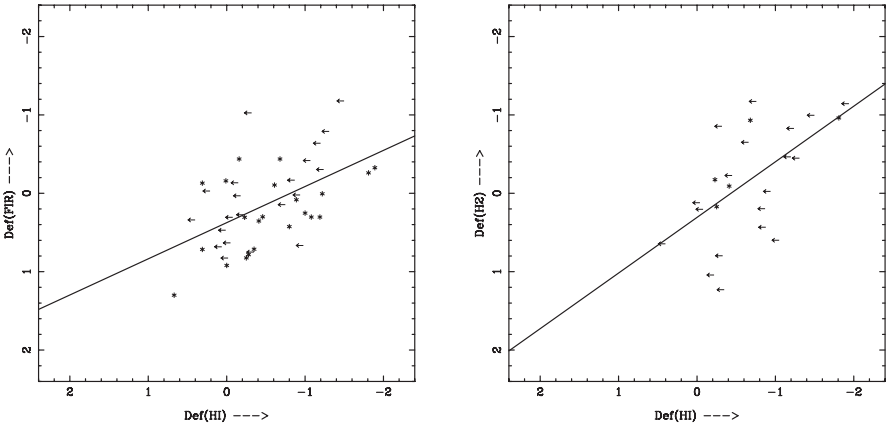

Fig. 3. FIR (left) and H_2 (right) deficiency as a function of HI deficiency for the HCG galaxies in our sample. The fits to the data are represented by the lines.

References

1. Espada, D., Bosma, A., Verdes-Montenegro, L., Athanassoula, E., Leon, S., Sulentic, J., Yun, M. S. 2005, A&A 442, 455
2. Iglesias-Paramo, J., Vilchez, J. M, 1999, ApJ 518, 94
3. Karachentseva, V. E. 1973, Comm. Spec. Ap. Obs., USSR 8, 1
4. Leon, S., Verdes-Montenegro, L. 2003, A&A, 411, 391
5. Mahdavi, A., Finoguenov, A., Bohringer, H., Geller, M. J., Henry, J. P. 2005, ApJ 622,187
6. Sulentic, J. W. 1976, ApJS, 32, 171
7. Sulentic, J. W. 1989, AJ, 98, 2066
8. Sulentic, Jack W., Rosado, M., Dultzin-Hacyan, D., Verdes-Montenegro, L., Trinchieri, G., Xu, C. Pietsch, W. 2001, AJ 122, 2993
9. Sulentic J. W., Verdes-Montenegro, L., Bergond, G., Lisenfeld, U., Durbala, A., Espada, D., Garcia, E., Leon, S., Sabater, J., Verley, S., Casanova, V., Sota, A. 2006, A&A in press
10. Trinchieri, G., Sulentic, J., Pietsch, W., Breitschwerdt, D. 2005, A&A 444, 697
11. Verdes-Montenegro, L., Del Olmo, A., Iglesias-Paramo, J., Perea, J., Vilchez, J. M, Yun, M. S.,Huchtmeier, W. K. 2002, A&A 396, 815
12. Verdes-Montenegro, L., Sulentic, J., Lisenfeld, U., Leon, S., Espada, D., Garcia, E., Sabater, J., Verley, S. 2005, A&A 436, 443
13. Verdes-Montenegro, L., Yun, M. S., Perea, J., Del Olmo, A., & Ho, P. T. P. 1998, ApJ 497, 89
14. Verdes-Montenegro, L., Yun, M. S., Williams, B. A., Huchtmeier, W. K., Del Olmo, A., Perea, J. 2001, A&A 377, 812
15. Verley 2006, PhD
16. Williams, B. A., Yun, Min S., Verdes-Montenegro, L. 2002,AJ 123, 2417
17. Xu, C., Sulentic, J. W. 1991, ApJ, 374, 407

Comparing Semi-Analytical and Numerical Modelling of the ICM Chemical Enrichment

S.A. Cora[1], L. Tornatore[2] and S. Borgani[2]

[1] Facultad de Ciencias Astronómicas y Geofísicas de la Universidad Nacional de La Plata, Argentina
sacora@fcaglp.unlp.edu.ar
[2] Dipartamento di Astronomia dell'Universita di Trieste, Italy
torna@sissa.it,borgani@oats.inaf.it

The dependence of iron abundance on cluster temperature is subject to continuous debate. There are some evidences of decreasing abundances from $\sim$0.7 to $\sim$0.3 times the solar metallicity in the temperature range of $\sim 3 - 10$ keV [1], while a roughly constant value of $\sim$0.3 times solar is claimed [2]. Physical interpretation of these ambiguous observational results calls for robust theoretical models that can predict systematic trends for the enrichment of clusters of different masses.

We use both semi-analytical and numerical modelling to investigate the relationship between metal enrichment of the intracluster/intragroup medium and the mass of the system. On one hand, the hybrid model combines a cosmological non-radiative *N*-Body/SPH simulation of a galaxy cluster (code GADGET, [3]) and a semi-analytic model of galaxy formation [4]; metals ejected from the galaxies of the semi-analytic model are distributed among gas particles in the underlying hydrodynamic simulation. On the other, the metal pollution of the intracluster gas has been implemented self-consistently in a *N*-Body/SPH simulation of a galaxy cluster [5], which uses a recent version of GADGET [6]. The comparison between these two numerical techniques will help to improve the modellization of the physical processes involved in galaxy formation and the consequent metal enrichment of the intracluster/intragroup gas.

The chemical model implemented in both models considers the contribution of different chemical elements provided by low- and intermediate-mass stars and core-collapse and type Ia supernovae, for which we have used analytical fitting formulas [7]. We adopt a Salpeter IMF and relax the IRA approximation by taking into account the different stellar lifetimes [8].

We present preliminary results on the spatial distribution of different chemical element abundances in the intracluster medium of a massive cluster provided by our models. They give similar Fe profiles, as shown in Figure 1. However, O and Si abundances given by the self-consistent code are lower than those obtained from the hybrid one. Thus, differences between these two models become evident in the results obtained for those species mainly produced by core-collapse supernovae. The impact of star formation and supernovae feedback prescriptions included in both numerical techniques will

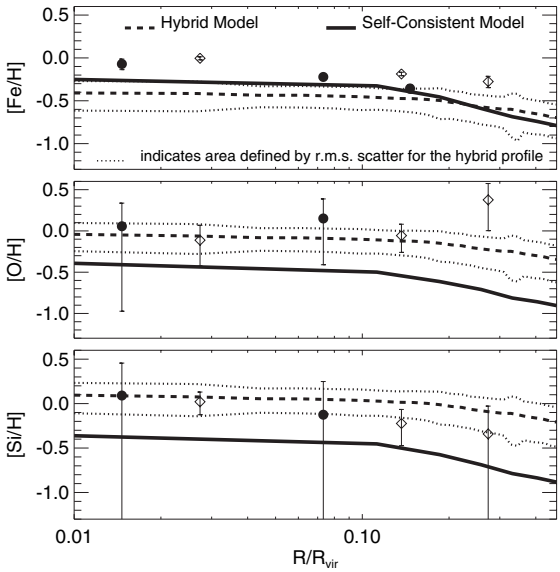

Fig. 1. Abundance profiles of Fe, O and Si relative to H, respect to the solar value [9] for the self-consistent simulation (solid line) and the hybrid model (dashed line). Symbols with error bars are observational data [10] for hot clusters ($k_{\rm B}T > 6\,{\rm keV}$, filled circles) and medium-temperature clusters ($3 < k_{\rm B}T < 6\,{\rm keV}$, open diamonds).

be analysed in detail to find out about the origin of these differences. We will extend this analysis in order to understand the developement of abundance patterns in a set of clusters with different temperatures.

S.A.C. thanks the LOC of this Conference for their financial support, and acknowledge Fundación Antorchas and CONICET for their grants.

References

1. W.H. Baumgartner, M. Loewenstein, D.J. Horner et al.: ApJ **620**, 680 (2005)
2. A. Renzini: ApJ **488**, 35 (1997)
3. V. Springel, N. Yoshida, S.D.M. White: New Astronomy **79**, 117 (2001)
4. S.A. Cora: MNRAS, accepted (2006)
5. L. Tornatore, S. Borgani, F. Matteucci et al.: MNMRAS **349**, L19 (2004)
6. V. Springel: MNRAS **364**, 1105 (2005)
7. S. Recchi, F. Matteucci, A. D'Ercole: MNRAS **322**, 800 (2001)
8. F. Matteucci, P. Padovani: ApJ **419**, 485 (1993)
9. M. Asplund, N. Grevesse, A.J. Sauval: The solar chemical composition. In: *Cosmic Abundances as Records of Stellar Evolution and Nucleosynthesis, ASP Conference Series*, vol 336, ed by T.G. Barnes III, F.N. Bash (Astronomical Society of the Pacific, San Francisco 2005) pp 25–35
10. T. Tamura, J.S. Kaastra, J.W.A.den Herder et al.: A&A **420**, 135 (2004)

Groups and Clusters of Galaxies in Cosmological Context

S. Borgani

Department of Astronomy, University of Trieste, via Tiepolo 11,
I-34131 Trieste, Italy
borgani@oats.inaf.it

Summary. In this contribution I will review the current status of cosmological constraints based on the determination of the mass function of galaxy groups and clusters, and its redshift evolution. After describing the approaches to calibrate an analytical expression for the cosmological mass function of collapsed dark matter halos, I will discuss the methods, based on X-ray observations, to compute cluster masses. I will then critically discuss the constraints on cosmological parameters, which have been derived so far, and the future perspectives from upcoming surveys from Sunyaev–Zeldovich and X-ray observations.

1 Introduction

Clusters of galaxies occupy a special place in the hierarchy of cosmic structures. They arise from the collapse of initial perturbations having a typical comoving scale of about $10\,h^{-1}$Mpc[1]. According to the standard model of cosmic structure formation, the Universe is dominated by gravitational dynamics in the linear or weakly non–linear regime on scales larger than this. In this case, the description of cosmic structure formation is relatively simple since gas dynamical effects are thought to play a minor role, while the dominating gravitational dynamics still preserves memory of initial conditions. On smaller scales, instead, the complex astrophysical processes, related to galaxy formation and evolution, start being relevant. Gas cooling, star formation, feedback from supernovae (SN) and active galactic nuclei (AGN) significantly change the evolution of cosmic baryons and, therefore, the observational properties of the structures. Since clusters of galaxies mark the transition between these two regimes, they have been studied for decades both as cosmological tools and as astrophysical laboratories.

In this contribution, I concentrate on the role that clusters play for cosmology. I will highlight that for them to be calibrated as cosmological tools, one needs to understand in details the astrophysical processes which determine their observational characteristics, i.e. the properties of the cluster galaxy population and the those of the diffuse intra–cluster medium (ICM).

[1]Here h is the Hubble constant in units of $100\,\mathrm{km\,s^{-1}}$ Mpc^{-1}

Constraints of cosmological parameters using galaxy clusters have been placed so far by applying different of methods.

1. The mass function of nearby galaxy clusters provides constraints on the amplitude of the power spectrum at the cluster scale [57, 68]. At the same time, its evolution provides constraints on the linear growth rate of density perturbations, which translate into dynamical constraints on the matter and Dark Energy (DE) density parameters.
2. The clustering properties (i.e., correlation function and power spectrum) of the large–scale distribution of galaxy clusters provide direct information on shape and amplitude of the power spectrum of the underlying DM distribution. Furthermore, the evolution of these clustering properties is again sensitive to the value of the density parameters through the linear growth rate of perturbations [9, 44].
3. The baryon fraction in nearby clusters provides constraints on the matter density parameter, once the cosmic baryon density parameter is known, under the assumption that clusters are fair containers of baryons [22]. Furthermore, the baryon fraction of distant clusters provide a geometrical constraint on the DE density parameter under the additional assumption that the baryon fraction within clusters does not evolve [3].

In this contribution I will mostly concentrate on the method based on the evolution of the cluster mass function. A substantial part of this contribution will concentrate on the different methods, based on X-ray observations, that have been applied so far to weight galaxy clusters. Since all the above cosmological applications rely on precise measurements of cluster masses, this part of my contribution will be of general relevance for cluster cosmology.

The structure of this paper will be as follows. I provide in Section 2 a review of the cosmological mass function, by discussing the corrections to the Press–Schechter formalism and the most recent calibrations based on large N–body simulations. Section 3 is devoted to the discussion of the hydrostatic equilibrium method to estimate cluster masses from gas temperature, and of the calibration based on scaling relations between X-ray luminosity and mass. In Section 4 I will describe the cosmological constraints, which have been obtained so far by tracing the cluster mass function with a variety of methods: distribution of velocity dispersions, X-ray temperature and luminosity functions, and gas mass function. In this Section I will also critically discuss the reasons for the different, sometimes discrepant, results that have been obtained in the literature and I will highlight the relevance of properly including the analysis of the cluster mass function all the statistical and systematic uncertainties in the relation between mass and observables. Finally, I will describe in Section 5 the future perspectives for cosmology with galaxy clusters and which are the challenges for clusters to keep playing an important role in the era of precision cosmology.

2 The mass function

The mass function (MF) at redshift z, $n(M,z)$, is defined as the number density of virialized halos found at that redshift with mass in the range $[M, M+dM]$. Press & Schechter [52] originally derived the following expression for the mass function arising from the collapse of cosmological density perturbations, in the form

$$\frac{dn(M,z)}{dM} = \sqrt{\frac{2}{\pi}} \frac{\bar{\rho}}{M^2} \frac{\delta_c}{\sigma_M(z)} \left| \frac{d\log\sigma_M(z)}{d\log M} \right| \exp\left(-\frac{\delta_c^2}{2\sigma_M(z)^2} \right) . \qquad (1)$$

In the above equation, $\bar{\rho}$ is the mean matter density at $z=0$, δ_c is the critical density contrast for spherical collapse ($\delta_c \simeq 1.69$, independent of redshift for an Einstein–de-Sitter cosmology, with a weak dependence on redshift and on Ω_m for more general cosmologies [16], and σ_M is the variance of density perturbations at the mass–scale M. Already this equation demonstrates the reason why the mass function of galaxy clusters is a powerful probe of cosmological models. Cosmological parameters enter in eq. (1) through the mass variance σ_M, which depends on the power spectrum and on the cosmological density parameters, through the linear perturbation growth factor, and, to a less degree, through the critical density contrast δ_c. Taking this expression in the limit of massive objects, the MF shape is dominated by the exponential tail. This implies that the MF becomes exponentially sensitive to the choice of the cosmological parameters. In other words, a reliable observational determination of the MF of rich clusters would allow us to place tight constraints on cosmological parameters.

Following Jenkins et al. [30], an alternative way of recasting the mass function is

$$f(\sigma_M, z) = \frac{M}{\bar{\rho}} \frac{dn(M,z)}{d\ln\sigma_M^{-1}} . \qquad (2)$$

In this way, the PS expression is recovered by setting $f(\nu,z) = \sqrt{2/\pi}\nu \exp(-\nu^2/2)$ with $\nu = \delta_c/\sigma_M$. The PS MF has served for more than a decade as a guide to constrain cosmological parameters from the mass distribution of galaxy clusters. Only with the advent of a new generation of N–body simulations, which are able to cover a very large dynamical range, have significant deviations of the PS expression from the exact numerical description been noticed [21, 62, 69]. Such deviations have been usually interpreted in terms of corrections to the PS approach.

Incorporating the effect of non–spherical collapse, Sheth & Tormen [61] have generalized the PS expression to

$$f(\sigma_M, z) = \sqrt{\frac{2a}{\pi}} C \left[1 + \left(\frac{\sigma_M^2}{a\delta_c^2} \right)^q \right] \frac{\delta_c}{\sigma_M} \exp\left(-\frac{a\delta_c^2}{2\sigma_M^2} \right) . \qquad (3)$$

These authors also compared this expression with results from N–body simulations, in which the mass of the clusters have been estimated with a spherical

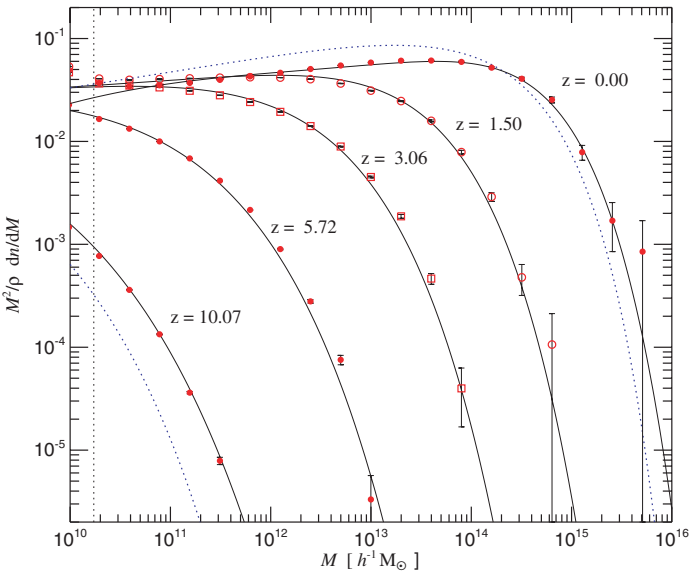

Fig. 1. The mass function of DM halos (dots with errorbars) identified at different redshifts in the Millenniun Run [62], compared to the predictions of the mass function by [30] and by [52]. The two model mass functions are plotted with solid and dotted curves, respectively.

overdensity (SO) algorithm, by computing the mass within the radius encompassing a mean overdensity equal to the virial one. As a result, they found the best–fitting values $a = 0.707$, $q = 0.3$, with the normalization constant $C = 0.3222$ obtained from the normalization requirement $\int_0^\infty f(\sigma_M)d\nu = 1$.

Jenkins et al. [30] proposed an alternative expression for the mass function,

$$f(\sigma_M, z) = 0.315 \exp(-|\ln \sigma_M^{-1} + 0.61|^{3.8}) , \qquad (4)$$

which has been obtained as the best fit to the results of a combination of different simulations, covering a wide dynamical range. More recently, Springel et al. [62] (see also [70]) used the largest available single N–body simulation to verify in detail the accuracy of eq. (4). The result of this comparison, which is reported in Figure 1, demonstrates that this mass function reproduces remarkably well numerical results over a wide range of sampled halo masses and redshifts, thereby representing a substantial improvement with respect to the PS mass function.

In practical applications, the observational mass function of groups and clusters is usually determined over about one decade in mass. Therefore, it probes the power spectrum over a relatively narrow dynamical range. This normalization is usually expressed in terms of σ_8, the r.m.s. value of density perturbations within a top–hat sphere with comoving radius of $8\,h^{-1}$Mpc.

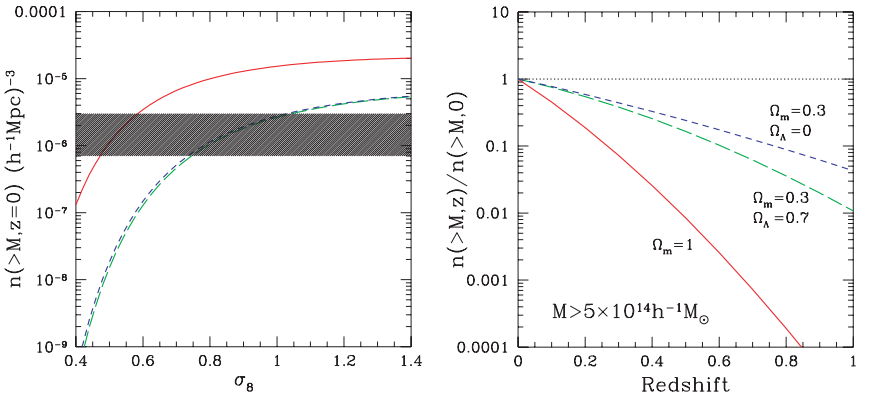

Fig. 2. The sensitivity of the cluster mass function to cosmological models [57]. *Left panel*: The cumulative mass function at $z = 0$ for $M > 5\times10^{14}h^{-1}M_{\odot}$ for three cosmologies, as a function of σ_8, with shape parameter $\Gamma = 0.2$; solid line: $\Omega_m = 1$; short–dashed line: $\Omega_m = 0.3$, $\Omega_\Lambda = 0.7$; long–dashed line: $\Omega_m = 0.3$, $\Omega_\Lambda = 0$. The shaded area indicates the observational uncertainty in the determination of the local cluster space density. *Right panel*: Evolution of $n(>M, z)$ for the same cosmologies and the same mass–limit, with $\sigma_8 = 0.5$ for the $\Omega_m = 1$ case and $\sigma_8 = 0.8$ for the low–density models.

In the left panel of Figure 2 we show that, for a fixed value of the observed cluster mass function, the implied value of σ_8 from eq. (3) increases as the density parameter decreases. Determinations of the cluster mass function in the local Universe using a variety of samples and methods indicate that $\sigma_8\Omega_m^\alpha = 0.4-0.6$, where $\alpha \simeq 0.4-0.6$, almost independent of the presence of a cosmological constant term providing spatial flatness. As for the evolution with redshift, the growth rate of the density perturbations depends primarily on Ω_m and, to a lesser extent, on Ω_Λ, at least out to $z \sim 1$, where the evolution of the cluster population is currently studied. Therefore, following the evolution of the cluster space density over a large redshift baseline, one can break the degeneracy between σ_8 and Ω_m. This is shown in the right panel of Figure 2: models with different values of Ω_m, which are normalized to yield the same number density of nearby clusters, predict cumulative mass functions that progressively differ by up to orders of magnitude at increasing redshifts.

3 Cluster masses from hydrostatic equilibrium

The condition of hydrostatic equilibrium determines the balance between the pressure force and the gravitational force. Its application to a spherically symmetric distribution of an ideal gas gives the total mass contained within the distance r from the cluster center as

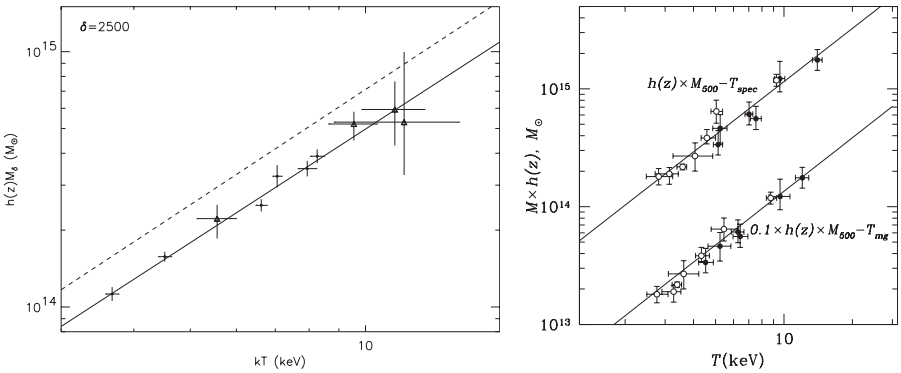

Fig. 3. The mass-temperature relation for nearby clusters (from [5]) and for distant clusters (from [33]), based on a combination of Chandra and XMM–Newton data.

$$M(< r) = -\frac{r}{G}\frac{k_B T}{\mu m_p}\left(\frac{d\ln\rho_{\rm gas}}{d\ln r} + \frac{d\ln T}{d\ln r}\right) . \tag{5}$$

Here μ is the mean molecular weight of the gas ($\mu \simeq 0.59$ for primordial composition) and m_p is the proton mass. An often used mass estimator is based on assuming the β–model for the gas density profile,

$$\rho_{\rm gas}(r) = \frac{\rho_0}{[1+(r/r_c)^2]^{3\beta/2}} \tag{6}$$

[14]. In the above equation, r_c is the core radius, while β is the ratio between the kinetic energy of any tracer of the gravitational potential (e.g. galaxies) and the thermal energy of the gas, $\beta = \mu m_p \sigma_v^2/(k_B T)$ (σ_v: one–dimensional velocity dispersion). By further assuming a polytropic equation of state, $\rho_{\rm gas} \propto P_{\rm gas}^{\gamma}$ (γ: polytropic index), eq. (5) becomes

$$M(< r) \simeq 1.11\times 10^{14}\beta\gamma\frac{T(r)}{\rm keV}\frac{r}{h^{-1}{\rm Mpc}}\frac{(r/r_c)^2}{1+(r/r_c)^2}\, h^{-1} M_\odot\,, \tag{7}$$

where $T(r)$ is the temperature at the radius r. In the absence of accurately resolved temperature profiles from X-ray observations, eq. (7) has been used to estimate cluster masses both in its isothermal [56] and in its polytropic [23, 18].

Thanks to the much improved sensitivity of the Chandra and XMM–Newton X-ray observatories, temperature profiles are now resolved with high enough accuracy to allow the application of more general methods of mass estimation, not necessarily bound to the assumptions of β–model and of an overall polytropic form for the equation of state [18, 5, 67].

It is clear that the two crucial assumptions underlying any mass measurements based on the ICM temperature concerns the existence of hydrostatic

equilibrium and of spherical symmetry. While effects of non–spherical geometry can be averaged out by performing the analysis over a large enough number of clusters, the former can lead to systematic biases in the mass estimates [53]. So far, ICM temperature measurements have been based on fitting the observed X-ray spectra of clusters to plasma models, which are dominated at high temperature by thermal bremsstrahlung. However, local deviations from isothermality, e.g. due to the presence of merging cold gas clumps, can bias the spectroscopic temperature with respect to the actual electron temperature [41, 43, 66]. This bias directly translates into a comparable bias in the mass estimate through hydrostatic equilibrium.

4 Phenomenological X-ray scaling relations

The relation between X-ray luminosity and temperature of nearby clusters is considered as one of the most robust observational facts against the self–similar model of the ICM. A number of observational determinations now exist, pointing toward a slope $L_X \propto T^{\alpha}$, with $\alpha \simeq 2.5$–3 [73], possibly flattening towards the self–similar scaling only for the very hot systems with $T \gtrsim 10$ keV [1]. While in general the scatter around the best–fitting relation is non negligible, it has been shown to be significantly reduced after excising the contribution to the luminosity from the cluster cooling regions [39] or by removing from the sample clusters with evidence of cooling flows [4]. As for the behaviour of this relation at the scale of groups, $T \lesssim 1$ keV, the emerging picture is now that it lies on the extension of the L_X–T relation of clusters, with no evidence for a steepening [45], although with a significant increase of the scatter [48], possibly caused by a larger diversity of the groups population when compared to the cluster population.

As for the evolution of the L_X–T relation, a number of analyses have been performed, using Chandra [19, 42] and XMM–Newton [33, 36] data. Although some differences exist between the results obtained from different authors, such differences are more likely due to the convention adopted for the radii within which luminosity and temperature are estimated. In general, the emerging picture is that clusters at high redshift are relatively brighter, at fixed temperature. The resulting evolution for a cosmology with $\Omega_m = 0.3$ and $\Omega_\Lambda = 0.7$ is consistent with the predictions of the self–similar scaling, although the slope of the high–z L_X–T relation is steeper than predicted by self–similar scaling, in keeping with results for nearby clusters. However, the uncertainties are still large enough not to allow to work out a precise redshift dependence of the L_X–T normalization.

As for the relation between X-ray luminosity and mass, its first calibration has been attempted by [56], for a sample of bright clusters extracted from the ROSAT All Sky Survey (RASS). In their analysis, these authors derived masses by using temperatures derived from ASCA observations and applying the equation of hydrostatic equilibrium of eq. (5) for an isothermal β–model.

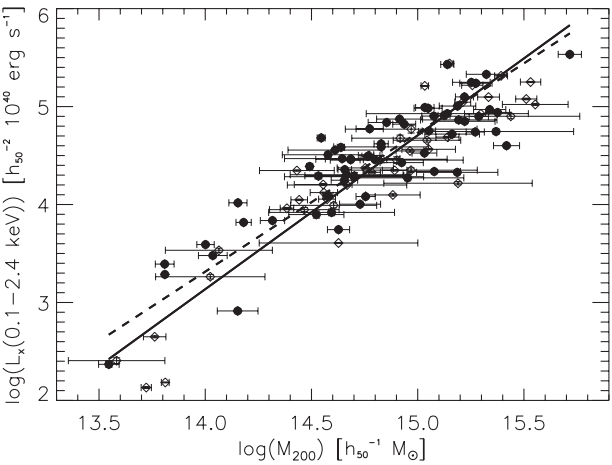

Fig. 4. The L_X–M relation for nearby clusters (from [56]). X–ray luminosities are from the RASS, while masses are estimated using ASCA temperatures and assuming hydrostatic equilibrium for isothermal gas.

The resulting M–L_X relation is shown in Figure 4. From the one hand, this relation demonstrates that a well defined relation between X-ray luminosity and mass indeed exist, although with some scatter, thus confirming that L_X can indeed be used as a proxy of the cluster mass. From the other hand, the slope of the relation is found to be steeper than the self–similar scaling, thus consistent with the observed L_X–T relation.

5 Constraints on cosmological parameters

5.1 The temperature function

The X-ray Temperature Function (XTF) is defined as the number density of clusters with given temperature, $n(T)$. As long as a one-to-one relation exist between temperature and mass, the XTF can be related to the mass function, $n(M)$, by the relation

$$n(T) \, = \, n[M(T)] \, \frac{dM}{dT} \, . \tag{8}$$

In this equation, the ratio dM/dT is provided by the relation between ICM temperature and cluster mass.

Measurements of cluster temperatures for flux-limited samples of nearby clusters were first made by Henry & Arnaud [28]. These results have been subsequently refined and extended to larger samples with the advent of *ROSAT*, *Beppo–SAX* and, especially, *ASCA*. XTFs have been computed for

both nearby [39, 51, 50, 29] and distant [17, 15, 26, 27] clusters, and used to constrain cosmological models. The starting point in the computation of the XTF is inevitably a flux-limited sample for which the searching volume of each cluster can be computed. Then the $L_X - T_X$ relation and its scatter is used to derive a temperature limit from the sample flux limit.

Once the XTF is measured from observations, eq. (8) is used to infer the mass function and, therefore, to constrain cosmological models. A slightly different, but conceptually identical approach, has been followed by Reiprich & Böhringer [56], who computed hydrostatic–equilibrium masses for a flux–limited sample of nearby bright RASS clusters, thereby expressing their results directly in terms of mass function, rather than of XTF.

Oukbir & Blanchard [49] have first suggested to use the evolution of the XTF as a way to constrain the value of Ω_m. Several independent analyses converge now towards a mild evolution of the XTF, which is interpreted as a case for a low–density Universe, with $0.2 \lesssim \Omega_m \lesssim 0.6$. An example is reported in the right panel of Figure 5 (from [27]), which shows the comparison between the XTFs of the sample of nearby clusters by Henry & Arnaud [28] and a sample of EMSS clusters with ASCA temperatures.

A limitation of the XTFs presented so far is the limited sample size (with only a few $z \gtrsim 0.5$ measurements), as well as the lack of a homogeneous sample selection for local and distant clusters. By combining samples with different selection criteria one runs the risk of altering the inferred evolutionary pattern of the cluster population. This can even give results consistent with a critical–density Universe [65, 7].

Besides the determination of the matter density parameter, the observational determination of the XTF also allows one to measure the normalization of the power spectrum, σ_8. Assuming a fiducial value of $\Omega_m = 0.3$, different

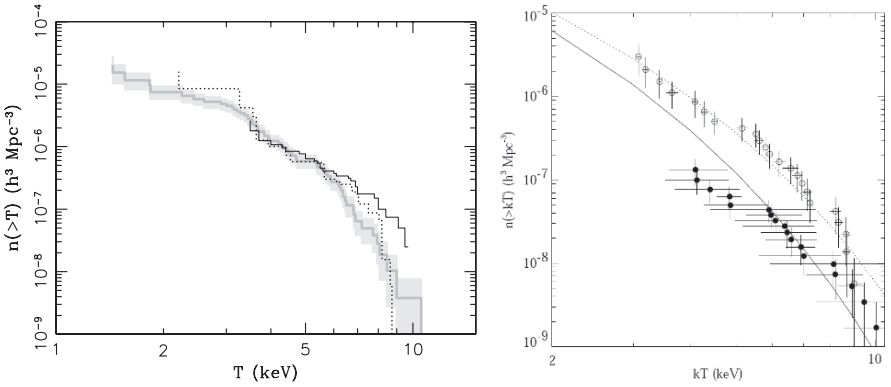

Fig. 5. *Left panel*: a comparison between the XTF for nearby clusters from [29] (shaded area), [39] (solid line) and [26] (dotted line). *Right panel*: the evolution of the XTF from [27]. Open and filled circles are for the local and the distant cluster sample, respectively.

(sometimes discrepant) determinations of σ_8 have been reported by different authors, ranging from $\sigma_8 \simeq 0.7$–0.8 [17, 56, 27] to $\sigma_8 \simeq 1$ [39, 51]. Ikebe et al. [29] compared different observational determinations of the XTF for nearby clusters (see left panel of Fig. 5) and established that they all agree with each other reasonably well. Although quite comfortable, this result highlights that the discrepant results on the normalization of the σ_8–Ω_m relation comes from the cosmological interpretation of the observed XTF, and not from observational uncertainties in its calibration. While the different model mass functions (i.e., whether Press–Schechter, Jenkins et al. or Sheth–Tormen) can in some cases account for part of the difference, more in general the different results are interpreted in terms of the different normalization of the M–T relation to be used in eq. (8) or to the way in which the intrinsic scatter and the statistical uncertainties in this relation are included in the analysis.

Substantially improved observational determinations of the XTF, and correspondingly tighter cosmological constraints, are expected to emerge with the accumulations of data on the ICM temperature from the Chandra and XMM–Newton satellites. Thanks to the much improved sensitivity of these X-ray telescopes with respect to ASCA, temperature gradients can be measured for fairly large sets of nearby and medium–distant ($z \lesssim 0.4$) clusters, thus allowing more precise determinations of cluster masses. At the same time, reliable measurements of global temperatures are now emerging for clusters out to the highest redshifts where they have been secured [58]. At the time of writing, several years after the advent of the new generation of X-ray telescopes, no determinations of the XTF from Chandra and XMM–Newton data have been presented, a situation that is expected to change quite soon.

5.2 The luminosity function

Another method to trace the evolution of the cluster number density is based on the X-ray luminosity function (XLF), $\phi(L_X)$, which is defined as the number density of galaxy clusters having a given X-ray luminosity. Similarly to eq. (8), the XLF can be related to the cosmological mass function of collapsed halos as

$$\phi(L_X) \, = \, n[M(L_X)] \, \frac{dM}{dL_X} \, , \tag{9}$$

where $M(L_X)$ provides the relation between the observable L_X and the cluster mass. The above relation needs to be suitably modified in case an intrinsic scatter exists in the relation between mass and temperature.

In general, the advantage of using X-ray luminosity as a tracer of the mass is that L_X is measured for a much larger number of clusters within samples with well-defined selection properties. The most recent flux–limited cluster samples contain now a fairly large ($\sim$100) number of objects, which are homogeneously identified over a broad redshift baseline, out to $z \simeq 1.3$. This

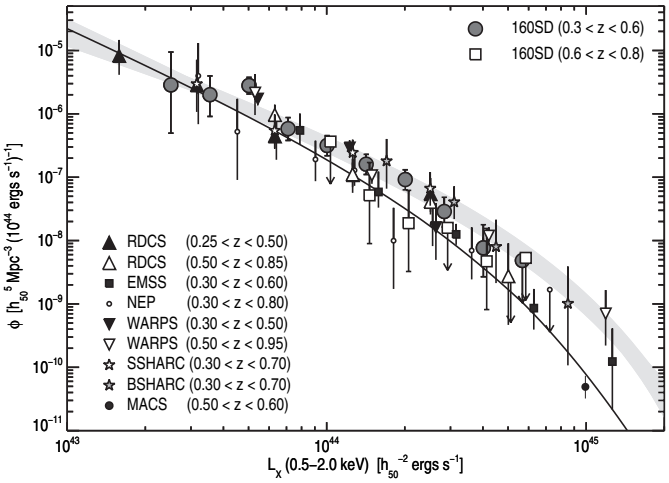

Fig. 6. A compilation of XLF within different redshift intervals for independent X-ray flux–limited surveys (from [47]). The shaded area shows the range of determinations of the local XLF, while the solid curve is the best–fitting evolving XLF discussed by Mullis et al. [47].

allows nearby and distant clusters to be compared within the same sample, i.e. with a single selection function. However, since the X-ray emissivity depends on the square of the gas density, the relation between L_X and $M_{\rm vir}$, which is based on additional physical assumptions and hence is more uncertain than the $M_{\rm vir}$–σ_v or the $M_{\rm vir}$–T relations.

A useful parametrization for the relation between temperature and bolometric luminosity can be casted in the form

$$L_{bol} \;=\; L_6 \left(\frac{T_X}{6\mathrm{keV}}\right)^{\alpha} (1+z)^A \left(\frac{d_L(z)}{d_{L,EdS}(z)}\right)^2 10^{44} h^{-2}\,\mathrm{erg\,s^{-1}}\,, \qquad (10)$$

with $d_L(z)$ the luminosity–distance at redshift z for a given cosmology.

Several authors [32, 40, 8] analyzed the number counts from different X-ray flux–limited cluster surveys and found that resulting constraints on Ω_m are rather sensitive to the evolution of the mass–luminosity relation. Other authors [59, 55, 64] analyzed different flux–limited surveys and found results to be consistent with $\Omega_m = 1$. Quite intriguingly, this conclusion is common to analyses which combine a normalization of the local mass function, using nearby clusters, to the evolution of the mass function using deep surveys. Clearly, any uncertainty in the calibration of the selection functions when combining different surveys may induce a spurious signal of evolution of the cluster population, possibly misinterpreted as an indication for high Ω_m.

In order to overcome this problem, Borgani et al. [12] analyzed the RDCS sample to trace the cluster evolution over the entire redshift range,

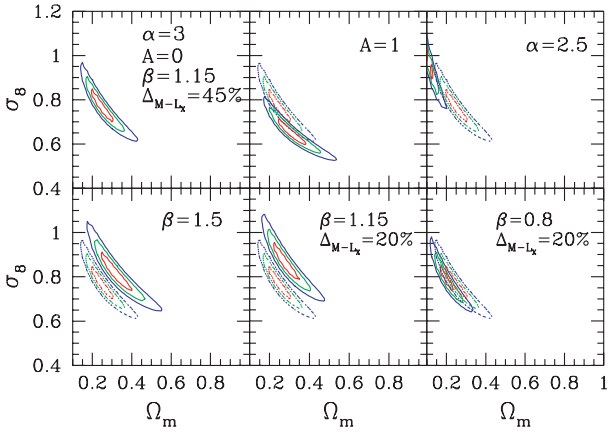

Fig. 7. Probability contours in the σ_8–Ω_m plane from the evolution of the X-ray luminosity distribution of RDCS clusters. The shape of the power spectrum is fixed to $\Gamma = 0.2$ [57]. Different panels refer to different ways of changing the relation between cluster virial mass, M, and X-ray luminosity, L_X, within theoretical and observational uncertainties (see also [12]). The upper left panel shows the analysis corresponding to the choice of a reference parameter set. In each panel, we indicate the parameters which are varied, with the dotted contours always showing the reference analysis.

$0.05 \lesssim z \lesssim 1.3$, probed by this survey, without resorting to any external normalization from a different survey of nearby clusters [11]. They found $0.1 \lesssim \Omega_m \lesssim 0.6$ at the 3σ confidence level, by allowing the M–L_X relation to change within both the observational and the theoretical uncertainties. In Figure 7 we show the resulting constraints on the σ_8–Ω_m plane (from [57]) and how they change by changing in different ways the parameters defining the M–L_X relation: the slope α and the evolution A of the L_X–T relation (see Equation 10), the normalization β of the M–T relation, and the overall scatter Δ_{M-L_X}. Flat geometry is assumed here, i.e. $\Omega_m + \Omega_\Lambda = 1$.

Constraints on Ω_m from the X-ray luminosity and temperature distribution of cluster are thus in line with the completely independent constraints derived from the baryon fraction in clusters, $f_{\rm bar}$ [71, 20, 2].

6 The future

A new era for cosmology with galaxy clusters is now starting. High sensitivity surveys for blind SZ identification over fairly large contiguous area, ∼100 deg^2, have have already started or are planned in the coming years. Also, the Planck satellite will survey the whole sky, although at a much lower sensitivity, and provide a large set of clusters identified through the SZ effect. These surveys promise to identify several thousands clusters, with a fair number of

objects expected to be identified at $z > 1$. In the optical band, CCD imaging with dedicated telescopes with large field of view will also allow to secure a large number of distant clusters. At the same time, X-ray observations over contiguous area [72] and "serendipitous" searches from XMM–Newton [46] and Chandra [13] archives will ultimately cover several hundreds deg^2 down to flux limits fainter than those reached by the deepest *ROSAT* pointings. Preliminary results suggest that identification of $z > 1$ clusters may eventually become routine [46]. Ultimately, they will lead to the identification of several thousands clusters.

Finally, technology of X-ray optics is now mature to plan a dedicated wide–field X-ray telescope, which should survey the sky over an area of several thousands deg^2, with a relatively good, XMM–like, point spread function and a lower background. This instrument would be invaluable for studies of galaxy clusters, thanks to its ability of both identifying extended sources with low surface brightness. Several missions with a similar profile have been proposed, although none has been approved so far. Still, the community working on galaxy clusters is keeping proposing this idea of satellite to different Space Agencies [25].

The samples of galaxy clusters obtainable from large–area SZ and X-ray surveys contain in principle so much information to allow one to constrain not only Ω_m and σ_8, but also the Dark Energy (DE) content of the Universe (see, e.g., [63, 60] for introductory reviews on Dark Energy). Constraining the nature of DE is now one of the most ambitious targets of modern cosmology.

As we have mentioned, the limited statistics prevents current cluster surveys to place significant constraints on Ω_Λ. Although this limitation will be overcome with future cluster surveys, the question remains as to whether the systematic effects can be taken under good enough control. Different lines of attack have been proposed in the literature, which should not considered as alternative to each other.

Majumdar & Mohr [38] have proposed the approach based on the so–called self–calibration (see also [37, 34, 35]). The idea underlying this approach is that of parametrizing in a sensible way the scaling relations between cluster observables and mass, including the corresponding intrinsic scatter and its distribution. In this way, the parameters describing these relations can be considered as fitting parameter to be added to the cosmological parameters. As long as the cluster statistics is large enough, one should be able to fit at the same time both cosmological parameters and those parameters related to the physical properties of clusters. Clearly, the reliability of this approach is inextricably linked to the possibility of accurately modeling the relations between mass and observables.

A line of attach to this problem is based on using detailed hydrodynamical simulations of galaxy clusters. The great advantages of using simulations is that both cluster mass and observable quantities can be exactly computed. Furthermore, the effect of observational set–ups (e.g., response functions of

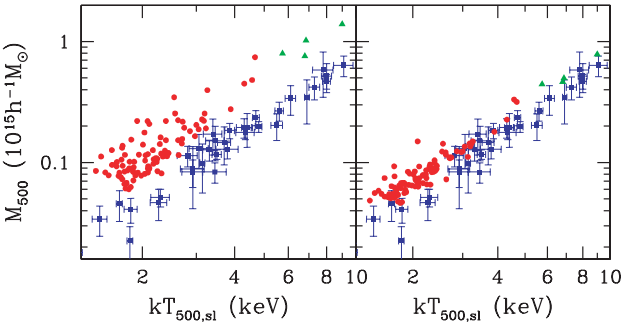

Fig. 8. The mass–temperature relation at $\bar{\rho}/\rho_{\rm cr} = 500$, in simulations (filled circles and triangles) and for the observational data by [23] (squares with errorbars). The left panel is for the true masses of simulated clusters; the right panel is for masses of simulated clusters estimated by adopting the same procedure applied by Finoguenov et al. to observational data (from [53]).

detectors, etc.) can be included in the analysis and their effect on the scaling relations quantified. This approach has been applied by different groups in the case of X-ray observations [24] to understand the relation between the ICM temperature, as measured from the fitting of the observed spectrum, and the "true" mass–weighted temperature [41, 43, 66]. Furthermore, simulations can also be used to verify in detail the validity of assumptions on which the mass estimators, applied to observations, are based. The typical example is represented by the assumption of hydrostatic equilibrium, discussed in Sect.3, for which violations in simulations at the 10–20 per cent level have been found [54, 10, 31].

An example of calibration of observational biases in the mass–temperature relation, using hydrodynamical simulations, is shown in Figure 8 (from [53]), which provides a comparison between the observed and the simulated M–T relation. Simulations here include radiative cooling, star formation and the effect of galactic winds powered by supernovae, and, as such, provide a realistic description of the relevant physical processes. The observational results, which are taken from Finoguenov et al. [23], corresponds to mass estimates based on the hydrostatic equilibrium for a polytropic β–model of the gas distribution [eq. (5)]. In both panels, the temperature has been computed by using a proxy to the actual spectroscopic temperature, the so–called spectroscopic–like temperature [43]. The left panel shows the results when exact masses of simulated clusters are used for the comparison. Based on this result only, the conclusion would be that simulations do indeed produce too high a M–T relation, even in the presence of a realistic description of gas physics. In the left panel masses of simulated clusters are computed instead by using the same procedure as for observed clusters, i.e. by applying eq. (6) for the hydrostatic equilibrium of a polytropic β–model. Quite remarkably, the effect of applying the observational mass estimator has two effects. First,

the overall normalization of the M–T relation is decreased by the amount required to attain a reasonable agreement with observations. Second, the scatter in the simulated M–T relation is substantially suppressed. This is the consequence of the fact that eq. (6) provides a one-to-one correspondence between mass and temperature, while only the cluster-by-cluster variations of β and γ account for the intrinsic diversity of the cluster thermal structure.

This example illustrates how simulations can be usefully employed as guidelines to study possible biases in observational mass estimates. However, it is worth reminding that the reliability of simulation results depends on our capability to correctly provide a numerical description of all the relevant physical process. In this sense, understanding in detail the (astro)physics of clusters is mandatory in order to calibrate them as tools in the era of precision cosmology.

References

1. Allen S. W., Fabian A. C., 1998, MNRAS, 297, L57
2. Allen S. W., Schmidt R. W., Ebeling H., Fabian A. C., van Speybroeck L., 2004, MNRAS, 353, 457
3. Allen S. W., Schmidt R. W., Fabian A. C., 2002, MNRAS, 334, L11
4. Arnaud M., Evrard A. E., 1999, MNRAS, 305, 631
5. Arnaud M., Pointecouteau E., Pratt G. W., 2005, A&A, 441, 893
6. Bahcall N. A., Cen R., Davé R., Ostriker J. P., Yu Q., 2000, ApJ, 541, 1
7. Blanchard A., Sadat R., Bartlett J. G., Le Dour M., 2000, A&A, 362, 809
8. Borgani S., Girardi M., Carlberg R. G., Yee H. K. C., Ellingson E., 1999, ApJ, 527, 561
9. Borgani S., Guzzo L., 2001, Nature, 409, 39
10. Borgani S., Murante G., Springel V., Diaferio A., Dolag K., Moscardini L., Tormen G., Tornatore L., Tozzi P., 2004, MNRAS, 348, 1078
11. Borgani S., Rosati P., Tozzi P., Norman C., 1999, ApJ, 517, 40
12. Borgani S., Rosati P., Tozzi P., Stanford S. A., Eisenhardt P. R., Lidman C., Holden B., Della Ceca R., Norman C., Squires G., 2001, ApJ, 561, 13
13. Boschin W., 2002, A&A, 396, 397
14. Cavaliere A., Fusco-Femiano R., 1976, A&A, 49, 137
15. Donahue M., Voit G. M., 1999, ApJl, 523, L137
16. Eke V. R., Cole S., Frenk C. S., 1996, MNRAS, 282, 263
17. Eke V. R., Cole S., Frenk C. S., Patrick Henry J., 1998, MNRAS, 298, 1145
18. Ettori S., De Grandi S., Molendi S., 2002, A&A, 391, 841
19. Ettori S., Tozzi P., Borgani S., Rosati P., 2004, A&A, 417, 13
20. Ettori S., Tozzi P., Rosati P., 2003, A&A, 398, 879
21. Evrard A. E., MacFarland T. J., Couchman H. M. P., Colberg J. M., Yoshida N., White S. D. M., Jenkins A., Frenk C. S., Pearce F. R., Peacock J. A., Thomas P. A., 2002, ApJ, 573, 7
22. Fabian A. C., 1991, MNRAS, 253, 29P
23. Finoguenov A., Reiprich T. H., Böhringer H., 2001, A&A, 368, 749
24. Gardini A., Rasia E., Mazzotta P., Tormen G., De Grandi S., Moscardini L., 2004, MNRAS, 351, 505

25. Haiman Z., Allen S., Bahcall N., et al. 2005, ArXiv Astrophysics e-prints
26. Henry J. P., 2000, ApJ, 534, 565
27. Henry J. P., 2004, ApJ, 609, 603
28. Henry J. P., Arnaud K. A., 1991, ApJ, 372, 410
29. Ikebe Y., Reiprich T. H., Böhringer H., Tanaka Y., Kitayama T., 2002, A&A, 383, 773
30. Jenkins A., Frenk C., White S., Colberg J., Cole S., Evrard A., Couchman H., Yoshida N., 2001, MNRAS, 321, 372
31. Kay S. T., Thomas P. A., Jenkins A., Pearce F. R., 2004, MNRAS, 355, 1091
32. Kitayama T., Suto Y., 1997, ApJ, 490, 557
33. Kotov O., Vikhlinin A., 2005, ApJ, 633, 781
34. Lima M., Hu W., 2004, Phys. Rev. D, 70, 043504
35. Lima M., Hu W., 2005, Phys. Rev. D, 72, 043006
36. Lumb D. H., Bartlett J. G., Romer A. K., Blanchard A., Burke D. J., Collins C. A., Nichol R. C., Giard M., Marty P. B., Nevalainen J., Sadat R., Vauclair S. C., 2004, A&A, 420, 853
37. Majumdar S., Mohr J. J., 2003, ApJ, 585, 603
38. Majumdar S., Mohr J. J., 2004, ApJ, 613, 41
39. Markevitch M., 1998, ApJ, 504, 27
40. Mathiesen B., Evrard A. E., 1998, MNRAS, 295, 769
41. Mathiesen B. F., Evrard A. E., 2001, ApJ, 546, 100
42. Maughan B. J., Jones L. R., Ebeling H., Scharf C., 2006, MNRAS, 365, 509
43. Mazzotta P., Rasia E., Moscardini L., Tormen G., 2004, MNRAS, 354, 10
44. Moscardini L., Matarrese S., Mo H. J., 2001, MNRAS, 327, 422
45. Mulchaey J. S., Zabludoff A. I., 1998, ApJ, 496, 73
46. Mullis C. R., Rosati P., Lamer G., Böhringer H., Schwope A., Schuecker P., Fassbender R., 2005, ApJl, 623, L85
47. Mullis C. R., Vikhlinin A., Henry J. P., Forman W., Gioia I. M., Hornstrup A., Jones C., McNamara B. R., Quintana H., 2004, ApJ, 607, 175
48. Osmond J. P. F., Ponman T. J., 2004, MNRAS, 350, 1511
49. Oukbir J., Blanchard A., 1992, A&A, 262, L21
50. Pierpaoli E., Borgani S., Scott D., White M., 2003, MNRAS, 342, 163
51. Pierpaoli E., Scott D., White M., 2001, MNRAS, 325, 77
52. Press W., Schechter P., 1974, ApJ, 187, 425
53. Rasia E., Mazzotta P., Borgani S., Moscardini L., Dolag K., Tormen G., Diaferio A., Murante G., 2005, ApJl, 618, L1
54. Rasia E., Tormen G., Moscardini L., 2004, MNRAS, 351, 237
55. Reichart D. E., Nichol R. C., Castander F. J., Burke D. J., Romer A. K., Holden B. P., Collins C. A., Ulmer M. P., 1999, ApJ, 518, 521
56. Reiprich T., Böhringer H., 2002, ApJ, 567, 716
57. Rosati P., Borgani S., Norman C., 2002, ARAA, 40, 539
58. Rosati P., Tozzi P., Ettori S., Mainieri V., Demarco R., Stanford S. A., Lidman C., Nonino M., Borgani S., Della Ceca R., Eisenhardt P., Holden B. P., Norman C., 2004, AJ, 127, 230
59. Sadat R., Blanchard A., Oukbir J., 1998, A&A, 329, 21
60. Sahni V., 2005, LNP Vol. 653: The Physics of the Early Universe, 653, 141
61. Sheth R., Tormen G., 1999, MNRAS, 308, 119
62. Springel V., White S. D. M., Jenkins A., Frenk C. S., Yoshida N., Gao L., Navarro J., Thacker R., Croton D., Helly J., Peacock J. A., Cole S., Thomas P., Couchman H., Evrard A., Colberg J., Pearce F., 2005, Nature, 435, 629

63. Steinhardt P. J., 2003, Royal Society of London Philosophical Transactions Series A, 361, 2497
64. Vauclair S. C., Blanchard A., Sadat R., Bartlett J. G., Bernard J.-P., Boer M., Giard M., Lumb D. H., Marty P., Nevalainen J., 2003, A&A, 412, L37
65. Viana P. T. P., Liddle A. R., 1999, MNRAS, 303, 535
66. Vikhlinin A., 2005, ArXiv Astrophysics e-prints
67. Vikhlinin A., Kravtsov A., Forman W., Jones C., Markevitch M., Murray S. S., Van Speybroeck L., 2005, ArXiv Astrophysics e-prints
68. Voit G. M., 2005, Reviews of Modern Physics, 77, 207
69. Warren M. S., Abazajian K., Holz D. E., Teodoro L., 2005, ArXiv Astrophysics e-prints
70. White M., 2002, ApJs, 143, 241
71. White S. D. M., Navarro J. F., Evrard A. E., Frenk C. S., 1993, Nature, 366, 429
72. Willis J. P., Pacaud F., Valtchanov I., Pierre M., Ponman T., Read A., Andreon S., Altieri B., Quintana H., Dos Santos S., Birkinshaw M., Bremer M., Duc P.-A., Galaz G., Gosset E., Jones L., Surdej J., 2005, MNRAS, 363, 675
73. Xue Y.-J., Wu X.-P., 2000, ApJ, 538, 65

The Association of Compact Groups of Galaxies with Large-scale Structures

H. Andernach and R. Coziol

Departamento de Astronomía, Universidad de Guanajuato, Mexico
heinz@astro.ugto.mx, rcoziol@astro.ugto.mx

Summary. We use various samples of compact groups (CGs) to examine the types of association CGs have with rich and poor clusters of galaxies at low ($z \simeq 0.04$) and intermediate ($z \simeq 0.1$) redshifts. We find that ∼10–20% of CGs are associated with rich clusters and a much larger fraction with poorer clusters or loose groups. Considering the incompleteness of catalogs of poorer systems at intermediate redshift, our result is consistent with *all* CGs at intermediate redshift being associated with larger-scale systems. The richness of the clusters associated with CGs significantly increases from $z \simeq 0.04$ to $z \simeq 0.1$, while their Bautz-Morgan type changes from early to late type for the same range in z. Neither trend is compatible with a selection effect in the cluster catalogs used. We find earlier morphological types of galaxies to be more frequent in CGs associated with larger-scale structures, compared to those in CGs not associated to such structures. We consider this as new evidence that CGs are part of the large-scale structure formation process and that they may play an important role in the evolution of galaxies in these structures.

1 Motivation and method

Although groups of galaxies form the principal environment of most galaxies in the Universe, their origin and evolution are still poorly understood. Theoretically, the resolution of numerical simulations is still insufficient to understand the formation of such small-scale structures. Observationally, the intrinsic low richness of groups makes them more difficult to detect and study than richer systems like cluster of galaxies, especially at intermediate and high redshift.

Within the Hierarchical Structure Formation paradigm (based on CDM models) we would like to address questions like e.g. "When do groups form and what IMF do they follow?", or "Assuming galaxy formation is biased, should we expect a sort of downsizing effect for groups, i.e. high-mass groups at high z forming before lower-mass ones at lower z?" What is the role of groups in the formation of large-scale structures? If groups were merging together to form larger-scale structures, how long can we expect them to retain their dynamical characteristics and be distinguished from the larger, more massive structure? Finally, following the merging scenario, what is the

importance of groups in the evolution of galaxies located in large-scale structures?

Here we concentrate on Compact Groups of galaxies (CGs). The advantage of CGs over other groups is that they reach galaxy densities comparable to those of clusters, and are consequently easier to identify in the sky, even at moderate redshift. From their relation with larger-scale structures [9],[12],[10],[2] it seems clear also that CGs form part of the large-scale structure formation process. Finally, it is expected that such compact configurations should have some distinctive and recognizable impact on the evolution of their galaxy members (see e.g. Plauchu Frayn et al., these proceedings). A more detailed study of the relation of CGs with large-scale structures may yield new insights on some of the above questions.

To examine the relation CGs have with large-scale structures we compiled a list of possible associations of CGs with rich and poor clusters of galaxies and with loose groups of galaxies. The CG samples we use are the HCGs [5], the SCGs [6], the SDSSCGs [8], and the PCGs [3]. Note that in our previous analysis [2] only the preliminary PCG sample by [7] was available. As samples of rich clusters we use the Abell catalog [1], and for poorer clusters and loose groups we take the NSC [4] and USGC [11] samples, respectively. The association method we use is described in detail in [2].

Based on the position of the groups relative to the center of the associated larger-scale structure and on a comparison of the apparent magnitude of galaxies in both structures we identified three types of such associations: ML or AML indicate that the galaxies in the CG are either the "Most Luminous" or "Among the Most Luminous" ones of the associated larger-scale structure, and SS if the group forms some sort of substructure at the periphery of a larger system. Examples of each association class can be found in [2].

2 Results

2.1 Associations of CGs with rich clusters

The associations of CGs with Abell clusters are described in Table 1. Columns are the CG sample name, total number of CGs in each sample (note that on

Table 1. Associations of CGs with Abell clusters

CG	N_{CG}^{tot}	N_{ass}	%	$\langle z \rangle$	Ass. type			Richness				BM type		
					SS	ML	AML	0	1	2	3	undef.	early	late
HCG	100	6	6	.04	5	1	...	5	...	...	1	...	2	3
SCG	121	21	17	.04	9	12	...	18	2	1	...	2	14	5
PCG	407	71	17	.12	20	...	51	23	34	12	3	12	5	54
SDSSCG	177	16	9	.12	11	...	5	5	9	1	1	4	...	12

the basis of our optical inspection of all 459 published PCGs we discarded 52, mostly for stellar contamination), the number of CGs associated with an Abell cluster, the percentage of associated CGs, their mean redshift, the number distribution of associated CGs among the different association types, and the Abell richness classes as well as the Bautz-Morgan (BM) types of the associated clusters. Interesting differences are observed, which can easily be related to the different group selection methods. Eye selection of the CG candidates, like HCGs and visual inspection of the otherwise automatically selected groups like the SDSSCGs, seem to discard most associations of CGs with larger-scale structures: 83% of HCGs and 69% of the SDSSCG are SS, while 57% are ML type in the SCGs and 72% are AML in the PCGs. This difference in the selection method may also explain why we found only one coincidence of a SDSSCG with a PCG. Based on the surface density of SDSSCGs and PCGs and their region of overlap, one would expect about 10 coincidences if the two selection methods were identical.

Despite the difference in group selection techniques the CG-cluster association rates seem quite similar at low ($z = 0.04$) and intermediate ($z = 0.12$) redshifts.

Other differences observed are more difficult to explain. We note for example that the richness of the associated clusters rises with redshift: the fraction of R = 1 cluster rises from 14% in the SCGs to 69% in the PCGs and SDSSCGs. The average BM type also seems to change with redshift: passing from 74% early types (I, I-II, II) in the SCGs to 92% late types (II-III, III) in the PCG and 100% late types in the SDSSCG.

We already observed these differences in our first examination of these samples [2]. The fact that we observe the same phenomenon using the complete (and revised) sample of PCGs and the SDSSCG sample, confirms that these differences occur in relation with the increase in redshift. In [2] we verified that these differences cannot be due to an incompleteness in richness of the Abell/ACO sample at intermediate redshift, nor to some sort of luminosity bias affecting clusters with different BM types. These differences are consistent with an increase of the mass of the associated structures at increasing redshift.

2.2 Associations of CGs with poorer structures

The associations of CGs with large-scale structures poorer than Abell clusters are described in Table 2. Columns are the CG sample name, the sample name of the associated structure, the number and percentage of CGs associated with that structure, the mean redshift of the CG-associated structures, their distribution among the three association types defined earlier, and the average richness of the associated structure.

Comparing with Table 1 we see that CGs are much more frequently associated with poorer than with richer structure. This increase in the number of associations is significant: a factor of 2 to 6 for the SCG and HCG at low

Table 2. Associations of CGs with poorer structures

CG	LSS	N_{CG}^{assoc}	%	$\langle z \rangle$	Assoc. type			$\langle N_{gal} \rangle$
					SS	ML	AML	
HCG	USGC	37	37	0.02	2	30	5	6
SCG	USGC	33	27	0.02	8	22	3	8
PCG	NSC	195	62	0.13	55	10	130	35
SDSSCG	NSC	21	25	0.13	5	...	14	40

z, and a factor of 3 to 4 for the SDSSCG and PCG at intermediate z. Note that the severe incompleteness of the NSC in low-richness structures (cf. [4]) implies that at higher redshifts almost all CGs may be part of a larger-scale system.

In Table 2 we also observe a significant increase in the number of ML- and AML-type association which indicates that CGs may generally form important "substructures" in these poorer, larger-scale systems.

2.3 Variation of galaxy morphologies with CG environment

In Table 3, we compare the number of galaxies of early (E-S0-S0/a), intermediate (Sa-Sab-Sb) and late (Sbc and later) morphological type in CGs located in different large-scale environments. For both HCGs and SCGs, distinguishing whether they are or not associated with clusters or loose groups (LGs), we list the number and percentages of galaxies of different morphological types. N_{gal} is the number of galaxies for which we could find a morphological type in NED (`nedwww.ipac.caltech.edu`). As expected, we find a significant increase of earlier morphological types in CGs associated with large-scale structures. This result suggests that in general the associations we found are physically real.

On the other hand, it is also quite interesting to note how rich in early-type galaxies the isolated CGs already are. Note that there seems to be no difference between isolated CGs and those associated with loose groups (LG). These results suggest that compact configurations like CGs have a great influence on galaxy evolution. This may be independent of the environment

Table 3. Distribution of galaxy morphologies as a function of CG environment

Morphological type	HCG out of cl.		HCG in LGs		HCG in cl.		SCG out of cl.		SCG in cl.	
	N_{gal}	%	N_{gal}	%	N_{gal}	%	N_{gal}	%	N_{gal}	%
Early	142	54.4	73	46.8	17	65.4	72	45.0	22	64.7
Intermediate	33	12.6	28	17.9	2	7.7	49	30.6	7	20.6
Late	86	33.0	55	35.3	7	26.9	39	24.4	5	14.7

or it may depend on some threshold mass of the larger-scale structure with which the CG is associated.

3 Conclusions

Despite the obvious biases introduced by the different selection methods, the high number of associations of CGs with larger-scale structures encountered in our analysis indicates that these systems must form naturally during the large-scale structure formation process. Both, the increase of mass of the associated structures at intermediate redshift, and the variation of galaxy morphologies with CG environment, are consistent with biased galaxy formation, which implies some sort of downsizing effect for groups: more massive groups form before less massive ones. Compact groups may affect galaxy evolution independently of environment, and/or the CG environment may affect galaxies more strongly above some threshold mass of the structures in which the groups form.

References

1. Abell G.O., Corwin Jr. H.G., Olowin R.P.: ApJS, **70**, 1 (1989)
2. Andernach H., Coziol R.: in *Nearby Large-Scale Structures and the Zone of Avoidance*, ASP Conf. Ser., **239**, eds. A.P. Fairall & P.A. Woudt, p. 67 (2005)
3. de Carvalho R.R., Gonçalves T.S., Iovino A., et al.: AJ, **130**, 425 (2005)
4. Gal R.R., de Carvalho R.R., Lopes P.A.A., et al.: AJ, **125**, 2064 (2003)
5. Hickson P., Mendes de Oliveira C., Huchra J.P., et al.: ApJ, **399**, 353 (1992)
6. Iovino A.: AJ, **124**, 2471 (2002)
7. Iovino A., de Carvalho R.R., Gal R.R., et al.: AJ, **125**, 1660 (2003)
8. Lee B.C., Allam S.S., Tucker D.L., et al.: AJ, **127**, 1811 (2004)
9. Mamon G.A.: A&A, **219**, 98 (1989)
10. Ramella M., Diaferio A., Geller M.J., Huchra J.P.: AJ, **107**, 1623
11. Ramella M., Geller M.J., Pisani A., da Costa L.N.: AJ, **123**, 2976 (2002)
12. Rood H.J., Struble M.F.: PASP, **106**, 413 (1994)

Probing the Environment with Galaxy Dynamics

A.J. Romanowsky

Departamento de Física, Universidad de Concepción, Casilla 160-C, Concepción, Chile
romanow@astro-udec.cl

Summary. I present various projects to study the halo dynamics of elliptical galaxies. This allows one to study the outer mass and orbital distributions of ellipticals in different environments, and the inner distributions of groups and clusters themselves.

1 Introduction: Halos and the environment

Elliptical galaxies are intriguingly homogeneous. Besides being more prevalent in high density regions, low-redshift ellipticals have observable central properties (e.g. color, velocity dispersion, metallicity, star formation history) whose environmental dependencies are relatively subtle (e.g. [1, 2]), in contrast to the case of spiral galaxies. Larger differences might be found in the ellipticals' outer parts, which should be the most strongly affected by environmental influences. For example, the tidal fields in higher-density environments could cause stripping of the galaxies' stellar and dark matter (DM) halos, and of their globular cluster (GC) systems – also affecting the anisotropy of the remaining halo stars and GCs. Indeed, a deep Virgo Cluster image seems to show stellar halo stripping in progress, a process which may be facilitated by dynamical halo heating in the pre-infall groups [3]. Gravitational lensing studies also indicate some DM halo stripping in high-density environments [4, 5, 6, 7].

The large radial extent of GC systems makes them handy tracers for halo stripping, and in fact it may be possible to use GCs as a proxies for the DM itself [8]. Very extended GC systems are found in cluster-dominant ellipticals (such as M87, M49, and NGC 1399) [9], which is consistent with them being agents rather than victims of stripping. Wide-field studies of more normal ellipticals are now getting underway – and provocatively, the Virgo galaxy NGC 4636 turns out to have a GC system with a sharp edge [10].

Groups should dominate the error budget of the Universe, but their mass distributions are among the most poorly determined. Observations from weak lensing and internal group dynamics don't agree on their total masses, much less the detailed distribution with radius (e.g. [11, 12, 13, 14]). Additional constraints, especially nearer the group centers, are essential. Fortunately,

studies of elliptical galaxy halos allow one to probe the mass distributions in galaxy groups as well as in individual galaxies. This is because many of the easiest-studied ellipticals are central group or cluster galaxies (e.g. [15, 16, 17]) – a frustration for galaxy research but a boon for group studies.

Whether in galaxies or in groups, there are several useful independent dynamical tracers: GCs, X-ray gas, and planetary nebulae (PNe), which are a powerful proxy for faint starlight. In groups with only a handful of galaxy velocities, there may be hundreds or thousands of GC and PN velocities attainable (albeit at relatively small radii). In M49 and M87, massive DM halo cores are found from constant-to-rising profiles of gas temperature, and of velocity dispersion profiles of PNe and GCs [18, 19, 20, 17, 21]. Different orbital properties are implied between the PNe and GCs, which should constrain central galaxy evolution scenarios. NGC 4636 has a constant GC dispersion profile, implying a fairly normal DM halo [22] – unsurprisingly different from X-ray results, given the evident departures from gas equilibrium [23]. NGC 1399 has a rising PN and GC dispersion profile, indicating either the DM core of the Fornax Cluster, or a recent interaction with another galaxy [24, 25]. Note that for halo tracers to be fruitful, it is imperative to combine them with constraints on the central galaxy's stellar mass, which is otherwise a major source of systematic uncertainty [17].

2 The Eridanus A group

Based on its X-ray gas and member galaxy velocities, Eridanus A appears to be a "dark cluster" with a virial mass $\sim 10^{14} M_{\odot}$ and mass-to-light ratio $\Upsilon_B \sim 1500\ \Upsilon_{B,\odot}$ [26, 27, 17, 28]. To probe this possibility further, we have acquired velocities of ~ 100 GCs around the central giant elliptical NGC 1407, using LRIS, FLAMES, and LDSS-3. Initial results with 36 GCs, comparing the GC dispersion profile to various models, do indeed support the presence of a super-halo (see Fig. 1). Based on typical empirical and theoretical values for the virial Υ of a group like Eri A [29, 14, 30], the profile should decrease outside 10 kpc – but a flat dispersion is observed. Combining more constraints from stellar, GC, X-ray, and group galaxy dynamics will allow us to trace the mass profile in more detail.

3 The Leo I group

Leo I is the nearest (10 Mpc) example of a group containing multiple giant early-type galaxies, including the "archetypal" L^* elliptical at its center, NGC 3379. It is unclear if the group is reasonably relaxed, with a group halo centered on NGC 3379. This galaxy has been the focus of numerous dynamical studies, most recently employing PNe [32, 33] and GCs [34, 35, 36]. The PNe imply surprisingly little DM inside 15 kpc, but leave the possibility that

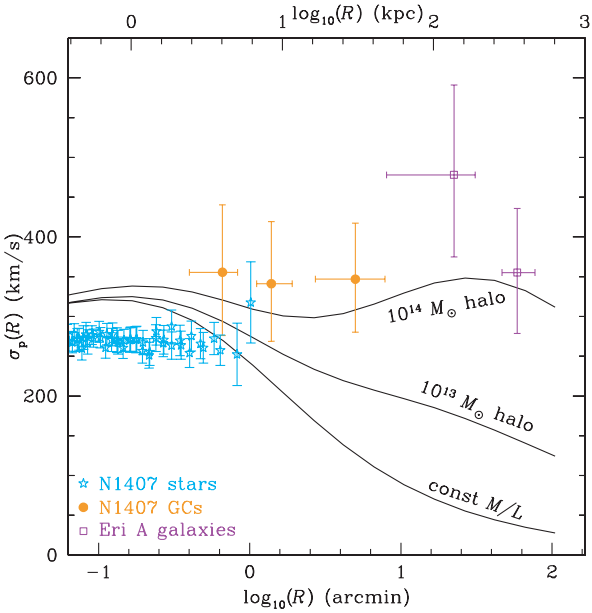

Fig. 1. Projected velocity dispersion radial profiles in the Eridanus A group. Points with error bars show data for stars and GCs in NGC 1407 [31], and for group galaxies. Curves show model predictions for the GCs, for a spherical isotropic assumption, and either no dark matter, a "normal" halo, or a "super" halo.

there are large amounts of DM spread further out in a massive, diffuse halo. The GC kinematics reach to 40 kpc, and do suggest a massive, even group-sized, halo (see Fig. 2). Another remarkable constraint comes from the HI gas ring which appears to orbit the core of the group, and implies $\Upsilon_B \sim 30$ inside 100 kpc [37]. This suggests a lot of DM, but much less than one would expect for a ΛCDM halo (whether galaxy- or group-sized), and appears to be at odds with the GC results (the PNe are technically compatible with either the GCs or the HI). However, the GC constraints are hampered by small-number statistics (49 velocities), and newly-acquired FLAMES data should clarify the situation with a doubled or tripled data set. As an interesting note of comparison, Leo I and Eri A are groups with nearly the same optical luminosity, but apparently differ in mass by at least a factor of 10.

4 Mass profiles of ordinary ellipticals

The halo mass profiles of "ordinary" ($\sim L^*$) ellipticals have long been elusive. The first inroads have come from new data on halo PN kinematics [38, 32, 39]. The first 5 ellipticals studied all have a projected velocity dispersion profile which declines markedly with radius. The obvious implication is

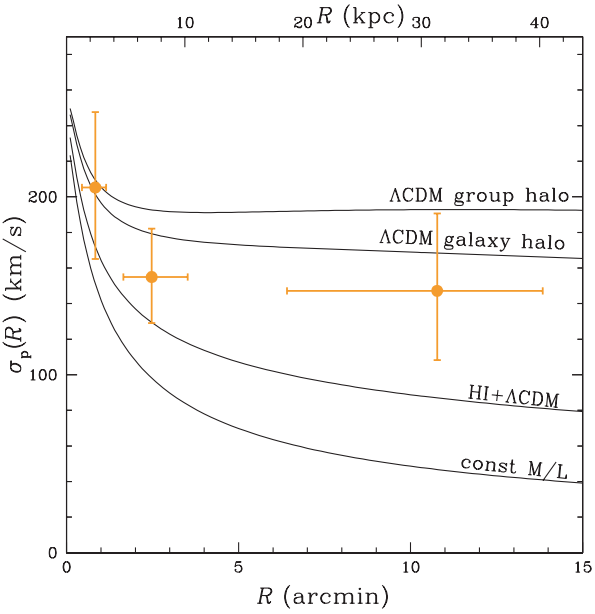

Fig. 2. Dispersion profile of GCs in the Leo I group. Error-bars show the data, and curves show spherical isotropic model predictions. The typical early-type galaxy halo mass comes from weak lensing results [7], and group mass from luminosity-function studies [29, 30]. A halo consistent with the HI ring constraint is also shown [37].

that the measurable DM content of these galaxies is remarkably low, as discussed above for NGC 3379. One might expect this effect to be strongest for the highest-density environments, where DM stripping could have occurred, but this does not appear to be the case. An alternative possibility is that the galaxy halo concentrations are lower than expected with ΛCDM, a possibility strengthened by analysis of literature data on early-type galaxies [40]. This is supported by some independent studies of ellipticals [41, 42, 15], and is paralleled by many studies of late-type galaxies.

Theoretical studies [43, 44] have pointed out various effects which could contribute to the declining dispersions, including oversimplified DM profiles, radial anisotropy variations, galaxy flattening, and biased PN-stellar correspondence. There are reasons to doubt that these effects could entirely explain the observations – for example, the modeling of NGC 3379 already incorporated a direct derivation of the (radial) anisotropy profile from the data. But certainly much more clarification is needed. Current work focuses on obtaining a large, systematic sample of independent mass tracers around ordinary ellipticals in different environments, and on refining the modeling – including direct calibratory comparisons with simulations.

References

1. F.M. Reda, D.A. Forbes, G.K.T. Hau: MNRAS **360**, 693 (2005)
2. M.S. Clemens, A. Bressan et al.: MNRAS, submitted (astro-ph/0603714)
3. J.C. Mihos, P. Harding et al.: ApJ **631**, L41 (2005); C.S. Rudick et al., this vol.
4. P. Natarajan, J.-P. Kneib, I. Smail: ApJ **580**, L11 (2002)
5. R. Gavazzi, Y. Mellier, B. Fort et al.: A&A **422**, 407 (2004)
6. P. Natarajan, J.-P. Kneib, I. Smail, R. Ellis: ApJ, submitted (astro-ph/0411426)
7. R. Mandelbaum, U. Seljak et al.: MNRAS, submitted (astro-ph/0511164)
8. K. Bekki, M.A. Beasley, J.P. Brodie, D.A. Forbes: MNRAS **363**, 1211 (2005)
9. D.E. McLaughlin: AJ **117**, 2398 (1999)
10. B. Dirsch, Y. Schuberth, T. Richtler: A&A **433**, 43 (2005)
11. R.G. Carlberg, H.K.C. Yee, S.L. Morris, H. Lin et al.: ApJ **552**, 427 (2001)
12. R.B. Tully: ApJ **618**, 214 (2005)
13. I.D. Karachentsev: AJ **129**, 178 (2005)
14. L.C. Parker, M.J. Hudson, R.G. Carlberg, H. Hoekstra: ApJ **634**, 806 (2005)
15. Y. Fukazawa, J.G. Botoya-Nonesa, J. Pu et al.: ApJ **636**, 698 (2006)
16. C.S. Kochanek, N.D. Morgan, E.E. Falco et al.: ApJ **640**, 47 (2006)
17. P.J. Humphrey, D.A. Buote et al.: ApJ, in press (astro-ph/0601301)
18. A.J. Romanowsky, C.S. Kochanek: ApJ **553**, 722 (2001)
19. K. Matsushita, E. Belsole, A. Finoguenov, H. Böhringer: A&A **386**, 77 (2002)
20. P. Côté, D.E. McLaughlin, J.G. Cohen, J.P. Blakeslee: ApJ **591**, 850 (2003)
21. G. Bergond et al.: in prep; N.G. Douglas, A.J. Romanowsky, K. Kuijken: in prep
22. Y. Schuberth, T. Richtler, B. Dirsch et al.: A&A, in press (astro-ph/0604309)
23. E. O'Sullivan, this vol.
24. N.R. Napolitano, M. Arnaboldi, M. Cappacioli: A&A **383**, 791 (2002)
25. T. Richtler, B. Dirsch et al.: AJ **127**, 2094 (2004); Y. Schuberth et al., in prep
26. A. Gould: ApJ **403**, 37 (1993)
27. H. Quintana, P. Fouqué, M.J. Way: A&A **283**, 722 (1994)
28. S. Brough, D.A. Forbes et al.: MNRAS, submitted (astro-ph/0603778)
29. F.C. van den Bosch, H.J. Mo, X. Yang: MNRAS **345**, 923 (2003)
30. V.R. Eke, C.M. Baugh, S. Cole et al.: MNRAS, submitted (astro-ph/0510643)
31. G.K.T. Hau: in prep; P. Sánchez-Blázquez et al.: in prep
32. A.J. Romanowsky, N.G. Douglas, M. Arnaboldi et al.: Science **301**, 1696 (2003)
33. A.P.N. Sluis, T.B. Williams: AJ **131**, 2089 (2006)
34. T.H. Puzia, M. Kissler-Patig, D. Thomas et al.: A&A **415**, 123 (2004)
35. M. Pierce, M.A. Beasley, D.A. Forbes et al.: MNRAS **366**, 1253 (2006)
36. G. Bergond, S.E. Zepf, A.J. Romanowsky et al.: A&A **448**, 155 (2006)
37. S.E. Schneider: ApJ **288**, L33 (1985)
38. R.H. Méndez, A. Riffeser, R.-P. Kudritzki et al.: ApJ **563**, 135 (2001)
39. A.M. Teodorescu, R.H. Méndez, R.P. Saglia et al.: ApJ **635**, 290 (2005)
40. N.R. Napolitano, M. Capaccioli et al.: MNRAS **357**, 691 (2005)
41. A. Borriello, P. Salucci, L. Danese: MNRAS **341**, 1109 (2003)
42. D. Rusin, C.S. Kochanek, C.R. Keeton: ApJ **595**, 29
43. G.A. Mamon, E.L. Łokas: MNRAS **363**, 705 (2005)
44. A. Dekel, F. Stoehr, G.A. Mamon, T.J. Cox et al.: Nature **437**, 707 (2005)

The Internal Dynamics of A115 Nearby Cluster of Galaxies

R. Barrena[1], W. Boschin[2] and M. Girardi[3]

[1] Instituto de Astrofisica de Canarias
rbarrena@iac.es
[2] Fundación Galileo Galilei - INAF
boschin@tng.iac.es
[3] Dipartimento di Astronomia, Università di Trieste
girardi@ts.astro.it

Summary. Based on optical data we propose a dynamycal model for A115. From spatial and radial velocity distributions we find three massive subsclusters that configure a pre-merging scenario. On this basis, we discuss on the origin of the radio emission and its correlation with X-rays.

1 Introduction

A115 is a hot Abell cluster ($kT_X \sim 8$ KeV, see [7] with an unusual arc-shape radio emission and other several asymmetric features [5]. Previous works (see e.g. [2], [7]) show this cluster as an ideal scenario where study the key aspects of the process of structure formation in mergers where the "ecosystems" (dark matter halos, ICM, galaxies, etc) play an important role. Now, using 96 radial velocities and $B-$ and $R-$band photometry we study the collision of three large substructures of A115. We also estimate the characteristic time of these interactions and its relation with the diffuse radio emission.

2 Results of the dynamical analysis

We select 96 galaxies (of 161 observed) recognized as cluster members via the adaptive–kernel analysis (see e.g. [8]). We find that A115 appears as a well isolated peak in the redshift space at $<z> = 0.193$ located at $(\alpha, \delta)_{J2000}$=(00:56:02,+26:23:00). It presents a velocity dispersion of $\sigma_V = 1353$ km s^{-1}, in agreement with the high average X-ray temperature. However, we find evidences that the cluster possess a three colliding substructures:

– Considering galaxies within the red sequence ($2 < B - R < 3$, $R < 21$) and using KMM test [1] we separate three clear clumps located $2'$ at the north (A), $3'$ at the south (B) and $4.5'$ at the SE (C) of the cluster center;

- a no uniform velocity distribution. The KMM analysis of the velocity field allows to separated two clumps at 95% confidence level. These peaks are coincident with the substructures A and C;
- we identify apparent cD galaxies in each clump, sign of evolved systems;
- the X-ray surface brightness shows two peaks (centred on A and B clumps) and a elongated profile toward the C substructure.

2.1 The virial masses and a collision model

Because A115 is far from virial equilibrium, we estimate virial mass assuming equilibrium in each clump separately. A, B and C substructures present velocity dispersions of 1061 km s^{-1}, 1464 km s^{-1} and 1034 km s^{-1}, which yields masses of 1.4, 1.9 and $1.3{\cdot}10^{15}$ $M_{\odot}$, respectively. Our analysis also shows the presence of a difference in mean velocities of $\Delta V = 960$ km s^{-1} between C and A+B system. A and B systems present the same mean velocities.

Taking into account relative velocities and distances between clumps we are able to estimate the time of the encounters solving the Two-Body problem [3]. We separate two collisions: A and B collision, and C versus A+B system. The first collision is contained in the plane of the sky (POS) and we find the susbtructures will be completely encountered in ∼0.15 Gyr. For the second encounter, (C, A+B), we estimate 0.3 Gyr and the merge axis is estimated to be around 10° out of the POS. The only possible solutions are in agreement with bounded systems in pre-merging state.

3 Conclusions

Our results suggest a merging scenario of three clumps with a mass ratio of 1:1:1 within the POS. We find the three substructures will be encountered in 0.3 Gyr. The proposed model supports recent Chandra observations, which reveal no front-shocks. On the other hand, according to the model of [4], the radio-halos take >0.6 Gyr after becoming evident. For this reason, the radio relic of A115 could have been powered by other major subcluster collisions in the recent past or may be a large radio-tail origined by the 3C28.0 AGN [6].

References

1. K.M. Ashman, C.M. Bird, & S.E. Zepf: AJ, **108**, 2348 (1994)
2. T.C. Beers, J.P Huchra & M.J. Geller: ApJ **264**, 365 (1983)
3. T.C. Beers, K. Gebhardt, W. Forman, et al.: AJ **102**, 1581 (1991)
4. G. Brunetti, G. Setti, L. Feretti, et al.: MNRAS **320**, 365 (2001)
5. L. Feretti, I.M. Gioia, G. Giovannini, et al.: AA **139**, 50 (1984)
6. G. Giovannini, L. Feretti, L. & L. Gregorini: AAS **69**, 111 (1987)
7. K. Gutierrez & H. Krawczynski: ApJ **619**, 161 (2005)
8. A. Pisani: MNRAS, **278**, 697 (1996)

Dynamics of the Radio–halo Cluster A2744: An Optical Study

W. Boschin[1], R. Barrena[2], M. Girardi[3] and M. Spolaor[3]

[1] Fundación Galileo Galilei - INAF
boschin@tng.iac.es
[2] Instituto de Astrofisica de Canarias
rbarrena@iac.es
[3] Dipartimento di Astronomia, Università di Trieste
girardi@ts.astro.it

Summary. We present the results of a dynamical analysis of the radio–halo cluster A2744 based on optical data. We find that this cluster is in an advanced merging phase, with two galaxy subsystems impacting along a direction close to the line–of–sight, likely observed just after the core passage.

1 Introduction

Abell cluster A2744 is a rich (Abell class=3; [1]), X–ray luminous ($L_{\rm X}$(0.1–2.4 keV)$\sim 2{\times}10^{45}\, h_{50}^{-2}$ erg s^{-1} [2]), and hot cluster ($T_{\rm X} \sim 8$ keV; [3]) at $z \sim 0.3$. It hosts one of the most luminous known radio–halos which covers the central cluster region with a radius of ~ 1 h$_{50}$ Mpc [4]. Previous works suggested that this cluster has a complex internal structure. In particular, Kempner & David [5] analyzed Chandra X–ray data and found a strong evidence for an ongoing major merger detecting two secondary X–ray peaks in the central cluster region and a third subcluster about 2 arcmin NW of the central core. In view of the availability of unexplored spectroscopic data in the ESO archive we study the internal dynamics of A2744 analyzing data of member galaxies.

2 Results of the dynamical analysis

Our analysis is based on redshift data for 102 galaxies. Of these, we select 85 galaxies recognized as cluster members via the adaptive–kernel analysis [6], [7] and the shifting–gapper technique [8]. We find that A2744 appears as a well isolated peak in the redshift space at $\langle z \rangle = 0.306$. It presents a line–of–sight (LOS) velocity dispersion very high for a cluster ($\sigma_{\rm V} = 1750$ km s^{-1}), significantly larger than what is expected in the case of a relaxed cluster with $T_{\rm X} \sim 8$ keV. Moreover, we find evidence that the cluster is far from dynamical equilibrium, as shown by:

- the non Gaussianity of the velocity distribution according to different statistical tests;
- the presence of a velocity gradient at the >98% c.l.;
- the presence of significant substructures at the ∼99% c.l. (see below).

2.1 Detection of substructures

To detect and analyze possible subsystems we use different methods coupling galaxy position and velocity information: the KMM method [9], the kinematical analysis of galaxy populations located in different spatial regions, and the Δ statistics [10]. Our analysis shows the presence of two galaxy clumps having:

- a difference in mean velocities of $\Delta V \sim 4000$ km s^{-1};
- a value of $\sigma_V \sim 1200$–1300 km s^{-1} for the main, low-velocity clump and a value of $\sigma_V \sim 500$–800 km s^{-1} for the secondary, high velocity clump;
- a remarked spatial segregation, with the galaxies of the high velocity clump mainly populating the S–SW cluster region.

3 Conclusions

Our results suggest a merging scenario of two clumps with a mass ratio of 3:1 and an high LOS impact velocity of $\Delta V_{\rm rf} \sim 3000$ km s^{-1}, likely observed just after the core passage. The merging axis, close to the LOS, is roughly along the NS direction. This scenario supports recent Chandra results although points out for a somewhat more advanced merging phase. For the final product of the merger we estimate a mass within 1 Mpc of 1.4–$2.4 \times 10^{15}\, M_{\odot}$, depending on the model adopted to describe the cluster dynamics. Such values are comparable to those of very massive clusters at lower redshifts. Our conclusion supports the view of the connection between extended radio emission and energetic phenomena in galaxy clusters.

References

1. G.O. Abell, H.G. Corwin Jr., & R.P. Olowin: ApJS, **70**, 1 (1989)
2. H. Ebeling, W. Voges, H. Böhringer, et al.: MNRAS, **281**, 799 (1996)
3. S.W. Allen: MNRAS, **296**, 392 (1998)
4. F. Govoni, T.A. Ensslin, L. Feretti, & G. Giovannini: A&A, **369**, 441 (2001)
5. J.C. Kempner, & L.P. David: MNRAS, **349**, 385 (2004)
6. A. Pisani: MNRAS, **265**, 706 (1993)
7. A. Pisani: MNRAS, **278**, 697 (1996)
8. D. Fadda, M. Girardi, G. Giuricin, F. Mardirossian, & M. Mezzetti: ApJ, **473**, 670 (1996)
9. K.M. Ashman, C.M. Bird, & S.E. Zepf: AJ, **108**, 2348 (1994)
10. A. Dressler, & S.A. Schectman: AJ, **95**, 985 (1988)

Dynamics and Shape of Brightest Cluster Galaxies

H. Andernach[1], K. Alamo-Martínez[1], R. Coziol[1] and E. Tago[2]

[1] Departamento de Astronomía, Universidad de Guanajuato, Mexico
heinz@astro.ugto.mx, karla@astro.ugto.mx, rcoziol@astro.ugto.mx
[2] Tartu Observatory, Tõravere, Estonia
erik@aai.ee

Summary. We identified Brightest Cluster Members (BCM) on DSS images of 1083 Abell clusters, derived their individual and host cluster redshifts from literature and determined the BCM ellipticity. Half the BCMs move at a speed higher than 37% of the cluster velocity dispersion $\sigma_{\rm cl}$, suggesting that most BCMs are part of substructures falling into the main cluster. Both, the BCM's velocity offset in units of $\sigma_{\rm cl}$, and BCM ellipticity, weakly decrease with cluster richness.

If BCMs formed "in-situ" they should "rest" at the bottom of the potential well of the cluster and have a radial velocity equal to the cluster mean. Previous studies, e.g. [4], based on small samples of clusters dominated by a cD galaxy, showed that this is far from reality. Here we extend these studies to 1083 Abell clusters likely to have a dominant galaxy, namely all clusters with Bautz-Morgan (BM) types I or I-II, all with Rood-Sastry (RS) type cD, and all clusters with notes in [1] indicating a "corona" of the first-ranked galaxy. From DSS images we derived positions for 1329 BCM candidates in 1076 clusters (occasionally more than one candidate per cluster), retrieved their basic parameters from NED, and extracted cluster mean redshifts, $z_{\rm cl}$, and velocity dispersions, $\sigma_{\rm cl}$, from the compilation maintained by two of us [2]. Deleting all foreground/background BCM candidates and restriction to clusters with $\geq$10 measured redshifts, yielded a sample of 385 BCMs in 326 Abell clusters for which we derived the relative velocity offset, $v_{\rm off}/\sigma_{\rm cl} = (v_{\rm BCM} - cz_{\rm cl})/(1 + z_{\rm cl})/\sigma_{\rm cl}$, with $v_{\rm BCM}$ the BCM radial velocity.

In Figure 1 we show that half of the BCMs in our sample move at peculiar velocities $> 0.37\,\sigma_{\rm cl}$. There is a trend for a smaller $v_{\rm off}/\sigma_{\rm cl}$ in richer clusters which is expected if the latter are dynamically more evolved.

We also determined BCM ellipticities using IRAF's `ellipse` for 1193 BCM candidates in 1012 clusters, but restricted our statistical analysis to the same sample of 385 BCMs mentioned above. Figure 2 shows that BCM ellipticity increases with richness. This may suggest that BCMs in richer clusters grow more likely by anisotropic mergers.

Our observations are consistent with a model where most BCM form during the collapse and virialization of poor clusters or compact groups with low velocity dispersions [3]. This supports the view that most galaxies formed in

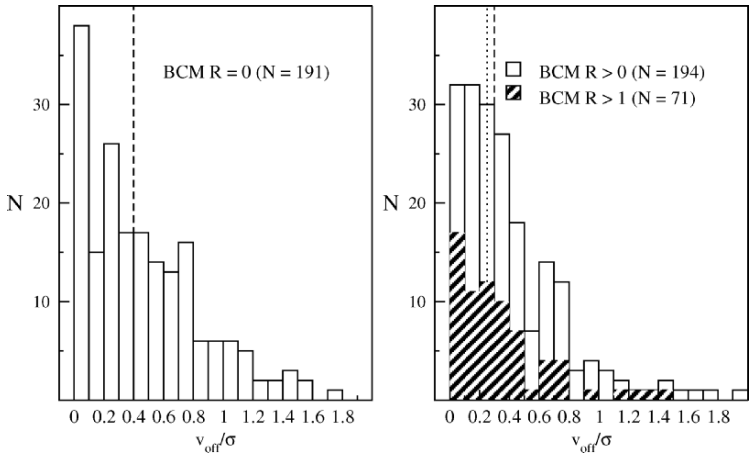

Fig. 1. Relative velocity offset for clusters with different Abell richness R. Median values are indicated with dashed lines or a dotted line for the shaded histogram.

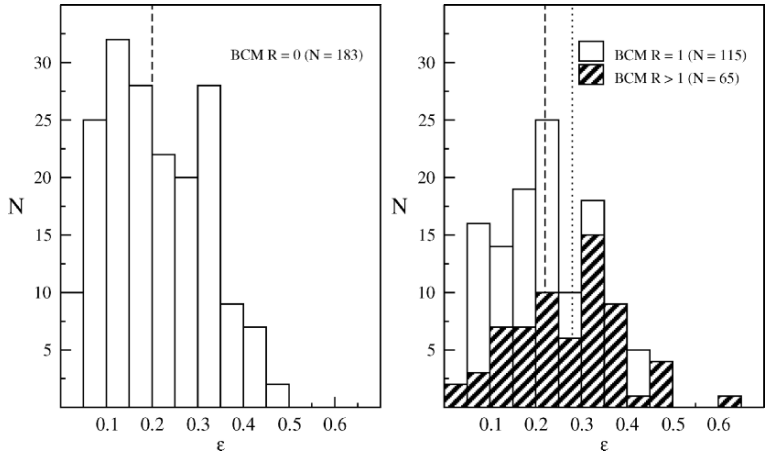

Fig. 2. BCM ellipticity distribution in clusters of different Abell richness. Median values are indicated with dashed lines or a dotted line for the shaded histogram.

groups (and not in rich clusters) with a common dark halo and/or individual halo of each galaxy which form(s) a local potential minimum for the BCM.

References

1. Abell G.O., Corwin Jr. H.G., Olowin R.P.: ApJS **70**, 1 (1989)
2. Andernach H., Tago E., Einasto M., Einasto J., Jaaniste J.: ASP Conference Series, Vol. 239, eds. A.P. Fairall & P.A. Woudt, p. 283 (2005)
3. Merritt D.: ApJ, **289**, 18 (1985)
4. Zabludoff A.I., Geller M.J., Huchra J.P., Vogeley, M.S.: AJ, **106**, 1273 (1993)

Author Index

Adami, C. – 267
Alamo-Martínez, K. – 395
Alves, D. – 45
Andernach, H. – 379, 395
Aruta, C. – 109
Athanassoula, E. – 349
Balogh, M. L. – 145
Barbuy, B. – 175
Barnes, D. G. – 33
Barrena, R. – 391, 393
Basilakos, S. – 285
Bassino, L. P. – 109
Bergond, G. – 349
Bomans, D. J. – 157
Borgani, S. – 355, 361
Borissova, J. – 45
Borthakur, S. – 349
Boschin, W. – 391, 393
Bosma, A. – 349
Bower, R. G. – 145
Bravo-Alfaro, H. – 193, 319
Brough, S. – 261
Buzzoni, A. – 91
Cannon, J. M. – 181
Carigi, L. – 241
Carlberg, R. G. – 145
Cellone, S. A. – 91, 109, 113
Chiosi, C. – 151
Cifuentes Cárdenas, A. – 113
Cigan, P. J. – 291
Colín, P. – 241
Combes, F. – 349
Conselice, C. J. – 123
Cora, S. A. – 355
Cortese, L. – 319
Cortés, J. R. – 343
Covone, G. – 267, 319
Coziol, R. – 163, 193, 379, 395
de Carvalho, R. R – 85, 175
de la Fuente, E. – 115, 139
de la Rosa, I. G. – 175
del Olmo, A. – 163, 301
De Rossi, M. E. – 239, 243
Dettmar, R.-J. – 157
Díaz, E. – 111
Dirsch, B. – 109
Durbala, A. – 301
Durret, F. – 267
Ebeling, H. – 67
Eke, V. R. – 53, 233
Espada, D. – 349
Flores-Fajardo, N. – 47
Forbes, D. – 97
Forte, J. C. – 113
Franco-Balderas, A. – 115, 139
Freeland, E. E. – 307
Freeman, K. C. – 33
Gallagher, J. S. – 291
Garcia, E. – 349
Gehrz, R. D. – 181
Geisler, D. – 41
Gibson, B. K. – 33
Girardi, M. – 391, 393
Gómez, M. – 109
Goto, T. – 79
Grebel, E. K. – 4
Gullieuszik, M. – 39
Hardy, E. – 343
Harris, W. E. – 41
Held, E. V. – 39
Hidalgo-Gámez, A. M. – 47
Hornstrup, A. – 67
Huchtmeier, W. K. – 349
Hwang, H. S. – 41
Infante, L. – 109
Iovino, A. – 85

Jackson, D. C. – 181
Kapferer, W. – 273
Katsiyannis, A. C. – 115
Kemp, S. N. – 115, 139
Kenney, J. D. P. – 343
Kilborn, V. A. – 33, 313
Kim, S. C. – 41
Kitzbichler, M. – 233
Kneib, J.-P. – 319
Koribalski, B. S. – 27
Kotov, O. – 67
Krusch, E. – 157
Lambas, D. G. – 239
Lee, H. – 181
Lee, M. G. – 41
Leon, S. – 349
Lima Neto, G. B. – 267
Lisenfeld, U. – 349
Loera-González, P. – 73
Magris C., G. – 197
Mamon, G. A. – 204
Martinez, M. A. – 163
McBride, C. – 227
Meaburn, J. – 115, 139
Mendes de Oliveira, C. – 103
Merlin, E. – 151
Mieske, S. – 103
Mihos, J. C. – 221, 227
Miles, T. A. – 279
Minniti, D. – 45
Molina, F. – 197
Möller, O. – 233
Mulchaey, J. S. – 145
Müller, V. – 157
Muriel, H. – 111
Natarajan, P. – 233
Odewahn, S. – 349
Oemler Jnr, A. – 145
O'Sullivan, E. – 331
Padilla, N. – 187
Park, H. S. – 41
Parravano, A. – 197
Pedersen, K. – 67
Peimbert, M. – 241
Perea, J. – 163, 301
Pérez Grana, J. A. – 115
Pérez, J. – 239
Pisano, D. J. – 33
Plana, H. – 301
Plauchu-Frayn, I. – 193
Plionis, M. – 285
Polomski, E. – 181
Pompei, E. – 85
Ponman, T. J. – 325, 349
Quintana, H. – 67
Ragone, C. – 111, 285
Rasmussen, J. – 67, 325, 349
Raychaudhury, S. – 279
Rejkuba, M. – 45, 169
Richtler, T. – 109
Rizzi, L. – 39
Burenin, R. – 67
Romanowsky, A. J. – 385
Rosado, M. – 301
Roychowdhury, S. – 337
Rudick, C. S. – 227
Rudie, G. C. – 291
Sabater, J. – 349
Sarajedini, A. – 41
Saucedo-Morales, J. – 73
Saviane, I. – 39
Scannapieco, C. – 239, 243
Sellim, I. – 349
Seguel, J. C. – 41
Skillman, E. D. – 22, 181
Smith Castelli, A. V. – 109
Spolaor, M. – 393
Staveley-Smith, L. – 33
Sulentic, J. – 301, 349
Tago, E. – 119, 395
Taylor, C. – 157
Temporin, S. – 273
Tissera, P. B. – 239, 243
Tornatore, L. – 355
Ulmer, M. P. – 267
Vazdekis, A. – 175
Vennik, J. – 119
Verdes-Montenegro, L. – 349
Verley, S. – 349
Vikhlinin, A. – 67
Vrtilek, J. M. – 331
Wehner, E. H. – 291
West, M. J. – 103
Wilman, D. J. – 145
Woodley, K. A. – 297
Woodward, C. E. – 181
Yun, M. S. – 349
Zabludoff, A. – 250
Zier, C. – 195

ESO ASTROPHYSICS SYMPOSIA
European Southern Observatory

Series Editor: Bruno Leibundgut

R. Morganti, W.J. Couch (Eds.),
Looking Deep in the Southern Sky
Proceedings, 1997. XXIII 336 pages. 1999.

J.R. Walsh, M.R. Rosa (Eds.),
Chemical Evolution from Zero to High Redshift
Proceedings, 1998. XVIII, 312 pages. 1999.

J. Bergeron, A. Renzini (Eds.),
From Extrasolar Planets to Cosmology: The VLT Opening Symposium
Proceedings, 1999. XXVIII, 575 pages. 2000.

A. Weiss, T.G. Abel, V. Hill (Eds.),
The First Stars
Proceedings, 1999. XIII, 355 pages. 2000.

A. Fitzsimmons, D. Jewitt, R.M. West (Eds.),
Minor Bodies in the Outer Solar System
Proceedings, 1998. XV, 192 pages. 2000.

L. Kaper, E.P.J. van den Heuvel, P.A. Woudt (Eds.),
Black Holes in Binaries and Galactic Nuclei: Diagnostics, Demography and Formation
Proceedings, 1999. XXIII, 378 pages. 2001.

G. Setti, J.-P. Swings (Eds.)
Quasars, AGNs and Related Research Across 2000
Proceedings, 2000. XVII, 220 pages. 2001.

A.J. Banday, S. Zaroubi, M. Bartelmann (Eds.),
Mining the Sky
Proceedings, 2000. XV, 705 pages. 2001.

E. Costa, F. Frontera, J. Hjorth (Eds.),
Gamma-Ray Bursts in the Afterglow Era
Proceedings, 2000. XIX, 459 pages. 2001.

S. Cristiani, A. Renzini, R.E. Williams (Eds.),
Deep Fields
Proceedings, 2000. XXVI, 379 pages. 2001.

J.F. Alves, M.J. McCaughrean (Eds.),
The Origins of Stars and Planets: The VLT View
Proceedings, 2001. XXVII, 515 pages. 2002.

J. Bergeron, G. Monnet (Eds.),
Scientific Drivers for ESO Future VLT/VLTI Instrumentation
Proceedings, 2001. XVII, 356 pages. 2002.

M. Gilfanov, R. Sunyaev, E. Churazov (Eds.),
Lighthouses of the Universe: The Most Luminous Celestial Objects and Their Use for Cosmology
Proceedings, 2001. XIV, 618 pages. 2002.

R. Bender, A. Renzini (Eds.),
The Mass of Galaxies at Low and High Redshift
Proceedings, 2001. XXII, 363 pages. 2003.

W. Hillebrandt, B. Leibundgut (Eds.),
From Twilight to Highlight: The Physics of Supernovae
Proceedings, 2002. XVII, 414 pages. 2003.

P.A. Shaver, L. DiLella, A. Giménez (Eds.),
Astronomy, Cosmology and Fundamental Physics
Proceedings, 2002. XXI, 501 pages. 2003.

M. Kissler-Patig (Ed.),
Extragalactic Globular Cluster Systems
Proceedings, 2002. XVI, 356 pages. 2003.

P.J. Quinn, K.M. Górski (Eds.),
Toward an International Virtual Observatory
Proceedings, 2002. XXVII, 341 pages. 2004.

W. Brander, M. Kasper (Eds.),
Science with Adaptive Optics
Proceedings, 2003. XX, 387 pages. 2005.

A. Merloni, S. Nayakshin, R.A. Sunyaev (Eds.),
Growing Black Holes: Accretion in a Cosmological Context
Proceedings, 2004. XIV, 506 pages. 2005.

L. Stanghellini, J.R. Walsh, N.G. Douglas (Eds.)
Planetary Nebulae Beyond the Milky Way
Proceedings, 2004. XVI, 372 pages. 2006.

S. Randich, L. Pasquini (Eds.)
Chemical Abundances and Mixing in Stars in the Milky Way and its Satellites
Proceedings, 2004. XXIV, 411 pages. 2006.

A.P. Lobanov, J.A. Zensus, C. Cesarsky, P.J. Diamond (Eds.)
Exploring the Cosmic Frontier
Astrophysical Instruments for the 21st Century.
XXVI, 270 pages. 2006.

I. Saviane, V.D. Ivanov, J. Borissova (Eds.)
Groups of Galaxies in the Nearby Universe
Proceedings, 2005. XX, 390 pages. 2007.